Development of small-molecule, peptide-mimetic, activating ligands of the potassium efflux (Kef) system



Holly Alice Philippa Bunce

Lady Margaret Hall, University of Oxford

Thesis submitted for the degree

Doctor of Philosophy in Organic Chemistry

Hilary Term 2021

Under the supervision of

Professor Stuart Conway (University of Oxford)

Dr Alastair Parkes (Evotec)

Dr Helen Horsley (UCB Pharma)

Name: HOLLY BUNCE Candidate number: 1012360

College: LADY MARGARET HALL Supervisor: PROF. STUART CONWAY

Title of thesis: Development of small-molecule, peptide-mimetic, activating ligands of the potassium efflux (Kef) system

Please tick to confirm the following:

I have read and understood the University's disciplinary regulations concerning conduct in examinations and, in particular, the regulations on plagiarism (*The University Student Handbook* Section 8.7; available at https://www.ox.ac.uk/students/academic/student-handbook). ☑

I have read and understood the Education Committee's information and guidance on academic good practice and plagiarism at

https://www.ox.ac.uk/students/academic/guidance/skills?wssl=1. ☑

The [thesis/dissertation/extended essay/assignment/project/other submitted work] I am submitting is entirely my own work except where otherwise indicated. ☑

It has not been submitted, either partially or in full, either for this Honour School or qualification or for another Honour School or qualification of this University (except where the Special Regulations for the subject permit this), or for a qualification at any other institution. ☑

I have clearly indicated the presence of all material I have quoted from other sources, including any diagrams, charts, tables or graphs. ☑

I have clearly indicated the presence of all paraphrased material with appropriate references. ☑

I have acknowledged appropriately any assistance I have received in addition to that provided by my [tutor/supervisor/adviser]. ☑

I have not copied from the work of any other candidate. ☑

I have not used the services of any agency providing specimen, model or ghostwritten work in the preparation of this thesis/dissertation/extended essay/assignment/project/other submitted work. (See also section 2.4 of Statute XI on University Discipline under which members of the University are prohibited from providing material of this nature for candidates in examinations at this University or elsewhere: http://www.admin.ox.ac.uk/statutes/352-051a.shtml). ☑

I agree to retain an electronic copy of this work until the publication of my final examination result, except where submission in hand-written format is permitted. ☑

I agree to make any such electronic copy available to the examiners should it be necessary to confirm my word count or to check for plagiarism. ☑

Candidate's signature:  Date: 03-Mar-21

Table of Contents

Abstract i

Acknowledgements iii

Abbreviations vii

Chapter 1: Introduction 1

1.1 Antimicrobial Resistance 1

1.2 Antibiotic Classes 4

1.2.1 Types of Antibiotics 4

1.2.2 Antibiotic Resistance 8

1.2.2.1 Horizontal gene transfer 9

1.2.2.2 Inactivation of the antibiotic 9

1.2.2.3 Target modification 10

1.2.2.4 Efflux pumps 10

1.2.3 Resistance exhibited by the ESKAPE pathogens 11

1.3 Chemical Diversity Within Antibiotics 12

1.3.1 Antibiotic peptides 14

1.3.2 Amide isosteres in peptide-mimetics 15

1.4 The Potassium (K^+) Efflux System (Kef) 17

1.4.1 Structure and function 18

1.4.2 Clinical relevance of Kef 22

1.4.2.1 The role of potassium Ions (K^+) in bacterial cell homeostasis 22

1.4.2.2 The ESKAPE pathogens 23

1.4.2.3 Kef in Gram-positive bacteria 25

1.4.2.4 Kef model system 25

1.5 Refinement of the known Kef ligands and SAR 26

1.6 Summary 35

1.7 Project Aims 36

Chapter Two: Investigation of Pyridinones as an Amide Replacement in *Sd*Kef Ligands 39

2.1 Introduction to the Pyridinone Scaffold 39

2.2 Synthesis of the Pyridinone 43

2.2.1 Synthesis of the peptide-mimetic ligand backbone 44

2.2.2 Introduction of a synthetic handle 48

2.2.3 Establishing coupling conditions to install the headgroup 51

2.2.4 Exploration of new headgroups 55

2.2.5 Work towards a pyridinone with a known activating headgroup 59

2.3 Biophysical Assays with *Sd*KefQCTD 63

2.3.1 WaterLOGSY 63

2.3.2 DSF 74

2.3.3 Towards quantification of a K_d of the pyridinone ligand using NMR 82

2.4 Conclusions 89

Chapter Three: Investigation of Oxazoles as an Amide Replacement in *Sd*Kef Ligands 91

3.1 Introduction to the Oxazole Scaffold 91

3.2 Synthesis of the Oxazole Peptide-Mimetic Ligand 94

3.2.1 Formation of the dipeptide backbone 95

3.2.2 Cyclisation optimisation 96

3.2.3 Oxidation to the desired oxazole 99
3.2.4 One-pot coupling step 100
3.2.5 Attempts to deprotect the methyl ester **148** 102
3.2.6 Investigating an alternative ester protecting group 104
3.2.7 Synthesis of the (*S*)-cysteine enantiomer **165** 109
3.3 Biophysical Assays with *Sd*KefQCTD 111
3.3.1 WaterLOGSY 111
3.3.2 DSF 115
3.4 Conclusions 117

Chapter Four: Investigation of Imidazopyridines as an Amide Replacement in *Sd*Kef Ligands 119
4.1 Introduction to the Imidazopyridine Scaffold 117
4.2 Synthesis of the Imidazopyridine Ligand 122
4.2.1 Formation of the ring system 123
4.2.2 Optimisation of the acetylation reaction 126
4.2.3 Headgroup installation 127
4.2.4 Iodination of **180** 128
4.2.5 Carboxylation of the imidazopyridine scaffold 129
4.2.6 Synthesis of analogues of the imidazopyridine **73** 131
4.3 Biophysical Assays with *Sd*KefQCTD 132
4.3.1 WaterLOGSY 132
4.3.2 DSF 134
4.4 Conclusions 135

Chapter Five: Identification and Evaluation of Peptide Isosteres Using Scaffold Hopping 137

5.1 Introduction to Scaffold Replacement 137

5.2 Scaffold Hopping Experiments 140

5.3 Synthesis of the Selected Dipeptide Mimic, **74** 143

5.4 Biophysical and Cell-Based Assays 146

5.4.1 WaterLOGSY 146

5.4.2 Kirby-Bauer disc assay 149

5.5 Conclusions 152

Chapter Six: Conclusions and Future Work 155

6.1 Conclusions 155

6.2 Future Work 161

Chapter Seven: Experimental 165

7.1 General Chemistry Experimental 165

7.2 Compound Synthesis Procedures and Data 170

7.3 Biology Experimental 239

7.3.1 General biology experimental 239

7.3.2 Protein expression and purification 240

7.3.3 SDS-PAGE 242

7.3.4 Water-ligand observed via gradient spectroscopy (WaterLOGSY) NMR 243

7.3.5 DSF 244

7.3.6 Kirby-Bauer disc assay 245

References 247

Appendices 282

A: Supplementary Figures 282

B: *Sd*KefQCTD Protein Characterisation 283

C: WaterLOGSY Full Spectra 291

D: Thermal Shift Data 301

E: Kirby-Bauer Disc Assay 305

F: Computational Chemistry 307

G: NMR Spectra of Novel Compounds 309

H: Image Permissions 435

Abstract

More people are expected to die of antibiotic resistant infections than cancer by 2050. Resistance is seen in virtually all currently available antibiotics, and only two new classes have been developed since the 1960s. The Kef system is a novel prospective antibiotic target for a new antibiotic class. Kef is a H^+/K^+ antiporter found in Gram-negative bacteria including the ESKAPE pathogens, which are difficult to treat. Kef is involved in bacterial homeostasis and protection mechanisms against electrophiles. Glutathione (GSH) is the native ligand of Kef and can react with electrophiles in the cell to form adducts (GSX) which activate the Kef system and protect the cell. The highest affinity GSX is ^{t}BuSG, a synthetic peptide-based ligand, from which was derived the dipeptide ligand **70**.

The focus of this research was to design peptide-mimetic Kef ligands based on **70**, that disrupt the function of the Kef system, and inhibit bacterial growth. The new scaffolds are designed to have improved chemical properties relative to the dipeptides and greater synthetic flexibility for ligand development. Three ligand scaffolds and analogues were designed using amide isosteres to replace the central amide bond: a pyridinone (**71**, Chapter 2), an oxazole (**72**, Chapter 3), and an imidazopyridine (**73**, Chapter 4).

Chapter 2 describes the synthesis of **71**, and ten carboxylic acid analogues, using a late stage diversification route. Varying the headgroups allowed exploration of the structure-activity relationship (SAR) around the ligand binding site. All the tested analogues were found to bind Kef using water-ligand observed *via* gradient spectroscopy

(waterLOGSY) NMR. Differential scanning fluorimetry (DSF) indicated different pyridinone headgroups stabilised and destabilised the Kef system. Chapter 3 describes the synthesis of **72** from an optimised route based on prior literature, however binding was not observed by waterLOGSY NMR or DSF. Chapter 4 describes the synthesis of **73** from a substituted pyridine. The acid showed promising initial results as a peptide mimetic and bound during waterLOGSY NMR analysis. Investigation of the magnitude of stabilisation using DSF was inconclusive, suggesting **73** is weakly binding, and below the DSF detection limit.

Chapter 5 describes the use of the computational technique scaffold-hopping to try and identify a new Kef ligand scaffold. ROCS, Spark, Blaze, and MOE programmes were used to search databases for a mimetic of the GSH backbone. A synthetically attractive hit **74** was selected and synthesised with three analogues, but these were not found to bind or activate Kef, from analysis by waterLOGSY NMR and Kirby-Bauer disc assay.

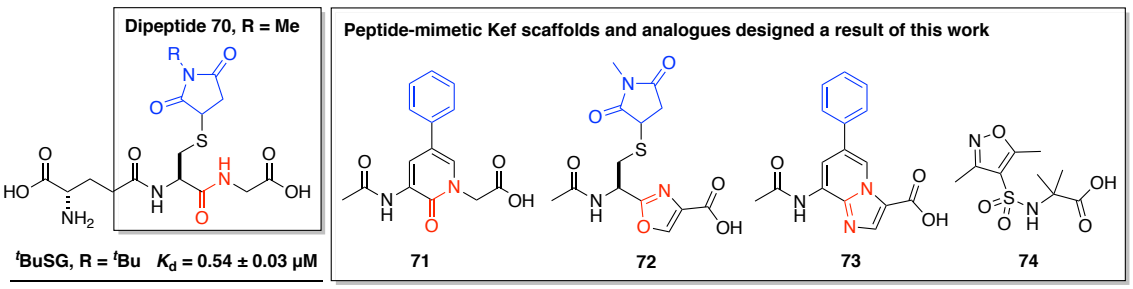


Figure 1. Examples of peptide and peptide-mimetic Kef ligands. Dipeptide **70** is derived from ^{t}BuSG and has the minimal structural requirement for activation of the Kef system. Peptide-mimetic scaffolds **71** and **73** were identified as the first peptide-mimetic ligands for the *Shewanella denitrificans* Q-linker C-terminal domain (*Sd*KefQCTD) Kef system.

The pyridinone and imidazopyridine scaffolds are the first peptide-mimetic ligand families for *Sd*KefQCTD. A high affinity Kef ligand could be developed into an antibiotic with a novel mode of action, providing a significant benefit to modern healthcare, with the increasing levels of antibiotic resistance.

Acknowledgements

First of all, I would like to thank my supervisor, Professor Stuart Conway for all your help and advice during this project. I am so pleased I got to work on something I believe is really important as with antibiotics, and to experience so much new chemistry and chemical biology that I hope will stand me in good stead for my career to come. I will always try to "be more stubborn than my chemistry" and apply the right amount of Cowboy to get the over future ~~herd~~ hurdles. Thank you for letting me join your fantastic group, from which I have gained many friends over the years.

Thank you to my industrial supervisors, Dr Helen Horsley and Dr Alastair Parkes, I enjoyed our meetings, and you were both always so helpful and full of ideas for the project. Thank you to Dr Michelle Southey and Dr Mike Bodkin for your support during my time at Evotec for Scaffold Hopping! Thank you to past Team Kef members, Catherine, Anthony, and Mary. Catherine, thank you for showing me the ropes, for all the good fun we had during your DPhil, and for your lab job Larry the Lyophiliser!

To Jess, my 'lil pal! Thank you for being my constant and wonderful friend, ready to bounce ideas and jokes off from. I enjoyed nearly every reason to tell you something funny from the other side of G11. I can think back on many a great joke or video: duck army, rollercoasters, and pulling things out of a hat. I hope we can continue to come up with more, Notebook: 2nd Ed.!

Thank you to the present members of the Conway Group. Adam, for your infectious joy for science and questionable humour, I enjoyed sharing G12 with you in 2020. Thank you to Katrina, Darius, Patrick, and Jenny, I enjoyed chatting with all of you about every topic under the sun, you are all great scientists and I hope the rest of your DPhils go well. To Alastair, Bernie, and Sophie, I am sad our overlap in the lab was so short, thank you all for being great and good luck with your DPhils. Thank you also to our post-docs not already mentioned: Maria, Pascal, Antoine, and unofficial Conway Group member Debs! I have appreciated all your advice, do not change your approachability and kindness! Aleksy, Ali, Max, and Sarah, good luck for the remainder of your Part IIs! Thank you to Ewen, Maze, Coco, and Joe for teaching me new things, and as well as Amy and Mus for all the good times in G11 and G12! Thank you to everyone who provided feedback on this thesis, I am very grateful for your time and good suggestions.

I would also like to thank the NMR staff of the CRL especially Professor Timothy Claridge, thank you all so much for being so helpful and approachable. I learned a lot during my DPhil, and you never made me feel like I was asking a silly question! Thank you also to Professor Christina Redfield for your accommodating me to use the Biochemistry 750 instrument when our 700 was unavailable. Thank you to the CRL support staff, you keep the building running and us all able to continue doing research! Thank you to Dr Adam Hardy, and the CJS group for all your help and advice during my wrestling with the equipment in Lower Ground. Thank you to Dr David Staunton for accommodating me in the Biochemistry Molecular Biophysics Suite, and to the AJR group for always letting me use your analytical balance!

Finally, I would like to thank my family especially Mum, Dad, and Nana. Thank you for all the encouragement even though you didn't have a clue what I was talking about. Thank you for the phone calls, posting things I needed, transport help, and personal bicycle repair! Thank you to all my friends, I've met such a wonderful group around the Gloucester Green gaming table, I am very grateful for all of you! Thank you to Loane, meeting you was one of the best things about Oxford, and dragging you to Comic con and other places round the UK made the DPhil experience better!

Last, but not least, thank you to my fiancé Sam. You are a miracle and I appreciate you so much. Our cohabitation adventure could not have been more successful, and you continue to support and care for me each day. Thank you for being there whilst I finished this work, and I look forward to the next bit!

Abbreviations

Abbreviation	Definition
3D	3-Dimensional
Ac_2O	Acetic anhydride
ACN	Acetonitrile
ADMET	Absorption, distribution, metabolism, excretion, and toxicity
APS	Ammonium persulfate
BLAST	Basic local alignment search tool
Boc	*Tert*-butyloxycarbonyl
CL	Cell lysate
*c*log*D*	Calculated log*D*
$_C$LogP	Calculated octanol/water partition coefficient
conc.	Concentrated
CPMG NMR	Carr-Purcell-Meiboom-Gill NMR
CTD	C-terminal domain
D	Distribution coefficient
DBU	1,8-Diazabicyclo[5.4.0]undec-7-ene
DCC	Dynamic combinatorial chemistry
DCL	Dynamic combinatorial library
DCM	Dichloromethane
DELTA-BLAST	Domain Enhanced Lookup Time Accelerated BLAST
DIAD	Diisopropyl azodicarboxylate

DIPEA	Diisopropylethylamine
DMAP	Dimethylaminopyridine
DMF	Dimethylformamide
DMSO	Dimethyl sulfoxide
DOS	Diversity-oriented synthesis
DPPA	Diphenylphosphoryl azide
DSF	Differential Scanning Fluorimetry
EDTA	Ethylenediaminetetraacetic acid
EPI	Efflux pump inhibitors
eq.	Equivalents
ESG	Ethyl succinimido glutathione
GSH	Glutathione
h	Hours
HBA	Hydrogen bond acceptors
HBD	Hydrogen bond donors
HEPES	4-(2-Hydroxyethyl)-1-piperazineethanesulfonic acid
IMAC	Immobilised metal affinity chromatography
IP	Intellectual property
ITC	Isothermal calorimetry
IV	Intravenous
K_d	Dissociation (equilibrium) constant
LiOH	Lithium hydroxide
MD	Molecular dynamics

MDR	Multi-drug (antibiotic) resistant
MeOH	Methanol
MG	Methylglyoxal
MOA	Mode of action
MS	Mass spectrometry
MW	Molecular weight
NaH	Sodium hydride, 60% dispersion with mineral oil
NBS	N-bromosuccinimide
NCS	N-chlorosuccinimide
NEB	New England Biolabs
NEM	*N*-ethylmaleimide
NEt_3	Triethylamine
NIS	N-iodosuccinimide
NMR	Nuclear magnetic resonance
NOE	Nuclear Overhauser Effect
PBP	Penicillin binding protein
PBS	Phosphate buffered saline, pH 7.4
PCR	Polymerase chain reaction
PD	Pharmacodynamics
PDB	Protein Data Bank
PDBID	Protein database identification number
PK	Pharmacokinetics
PMI	Principle moment of inertia

PPh_3	Triphenylphosphine
PSA	Polar surface area
ptfmF	p-Trifluoromethyl-L-phenylalanine
QCTD	Quaternary C-terminal domain
QCTD	(Kef) Q-linker C-terminal domain
RB	Rotatable bonds
rRNA	Ribosomal ribonucleic acid
RT	Room temperature
SAR	Structure-activity relationship
SDS-PAGE	Sodium dodecyl sulphate polyacrylamide gel electrophoresis
SEC	Size-exclusion chromatography
SFI	Solubility forecast index
TEMED	Tetramethylethylenediamine
TESH	Triethylsilane
TFA	Trifluoroacetic acid
THF	Tetrahydrofuran
TLC	Thin layer chromatography
T_m	Melting temperature
TMSCl	Trimethylsilyl chloride
TPSA	Topological polar surface area
waterLOGSY	Water-ligand observed *via* gradient spectroscopy
WL	WaterLOGSY
ΔT_m	Thermal shift (change in melting temperatures, °C)

Chapter One: Introduction

1.1 Antimicrobial Resistance

Antimicrobial resistance (AMR) is arguably the most serious threat to modern medicine. The current prediction is that more people will die of antibiotic resistant infections than cancer by 2050 (Figure 1.1).[1]

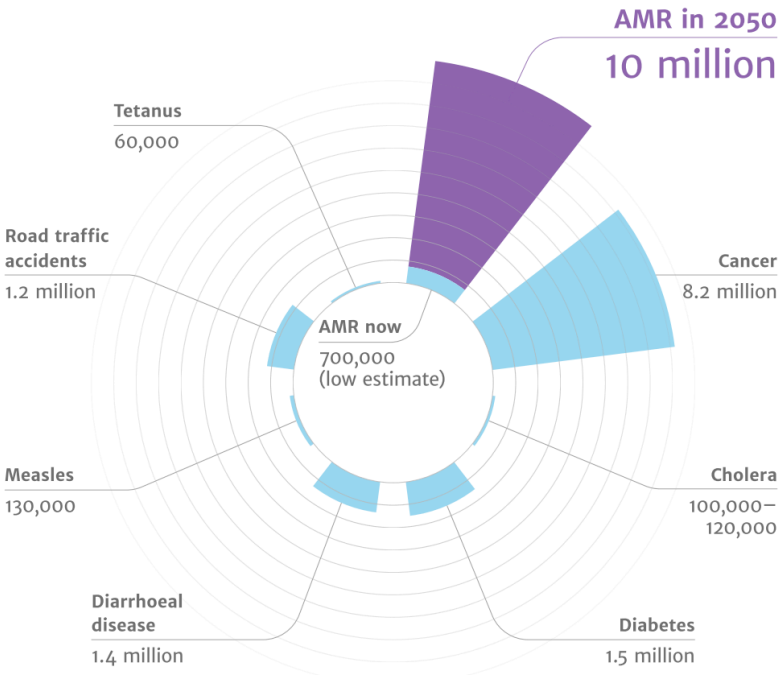


Figure 1.1. Graphical representation of the predicted increase in deaths from 2016 (blue) to 2050 (purple) due to antimicrobial resistance (AMR) compared to deaths by other causes. Figure reproduced with permission from Tackling Drug-Resistant Infections Globally - Final Report and Recommendations.[1]

In both developed and developing economies, the impact of AMR will render common surgeries impossible due to the risk of infection and will eradicate some of the most basic healthcare. Identification of the bacterial type responsible for an infection can be time consuming, and treatment must be administered as quickly as possible for patients with serious infections, and therefore the ideal anti-bacterial drug should be broad spectrum.[2]

Research into the development of new anti-infectives including antibiotics has slowed since the 1940s–1960s ("The Golden Age of Antibiotics"),[3] which is likely due to the decreased pharmaceutical investment into the development and sale of new medicines. New anti-infectives have several key challenges including expensive development, high likelihood of failure, and poor returns.[4,5]

Much antibiotic development in the 1990s and early 2000s used a genomics based approach for discovery, with a focus on identifying druggable targets only found in prokaryotes.[6,7] This type of discovery meant compound affinity was prioritised over other considerations such as: biased libraries towards hit compounds for human targets, properties including bacterial permeability, and minimising compound efflux. However, the fundamental problem associated with anti-infective drug discovery is resistance (covered in more detail in section 1.2.2), which will make a compound ineffective, and impacts returns on investment.[1,8] As antibiotics are typically taken as short courses, this also reduces profits compared to treatments for chronic medical problems.[5] Worldwide, science has a responsibility to develop new antibiotics for the global population, but making the discovery platform (a group of technologies) more accessible to pharmaceutical companies is one of the first challenges in increasing the development of new antibiotic medicines.[9,10]

Bacterial species are categorised as either Gram-negative or Gram-positive from their colour following the Gram-stain technique.[11] Gram-positive bacteria compromise 40% exposed peptidoglycans by mass, whereas Gram-negative bacteria have an outer membrane that encases the peptidoglycans in the periplasmic space (Figure 1.2). The

stain utilises a violet-iodide dye that is applied to the bacteria. The exposed peptidoglycans in Gram-positive bacteria retain the purple colouration from the dye, and Gram-negative bacteria do not (and are then often counterstained, with for example safranin).[12]

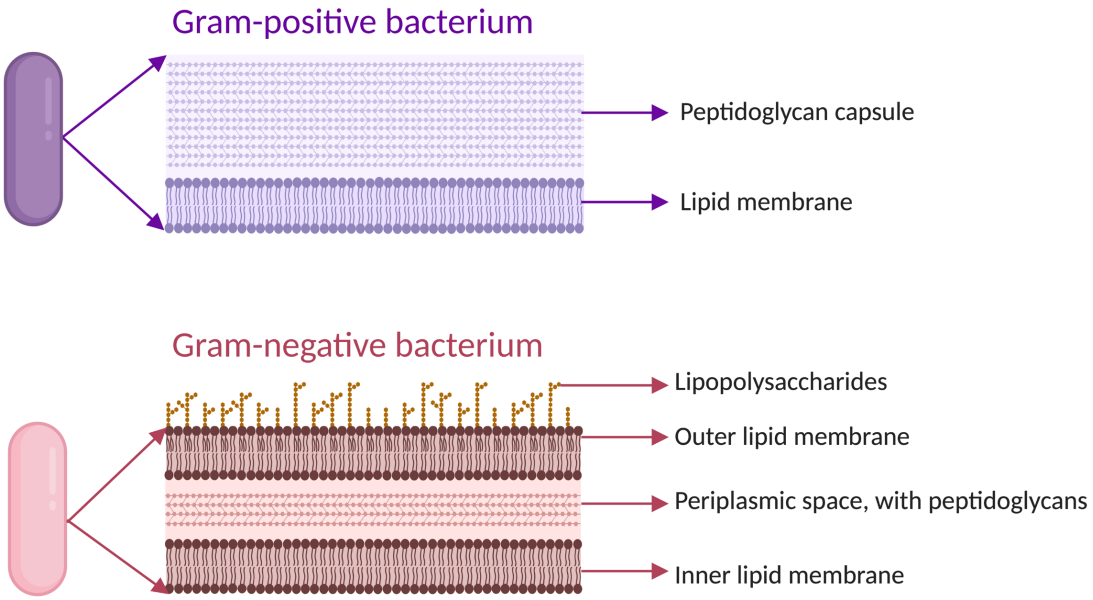


Figure 1.2. Structural differences between Gram-positive and Gram-negative bacteria.[13] Gram-positive bacteria have one lipid membrane and a thick peptidoglycan capsule, which absorbs the violet stain. Gram-negative bacteria have peptidoglycan found in the periplasmic space between the two membranes and can be decolorised.[11]

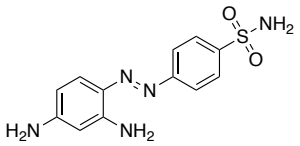
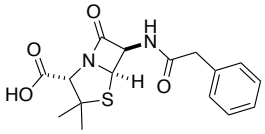
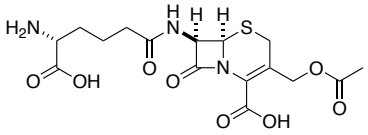
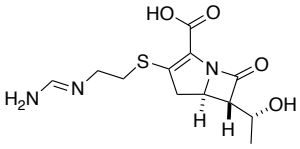
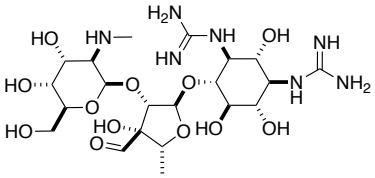
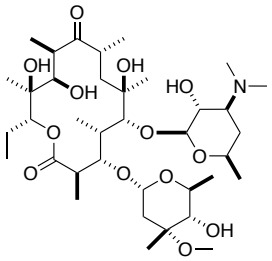
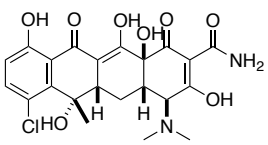
The ESKAPE pathogens are a group of bacteria responsible for up to 16% of hospital acquired infections (HAIs).[14] The ESKAPE pathogens include *Enterococcus faecium* (E), *Staphylococcus aureus* (S), *Klebsiella pneumoniae* (K), *Acinetobacter baumannii* (A), *Pseudomonas aeruginosa* (P), and the *Enterobacter* species (E) family.[15] Of these, *K. pneumoniae*, *A. baumannii*, *P. aeruginosa*, and all *Enterobacter* species are Gram-negative. Development of antibiotic drugs to target Gram-negative bacteria is especially important because of the clinical relevance of these species. However, it is especially difficult to deliver drugs to cytoplasmic targets within Gram-negative bacteria because of their two membranes and rapid compound expulsion from efflux pumps.[8,16,17]

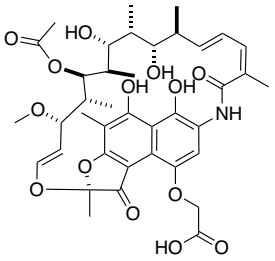
1.2 Antibiotic Classes

1.2.1 Types of antibiotics

The first antibiotic drug used clinically was Salvarsan in 1910. This compound is an organo-arsenic drug,[3,18] which shows toxicity to humans and is therefore no longer used.[19] However, one of the most ground-breaking medical advancements of the last 100 years was the discovery of the antibiotic Penicillin (**2**), in 1928.[20] This discovery heralded the beginning of the Golden Age of Antibiotics, which led to the discovery of many different classes of antibiotics.[3] A consequence of this progress was the start of the complacent belief that bacterial infections were a solved problem.[21,22] The flooding of new antibiotics into the market during the Golden Age resulted in the assumption that victory had been achieved against bacterial infection and abandonment of research in this area.[23,24] Multiple new classes of antibiotics with different modes of action were discovered from 1940–1970, with some resurgence from 2000,[25] the major established classes of which are detailed below with their modes of action (MOA, Table 1.1).[26,27]

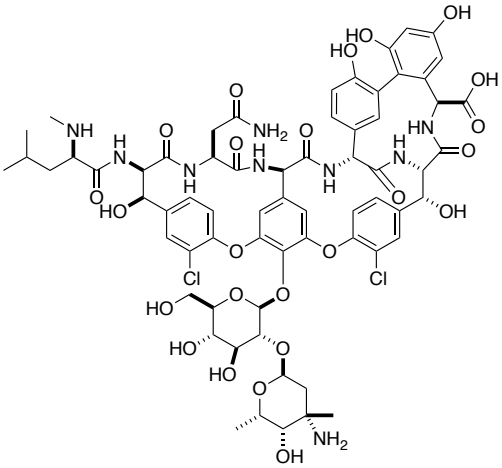
Table 1.1. Structure of the first discovered antibiotic as examples of each class, and summary information on their discovery and mode of action.

Antibiotic Structure	Summary
	**Sulfonamides** Discovered: 1932 (Prontosil, **1**)[27] by Domagk. MOA: Folate synthesis, inhibition of dihydropteroate synthetase
	**β-lactams** Discovered: 1928 (Penicillin, **2**)[20] by Fleming. MOA: Inhibition of cell wall biosynthesis.
	**Cephalosporins** Discovered: 1948 (cephalosporin C, **3**)[28] by Giuseppe Brotzu, (Edward Abraham and Guy Newton). MOA: Inhibition of cell wall biosynthesis.
	**Carbapenems** Discovered: 1976 (Imipenem, **4**)[29] by Miyadera *et al*. MOA: Inhibition of cell wall biosynthesis.
	**Aminoglycosides** Discovered: 1943 (Streptomycin, **5**)[30] by Waksman, Schatz, and Bugie . MOA: Mistranslation of proteins *via* binding to 30S ribosomal subunits.
	**Macrolides** Discovered: 1949 (erythromycin, **6**)[31] by Bunch and McGuire. MOA: Mistranslation of proteins *via* binding to 50S ribosomal subunits.
	**Tetracyclines** Discovered: 1945 (chlortetracycline, **7**)[32] by Duggar MOA: Mistranslation of proteins *via* binding to 30S ribosomal subunits.



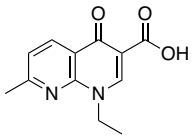
Rifamycins

Discovered: 1957 (rifamycin B, **8**)[33] by Sensi.
MOA: Transcription inhibitor, binds β-subunit of RNA polymerase



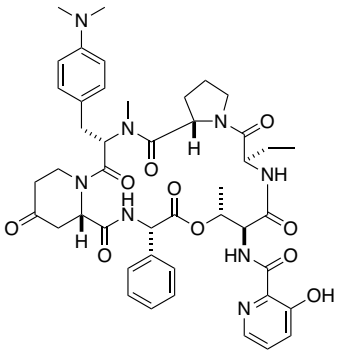
Glycopeptides

Discovered: 1952 (vancomycin, **9**)[34] by Kornfeld
MOA: Inhibition of cell wall biosynthesis.



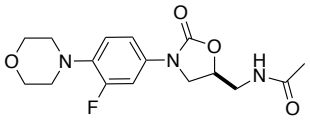
Quinolones

Discovered: 1962 (nalidixic acid, **10**),[35] by Lesher *et al*.
MOA: Inhibition of DNA gyrase



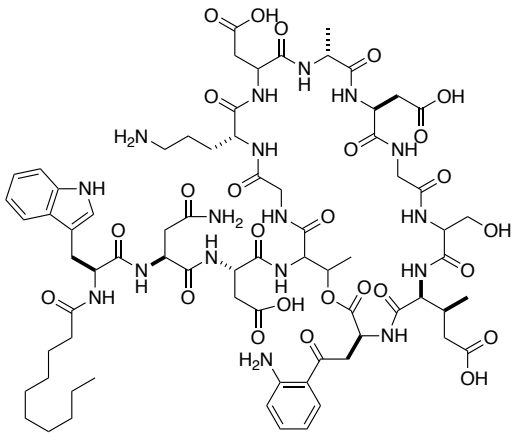
Streptogramins

Discovered: 1953 (streptogramin B, **11**),[36] by Charney *et al*.
MOA: Mistranslation of proteins *via* binding to 50S ribosomal subunits.



Oxazolidinones

Discovered: 1978 (class, DuPont, **12**),[37] 1996 (linezolid),[38] by Brickner *et al*.
MOA: Mistranslation of proteins *via* binding to 50S ribosomal subunits.



Lipopeptides
Discovered: 1985 (Daptomycin, **13**),[39] by Eliopoulos *et al.*
MOA: Disruption of cell-membrane, leading to cell lysis.

There are many other classes of antibiotics not included in Table 1.1,[3,40] but these examples have been selected because of their clinical relevance.[26,27] Co-amoxiclav (**14**, **15**) and piperacillin-tazobactam (**16**, **17** Figure 1.3) was the main β-lactam/β-lactamase inhibitor combination therapy used as front line antibiotic treatments in the UK in 2013.[41] The penicillin class accounts for approximately 50% of prescribed medicines from 2013–2015 in uncomplicated UK infections.[42,43] Vancomycin (**9**), daptomycin (**13**), colistin, and tigecycline are the current drugs of last resort, meaning they are not used for routine treatment to prevent accumulation of resistance for the treatment of only multi-drug resistant (MDR) infections,[44,45] and concerns over toxic side effects.[46]

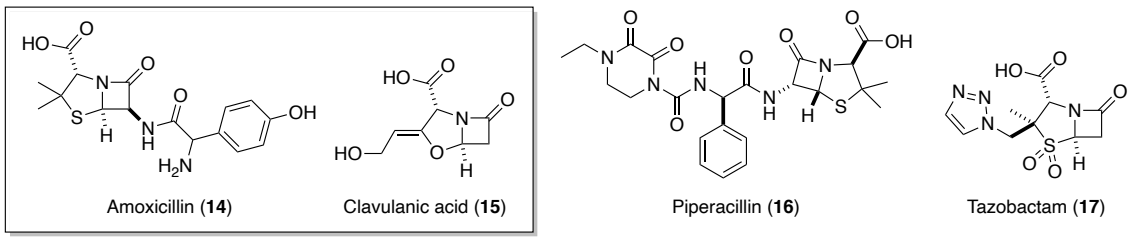


Figure 1.3. Structures of Co-amoxiclav (amoxicillin and clavulanic acid) and piperacillin-tazobactam.

1.2.2 Antibiotic resistance

Following the emergence of MRSA and other MDR Gram-positive infectious species, there was a large response from the research community in the development of antibiotics capable of combating Gram-positive bacterial infections.[47] However, Gram-negative infections have been somewhat neglected because of this publicity, and antibiotics capable of targeting these infections are increasingly needed with the emergence of resistant strains.[48]

The additional outer membrane of Gram-negative bacteria provides selective permeability, making these infections particularly difficult to treat. Hydrophobic antibiotics aim to penetrate the lipid membrane directly (for example aminoglycosides and macrolides), where hydrophilic antibiotics enter through porins (for example β-lactams). Resistance mechanisms to prevent both forms of entry have been observed,[49] and Gram-negative bacteria can have cooperative resistance systems.[49,50]

Common mechanisms of resistance include drug target modification, efflux pumps, and inactivation of the antibiotic (Figure 1.4). These mechanisms of resistance can be passed between bacteria by horizontal gene transfer,[26,51] which is a mechanism by which two organisms exchange genetic information where one is not ancestrally descended from the other.[52] Several other processes exist, such as that of *A. baumannii* which has intrinsically slow porins which decrease its permeability to antibiotics.[53]

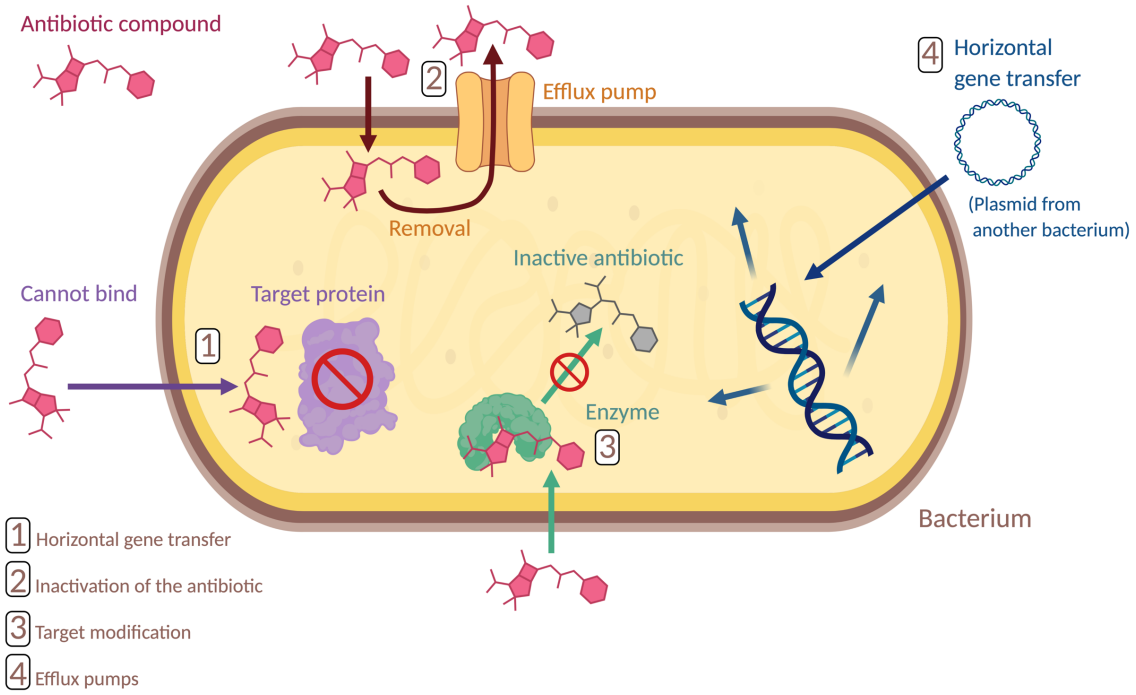


Figure 1.4. Bacterial resistance mechanisms cartoon.[13] Numbered representations: 1) target modification, where the target is modified so the antibiotic cannot bind; 2) efflux pumps, these remove the antibiotic after it has entered the cell; 3) inactivation of the antibiotic typically through degradation or reaction of the antibiotic; 4) horizontal gene transfer facilitates the fast accumulation of resistance mechanisms.

1.2.2.1 Horizontal gene transfer

Horizontal gene transfer exacerbates resistance, allowing for rapid exchange of genetic information between individual organisms that may not be from the same species.[54,55] Following an advantageous point mutation in one species, such transfer means that other species of bacteria do not have to arrive at this advantage through their own chance mutation. Antibiotic adjuvants and combination therapies can overcome some of these resistance mechanisms.[51,56]

1.2.2.2 Inactivation of the antibiotic

Exploitation of the chemical reactivity of an antibiotic, through degradation or reaction of a key structural feature, can lead to inactivation as a mechanism of resistance,[51] and

the penicillin family of antibiotics is one example of this.[55,57] The MOA of penicillins is the covalent binding of the compound to a transpeptidase responsible for the synthesis of peptidoglycan through reaction of a β-lactam ring, which inhibits the bacterial cell wall synthesis.[58,59] Lactamases exploit this mechanism by hydrolysing the β-lactam ring, either through a serine residue, or metalloenzymes using water and a zinc ion, rendering it inactive.[57] β-Lactamase inhibitors have been developed as a strategy to prevent this form of resistance, and are used in combination with β-lactam antibiotics, however multiple resistance mechanisms have evolved to combat this.[60]

1.2.2.3 Target modification

Bacterial resistance can be conferred through target modification. The biological target of the antibiotic is modified in a way that the antibiotic is no longer effective, often *via* a single change to the structure of the target. This modified structure usually retains cellular function but is less susceptible to the action of the antibiotic.[51] This type of resistance has been observed against aminoglycosides and macrolides.[30,61] Aminoglycosides bind to bacterial ribosomes resulting in a conformational change, negatively impacting their function.[30,62] Modification of the target ribosome by methylation reduces the affinity of the aminoglycoside.[55]

1.2.2.4 Efflux pumps

Efflux pumps are present in bacterial cell membranes and are used by bacteria to expel unwanted or toxic substances,[51] and these pumps present a particular hurdle for antibiotics with cytosolic targets.[51] Some efflux pumps are specific for one substrate class, whereas others can remove structurally different types of unwanted compounds, as

many as thousands.[51,63] Increased resistance is also seen with efflux mutant species that have permanently upregulated efflux pumps.[64,65] Examples of pumps that work in an organised manner with transporter proteins and other pumps to remove unwanted substances are known (such as the resistance nodulation division family).[64]

Blocking these efflux pumps is a way to re-sensitise bacteria to an antibiotic, using efflux pump inhibitors (EPIs). EPIs work in a number of ways including inhibiting pump expression, preventing pump assembly at the membrane, blocking the pump outlet, or depleting the energy the pumps require to function.[51] However, there are associated toxicity issues related to non-specificity with eukaryotic efflux pumps.[16,51]

1.2.3 Resistance exhibited by the ESKAPE pathogens

Resistance mechanisms have been observed in all the ESKAPE pathogens,[15,47,66,67] and the Gram-negative ESKAPE pathogens include clinically important MDR species. *Klebsiella pneumoniae* has acquired high resistance to previously effective carbapenem and cephalosporin antibiotic classes, and now the mortality rate often exceeds 40% of infections.[67] *A. baumannii* is capable of opportunistically causing a variety of infections,[47] and has a high natural resistance to antibiotics through decreased cell permeability through porins, and increased overexpression of efflux pumps.[53] *A. baumannii* can additionally acquire resistance genes very easily, making it a problematic candidate for MDR. One strain of *A. baumannii* was found to have 49 resistance genes against 7 different antibiotic classes within a single gene cluster.[47] *Pseudomonas aeruginosa* is also an opportunistic pathogen with many resistance mechanisms including promiscuous

efflux pumps and a plethora of advantageous mutations.[15] It can remain viable in the lungs of cystic fibrosis patients for over ten years.[67] *Enterobacter* species are showing increasing levels of resistance. Reports from 2013[15] and 2016[53] state some MDR species are resistant to almost all available antibiotics, except colistin and tigecycline reserved as drugs of last resort,[44] and a more recent report from 2020 states colistin resistance has now been observed.[67]

1.3 Chemical Diversity Within Antibiotics

Many antibiotics do not fall within traditional 'drug-like' chemical space,[68,69] as shown by the structures of the classes in Table 1.1. Antibiotics often have higher molecular weight, increased numbers of hydrogen bond donors and acceptors, and more rotatable bonds than non-antibiotic drugs.[70] The most well-known description of these desirable properties for oral bioavailability being Lipinski's Rule of Five.[71,72] The success of "privileged structures" that are more likely to generate hit compounds has led to reduced chemical diversity (Figure 1.5),[73–77] and excluded potential antibiotics.[78] Natural products are a source of discovery of antibiotics,[3,21,79] although the resulting challenges has reduced how many are pursued for development into drugs.[80]

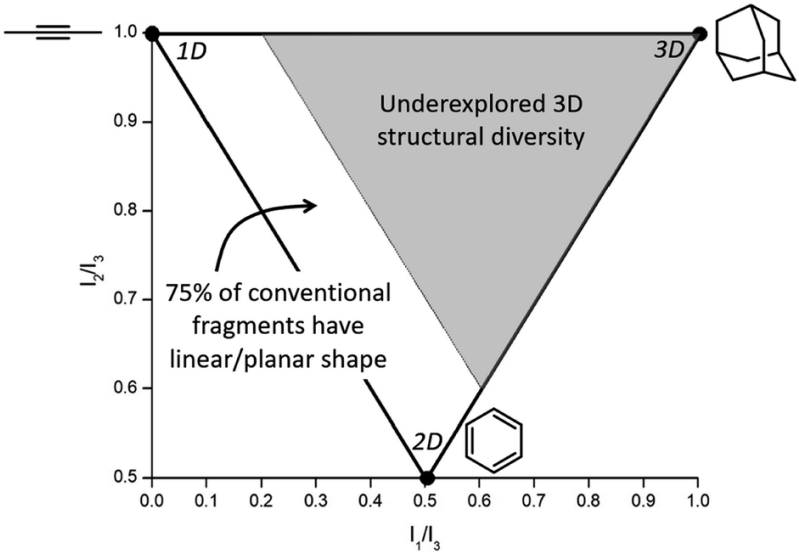


Figure 1.5. Example of lacking diversity in chemical space. Fragments from the ZINC[81] database are plotted according to the ratios of their normalised PMI (principle moment of inertia) values. This allows for the comparison of molecular shapes against the three molecular standards 2-butyne, benzene, and adamantane. Reproduced with permission from *Chem. Sci*., 2020, **11**, 1216–1225 - Published by the Royal Society of Chemistry.[82]

Out of the twelve approved antibiotics for Gram-negative infections between December 2014 and December 2019, only one drug belonged to a new antibiotic class, the pleuromutilins.[83,84] This exacerbates the problem of resistance as many protective mechanisms work against multiple classes of antibiotics, such as the β-lactam containing classes, thereby contributing to MDR of these organisms.[15]

Overall, there are many important properties that need to be considered in the structure of a lead compound to result in an active final drug. This includes bioavailability in humans (depending on how the drug will be administered),[85] the permeability of the drug into the bacteria, and the affinity of the compound for the pathogenic target. For Gram-negative bacteria, accumulation of the drug inside the cell is increased when molecules have an ionisable nitrogen, are polar (an average log$D_{7.4}$ −2.8)[86] but have hydrophobic functionality, high rigidity, and low globularity.[17,87,88] Designing a drug for a prokaryotic structure is challenging, but this provides an opportunity for selectivity over

a eukaryote,[89] which was one of the reasons behind the success of penicillin.[90] Design of a new antibiotic from a naturally occurring compound offers exploration of new chemical diversity,[69,86,91] and discovery of new antibiotics with new modes of action (MOA) is key.

1.3.1 Antibiotic peptides

Antibiotic peptides make an important contribution to the available drugs to tackle infections.[92] Three out of four of the drugs of last resort (as mentioned in section 1.2.1) are peptide-based, and these are vancomycin, daptomycin, and colistin. They show selectivity, efficacy, and low potential for developing resistance when compared to other small molecule antibiotics, although this can still occur such as Enfuvirtide used for HIV.[21,92,93] However, antibiotic peptides experience many of the same drawbacks as other peptide based drugs including bioavailability, stability, oxidation susceptibility, clearance mechanisms, toxicity, and expensive production.[21,94,103,104,95–102] They can be easily cleaved by peptidases, with specificity dependent on the sequence of the peptide.[105] A solution to these challenges are peptide derived drugs including modified peptides, pseudopeptides, and peptide-mimetics.[99,106] Modified peptides contain small changes without altering the peptide bond and are still essentially peptidic, such as unnatural amino acids, and cyclisation. Pseudopeptides are partial peptides where some of the chemical groups have been changed, such as peptoids which have the chosen amino acid side chain now swapped to the nitrogen, to form a *N*-alkylated glycine. Peptide-mimetics are organic molecules that mimic the activity of peptides but are no longer peptidic.[106] Morphine was identified as the first peptide-mimetic molecule following the identification of two endogenous penta-peptides with the same activity.[106,107]

1.3.2 Amide isosteres in peptide-mimetics

Isosteres are chemical moieties that mimic the steric and electronic properties of other functional groups, but have a different chemical structure,[108] and peptide-mimetics are a type of amide isostere.[109] Bioisosteres have similar chemical properties to their parent compound and exhibit comparable biological activity.[109,110] They are used to improve the PD/PK properties of drug compounds, while still having affinity and efficacy in the target setting.[111,112] Two examples of mimetic groups used in compounds include fluorine and methyl groups. Fluorine is often used to block a metabolically labile C-H site that would be oxidised by a P450 cytochrome, to improve bioavailability such as in Ezetimibe,[113] and methyl groups that can prevent hydrolysis by amidases such as in Lidocaine.[114] Amide isosteres can contribute to the structures of pseudopeptides and peptide-mimetics (Figure 1.6).[115–117]

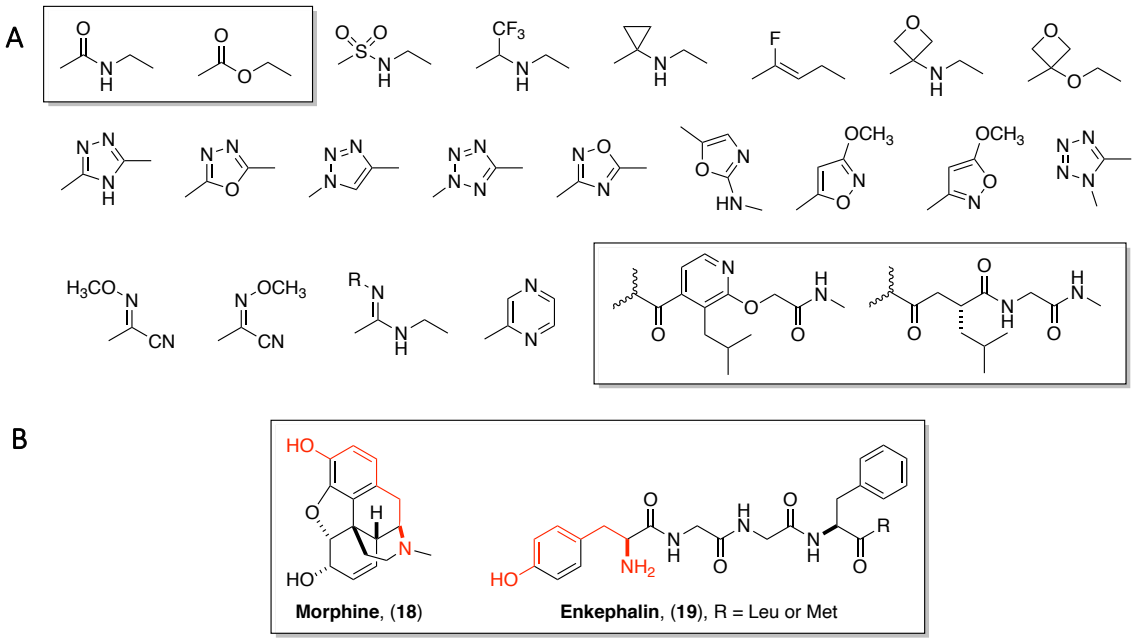


Figure 1.6. Examples of isosteric groups: A) amide and ester mimetics; B) Morphine (18) as a peptide-mimetic. A) Reprinted (adapted) with permission from Meanwell, N. A. *J. Med. Chem.* **2011**, 54, 2529–2591. Copyright (2011) American Chemical Society.[109] B) Morphine (**18**) and the endogenous penta-peptide (**19**) with the same activity, with the isosteric group highlighted in red.

The amide bond exists in peptides from the linkage of the carboxylic acid and amine of two amino acids, and is capable of existing in two tautomers, the keto and enol forms (Figure 1.7).[118] As a result of this the amide bond has partial double bond character and a dipole (represented by ∂+/∂−). The amide group has a hydrogen bond acceptor (HBA) and hydrogen bond donor (HBD) pointing in opposite directions from the oxygen and amide proton respectively. The amide bond can exist in the trans or cis conformation, however it is found primarily in the trans conformation to avoid steric clash. Rotation about the C–N bond is possible although slow due to the partial double bond character.[119]

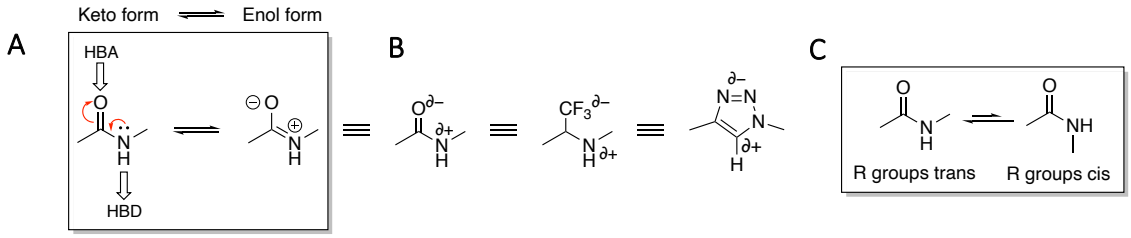


Figure 1.7. Amide bond illustration and comparison to some amide isosteres. A) Illustration of the keto and enol tautomers of the amide bond. B) Examples of amide bond isosteres. C) Illustration of the trans and cis geometric amide isomers. Amide bonds have partial double bond character and a dipole. The relative directions of its hydrogen bond acceptor (HBA) and hydrogen bond donor (HBD) groups are opposite, this is satisfied by the trifluoromethyl and triazole isosteric groups shown. Amide groups predominantly exist trans to avoid steric clash.

Backbone modifications have been used to improve drug stability of peptidomimetics.[120] Isosteres of the amide bond mimic this dipole and partial double bond character while reducing the potential of cleavage by peptidases.[109,121] The rigidity of ring systems may additionally help a ligand make the required polar interactions for binding by removing the rotation about the C–N bond. There is extensive use of 1,2,3-triazoles in the literature as a cyclic amide bond replacement to increase metabolic stability, and 1,2,4-oxadiazoles which also grant increased membrane permeability and bioavailability.[121] These cyclic isosteres have increased rigidity and constrain the amide bond replacements into the desired orientation, as well as reducing their susceptibility to cleavage.[117]

Examples of peptide-mimetic compounds with antimicrobial activity have been reported.[122–126] These examples illustrate how the replacement of amide bonds with appropriate isosteres in peptide-based antibiotics can help overcome the deficiencies of these compounds and improve them as potential drug candidates. Using amide bond isosteres increases the available chemistry when designing and building a molecule. Small molecules arguably have more flexibility in their synthesis than peptides because they include a greater variety of functional groups including unnatural ones, and typically have less linear synthetic routes. The broader available synthetic chemistry also gives opportunities to tailor a drug compound to overcome the challenges associated with antibiotics, such as accumulation in Gram-negative bacteria (Section 1.3).[88] Antibiotic peptide-mimetics should still invoke the same activity while having an altered chemical structure.

1.4 The Potassium (K^+) Efflux System (Kef)

The Kef system is a proton-potassium ion antiporter found in the membrane of Gram-negative bacteria.[127–130] The role of this system in K^+ efflux was identified by Bakker *et al.* in 1987,[131] and the gene sequence for KefC was identified in *E. coli* (*Ec*KefC) by Munro *et al*. in 1991.[132] These reports classified KefC as a membrane protein, with a native ligand of L-glutathione (GSH, **20**),[132,133] that is responsible for regulation of intracellular pH.[134] *Ec*KefC and *Ec*KefB (another related Kef system) are part of the protein family related to Trk, which are potassium uptake proteins.[131,135] *Ec*KefC is thought to be located in the cytoplasmic membrane, with other proteins involved in K^+ regulation including Trk located here. The Kef system is part of a protective mechanism for the

bacteria against toxic electrophiles.[136–138] Control of intracellular pH protects nucleophilic groups (found in proteins and deoxyribonucleic acid (DNA)) and reduces their reactivity with electrophiles.

1.4.1 Structure and function

The Kef system is a homodimer, the X-ray crystal structure of *Ec*KefC was first elucidated in 2009 by Roosild *et al*. The structure of KefC contains a K^+ transport nucleotide binding (KTN) C-terminal domain (CTD), and it is bound to its ancillary protein (KefF). KefF is responsible for stabilising the dimeric structure, and is required for full activation of the protein (Figure 1.8).[139] Kef systems with an ancillary protein exist as a dimer of dimers, the binding site for GSH is at the KefC dimer interface. [139] Three X-ray crystal structures have been obtained for the CTD of *Ec*KefC (PDB ID: 3EYW,[139] 3L9W,[128] and 3L9X[128]) and one for the CTD of the Kef system from another Gram-negative organism *Shewanella denitrificans*, *Sd*Kef (PDB ID: 5NC8).[140]

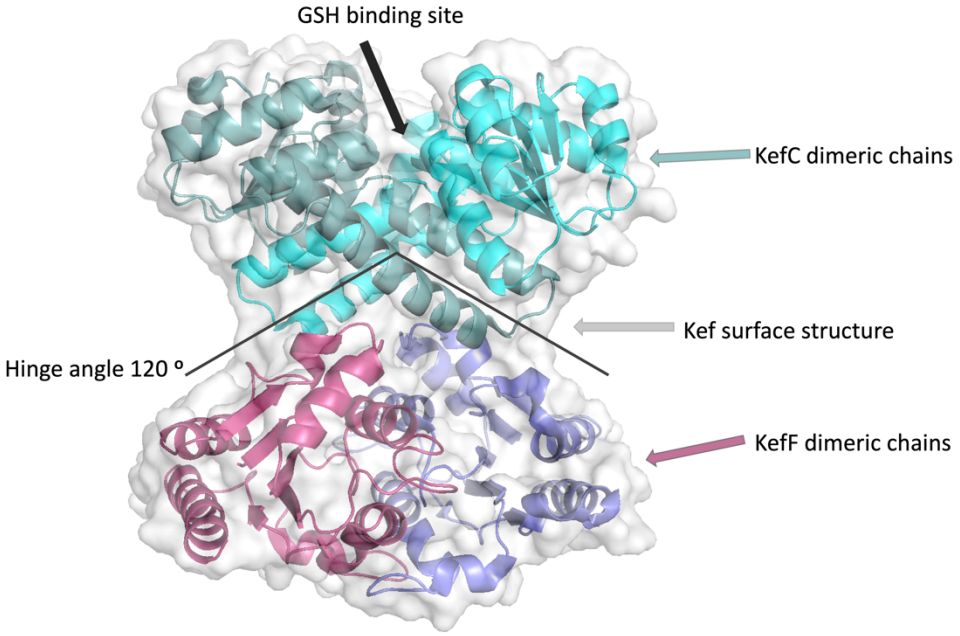


Figure 1.8. The *apo* X-ray crystal structure of *Ec*KefC (PDB ID: 3EYW). The structure is a dimer of dimers. The image is coloured as follows: KefC dimeric chains (blue, green), KefF dimeric chains (pink, purple), resolved to 2.4 Å resolution.

The *Ec*KefC-KefF dimer is tightly associated *via* an exposed hydrophobic surface, and each contains a Rossman fold,[129] which forms the nucleotide binding domain.[139–141] The KTN domain is regulated *via* the hinge angle between the KTN domains forming the dimer.[139] This hinge allows for significant conformational change, and can constrict to such an extent to expose two hydrophobic patches on the KTN dimer. This allows a hydrophobic surface interaction between the KefC and KefF dimers, thus forming the tetrameric dimer of dimers.[129] In an alignment of known KTN domains, the hinge angle of the open conformation was approximately 120 °, and the closed angle was approximately 90 °. The structure observed for *Ec*KefC had a hinge angle of 120 °, which suggests that KefF stabilises KefC in an open conformation.[142] The KTN domain and transmembrane portion are connected by a flexible linker.[129] The full length Kef protein including the membrane portion has not yet been crystallised.

The Kef inhibitor GSH (**20**) is present at ~17 mM in *E. coli*,[143] it has a K_d of 900 ± 200 µM, and holds the protein in the closed conformation. K^+ regulation has several important roles in bacteria (Section 1.4.2.1), and in the absence of GSH, K^+ leakage is observed.[139] GSH can react with electrophiles to form GSX adducts (**21**), such as *N*-ethylmaleimide (NEM, **22**), to form ethyl succinimido glutathione (ESG, **23**), (Figure 1.9).

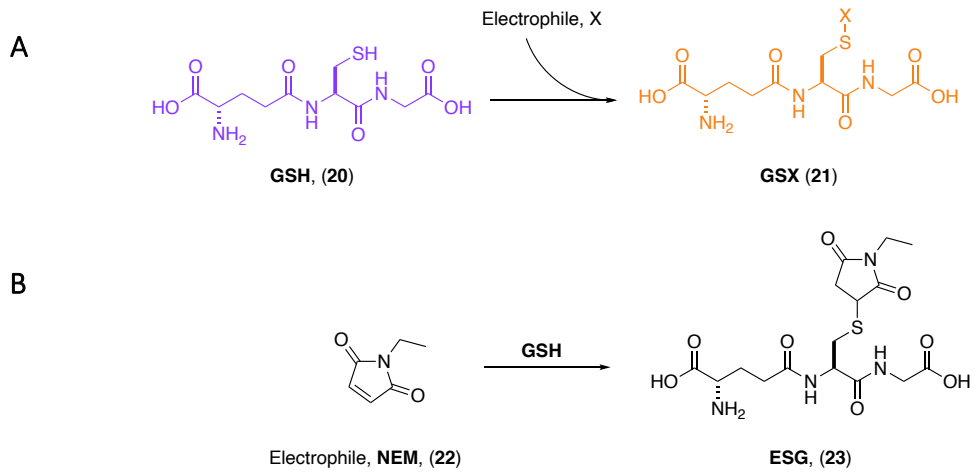


Figure 1.9. Reaction of GSH with electrophiles to form GSX adducts. A) Reaction of GSH with an electrophile, X to form a GSX adduct. B) An example of an electrophile, NEM which forms GSX adduct ESG.

Binding of bulky GSX adducts causes a conformational change in the KTN domain, through displacement of the capping residue (the terminal residue of an alpha helix)[144] phenylalanine (F)441 (Figure 1.10).[128,129] The flexible hinge region is postulated to facilitate the conformational change of the KTN domain dimer to the transmembrane portion, resulting in activation of the Kef system by H^+ influx and K^+ efflux.[129]

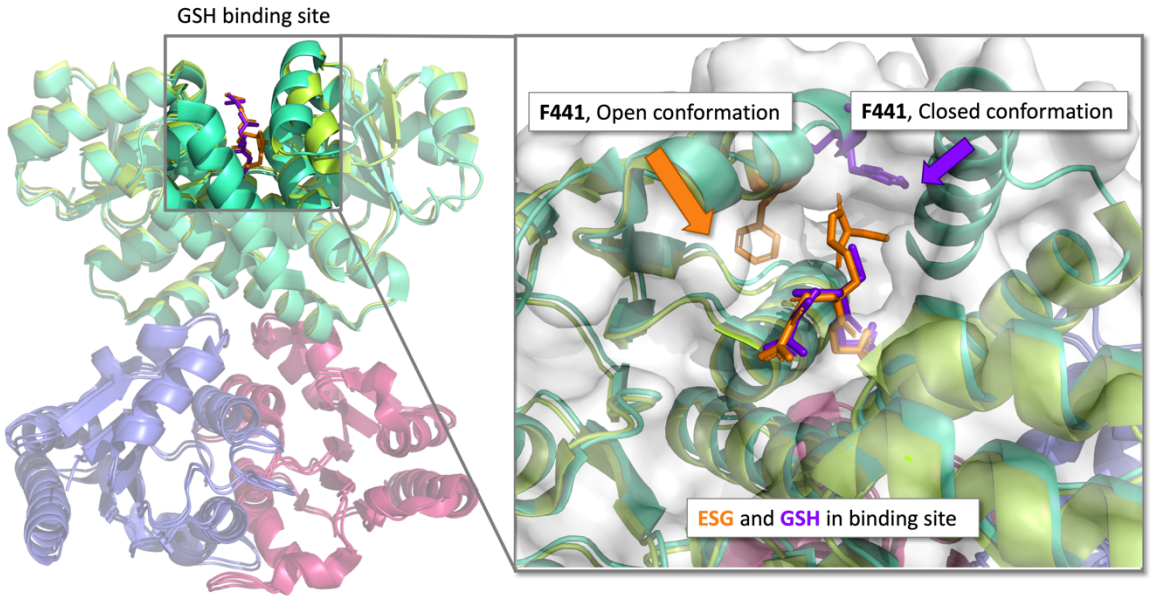


Figure 1.10. X-ray crystal structures 3L9W (GSH-bound) and 3L9X (ESG-bound),[128] of *E. coli* KefC and KefF. 3L9W: KefC = blue-green, KefF = purple and pink, GSH = purple, capping residue F441 = purple; 3L9X: KefC = yellow-green, KefF = purple and pink, ESG = orange, capping residue F441 = orange. Displacement of F441 by ESG is evident from the two X-ray crystal structures, which is believed to result in the conformational change of Kef and Kef activation (K^+ efflux).

Methylglyoxal (MG, **24**) is an electrophile produced by bacteria from dihydroxyacetone phosphate in a pathway related to glycolysis, to remove toxic phosphorylated intermediates.[145–147] However, build up can cause cell death through reaction with macromolecules such as proteins and DNA.[146–148] The removal mechanism of MG is well established in Gram-negative bacteria, it is known to react with GSH followed by a detoxification pathway catalysed by glyoxalase I and II (Figure 1.11). The resulting GSX ((*S*)-lactoyl glutathione for MG and GSH) binds to the Kef system and activates it, protecting the DNA and proteins in the cell. Treatment of *E. coli* cells with MG causes loss of potassium, which is later recovered when the activator is no longer present.[148]

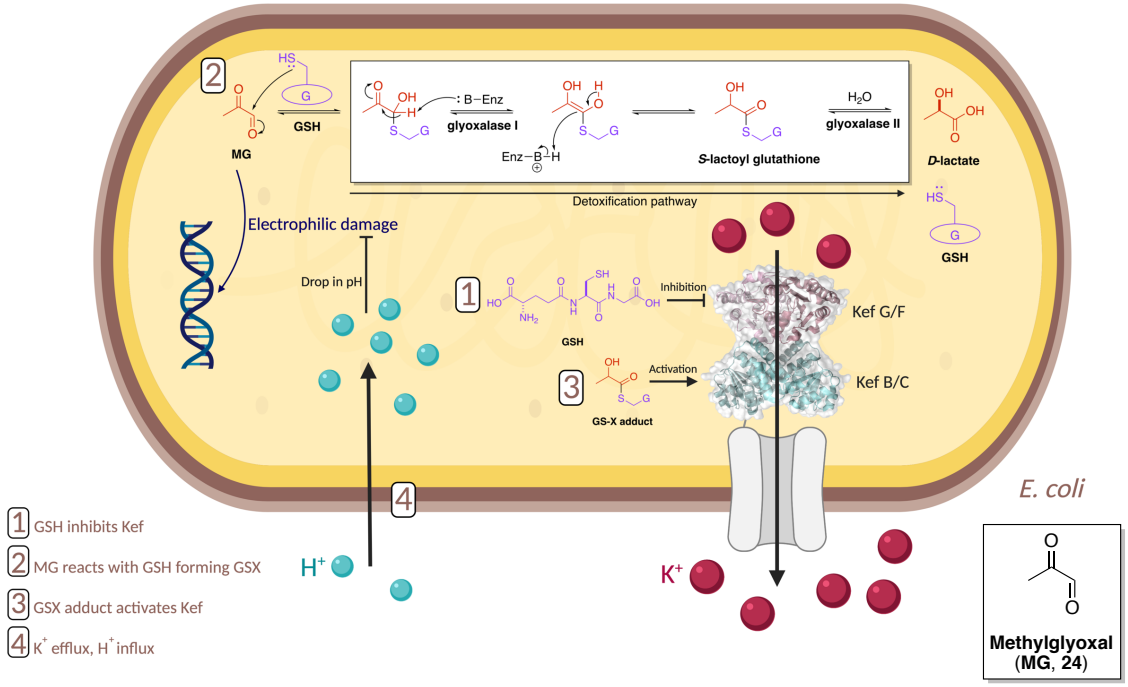


Figure 1.11. Kef detoxification pathway with MG.[13,145] The pathway consists of: 1) GSH acts as an inhibitory ligand of Kef keeping the system closed; 2) Example reaction mechanism with an electrophile (MG) and GSH to produce an activating GSX adduct ((*S*)-lactoyl glutathione), as part of an *E. coli* detoxification pathway; 3) binding of the GSX adduct activating the Kef system; 4) activation causes potassium efflux and concomitant proton influx, the drop in pH protonates potential nucleophiles protecting them from electrophilic damage.

Further evidence for this activation mechanism was shown through the mutation of the phenylalanine (F) capping residue of the *Sd*Kef system with 4-trifluoromethyl-L-phenylalanine (ptfmF). Conformational changes were observed using ^{19}F NMR when activating Kef ligands were added, and not for inhibitory ligands (Dr Anthony Chan and Dr Catherine Haslam, unpublished work).[149]

1.4.2 Clinical relevance of Kef

1.4.2.1 The role of potassium Ions (K^+) in bacterial cell homeostasis

K^+ have four major roles in bacteria: activation of cellular enzymes, osmotic functions, pH regulation, and acting as a secondary messenger.[131,150,151] Many bacterial enzymes

including peptide transferases, kinases, and synthases are activated by K^+, although the range of concentrations across different species is large, from 18 mM to 4 M.[150] Osmotic functions include the regulation of turgor pressure and cell osmolarity (solute concentration).[151] Levels of K^+ are used to regulate upshock and downshock to control turgor pressure relative to the osmolarity of the environment. Osmotic downshock can result in greater turgor pressure than the cell envelope can withstand, resulting in loss of integrity and consequently small molecules, periplasm, and intracellular proteins.[150] Regulation of pH by movement of protons across the membrane is primarily performed using K^+, as these are the other major cellular cations. This allows cells to respond to changes in internal or external pH, for example to maintain the structural role of charged groups in proteins and nucleic acids.[151] The secondary messenger function of K^+ is the uptake of compatible solutes (neutral, polar molecules) at high osmolarity.[151] K^+ gradients are rarely used as an energy source, because of the typically small energy in the K^+ gradient in most bacteria.[150]

1.4.2.2 The ESKAPE pathogens

Kef is a prospective novel antibacterial target, and it has been proposed that interference with the protective mechanism may inhibit the growth of, or kill, bacteria that express the system. Interference with the intracellular K^+ concentration, key to many aspects of bacterial physiology, may be detrimental to the bacteria,[131,150,151] or sensitise cells to electrophiles and antibiotics as part of a co-therapy.[137,152]

The Kef system has homologues in non-pathogenic and pathogenic bacteria. Results from a BLAST (basic local alignment search tool) search of the primary sequence of *Sd*Kef

showed a 45% and 44% %identity, and 64% and 65% %similarity, to *Ec*KefC and *Ec*KefB respectively.[145] A DELTA-BLAST (domain enhanced lookup time accelerated BLAST) of the primary sequence of *Sd*Kef showed there are homologues present in other human pathogens including *Salmonella*, *Yersinia pestis* (responsible for the Black Death), and *Burkholderia pseudomallei* (responsible for melioidosis).[149,153,154] There are however, no homologues in humans, which makes Kef an excellent target for a new antibiotic, reducing toxic side effects from affinity for human biological structures.[51,55]

Inhibition of over-expressed Kef has been shown to be bacteriostatic, meaning that it prevents bacterial growth but does not kill the bacteria.[149] Experiments to identify the minimum inhibitory concentration (MIC) were performed on an *E. coli* strain MJF645. This is a mutant strain with no genes for endogenous Kef proteins or glutathione biosynthesis, making it ideal for expression and investigation of non-native Kef systems. In this experiment, the MIC was defined as the concentration required to inhibit bacterial growth to less than 20% of the negative control well, where no compound was present. MJF645 overexpressing the *Y. pestis* Kef system had an MIC of 15.6 μg mL^{-1}. All subcultures from the inhibited wells of *E. coli* from this experiment grew when transplanted into fresh media.[149] Currently there is no compound capable of inhibiting the growth of bacteria expressing wild type levels of Kef, but it is possible a high affinity ligand could achieve this result. The stress of interference with a protective and homeostatic system on the bacteria used in combination with another drug could be developed into an effective antibiotic treatment.

1.4.2.3 Kef in Gram-positive bacteria

An equivalent protective system is found in Gram-positive bacteria, the KhtSTU K^+ efflux pump, identified in *Bacillus anthracis* that shows poor homology (17% identity, 35% positives) to *Sd*Kef.[149,153] The firmicutes phylum of Gram-positive bacteria does not produce GSH, and so bacillithiol (BSH, **25**) is used as the major low molecular weight thiol.[155] The BSH adduct of MG ((*S*)-lactoyl-BSH, BSL, **26**) binds to KhtSTU causing cellular acidification (Figure 1.12).[156]

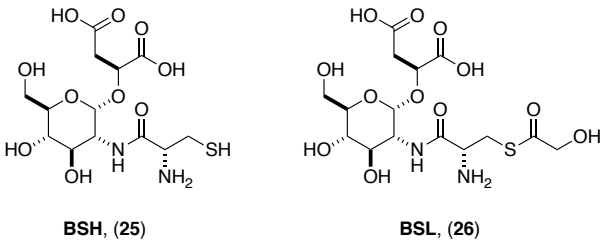


Figure 1.12. Structures of BSH and BSL. BSH is the low-weight molecular thiol in Gram-positive bacteria. BSH can react with MG to form the activating adduct BSL.

1.4.2.4 Kef model system

The model system chosen for this research is *Sd*Kef, which is the Kef system from *Shewanella denitrificans*, a non-pathogenic marine bacterium.[157] *Sd*Kef shows high homology to *Ec*KefC (Section 1.4.2.2), and does not have an ancillary protein which makes expression and solubilisation of the protein easier (Figure 1.13). To form a soluble construct for biophysical assays, a highly charged 10 amino acid Q-linker was used. The linker is comprised of residues 391–408 (GHELEVDIEP).[145] For *Sd*Kef the KTN domain construct is also referred to as the Q-linker C-terminal domain (QCTD) and has been used in biophysical assays with Kef ligands.[140,153] The equivalent of the capping residue F441 in *Ec*KefC is missing from the crystal structure for *Sd*Kef, and due to poor resolution of this region, docking opportunities with this structure would be limited.

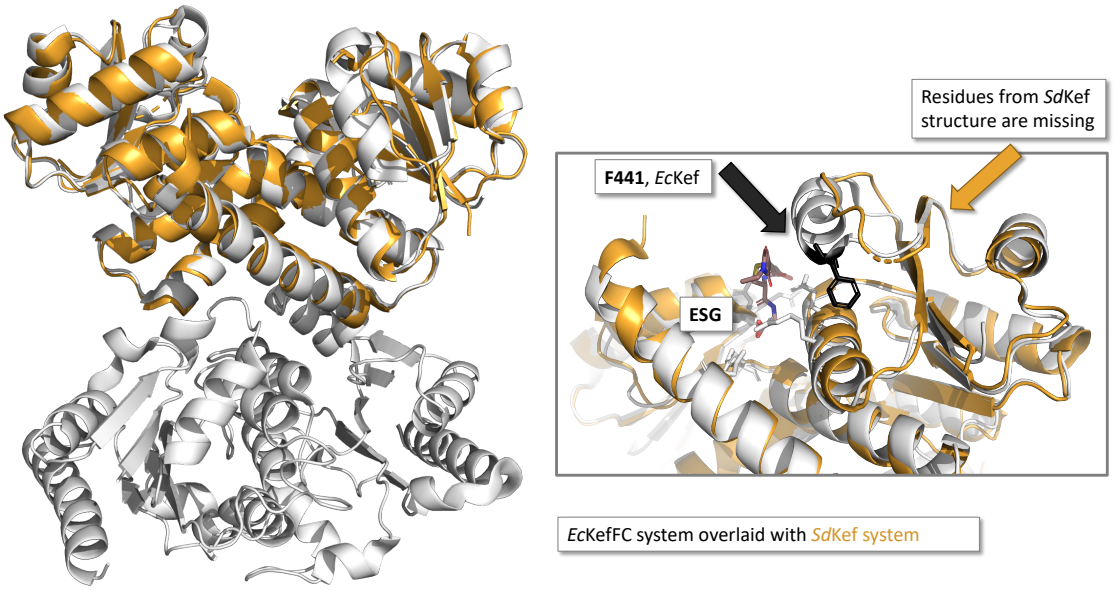


Figure 1.13. Overlay of X-ray crystal structurea of *Sd*Kef KTN domain (PDB ID: 5NC8, orange) and *Ec*KefFC (PDB ID: 3L9X, white) with ESG (pink brown), and an expansion showing the missing residues.[140] The two proteins have a high shape similarity, although the equivalent of the capping residue F441 in *Ec*KefFC is missing in the *Sd*Kef structure, and is visible as a broken loop.

1.5 Refinement of the known Kef ligands and SAR

The first synthetic Kef ligands were based on GSH. It has been shown that the GSX adduct with NEM activated the *Ec*Kef system.[129,133,136,137,152] Consequently, different electrophiles were explored to investigate the structural requirements for Kef activation.[145,158] The dissociation constant (K_d) of these ligands was measured for *Sd*KefQCTD (**ESG**, *N*-*tert*-butylsuccinimido-(*S*)-glutathione ^{t}BuSG (**27**), (*S*)-lactoyl glutathione (**28**), and 1-(octen-3-one)-SG (**29**), Figure 1.14).

With the confirmation of the binding and activation of *Sd*Kef, several new ESG analogues were synthesised from GSH. Enone conjugate addition reactions installed cyclic and acyclic headgroups including varied *N*-alkyl succinimido groups, cyclopentanes with

mono and diketones, and three different length linear ketone chains (Figure 1.14 A, B). Thiol-ene coupling reactions installed hydrophobic headgroups with linear, multicyclic saturated structures and aromatic moieties (Figure 1.14, A, C).

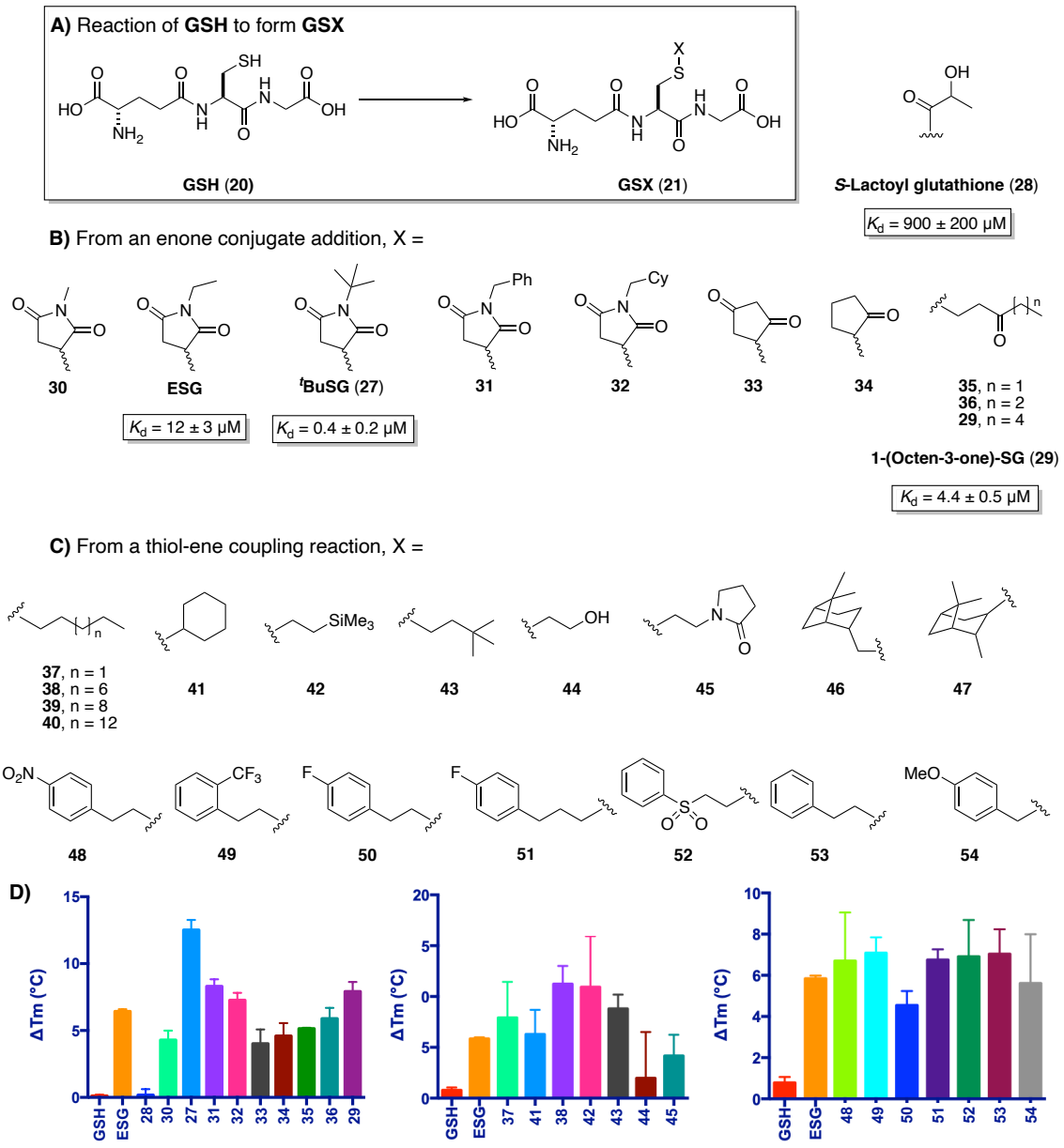


Figure 1.14. New headgroups for GSX adducts. A) Reaction of glutathione with electrophiles to form GSX adducts; B) enone conjugate addition headgroups; C) thiol-ene coupling reaction headgroups. K_d values were obtained from fluorescence emission spectra, fluorescence anisotropy, or isothermal calorimetry (ITC).[145] The ability of the headgroups to activate Kef was investigated through various biophysical assays;[145,159] D) Differential scanning fluorimetry (DSF) results illustrating the SAR around the GSX headgroup (a greater ΔTm means the ligand has greater affinity). Reproduced and adapted with permission from Healy, J.; Ekkerman, S.; Pliotas, C.; Richard, M.; Bartlett, W.; Grayer, S. C.; Morris, G. M.; Miller, S.; Booth, I. R.; Conway, S. J.; Rasmussen, T. *Biochemistry* **2014**, *53*, 1982–1992,[145] and Healy, J.; Rasmussen, T.; Miller, S.; Booth, I. R.; Conway, S. J.. *Org. Chem. Front*. **2016**, *3*, 439.[159]

All of the tested structures showed stabilisation of *Sd*Kef in a thermal shift assay relative to GSH.[160] The general trend showed bulky, rigid headgroups to have the greatest stabilisation (Figure 1.14, D). The succinimide headgroups generally had higher affinity than the linear, flexible headgroups, and the most stabilising ligand tested was ^{t}BuSG.[145] The succinimide headgroups had the highest rate and extent of activation which correlated with this trend,[145] whereas the more flexible linear chains had similar affinities but showed reduced K^+ release, suggesting these were inhibitors. ^{t}BuSG is also the highest affinity Kef ligand measured to date with the lowest K_d (Figure 1.14).[145] It is hypothesised that the electrophile contributes some affinity to the Kef ligand, either through direct hydrophobic interactions, an enthalpic increase as a result of the conformational change of the protein, or an entropic increase due to the displacement of structured water molecules lodged in the protein.[145] The data was consistent with previous observations of bulky, rigid, hydrophobic headgroups having greater affinity for *Sd*Kef.[159]

To explore Kef structure-activity relationships (SAR), the interactions between the GSH and ESG backbones and *Ec*KefCCTD were analysed. The X-ray crystal structure of *Ec*KefCCTD and ESG (PDB ID: 3L9X) showed polar contacts between seven residues in the binding site (Figure 1.15).

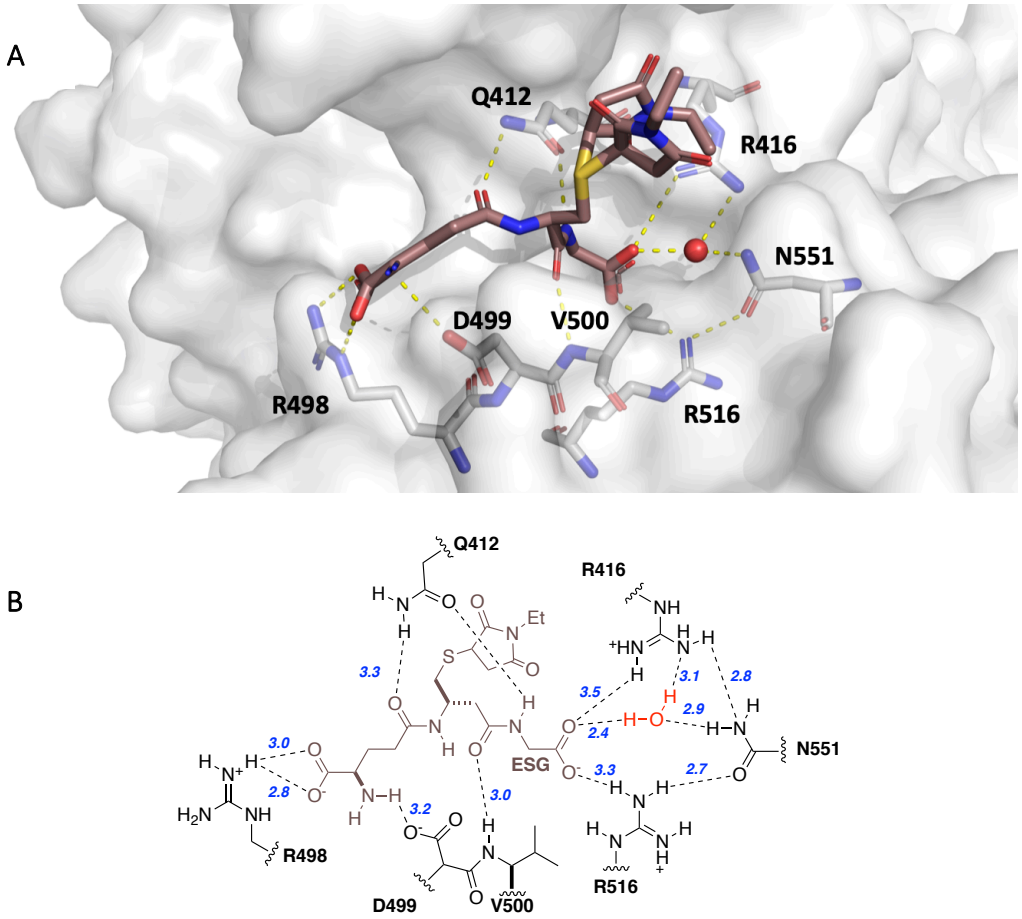


Figure 1.15. X-ray crystal structure of *Ec*KefCCTD with ESG (PDB ID: 3L9X). A) Pymol generated image showing important residues interacting with the ESG (pink-brown), Kef backbone in white, polar contacts indicated by yellow dashed lines, and a well-structured water molecule (red sphere). Two diastereomers of ESG are shown. Residues making polar contacts and thought to be important for binding interactions include Q412, R416, R498, D499, V500, R516, and N551.[128] B) Chemdraw image illustrating these interactions. Reproduced and adapted with permission from Roosild, T. P.; Castronovo, S.; Healy, J.; Miller, S.; Pliotas, C.; Rasmussen, T.; Bartlett, W.; Conway, S. J.; Booth, I. R. *Proc. Natl. Acad. Sci.* **2010**, *107*, 19784–19789.[128]

Each amino acid section present in the tripeptide backbone was removed or changed to investigate their effect on the affinity of the ligand.[153,158] Peptide analogues of GSH replacing the three different parts of the peptide backbone with alternative amino acids were synthesised and tested in biophysical assays (Figure 1.16).[158]

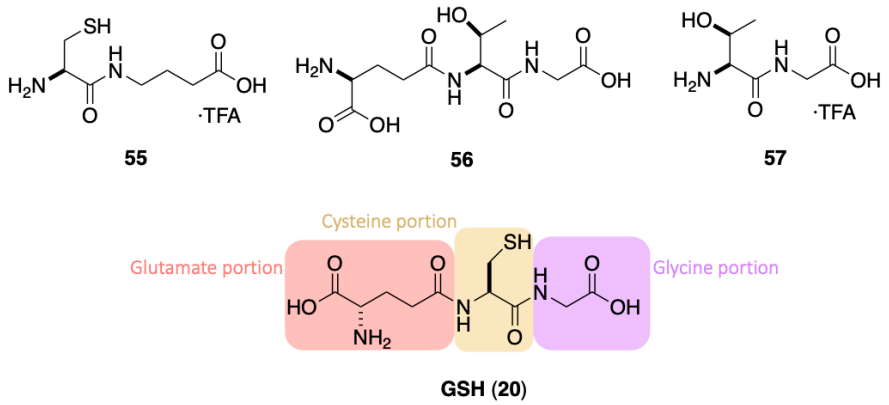


Figure 1.16. Analogues of GSH. Consisting of alternative amino acids, to assess the structural importance of the components of ESG and GSH. **55** is a glycine modification (with no glutamic acid), **56** is a cysteine modification, and **57** is a cysteine modification with no glutamic acid. Further examples of modifications were made, but only **55**–**57** were tested.[158]

55 investigated the importance of hydrogen bonds made by the glutamic acid and whether the structured water could be displaced by lengthening the alkyl chain. **56** investigated the importance of the cysteine on stabilising the closed conformation of Kef by the proposed replacement of a water molecule. **57** investigated the importance of the glutamic acid and cysteine. As none of these structures (**55**–**57**) bound to Kef, this showed that there were key binding interactions made by each amino acid in GSH.

To investigate which individual binding interactions were crucial, the glutamic acid, cysteine, and glycine regions of ^{t}BuSG were modified in turn to generate a range of truncated analogues. The analogues were tested in biophysical assays to measure their K_d values for *Sd*KefQCTD.[153] By examining the K_d values of dissected segments of ^{t}BuSG, the critical polar interactions were used to generate a truncated Kef dipeptide ligand **58**.[153] An example of replacements of the glycine portion are shown below (Figure 1.17).[153]

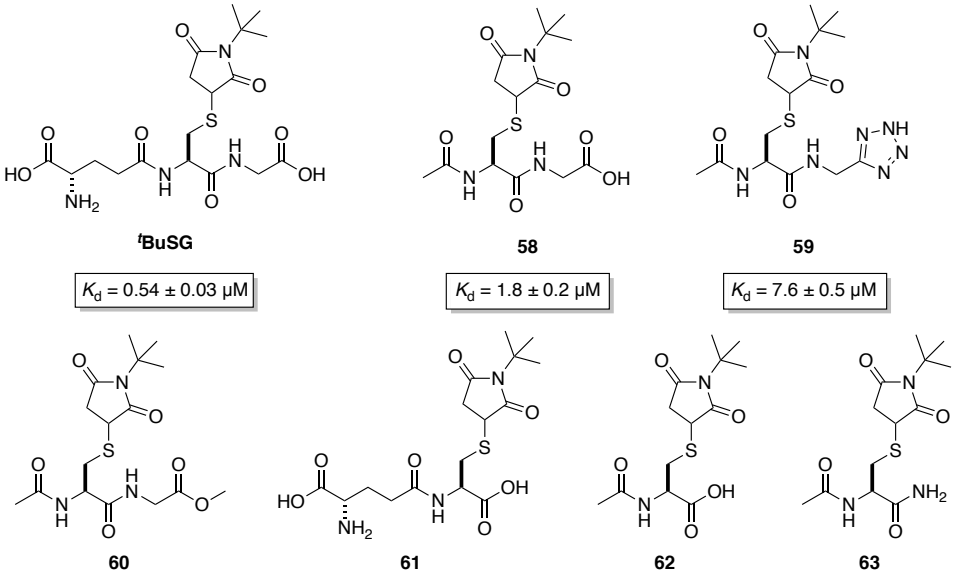
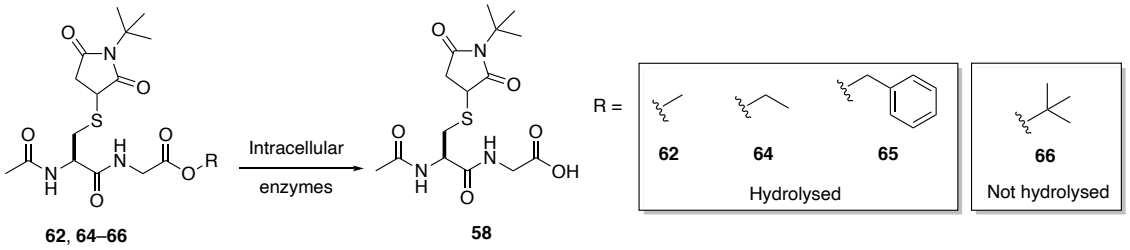


Figure 1.17. Truncated dipeptide structures generated as analogues of ^{t}BuSG. Structures outlined in boxes had comparable K_d values, and demonstrate **58** as having the minimum structural requirements required for binding to the Kef system.[153]

K_d values were obtained for ^{t}BuSG, **58**, and **59** using ^{1}H Carr-Purcell-Meiboom-Gill (CPMG) NMR, but not for the other compounds. This research showed the glycine portion is fundamental for affinity to the Kef protein. The methyl ester **60**, structures **61**, **62**, and **63**, completely lost affinity with removal of the polar interaction made by the carboxylic acid. However, the tetrazole **59** which is a carboxylic acid mimetic, was tolerated as shown by ^{1}H CPMG NMR and a competition fluorescence assay.[153] The truncated dipeptide **58** includes groups capable of making the key binding interactions with *Sd*Kef, and maintains approximate affinity compared to ^{t}BuSG. The (*R*)-enantiomer of **58** activates Kef, while the corresponding (*S*)-enantiomer loses affinity and is inactive.[149,153,161]

The binding site for the Kef system is intracellular, so any antibiotic targeting the Kef system needs to be cell permeant. While the tripeptide carboxylic acids of GSH and ESG were not cell permeant, however, the corresponding methyl, ethyl, and benzyl esters

could permeate the cell membrane.[153,158,162] Once the esters **62**, **64**–**66** had permeated the *E. coli* cells, they were hydrolysed *in vivo* to the carboxylic acid **58** (HPLC analysis, Scheme 1.1).[120] It can be concluded that these compounds are substrates for promiscuous esterases.



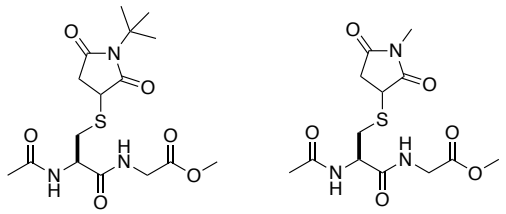
62, 64–66 58

Scheme 1.1. Analysis of hydrolysis of various ester groups on the dipeptide ligands. Cell lysates (CL) were exposed to the ester compounds **62**,**64**–**66** and compared to standards for the ester and carboxylic acid compounds. The methyl **62**, ethyl **64**, and benzyl **65** esters all showed hydrolysis in *E. coli* from HPLC analysis, while the *tert*-butyl ester **66** did not.

The methyl ester **62** activated *E. coli* expressing *Sd*Kef in the K^+ efflux assay.[153] The *in vitro* and bacterial data together suggest that the ester compounds are acting as prodrugs. The rate of potassium efflux of **62** was slower than the rate for NEM, likely due to dependency on the rate of hydrolysis of the methyl ester.[153]

The dipeptide methyl esters **62** and **67** (Figure 1.18) were tested on *E. coli* cells over-expressing *Sd*Kef using the Kirby-Bauer disc diffusion assay, to see if they could inhibit the growth of, or kill, bacteria.[153,161] In this assay, bacteria on an agar plate are treated with a paper disc containing a solution of compound.[163] The bacteria were unable to grow in zones around the paper discs, therefore activation of Kef as shown by potassium efflux measurements,[145] inhibits the growth of bacteria. This research identified **67** as the illustrative compound for the minimal structural requirement for activation of the Kef system. The (*S*)-enantiomers of **62** and **67** did not inhibit or kill the

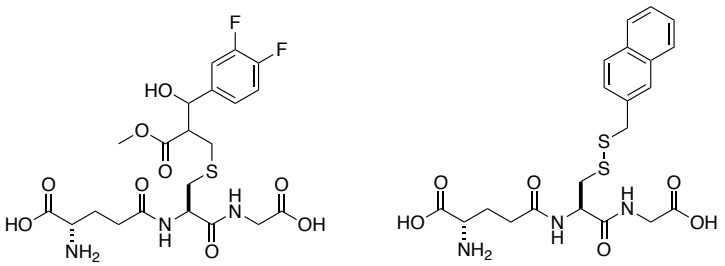
bacteria, showing the importance of the (*R*)-stereochemistry in the cysteine portion of the truncated dipeptide.[161]



62 **67**

Figure 1.18. Truncated dipeptides 62 and 67. Both dipeptides inhibited the growth of *E. coli* over-expressing *Sd*Kef, and the structure of **67** represents the minimal chemical structural requirement for activation of the Kef system, with the methyl ester for cell permeability.

To identify new headgroups capable of activating the Kef system, a dynamic combinatorial chemistry (DCC) approach was used.[164] DCC involves generating new ligands using thermodynamic control of a reversible reaction and used protein-directed headgroup selection for GSH. An equilibrating mixture of GSH and potential electrophiles that could react to form GSX adducts were analysed during stirring in the presence of *Sd*KefQCTD. A high-affinity headgroup GSX adduct would spend more time bound to the protein, and consequently would be present in a higher proportion than a lower-affinity compound. Lower-affinity GSX adducts spend more time in solution and are therefore more likely to undergo the reverse reaction, reforming GSH. Two dynamic combinatorial libraries (DCL) were set up with GSH: conjugate addition to enones and disulphide exchange (Figure 1.19).[165] The libraries amplified two ligands (**68** and **69**) which consequently showed binding to the *Sd*KefQCTD during NMR binding experiments. This approach validates DCC as a method to generate new Kef ligands and provides evidence that bulky, rigid headgroups are required for high affinity for Kef.



68 69

Figure 1.19. DCC Experiments with GSH. **68** generated from enone reversible reaction from GSH, **69** generated from disulphide exchange reversible reaction from GS-SG.

1.6 Summary

The emergence of antibacterial resistance to existing medicines, the lack of success of recent compounds in clinical trials, and the reduction of industry research in the field of anti-infectives, demonstrates the need for novel antibiotic drug classes and targets such as Kef. Kef has clinical significance due to its presence in Gram-negative bacteria, including some of the ESKAPE pathogens, *Y. pestis*, and *B. pseudomallei*. It plays a fundamental role in native protective mechanisms and bacterial homeostasis, and disruption has been shown to lead to inhibition of cell growth. The native ligands for Kef are currently peptidic and of low micromolar affinity. Recent research has identified the key structural requirements for binding and the most effective headgroups for activation of the Kef system.

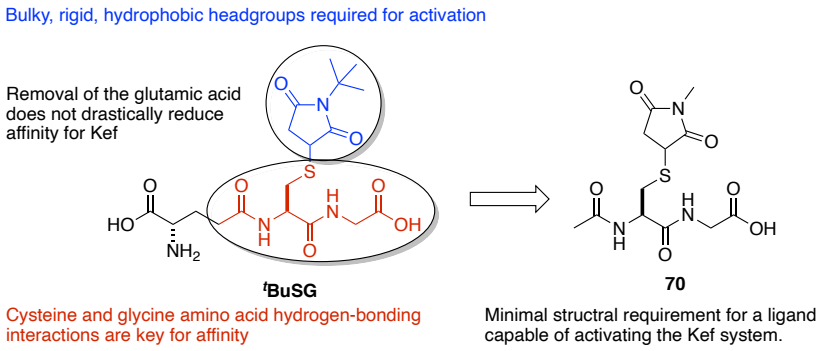


Figure 1.20. Summary of SAR investigation of the peptide based Kef ligands.[145,153,158,159] There are key hydrogen bonding interactions made by the cysteine and glycine portions of the peptide backbone that will be required by the next generation of Kef ligands however, it is possible to remove the glutamic acid without drastic loss of affinity. The *tert*-butyl succinimide headgroup is the currently best identified headgroup for activation of the Kef system. Requirements for the headgroup to activate the Kef system are large steric bulk, rigidity, and increased hydrophobicity.

It has been shown that these ligands can permeate the Gram-negative cell membrane and initiate potassium efflux as an ester prodrug. The next-generation ligands need to build on the known structural requirements as identified from these small peptides, while incorporating desirable chemical properties.

1.7 Project Aims

Peptide-based ligands for Kef have several problems associated with their development as outlined in section 1.3, and the focus of this research is to investigate possible isosteric replacements for the central amide bond in **70.** The chosen scaffolds are a pyridinone (**71**), oxazole (**72**), imidazopyridine (**73**), and scaffold hopped structure (**74**) (Figure 1.21). The peptide-mimetic amide group replacements were chosen to combine mimicry of the binding contributions provided by the amide bond, with greater synthetic flexibility provided by the organic molecule, and the proposed scaffolds must be synthetically tractable.

Pyridinones (Chapter 2) have some precedent as peptide-mimetic scaffolds.[112,166–169] This moiety was chosen for the different reactivity due to the heterocyclic nature of the ring, and the possibility of simple diversification for SAR exploration. The oxazole (Chapter 3) has substantial precedent as a peptide-mimetic and was chosen as it replaced the amide portion of the molecule but retained the key cysteine stereocentre.[170–174] The imidazopyridine (Chapter 4) has little literature precedent as a peptide-mimetic,[175,176] but this scaffold was chosen to investigate a different vector for the important carboxylic acid polar interaction, in addition to the synthetic flexibility of the headgroup installation. The increased rigidity of these ligands may help their uptake and accumulation into Gram-negative bacteria. Scaffold hopping (Chapter 5) was also investigated as a strategy to generate a new ligand scaffold, capable of acting as a peptide-mimetic for Kef, using computational chemistry methods.

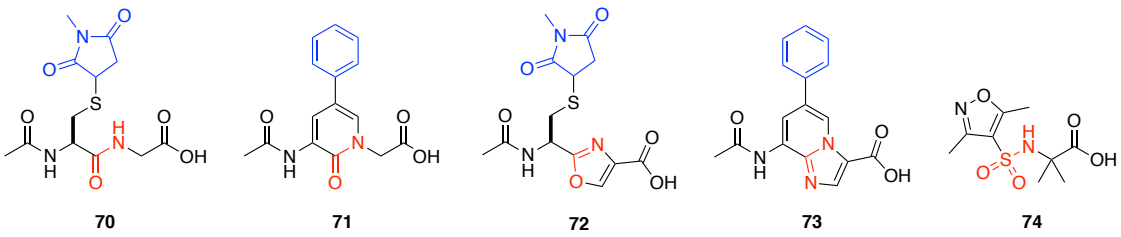


Figure 1.21. Structures of known dipeptide Kef ligand, 70, and proposed peptide-mimetic ligands 71, 72, 73, and scaffold hopped structure 74. The headgroup replacement moieties are coloured blue, and the amide bond replacements in red.

71–**73** will explore the replacement of the central amide bond in **70**. The dipoles in **70** and **71** are the most similar due to both having a planar N-C=O containing functional group with partial double bond character,[177,178] as the pyridinone exists predominantly in the keto form. **71** will adopt a flat, rigid conformation with torsion angles closer to 180 ° than 109 ° around the cysteine replacement part of the molecule,[178] which has changed from an sp^3 to an sp^2 hybridised carbon atom. The oxazole and imidazole rings in **72** and **73** respectively will change the properties of the dipole around the N and O/N atoms compared to an amide.[179–182] Although the conformational restriction of the five-membered ring, a smaller N-C-O/N bond angle, and reduced electronegativity of N compared to O in imidazole,[180] may result in less good amide bond mimic, this is balanced by the synthetic tractability.[183–185] **72** and **73** have reduced flexibility compared to **70** due to the removal of the glycine methylene group, and **73** will also investigate whether a bicyclic backbone is tolerated by the *Sd*KefQCTD system.

The kef system is important for bacterial homeostasis and protection against electrophiles, and consequently interfering with this system has the potential to be detrimental to the growth of the bacteria. Kef ligands have the potential to act as broad-spectrum Gram-negative antibiotics or adjuvants, as many clinically relevant Gram-negative bacteria including the ESKAPE pathogens, express a Kef system.

Antibiotics that target the Kef system would function *via* a new MOA for which bacteria do not currently have resistance. As our collective understanding of AMR has developed, new classes of antibiotics can be used more judiciously and sparingly to prevent their loss of efficacy.

The aim is to develop a peptide-mimetic, activating ligand for the Kef system in Gram-negative bacteria. All these ligand designs are novel scaffolds for the Kef system, and the focus of this research is to develop synthetic routes for the three amide isostere scaffolds and scaffold hopped structure, followed by the optimisation of biophysical assay conditions for testing in our model system *Sd*KefQCTD. The four ligand scaffolds (Figure 1.22) will be synthesised along with their analogues, subjected to biophysical assays, and evaluated as suitable peptide-mimetics of **70** for the *Sd*Kef system.

Chapter Two: Investigation of Pyridinones as an Amide Replacement in *Sd*Kef Ligands

2.1 Introduction to the Pyridinone Scaffold

The pyridinone is a six-membered heterocycle that has been used in a number of drug scaffolds, including those targeting kinases,[186,187] and for metal chelation.[188] It can exist in two tautomers, the 2-hydroxypyridine and the pyridinone cyclic amide (Figure 2.1). Examples exist of pyridinones being used as a peptide mimetic group.[73,112,166–168,189–191] A pyridinone moiety as a replacement for an amide can improve drug-like properties such as oral bioavailability; one of the first examples of this replacement was for a proline group by Brown *et al,*[168] and Sanderson *et al*.[169] The peptide inhibitor ICI 200880 (**75**) suffered from rapid elimination following IV administration, and none was detected after oral delivery.[192] A peptide-mimetic pyridinone analogue **76** of peptide derivative **L-371,912** (**77**), was orally bioavailable and resulted in the desired biological activity (Figure 2.1).[169,190,193]

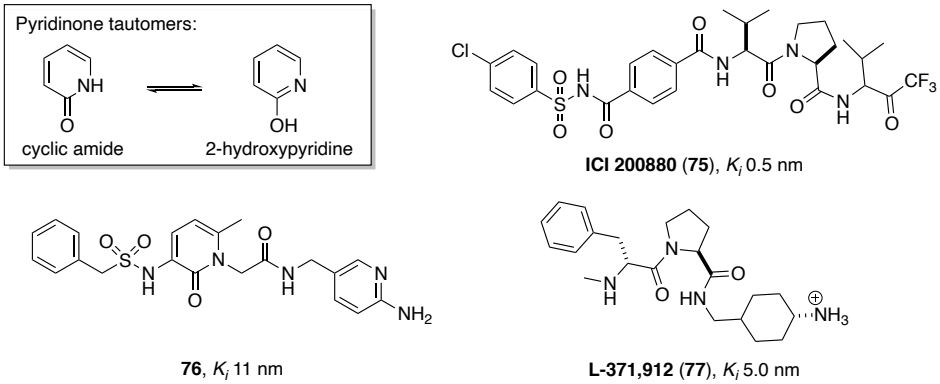


Figure 2.1. Illustration of the two pyridinone tautomers and an example of a pyridinone peptide mimetic. **76** was able to form the same amide bond interactions as its parent compounds ICI 200880 (**75**) and L-371,912. **76** had improved properties to the peptide compounds.

The pyridinone was selected as part of this research as a peptide-mimetic for the Kef dipeptides. As discussed previously (section 1.7), the aim of this work was to design a peptide mimetic Kef ligand and replace the central amide bond of **70**. The aromatic properties of the ring system change the nature of the central amide bond, and this scaffold introduces synthetic flexibility for installing a variety of different headgroups in the 5-position *via* cross coupling reactions (Figure 2.2). Synthesis of the carboxylic acid and methyl ester would permit investigation of the binding and pro-drug approach of this structure.

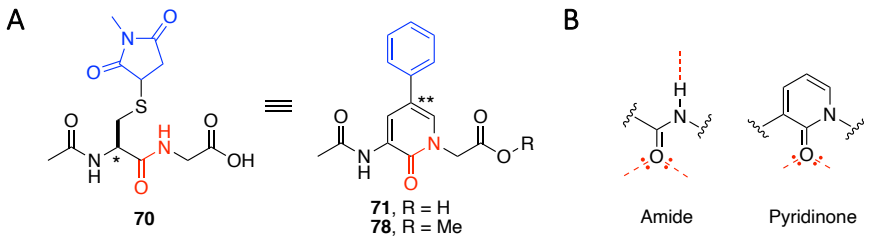


Figure 2.2. Representation of the pyridinone ligand as a peptide mimetic for the dipeptide structure 70. A) 2D-diagram of the replacement moieties for the dipeptide with the amide bond replacement in red, and the headgroup in blue. * labels the important stereocentre in **70**, ** labels the group which can be easily varied as part of SAR exploration *via* different cross-coupling reactions. B) Diagram comparing the hydrogen bond acceptor/donor interactions of an amide and pyridinone group.

The pyridinone **71** maintains the same relative positions of the heteroatoms as in **70** and has reduced peptide characteristics due to the aromatic nature of the central ring. There is more rigidity due to the lack of rotatable bonds compared to the analogous dipeptide

70.[191] The pyridinone can make the same hydrogen bond acceptor interaction as the amide but not the hydrogen bond donor interaction. This could reduce affinity and the importance of this interaction will be investigated through this scaffold. The physicochemical properties of **71**, **78**, and **70** were compared including the molecular weight (MW), number of hydrogen bond donors (HBD) and acceptors (HBA), number of rotatable bonds (RB), calculated (*c*)log$D_{pH7.4}$, solubility forecast index (SFI), and topological polar surface area (TPSA) from calculations by ACD/I-labs (Table 2.1).[194] The SFI is calculated as the sum of the *c*log$D_{pH7.4}$ and the number of aromatic rings in a molecule, and if the result is < 5 then the compound is likely to be water soluble.[195] The TPSA describes the calculation of the topological polar surface area (PSA), which is the area of the van der Waals surface of the compound that is comprised of oxygen, nitrogen, or protons attached to oxygen or nitrogen atoms. Higher TPSA values means lower lipophilicity, and compounds that have PSA values ≥ 140 Å^2 are absorbed poorly in the intestines, so this parameter is used to predict bioavailability. Compounds that show activity in Gram-negative bacteria have a higher average TPSA (100–200 Å^2) compared to drugs from other therapeutic areas (68 Å^2).[70,196–198]

Table 2.1. Physiochemical properties calculated from ACD/I-labs to compare the properties of 71 and 70.

Property	Value **70**, Comments	Value **71**, Comments	Value **78**, Comments
MW/ gmol^{-1}	331.35	286.28	300.31
HBD	3	2	1
HBA	9	6	6
RB	7	4	5
*c*log$D_{pH7.4}$	–6.4	–3.3	0.7
SFI	–6.4, predicted to be soluble	–1.3, predicted to be soluble	2.7, predicted to be soluble
TPSA/ Å^2	158.2	86.7	75.7

70, **71**, and **78** are predicted to be soluble with SFI values much less than 5. The pyridinone compounds **71** and **78** have a lower TPSA than **70**, more similar to the majority of drug compounds. This could predict improved accumulation in Gram-negative bacteria, as hydrophobic functionality is known to be important.[87] The pyridinone **71** does not contain the important stereocentre present in the cysteine part of the dipeptide Kef ligands. This presents an interesting opportunity to investigate this feature, to see if the stereocentre is necessary for a ligand with good affinity or efficacy (for activation of the Kef system over inhibition). Activating aromatic headgroups are known in the literature for the Kef system.[149,159] If the pyridinone backbone acts as a peptide mimetic, then aromatic headgroups with electron withdrawing and donating functional groups, different substitution patterns, and different sized hydrophobic groups can be attached to explore the SAR around the Kef binding site. They also introduce significant synthetic flexibility for elaboration of the scaffold.

This chapter reports the investigation of the pyridinone scaffold as a peptide mimetic ligand for the Kef system. The pyridinone scaffold **71** was synthesised, along with nine elaborated analogues, which were tested in biophysical assays to assess their suitability as a new peptide-mimetic ligand scaffold for the Kef system. The pyridinone ligand was found to have potential as a scaffold and bound to the Kef system.

2.2 Synthesis of the Pyridinone

The synthesis strategy first forms the pyridinone backbone based on literature precedent,[166] followed by a late stage diversification step for SAR exploration around the headgroup (Figure 2.3). The nitropyridinone **79** is alkylated to give compound **80**, followed by reduction of the nitro group to give a free amine **81**, that is then acetylated to give the pyridinone backbone **82**. The backbone is iodinated to give **83** to provide a synthetic handle for diversification with cross-coupling reactions to synthesise **78** and potential analogues. This step is incorporated late in the route for efficient large scale synthesis of the pyridinone compound series. The final step is the deprotection of the methyl ester to give the carboxylic acid compound **71**.

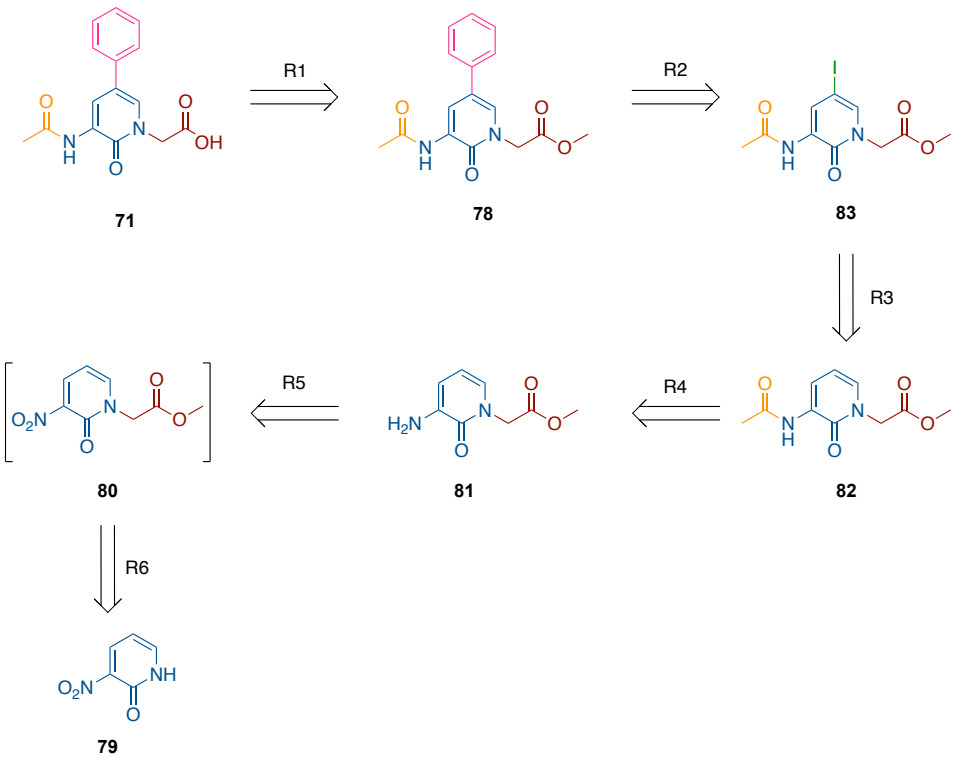
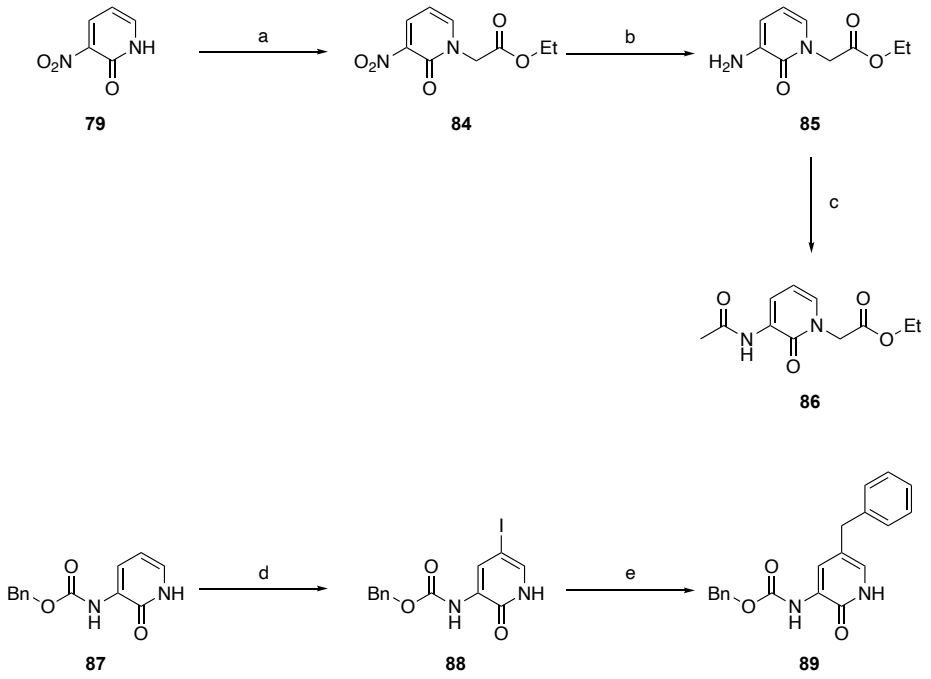


Figure 2.3. Retrosynthesis plan for the pyridinone ligand, 71. The strategy uses a nitropyiridnone (**79**, blue) that is alkylated (**80**, red), reduced (**81**), and acetylated (orange) to form the pyridinone backbone **82**. The backbone is then iodinated (**83**, green) to install different headgroups (pink) *via* cross coupling reactions. The final step of the synthesis is hydrolysis of **78** to give the carboxylic acid **71**. Formation of **82** is based on literature precedent.[166]

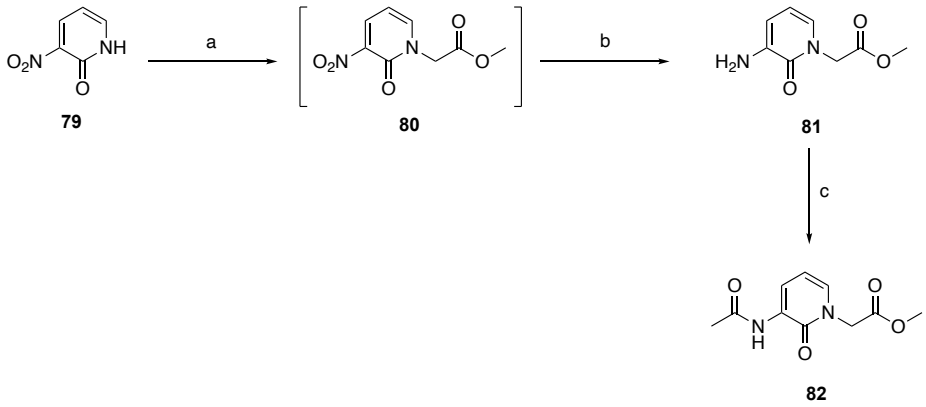
2.2.1 Synthesis of the peptide-mimetic ligand backbone

Warner *et al* have previously reported the synthesis of pyridinone containing molecules **86** and **89** (Scheme 2.1.) and this procedure was adapted for the synthesis of the pyridinone Kef ligand.[166] The route starts with preparation of the acetylated amine, followed by the cross-coupling reaction, and finally the alkylation on nitrogen.



Scheme 2.1. Route for synthesis of related pyridinone structures by Warner *et al.* *Reagents and conditions*: a) i) NaH, DMF, ii) Ethyl iodoacetate, no reported yield; b) H_2, 10% Pd-C, EtOH, no reported yield; c) Acetic anhydride, Na_2CO_3, no reported yield; d) *N*-Iodosuccinimide, DCM, 46%; d) Zn, BnBr, THF, dichloro[1,1'-bis(diphenylphosphino)ferrocene]Pd(II), no reported yield.

An adapted version of these routes was used for this research. For synthesis of a series of pyridinones, it was preferable to have the last common intermediate **82** (Figure 2.3) at a late stage of the synthetic route to enable efficient diversification. To avoid unwanted reactivity during the acetylation or alkylation steps with a diamine in the route, the alkylation was performed first, followed by the reduction and acylation (Scheme 2.2).



Scheme 2.2. Synthesis of the pyridinone backbone using literature conditions. *Reagents and conditions:* a)i) NaH, DMF, 0 °C to RT, 1 h, ii) Methyl bromoacetate, RT, 18 h, (4–24 h); b) H_2, Pd/C, methanol/THF, 3:1, RT, 1–2 h, n = 4, 60–>99% c) Acetic anhydride, pyridine, DMAP, THF, RT, 18 h, (15–24 h), n = 5, 61–74%.

This synthesis proceeded *via* a deprotonation of the nitroaminopyridine **79** (Fluorochem, CAS: 6332-56-5) with sodium hydride at 0 °C, followed by alkylation with methyl bromoacetate at room temperature. The work-up of the alkylation step was first attempted with a lithium chloride (0.5 M) wash, as this is known to remove dimethylformamide (DMF) well, however, this resulted in a loss of the product **80**. The polar nature of this compound meant it partitioned more towards the aqueous components (*c*log$D_{7.4}$ –0.31), so using water and brine for washes reduced the partitioning of **80** into the aqueous layer. **80** was a poorly soluble, yellow, crystalline solid, which meant purification *via* crystallisation or flash column chromatography was difficult. Telescoping this step and the following step avoided solubility issues during purification and provided access to **81**. The alkylation also gives a bright pink side compound that is a slightly more water-soluble amorphous solid/oil. When this was extracted from the aqueous components during the work up, the ^{1}H NMR was very similar to that of **80** (Figure 2.4). It was hypothesised the identity of this pink compound was the O-alkylated product **90**.

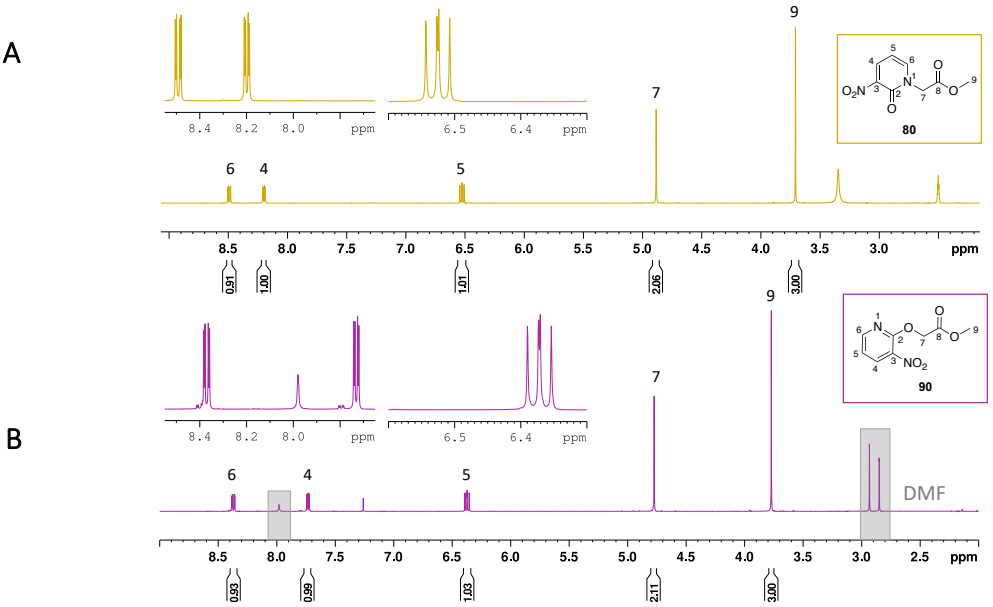


Figure 2.4. Stack of isolated 80 (A) and pink extracted compound 90 (B). Both spectra have expanded sections to show the multiplicities. The spectra have been run in two different solvents (A, D_6-DMSO and B, $CDCl_3$). The coupling patterns are similar for the two species, with slight differences in chemical shift.

The yellow needles suspected to be **80** dissolved only in dimethyl sulfoxide (DMSO) with heat, whereas **90** dissolved in $CDCl_3$ providing further evidence of two different compounds being formed. The compound is also a notably different colour (Figure 2.5).

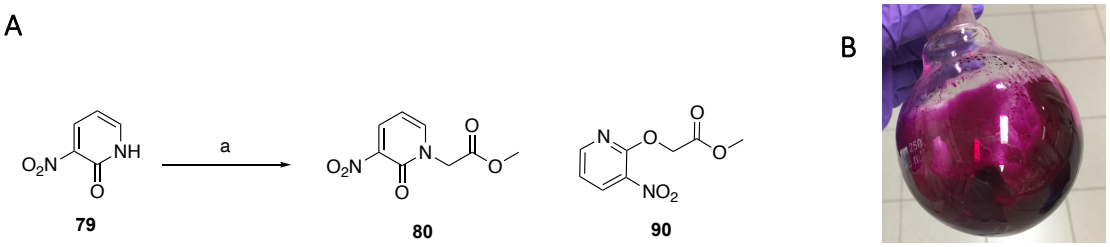
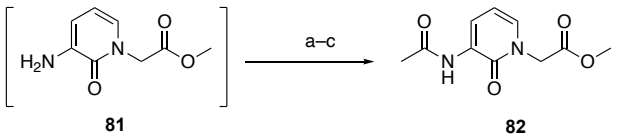


Figure 2.5. Alkylation of nitropyridinone 79. A) Scheme showing the two possible products, B) Image showing intense pink colour of isolated side product. A) *Reagents and conditions:* a)i) NaH, DMF, 0 °C to RT, n = 7, 27–85% of **80**, ii) Methyl bromoacetate RT. The desired *N*-alkylated product is **80**, and possible O-alkylated product **90**.

There is additional evidence for the O-alkylation of **80**. When the pink by-product was isolated from the aqueous work-up components, 2D-TLC (thin-layer chromatography) on silica indicated substantial decomposition of this compound. A new bright yellow spot was formed that matched the R_f and colour of the starting nitropyridinone **79**, which is neon yellow. The IR spectra for the isolated **80** showed two stretches at 1746 cm^{-1} and

1673 cm^{-1} providing evidence that the *N*-alkylated product was the major product formed and isolated during this step. **90** was unable to be isolated alone because of the decomposition on silica.

The second step was a reduction of the nitro group with hydrogen, which proceeded with complete consumption of the starting material, as shown by TLC monitoring of the reaction to give **81**. The acetylation step used conditions from the literature,[166] however the reaction did not progress which was assumed to be a result of the insolubility of the Na_2CO_3 under the reaction conditions (Scheme 2.3., Table 2.2. a).



81 **82**

Scheme 2.3. Acetylation of the free amine 81. *Reagents and conditions:* see Table 2.2.

Table 2.2. Conditions for the acetylation of 81 to give 82 (Scheme 2.3.). Conditions a were taken directly from the literature.

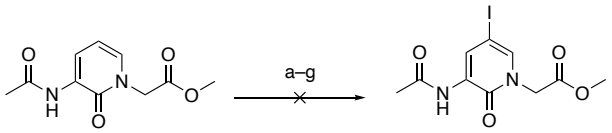
Acetylation method	Reagents and conditions	Outcome
a	Ac_2O, Na_2CO_3, MeOH, RT, 5 h	No reaction
b	**a**, added Ac_2O, DMAP, 50 °C, 5 h	10% yield over the three steps
c	Ac_2O, Pyridine, DMAP, THF, RT, 15–24 h	6–74% over three steps

To overcome this issue, two additional equivalents of both acetic anhydride (Ac_2O) and dimethylaminopyridine (DMAP) were added to the reaction (Table 2.2. b), which was warmed to 50 °C. Some **82** was formed but the reaction did not go to completion. Conditions using an organic base were therefore investigated (Table 2.2. c). Use of pyridine resulted in formation of **82,** albeit in poor yield (6% over three steps). The poor yield was due to the reaction being incomplete as there was an additional unidentified

side product spot following TLC analysis. Subsequent attempts at this reaction were left stirring longer to ensure **81** was completely consumed and had reproducible yields of 60–74%.

2.2.2 Introduction of a synthetic handle

The next step from the synthesis by Warner *et al.*[166] is an iodination of **82** in the 5-position using *N*-iodosuccinimide (NIS) in dichloromethane (DCM). The next planned step was to install various aromatic headgroups using Negisihi couplings which give the synthetic flexibility desired for this ligand series. The iodination was attempted directly on the pyridinone backbone **82** but did not form the desired product (Scheme 2.4, Table 2.3).



82 **83**

Scheme 2.4. Iodination attempts on 82. None of the reagents and conditions outlined in Table 2.3 were able to install the desired iodo group.

Table 2.3. Summary of iodination reaction attempts on 82. See Scheme 2.4.

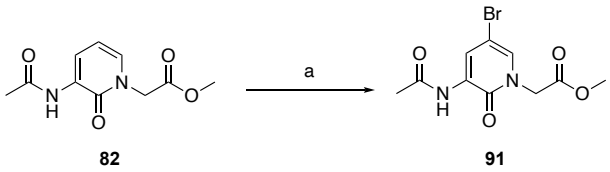
Iodination method	Reagents and conditions	Outcome
a	NIS, DCM, RT, 24 h	Starting material recovered, complicated reaction mixture by TLC.
b	i) NCS, NaI, MeCN ii) **82**, DCM, 7 h iii) $FeCl_3$ 5%, RT, 36 h	Starting material consumed, complicated reaction mixture, no formation of **83**.
c	NIS, DCM, RT to 40°C, 24 h	Starting material recovered, complicated reaction mixture by TLC
d	NIS, imidazole, DCM, RT, 24 h	Starting material recovered
e	NIS, pyridine, RT, 24 h	Starting material recovered
f	NIS, acetic acid, DCM, RT, 23 h	Incomplete consumption of starting material by TLC, crude NMR shows no characteristic pyridinone peaks.
g	NIS, TFA, DCM, RT, 23 h	Incomplete consumption of **82** by TLC, crude NMR shows no characteristic pyridinone peaks.

The NIS was then generated *in situ* from *N*-chlorosuccinimide (NCS) and NaI in acetonitrile (MeCN) (so the reaction could be attempted with fresh NIS as it is known to decompose if stored incorrectly),[199] before being concentrated and added to a solution of **82** in DCM (Table 2.3, b). Side reactions were occurring as indicated by multiple spots observed using TLC analysis. For the second step, sub-stoichiometric iron(III) chloride was added to the reaction mixture as this is known as a catalyst for the halogenation of aromatics from iodosuccinimide.[200,201] The addition did show consumption of **82**, but no formation of **83**, and the reaction mixture contained multiple compounds as evident by TLC. NIS in DCM was also heated to reflux (Table 2.2, c) to accelerate the reaction, but no **83** was formed.

Next the addition of base to aid in the deprotonation step of the reaction was investigated, although only **82** was isolated (Table 2.3, d and e). There is some precedent in the literature for iodination of related *N*-alkylated pyridinone systems under acidic

conditions as well with acetic acid[202] and TFA,[203] and so these acids were used to attempt to form **83** (Table 2.3, f and g). However, there was no observed formation of **83**.

Given the difficulties encountered with installing an iodo group, bromination with *N*-bromosuccinimide (NBS) would still provide a good synthetic handle with which to install headgroups, so this was investigated as an alternative to iodination (Scheme 2.5). This reaction gave the bromide-containing **91** in 65% yield (Figure 2.6).



Scheme 2.5. Bromination of the pyridinone backbone 82 with NBS. *Reagents and conditions:* a) NBS, DCM, RT, 3 h, n = 4, 23–65%.

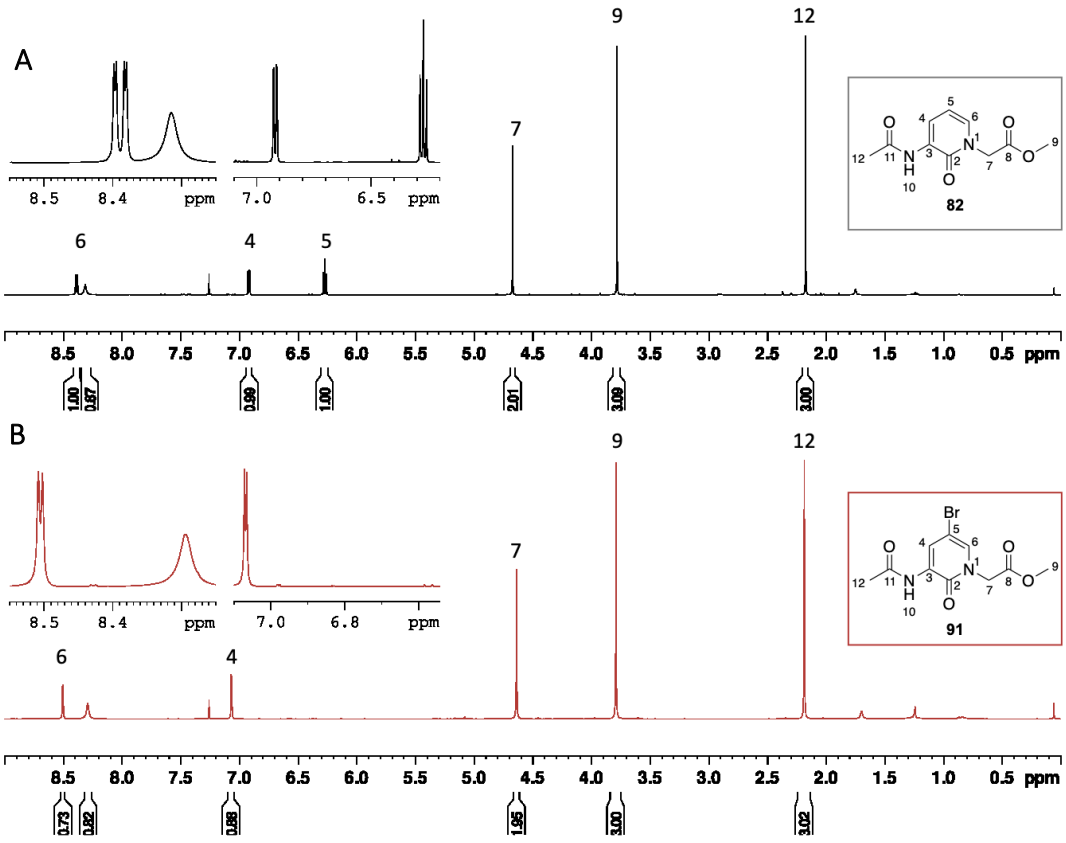


Figure 2.6. ^{1}H NMR stack of A) pyridinone backbone 82 and B) bromopyridinone 91. Doublet of doublets in A indicating the proton at position 5, is no longer present in B. The *J* values for the two doublets in **91** are 2.4 Hz, which is consistent with the proposed regioselectivity.

All of the literature precedent for similar bromination and iodination reactions show the bromine adding to the 5-position of the pyridinone. This regioselectivity is expected from the pyridinone nitrogen being able to donate electrons to the 5 and 3-positions of the ring (Figure 2.7).[204] As the pyridinone **82** has a substituent at the 3-position and none at the 4 or 6-position, the 5-position is also the least sterically hindered. Reactivity at the 5-position is expected, and the *J* values calculated from the ^{1}H NMR spectra provides evidence for this. The coupling constant of 2.4 Hz for the two doublets in **91** is in the expected range for a 4-bond coupling.

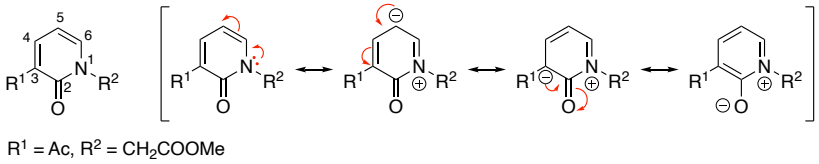
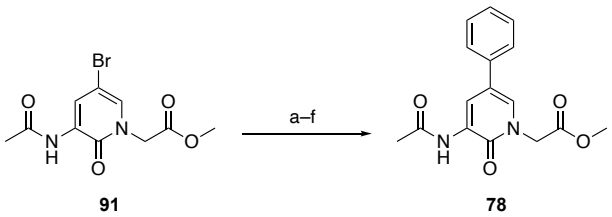


Figure 2.7. Diagram of the pyridinone core in 82 showing resonance forms. The resonance forms illustrate the regioselectivity for reactivity at positions 3 and 5 of the pyridinone ring as a result of the pyridine-like nitrogen. The aniline-like nitrogen in R^1 favours reactivity in the 4 and 6 position of the pyridinone ring, but the contribution is much less than the pyridine-like nitrogen, due to the nitrogen lone pair being less available as part of an amide bond.

2.2.3 Establishing coupling conditions to install the headgroup

With a reproducible route to the backbone established for **91**, there was an opportunity to explore the SAR around the headgroup. **91** can potentially be modified with a variety of different headgroups at the 5-position using Suzuki-Miyaura coupling reactions. It was therefore necessary to identify conditions that can couple boronic acids and esters to **91** (Scheme 2.6). Phenyl boronic acid was used for the screen, as identification of robust conditions for coupling of bulky, hydrophobic headgroups was an objective towards discovery of a high affinity Kef ligand, and this provided an inexpensive and readily sourced example.



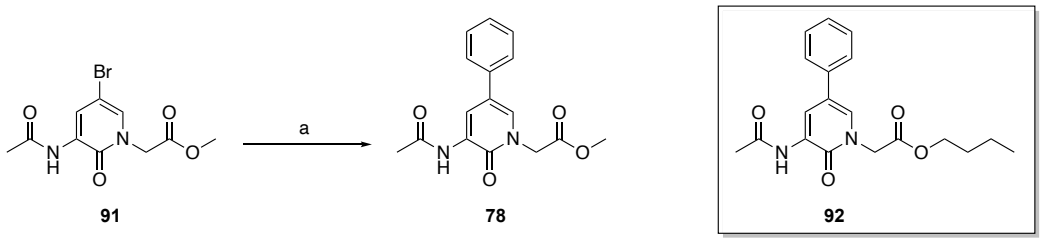
Scheme 2.6. Suzuki conditions screen. *Reagents and conditions:* a) Phenyl boronic acid, catalyst, base, and solvent, 100 °C, 21 h. See Table 2.4 for reagents and outcomes.

Table 2.4. Summary of reagents and outcomes from Scheme 2.6 for Suzuki reaction. The reactions were conducted on 0.07 mmol scale, and the outcome of each is outlined below.

	Catalyst	Base	Solvent	Outcome
a	$PdCl_2$[dppf]	K_2CO_3	DMF	No reaction, **91** unchanged
b	$PdCl_2$[dppf]	K_3PO_4	DMF	No reaction, **91** unchanged
c	$PdCl_2$[dppf]	$CeCO_3$	Dioxane	De-halogenation, **82** formed
d	$PdCl_2(PPh_3)_2$	K_2CO_3	DMF	No reaction, **91** unchanged
e	$PdCl_2$(Amphos)	K_2CO_3	Dioxane	De-halogenation, **82** formed
f	$Pd(OAc)_2$, XPhos	K_3PO_4	*n*-Butanol	Consumption of **91**

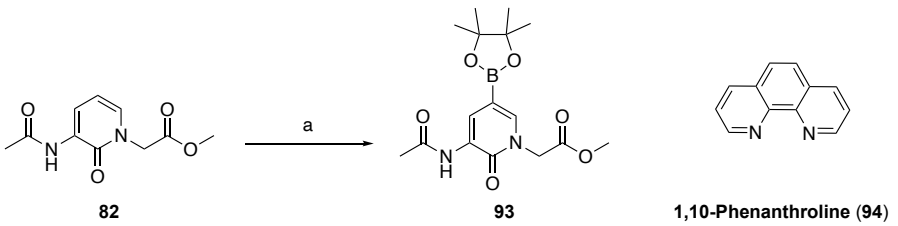
When DMF was used as a solvent there was no reaction, with the pyridinone and boronic acid both visible by TLC analysis (Table 2.4, a, b, d). When dioxane was used as a solvent (Table 2.4, c and e) **91** was consumed to form the dehalogenated pyridinone **82**. When *n*-butanol was used as a solvent (Table 2.4, f) **91** was consumed, and TLC analysis suggested a coupled product had formed, as a new spot with a higher R_f was observed. There is a clear solvent effect on the cross-coupling reaction. A strongly co-ordinating solvent such as DMF favours S_N2 over three-membered oxidative addition steps,[205] which may be preferred for **91** if the activated complex of the S_N2 mechanism is highly distorted.[205] Dioxane facilitates the oxidative addition step as shown by the de-halogenated side product, however the reductive elimination step did not occur, possibly due to electron rich ligands reducing rate of this step.[205] After purification, the isolated compound contained the correct aromatic proton ^{1}H NMR signals for the phenyl ring. However, a transesterification had occurred during the reaction between the *n*-butanol

and the methyl ester of the pyridinone, to give the butyl ester compound **92** in 41% yield. Replacing the solvent with *tert*-butanol stopped the transesterification and gave the desired **78** in 69% yield (Scheme 2.7).



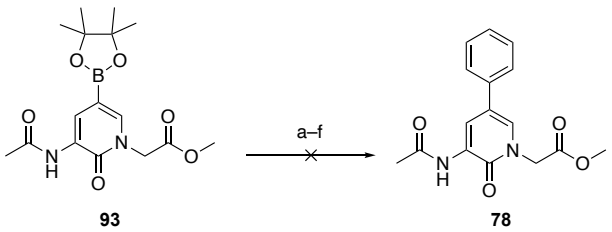
Scheme 2.7. Suzuki coupling conditions compatible with the pyridinone. *Reagents and conditions:* a) Phenyl boronic acid, $Pd(OAc)_2$, XPhos, K_3PO_4, ^tBuOH, 100° C, 21 h, 69%. These conditions prevented the formation of the transesterified product **92**.

Suzuki couplings with the boronic pinacol ester in the 5-position would allow coupling with aromatic bromides increasing the range of possible analogues that could be synthesised. Literature precedent for this reaction described using a C-H functionalisation process to install a boronic pinacol ester at the 5-position of a similar pyridone core.[206] The conditions were repeated with **82** to give the desired compound **93** (Scheme 2.8). This reaction resulted in a variable yield as **93** was unstable to silica.



Scheme 2.8. Installation of the boronic pinacol ester in the 5-position. *Reagents and conditions*: a) $(Bpin)_2$, $[Ir(OMe)(Cod)]_2$, 1,10-phenanthroline (**94**), THF, 80 °C, 18–24 h, n = 3, 41–64%.

With the pinacol ester **93,** a new set of conditions could be screened for coupling to a variety of commercially available bromides (Scheme 2.9, Table 2.5).



Scheme 2.9. Screen of reagents and conditions for Suzuki cross-coupling reaction. *Reagents and conditions:* a) Phenyl bromide, catalyst, base, and solvent, 100 °C, 21 h. For outcomes see Table 2.5.

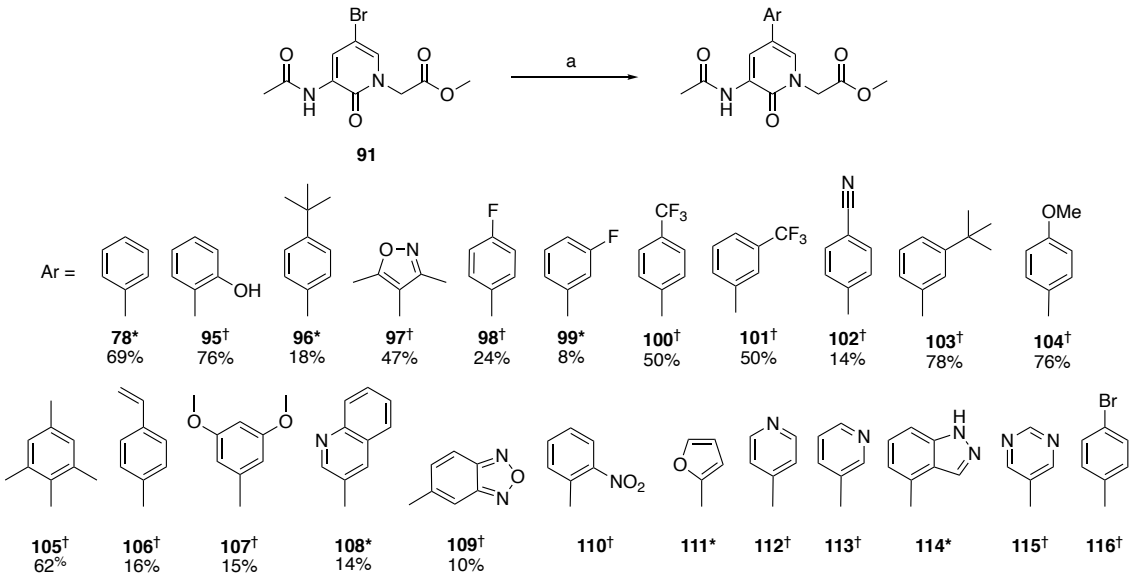
Table 2.5. Summary of reagents and conditions screened for new Suzuki reaction conditions for 93. See Scheme 2.9.

Suzuki coupling conditions	Catalyst	Base	Solvent	Time /h	Outcome
a	$Pd(PCy_3)_2$	Cs_2CO_3	Dioxane	20	No reaction
b	$PdOAc_2$[dppf]	K_3PO_4	MeCN	20	No reaction
c	$PdCl_2$[dppf]	K_3PO_4	Dioxane	20	No reaction
d	$PdCl_2(PPh_3)_2$	K_2CO_3	DMF	2	Consumption of **93**
e	$PdCl_2$(Amphos)	K_2CO_3	Dioxane	20	No reaction
f	$PdCl_2$[dppf]	K_2CO_3	DMF	2	Consumption of **93**
g	$Pd(OAc)_2$ XPhos	K_2CO_3	*tert*-butanol	24	No reaction

None of the conditions screened led to the formation of **78**. Reactions d and f had a new peak in the ^{1}H NMR spectrum at approximately 8.0 ppm for approximately two protons. While formation and subsequent deacetylation of **78** is a possibility, the mass spectrum of the crude mixture showed no evidence of this. The free amine **81** has previously been observed by MS. Further screening is required to identify effective coupling conditions, and this approach was not pursued further.

2.2.4 Exploration of new headgroups

To explore the SAR for new headgroups capable of activating *Sd*Kef, the bromopyridinone **91** was coupled to a range of boronic acids and esters (see Scheme 2.10) using the established Suzuki conditions (Scheme 2.7).



Scheme 2.10. All headgroups coupled on to the pyridinone backbone 91. *Reagents and conditions*: a) Het/ArB(OH)$_2$, Pd(OAc)$_2$, XPhos, $K_3PO_4.H_2O$, *tert*-butanol, 18 h, (2–24 h), 100 °C (*) or 80 °C (†). All coupling reactions were performed with the conditions listed above, with percentage yields for each compound listed underneath their number, reactions with **110**–**116** did not result in isolation of coupled product, so are listed with no yield.

Different moieties have been incorporated onto the pyridinone backbone including bulky lipophilic groups (such as **96** and **105**), electron donating groups (**95** and **107**), and electron withdrawing groups (**102** and **109**). The peptide ligands been shown to bind to the Kef system as GSX adducts with aromatic headgroups, and they included NO_2, CF_3, F, and MeO groups (Section 1.5).[159] Therefore headgroups with these moieties to assess the contribution of the pyridinone backbone to binding were included. The highest affinity ligands to date are GSX adducts with *N*-alkyl succinimide headgroups. Aromatic rings with *tert*-butyl groups had not yet been investigated, and were of interest because ^{t}BuSG shows the most stabilisation and greatest activation of *Sd*Kef (Section 1.5).[145] It

was speculated **96** and **103** may have potential to activate the Kef system, with bulky hydrophobic groups attached to the headgroup.

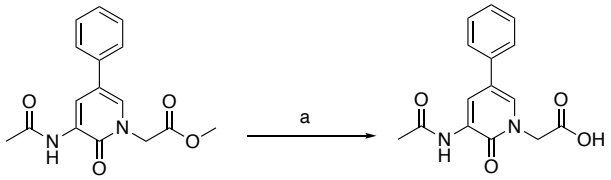
Fluorine containing ligands with F or CF_3 groups were included for use in ^{19}F NMR binding assays. The quinoline headgroup was of interest following dynamic combinatorial chemistry experiments run by Mary Wilson[165] showing naphthalene as a headgroup for a GSX adduct that was capable of binding to Kef (Section 1.5). The napthalene pyridinone compound had a *c*log$D_{pH7.4}$ value of –2.8,[194] where the quinoline had a *c*log$D_{pH7.4}$ value of –3.1 and consequently greater solubility. Some additional headgroups were installed to further probe the SAR of the dipeptide binding site, including a nitrile and vinyl group for coupling reactions such as Click or thiol-ene to form probes,[207–211] a dimethylisoxazole to explore whether a polar headgroup could bind with the pyridinone backbone, and the 2,4,6-trimethylphenyl headgroup to explore the effect of steric bulk closer to the ligand backbone.

Most of the reactions performed at 80°C have higher yields than those performed at 100 °C which was the initial temperature used for the reaction. Couplings done at 100 °C have many more side reactions as shown by TLC than at 80 °C, and so the procedural temperature was decreased to 80 °C.

The coupling reactions using amine boronic acids (**112**–**115**) did not yield any of the desired product, as these boronic acids had poor solubility in *tert*-butanol. Nitrogen lone pairs are also known to coordinate to the palladium catalysts, and this may be another reason for their poor reactivity. The furyl group (**111**) was unstable to the reaction

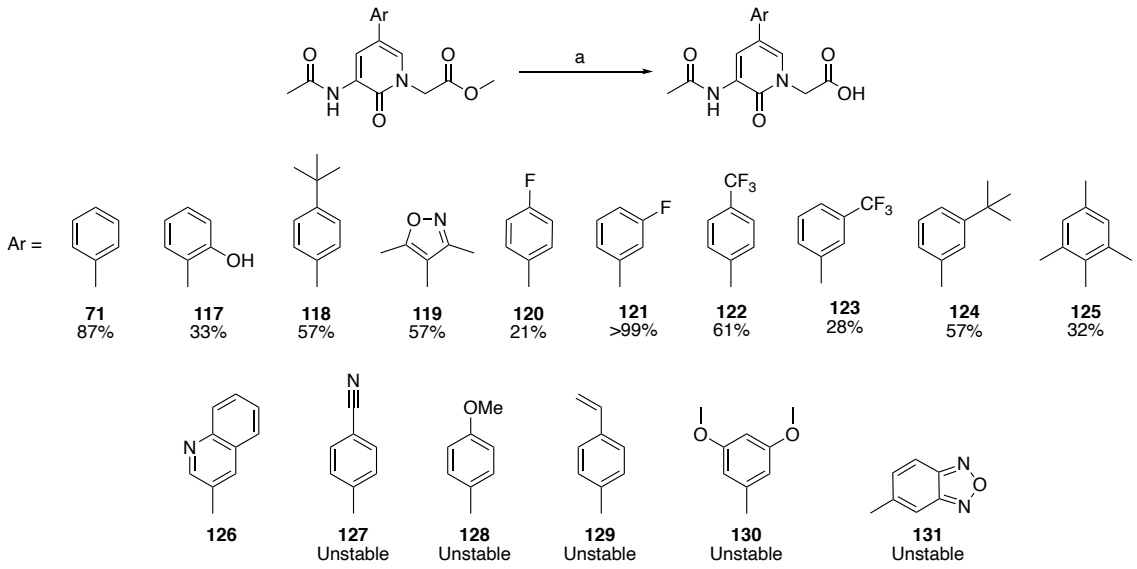
conditions, and the nitrophenyl (**110**) appeared to couple with consumption of **91** by TLC, but **110** was so insoluble in all common organic solvents tried (including DMSO, at RT) that it could not be purified. The SFI value of **110** is 2.63 which is predicted to be soluble, showing a limitation of these calculations.[194,195] The value is similar to soluble compounds such as **71** (SFI = 2.72) and **97** (SFI = 2.41), and is less than **96** (SFI = 4.28) which did not experience solubility problems.

With these sixteen coupled pyridinone products in hand, the next step was to deprotect the methyl ester groups to reveal the carboxylic acid, which is required to bind to Kef (see Section 1.5). Hydrolysis conditions have been established for the Kef dipeptides using lithium hydroxide in THF/MeOH/H_2O 3:2:1,[149] and these were applied first on the peptide mimetic compounds (Scheme 2.11).



Scheme 2.11. Hydrolysis conditions for the phenyl pyridinone compound 78. *Reagents and conditions*: a) Lithium hydroxide, THF/MeOH/H_2O 3:2:1, RT, 5 h, 87%.

Starting with **78**, these conditions gave the desired carboxylic acid **71** in 87% yield. Ten of the isolated methyl ester compounds were also hydrolysed using this method (Scheme 2.12).



Scheme 2.12. Examples of hydrolysis reactions performed on pyridinone compounds. *Reagents and conditions*: LiOH, THF/MeOH/H_2O 3:2:1, RT, 2 h (0.2–18 h). The percentage yields are listed below the compound name in each example.

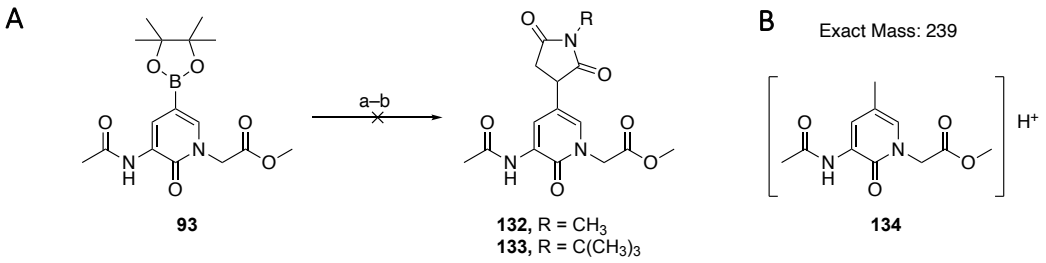
The hydrolysis conditions were applied to sixteen of the pyridinone esters (**71**, **117**–**131**) to give ten pyridinone acids with new headgroups to explore the SAR of the pyridinone compound as a Kef ligand. **108** was hydrolysed to afford **126**, however **126** could not be isolated in >95% purity for biophysical testing. **108** was consistently isolated in poor purity by NMR analysis (the cleanest by ^{1}H NMR was measured by RP analytical HPLC to be 92%). The zwitterionic nature of **126** resulted in difficulties with extraction of the acid and removal of impurities by flash silica column and capture/release chromatography.

Compounds **127**–**131** were also formed from hydrolysis of the respective methyl esters, however, proved to be unstable on silica and so could not be purified by flash column chromatography.

2.2.5 Work towards a pyridinone with a known activating headgroup

To obtain evidence that the pyridinone is binding in the same binding site as GSH, it was of interest to synthesise a pyridinone ligand with a succinimide headgroup. This would investigate the binding interactions made of the pyridinone backbone. Known *Sd*Kef ligands such as **70**, and ESG contain succinimide headgroups, and so this moiety is known to be tolerated and capable of activating the Kef system.

The boronic pinacol ester compound **93** was investigated in a cross coupling reaction based on an oxidative Heck reaction from the literature,[212] using a cyclopentene-1,3-dione with palladium acetate and 1,10-phenanthroline (**94**). These conditions were tolerant of electron donating and withdrawing groups on the aryl ring, and it was thought they may be compatible with the pyridinone system (Scheme 2.13).



Scheme 2.13. Attempts towards a cross coupling reaction with pyridinone compound 93 to install maleimide headgroup. A) *Reagents and conditions*: maleimide, $Pd(OAc)_2$, 1,10-phenanthroline (**94**), DMF, O_2, 72 °C, 4–23 h, with a) *N*-methylmaleimide (**132**) or b) *N-tert*-butylmaleimide (**133**); B) Compound **134** detected by MS from reagents and conditions a.

The reaction conditions for Scheme 2.13 a with *N*-methylmaleimide consumed the starting material **93**, however, no **132** was isolated. The single most prominent spot as analysed by TLC did not have any characteristic pyridinone peaks following analysis by ^{1}H NMR, although the mass-spectrum of this compound showed a peak for $[239]^+$. This mass corresponds to methylation of the pyridinone backbone in the 5-position, **134**. The

reaction was repeated with *tert*-butylmaleimide (Scheme 2.13 b) to stop the possible alkylation side reaction, however this just returned starting material **93**.

As the literature conditions used a cyclopentene-1,3-dione for the coupling reaction, this group was considered of interest as it was sterically similar to the *N*-methylmaleimide. The pentenedione would make an interesting comparison sterically and electronically when investigated if it was capable of activating Kef (Figure 2.8).

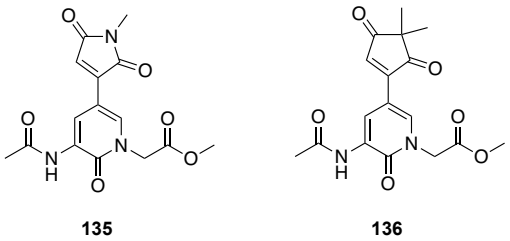
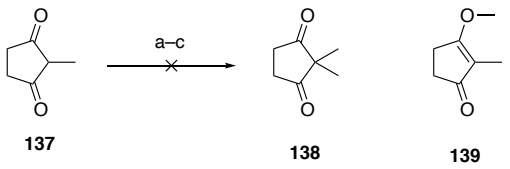


Figure 2.8. 3D-comparison of *N*-methylmaleimide headgroup (135) and dimethylcyclopentenedione headgroup (136) on the pyridinone backbone.

The synthesis of this headgroup had been reported by Lamb *et al* and the conditions were attempted (Scheme 2.14, Table 2.6).[213]



Scheme 2.14. Attempts to synthesise the cyclopentanedione 138. For full reagents and conditions see Table 2.6.

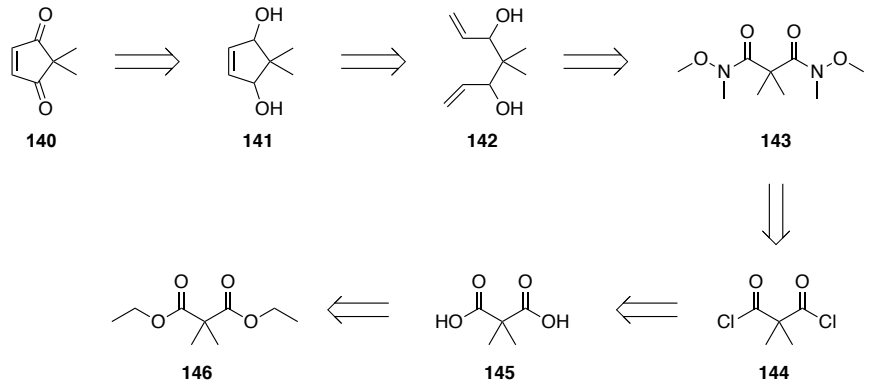
Table 2.6. Reagents and conditions for the attempted synthesis of dimethylcyclopentanedione, 138 (Scheme 2.14).

Method	Reagents and conditions	Outcome
a	MeI, DBU, MeCN, 82 °C, 24 h	Formation of **139**
b	KOH (1.0 eq), MeI (1.0 eq), dioxane:water 3:1, 105 °C, 90 h	Formation of **139**
c	KOH (4.0 eq), MeI (4.0 eq), dioxane:water 3:1, 105 °C, 94 h	Formation of **139**

The conditions taken from the literature[212] use an alkyl bromide with DBU in acetonitrile (MeCN) (Table 2.6, a), however, when this was attempted with MeI, the only isolated product was **139** with alkylation on oxygen (see Appendix Figure S.1.).

Another literature synthesis by Brun *et al.* for **138** was investigated that used KOH in water/dioxane,[214] (Scheme 2.14, Table 2.6 b) so the reflux temperature was higher (105 °C) than for MeCN (82 °C), however, this also gave only **139**. KOH and DBU are clearly able to deprotonate **137**, however, the resulting enolate was very stable and so preferentially reacted on oxygen. The reaction was repeated (Scheme 2.14, Table 2.6, c), with three equivalents of the MeI and KOH instead of one initially, to try and force a second deprotonation and achieve alkylation on the carbon. The reaction was additionally fed with 3 × 0.3 equivalents of MeI and KOH to try to push the reaction to completion but only **139** was isolated. A screen of different electrophiles could reveal a new strategy for this alkylation for a softer and sterically unhindered electrophile that is able to react at carbon.

A new synthesis route for this compound is required, or a screen for an alternative electrophile or deprotonation strategy which will be the subject of future work (Scheme 2.15).



Scheme 2.15. Proposed retrosynthesis of the cyclopentenedione 140 required for the Heck coupling reaction. This route was chosen as it utilises an orthogonal cyclisation approach to that trialled previously.

Starting the synthesis with an existing dimethyl substituted methylene will be investigated to avoid the tricky installation requiring very forcing conditions. **146** is the simplest commercial dimethyl malonate moiety and will require three steps to reach the Weinreb amide **143** required to prevent over-addition of the Grignard during the formation of **142**. An alkene ring closing metathesis reaction to form the unsaturated diol should be successful due to the favoured five membered ring, and entropically favourable formation of ethylene.

2.3 Biophysical Assays with *Sd*KefQCTD

To determine the suitability of the pyridinone **71** as a peptide mimetic, the compound was subjected to biophysical assays to determine whether it was capable of binding to *Sd*KefQCTD.

2.3.1 WaterLOGSY

Water-ligand observed *via* gradient spectroscopy (waterLOGSY, WL) is a ^{1}H NMR based assay that relies on the transfer of intermolecular Nuclear Overhauser Effects (NOEs) from the bulk water to the ligand, and can provide qualitative evidence of ligand binding to a protein of interest.[111,215–218] The ligand must be experiencing fast binding exchange with the protein, and be in excess (this protocol has a ligand excess of 25:1). The magnetisation can be transferred directly from the bulk water, which is a positive NOE effect, or *via* the protein which is a negative NOE effect. The magnetisation can be transferred either through the protein from the bulk water bound at the protein surface, directly from water bound to the protein near the ligand, or through exchangeable protons exchanged from the bulk water with exchangeable groups on the protein surface.[218] Molecules that do not interact with the protein tumble quickly and display a positive NOE, whereas those that do interact tumble slowly like the protein and display a negative NOE. DMSO is used as the reference resonance for the assay and is present in the assay at 1% by volume. If the ligand is behaving like a small molecule in solution and not interacting with the protein, it will have resonances with the same sign as DMSO, as it experiences direct magnetisation transfer from the bulk water. If the ligand is

interacting and binding to the protein, it will have the opposite sign to DMSO. Exchangeable protons such as NH and OH always have a positive NOE.[215,219] The overall signal intensity is a result of the combination of these NOE effects. WaterLOGSY is an ideal assay because it is capable of detecting low micromolar affinity ligands. It is thus suitable for detecting weak binders like the Kef dipeptides, and any potential peptide mimetics are also likely to be binding with similar affinity.[216]

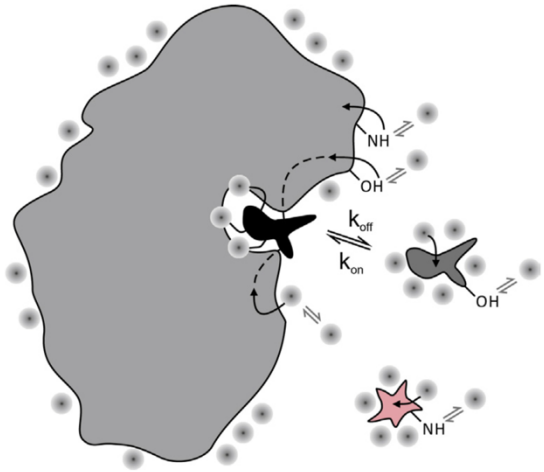


Figure 2.9. WaterLOGSY cartoon showing possible magnetisation transfer pathways between a ligand and a protein receptor. The bulk water (grey circles) can transfer magnetisation to the protein (large grey shape) and unbound ligands *via*: exchangeable protons (double arrows); direct NOEs (solid black arrows) from water bound near the binding site; spin-diffusion through the receptor (dashed lines) as indirect transfer from the bulk water. Binding ligands (grey and black) have a proportion of magnetisation transferred through the protein, which means negative NOE effects consist of a large proportion of the final signal, as well as directly from bulk water. Non-binding ligands (pink) only have direct transfer from the bulk water and therefore exhibit positive NOE effects. Figure reproduced with permission from High-Resolution NMR Techniques in Organic Chemistry 3rd edition, Prof T. Claridge.[218]

The waterLOGSY assay comprises three separate experiments. Firstly, a ^{1}H NMR experiment of the ligand in the absence of protein is run to look for identifiable resonances for the compound being tested. Secondly, a waterLOGSY experiment of the ligand without protein is run as a negative control to look for false positives, to check the compound is properly dissolved to the correct concentration. Insoluble compounds can form aggregates in solution that tumble slowly and appear as large molecules with the opposite sign to DMSO even when protein is not present. Finally, a waterLOGSY with

protein is run to identify if the ligand is binding *via* any inverted resonances relative to DMSO.

As WaterLOGSY has not been used for the Kef system prior to this research, a positive control was selected that is a known binder (**58**, supplied by Dr Catherine Haslam) to the protein of interest, with *Sd*KefQCTD being used as the model Kef system (Section 1.4.2.4). The *tert*-butyl group on the maleimide gives a clear resonance as it integrates for 9H and is easy to visualise. The known binder functions as a positive control to check the protein has not degraded and is folded properly, and the instrument is acquiring data as expected (Figure 2.10). A known binder was run for every tube of protein used in the assay.

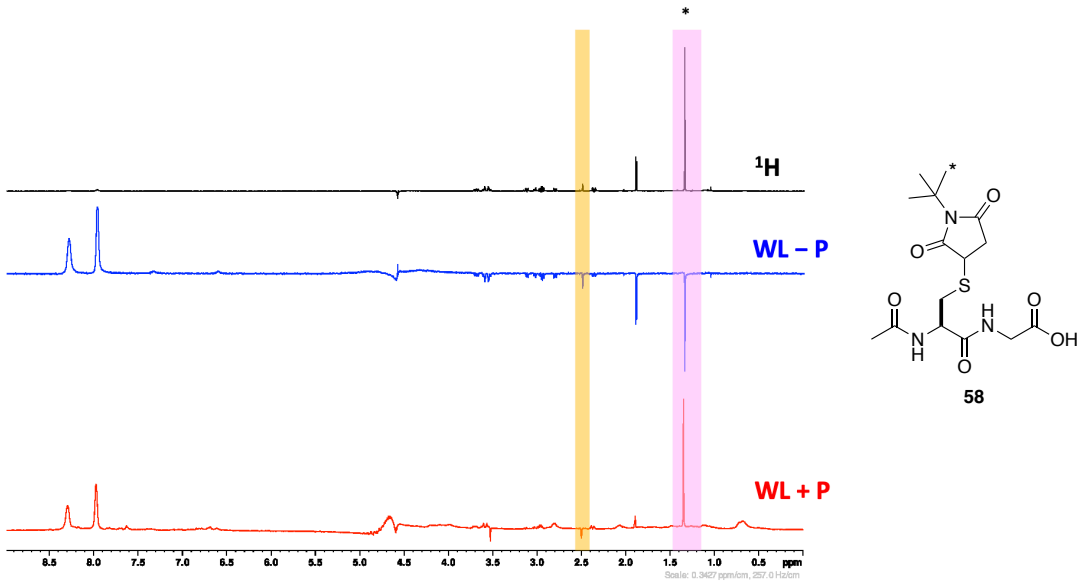


Figure 2.10. Full waterLOGSY spectrum of positive control dipeptide 58. Stack top to bottom: black, water-supressed ^{1}H NMR of **58**; blue, waterLOGSY spectrum without protein; red, waterLOGSY spectrum with *Sd*KefQCTD protein. DMSO is highlighted at 2.50 ppm in yellow and is the sample reference. The compound peak of interest (^{t}Bu, *) is highlighted in pink. The red spectrum shows characteristic inversion of the ligand peaks relative to DMSO, which indicates ligand binding to the protein.

The dipeptide **58** shows the characteristic inversion of peaks showing that **58** is behaving like a large protein molecule and is binding to *Sd*KefQCTD. WaterLOGSY spectra for **58** had not previously been obtained prior to this research. As these conditions were suitable

for detecting weakly binding ligands (**58** has a K_d of 1.8 ±0.2 µM) the experiment was run on the pyridinone ligand **71** (Figure 2.11).

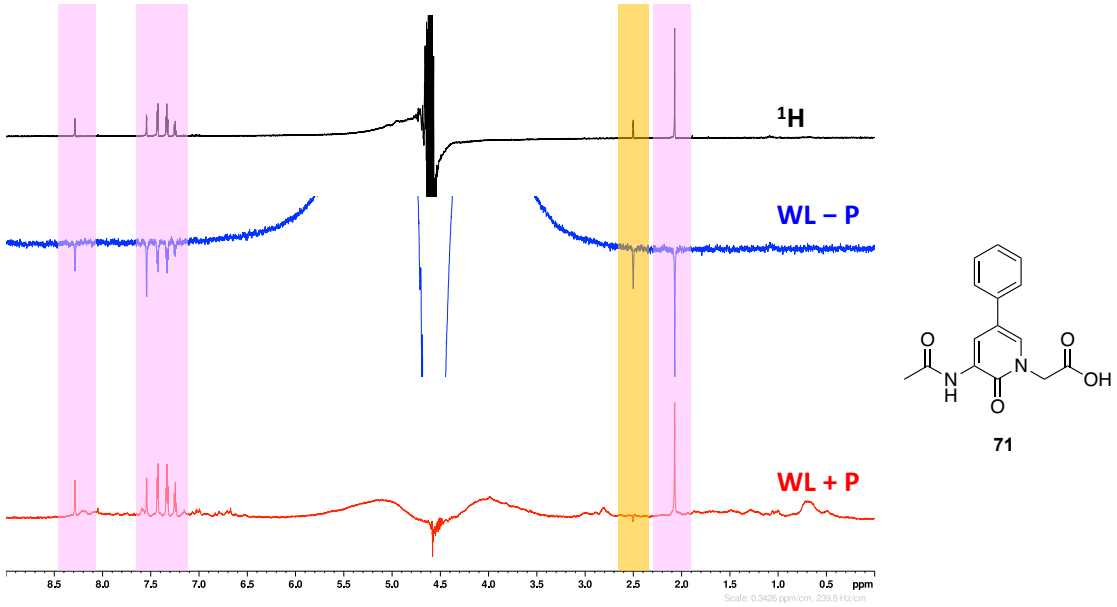


Figure 2.11. Full waterLOGSY spectrum of pyridinone compound 71. Stack top to bottom: black, water-supressed ^{1}H NMR of **71**; blue, waterLOGSY spectrum without protein; red, waterLOGSY spectrum with *Sd*KefQCTD protein. DMSO is highlighted at 2.50 ppm in yellow and is the sample reference. The compound peak of interest is highlighted in pink. The red spectrum shows characteristic inversion of the ligand peaks relative to DMSO, which indicates ligand binding to the protein.

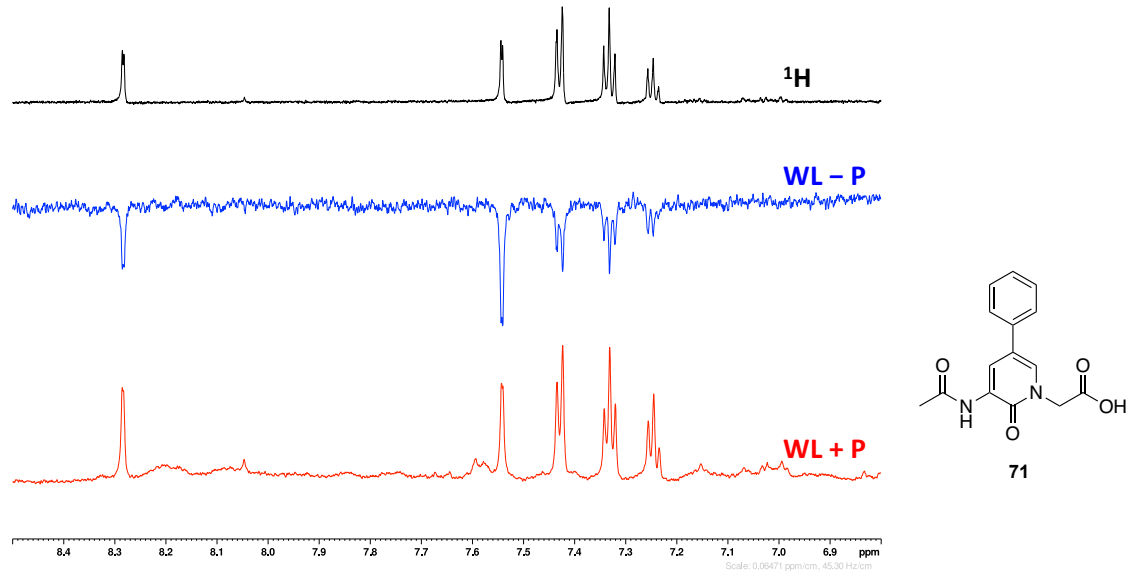
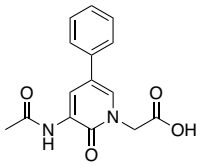
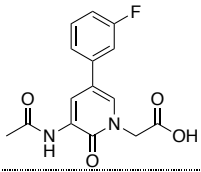
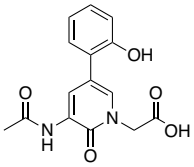
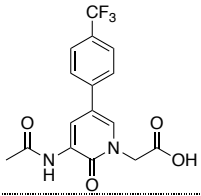
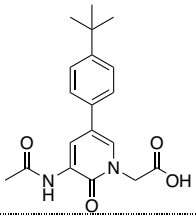
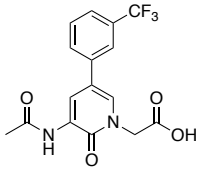
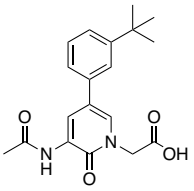
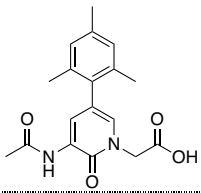
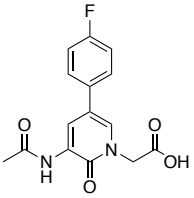
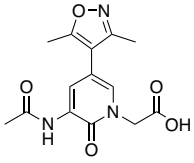


Figure 2.12. Expanded section of the waterLOGSY spectrum of 71. Stack top to bottom: ^{1}H, water-supressed ^{1}H NMR of **71**; WL–P, waterLOGSY spectrum without protein; WL+P, waterLOGSY spectrum with *Sd*KefQCTD protein. This is an expansion of the full spectrum (Figure 2.11).

There is very little protein background around the chemical shift upwards of 7.0 ppm, so aromatic peaks are typically the easiest to observe. The waterLOGSY spectra of **71** show

the clear inversion of ligand peaks relative to DMSO, with these resonances between 7.0–8.5 ppm easiest to observe, suggesting that **71** can bind to *Sd*KefQCTD. This experiment is the first evidence of a non-peptide ligand that binds to *Sd*KefQCTD. With this promising initial result, nine more pyridinone ligands with different aromatic headgroups were tested using waterLOGSY (Table 2.7).

Table 2.7. Summary of waterLOGSY observable binding for pyridinone compounds. A diverse range of groups were investigated as potential headgroups for the pyridinone backbone. Electron donating and withdrawing groups, and substitutions at the 2, 3 and 4-positions were investigated. ✓ = compound binds.

Compound	Structure	Binds *Sd*KefQCTD by WL	Compound	Structure	Binds *Sd*KefQCTD by WL
71		✓	**121**		✓
117		✓	**122**		✓
118		✓ (experiment run at 125 µM to avoid aggregation)	**123**		✓
119		✓	**124**		✓
120		✓	**125**		✓

The following spectra show the results for the different headgroups (Figures 2.13–2.21).

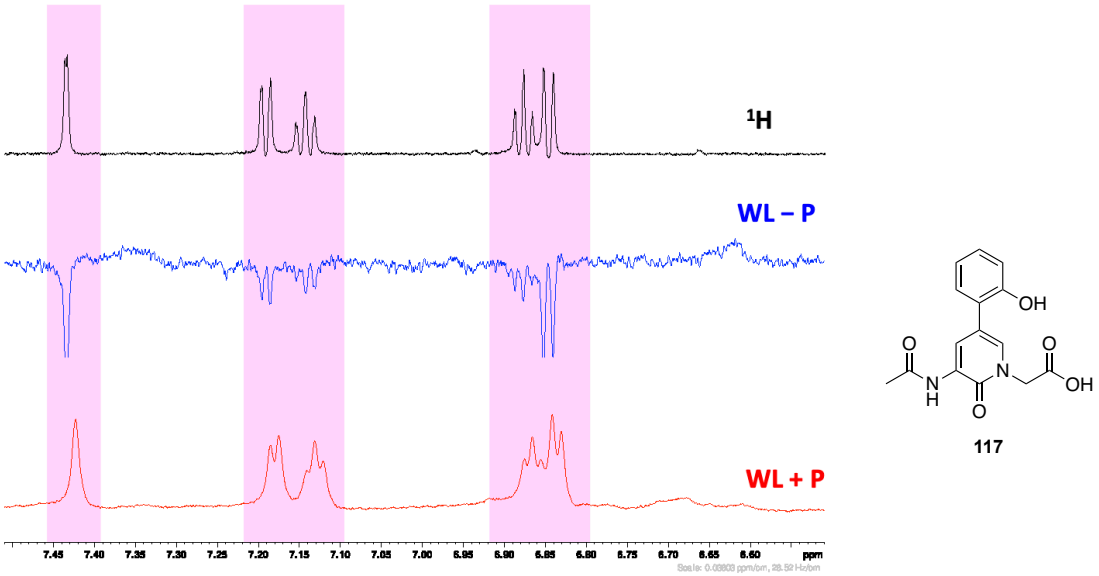


Figure 2.13. Expanded section of the waterLOGSY spectrum of 117. Stack top to bottom: ^{1}H, water-supressed ^{1}H NMR of **117**; WL–P, waterLOGSY spectrum without protein; WL+P, waterLOGSY spectrum with *Sd*KefQCTD protein. This is an expansion of the full spectrum (see appendix for full spectrum). The compound peaks of interest are highlighted in pink.

The 2-hydroxyphenypyridinone **117** shows the same inversion, most clearly observed by the aromatic resonances shown in Figure 2.13. This shows that additional functionality is tolerated in the 2-position of the phenyl ring.

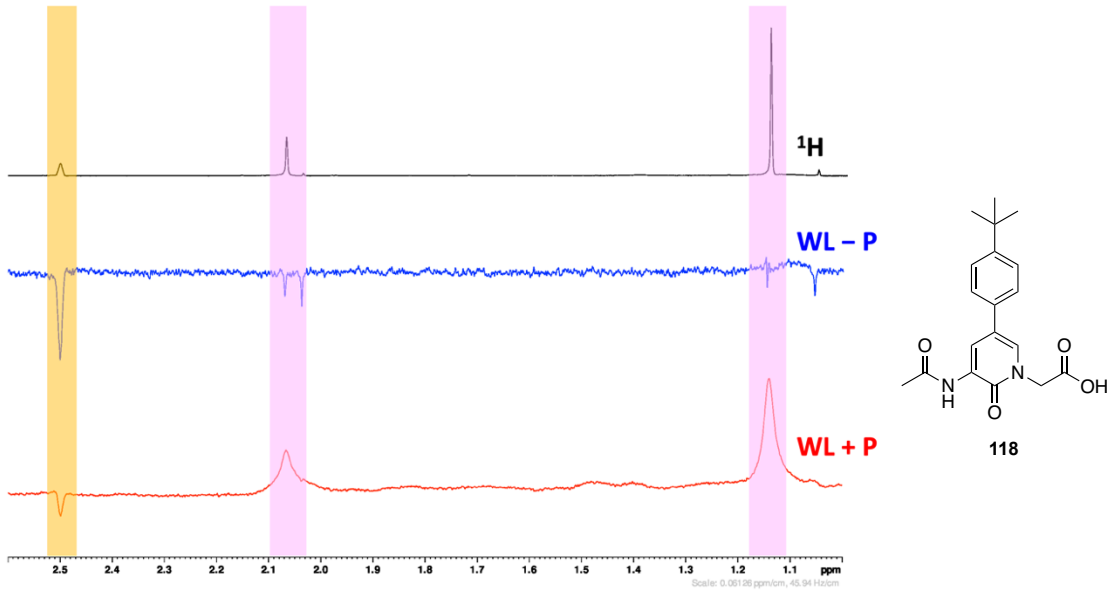


Figure 2.14. Expanded section of the waterLOGSY spectrum of 118. Stack top to bottom: ^{1}H, water-supressed ^{1}H NMR of **118**; WL–P, waterLOGSY spectrum without protein; WL+P, waterLOGSY spectrum with *Sd*KefQCTD protein. This is an expansion of the full spectrum (see appendix for full spectrum). DMSO is highlighted at 2.50 ppm in yellow and is the sample reference. The compound peaks of interest are highlighted in pink.

The *tert*-butylphenylpyridinone ligand **118** also shows the characteristic inversion relative to DMSO showing it also binds to *Sd*KefQCTD. The spectrum for **118** also has a 9H alkyl resonance for the *tert*-butyl group and so this was used as a diagnostic peak for the waterLOGSY assay. The *tert*-butyl functional group was also tolerated in the 3-position of the phenyl ring in **119** which also showed evidence of binding *via* waterLOGSY (Fig 2.15).

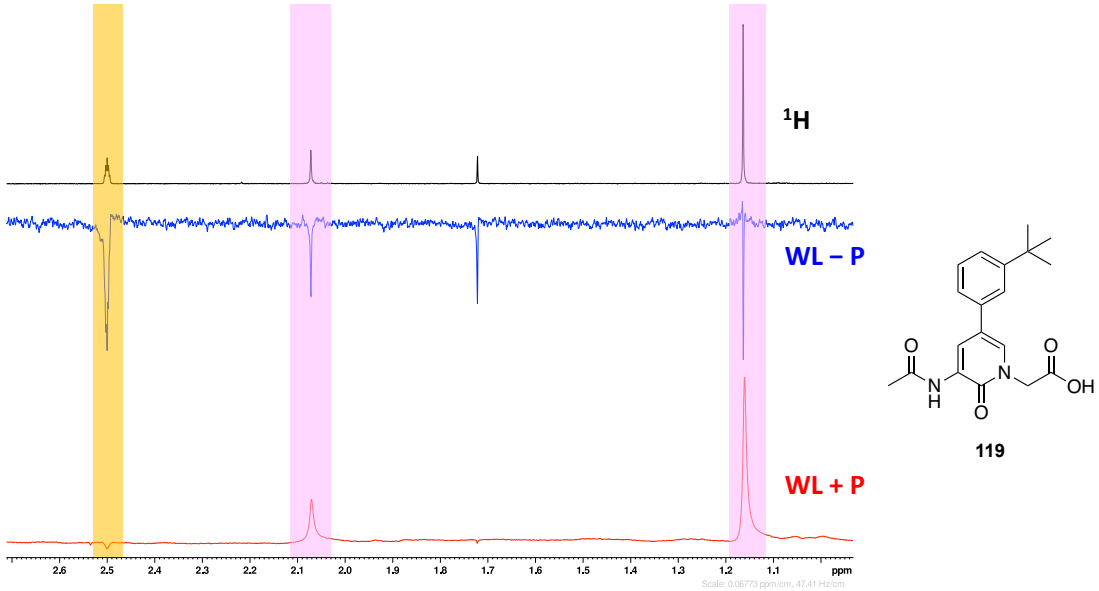


Figure 2.15. Expanded section of the waterLOGSY spectrum of 119. Stack top to bottom: ^{1}H, water-supressed ^{1}H NMR of **119**; WL–P, waterLOGSY spectrum without protein; WL+P, waterLOGSY spectrum with *Sd*KefQCTD protein. This is an expansion of the full spectrum (see appendix for full spectrum). DMSO is highlighted at 2.50 ppm in yellow and is the sample reference. The compound peaks of interest are highlighted in pink.

119 also shows the clear inversion with the opposite sign of the 9H peak to that of DMSO, suggesting this molecule is also capable of binding to *Sd*KefQCTD.

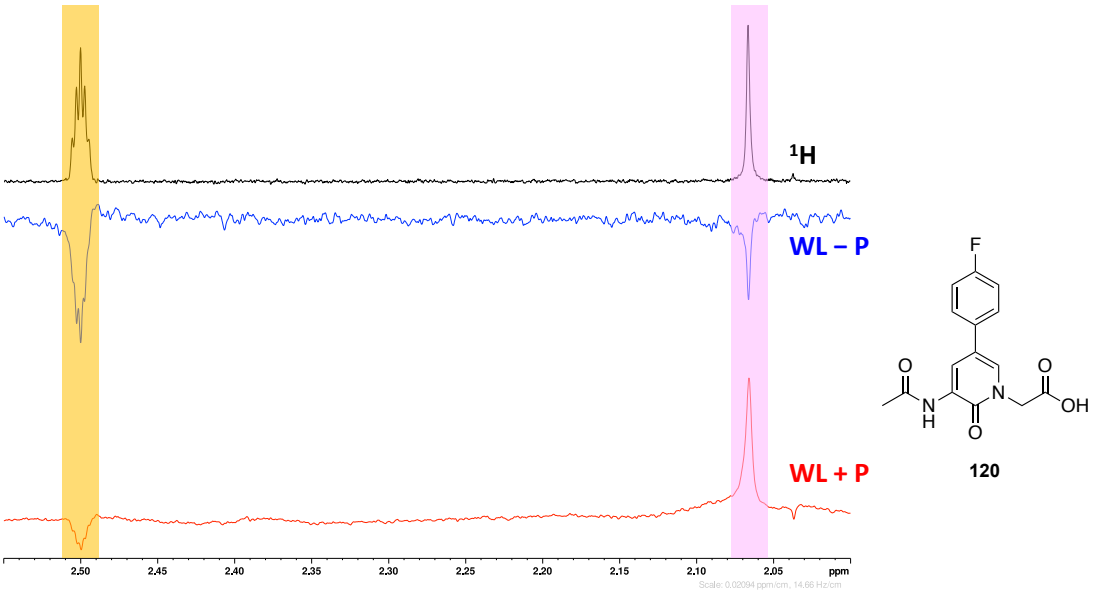


Figure 2.16. Expanded section of the waterLOGSY spectrum of 120. Stack top to bottom: ^{1}H, water-supressed ^{1}H NMR of **120**; WL–P, waterLOGSY spectrum without protein; WL+P, waterLOGSY spectrum with *Sd*KefQCTD protein. This is an expansion of the full spectrum (see appendix for full spectrum). DMSO is highlighted at 2.50 ppm in yellow and is the sample reference. The compound peak of interest is highlighted in pink.

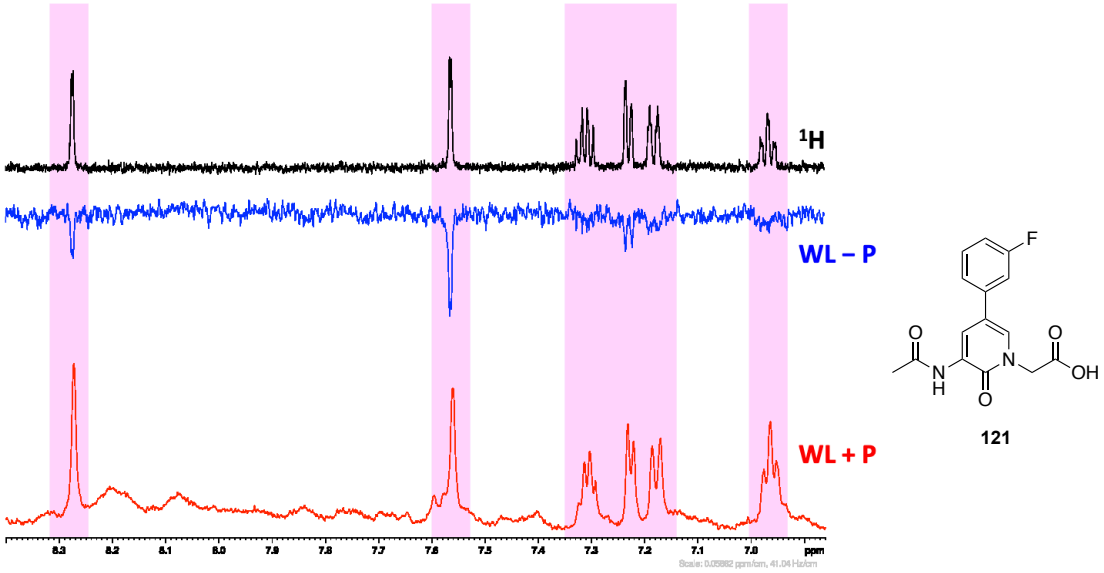


Figure 2.17. Expanded section of the waterLOGSY spectrum of 121. Stack top to bottom: ^{1}H, water-supressed ^{1}H NMR of **121**; WL–P, waterLOGSY spectrum without protein; WL+P, waterLOGSY spectrum with *Sd*KefQCTD protein. This is an expansion of the full spectrum (see appendix for full spectrum). The compound peaks of interest are highlighted in pink.

It was hypothesised that trifluoro analogues of **118** and **119** would bind to *Sd*KefQCTD, by replacing the *tert*-butyl group with a CF_3 moiety in **122** and **123**.

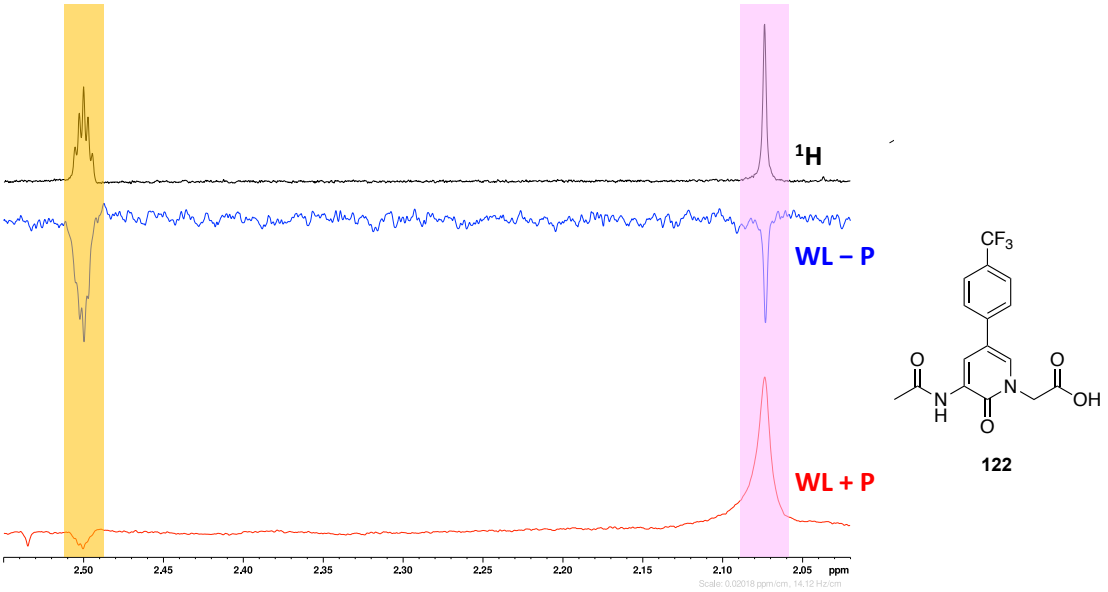


Figure 2.18. Expanded section of the waterLOGSY spectrum of 122. Stack top to bottom: ^{1}H, water-supressed ^{1}H NMR of **122**; WL–P, waterLOGSY spectrum without protein; WL+P, waterLOGSY spectrum with *Sd*KefQCTD protein. This is an expansion of the full spectrum (see appendix for full spectrum). DMSO is highlighted at 2.50 ppm in yellow and is the sample reference. The compound peak of interest is highlighted in pink.

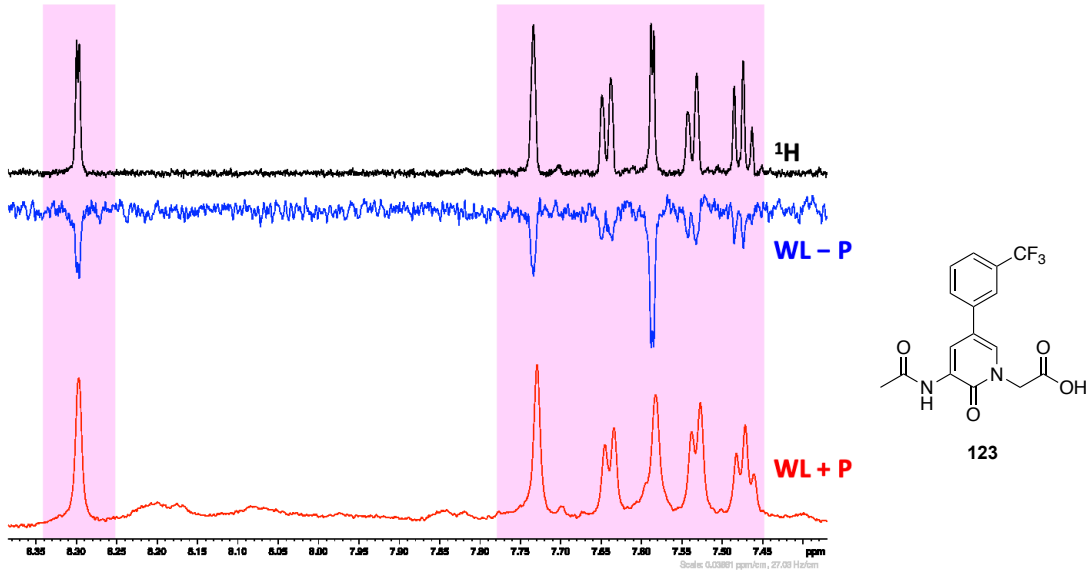


Figure 2.19. Expanded section of the waterLOGSY spectrum of 123. Stack top to bottom: ^{1}H, water-supressed ^{1}H NMR of **123**; WL–P, waterLOGSY spectrum without protein; WL+P, waterLOGSY spectrum with *Sd*KefQCTD protein. This is an expansion of the full spectrum (see appendix for full spectrum). The compound peaks of interest are highlighted in pink.

All the pyridinone ligands with fluorine-containing headgroups bound to the *Sd*KefQCTD protein, showing that the CF_3 and F moieties were not too bulky or lipophilic to interfere with binding.

The trimethylphenyl headgroup in **124** was one of the bulkiest hydrophobic headgroups installed in a pyridinone compound, to explore the tolerance of a wider aromatic headgroup (Figure 2.20).

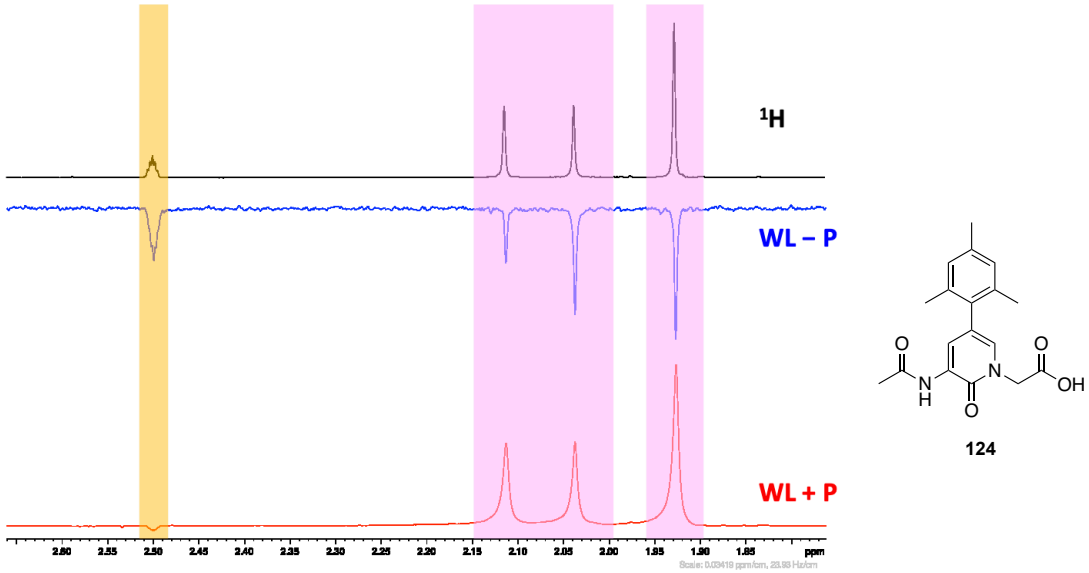


Figure 2.20. Expanded section of the waterLOGSY spectrum of 124. Stack top to bottom: ^{1}H, water-supressed ^{1}H NMR of **124**; WL–P, waterLOGSY spectrum without protein; WL+P, waterLOGSY spectrum with *Sd*KefQCTD protein. This is an expansion of the full spectrum (see appendix for full spectrum, Figure S.13). DMSO is highlighted at 2.50 ppm in yellow and is the sample reference.

124 shows inversion of the compound peaks relative to DMSO and shows binding to the *Sd*KefQCTD system. The results for the compound suggests that large, bulky headgroups are tolerated within the binding site of *Sd*KefQCTD. The dimethyl isoxazole in **125** was a considerably more polar headgroup than had previously been incorporated into the pyridinone compounds and offered an opportunity to investigate the impact of hydrogen bonding interactions around the headgroup, rather than just displacement of the capping residue (Figure 2.21).

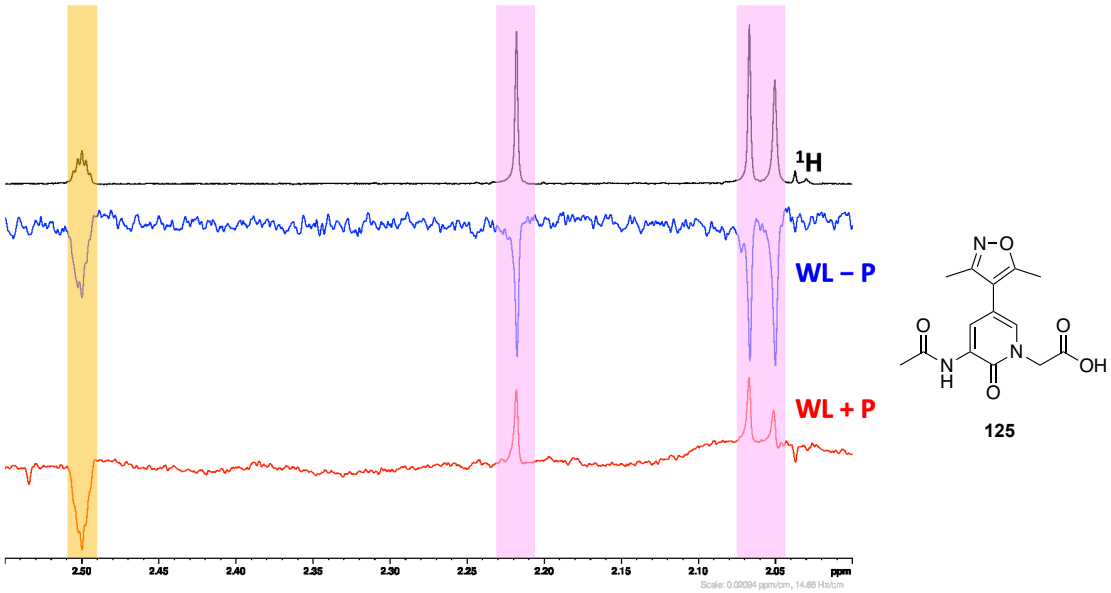
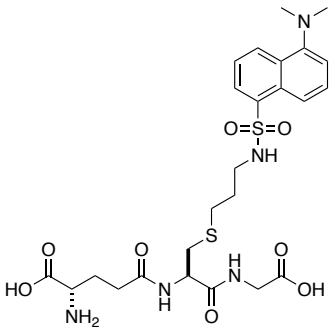


Figure 2.21. Expanded section of the waterLOGSY spectrum of 125. Stack top to bottom: ^{1}H, water-supressed ^{1}H NMR of **125**; WL–P, waterLOGSY spectrum without protein; WL+P, waterLOGSY spectrum with *Sd*KefQCTD protein. This is an expansion of the full spectrum (see appendix for full spectrum).

125 also showed binding to the *Sd*KefQCTD system, suggesting that hydrogen bonding interactions may be tolerated with the pyridinone headgroup, and could potentially be a way to increase affinity when included within a large bulky headgroup required for displacement of the capping residue.

These new ligands provide further evidence for the tolerance of aromatic headgroups by the *Sd*KefQCTD system. **118** and **119** provide new SAR information as the bulky *tert*-butyl group attached to a phenyl ring is tolerated by *Sd*KefQCTD. Several bulky headgroups have been identified by previous work including the fluorescent *S*-((5-(dimethylamino)naphthalen-1-yl)sulfonylaminopropyl) glutathione (DNGSH (**147**), Figure 2.22).[145] The fluorine containing ligands, **120**, **121**, **122**, and **123** would be useful probes for the *Sd*KefQCTD system and could be used in ^{19}F NMR experiments for K_d determination.



DNGSH (147)

Figure 2.22. Fluorescent competition ligand DNGSH (147) with a K_d value of 6–19 μM.[145] This ligand is an example of a bulky headgroup (dansyl) that is able to bind to Kef.

The pyridinone backbone should improve the physiochemical properties of these ligands, while introducing synthetic flexibility for SAR exploration. They do not contain the central amide bond which is a possible site of cleavage by peptidases and have removed the cysteine stereocentre which could be epimerised causing loss of ligand affinity. The pyridinone ligands are also the first examples of aromatic headgroups joined directly to the ligand backbone, capable of binding to the *Sd*KefQCTD system, rather than connected *via* a flexible aromatic linker.[145,149] They also provide a new chemical space for Kef ligands, with increased aromaticity.

2.3.2 DSF

Differential scanning fluorimetry (DSF) was chosen as an orthogonal assay to waterLOGSY to test the binding of **71**, **117-125** to *Sd*KefQCTD.[220] DSF has the advantage of being higher throughput than waterLOGSY, so more compounds can be tested quickly. Confirmation of ligands binding *via* DSF validates the results from waterLOGSY. Proteins denature or 'melt' when heated to a characteristic melting temperature (T_m), which is measured by the assay. When a ligand binds to a protein there will be a change in the melting

temperature called a thermal shift (ΔT_m). An increase in the melting temperature suggests the ligand is stabilising the protein, and a decrease shows destabilisation, which is less frequent but known to occur.[221] The greater the stabilisation effect the greater the thermal shift.

This DSF assay protocol works by detecting fluorescence from Sypro™ Orange dye, which is strongly quenched by water. An increase in fluorescence is detected as the dye can bind non-specifically to hydrophobic regions of a protein, which stops water quenching the fluorescence. With increasing temperature, the protein sample will denature, enabling the dye to bind, until it is fully unfolded giving a fluorescence peak with maximum dye binding. Further increase in temperature causes aggregation of the protein and dissociation of the dye, and so fluorescence decreases. The melting temperature of the protein (T_m) is calculated from the steepest part of the gradient (Figure 2.23).

DSF is effective for comparison only between ligands of the same series with the same protein. The melting temperatures of ligands with different proteins, or different ligand scaffolds with the same protein, cannot be used to draw conclusions on their relative affinities. The melting temperature depends on the structure of the protein and the fluorescence on the proportion of hydrophobic regions that the dye can bind to. Hydrophobic ligands show a thermal shift of greater magnitude when compared to hydrophilic ligands because of the larger entropy component.

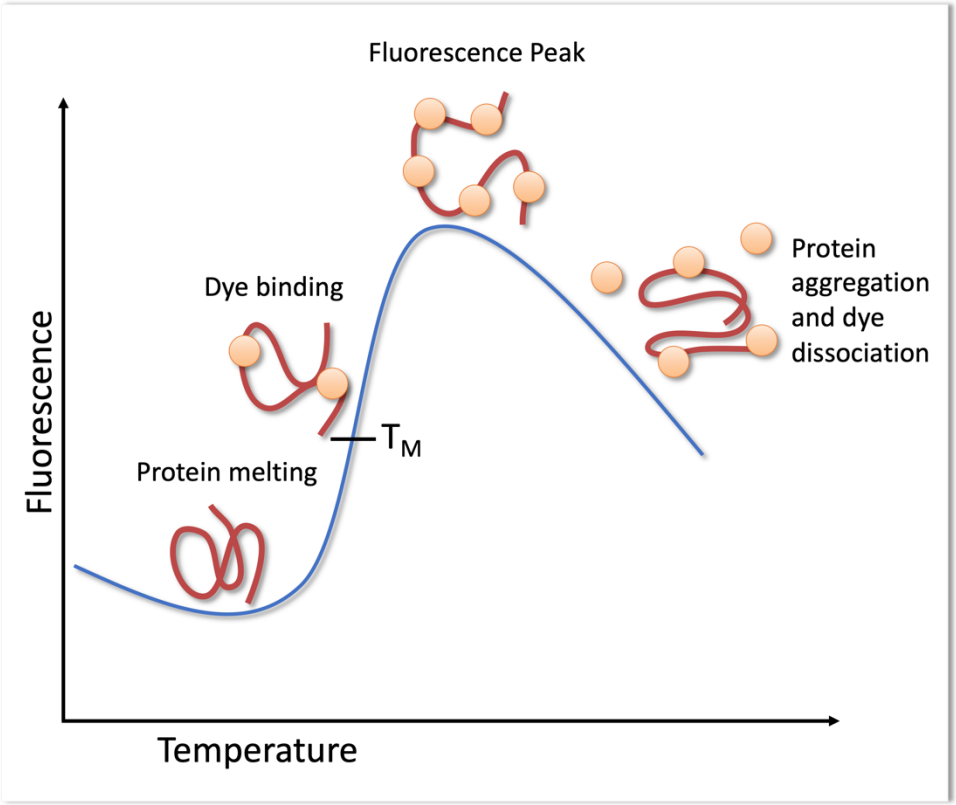


Figure 2.23. Cartoon illustration of DSF thermal shift. The graph shows the measure of fluorescence with change in temperature shown as a blue line, the protein of interest represented in red and Sypro™ Orange dye as orange circles.[160]

Glutathione S-conjugates have large ΔT_m values (approximately 5–13°C) for *Sd*KefQCTD, with ^{t}BuSG giving a ΔT_m of ~12°C.[145] The dipeptides are expected to have smaller ΔT_m values, corresponding to their larger K_d values. DSF was therefore a suitable choice of assay to detect a ligand with similar affinity to the peptides and provide comparison with other Kef binders of the same series. The results from the assay are shown below (Figure 2.24).

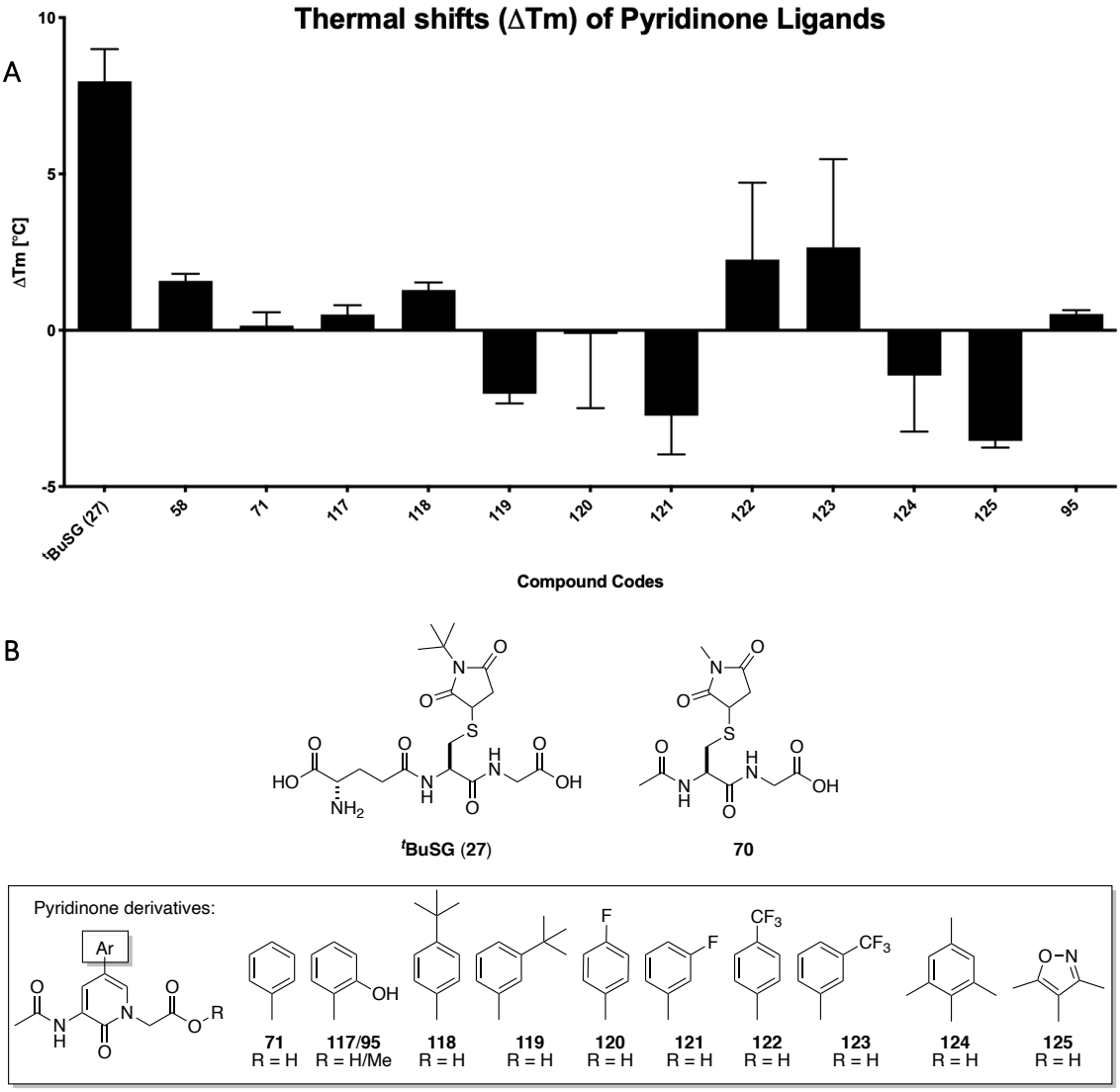


Figure 2.24. DSF Assay results with *Sd*KefQCTD. A) DSF assay thermal shift results, error bars are standard error from triplicate except ^{t}BuSG (eight repeats); B) Structures of compounds used in DSF. Thermal shift results (^{t}BuSG, **27**, and **70**, supplied by Dr Catherine Haslam) were used as positive controls. **71**, **117**, and **120** showed a negligible change in melting temperature, suggesting that they have weak or no binding interaction to *Sd*KefQCTD, but **118**, **122**, and **123** show stabilisation of *Sd*KefQCTD. Destabilising effects are seen with **119**, **121**, **124**, and **125**. **95** was run as a negative control as the methyl ester was not expected to bind.

The ΔT_m values of the *N*-methylsuccinimido dipeptide was unknown prior to undertaking this assay. As expected, there is a large ΔT_m for ^{t}BuSG (10 °C, literature value is ~12 °C).[145] The value for the dipeptide **70** is smaller at 2 ±0.4 °C. **70** is suspected to have a low micromolar K_d (based upon that of its analogue **58** (supplied by Dr Catherine Haslam), the *N-tert*-butylsuccinimido-dipeptide, which has a K_d of 1.8 ±0.2 μM). **70** was chosen as a positive control as it constitutes the minimal structural requirement for activation of the

Kef system (Section 1.5) and may provide a detection limit as a weakly binding ligand. The two thermal shift results of **70** and ^{t}BuSG suggests that they both bind to and stabilise the *Sd*KefQCTD protein, but to different extents.

71 shows a negligible ΔT_m of 0.2 ±0.4 °C, which was unexpected as this compound had been shown to bind to *Sd*KefQCTD *via* waterLOGSY. It is possible that as waterLOGSY can detect very weakly binding ligands, that **71** is too weak a binder to produce a detectable ΔT_m in this DSF assay. The same was observed for **117** which also showed binding in the waterLOGSY assay, but a negligible effect in DSF. However, the ΔT_m for **118** was comparable to that of **70** suggesting that this ligand is producing a similar stabilising effect to that of **70**, and could be binding with similar affinity, within the detection limit of waterLOGSY and DSF. **125**, **119**, and **121** destabilise *Sd*KefQCTD, this could be due to these ligands acting as inhibitors and causing an different conformational change to the displacement of the capping residue caused by ^{t}BuSG and **70**. The thermal shifts for **122**, **123** and **124** have large associated standard errors and the data are inconclusive. The methyl ester **95** also shows no stabilisation to the *Sd*KefQCTD system, however, the results of this as a negative control are inconclusive because **117** also showed no observable stabilisation as it is below the detection limit.

The initial results suggest that the different pyridinone headgroups have a mixture of stabilising and de-stabilising effects, possibly due to the different sizes and polarities of moieties within the headgroups. The standard error is particularly high for compounds that are the most lipophilic, with the least polar headgroups.

To investigate whether poor solubility of the more lipophilic compounds was causing the variation, the assay was repeated at half concentration of the ligands (500 µM, Figure 2.25). It was observed that the compounds were soluble at 500 µM during the waterLOGSY assay, as no aggregation (and therefore false positives) were detected in the waterLOGSY experiment without the presence of *Sd*KefQCTD (see Section 2.3.1). Both DSF and waterLOGSY were run in a solution of 1% DMSO in an aqueous phosphate buffer.

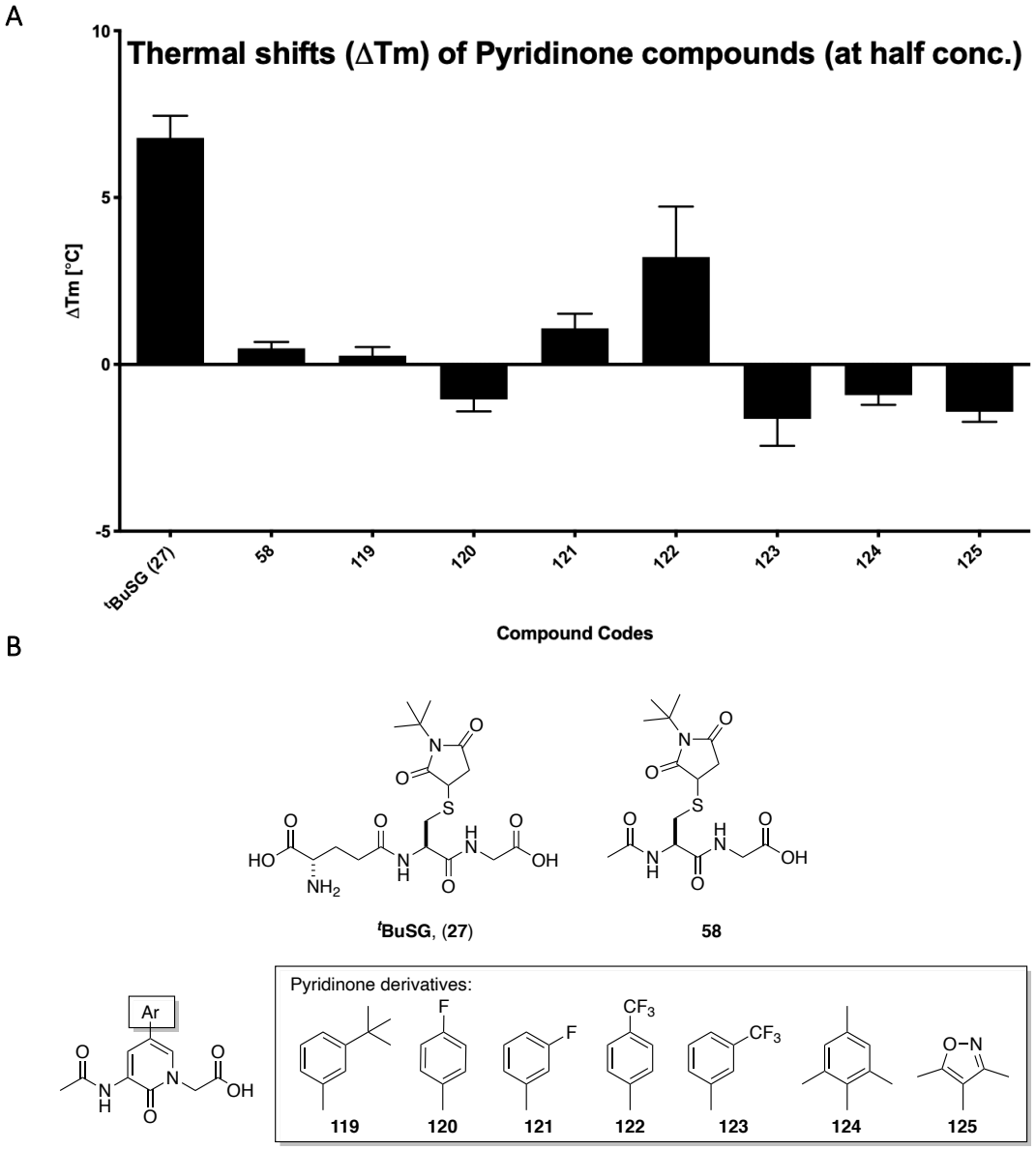
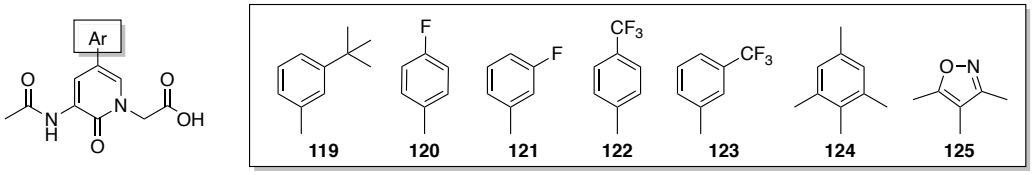


Figure 2.25. DSF Assay results with *Sd*KefQCTD. A) DSF assay thermal shift results, error bars are standard deviation from triplicate; B) Structures of compounds used in DSF. Thermal shift results ^{t}BuSG (**27**) was used as a positive control. The dipeptide **58** was also tested for comparison. The thermal shifts show a mixture of stabilisation and destabilisation of the *Sd*Kef system.

The experiment with ligand concentrations of 500 µM had lower standard error values than 1 mM of ligand. However, because the variability is still high this is unlikely to be caused by solubility, and no precipitation or insolubility was seen during the preparation of the samples. Some of the thermal shift results (stabilising and destabilising) were consistent, and the full comparisons are summarised below (Table 2.8). The mixture of stabilising and destabilising effects of the binding *Sd*KefQCTD ligands could suggest that stabilising ligands are potential activators of the protein, and destabilising ligands are inhibitors. However, GSH is a known inhibitor of Kef, but shows no ΔT_m because it is too low affinity.[145] It is possible the destabilising ligands are causing a different conformational change to that of activating *Sd*KefQCTD ligands, or they are binding to a different part of the protein.

Table 2.8. Summary of results of DSF experiments. The summary is a comparison of DSF experiments run at 1 mM or 500 µM ligand concentration, with 12 µM *Sd*KefQCTD. The ligand-protein interaction is thought to be stabilising if the melting temperature of the protein increases in the presence of the ligand or destabilising if the melting temperature decreases.

Compound	Thermal Shift	Comments
^{t}BuSG	Stabilising	Matches that observed in the literature.[145]
70	Stabilising	Matches that observed in the literature.[145]
58	Stabilising	Matches that observed in the literature.[145]
119	Inconclusive	A small stabilising or destabilising effect is seen, so **119** is binding around or below the detection limit.
120	Destabilising	Unexpected result of destabilisation, as fluorine is often used as an isostere of hydrogen,[109] and **71** does not show an observable thermal shift.
121	Inconclusive	Both experiments show **121** as having an inconsistent destabilising or stabilising effect, so the effect is unclear.
122	Stabilising	**122** shows a consistent stabilising effect, similar to that of **118**. CF_3 moieties are sometimes used as methyl or ^{t}Bu isosteres, and are considered to be in-between these in size, so a similar effect is expected.[109]
123	Inconclusive	**123** shows an inconsistent, destabilising or stabilising effect, so the effect is unclear.
124	Destabilising	Consistent destabilisation.
125	Destabilising	Consistent destabilisation.



DSF shows high variability limiting its use as an assay to rank weakly binding ligands identified by waterLOGSY, as many are below the detection limit for an observable ΔT_m. DSF has confirmed that the pyridinone compounds can bind to *Sd*KefQCTD, supporting the pyridinone scaffold as a suitable peptide mimetic for the peptide ligands. **118** and **122** have been identified as potential activators, following the highest observed stabilisation of *Sd*KefQCTD.

2.3.3 Towards quantification of a K_d of the pyridinone ligand using NMR

As qualitative binding confirmation had been observed for multiple pyridinone compounds, ranking of this new series as *Sd*KefQCTD ligands was important for directing future structural alterations to improve affinity. K_d calculation can be used to rank identified *Sd*Kef ligands. As **71** had exhibited good properties for the waterLOGSY NMR assay, this ligand was selected for initial experiments.

NMR titration experiments have been used previously in the group to determine K_d values, and it has worked for the peptide ligands for the *Sd*KefQCTD system.[149,153] Ligands often display a change in chemical shift, or line width change, as they bind to a protein.[219,222] NMR techniques are useful as they allow direct observation of ligand binding. The change in chemical shift or line width was monitored against changing the protein or ligand concentration The following assumptions are made for the binding of ligands using a linear graphical model for the determination of K_d.[217,223]

Ligand L, binds to protein P, to form Ligand-Protein complex LP:

Equation 1: $$L + P \underset{k_{off}}{\overset{k_{\mathrm{on}}}{\rightleftharpoons}} LP$$

The rates of dissociation and association of the ligand, give the K_d:

Equation 2: $$\frac{k_{\mathrm{off}}}{k_{on}} = K_{\mathrm{d}}$$

Ligand-protein exchange systems exist on a spectrum, from fast to slow exchange.[217] Slow exchange systems show distinct resolved NMR resonances for the free and bound

states, and so the K_d could be obtained from the integration of the two separate resonances. For fast exchange the observed resonance should be a weighted average of the free and bound states according to the relative populations of each. Intermediate cases between these two extremes are complex and more difficult to interpret.[224]

The NMR observed parameter for a fast exchange system Δ_{obs} (chemical shift, line width, etc.) is the sum of the parameter in the free mole fraction $X_{L(free)}$ and bound $X_{L(bound)}$ states:

Equation 3: $\Delta_{obs} = \Delta_{free}X_{L(free)} + \Delta_{bound}X_{L(bound)}$

As the pyridinone ligands show an observable effect in waterLOGSY experiments, it was assumed they would exhibit fast exchange with the *Sd*KefQCTD system, so it was expected that a single resonance of the average population would be observed.

For the titration experiment, several water-suppressed proton experiments were run with increasing concentrations of *Sd*KefQCTD to a set concentration of ligand similar to the set up for waterLOGSY. The strongest singlet resonance from **71** (the acetyl methyl CH_3) would be followed throughout the titration experiment. Peak width and chemical shift were used to track the binding of the ligand (Figure 2.26).

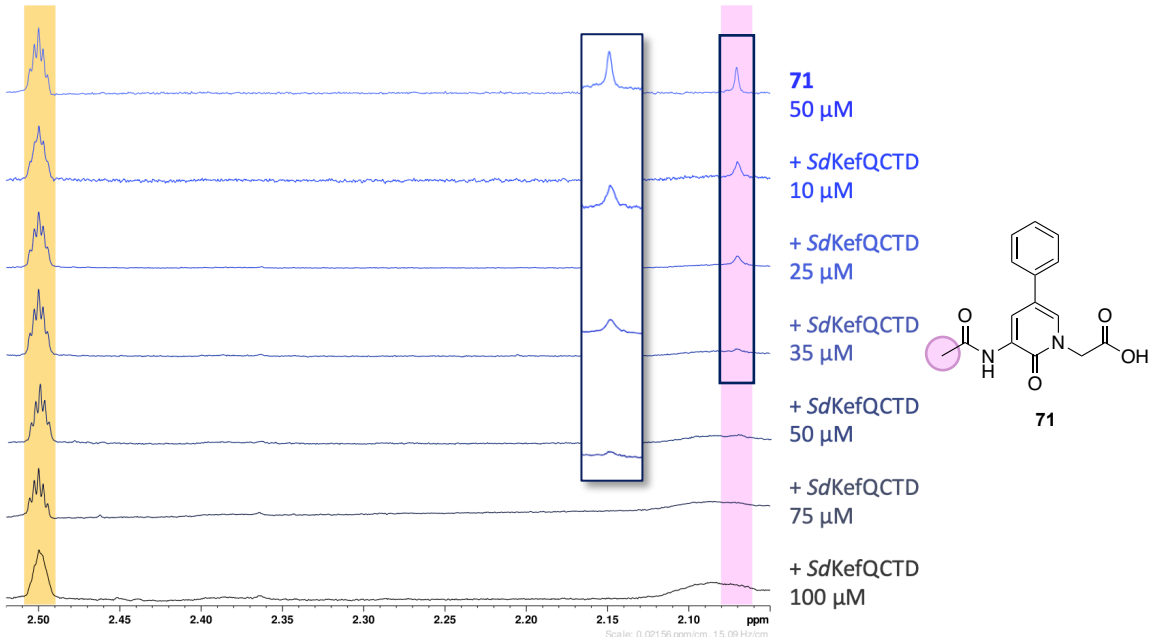


Figure 2.26. NMR titration experiment with set 71 concentration (50 µM) and increasing ligand concentration (10–100 µM). The inset shows an expansion of the resonance at 2.09 ppm. The spectra are calibrated against DMSO at 2.50 ppm (highlighted in yellow) and the **71** CH_3 is highlighted in pink. A magnification of the resonance assigned as the CH_3 singlet showed slight broadening, but there is very little change or movement in chemical shift.

The spectra for **71** showed slight broadening, although unfortunately a protein peak was present at the same chemical shift for the strongest singlet resonance, and this made analysis of the resulting spectra difficult.

The experiment was repeated with a *tert*-butanol standard for comparison of any ligand peak broadening, varying the concentration of **71**, with a lower constant concentration of *Sd*KefQCTD to avoid protein peaks interfering with the analysis. Nine water-supressed proton experiments were run with increasing concentrations of ligand (20–200 µM) with a set concentration of protein (20 µM) (Figure 2.27).

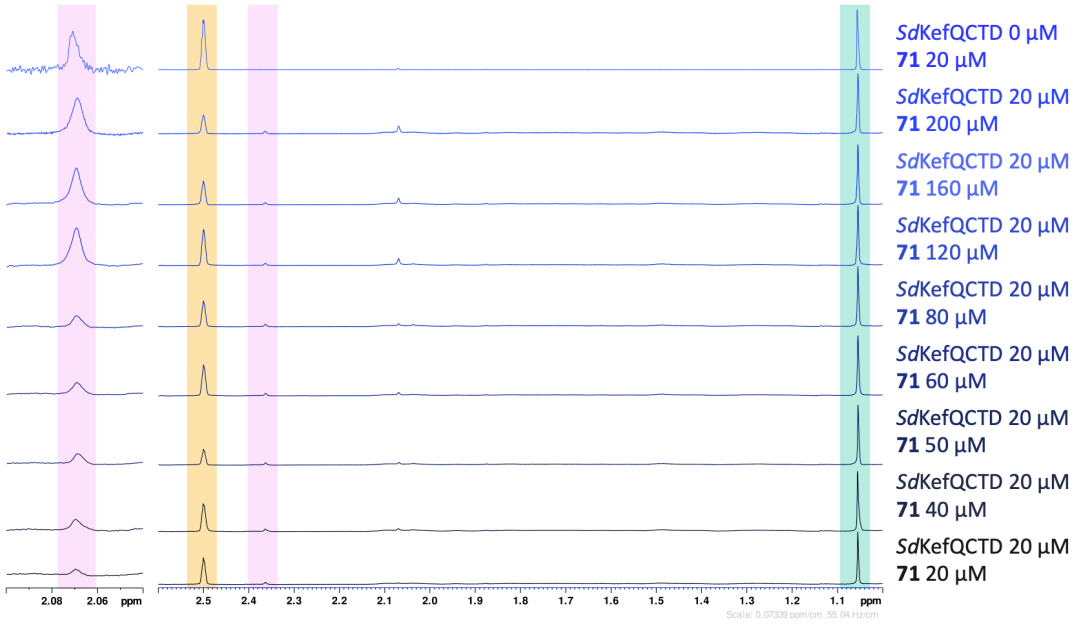


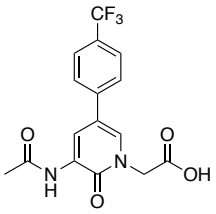
Figure 2.27. NMR titration experiment with set *Sd*KefQCTD concentration (20 µM) and decreasing ligand concentration (200–20 µM). The spectra are calibrated against DMSO at 2.50 ppm (highlighted in yellow) and the **71** CH_3 is highlighted in pink. Peak broadening was measured against *tert*-butanol used as a standard (highlighted in green). A magnification of the CH_3 singlet resonance is shown on the left where there is no observable broadening or change in chemical shift.

The change in line width of the acetyl methyl CH_3 of **71** was compared *tert*-butanol and did not show any progressive change with decreasing concentration of the ligand. There was also no observable change in chemical shift of the resonance, so this could not be used to determine a K_d. This suggests that the binding interaction is too weak to be detectable with ^{1}H NMR.

It was hypothesised that using ^{19}F NMR could provide a method to obtain a K_d through NMR titration. ^{19}F NMR has comparable signal abundance to ^{1}H, signals occur over a larger range of chemical shifts to that of ^{1}H NMR,[218] and *Sd*KefQCTD does not contain any fluorine, which made it a suitable choice to quantify binding of the pyridinone scaffold to the *Sd*KefQCTD system.[219,225] It was likely that a binding interaction between ligand and protein would therefore result in an observable change in chemical shift for ^{19}F, so ppm

or line width changes could provide two opportunities to observe an Δ_{obs} effect from binding.

The ligand selected for these experiments was **122**, as this ligand included a CF_3 group which would give a large ^{19}F signal for observation, as well as **122** having one of the greatest stabilising effects in DSF experiments. **122** would ideally have sufficiently high binding affinity to produce an observable effect in an NMR observable parameter Δ_{obs} (Figure 2.28).



122

Figure 2.28. 122 used for NMR titration experiments. This ligand has the CF_3 moiety for the largest ^{19}F signal, and had a similar stabilising thermal shift to that observed for **118** which were two of the highest observed for the pyridinone ligands.

A titration experiment was run with a set concentration of ligand (10 µM), and increasing concentrations of protein (*Sd*KefQCTD, 0–40 µM) to try and capture the maximum observable change of chemical shift or line width during binding of **122** (Figure 2.29).

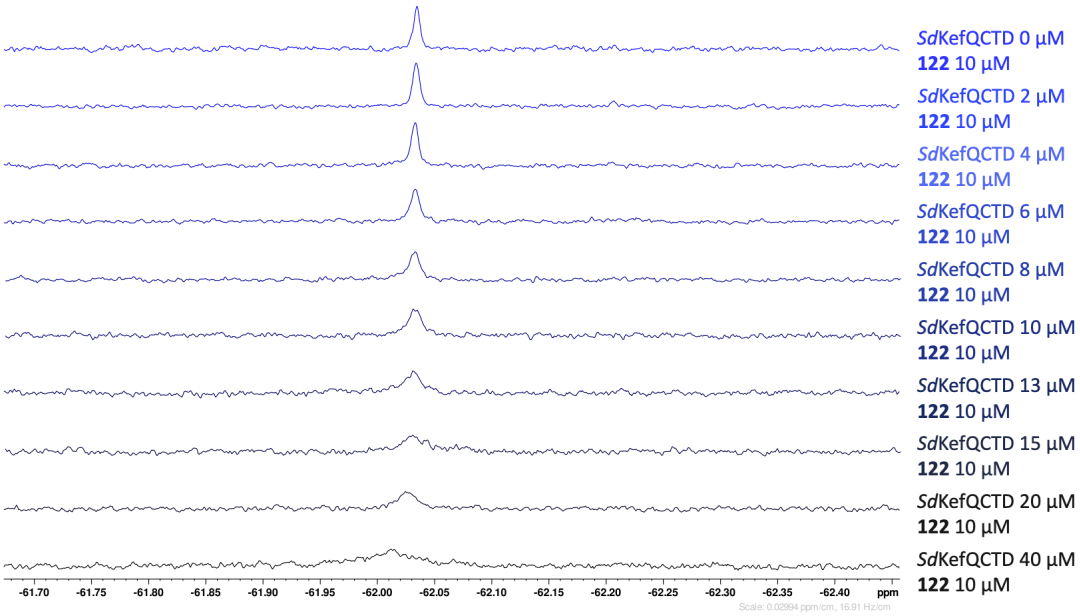


Figure 2.29. ^{19}F NMR titration experiment showing broadening and chemical shift change of CF_3 peak. The titration experiment was run with 1,1,1-trifluoroacetone as a standard, and the *Sd*KefQCTD protein.

Both a line width increase and chemical shift change was observed for this resonance with increasing concentration of protein. The line-fitting function from the MestReNova[226] programme was used to calculate the width of the resonance in Hz, and the change in chemical shift of the CF_3 resonance was also recorded (Figures 2.30, 2.31).

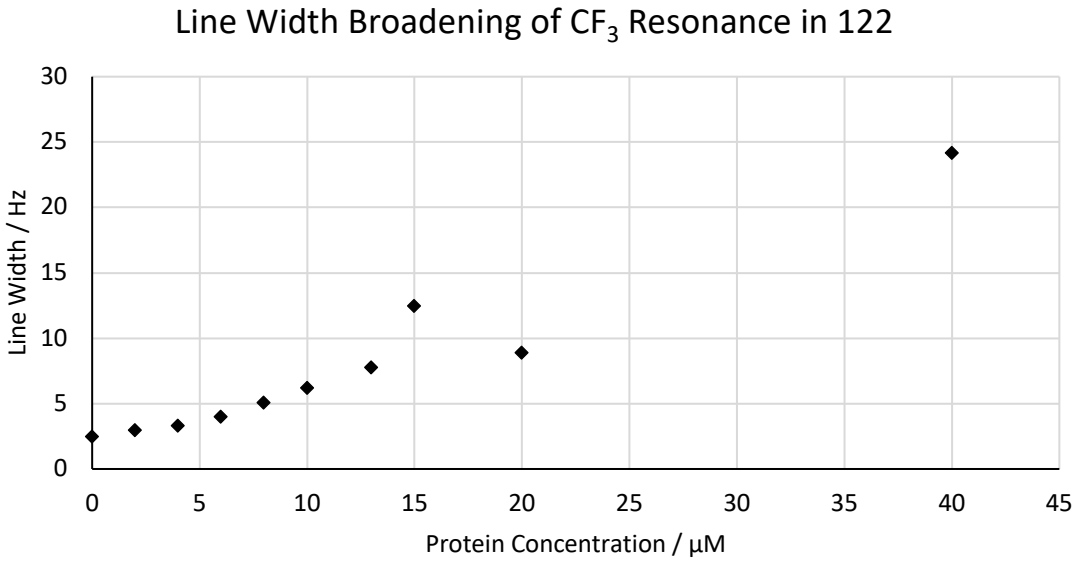


Figure 2.30. Graph displaying the changing broadening of the resonance line width with changing protein concentration. The typical profile should show a decreasing rate of change until the maximum change in line width is reached.

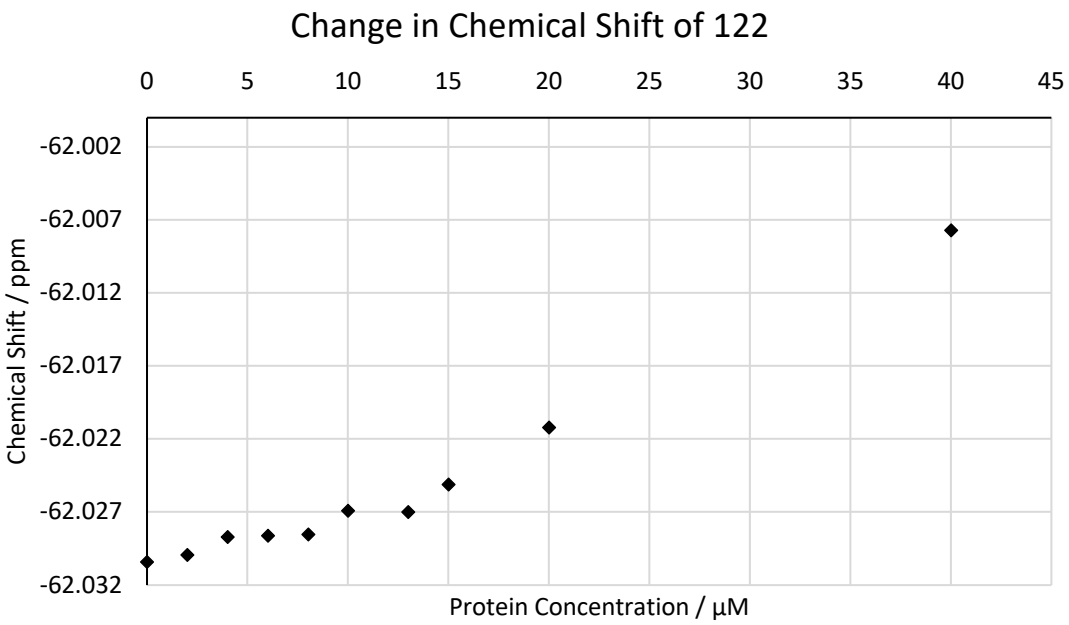


Figure 2.31. Graph displaying the changing chemical shift of the resonance with changing protein concentration. The typical profile should show a decreasing rate of change in chemical shift until the maximum change in chemical shift is reached.

Both Δ_{obs} for this system (line width and chemical shift) display an unexpected profile. A typical profile should show a decreasing rate of change of Δ_{obs} with increasing quantities of protein as the maximum observed change Δ_{max} is reached.[217,223] It is unclear whether the maximum change in line width or change in chemical shift was reached, and more data points are required to plot the relationship between chemical shift and protein concentration. The rate of change of both Δ_{obs} show an increase with increasing concentrations of *Sd*KefQCTD.

Non-linear effects such as the Δ_{obs} of chemical shift and line width from this experiment can be indicative of multiple binding modes.[224] Non-linear effects being observed can also suggest that the exchange system changes between fast and slow dependent on [P], and as the linear analysis depends on fast exchange these methods are not suitable for analysing these data.

The *Sd*KefQCTD system exists as a dimer, with the binding site at the interface of these dimers as discussed previously in Section 1.4.1.[140] It is unknown currently whether the pyridinone series is binding at the same site at the dimer interface, whether it is binding non-specifically to another part of the protein, or what binding mode it occupies. These data suggest that this system is exhibiting a more complicated binding effect, and so further analysis is required.

2.4 Conclusions

This work has shown that the pyridinone is a suitable peptide mimetic for the Kef system. The pyridinone compounds have been used to replace the central amide bond moiety from the dipeptides. They have introduced new synthetic flexibility to allow the coupling of sixteen different headgroups for SAR exploration, that had not previously been used in Kef ligands. The pyridinone scaffold was synthesised from the nitropyridinone core, and Suzuki conditions that are compatible with a variety of moieties have been developed to install headgroups onto this backbone. Ten different carboxylic acids have been tested in biophysical assays, leading to the identification of promising pyridinone compounds **118** and **122**. This work has obtained the first waterLOGSY and DSF evidence of binding of dipeptide **70**. Future work will include quantification of the binding of the pyridinone series using a different technique such as isothermal calorimetry, the conclusion of the synthesis of a pyridinone with a maleimide headgroup, and the biophysical testing of future pyridinone carboxylic acids.

Chapter Three: Investigation of Oxazoles as an Amide Replacement in *Sd*Kef Ligands

3.1 Introduction to the Oxazole Scaffold

Oxazoles and isoxazoles have been an important functional group in drug scaffolds as an acetylated lysine mimic,[227] and valuable isosteres for: carboxylic acids, other five-membered heterocycles, and amides.[109,121] Oxazoles have been used as amide bond replacements in the literature,[121,170–174] with examples being used for restraint of torsion angles,[171] and mimics of biological peptides such as Substance P (a neuropeptide) with increased potency.[172,173] An oxazole was chosen as a suitable mimetic group to replace the amide in **70** (Figure 3.1, A), since it can mimic the HBA interaction of the dipeptide, reduces rotation of the carboxylic acid, and has the advantage of increased stability. An oxazole was chosen over an isoxazole for this work because it more closely mimics the electronic arrangements of the amide bond. The polar oxygen and nitrogen atoms are on opposite sides of the ring, whereas an isoxazole has both polar atoms on the same side (Figure 3.1, B). The 1,2,3-triazole moiety has much more literature precedent as a successful amide bond replacement,[121,228]however, the oxazole facilitated a convenient synthesis from the parent dipeptide to retain the key cysteine stereocentre. Synthesis of the carboxylic acid and methyl ester would permit investigation of the binding and pro-drug approach of this structure.

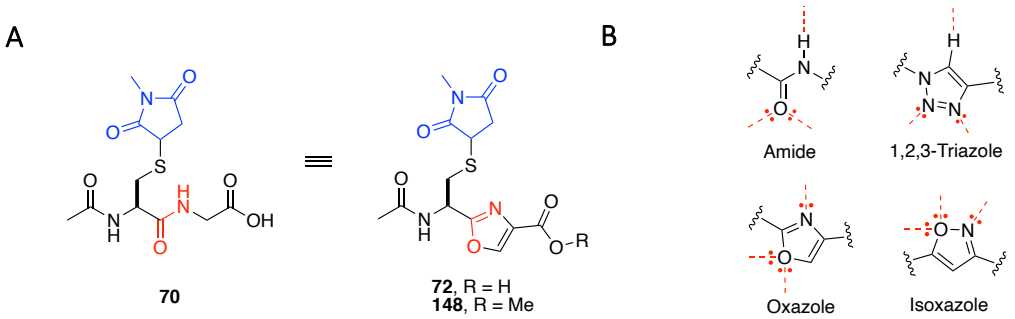


Figure 3.1. Representations of the oxazole-containing dipeptide mimic 72; A) 2D structures of dipeptide **70** and the oxazole peptide mimetic **72**. In each structure, the central amide bond or replacement is highlighted in red, and the same methylmaleimide headgroup chosen, highlighted in blue; B) Electronic arrangement of H-bonds (red) in the amide bond and possible replacement groups, an oxazole, isoxazole, or 1,2,3-triazole.

It is possible for the oxazole to make the hydrogen bond acceptor interaction made by the amide, but not the hydrogen bond donor interaction. The structure of **72** replaces the central amide bond with an oxazole group, but the rest of the molecule is unchanged. The (*R*)-stereochemistry of **70** from the cysteine portion of the molecule is conserved, as this is known to be important for activity. The *N*-methylsuccinimide headgroup is included as this provides a contribution to ligand affinity and activates Kef, therefore any comparative difference is due to the amide bond replacement. The synthesis of **72** will have a late stage diversification step to allow installation of alternate headgroups for SAR exploration, in an otherwise identical synthetic route, should the oxazole moiety be a successful peptide mimetic.

The physicochemical properties of **72**, **148**, and **70** were compared including the $clogD_{pH7.4}$, SFI,[195] and TPSA from calculations by ACD/I-labs (Table 3.1).[194]

Table 3.1. Physiochemical properties calculated from ACD/I-labs to compare the properties of 70, 72 and 148.

Property	Value **70**, Comments	Value **72**, Comments	Value **148**, Comments
MW/ $gmol^{-1}$	331.35	341.34	355.37
HBD	3	2	1
HBA	9	9	9
RB	7	6	7
*c*log$D_{pH7.4}$	–6.4	–3.9	–0.3
SFI	–6.4, predicted to be soluble	–2.9, predicted to be soluble	0.7, predicted to be soluble
TPSA/ $Å^2$	158.2	155.1	144.1

The oxazole ligands are predicted to be water soluble with SFI values less than 5. The TPSA of **72** and **148** were calculated to be 155.1 $Å^2$ and 144.1 $Å^2$ respectively. This is comparable to **70**, and is a parameter for which the oxazole is a good mimic, as well as falling within the range of other known antibiotic compounds (TPSA 100–200 $Å^2$).[195–198] This chapter reports the investigation of the oxazole scaffold as a peptide mimetic ligand for the Kef system. Both enantiomers of the oxazole ligand were synthesised and tested in biophysical assays to assess the suitability of the oxazole as a new ligand scaffold for the Kef system.

3.2 Synthesis of the Oxazole Peptide-Mimetic Ligand

The first step in the synthesis of **72** is the coupling of two protected amino acids to form the dipeptide **150**. This "chiral pool" strategy means the stereocentre is incorporated from a starting compound that occurs in nature and there is no enantioselective step required.[229] The dipeptide **150** can be cyclised to form the oxazoline **151**, which can be oxidised to the oxazole **152**. This positions the ester at the desired ring position to mimic the structure of **70**. The two protecting groups are then removed in a global deprotection step, followed by a selective installation of the maleimide on the thiol using literature precedent,[145,149] and acetylation on the free amine to give the ester **148**. The maleimide headgroup can be changed during this late stage diversification step to explore the SAR around the oxazole ligand. The final step is deprotection of the methyl ester to form the carboxylic acid **72** (Figure 3.2).

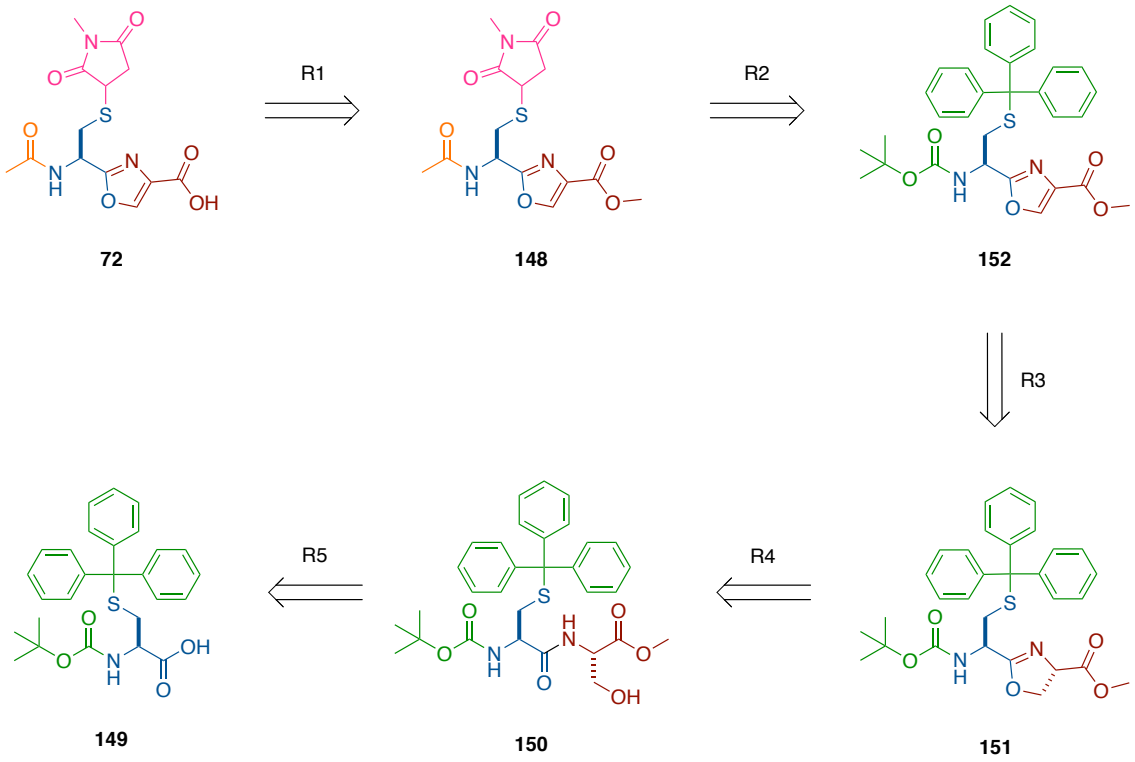
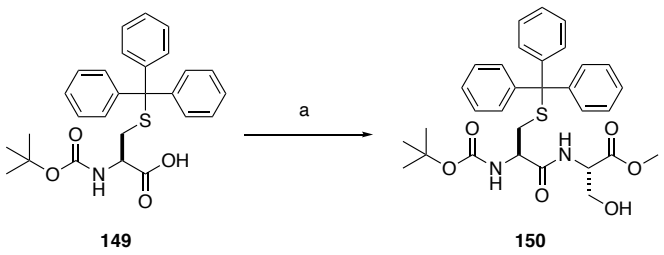


Figure 3.2. Retrosynthesis plan for the oxazole ligand, 72. The strategy uses two protected amino acids cysteine (**149**, blue) and serine (red), that are coupled (**150**) to form an oxazoline (**151**), and then oxidised to the oxazole backbone (**152**). The protecting groups (green) are removed as part of a global deprotection strategy. This is followed by installation of the headgroup (pink) which can be changed to explore SAR of the ligand, and acetylation (orange), to give the oxazole ligand ester (**148**). The final step is hydrolysis to give the carboxylic acid (**72**). Formation of **152**, and **148**, is based on literature precedent.[230]

3.2.1 Formation of the dipeptide backbone

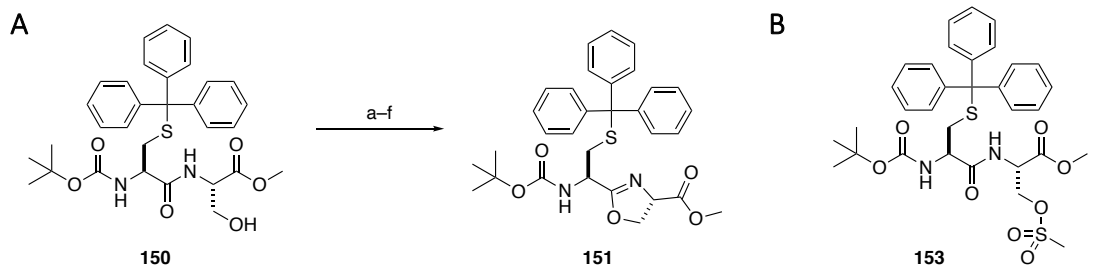
The route proceeded *via* a reaction of dipeptide **150** (Scheme 3.1) to give the oxazole moiety as the new backbone. Formation of **150** from a simple amide coupling reaction of **149** (Novabiochem, CAS: 21947-98-8) with serine methyl ester hydrochloride (Fluka, CAS: 5680-80-8) proceeded in 55–70% yields. Neutral reaction conditions (diphenylphosphoryl azide, DPPA) and a mild base (triethylamine) were used to avoid epimerisation of the stereocentres in the amino acids (Scheme 3.1).[230]



Scheme 3.1. Synthesis of the dipeptide 150. *Reagents and conditions*: a) Serine methyl ester hydrochloride, DPPA, NEt_3, DMF, 0 °C, 18 h (16–32 h), n = 9, 53–85%.

3.2.2 Cyclisation optimisation

Using the Boc-protected **150**, the first cyclisation method investigated to give the oxazoline **151** (Scheme 3.2 A, Table 3.2 a) involved converting the serine alcohol to the chloride.[231] The maximum yield of the oxazoline was only 5%, and so this method was too poor yielding to be used in the synthesis. Converting the alcohol **150** to the activated mesyl compound was also investigated (Table 3.2 b).[232] However, these conditions yielded only the activated dipeptide **153** and cyclisation to the oxazoline did not occur, even when the reaction was heated under reflux. The final cyclisation methods (Table 3.2 c and d) investigated were converting the alcohol to either the bromide using $BrCCl_3$,[233] or iodide using iodine and PPh_3,[234] although only starting material was recovered from both reactions.



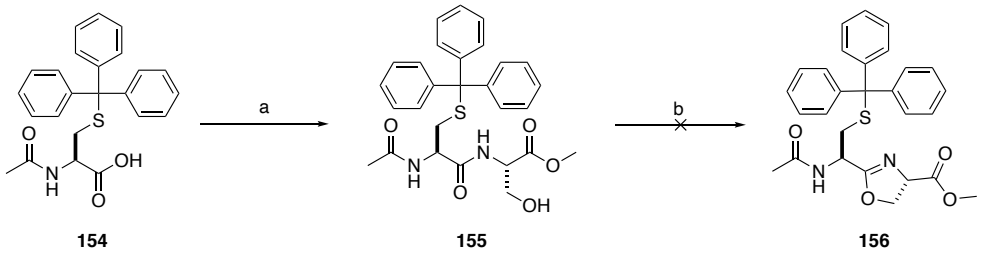
Scheme 3.2. Cyclisation conditions investigated to yield the desired oxazoline 151. A) For full reagents and conditions, see Table 3.2. B) Mesylated dipeptide **153** from alternative cyclisation methods. See Table 3.2 entry c, this was the only isolated product obtained rather than the desired oxazoline **151**.

Table 3.2. Cyclisation conditions for reaction of the dipeptide 150 to the oxazoline 151.

Method	Reagents and Conditions	Outcome
a	$SOCl_2$, pyridine, diethyl ether/THF, RT, 4 h	5% yield of **151**
b	i) NEt_3, 0 °C; ii) Mesyl chloride, 0 °C to RT, 6 h, then 40 °C, 1 h	Mesylated dipeptide **153** only
c	i) Iodine, PPh_3, imidazole, DCM, RT, 15 min; ii) DMF, RT 15 h	Starting material **150** isolated
d	$BrCCl_3$, PPh_3, DCM, RT, 30 h	Starting material **150** isolated
e	DIAD, PPh_3, THF, 0 °C to RT, 17–73 h	n = 3, 0–51% yield of **151**
f	DEAD, PPh_3, THF, RT, 18–22 h	n = 4, 68–91% yield of **151**

The Mitsunobu reaction was investigated to cyclise the dipeptide **150** to **151**. This step avoids any harsh conditions that could epimerise the stereocentres or degrade the sensitive oxazoline ring, (Table 3.2 e). However, **150** was very slow to react and many side products were produced, as shown by TLC analysis. It was necessary to add two additional equivalents of DIAD and PPh_3 over 48 h to completely consume the starting material **150**. During purification by flash column chromatography, the oxazoline compound **151** frequently co-eluted with $OPPh_3$ and therefore several purifications were required to finally obtain **151** in the necessary purity (95% by reverse phase (RP) analytical HPLC). There was significant variation in the yield (0–51%) as a result of how many purifications were required to remove $OPPh_3$.

Whether using the *N*-acyl protected cysteine **154** as a starting material would improve purification after the DIAD-mediated Mitsunobu reaction was investigated. This could avoid some of the co-elution problems by changing the polarity of the product **156** from that of $OPPh_3$ and the other side products. The synthesis from **154** is shown in Scheme 3.3.



Scheme 3.3. Synthesis of the acyl-protected dipeptide 156. *Reagents and conditions*: a) Serine methyl ester hydrochloride, DPPA, NEt_3, DMF, 0 °C, 24 h, 72%; b) DIAD, PPh_3, THF, 0 °C, 72 h, no formation of **156**.

The amide coupling reaction with **154** proceeded as with the Boc-protected starting material **149** (Scheme 3.1), and a single purification gave the product **155** in the required purity. The differing polarity between **155** and $OPPh_3$ improved their separation by flash column chromatography. However, during the cyclisation step, several additional equivalents of DIAD and PPh_3 were required for complete consumption of the starting material **155** by TLC analysis, compared to the Boc protected **150**. The product(s) of the reaction could not be identified, as part of a very complicated mixture by ^{1}H NMR analysis. It is likely that the large steric bulk and carbamate electronics of the Boc group is required for the Mitsunobu reaction, and the acyl group was unable to facilitate the reaction, and so the desired product **156** was not formed.

Diethyl azodicarboxylate (DEAD) was used instead of DIAD in the reaction of **150**, DEAD is more reactive than DIAD (Table 3.2 f) as it is less hindered. It was hoped that increasing the rate of reaction would yield the desired product before any degradation or slower side reactions occurred. The reaction with DEAD yielded the desired **151** in 68–91% yield and could be performed at room temperature. The reaction also did not form any side products following TLC analysis, and the yield was reproducible. However, the DEAD by-product **158** coeluted during purification and since it is not visible by UV light or by staining (Figure 3.3) it can be assumed to be present as a contaminant in all isolated **151**.

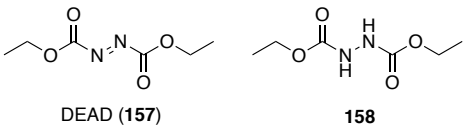
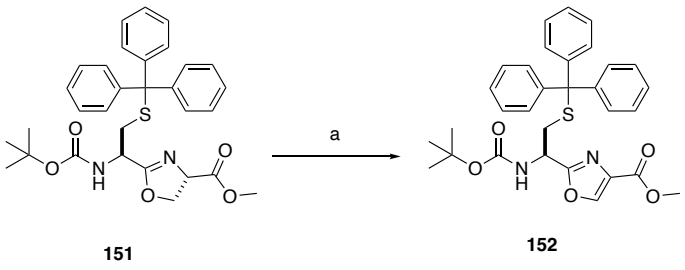


Figure 3.3. Structures of DEAD and DEAD by-product (diethyl 1,2-hydrazinedicarboxylate) contaminant.

158 is insoluble in toluene and is easily separated from the oxazoline by washing with water, with three washes reducing the proportion of side product to approximately 5% of the total mass, as estimated by ^{1}H NMR.

3.2.3 Oxidation to the desired oxazole

To synthesise the oxazole **152** from the oxazoline **151,** a mild oxidation method was required, so as not to degrade the various protecting groups in **151,** or racemise the cysteine stereogenic centre. A mild dehydrogenation method from the literature,[235] using bromotrichloromethane ($BrCCl_3$) and 1,8-diazabicyclo[5.4.0]undec-7-ene (DBU), was selected. This approach was chosen as it does not react with the Boc, trityl, or ester protecting groups on **151** and gave excellent yields of 75–95% for other oxazoline ester systems. Subjecting the oxazoline **151** to these conditions gave the oxazole **152** in 30–71% yields (Scheme 3.4).



Scheme 3.4. Synthesis of the oxazole 152 from the oxazoline 151. *Reagents and conditions*: a) $BrCCl_3$, DBU, DCM, 0 °C, 2–4 h, n = 8, 30–71%.

The reaction shown in Scheme 3.4 is speculated to occur *via* a radical-initiated dehydrogenation, followed by a second to give the oxazole **152** (Figure 3.4) as "no initial bromination is observed" (described in the original literature).[235] Repeated attempts at this reaction show that the reaction proceeds better on a smaller scale (0.02–0.07 mmol gave 51–71%, 0.33–0.42 mmol gave 30–33%). This is possibly due to localised heating on a larger scale, with reduced cooling efficiency from the ice bath in a larger solvent volume over a larger flask with reduced relative surface area.

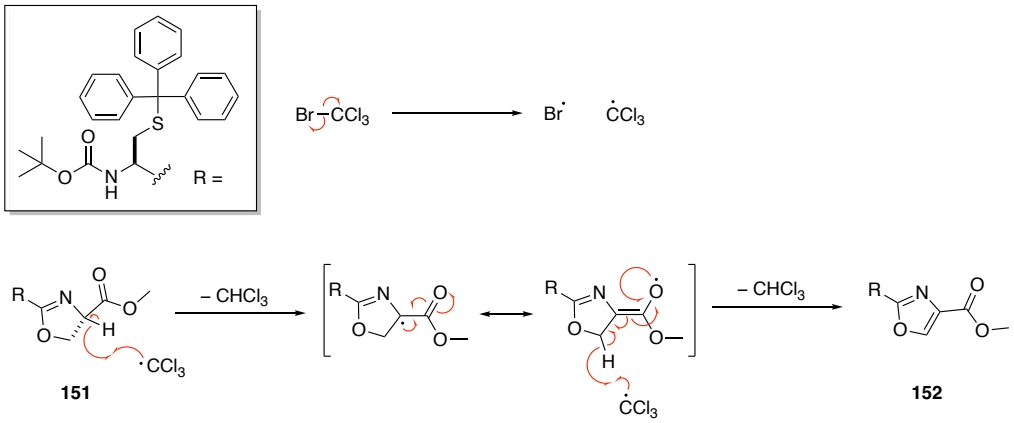
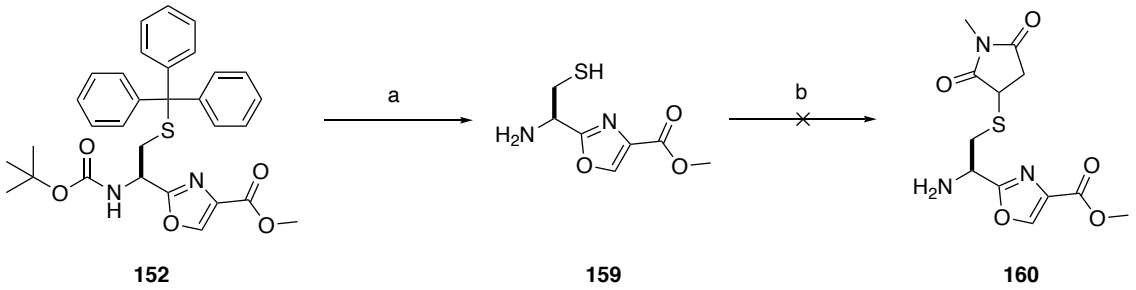


Figure 3.4. Our speculated radical oxidation mechanism *via* a dehydrogenation.[235]

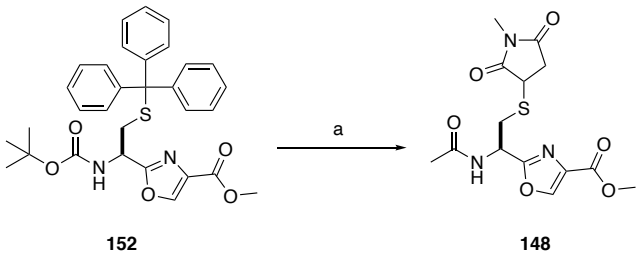
3.2.4 One-pot coupling step

Following the oxidation, the final stages of the synthesis were deprotection of the thiol and amine, functionalisation of the thiol, and acetylation of the amine. To remove the Boc and trityl groups, **152** was treated with trifluoroacetic acid and triethylsilane. The reaction appeared to go to completion by TLC analysis with the consumption of the spot corresponding to **152**, but very little of the product **159** was isolated following purification (Scheme 3.5).



Scheme 3.5. Attempted synthesis of the maleimide coupled oxazole 160. *Reagents and conditions*: a) TFA, TESH, DCM, 0 °C, 2 h, 6%; b) *N*-Methylmaleimide, MeOH, RT, 15 h.

Given this low yield, it was hypothesised that compound **159** may be unstable, due to the free amine and thiol groups, or that **160** degraded during isolation. Consequently, this deprotection step was telescoped into the next, which was conjugate addition of the thiol to *N*-methylmaleimide. However, all attempts to isolate the free amine after this step also resulted in loss of the product during purification. These reactions were therefore combined into a three-step, one-pot, reaction that avoided isolation of any potentially unstable intermediates (Scheme 3.6).

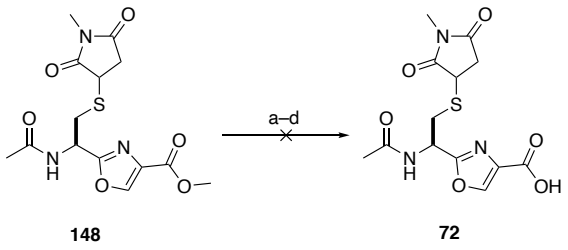


Scheme 3.6. Three-step one-pot reaction to form the final oxazole methyl ester compound 148. *Reagents and conditions*: a) i) TFA, TESH, DCM, RT, 0.5–1 h; ii) *N*-Methylmaleimide, MeOH, RT, 4 h; iii) Acetyl chloride, NEt_3, THF, RT, 19–27 h; n = 3, 13–70% (over three steps).

During optimisation of this one-pot synthesis, acetylation of the amine **160** was first tried with acetic anhydride, pyridine, and DMAP in DCM at RT. These conditions did not yield **148**, even though consumption of the starting material was observed by TLC analysis. More forcing conditions (acetyl chloride and NEt_3) were investigated to increase the rate of acetylation and reduce any risk of product degradation in solution. This yielded the desired final ester **148** in 13–70% yield (over 3 steps).

3.2.5 Attempts to deprotect the methyl ester 148

The final step for the synthesis of the oxazole derivative **72** was hydrolysis of the methyl ester in **148**, to give the carboxylic acid (Scheme 3.7). Standard conditions for the hydrolysis of an organic ester are lithium hydroxide in THF/MeOH/H_2O 3:2:1, which have been used in the synthesis of other similar dipeptides.[149] This hydrolysis is typically fast (<2 h)[149] and avoids epimerisation of the cysteine stereocentre.[149] When **148** was exposed to these conditions, an immediate colour change of the solution occurred from pale yellow to red. Lithium hydroxide degraded the succinimide ring and cysteine part of the molecule following analysis by ^{1}H NMR (Figure 3.5), and did not give the desired oxazole **72**. Some of the characteristic chemical shifts and multiplicities were missing, there is no longer a singlet for the aromatic proton, with several other resonances present in this region. Several other hydrolysis attempts with milder conditions were investigated and the results are summarised in Table 3.3.



Scheme 3.7. Hydrolysis attempts of the methyl ester 148 to yield the final carboxylic acid 72. The summary of conditions and outcomes is outlined in Table 3.3.

Table 3.3. Summary of hydrolysis conditions attempted for the oxazole methyl ester 148. For the corresponding scheme, see scheme 3.7, (PBS, phosphate buffered saline).

Hydrolysis Method	Reagents and Conditions	Outcome
a	LiOH (10 eq.), THF/MeOH/H_2O 3:2:1, RT, immediate	Degradation of **148**
b	LiOH (1 eq.), THF/MeOH/H_2O 3:2:1, 0 °C, immediate	Degradation of **148**
c	LiBr, NEt_3, THF, RT, 2 h	Degradation of **148**
d	Hog pancreas lipase, 5% DMSO in PBS, RT, 18 h	Starting material **148** isolated

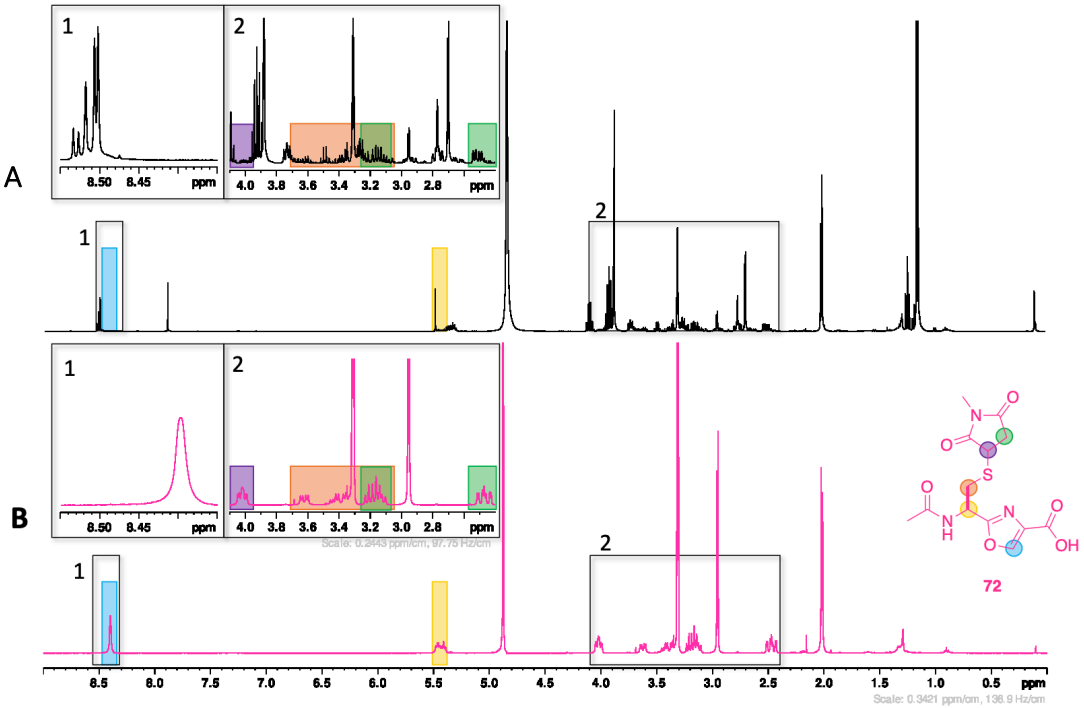


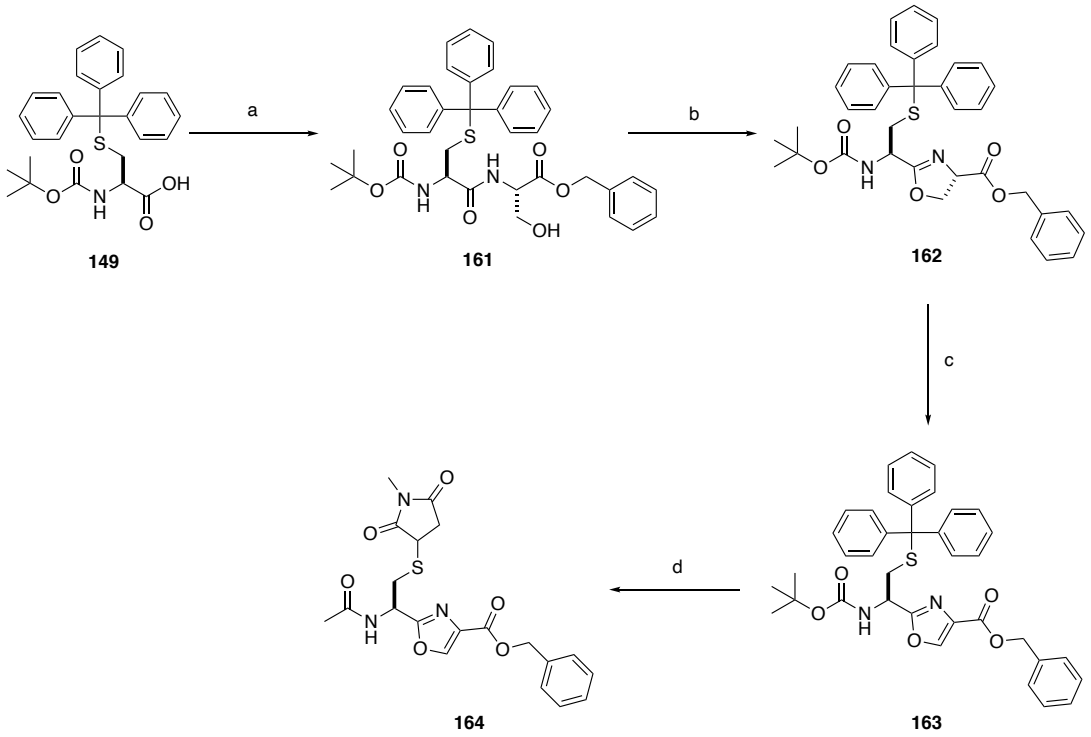
Figure 3.5. Overlay of ^{1}H NMR spectra: A) product from lithium hydroxide hydrolysis attempt with 148; B) Spectrum of an authentic sample of the oxazole acid 72. Magnified section shows that the oxazole, succinimide ring, and cysteine portion of the molecule have been degraded by the LiOH reaction conditions.

The reaction was repeated with a single equivalent of lithium hydroxide and at 0 °C to slow any side reactions (Table 3.3 b).[236] However, these conditions also degraded the starting material. Attempts to generate a small amount of hydroxide *in situ* with lithium bromide[237] also led to degradation of the starting material (Table 3.3 c).

As the hydroxide hydrolysis conditions caused compound degradation, a mild enzymatic approach was investigated to hydrolyse the methyl ester (Table 3.3 d). Lipases have been shown to remove ester groups without affecting the rest of the molecule and provided some mild conditions to investigate.[238,239] Hog pancreas lipase was chosen as a suitably promiscuous enzyme,[238] it was hoped that **148** would be compatible with the active site, and the reaction could take place in neutral conditions that would avoid epimerisation of the stereogenic centre. However, this approach did not hydrolyse the ester and instead returned the starting material **148**. This was likely due to incompatibility between **148** and the active site, and no insolubility of **148** was observed.

3.2.6 Investigation of an alternative ester protecting group

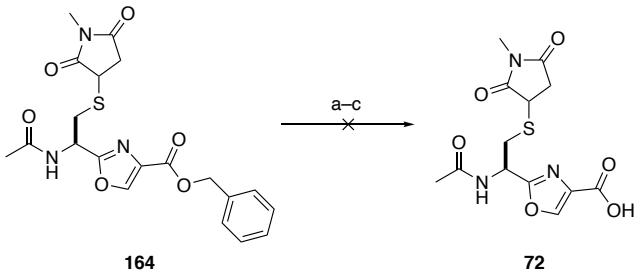
Due to the problems encountered with this ester hydrolysis, it was proposed that using an alternative ester might facilitate deprotection at the end of the synthesis. Ideally, the protecting group would deprotect under neutral conditions to avoid degrading the rest of the molecule. The benzyl ester was selected because it could be deprotected using hydrogenolysis.



Scheme 3.8. Synthesis of the benzyl ester protected oxazole 164 using the previously established route. *Reagents and conditions*: a) Serine benzyl ester hydrochloride, DPPA, NEt_3, DMF, 0 °C, 18–25 h, n = 5, 71–92%; b) DEAD, PPh_3, THF, RT, 18 h (2–24 h), n = 5, 61–81%; c) $BrCCl_3$, DBU, DCM, 0 °C, 3 h (1–7 h) n = 3, 61–64%; d) i) TFA, TESH, DCM, RT, 1 h ii) *N*-Methylmaleimide, MeOH, RT, 4 h, iii) AcCl, NEt_3, THF, RT, 22–27 h, n = 3, 17–68% (over 3 steps).

The synthesis of **164** proceeded using the optimised conditions from the synthesis of the methyl ester compounds (Scheme 3.8). The amide coupling of **149** and the protected serine (Alfa Aesar, CAS: 60022-62-0) gave the dipeptide **161** in 71–92% yields. The cyclisation of the dipeptide gave the oxazoline **162** in 43–81% yields. The reaction was easier to purify than those using previous substrates, as the benzyl-protected oxazoline **162** did not co-elute with the reduced DEAD and so no additional purification or washing was required. The oxidation reaction gave the oxazole **163** in 61–79% yield. While the reaction gave multiple side products, which complicated purification by flash column chromatography, the oxazole **163** was isolable from the mixture. Changing flash column chromatography conditions from a petroleum ether 40–60/ethyl acetate mixture to a toluene/acetone mixture improved separation of the compounds in the crude mixture. The final step gave the *N*-methylsuccinimido substituted derivative **164** in 17–68% yield

over three steps. The final step in this synthesis was the removal of the benzyl ester protecting group in **164** using hydrogenolysis. Three sets of conditions were investigated (Scheme 3.9).



Scheme 3.9. Hydrogenolysis attempts to cleave the benzyl ester in 164 to give the desired compound 72. *Reagents and conditions*: a) H_2, Pd/C (10% By weight), ethyl acetate, RT, 18 h; b) H_2, Pd/C, Ethanol, acetic acid, RT, 22 h; c) H_2, Palladium black, ethanol, RT, 4 h.

Standard hydrogenolysis conditions (palladium on carbon) were tried initially, however, this returned starting material, indicating that the conditions were not forcing enough. These conditions were repeated with ethanol and acetic acid, which are frequently used in the literature to avoid nucleophiles poisoning the palladium catalyst.[240,241] These conditions also returned the starting material **164**.

A more reactive form of palladium, palladium black, was then investigated for the hydrogenolysis reaction. Consumption of the starting material was observed by TLC analysis, and a new spot appeared, which stained yellow with bromocresol green (which detects carboxylic acids). The ^{1}H NMR spectrum of the reaction mixture suggested the conditions had not degraded the cysteine or succinimide moieties, however the yield was poor with only a 36% crude yield (Figure 3.6).

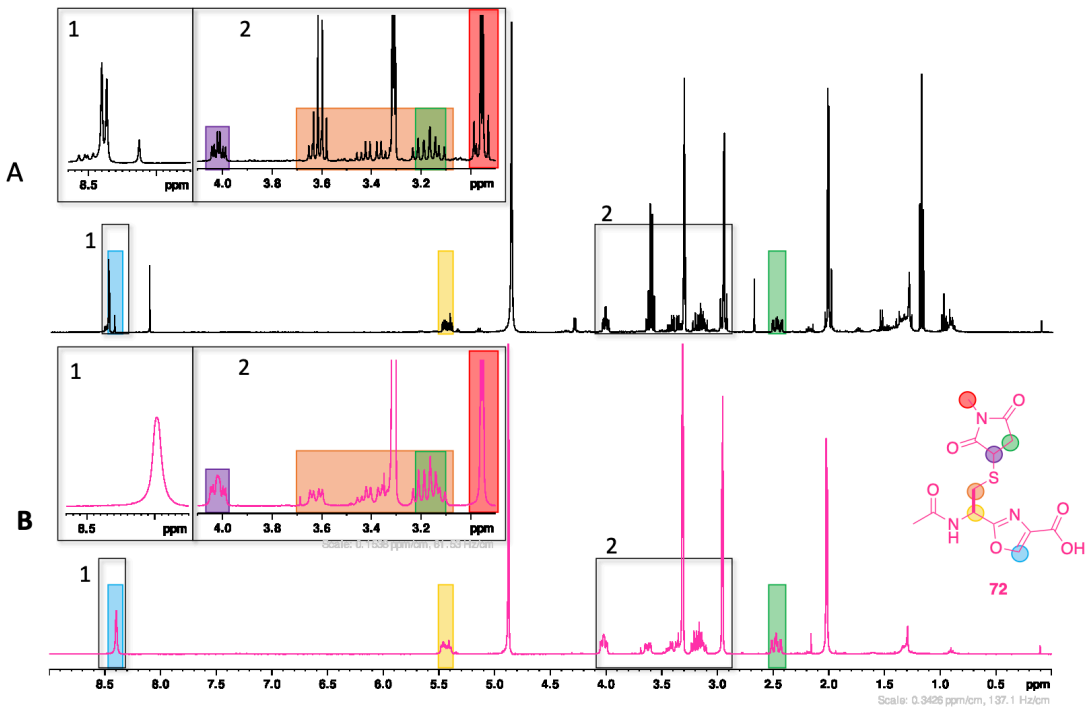
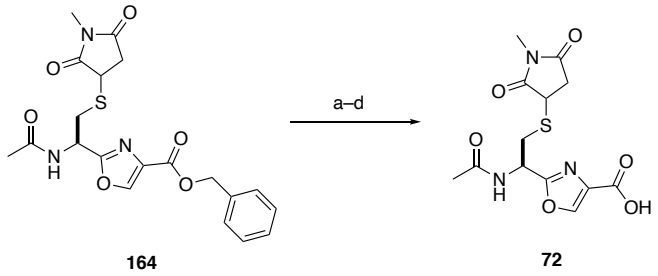


Figure 3.6. Stacked ^{1}H NMR spectra showing the outcome of the hydrogenolysis with palladium black. A) Palladium black hydrogenolysis reaction mixture. These conditions suggest having deprotected the benzyl ester. The resonances corresponding to the cysteine and succinimide portion of the molecule are present, however higher yielding conditions were desired. B) Spectrum of an authentic sample of the oxazole acid **72**.

Bromotrimethylsilane (TMSBr) is a mild method for deprotection of benzyl esters,[242] and so this reagent was investigated on **164** (Scheme 3.10, Table 3.4). Iodotrimethylsilane (TMSI) was also tried as a more reactive alternative to TMSBr.



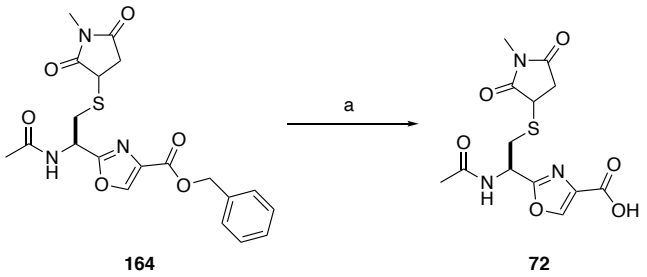
Scheme 3.10. Further hydrolysis attempts to remove the benzyl ester of 164. See Table 3.4 for summary of these reaction conditions and outcomes.

Table 3.4. Summary of outcomes of screening TMSBr and TMSI for cleavage of the benzyl ester in 164. All reactions were conducted on a 0.05 mmol scale, RT.

Deprotection Method	Reagents and Conditions	Outcome
a	TMSBr, DCM, 16 h	Starting material remaining and baseline spot appeared
b	TMSBr, toluene, 16 h	Starting material present only
c	TMSI, DCM, 3 h	Baseline spot appeared
d	TMSI, toluene, 16 h	Starting material remaining and baseline spot appeared

The oxazole **164** was subjected to TMSBr and TMSI in dichloromethane (DCM) and toluene (Table 3.4). The reaction with TMSBr in toluene showed no conversion, possibly due to poor solubility of **164**, whereas TMSBr in DCM showed partial conversion to the acid. TMSI is known to be more reactive, and so TMSI in toluene also showed partial conversion to the acid. The partial conversion is also likely due to the solubility problems of **164** in toluene, and it is possible that the reaction would have gone to complete conversion were it not for the solubility problems. As there were no such solubility problems of **164** with DCM, full conversion to the acid was achieved with TMSI.

The material isolated from the TMSI in DCM reaction looked promising from analysis by ^{1}H NMR, but because of the very small quantity of material isolated it could not be confirmed that the desired product **72** had been obtained. Based on the results of these small-scale reactions, it was decided to repeat the reaction with TMSI in DCM with a larger quantity of starting material **72** to enable isolation of a larger amount of material after purification (Scheme 3.11).

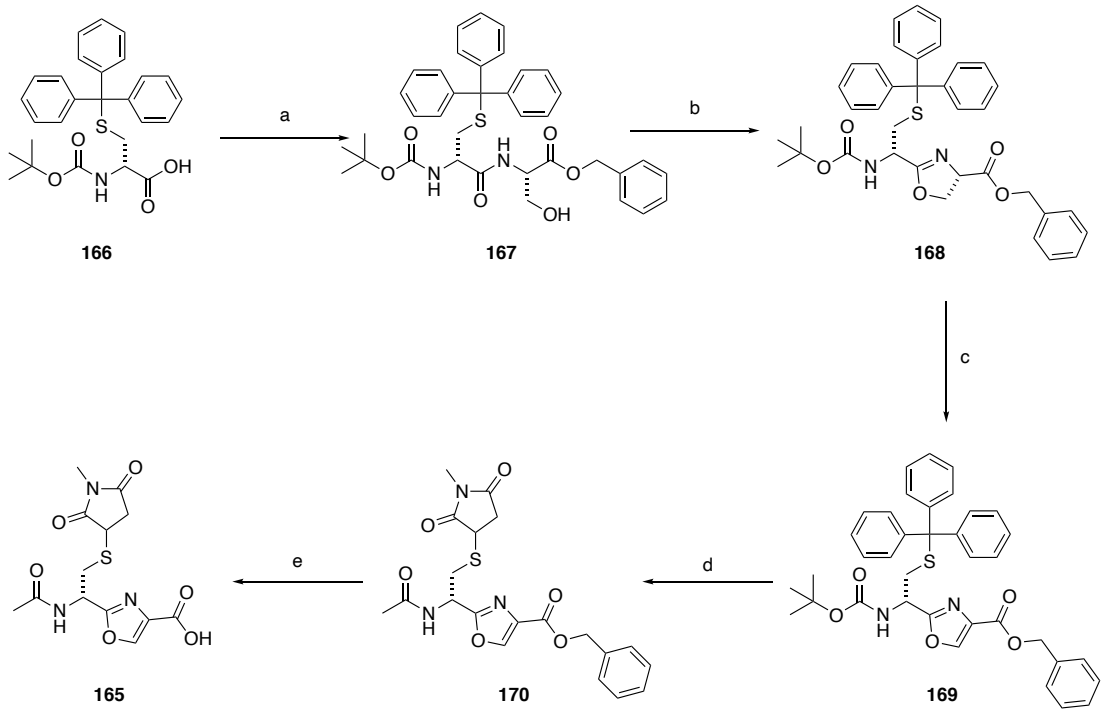


Scheme 3.11. Cleavage of the benzyl ester protecting group in 72 on a 0.08 mmol scale with TMSI in DCM.
Reagents and conditions: a) TMSI, DCM, RT, 16 h, 60%.

From the material isolated from this reaction, the product **72** was found to contain approximately 15% of the methyl ester **148** by NMR, presumably from the reaction quench with methanol. In future reactions, the formation of this by-product could be avoided by using water for the quenching step instead. Purification by flash column chromatography removed the methyl ester **148** to yield the final oxazole carboxylic acid compound **72** in a 60% yield.

3.2.7 Synthesis of the (*S*)-cysteine enantiomer 165

The (*R*)-stereochemistry in the cysteine portion of the dipeptides is necessary for binding to *Sd*KefQCTD, while the (*S*)-enantiomer does not bind. The (*S*)-enantiomer (**165**, Scheme 3.12) of the oxazole carboxylic acid **72** was synthesised as a negative control for the biophysical assays. The synthesis of **165** was completed using the route optimised for the (*R*)-enantiomer **72** (Scheme 3.12).



Scheme 3.12. Synthesis of the (*S*)-enantiomer 165 for use as a negative control. *Reagents and conditions*: a) Serine benzyl ester hydrochloride, DPPA, NEt_3, DMF, 0 °C, 5–24 h, n = 2, 82–85%; b) DEAD, PPh_3, THF, RT, 2–20 h, n = 4, 54–92%; c) $BrCCl_3$, DBU, DCM, –8 °C or 0 °C, 18 h, n = 2, 29% (–8 °C), or 36% (0 °C); d) i) TFA, TESH, DCM, RT, 1 h, ii) *N*-Methylmaleimide, MeOH, 4 h, iii) AcCl, NEt_3, THF, RT, 23 h, 79%; e) TMSI, DCM, RT, 1 h, 22%.

The coupling of **166** and the protected serine using DPPA gave the dipeptide **167** in 82–85% yields. The cyclisation gave the desired oxazoline **168** in 54–92% yields. The cyclisation reaction proceeded more quickly on a smaller scale, in 4 h for 0.2 mmol scale, or 19 h for a 2.3 mmol scale. The oxidation of **168** gave the oxazole **169** in 29–36% yields. A complicated mixture as analysed by TLC was isolated after attempting the reaction at 0 °C, so a lower temperature of –8 °C was used for the reaction to try and reduce this and improve the yield of 36%. The was no reduction in the number of side products formed and the yield did not improve (29%), suggesting that the increased rate of reaction at a higher temperature had reduced the number of side products.

The one-pot coupling reaction of **169** gave the benzyl ester **170** in a 79% yield. The increased yields for **170** compared to the (*R*)-enantiomer **164** may have been because

the Boc-protected (*R*)-precursor **163** was not dry. The final ester deprotection gave the final compound **165** in a 22% yield and in the required purity for biophysical testing (95% by RP analytical HPLC). The reaction did not go to completion as shown by the ^{1}H NMR spectrum of the crude product, although TLC analysis appeared to show consumption of the benzyl ester **170**. It is likely that some material was lost during purification by flash column chromatography, as the acid **165** streaked heavily, resulting in a low yield. Further optimisation of column solvents could help to reduce the streaking and improve the yield.

3.3 Biophysical Assays

With the (*R*)-(**72**) and (*S*)-enantiomers (**165**) of the oxazole carboxylic acid in hand, these compounds were tested in biophysical assays to determine if they could bind to *Sd*KefQCTD. As for the pyridinone compounds (Chapter 3), the biophysical assays chosen were the waterLOGSY NMR assay and DSF, which provide two orthogonal approaches for qualitative determination of binding.

3.3.1 WaterLOGSY

WaterLOGSY[216] was chosen to investigate whether **72** and **165** were able to bind to the *Sd*KefQCTD system (section 2.3.1). The waterLOGSY experiment for this ligand was run with the dipeptide **70** (supplied by Dr Catherine Haslam) as a positive control (Figures 3.7, 3.8).

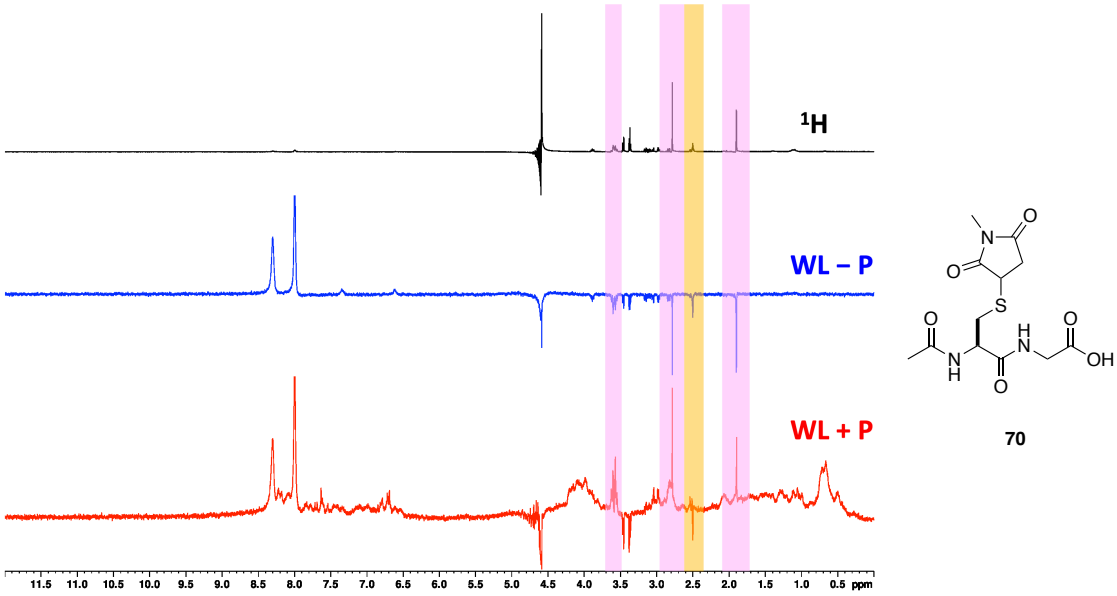


Figure 3.7. Full waterLOGSY spectrum of positive control dipeptide 70. Stack top to bottom: ^{1}H, water-supressed ^{1}H NMR of **70**; WL–P, waterLOGSY spectrum without protein; WL+P, waterLOGSY spectrum with *Sd*KefQCTD protein. DMSO is highlighted at 2.50 ppm in yellow and is the sample reference. Compound peaks are highlighted in pink. The red spectrum shows characteristic inversion of the ligand peaks relative to DMSO, which indicates ligand binding to the protein.

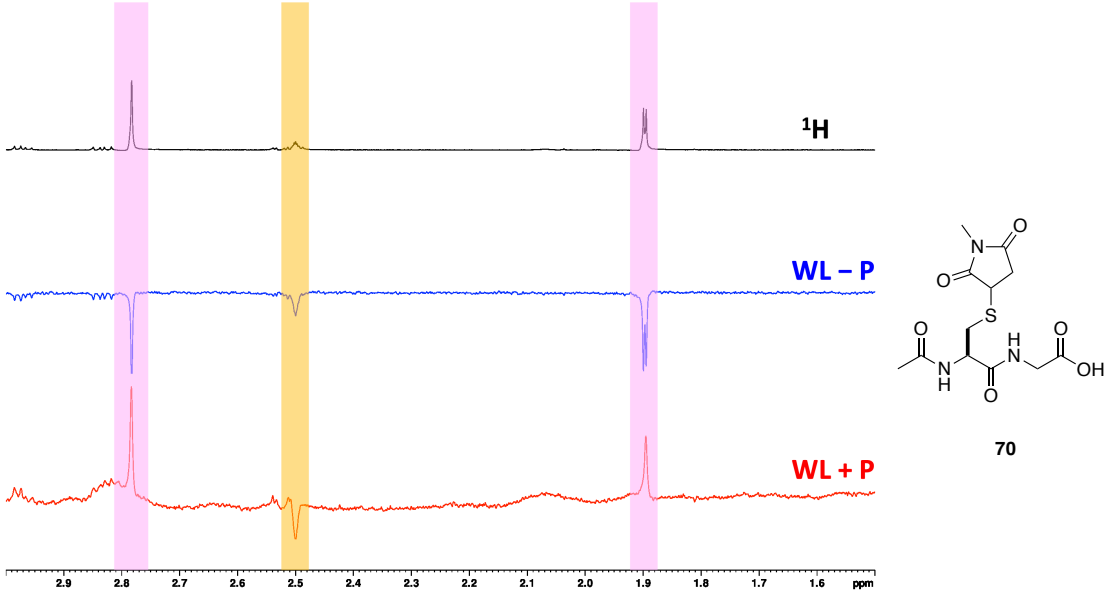


Figure 3.8. Expanded section of the waterLOGSY spectrum of the dipeptide positive control 70. Stack top to bottom: ^{1}H, water-supressed ^{1}H NMR of **70**; WL–P, waterLOGSY spectrum without protein; WL+P, waterLOGSY spectrum with *Sd*KefQCTD protein. DMSO is highlighted at 2.50 ppm in yellow and is the sample reference. Compound peaks are highlighted in pink. The spectrum shows the characteristic inversion of the ligand peaks relative to DMSO, which indicates ligand binding to the protein.

The positive control **70** shows the expected binding response with inversion of the compound peaks relative to DMSO, suggesting that the compound has received magnetisation transfer *via* the protein which is present giving a negative NOE effect.

The waterLOGSY experiment was also run on the peptide-mimetic ligand **72** (Figures 3.9, 3.10).

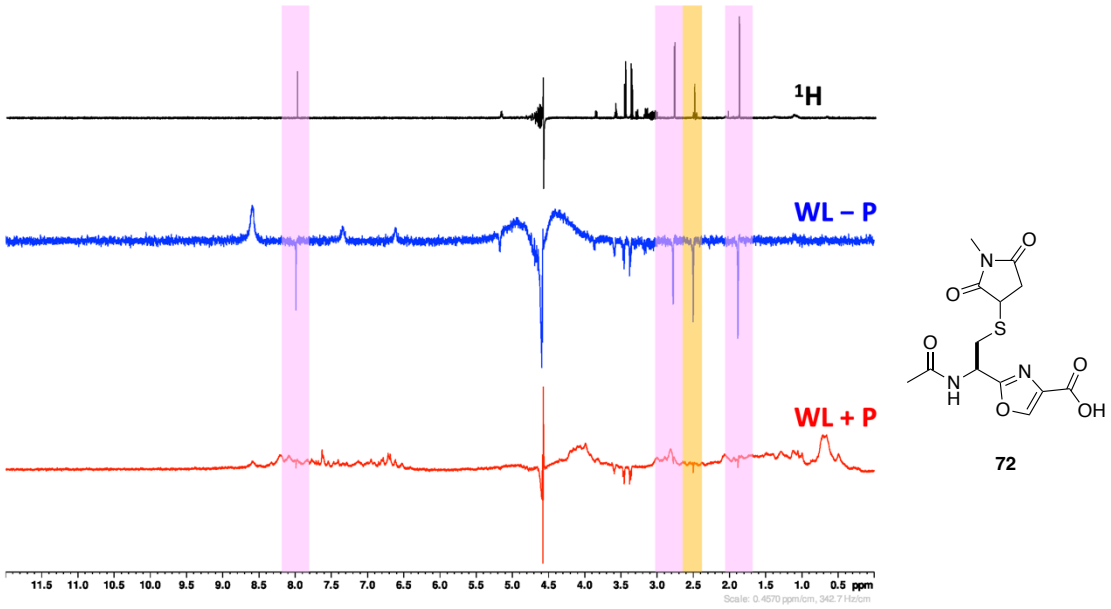


Figure 3.9. Full waterLOGSY spectra of the oxazole peptide mimetic compound 72. Stack top to bottom: ^{1}H, water-supressed ^{1}H NMR of **72**; WL–P, waterLOGSY spectrum without protein; WL+P, waterLOGSY spectrum with *Sd*KefQCTD protein. DMSO is highlighted at 2.50 ppm in yellow and is the sample reference. Compound peaks are highlighted in pink. The compound peaks in the waterLOGSY spectrum with protein do not show inversion relative to DMSO, which indicates no binding of **72**.

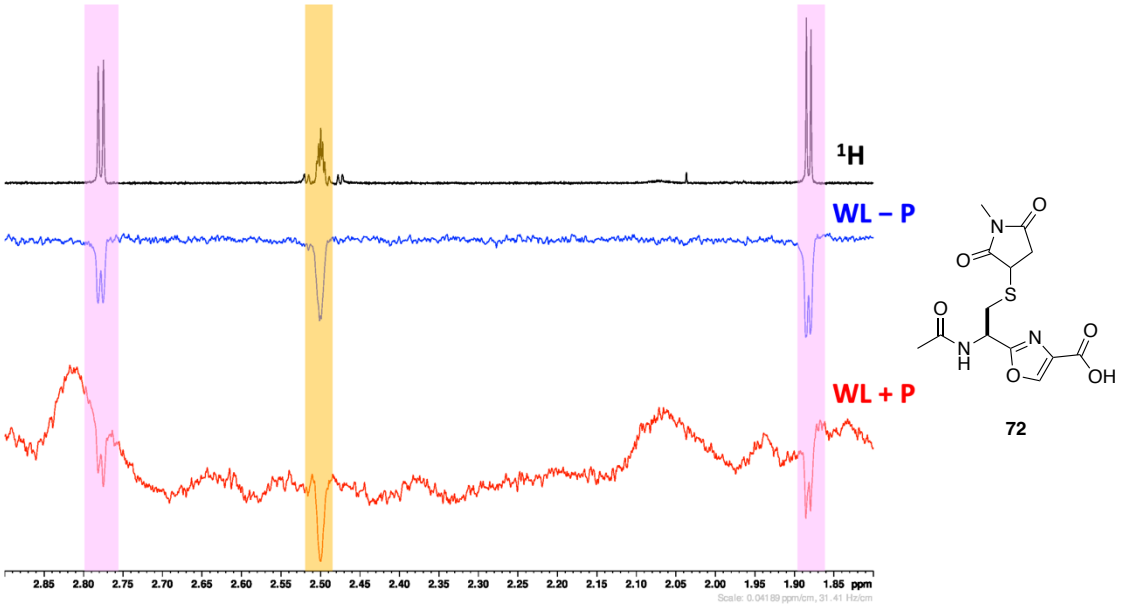


Figure 3.10. Expanded section of the waterLOGSY spectrum of 72. Stack top to bottom: ^{1}H, water-supressed ^{1}H NMR of **72**; WL–P, waterLOGSY spectrum without protein; WL+P, waterLOGSY spectrum with *Sd*KefQCTD protein. DMSO is highlighted at 2.50 ppm in yellow and is the sample reference. Compound peaks are highlighted in pink. The compound peaks in the waterLOGSY spectrum with protein do not show inversion relative to DMSO, which indicates no binding of **72**.

The waterLOGSY spectrum of **72** without protein shows that the compound is soluble, as there is no aggregation. When the *Sd*KefQCTD is present, there is no inversion relative to DMSO, suggesting that the oxazole **72** is not binding to the protein. The negative control **165** was also tested in this assay, binding was not expected due to the inverted stereocentre in the cysteine portion of the molecule as mentioned previously.

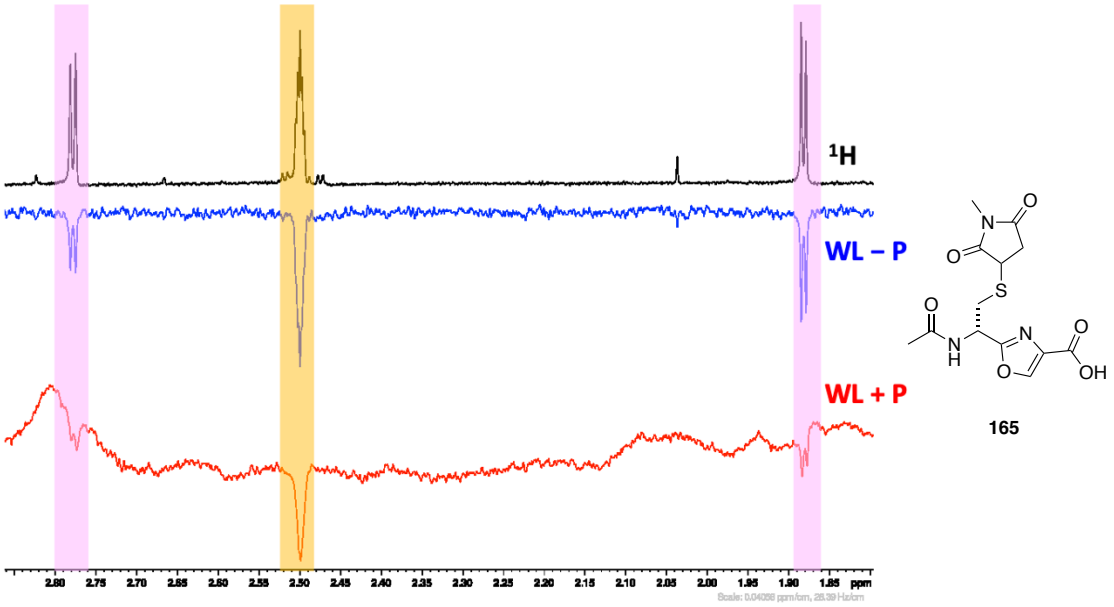


Figure 3.11. Expanded section of the waterLOGSY spectrum of 165. Stack top to bottom: ^{1}H, water-supressed ^{1}H NMR of **72**; WL–P, waterLOGSY spectrum without protein; WL+P, waterLOGSY spectrum with *Sd*KefQCTD protein. DMSO is highlighted at 2.50 ppm in yellow and is the sample reference. Compound peaks are highlighted in pink. The compound peaks in the waterLOGSY spectrum with protein do not show inversion relative to DMSO, which indicates no binding of **165**.

165 showed no indication of binding with the compound peaks showing the same sign as DMSO, suggesting that **165** is also not a suitable peptide mimetic of **70**.

3.3.2 DSF

As an orthogonal assay, DSF was used to determine whether the oxazole acid **72** or the negative control compounds **165** binds to the Kef protein. The DSF assay detects a change in melting temperature (ΔT_m) of the protein in the absence and presence of a potential ligand.[220] An increase in the melting temperature suggests that the ligand is stabilising the protein and is therefore binding to it (Section 2.3.2). The oxazole carboxylic acid **72** was tested along with two positive controls ^{t}BuSG and **70**, and **165** with ^{t}BuSG. As mentioned previously, the GSX (**21**) and dipeptides have known thermal shifts up to ~13 °C.[145] This assay was a suitable choice to observe an effect for a new scaffold type as

weakly binding ligands produce detectable ΔT_m, and could provide comparison with other Kef binders. The results from the assay are shown below (Figure 3.12).

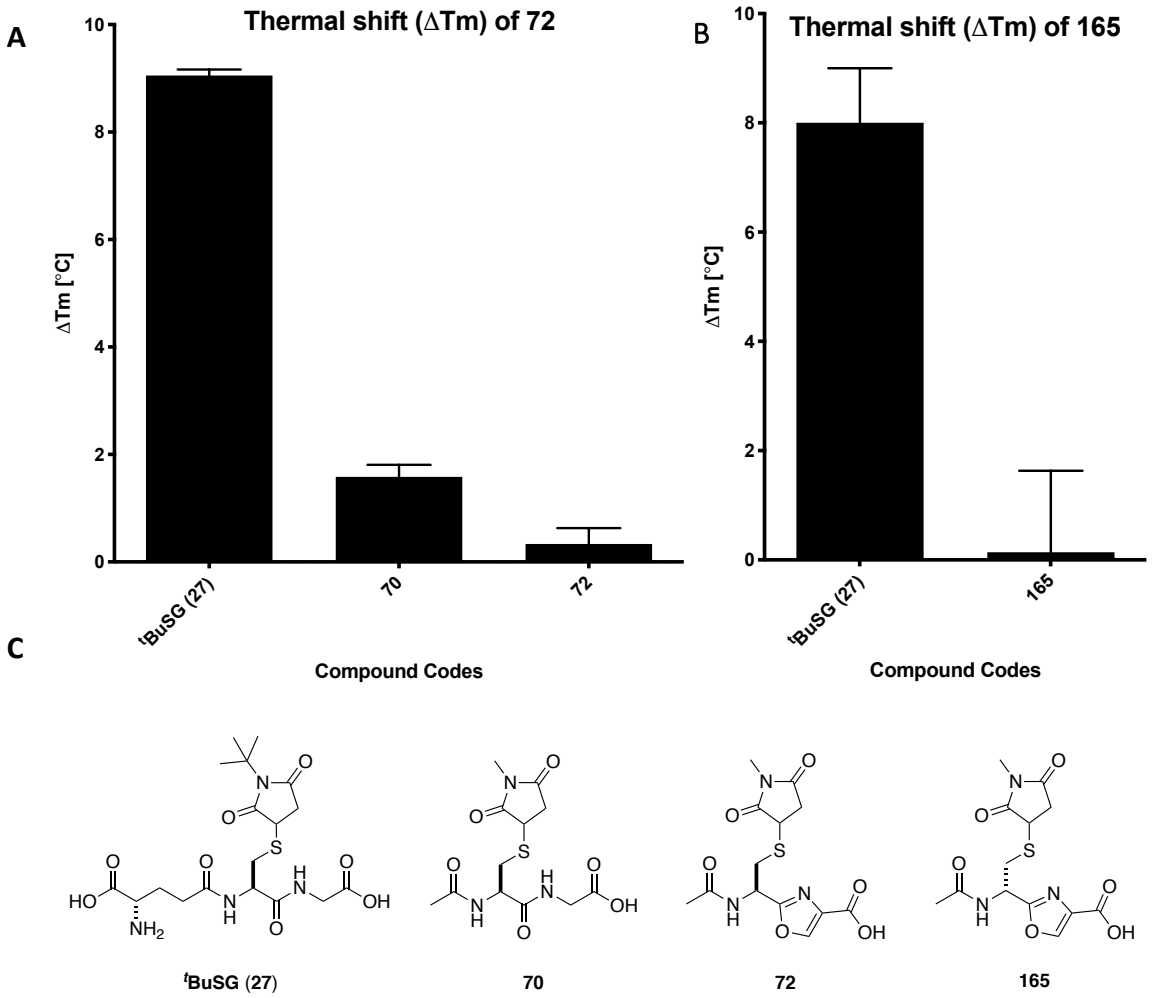


Figure 3.12. DSF Assay results with *Sd*KefQCTD. A) **72** thermal shift results. (^{t}BuSG (**27**) was used as a positive control. The dipeptide **70** was also tested for comparison. **72** showed a negligible change in melting temperature, consistent with it not binding to Kef. B) **165** thermal shift results. **165** also showed a negligible change in melting temperature of *Sd*Kef. C) Structures of tested compounds.

The ΔT_m values of the dipeptide **70** and for ^{t}BuSG are as expected, and match the literature.[145] The ΔT_m for the oxazole ligands **72** and **165** are <1 °, these data suggest that both enantiomers **72** and **165** do not bind to the *Sd*KefQCTD, and this result matches that seen by waterLOGSY.

The oxazole may have inadvertently removed some of the important features of the dipeptide ligand that factor into its affinity. These could be the arrangement and direction of functional groups that make necessary interactions in the binding, a change in polarity that has negatively affected hydrogen-bond interactions, or a 3D-conformation change so the ligand is no longer able to fit in the binding pocket.

3.4 Conclusions

A peptide mimetic ligand was designed based on the usage of oxazoles as amide bond replacement moieties for the Kef system. The carboxylic acid compound **72** was synthesised through an optimised route from the protected cysteine and serine amino acids *via* deprotection of the benzyl ester. **72** was then tested in two biophysical assays (waterLOGSY and DSF), that showed **72** was not capable of binding to Kef. Therefore, it can be concluded that in this instance the oxazole carboxylic acid is not a suitable peptide mimetic ligand. Chiral HPLC analysis of **72** would provide evidence that the stereocentre was intact and degradation had not cause loss of binding with the opposite stereochemistry. Further investigation of the binding properties of this ligand could include computational molecular dynamics (MD) experiments that could evaluate why **72** cannot bind to Kef. Novel thermal shift results for the dipeptide **70** have also been obtained as a result of this work.

Chapter Four: Investigation of Imidazopyridines as an Amide Replacement in *Sd*Kef Ligands

4.1 Introduction to the Imidazopyridine Scaffold

The imidazopyridine scaffold has little precedent as a peptide mimetic compared to the oxazole or pyridinone scaffolds. One example of the imidazopyridine system being used as a replacement of an amide bond is in the development of compounds with activity against psoriasis in a mouse model.[175] Despite this, imidazopyridine scaffolds are present in a number of important biologically-relevant compounds with examples used to treat inflammation, cancer, and psychiatric conditions (the latter two especially because of their structural similarity to purines and pyrimidines).[243] Zolpidem is a commonly used sedative and is a well-known example.[243–246] The imidazo[1,2-a]pyridine has been used as a peptide mimetic for a serine-serine segment of a peptide for Akt (protein kinase B, an AGC group kinase).[176] The peptide-mimetic scaffold was able to bind to Akt with improved proteolytic stability.

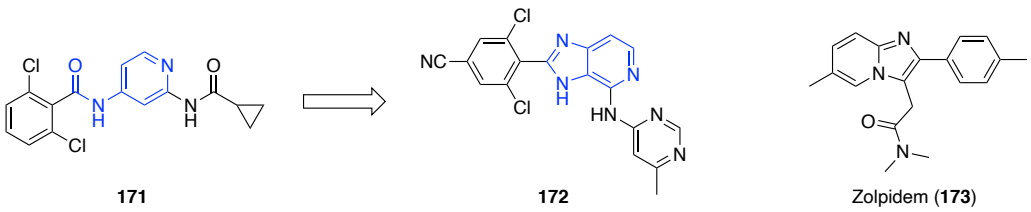


Figure 4.1. An example of an amide bond replacement ligand 172 with an imidazopyridine scaffold from 171,[175] and a commonly used imidazopyridine drug, Zolpidem (173).[243,246] **172** is a reported Tyrosine Kinase 2 inhibitor developed from **171**. The imidazopyridine core was used to constrain the amide bond, and increase affinity and selectivity.[175]

The aim of this work is to develop a peptide mimetic Kef ligand based on **70** by replacing the central amide bond. The imidazopyridine **73** has potentially improved synthetic

flexibility over **70**, similar to the pyridinone **71**, with the possibility to undergo cross coupling reactions to install different headgroups (Figure 4.2). Synthesis of the carboxylic acid and methyl ester would investigate the binding and pro-drug approach of this structure.

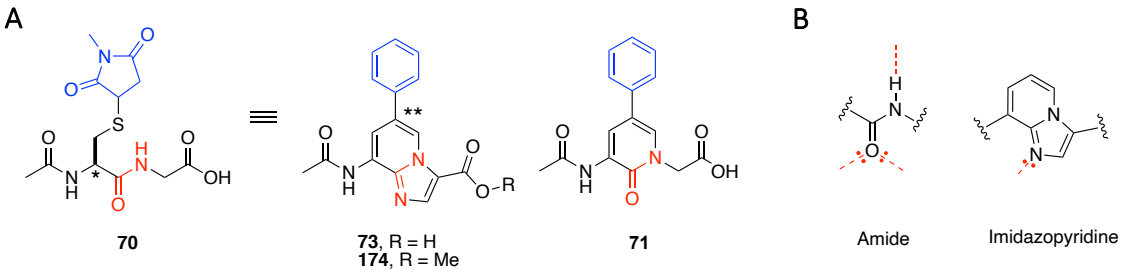


Figure 4.2. Representation of the imidazopyridine ligand as a peptide mimetic for the dipeptide structure 70. A) 2D-diagram of the replacement scaffolds for the dipeptide with the amide bond replacement in red, and the headgroup in blue, * labels the important stereocentre in **70**, ** labels the group which can be easily varied as part of SAR exploration *via* different cross-coupling reactions. B) Diagram comparing the hydrogen bond acceptor/ hydrogen bond donor interactions of an amide and imidazopyridine group.

The imidazopyridine ring system can make one hydrogen bond acceptor interaction like that of an amide bond with the imidazole-like nitrogen. The nitrogen lone pair is contained in an sp^2 orbital like that of the amide oxygen atom, however, the other two sp^2 and p orbitals are contributing to the ring system. The imidazopyridine does not have the hydrogen bond donor amide proton replacement, which could be detrimental to binding, and so this scaffold will explore the importance of this interaction as part of the amide bond replacement. **73** also has increased rigidity, as it has three rotatable bonds compared to seven in **70**,[194] which is an important feature for the uptake into Gram-negative bacteria.[17] **73** also does not contain the important cysteine stereocentre as is also the case for **71**. The loss of this stereocentre did not prohibit the binding of **71**, although the affinity was reduced compared to **70**, therefore it was hypothesised that **73** should also bind to *Sd*KefQCTD. The physicochemical properties of **73**, **174**, and **70** were compared including the molecular weight, hydrogen bond donor/acceptor interactions,

rotatable bonds, *c*log$D_{pH7.4}$, SFI,[195] and TPSA from calculations by ACD/I-labs (Table 4.1).[194]

Table 4.1. Physiochemical properties calculated from ACD/I-labs to compare the properties of 70, 73 and 174.

Property	Value **70**, Comments	Value **73**, Comments	Value **174**, Comments
MW/ $gmol^{-1}$	331.35	295.29	309.32
HBD	3	2	1
HBA	9	6	9
RB	7	3	4
*c*log$D_{pH7.4}$	–6.4	–1.51	1.8
SFI	–6.4, predicted to be soluble	1.49, predicted to be soluble	4.8, predicted to be borderline soluble
TPSA/ $Å^2$	158.2	84.2	73.2

The imidazopyridine ligands are predicted to be water-soluble with SFI values less than 5, although **174** has a borderline value of 4.8 which may cause solubility issues in future cell-based assays. **73** and **174** are calculated to have lower TPSA values than **70** at 84.2 $Å^2$ and 73.2 $Å^2$ respectively. Similar to the pyridinone compounds, this may predict low accumulation in Gram-negative bacteria, and may need addressing for future generations of imidazopyridine ligands.[195–197]

To investigate the SAR around the imidazopyridine, the 4-trifluoromethylphenyl and 4-*tert*-butylphenyl headgroups are of interest. These are potentially useful tool ligands if the imidazopyridine backbone functions as a peptide mimetic. The 4-trifluoromethylphenyl derivative was of interest as a fluorine containing imidazopyridine ligand could be used to establish a K_d using ^{19}F NMR, as discussed in section 2.3.3. In addition, **122** provided the greatest stabilisation of *Sd*KefQCTD in a DSF

assay for the pyridinone series. The 4-*tert*-butylphenyl pyridinone derivative showed stabilisation in DSF (**118**), and the tert-butyl succinimide headgroups comprise part of the highest affinity peptide ligands. These headgroups are of interest for the imidazopyridine scaffold as well (Figure 4.3).

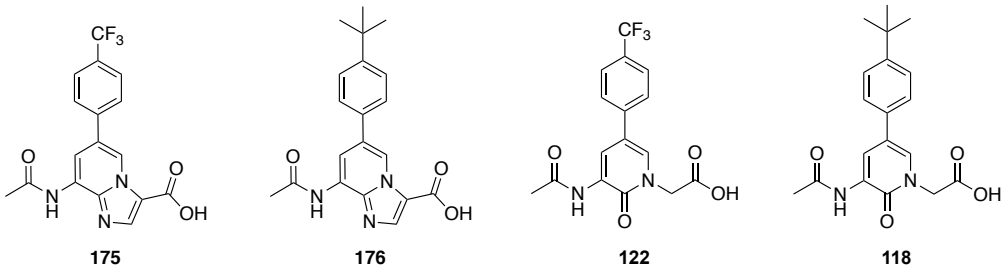


Figure 4.3. Comparison of imidazopyridine tool ligands and pyridinone tool ligands. The 4-trifluoromethylphenyl group was used for ^{19}F NMR K_d determination of **122**, and will be investigated for **175**. The *tert*-butylphenyl group showed the greatest stabilisation of the Kef system from the pyridinone ligands tested (**118**), and may provide affinity to **176**.

This chapter reports the investigation of the imidazopyridine scaffold as a peptide mimetic ligand for the Kef system. The imidazopyridine scaffold was synthesised, along with work towards two analogues. These compounds will be tested to assess their suitability as new ligands for the Kef system.

4.2 Synthesis of the Imidazopyridine Ligand

The first step in the synthetic route for **73** is a cyclisation to form the scaffold, then acetylation of the free amine. This is followed by the diversification step to install the desired headgroup for future SAR exploration, done before the iodination step to avoid any unwanted side product formation during the cross-coupling reaction. The final step was the installation of the carboxylic acid hypothesised to form a key hydrogen bonding interaction important for affinity.

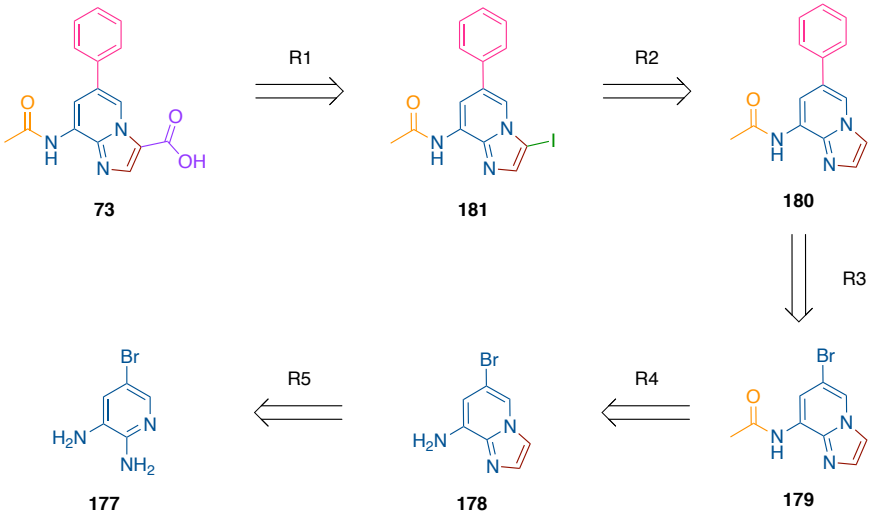
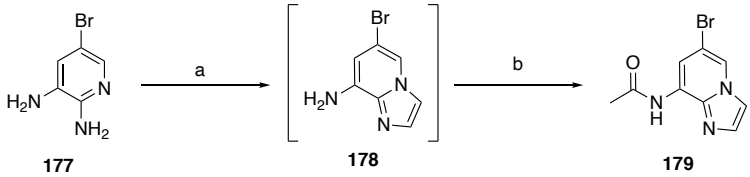


Figure 4.4. Retrosynthesis plan for the imidazopyridine ligand, 73. The strategy uses a diaminopyridine (blue) that is cyclised to form the imidazole ring (red) and acetylated (orange) to give the imidazopyridine core **179**. This core has a built in synthetic handle from the bromide to perform cross coupling reactions to install a variety of headgroups (pink). The final steps of the synthetic route are installation of an iodide as a second synthetic handle (green), to be used for a carboxylation to give the carboxylic acid ligand **73**.

4.2.1 Formation of the ring system

The synthesis of the imidazopyridine ligand scaffold **178** had been reported by Hill *et al.*[247] The ring system was formed using the diaminopyridine **177** (Fluorochem, CAS: 38875-53-5) in a cyclisation with chloroacetaldehyde. After obtaining **178**, it was intended to telescope the free amine into an acetylation reaction with acetyl chloride (AcCl), to avoid purification of a free amine (Scheme 4.1).

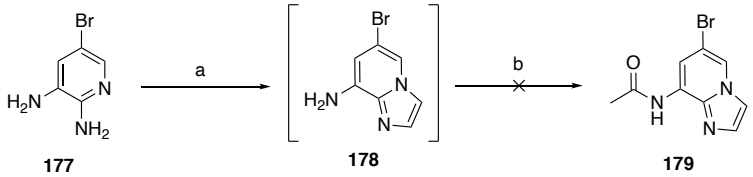


Scheme 4.1. Formation of the imidazopyridine scaffold, 179. *Reagents and conditions*: a) chloroacetaldehyde (50% in H_2O), IPA, 90 °C, 6 h; b) AcCl, NEt_3, pyridine, THF, RT, 4 h, 38% (over two steps).

The cyclisation was first performed on 200 mg, however ^{1}H NMR analysis of the resulting brown solid and a black residue constituting the crude residue gave no evidence of the

formation of **178**. The scale was increased to 1.0 g to facilitate handling of the crude material. This scale is closer to that of the literature (10 g)[247] and helped isolation of the poorly soluble and complex reaction mixture. The resulting crude material was easier to transfer to a flask for the subsequent reaction, and it was telescoped into the acetylation step. Typically, acetylation reactions using AcCl are performed in DCM, however, **178** had limited solubility and so THF was used for the reaction. The acetylation did not progress so NEt_3 was added to the mixture which resulted in no change. Pyridine (Py) was then added to catalyse the acetylation, after which analysis by TLC showed consumption of **178**, and **179** was isolated in 38% yield over the two steps.

When this reaction was doubled in scale to 2.0 g, no identifiable **179** was isolated. The literature reports cyclisation performed on a 10 g scale at 94% yield, and thus has been shown to work on larger scales.[247] Further attempts at this cyclisation did not consistently yield **179** due to the apparent sensitivity of the cyclisation, resulting in complex mixtures that did not contain the desired product (Scheme 4.2, Table 4.2). Analysis of the commercially obtained **177** showed some impurities, however, newly purchased precursor material (**177** and chloroacetaldehyde) did not improve the outcome of the reactions.



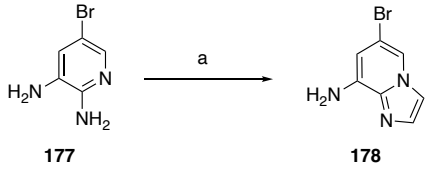
177 178 179

Scheme 4.2. Unsuccessful attempts at the formation of 179. *Reagents and conditions*: a) chloroacetaldehyde (50% in H_2O), IPA, 90 °C; b) see table.

Table 4.2. Reagents and conditions for the repeat attempts of cyclisation of the imidazopyridine scaffold 179.

Method	Scale	Cyclisation Conditions	Acetylation Conditions	Outcome
i	1.0 g	Chloroacetaldehyde (50% in H_2O), IPA, 90 °C, 18 h	AcCl, NEt_3, pyridine, THF, RT, 28 h	38% yield of **179**
ii	2.0 g	Chloroacetaldehyde (50% in H_2O), IPA, 90 °C, 15 h	Not attempted	Cyclisation reaction step (a) gave a complicated mixture including **177** and **178**.
iii	2.0 g	Chloroacetaldehyde (50% in H_2O), IPA, 90 °C, 22 h	AcCl, Py, THF, 30 °C, 24 h	No **178** or **179** formed.
iv	2.0 g	Chloroacetaldehyde (50% in H_2O), IPA, 90 °C, 16 h	AcCl, Py, THF, RT, 24 h	**177** consumed, **178/179** not formed.
v	0.5 g	Chloroacetaldehyde (50% in H_2O), IPA, 90 °C, 1 h μ-wave	AcCl, Py, NEt_3, THF, RT, 22 h	**177** consumed, **178/179** not formed.

With the cyclisation using chloroacetaldehyde proving unreliable, alternative conditions were sought to produce the imidazopyridine system. The use of bromoacetaldehyde or bromoacetaldehyde diethyl acetal instead of chloroacetaldehyde has precedent for such cyclisations (Scheme 4.3).[245,248,249]

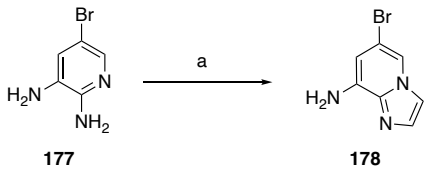


177 **178**

Scheme 4.3. Reported cyclisation example using bromoacetaldehyde.[245] *Reagents and conditions*: a) i) Bromoacetaldehyde diethyl acetal, conc. HCl, dioxane/water 2:1, reflux, 30 min; ii) $NaHCO_3$, **177** in dioxane/water 2:1, reflux 14 h, 92%. (1.5 g scale.)

These conditions generate the bromoacetaldehyde *in situ* by reaction of bromoacetaldehyde diethyl acetal with concentrated (conc.) HCl. The bromoacetaldehyde mixture is then neutralised through the addition of $NaHCO_3$, before addition of **177**. Bromoacetaldehyde reduces the number of side reactions compared to chloroacetaldehyde as it is more electrophilic due to the weak C–Br bond and reacts

faster.[250] Therefore cyclisation with *in situ* generated bromoacetaldehyde was investigated (Scheme 4.4).[245] These conditions reliably gave **178** in 57–73% yield.

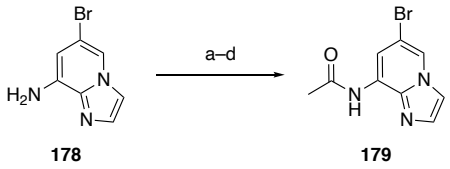


177 **178**

Scheme 4.4. New conditions for the formation of the imidazopyridine scaffold, 178. *Reagents and conditions*: a) i) Bromoacetaldehyde diethyl acetal, conc. HCl, dioxane/H_2O 2:1, 30 min, 88 °C to RT; ii) $NaHCO_3$, **177**, dioxane/H_2O 2:1 88 °C to RT, 21–23 h; n=2, crude yield 57–73%.

4.2.2 Optimisation of the acetylation reaction

The next step in the synthesis was the acetylation of **178** to give the acetylated imidazopyridine scaffold **179**. Four sets of conditions were investigated to optimise the acetylation (Scheme 4.5, Table 4.3, a). The acetyl chloride conditions led to a complicated product mixture upon analysis by TLC, with many side reactions occurring as shown by multiple spots.



178 **179**

Scheme 4.5. Acetylation of the free amine on imidazopyridine 178. For full reagents and conditions see Table 4.2.

Table 4.3. Reagents and conditions for the acetylation of the amine 179 (Scheme 4.5.).

Method	Reagents and Conditions	Outcome
a	AcCl, Py, DCM, RT, 15 h	Consumption of **178**,
b	AcCl, Py, DCM, 0 °C, 3 h	Consumption of **178**.
c	i) Ac_2O, DCM, RT, 22 h; ii) DMAP, RT, 7 h	25% yield of **179**.
d	Ac_2O, DMAP, Py, NEt_3, DCM, RT/30 °C, 48–96 h.	50–52% yield of **179**, n=2.

The acetyl chloride acetylation conditions were repeated at 0 °C (Scheme 4.5, Table 4.3, b) in an attempt to slow side reactions. However, the crude ^{1}H NMR showed a complicated mixture isolated from this reaction. Analysis by TLC showed a number of spots (absorbing at 365 nm), suggesting that **179** was unstable to these reaction conditions and/or multiple side reactions were occurring.

It was considered that the use of a less-reactive acetylating agent such as acetic anhydride (Ac_2O) would reduce the amount of side reactions occurring during this step. **178** was stirred with acetic anhydride in DCM at RT (Scheme 4.5, Table 4.3, c), and no reaction occurred. DMAP was added to accelerate the reaction, after which analysis by TLC showed consumption of **178**. The major product was isolated from the reaction mixture, providing of **179** in 25% yield.

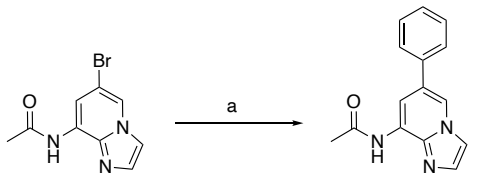
To improve the yield of the reaction (Scheme 4.5, Table 4.3, d), pyridine was added as an organic base. However, the reaction showed no consumption of **178** based on TLC analysis. NEt_3 and further Ac_2O was added, and the mixture was warmed to 30 °C which finally gave **179** in 52% yield. A repeat of the reaction included the complete mixture of DMAP, Py, and NEt_3, which was stirred at RT which also gave **179** in 50% yield.

4.2.3 Headgroup installation

Similar to the synthesis of the pyridinone ligand **71**, the imidazopyridine route includes an intermediate with a bromo moiety, allowing for the coupling of a variety of new headgroups. Of particular interest was investigation of the same headgroups as the

pyridinone series, especially those with the highest affinity or assay utility. This would allow comparison between the two backbone scaffolds.

Following the acetylation reaction to give **179**, a coupling reaction was used to install the phenyl headgroup. The Suzuki coupling conditions were taken from the literature,[251] with the pre-formed palladium(II) [1,1′-bis(diphenylphosphino)ferrocene] (dppf) dichloride complex, and caesium carbonate in toluene (Scheme 4.6).



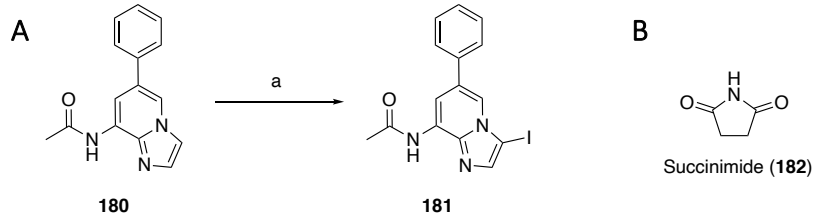
179 **180**

Scheme 4.6. Suzuki coupling conditions for the imidazopyridine 179. *Reagents and conditions*: a) Phenyl boronic acid, Pd[dppf]Cl_2, Cs_2CO_3, toluene, 90 °C, 18 h, (3–23 h), n=7, 36–97%.

The reaction had no observable side reactions following analysis by TLC, and only one product was isolated from the reaction mixture.

4.2.4 Iodination of 180

To functionalise the peptide mimetic backbone **180** with a carboxylic acid a versatile synthetic handle was required. There is literature precedent for the carboxylation of iodo-heteroaromatic using carbon dioxide,[252,253] therefore the scaffold was iodinated using NIS (Scheme 4.7).[254]



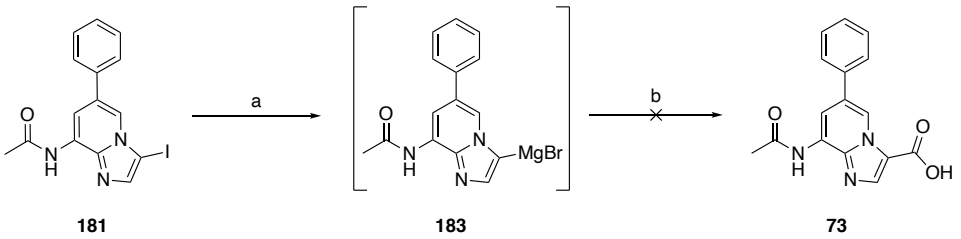
Scheme 4.7. Iodination of the imidazopyridine scaffold with headgroup, 180. A) Reaction scheme for the iodination, r*eagents and conditions*: NIS, DCM, 0 °C, 20 h, (2–24 h), n=5, 12–68%; B) Succinimide co-product produced from NIS.

The reaction produced succinimide (**182**) as a co-product, which was difficult to remove during purification using flash column chromatography on silica, as it eluted at the same time as **181**. Succinimide is poorly soluble in chloroform, however, the difference in solubility between **181** and succinimide was not enough to utilise chloroform as an extraction solvent. **181** is poorly soluble in acetonitrile and was washed with ice-cold solvent to remove the succinimide, which gave yields of **181** between 12–15%. An alternative wash of the dissolved organic components in ethyl acetate using saturated sodium bicarbonate, water, followed by brine was identified, and this removed the necessity of multiple purifications by flash column chromatography of **181**. This procedure had improved yields of 66–68% and removed the succinimide.

4.2.5 Carboxylation of the imidazopyridine scaffold

The final step in the synthesis of the imidazopyridine carboxylic acid scaffold **73** was the introduction of the carboxylic acid moiety. This group forms key binding interactions to Kef.[153]

The first approach was a metal-halogen exchange and carbon capture reaction to install the carboxylic acid in one step utilising the iodide handle in **181** (Scheme 4.8).[255]

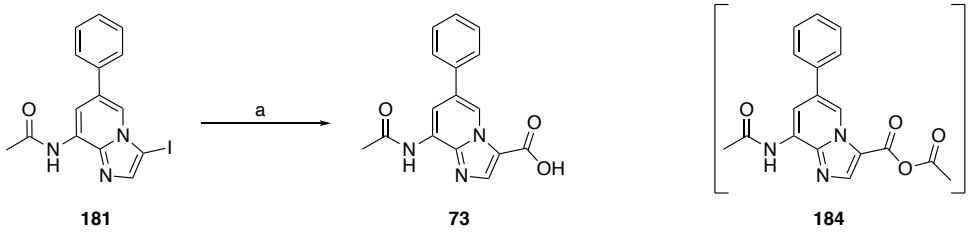


181 183 73

Scheme 4.8. Attempts to carboxylate the imidazopyridine 181. *Reagents and conditions*: a) i) EtMgBr, THF, –25 °C, 30 min; b) CO_2 (g), –78 °C; 3–18 h, n=3.

The metal-halogen exchange was carried out using the Grignard reagents at –25 °C, then CO_2 was bubbled through the solution at –78 °C. Consumption of **181** occurred and the formation of two new spots was observed following analysis by TLC. However, only the dehalogenated imidazopyridine **180** was isolated. This indicates that the metal-halogen exchange occurred, but the reaction may not have been dry, or that CO_2 was not a suitable electrophile.

Alternative conditions were investigated to install a carboxylic acid group on a heteroaromatic ring using hydroxycarbonylation conditions.[256–258] These conditions seemed suitable for **181** as the sodium formate coupling reaction started from the same iodinated imidazole ring system (Scheme 4.9).



181 73 184

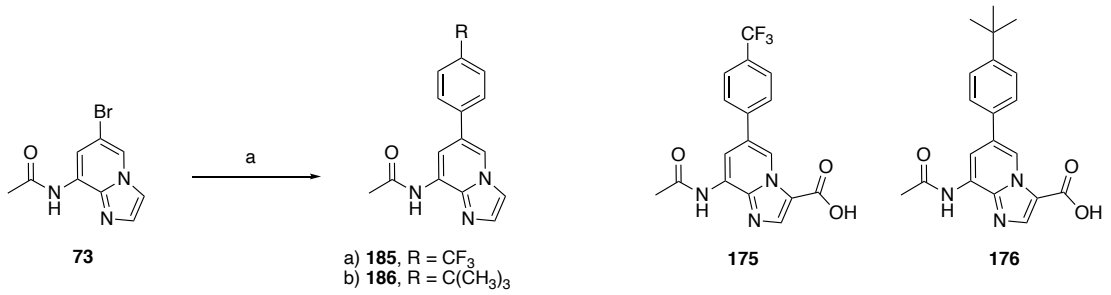
Scheme 4.9. Hydroxycarbonylation reaction to install the carboxylic acid and form 73. *Reagents and conditions*: a) Sodium formate, $Pd(OAc)_2$, LiCl, DIPEA, Ac_2O, DMF, 80 °C, 22 h, 71%. Mixed anhydride intermediate **184** formed during the reaction.

The reaction involves pre-stirring the sodium formate, acetic anhydride and diisopropylethylamine (DIPEA) in DMF, before addition of the iodide, LiCl, and palladium acetate. This ensures the mixed anhydride is formed to generate CO *in situ*, which is then

able to form another mixed anhydride **184** from **181**, before being hydrolysed to give the carboxylic acid **73**. Using these conditions, **73** was isolated in 71% yield.

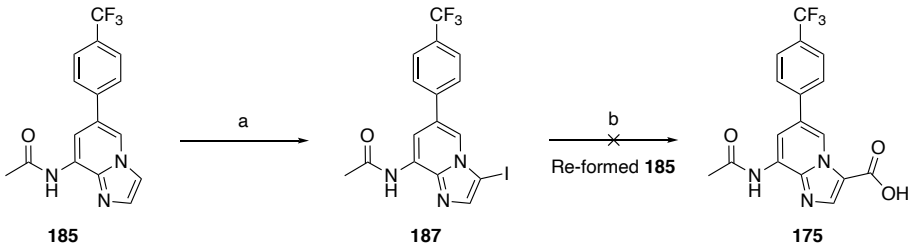
4.2.6 Synthesis of analogues of the imidazopyridine 73

Synthesis and testing of **175** and **176** began exploration of the SAR around the imidazopyridine scaffold, as discussed in section 4.1. The 4-trifluoromethylphenyl and *tert*-butylphenyl headgroups were coupled onto **179** using the same reaction conditions as the formation of **180** (Scheme 4.10).



Scheme 4.10. Coupling two additional headgroups onto the imidazopyridine scaffold. *Reagents and conditions*: $RB(OH)_2$, $Pd[dppf]Cl_2$, Cs_2CO_3, toluene, 90 °C, 19 h; R = 4-*tert*-butylphenylboronic acid, 29%; R = 4-trifluoromethylphenylboronic acid, 55%.

The next step in the synthesis of these useful tool ligands was to install the carboxylic acid group *via* the iodide (Scheme 4.11). The CF_3-containing headgroup was most of interest so only synthesis of **175** was attempted due to insufficent time to complete both syntheses. The iodination of **185** did not go to completion and gave **187** in 35% yield. For the final step the palladium coupling conditions to install the carboxylic acid were repeated. However, it did not result in the hydroxycarbonylation reaction, but instead dehalogenation to reform **185**, possibly due to insufficiently dry reaction conditions.



185 187 175

Scheme 4.11. Synthesis of the trifluoro tool compound 175. R*eagents and conditions*: a) NIS, DCM, 0 °C, 6 h, 35%; b) sodium formate, $Pd(OAc)_2$, LiCl, DIPEA, Ac_2O, DMF, 80 °C.

4.3 Biophysical Assays with *Sd*KefQCTD

To determine the suitability of the imidazopyridine scaffold present in **73** as a peptide mimetic, the compound was subjected to biophysical assays to determine whether it was capable of binding to the *Sd*KefQCTD. As for the pyridinone compounds (Chapter 2), the biophysical assays chosen were the waterLOGSY NMR, and DSF, which provide two orthogonal approaches for qualitative determination of binding to *Sd*KefQCTD.

4.3.1 WaterLOGSY

The waterLOGSY NMR assay (see section 2.3.1) was chosen to investigate the binding of **73** with *Sd*KefQCTD (Figure 4.5).

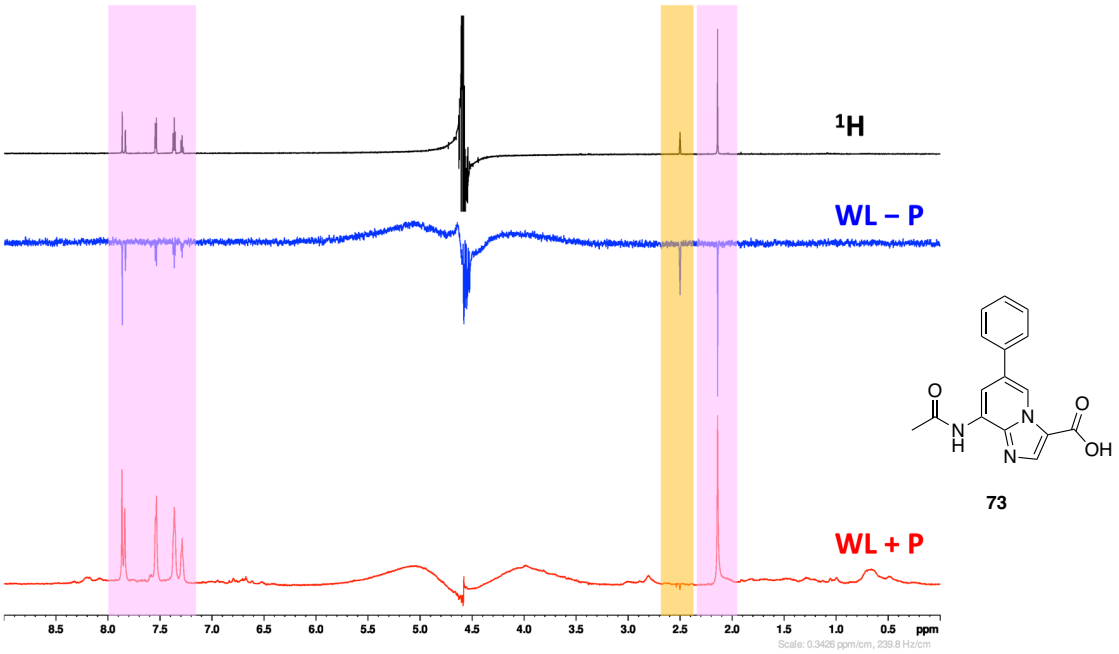


Figure 4.5. WaterLOGSY spectrum of 73. Stack top to bottom: ^{1}H, water-supressed ^{1}H NMR of **73**; WL–P, waterLOGSY spectrum without protein; WL+P, waterLOGSY spectrum with *Sd*KefQCTD protein. DMSO is highlighted at 2.50 ppm in yellow and is the sample reference, compound peaks are highlighted in pink. The spectrum shows the characteristic inversion of compound peaks relative to DMSO, indicative of binding to *Sd*Kef.

The spectrum shows the characteristic inversion of the compound peaks relative to DMSO in the waterLOGSY experiment in the presence of *Sd*Kef, suggesting that **73** is binding to *Sd*KefQCTD. This ligand shows there is some tolerance in the connections within the backbone for the formation of hydrogen-bonds to the protein, as comparing **73** with **71** there is the additional imidazole ring in **73**. **73** does not further explore the SAR around the headgroup as it includes an unsubstituted phenyl ring, although future ligands based on this scaffold may explore this. This experiment provides the first evidence of the imidazopyridine scaffold being a suitable peptide mimetic for the *Sd*KefQCTD system.

4.3.2 DSF

DSF was chosen as a suitable orthogonal assay to waterLOGSY as for the previous compounds tested in this work. The DSF assay detects a change in melting temperature (ΔT_m) of the protein in the absence and presence of a potential ligand.[220] An increase in the melting temperature suggests that the ligand is stabilising the protein and is therefore binding to it (see section 2.3.2). The imidazopyridine **73** was tested with ^{t}BuSG as a positive control (Figure 4.6). The assay was with two concentrations of ligand 1 mM and 0.5 mM, to identify any solubility issues.

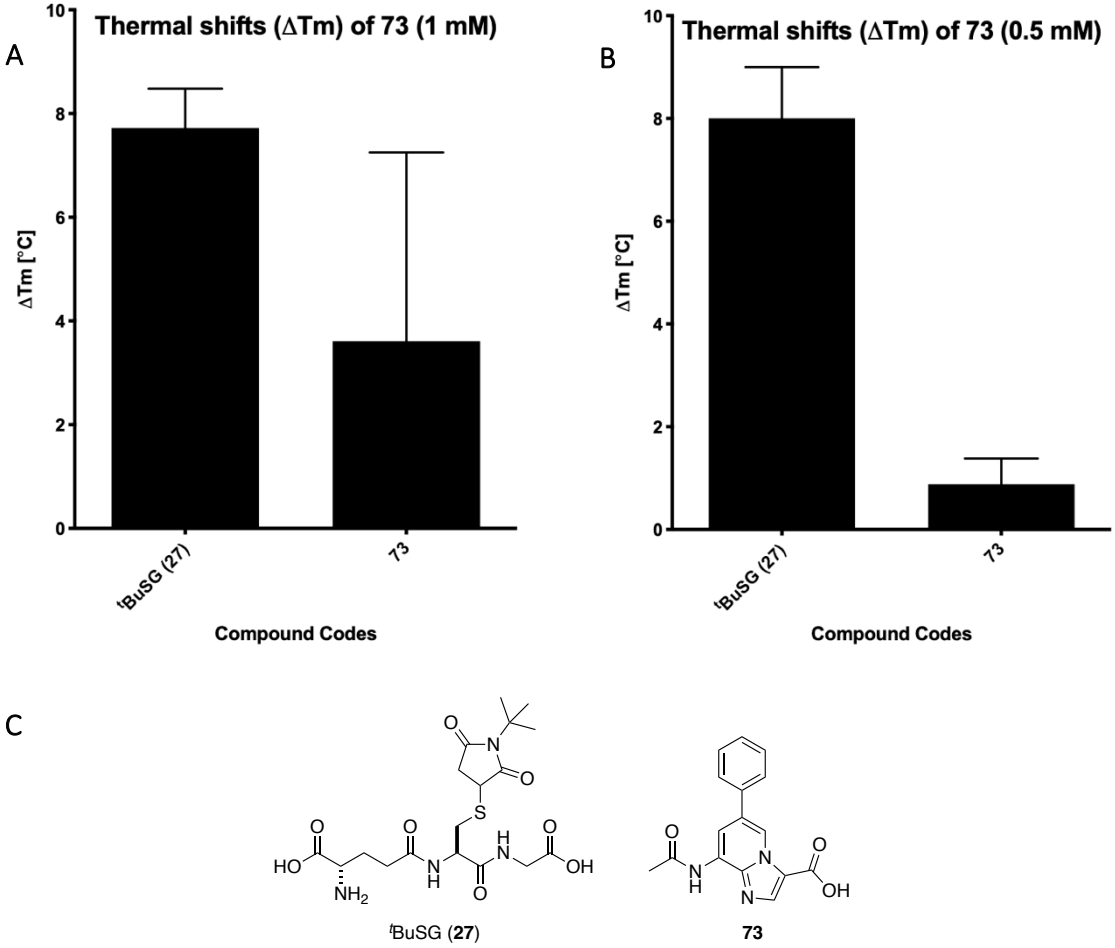


Figure 4.6. DSF Assay results with *Sd*KefQCTD. A) DSF assay thermal shift results at 1 mM **73**, error bars are standard error of the mean from a triplicate result; B) DSF assay thermal shift results at 0.5 mM **73**; C) Structures of compounds used in DSF. Thermal shift results ^{t}BuSG (**27**) was used as a positive control. There was considerable variation in the thermal shift results from **73**, so it is difficult to draw a conclusion from these data.

The DSF repeat at 500 μM showed a very small stabilisation of the protein when **73** was present. The associated standard error was much smaller, suggesting that the variation in melting temperatures could be due to insolubility of **73**, however DSF does exhibit high variability. It is possible that the affinity of **73** for *Sd*KefQCTD is at the threshold of detection for DSF, which may account for the small stabilisation, although it is difficult to draw a conclusion from these data.

The thermal shift data supports that of waterLOGSY that **73** is a suitable peptide mimetic compound for the *Sd*KefQCTD system, as both experiments show stabilisation of the protein.

4.4 Conclusions

The imidazopyridine ligand **73** was synthesised using a cyclisation reaction from diaminopyridine, followed by installation of the headgroup and carboxylation *via* an iodo group on the imidazole ring. The synthesis required optimisation of the cyclisation and acetylation steps, but suitable conditions compatible with the reactivities of the parent molecule were identified. Installation of the headgroup and carboxylic acid was undertaken with palladium-catalysed coupling reactions. The scaffold was tested in two orthogonal biophysical assays, waterLOGSY and DSF, to assess whether it was able to bind to the *Sd*KefQCTD. The assays suggested that the scaffold was capable of binding to *Sd*KefQCTD through a positive waterLOGSY result, but that it was possibly low affinity, and so only resulted in a borderline stabilisation of the protein in DSF. However, this is promising evidence that the imidazopyridine scaffold could be a suitable peptide mimetic

for the *Sd*KefQCTD system. The central amide bond has been replaced with this core, which has increased rigidity and hydrophobicity, which are factors that are important for the accumulation in Gram-negative bacteria.[17,87,88] Further investigation of the SAR with the completion of the synthesis of the CF_3 and *tert*-butyl containing aromatic headgroups **175** and **176** as well as others, followed by testing, will be useful for the confirmation of the imidazopyridine scaffold as a Kef ligand. Future work will include the synthesis of multiple new headgroups to explore the SAR, and affinity determination of this ligand series *via* ^{19}F NMR, fluorescence based competition assay,[158] or ITC experiments.[153,158]

Chapter Five: Identification and Evaluation of Peptide Isosteres Using Scaffold Hopping

5.1 Introduction to Scaffold Replacement

Scaffold replacement is a technique used to identify mimetic structures that conserve the steric or electronic properties of the molecule, often using isosteres (described in section 1.3.2). The technique aims to maintain the desired binding affinity or phenotype activity through a structurally different molecule that is capable of making similar interactions with the target. Ideally, a scaffold replacement would lead to improvements in physiochemical properties, such as structural rigidity, chemical stability, or solubility, amongst others.[259–262] This approach is also useful for ligand design, to not only access new chemical space, but also explore new chemical intellectual property (IP). The work described in this chapter was a preliminary study performed to explore an alternate approach to that presented in previous chapters. It applies a computational approach to identify a new peptide-mimetic ligand capable of activating Kef.

One of the first programmes to facilitate 'scaffold hopping' was SEAL,[263] which looked at the obvious replacements of the two most important properties of a ligand: steric and electronic properties. The programme scored, and hence ranked, hits *via* "the active site shape and charge distribution".[263] Compounds are scored based on their ability to meet set criteria (such as lipophilicity) and those that fulfil a high number of these criteria, compared to a reference compound, are deemed "hits". These hits are then ranked by

the chosen score to present the results in an order that identifies the most promising isostere. Modern programmes[264–268] use more complex scoring methods, that measure these two properties as well as the similarity to the reference ligand and its pharmacophore. Pharmacophores[269–272] define the essential requirements for a compound to bind to a target protein in terms of type and location. Scaffold replacement allows a large area of chemical space to be searched for these key interactions to identify diverse ligands that are still likely to bind to the protein of interest, while investigating novel chemical space. Scaffold hopping is also used to identify more lead-like scaffolds, which still maintain the key interactions and selectivity given by a native ligand or peptide.[97] (See Figure 5.1. below.)

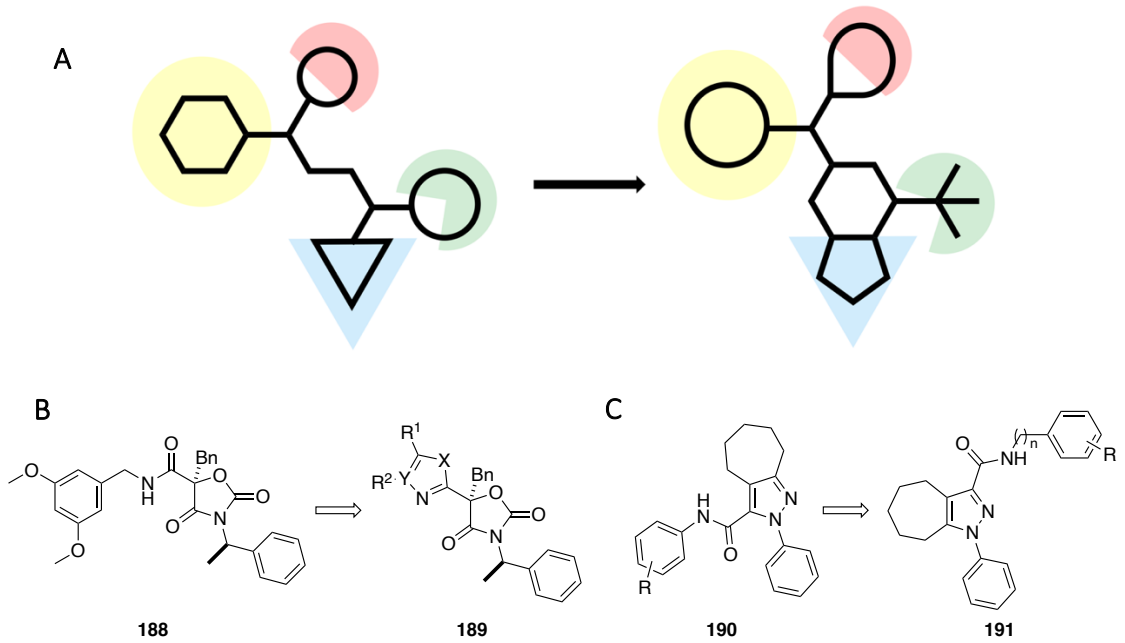


Figure 5.1. Cartoon and diagrams showing scaffold replacement. A) Cartoon illustration. Chemical moieties are switched that still maintain the desired steric and electronic properties of the parent molecule. This is used to improve the overall characteristics of the molecule. B) Example of scaffold hopping used by Cox *et al.* to stabilise metabolically labile groups.[273] C) Example of scaffold hopping by Jiang *et al*. used to identify a novel structure resulting in the desired phenotypic activity.[274]

The aim of this work is to identify a new chemical scaffold using the scaffold hopping technique capable of binding to and activating the *Sd*KefQCTD system. The current highest affinity activators of *Sd*KefQCTD are di- and tri-peptides and so have the inherent

instabilities associated with amide bonds and draw-backs of peptide based drugs.[95,98,100,104,106,275] The stereocentre derived from cysteine was identified as necessary for activation of Kef, however there is a risk of loss of affinity through racemisation.[153] Therefore, replacement of this stereocentre with a new backbone without loss of affinity is desirable. Protein-based drugs are susceptible to a number of pathways affecting their bioavailability and stability (discussed in section 1.3.3).[94] Although this is not unique to peptides and still affects small-molecule drugs, structural changes to reduce these can arguably be more easily incorporated into small organic molecules. It was thought that computer-aided design could identify replacement scaffolds for new Kef ligands that could fulfil the electronic and steric requirements of a binding ligand, while removing the potential instability and vulnerable stereocentres in the resulting lead molecule.

This chapter reports the investigation of the scaffold hopping techniques as a method to generate new peptide mimetic ligands for the Kef system. One new scaffold and three analogues were synthesised and tested to assess whether they could bind to the GSH-binding site of the Kef system.

5.2 Scaffold Hopping Experiments

Multiple methods were employed to perform scaffold-hopping from the dipeptide **70** backbone and GSH conjugate ESG.* A workflow was followed with three stages for the generation, filtering, and selection of compounds (Figure 5.2).



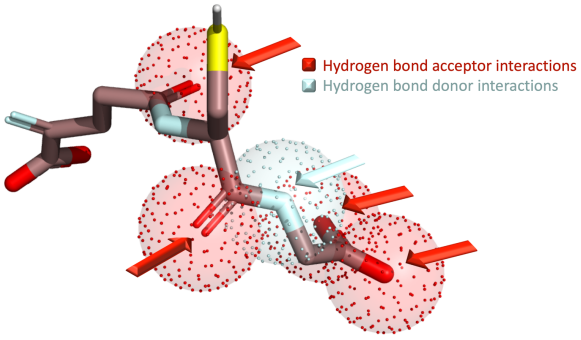
Figure 5.2. Workflow diagram for scaffold hopping experiments. Stage 1, generating: Spark™ and Blaze were used to generate libraries of suitable peptide mimics, ROCS was used to generate 3D-shape mimetics. Stage 2, filtering: the stage 1 libraries were filtered using a pharmacophore generated in ROCS and visualised with MOE to give the top hits. Stage 3, evaluation: the top hits were visually inspected to choose a suitable target compound for synthesis.

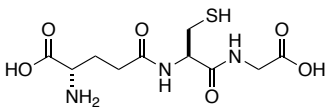
For stage 1, Spark™ was used to search the Zinc[81] library for compounds that would be suitable mimics of the electron cloud profile of the dipeptide **70** backbone (without the succinimide headgroup). The top 500 results were saved. Blaze was used to search the Evotec virtual library for electronic mimics of the ESG tri-peptide based structure, and the top 10% results saved. ROCS was used to search the OMEGA[276] library for a suitable mimic of the 3D-shape of GSH and ESG. This led to the generation of 40264 theoretical compounds that were suitable peptide analogues, and the mixture of techniques and databases ensured a large area of chemical space was explored. The backbone of **70** and GSH were used as the search query because it was desired to mimic interactions made by the backbone rather than the headgroup. A variety of headgroups have been shown

* Programmes and support from Dr Michelle Southey and Dr Mike Bodkin at Evotec (UK) Ltd: Spark,[264] ROCS,[265] and Blaze,[266] visualisation with MOE,[267] and using the Evotec_VS_7M, OMEGA,[276] and Zinc libraries.[81]

to be tolerated by the Kef system,[145,153] and the focus of this work was on replacing the central amide bond.

For stage 2, the search results were further refined using a pharmacophore query, based upon the minimum interactions required as made by the known dipeptide ligand **70**, from GSH (Figures 5.3, 5.4). The pharmacophore query used for potential ligands for *Ec*Kef featured: exclusion of amide bonds within same regions of the **70**; satisfaction of a minimum of three hydrogen bond donors and acceptors out of the five total present in **70**; no clashes within the excluded volume (volume that is occupied by the receptor from the protein crystal structure). This refined the results to 4923 compounds.





GSH (**20**)

Figure 5.3. 3D-GSH showing a diagram of the pharmacophore used in the selection process with MOE. Compounds were selected based on how many of the hydrogen bond donor and acceptor interactions were satisfied out of the five total.

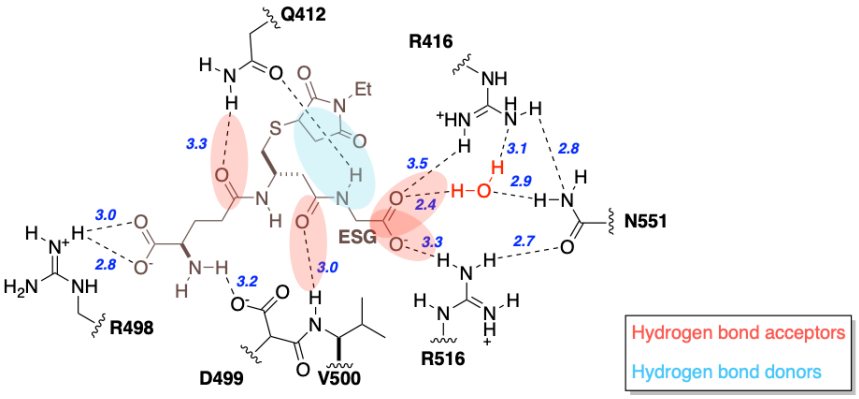
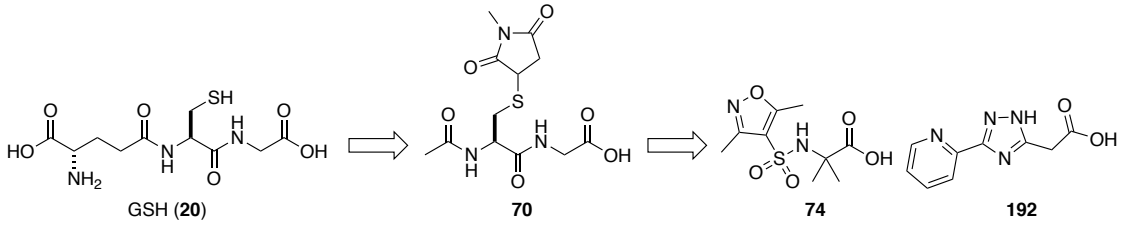


Figure 5.4. Figure showing ESG in the Kef binding site with potential hydrogen bonding interactions. Hydrogen bonds (quoted in Å in blue) required from truncated dipeptide region of ESG shown above, as well as removal of the central amide bond between the cysteine and glycine amino acids. Reproduced and adapted with permission from Roosild, T. P.; Castronovo, S.; Healy, J.; Miller, S.; Pliotas, C.; Rasmussen, T.; Bartlett, W.; Conway, S. J.; Booth, I. R. *Proc. Natl. Acad. Sci.* **2010**, *107*, 19784–19789.[128]

For stage 3 the results were ranked via the Tanimoto coefficient to their similarity to GSH, and prioritised *via* visual inspection to leave 35 compounds that satisfied 3–5 of the donor/acceptor interactions, and did not clash with the receptor. The results were manually inspected, and the most synthetically attractive hit (**74**) was selected for synthesis (Figure 5.5.). This ligand was generated from ROCS, a programme that screens databases against ligand shape.

A



B

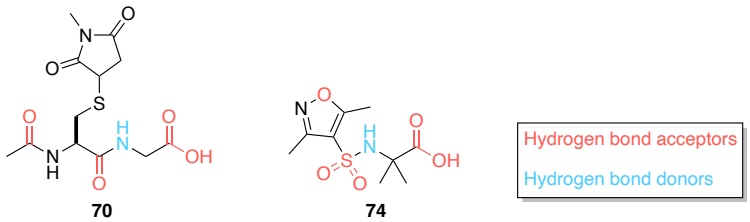


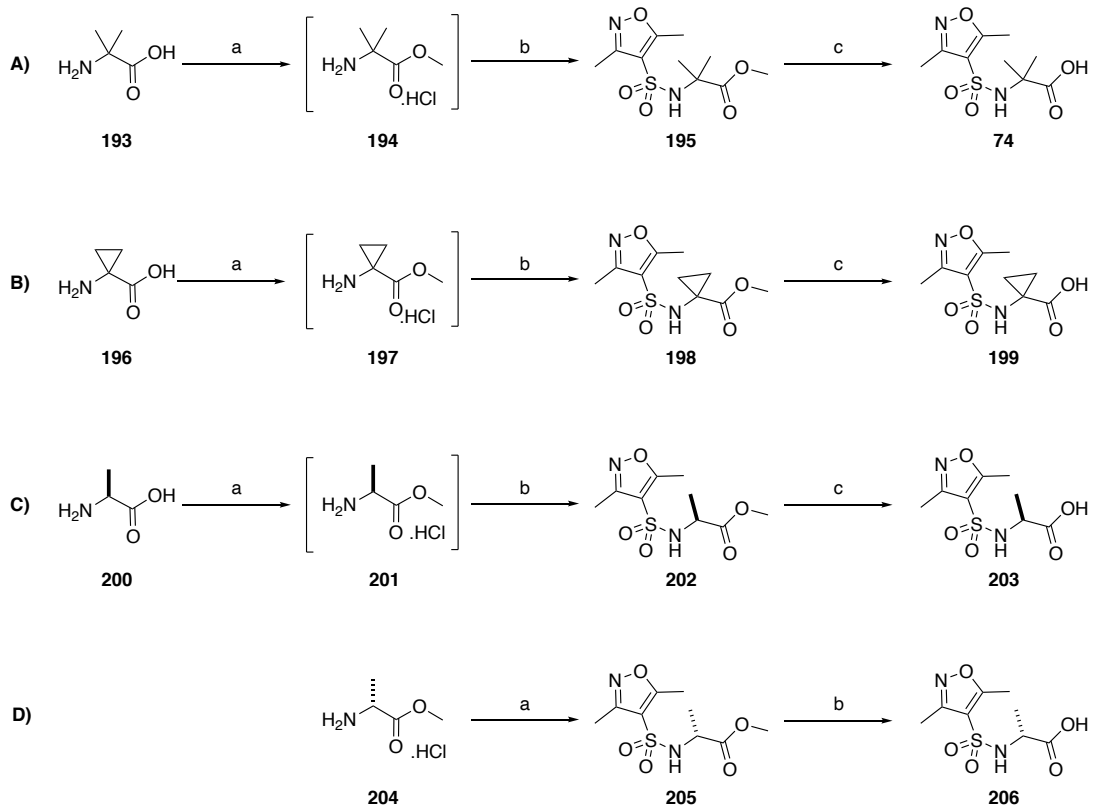
Figure 5.5. Examples of scaffold-hopping predicted structures derived from GSH and dipeptide 70 within *Ec*KefQCTD. A) Illustration showing how the structures were derived. Ligand **74** was chosen for synthesis as a synthetically attractive hit. B) Diagram of **74** with **70** showing the pharmacophore it mimics, including the hydrogen bond donors and acceptors in the backbone (blue and red).

The structure was predicted to make all five hydrogen bond donor and acceptor interactions made by the dipeptide backbone (Figure 5.3, 5.4), had no central amide

bond, and did not clash with the receptor excluded volume. The synthesis of three analogues of **74** was planned to explore the SAR within the glycine derived portion of **70**. The dimethyl groups may aid the structure in adopting the preferred conformation for binding, and analogues would identify if ligand affinity could be increased through further steric exploration of the active site. It is known that the (*R*)-enantiomer at the cysteine amino acid in **70** and ^{t}BuSG causes activation of Kef, whereas the (*S*)-stereochemistry cannot bind.[153] It was decided to investigate the effect of simple alkyl substitutions (one or two methyl groups, and a cyclopropyl ring) in the glycine portion of the scaffold-hopped molecule **74.** This would help to gain further understanding of what substituents are tolerated by *Sd*KefQCTD.

5.3 Synthesis of the Selected Dipeptide Mimic, 74

The dimethyl, cyclopropyl, (*R*)- and (*S*)- methyl analogues were synthesised to investigate the importance of the stereogenic centre next to the sulfonamide, (Scheme 5.1). The synthesis of **74** is three steps from the starting amino acid **193**, to give the carboxylic acid required for binding. The first step is a methyl esterification of the amino acid, followed by a coupling reaction to give the sulfonamide. Finally, a hydrolysis gave the carboxylic acids **74**, **199**, **203**, and **206**.



Scheme 5.1. Synthesis of the chosen dipeptide mimic 74 and analogues. A) *Reagents and conditions:* a) TMSCl, MeOH, RT; b) i) NEt_3, THF, RT, 22 h, ii) 2,5-Methyl-4-isoxazolesulfonyl chloride, RT, 14–24 h 26%; c) LiOH, THF/MeOH/H_2O 3:2:1, 22–24 h, 95%. B) *Reagents and conditions:* a) TMSCl, MeOH, RT; b) i) NEt_3, THF, RT, 22 h, ii) 2,5-Methyl-4-isoxazolesulfonyl chloride, RT, 14–24 h 24%; c) LiOH, THF/MeOH/H_2O 3:2:1, 22–24 h, 60%. C) *Reagents and conditions:* a) TMSCl, MeOH, RT; b) i) NEt_3, THF, RT, 22 h, ii) 2,5-Methyl-4-isoxazolesulfonyl chloride, RT, 14–24 h 73%; c) LiOH, THF/MeOH/H_2O 3:2:1, 22–24 h, 65%. D) *Reagents and conditions:* a) i) NEt_3, THF, RT, 22 h, ii) 2,5-Methyl-4-isoxazolesulfonyl chloride, RT, 14–24 h 59%; b) LiOH, THF/MeOH/H_2O 3:2:1, 22–24 h, 69%.

To install the methyl ester a robust method using trimethylsilylchloride (TMSCl) and methanol was used,[277] which gave complete conversion from the corresponding acid **193** (Sigma Aldrich, CAS: 62-57-7), **196** (Fluorochem, CAS: 22059-21-8), and **200** (Fluka, CAS: 56-41-7). These protected amino acids were then coupled with the sulfonyl chloride (Fluorochem, CAS: 80466-79-1). Under the literature conditions,[278] using DCM as a solvent, solubility problems with **194**, **197**, **201**, and **204** (Fluorochem, CAS: 14316-06-4) were encountered leading to no reactivity. Several different solvent and base combinations were investigated to find a suitable set of conditions (see Table 5.1.), that were effective for all coupling reactions.

Table 5.1. Summary of conditions screen to couple the sulfonyl chloride and amino acid.

Entry	Base	Solvent	Time /h	Outcome
1	Imidazole, 2 eq.	DCM	19	Imidazole adduct only
2	NEt_3, 2 eq.	DCM	7	6% desired product
3	NEt_3, 3 eq.	THF	72	30% desired product
4	NEt_3, 3 eq.	DMF	72	Not desired product
5	Pyridine, 3 eq.	DCM	72	Not desired product

Firstly, addition of imidazole (Table 5.1, entry 1) was investigated to attempt to activate the sulfonyl chloride for addition of the amino acid. However, the reaction did not go to completion, and only the sulfonyl imidazole adduct was isolated after purification with silica flash column chromatography. Repeating the literature conditions, with a second equivalent of triethylamine (Table 5.1, entry 2) to fully liberate the free amine from the hydrochloride salt, also resulted in an incomplete reaction with a poor 6% yield. To investigate if poor solubility in DCM was causing poor reactivity, THF was used (Table 5.1, entry 3) which visibly showed that the sulfonyl chloride was undissolved. However, after TLC analysis showed consumption of the sulfonyl chloride, there was a 30% yield of the desired product isolated. DMF was investigated to dissolve the sulfonyl chloride (Table 5.1, entry 4), and visually looked to have dissolved everything. However, the isolated crude mixture did not resemble the desired compound, this could be due to competing side reactions with contaminating dimethylamine from DMF. The compound of interest was not identified in the crude ^{1}H NMR. Finally, using pyridine as a base (Table 5.1, entry 5) also did not give the desired compound. The conclusions from this brief screen were that THF/ triethylamine conditions were the most suitable for the coupling reaction.

The coupling reaction forming the sulfonamides gave very variable yields (24–73%, Scheme 5.1) depending on the substrate, likely due to the varying steric demands of the

esters. An unexpected poorer yield of 59% was obtained for the coupling to form **205** compared to 73% for **202**, possibly due to impure starting material. The purchased starting material **204** showed some additional peaks in its ^{1}H NMR spectrum. Once these esters (**195**, **198**, **202**, and **205**) had been obtained they were hydrolysed to the corresponding acids (60–95%, Scheme 5.1) using lithium hydroxide in a polar solvent mixture. In summary, the carboxylic acid compounds **74**, three analogues **199**, **203**, and **206**, and the corresponding methyl esters were synthesised and obtained in sufficient purity to test in biophysical assays.

5.4 Biophysical and Cell-Based Assays

To assess whether the scaffold-hopped ligands were capable of binding and activating *Sd*Kef, they were tested in WaterLOGSY NMR assay,[216] and the Kirby-Bauer Disc assay.[163] WaterLOGSY identifies whether a ligand can weakly bind to *Sd*KefQCTD and the Kirby-Bauer disc assay can show the effect of ligand binding on the growth of *E. coli* cells expressing a protein of interest.

5.4.1 WaterLOGSY

WaterLOGSY was suitable as an initial assay to explore binding potential as it can detect weak ligands that bind with low micromolar affinity (section 2.3.1).[216] The ligands **74**, **199**, **203**, and **206** would be expected to be weakly binding as they are fragment based, and so waterLOGSY is a suitable screening assay for these ligands. The positive control used is a known binder (Figure 5.6), the dipeptide **58** .[145,153]

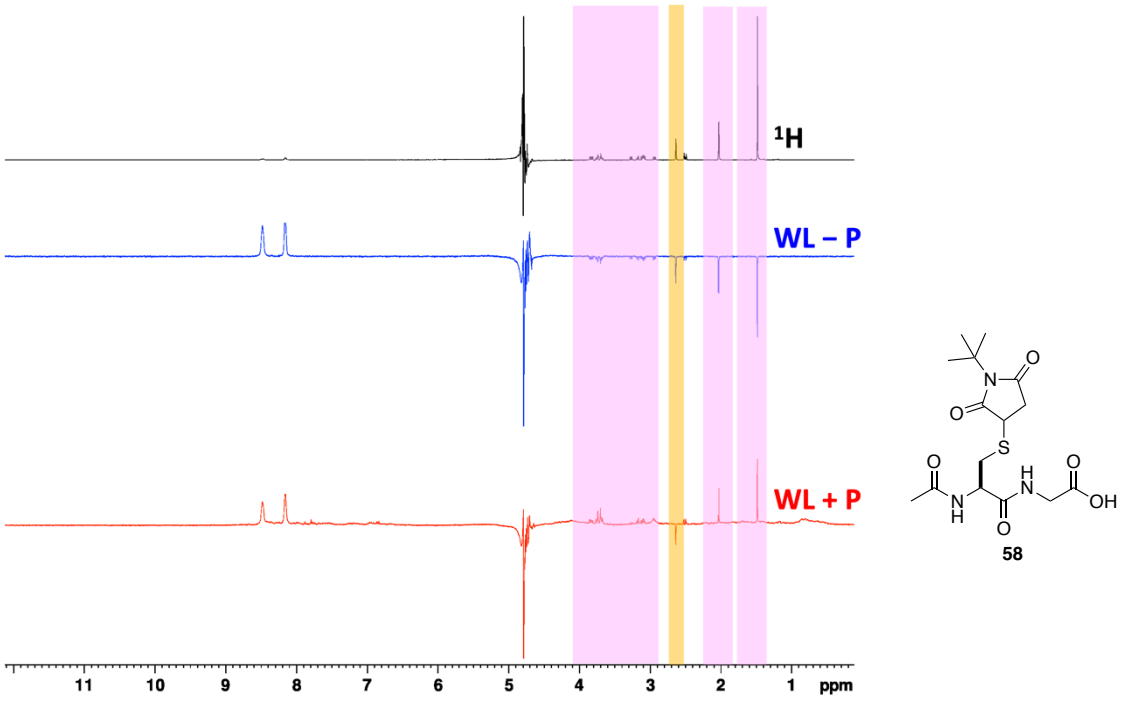


Figure 5.6. WaterLOGSY spectra stack of a positive control, 58. Stack top to bottom: ^{1}H, water-suppressed ^{1}H spectrum; WL–P, WaterLOGSY without protein present; WL+P, the compound with the protein of interest *Sd*KefQCTD. The area highlighted in yellow is DMSO at 2.5 ppm, and the compound peaks of interest are highlighted in pink.

The positive control experiment (Figure 5.6) shows the characteristic inversion of compound peaks compared to DMSO, as expected for a known binder. The spectra for the ligands **74, 199, 203, 206** (Figure 5.7) show no characteristic inversion of ligand peaks (pink) relative to DMSO (yellow), and so it can be concluded that these ligands show no observable binding to Kef.

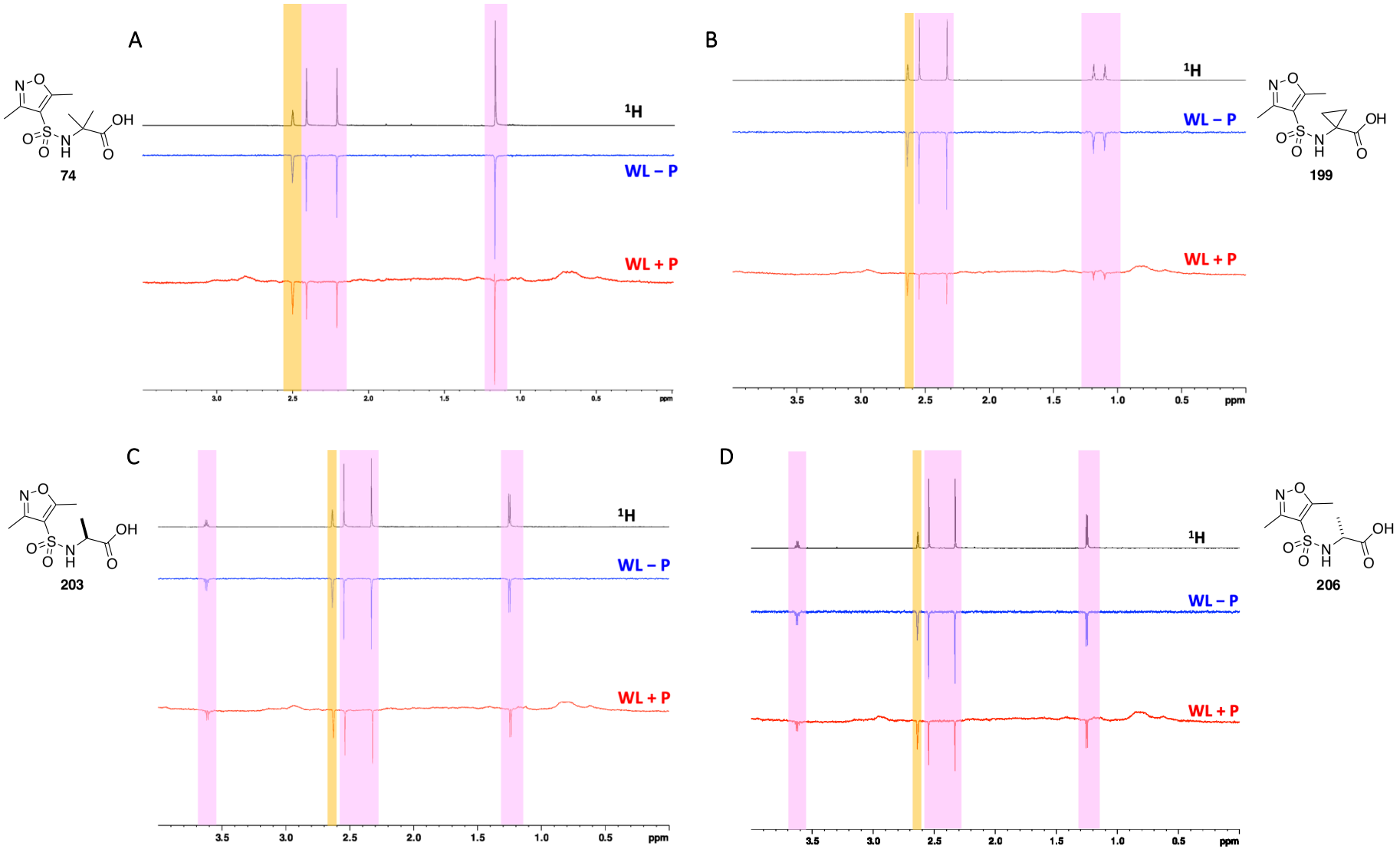


Figure 5.7. WaterLOGSY figures of the four scaffold-hopped ligands. **74** is the predicted structure, and **199**, **203**, and **206** are analogues. Stacks top to bottom: ^{1}H, water-suppressed ^{1}H spectrum; WL–P, WaterLOGSY without protein present; WL+P, the compound with the protein of interest *Sd*KefQCTD. The four ligands do not show the characteristic inversion of binding.

5.4.2 Kirby-Bauer disc assay

The compounds designed from the scaffold hopping **195**, **198**, **202**, and **205** were tested in an orthogonal cell-based assay. The Kirby-Bauer disc assay assesses whether the compound of interest inhibits the growth of the bacterial strain spread on the plate.[163] The bacteria expressing the protein of interest are streaked across an agar plate containing an antibiotic. The plasmid for the protein of interest also confers resistance against this antibiotic. Paper discs impregnated with a solution of the test compound are placed on the plate, and after a 24 h incubation period the inhibition zones are measured around the discs where the bacteria could not grow (Figure 5.8). It has been previously established that activation of over-expressed Kef in *E. coli* is bacteriostatic.[149] It has been shown compounds that activate Kef create a zone of inhibition around the disc impregnated with compound solution.[149,153]

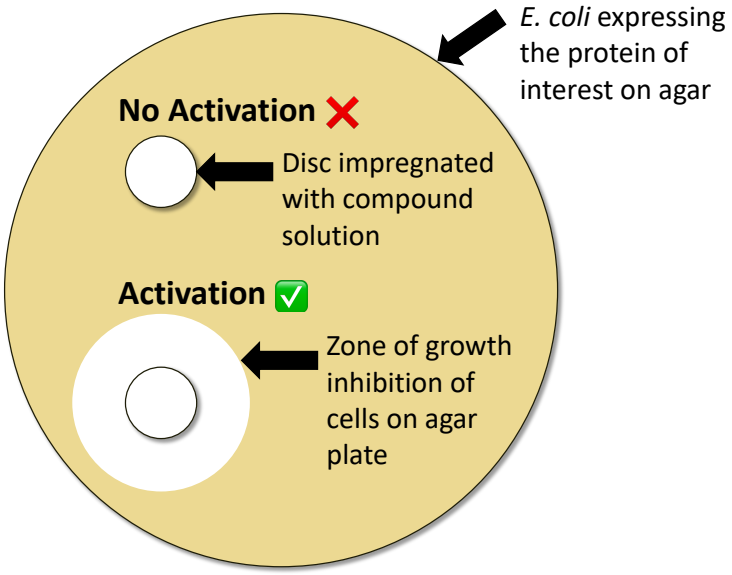


Figure 5.8. Diagram of the Kirby-Bauer disc assay illustrating an activating and non-activating Kef ligand effect on bacterial growth.

For the purposes of this assay, the *E. coli* strain MJF645 (supplied by Dr Catherine Haslam) was used which lacks chromosomal Kef systems *kef*F, *kef*C, *kef*G, *kef*B, and glutathione biosynthesis gshA.[145] This would assess whether the effects are only as a result of the plasmid-containing

Kef system without the native *E. coli* Kef systems. The removal of glutathione biosynthesis will allow weak ligands to bind without needing to out-compete the high internal GSH concentration in the cell. The cells over-express either the *Sd*Kef system using IPTG as a promoter (pTrc*Sd*KefH_6 plasmid), or the *E. coli* KefFC system (pKc11) which already contains a promoter. The ampicillin resistance gene is present in both plasmids and was used to select colonies during the transformation. (Summary of plate set up, Table 5.2.). Over-expression of Kef by the chosen cell line is hypothesised to make identification of a weakly binding, new ligand class easier.

Table 5.2. Summary of plasmids and corresponding agar additives used for the disc assay, Key: + = included, – = not included.

Plate number	Host	Plasmid	IPTG	Ampicillin
1, 4	MJF645	pTrc*Sd*KefH_6	+	+
2, 5	MJF645	pkC11	–	+
3, 6	MJF645	none	–	–

The bacteria were exposed to a disc impregnated with each of the methyl esters (**195**, **198**, **202**, and **205**) and the inhibition zones were measured after a 24 h incubation period (see Figure 5.9). The methyl ester compounds are used as they are more likely to be cell-permeable, and the peptide carboxylic acids are not.[161]

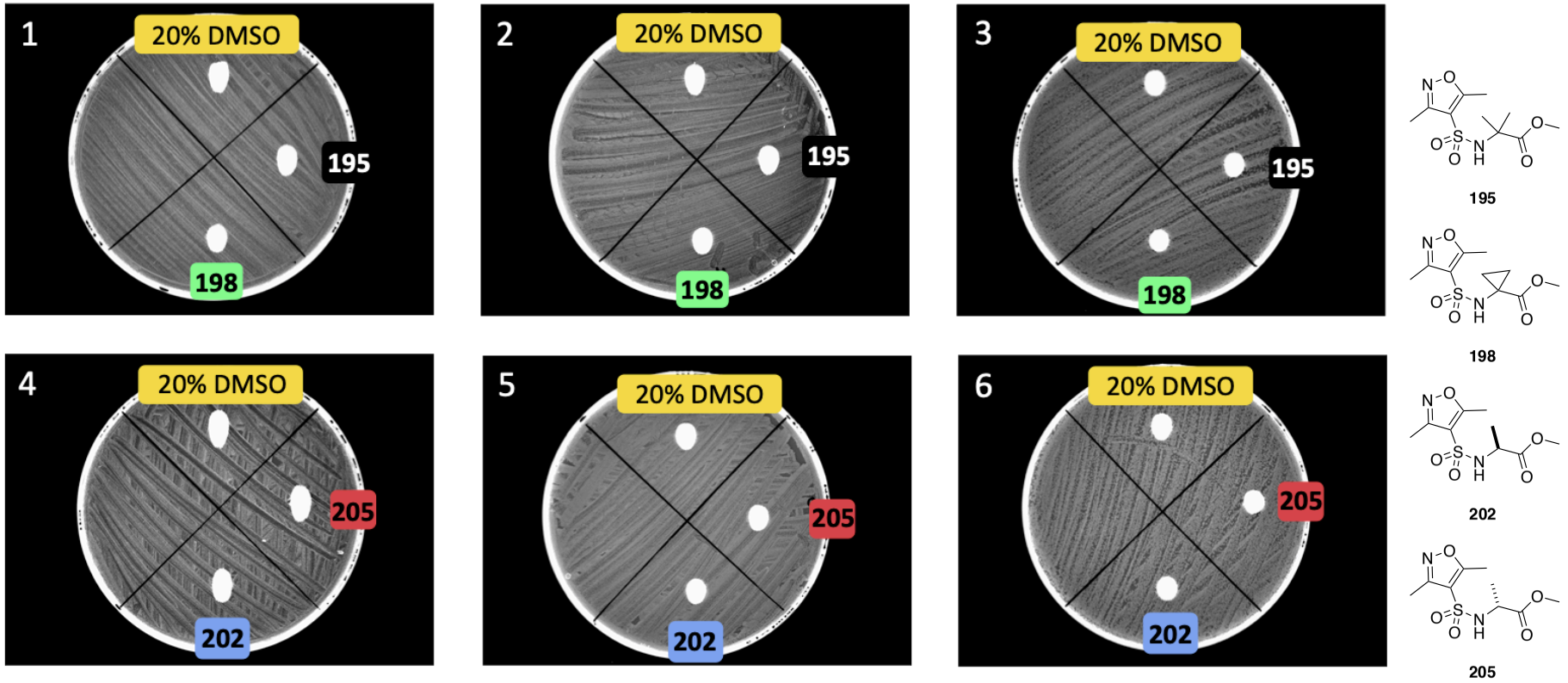


Figure 5.9. Kirby Bauer disc assay plates of *E. coli* expressing different Kef systems, and disc containing compounds of interest. Discs all have diameters of 6 mm with no zones of inhibition. Plates 1,4 *Sd*Kef, plates 2,5 *Ec*KefFC, plates 3,6 no Kef system.

The results show that the compounds are unable to activate Kef. A negative control of 20% DMSO in water is also added to an area of each of the plates, which also shows no effect. A negative control *E. coli* with no plasmid (and therefore no Kef systems) showed there was not an off-target effect resulting in inhibition of cell growth. A positive control was not run for this assay so limited conclusions can be drawn, as it is possible the Kef systems are not expressing correctly which could be a reason for seeing no growth inhibition.

5.5 Conclusions

A new ligand backbone was identified using scaffold hopping that was predicted to bind to the Kef protein. The ligand was synthesised, along with three analogues that explored some SAR around the new ligand scaffold. With the methyl ester compounds and carboxylic acids yielded in sufficient purity to test, the carboxylic acids were assessed using waterLOGSY NMR assay. The compounds did not appear to bind to *Sd*KefQCTD. The methyl esters were then tested on cells in the Kirby-Bauer disc assay but did not show evidence that they were able to activate the Kef systems, and therefore did not inhibit the bacterial growth. This result is unsurprising as these compounds were scaffold hopped from the dipeptide backbone only that is based on GSH which is a low affinity inhibitor. The waterLOGSY results suggested the compounds were either too low affinity for binding to be detected or did not bind.

Scaffold hopping is a valid technique for the generation of new ligand scaffolds, however this was preliminary work in the context of this research, and was unsuccessful in the

generation of a new ligand scaffold. To improve this method of scaffold discovery for activating *Sd*Kef ligands, the headgroup should be included in the query as a starting scaffold. Using a higher affinity scaffold as a starting point is a revised approach to generate ligands that would be sufficiently high affinity, and therefore detectable, with the binding assays available. After generating a list of new hits there should be improved refinement of the results. The scoring method used could be improved by ranking compounds according to a more important property or set tighter boundaries for the steric and electronic characteristics to match the dipeptide more closely. Docking experiments performed on the hit compounds would have further refined the existing hits and may have identified a scaffold with a higher affinity for Kef.

Chapter Six: Conclusions and Future Work

6.1 Conclusions

The aim of this research was to identify a novel, peptide mimetic scaffold for the Kef system. Previous work had identified **70** (Figure 6.1) as the minimal structural requirement for activation of the Kef system.[153] This compound is derived from known activators of the Kef system including ^{t}BuSG and ESG (Figure 6.1).

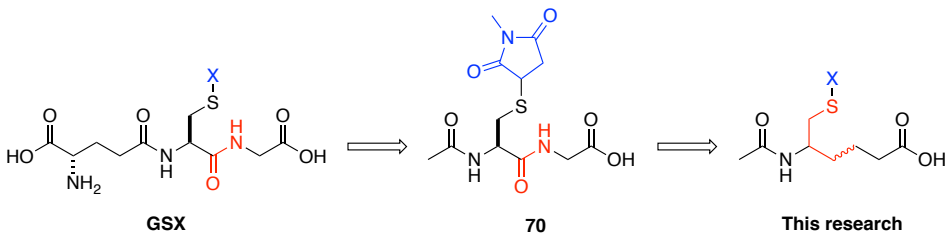


Figure 6.1. Structures of GSX, 70, and simplified target structure for this research. The amide bond, and the future replacement is shown in red, and the headgroup is shown in blue.

This research investigated replacement scaffolds to remove the central amide bond and reduce the peptide-like characteristics from Kef ligands. Three new ligand scaffolds: **71**, **72**, **73**, and one identified from scaffold hopping **74** (Figure 6.2) were synthesised and evaluated in biophysical assays for binding to the *Sd*KefQCTD system.

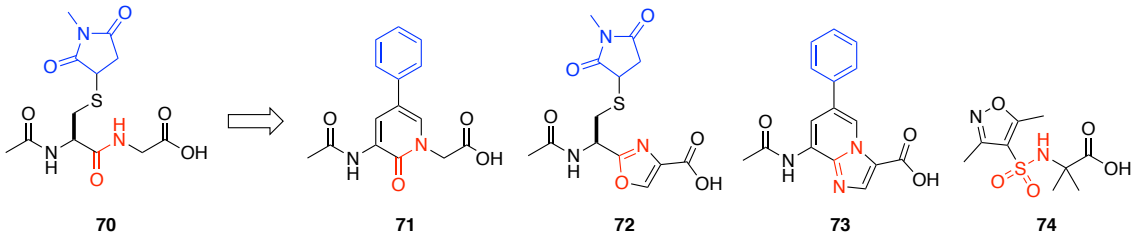


Figure 6.2. Structures synthesised during this work as potential replacement scaffolds for dipeptide 70. The amide bond replacement is shown in red, and the headgroup is shown in blue.

Chapter 2 summarises the synthesis and testing of the pyridinone ligand, **71**. The ligand was synthesised *via* a short route to a common intermediate, which was used in robust

coupling conditions to install 16 different headgroups, of which a further 10 were hydrolysed to give the desired carboxylic acid binding species. These carboxylic acids were then tested in waterLOGSY and DSF assays and found to bind to the *Sd*KefQCTD system. Previous research identified larger, bulkier, headgroups showed the most stabilisation of the protein *via* DSF,[145] and this finding was consistent with these results. Using DSF a mixture of stabilising and destabilising head groups were identified. This could be due to an alternative binding mode of the pyridinone backbone, off target binding to the protein, or a different conformational change than the displacement of the *Sd*KefQCTD capping residue. This SAR information will help to direct the design of future pyridinone Kef ligands, the most promising ligand was **122** (Figure 6.3), which showed binding and the greatest stabilisation of *Sd*KefQCTD *via* waterLOGSY and DSF of the series.

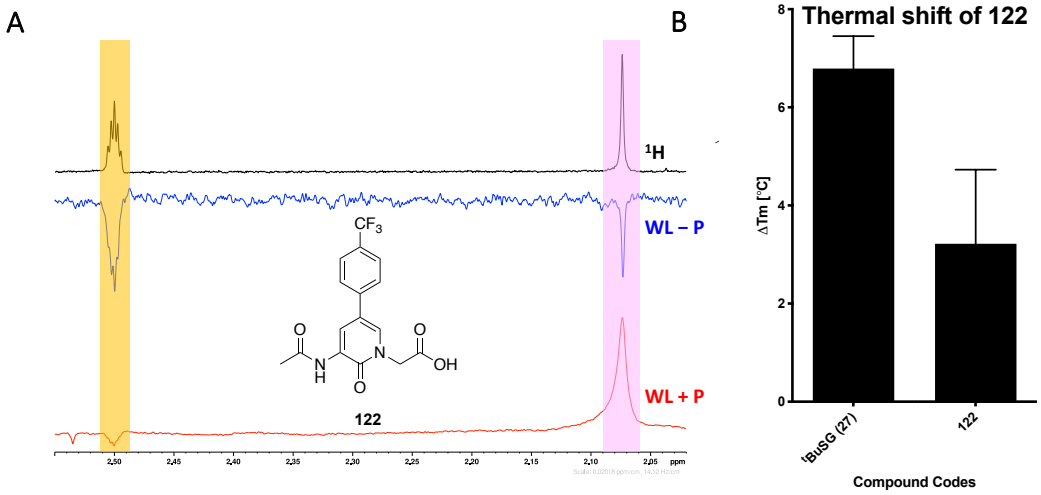


Figure 6.3. Biophysical assay results of 122. A) Expanded section of the waterLOGSY spectrum of **122.** Stack top to bottom: ^{1}H, water-supressed ^{1}H NMR of **122**; WL–P, waterLOGSY spectrum without protein; WL+P, waterLOGSY spectrum with *Sd*KefQCTD protein. DMSO is highlighted at 2.50 ppm in yellow and is the sample reference. The compound peak of interest is highlighted in pink. B) DSF results of **122**. ^{t}BuSG was used as a positive control.

NMR titration experiments to determine K_d were run with **71** but were unsuccessful as there was no trackable broadening or line width change for the observed peak. **122** was used in ^{19}F NMR titration experiments to determine K_d, an unexpected non-linear profile

was obtained, and thus this technique was not suitable for K_d determination. Despite this, the pyridinone is a suitable scaffold for a peptide mimetic for *Sd*KefQCTD, and future SAR exploration is possible. The pyridinone scaffold is the first non-peptide ligand identified for the Kef system. An alternative technique to NMR to obtain quantitative binding data will be the subject of future work. Novel NMR binding data including the first waterLOGSY results of **70**, **58**, and ^{t}BuSG (see appendix for full spectra) was also obtained as a result of this work.

Chapter 3 summarises the synthesis and testing of the oxazole scaffold ligand **72**, and the negative control **165**. The ligand was synthesised *via* an optimised literature based route to form the heterocyclic backbone from the dipeptide, followed by the deprotection and decoration of the ligand core. This route proved non-trivial when the final ester deprotection step resulted in either no reactivity or degradation of the starting oxazole. The synthesis was repeated with a benzyl ester protection group which provided a mild method of deprotection using TMSI (Figure 6.4) to obtain **72**, and this route was repeated to form the opposite enantiomer **165**.

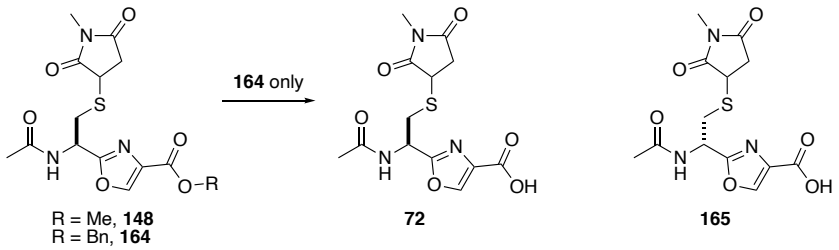
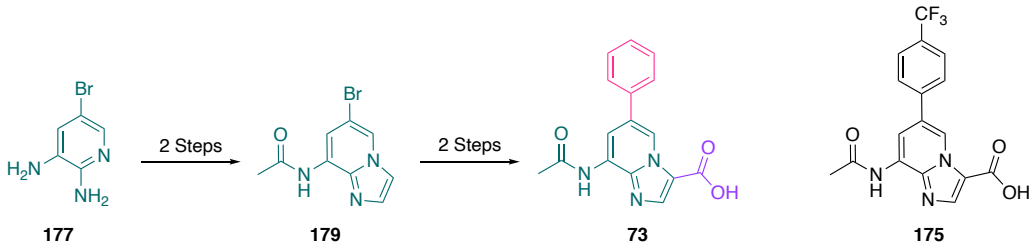


Figure 6.4. Summary of ester hydrolyses to form 72. 148 could not be hydrolysed successfully, while TMSI was able to deprotect **164** to give the desired carboxylic acid compound **72**. The opposite enantiomer **165** was synthesised from the same route.

Neither **72** and **165** were found to bind to *Sd*KefQCTD following investigation with waterLOGSY and DSF. This was an unexpected result as **72** had the smallest structural change from **70** out of the new scaffolds, including retention of the (*R*)-stereogenic centre

that is key for binding derived from the cysteine portion of the molecule. It is possible there was some degradation of this stereocentre, and analysis using chiral HPLC should be the subject of future work. As expected **165** did not bind, but because **72** also did not bind when expected, other factors (such as the new ligand shape and electronics) cannot be ruled out. The oxazole is not a suitable dipeptide mimetic ligand for *Sd*KefQCTD, as no binding of **72** was observed in two orthogonal assays. This could be due to the reduced flexibility in the ligand backbone, or the conformation of the ligand in solution meaning it cannot adopt the required pose required for binding. Computational analysis of **72** may help elucidate any structural changes that could increase affinity for the Kef system and should be the subject of future work.

Chapter 4 summarises the synthesis and testing of the imidazopyridine peptide mimetic scaffold, **73**. The synthesis of the ligand started with the cyclisation to form the bicyclic core, followed by the incorporation of the desired headgroup, and finally installation of the carboxylic acid. This route was less efficient than the synthetic routes for the other two scaffolds (**71** and **72**). The last common intermediate did not include the completed backbone before the installation of the headgroup, and so additional steps to complete the backbone could not be performed on large scale.



177 179 73 175

Figure 6.5. Summary of the synthesis route of 73 *via* the imidazopyridine core 179. The core is coloured green, with the final two steps of the coupling of the headgroup shown in pink, and the hydroxycarbonylation product coloured purple. The CF_3 containing ligand of interest **175** is also shown, for which the synthesis will be the subject of future work.

A more efficient route would install the headgroup as the final step, as for the pyridinone synthesis, which would be the subject of future work (Figure 6.5). The imidazopyridine scaffold was shown to be a suitable peptide mimetic ligand for *Sd*KefQCTD from biophysical assays, **73** bound during waterLOGSY experiments and showed slight stabilisation of the protein in DSF. This provides evidence that the scaffold can bind albeit weakly to the *Sd*KefQCTD, and the imidazopyridine is the second non-peptide scaffold identified as a ligand for the Kef system as a result of this work. To establish some SAR for this ligand series, synthesis of different headgroup analogues of **73** and testing in biophysical assays will be the subject of future work. For quantification of binding, completion of the synthesis of **175** would enable ^{19}F NMR studies, if the ligand binds in a non-linear way similar to **71**, an alternative technique such as ITC may be necessary.

Chapter 5 utilised scaffold hopping to identify a new non-peptide scaffold for ligands for the *Ec*Kef system. Various databases were searched for electronic and structural mimics of the backbones of **70** and GSH, and the top hits filtered by the desired pharmacophore. The pharmacophore included the key hydrogen bonding interactions, and structural clashes with the protein. The most synthetically attractive hit **74** was identified and synthesised, along with analogues exploring the stereochemistry at the glycine portion of the molecule (**199**, **203**, and **206**). The four compounds and their corresponding methyl

esters were tested in biophysical and cellular assays, but not found to bind to *Sd*KefQCTD in waterLOGSY, and did not inhibit cell growth of *E. coli* overexpressing *Sd*Kef in the Kirby-Bauer disc assay.

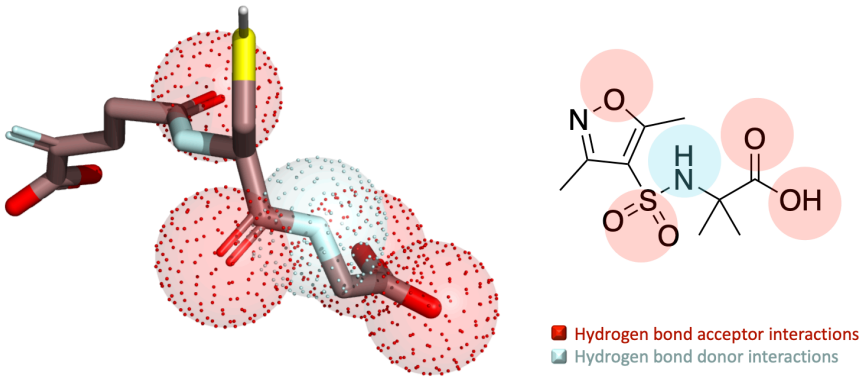


Figure 6.6. 3D-GSH showing a diagram of the dipeptide derived pharmacophore used in the selection process with MOE, alongside 74 with pharmacophore marked on the structure. Hydrogen bond acceptor interactions are shown in red, and hydrogen bond donor interactions are shown in blue.

The structures used were scaffold hopped from the dipeptide backbone, which is derived from the GSH backbone, a low affinity inhibitor of the Kef system. This structure may have been too low affinity as a starting point to generate a comparable affinity binder. Use of the full dipeptide with headgroup such as **70** or **58** for scaffold hopping may have generated a hit with higher affinity for the Kef system and will be the subject of future work. Selection of a higher affinity hit compound may also have been aided by more extensive screening or ranking and use of docking experiments with *Ec*Kef with the most promising hits would generate a better candidate for a non-peptide Kef ligand. Tighter constraints around the electronic or structural properties of the ligand backbone could identify compounds that were a closer mimic of the dipeptide.

6.2 Future Work

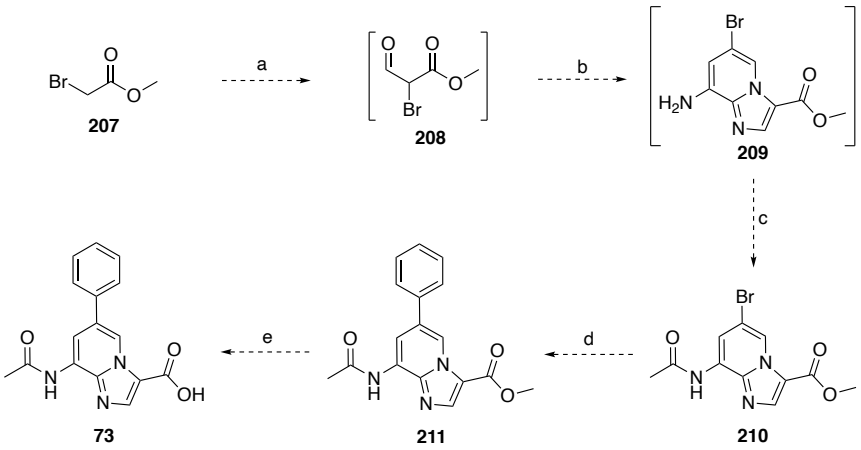
From this research, two scaffolds have been identified that constitute a novel series of peptide mimetic Kef ligands: the pyridinone and the imidazopyridine ligands. The oxazole and scaffold-hopped structure were not suitable peptide mimetics for this system.

The pyridinone ligands are the most promising non-peptide ligand series identified currently. For the next stage of their development as a ligand series, quantification of the binding is a priority. A fluorescence based competition assay was developed for the *Sd*KefQCTD system and is capable of detecting low micromolar ligands,[158] which is the approximate affinity typically detectable through waterLOGSY. Fluorescence could provide a suitable alternative to NMR measurements, as it has been used for K_d calculation on the *Sd*Kef system. ITC is has also been employed for the quantification of binding ligands to the Kef system,[153] and may provide an alternative method to fluorescence. Quantification of the affinity would allow ranking of the pyridinone ligands, thus directing the design for a higher affinity second-generation of pyridinone ligands. Conclusion of the synthesis of a pyridinone with a succinimide headgroup would investigate the contribution of the pyridinone backbone to binding to *Sd*Kef, providing an opportunity for comparison with peptide-ligands containing this head group.

To determine why the oxazole moiety is not currently a suitable peptide mimetic, computational analysis of this structure should be performed. It is not yet understood why **72** was unable to bind to the Kef system, and chiral HPLC analysis of possible degradation of the stereocentre will be carried out. Future work should include docking

experiments with the *Ec*Kef system, to help identify possible binding poses of **72**. Molecular dynamics (MD) experiments could be used to evaluate the stability of these poses in the binding site. Following the identification of the optimal **72** binding pose, opportunities to increase the affinity may be identified through new polar/hydrophobic interactions or removing structural clashes. These experiments may be non-trivial because of the known conformational change of the Kef protein as a result of ligand binding and displacement of the capping residue.

To progress the investigation of the imidazopyridine ligand, a more efficient synthesis should be developed. The current route for **73** performs the differentiating headgroup installation step before completion of the backbone, reversing this would allow for improved scale up. The following route is proposed (Scheme 6.1) for future work.



Scheme 6.1. Alternative proposed synthesis of 73. *Reagents and conditions*: a) i) LDA, THF, −78 °C, ii) Ethyl formate, −78 °C to RT;[279] b) 2,3-Diamino-5-bromopyridine, *n*-butanol, 100 °C;[280] c) Ac_2O, DMAP, Py, NEt_3, DCM, 30 °C; d) Phenyl boronic acid, Pd[dppf]Cl_2, Cs_2CO_3, toluene, 90 °C; e) Lithium hydroxide, THF/MeOH/H_2O 3:2:1. This route is the same length (five steps) as the current synthesis but is an improvement in several ways.

The route outlined in Scheme 6.1 would synthesise the entire imidazopyridine backbone on large scale (**207** to **210**) with fewer small-scale steps making the overall route more efficient. This route also has three telescoped steps (Scheme 6.1, a–c) before purification,

rather than after the second step as in the current procedure (Chapter 4, Schemes 4.4, 4.5). Finally, this route removes the iodination step, which although improved from 12–15% to 66–68%, does not give a high yield.

Following the optimisation of the imidazopyridine route, concluding the synthesis and testing of the CF_3 and *tert*-butyl containing ligands **175** and **176**, as well as a series of analogues will be the subject of future work. This will allow further investigation of the SAR of the imidazopyridine as a peptide mimetic Kef ligand.

Testing of the three ligands **71**–**73** in a cell-based assay such as the Kirby-Bauer disc assay is also of interest for future work. It has been established that examples of the pyridinone and imidazopyridine ligand series can bind to *Sd*KefQCTD in biophysical assays. Investigating the effect of **71** and **73** on the growth of bacteria expressing a Kef system is the next step in validating the mechanism of action of these scaffolds, and would provide further evidence for the inability of **72** to bind to *Sd*Kef. This work was not completed due to time constraints.

Extension of the scaffold hopping search, and further refinement of the hits will also be the subject of future work. To improve the affinity of the scaffold, the database search for a structure match would be based upon the dipeptide backbone and headgroup **70** or **58**, as the headgroup provides a significant portion of the binding affinity to the Kef system (GSH K_d = 900 ± 200 µM, ^{t}BuSG K_d = 0.4 ± 0.2 µM). Following the generation of new hit compounds, the refinement process should be subject to improvement. Stricter requirements for the pharmacophore will be set, controlling this will help identify

compounds that are closer mimics of the pharmacophore electronics and structure. The new hit compounds will better fulfil the required hydrogen bonding interactions made by the peptide backbone. To evaluate the molecules identified from the scaffold hopping and ranking, docking experiments with *Ec*Kef will further assess the proposed molecules suitability as Kef ligands.

This research has identified two new peptide mimetic scaffolds for the *Sd*Kef system, the pyridinone and imidazopyridine ligands. Future work will look to increase the affinity of ligands from these series and identify new scaffolds with the computational techniques described. Candidate ligands with high affinity will then be tested in cellular assays to assess whether there is any activation of the Kef system in over-expression mutants, followed by the wild type organisms. Further research on activators of the Kef system has the potential to develop a novel antibiotic treatment for Gram-negative bacterial infections with no known resistance mechanism. Peptide mimetic ligands have more flexible synthesis to improve their properties towards accumulation in Gram-negative bacteria, improved biophysical characteristics, and could offer a significant benefit to modern healthcare.

Chapter Seven: Experimental

7.1 General Chemistry Experimental

Reagents and solvents used were of commercially available reagent grade and were used without further purification, unless stated. All non-aqueous reactions were carried out under an argon atmosphere in a flame-dried flask. Anhydrous solvents were obtained from an MBRAUN Solvent Purification System 5 and stored under an argon atmosphere over 3 Å molecular sieves. Concentration *in vacuo* was performed at 40 ˚C for organic solvents using a Buchi™ rotary evaporator. Brine refers to a saturated aqueous solution of sodium chloride. Petroleum ether refers to the fraction of light petroleum ether boiling in the range 40–60 °C. Celite® refers to Celite® 545 filter aid, treated with sodium carbonate, flux-calcined (Sigma Aldrich).

Analytical Thin Layer Chromatography (using normal phase silica gel, NP TLC) was carried out on normal phase Merck silica gel 60 F254 aluminium-supported thin layer chromatography sheets. Visualisation was by absorption of UV light (λ_{max} 254 nm) or thermal development after staining in an aqueous solution of potassium permanganate, or ethanolic solution of ninhydrin.

Silica gel flash column chromatography was carried out manually on Merck Geduran® silica gel 60 (40–63 µm), eluting with solvents as supplied, under a positive pressure of compressed, gaseous N_2.

^{1}H NMR spectra were measured on a Bruker AV400 (400 MHz), Bruker DRX500 (500 MHz) or Bruker AVII 500 (500 MHz) spectrometer in the stated solvents as a reference for the internal deuterium lock. The chemical shift data for each signal are given as δ in units of parts per million (ppm) relative to tetramethylsilane (TMS) where δ(TMS) = 0.00. The spectra are calibrated using the solvent peak with the data provided by Fulmer *et al*.[281] The multiplicity of each signal is indicated by: s (singlet); d (doublet); t (triplet); q (quartet); m (multiplet) or combinations thereof. The number of protons (n) for a given resonance signal is indicated by nH. Where appropriate, coupling constants (*J*) are quoted in Hz, recorded to the nearest 0.1 Hz, and identical coupling constants are averaged. Where a mixture of diastereomers is observed they are assigned A and B, and these ABX systems and the corresponding coupling constants are labelled (H – 3''$_{x}$ and J_{AX}) in the reported ^{1}H NMR. Spectra were assigned using COSY, HSQC and HMBC experiments as necessary.

^{13}C NMR spectra were measured on a Bruker AVII 500 (126 MHz) or Bruker AV400 (101 MHz) spectrometer in the stated solvents as a reference for the internal deuterium lock using the standard ^{13}C experiment. The chemical shift data for each signal are given as δ in units of parts per million (ppm) relative to tetramethylsilane (TMS) where δ(TMS) = 0.00. The spectra are calibrated using the solvent peak with the data provided by Fulmer *et al*.[281] Signals are quoted to 1 decimal place unless peaks are indistinguishable, in which case 2 decimal places are used. Where a mixture of diastereomers is observed they are assigned A and B, with diastereomer A having a distinct resonance at the highest chemical shift.

^{19}F NMR spectra were recorded on a Bruker AVIII HD 400 (376 MHz) spectrometer in the solvent stated. Chemical shifts δ are quoted in parts per million (ppm), to the nearest 0.1 ppm. The multiplicity of each signal is singlet unless otherwise stated.

Mass spectra were acquired on either an Agilent 6120 (low resolution) or Bruker microToF spectrometer (high resolution) using electrospray ionisation (ESI) from solutions of methanol. *m/z* values are reported in Daltons and followed by their percentage abundance in parentheses.

Melting points were determined using a Griffin capillary tube melting point apparatus and are uncorrected. The solvent(s) from which the sample was crystallised is given in parentheses. For samples which decomposed, the decomposition point (d.p.) is reported.

Infrared spectra were obtained from neat samples, using a diamond ATR module. The spectra were recorded on a Bruker Tensor 27 spectrometer. Absorption maxima are reported in wavenumbers (cm^{-1}) and reported as s (strong), m (medium), w (weak), or br (broad).

Specific optical rotations were measured using a Schmidt Haensch Unipol polarimeter, using a sodium lamp at 589 nm and a path length of 1.0 dm at 25 °C. The concentration (c) is expressed in g/100 mL (equivalent to g/0.1 dm^3). Specific rotations are denoted $[\alpha]_D^T$ and are given in implied units of deg cm^2 g^{-1} (where T = ambient temperature in °C).

Analytical high performance liquid chromatography (HPLC) for methods 1–4 was carried out on a PerkinElmer Flexar system with a Binary LC Pump and UV/Vis LC Detector set at 220 nm or 254 nm. For determination of compound purity, a Dionex Acclaim reverse phase 120 column (C_{18}, 5 µm, 120 Å, 4.6 × 150 mm) was employed using a flow rate of 1.5 mL min^{-1} (methods 1–3) or an Atlantis T3 reverse phase column (C_{18}, 3 µm, 100 Å, 4.6 × 150 mm) using a flow rate of 1.0 mL min^{-1} (method 4). Samples were injected in methanol, or acetonitrile. A 'short run' (SR) or 'long run' (LR) method was used for each compound and the methods are described below:

Detail of the HPLC methods used to test the purity of the compounds.

Method	Start Time / min	End Time / min	Start % (A)	Finish % (A)
1	0	10	95	5
	10	15	5	5
2	0	20	95	5
	20	25	5	5

Mobile Phases: A = water, B = MeCN, wavelength 220 or 254 nm.

Method	Start Time / min	End Time / min	Start % (A)	Finish % (A)
3	0	10	95	5
	10	15	5	5
4	0	2	100	100
	2	15	100	5
	15	20	5	5

Mobile Phases: A = water + TFA (0.1%), B = MeCN + TFA (0.1%), wavelength 220 or 254 nm.

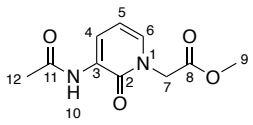
Method 5 was run on an agilent 1260 Infinity II fitted with a quaternary pump, vial sampler, DADWR, column chamber and an Agilent Infinity fraction collector at 220 nm and 254 nm. For analysis of compound purity an XBridge ($C_{18,}$ 5 µM, 4.6 × 150 mm) was employed using a flow rate of 1.0 mL min^{-1} (method 5). Samples were injected in methanol with up to 10% DMSO *v/v*.

Method	Start Time / min	End Time / min	Start % (A)	Finish % (A)
5	0	1	95	95
	1	11	95	5
	11	13	5	5
	13	14	5	95
	14	15	95	95

Mobile phases: A = H2O + TFA (0.1%), B = MeCN + TFA (0.1%), wavelength 220 and 254 nm.

7.2 Compound Synthesis Procedures and Data

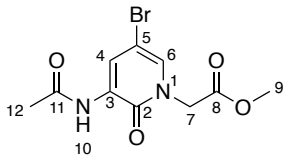
Methyl (3-acetamido-2-oxopyridin-1-yl)acetate, 82



Sodium hydride (60% dispersion in mineral oil, 600 mg, 15 mmol, 1.0 eq.) was added slowly to a stirred solution of 2-hydroxy-3-nitropyridine (2.5 g, 15 mmol, 1.0 eq.) in *N,N*-dimethylformamide (30 mL) at 0 °C and stirred for 30 min. Methyl bromoacetate (1.4 mL, 15 mmol, 1.0 eq.) was added to the reaction mixture and it was left to warm to RT. Complete consumption of the starting material was observed after 21 h following analysis by TLC, the mixture was concentrated *in vacuo* to approximately 5 mL remaining. The mixture was then diluted with ethyl acetate (100 mL). The organic component was washed with water (30 mL × 2) and brine (30 mL) and the organic components dried with magnesium sulfate, and concentrated *in vacuo* to afford the intermediate methyl (3-nitro-2-oxopyridin-1-yl)acetate (2.7 g) as a red residue. Methyl (3-nitro-2-oxopyridin-1-yl)acetate (2.7 g, 13 mmol, 1.0 eq.) and palladium on carbon (270 mg, 10% w/w) were stirred in methanol/tetrahydrofuran (3:1, 28 mL) under a hydrogen atmosphere. Complete consumption of the intermediate was observed after 2 h, was filtered through a syringe filter, and the solution concentrated *in vacuo* to afford the intermediate methyl (3-amino-2-oxopyridin-1-yl)acetate as a pale green residue which was assumed quantitative . The amine was dissolved in 28 mL of tetrahydrofuran (THF), followed by addition of dimethylaminopyridine (310 mg, 2.5 mmol, 0.20 eq.) and pyridine (2.0 mL, 25 mmol, 2.0 eq.). Acetic anhydride was added to the mixture (2.4 mL, 25 mmol, 2.0 eq.) followed by additional THF (28 mL) and the resulting mixture was

stirred under argon. Complete consumption of the amine was observed after 16 h, the reaction was quenched with water (20 mL) and concentrated *in vacuo*. The reaction mixture was diluted with ethyl acetate (150 mL) and washed with aqueous hydrochloric acid (1 M, 100 mL), water (100 mL) and brine (100 mL). The aqueous components were extracted with ethyl acetate (5 × 100 mL). The crude residue was purified by flash column chromatography on silica (ethyl acetate), to afford the title compound (1.6 g, 69% over two steps) as an off-white solid: R_f 0.35 (toluene/ethanol, 9:1); m.p. 144–145 °C (from toluene); $\tilde{\nu}_{max}$ (neat/cm^{-1}) 3261 (N-H, w), 1746 (C=O, m), 1689 (C=O, s), 1645 (C=O, s), 1589 (C=C, s), 1514 (C=C, s), 1371 (C-N, m), 1229 (C-O, s), 1209 (C-O, m), 772 (C-H, m), 751 (C-H, s); ^{1}H NMR (500 MHz, $CDCl_3$) δ 8.39 (1H, dd, *J* 6.5, 1.8, H - 6), 8.32 (1H, s, H - 10), 6.92 (1H, dd, *J* 6.5, 1.8, H - 5), 6.27 (1H, dd, *J* 6.5, 1.8, H - 4), 4.67 (2H, s, H - 7), 3.78 (3H, s, H - 9), 2.17 (3H, s, H - 12); ^{13}C NMR (126 MHz, $CDCl_3$) δ 169.5 (C-11), 168.1 (C-8), 157.8 (C-2), 130.4 (C-4), 129.8 (C-3), 122.9 (C-6), 107.5 (C-5), 53.2 (C-9), 51.4 (C-7), 25.1 (C-12). HRMS *m/z* (ESI$^+$) [Found: 247.06889, $C_8H_9N_2O_5$ requires [M+Na]$^+$ 247.06893]; LRMS *m/z* (ESI$^+$) 247 ([M+Na]$^+$, 39%); HPLC retention time 5.1 min (method 3), 98.5%.

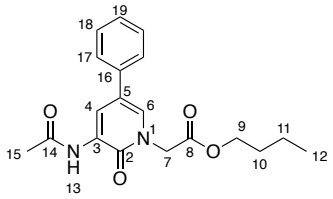
Methyl (3-acetamido-5-bromo-2-oxopyridin-1-yl)acetate, 91



N-Bromosuccinimide (480 mg, 2.7 mmol, 2.0 eq.) was added to a suspension of methyl (3-acetamido-2-oxopyridin-1-yl)acetate (300 mg, 1.4 mmol, 1.0 eq.) in DCM (6 mL) and the mixture stirred at RT. Complete consumption of the starting material was observed after 26 h following analysis by TLC, and the reaction mixture was concentrated *in vacuo*.

The residue was dissolved with ethyl acetate (30 mL) and washed with water (30 mL) and brine (30 mL) and then concentrated *in vacuo*. The crude mixture was purified by flash column chromatography on silica (chloroform) to afford the title compound (265 mg, 65%) as a brown solid: R_f 0.58 (ethanol 2% in chloroform); m.p. 168–169°C (from chloroform); $\tilde{\nu}_{max}$ (neat/ cm^{-1}) 3300 (N-H, w), 1739 (C=O, s), 1698 (C=O, m), 1644 (C=O, s), 1592 (C=C, m), 1515 (C=C, s), 1229 (C-N, s), 1190 (C-O, m), 774 (C-H, m); ^{1}H NMR (400 MHz, $CDCl_3$) δ 8.51 (1H, d, *J* 2.5, H - 6), 8.29 (1H, s, H - 10), 7.07 (1H, d, *J* 2.5, H - 4), 4.64 (2H, s, H - 7), 3.80 (3H, s, H - 9), 2.19 (3H, s, H - 12); ^{13}C NMR (101 MHz, $CDCl_3$) δ 169.2 (C-11), 167.3 (C-8), 156.3 (C-2), 129.8 (C-5), 129.6 (C-4), 125.3 (C-6), 99.9 (C-3), 53.1 (C-9), 51.0 (C-7), 24.8 (C-12); HRMS *m/z* (ESI^+) [Found: 324.97954 and 326.97745 $C_{10}H_{11}N_2O_4BrNa$ requires $[M+Na]^+$ 324.97944 and 326.97739]; LRMS *m/z* (ESI^+) 325 ($[M+Na]^+$, 100%, 327 ($[M+Na]^+$ 88%); HPLC retention time 6.7 min (method 3), 99.0%.

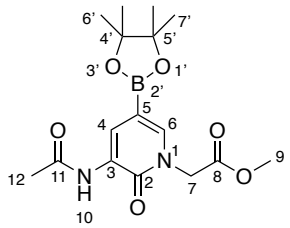
Butyl (3-acetamido-2-oxo-5-phenylpyridin-1-yl)acetate, 92



A mixture of methyl (3-acetamido-5-bromo-2-oxopyridin-1-yl)acetate (20 mg, 0.066 mmol, 1.0 eq.), phenyl boronic acid (8.9 mg, 0.073 mmol, 1.1 eq.), palladium diacetate (1.5 mg, 0.0066 mmol, 0.10 eq.), XPhos (3.2 mg, 0.0066 mmol, 0.10 eq.) and potassium phosphate tribasic hydrate (30 mg, 0.13 mmol, 2.0 eq.) in *tert*-butanol (0.66 mL) was heated to 100 °C in a sealed tube under argon. Complete consumption of the starting material was observed after 21 h following analysis by TLC. The reaction mixture was washed through a pad of Celite® with chloroform and concentrated *in vacuo* to afford

the crude product. The crude residue was purified by flash column chromatography on silica (chloroform) to afford the title compound (8.2 mg, 41%) as a colourless solid: R_f 0.57 (2% ethanol in chloroform); m.p. 123–125 °C (from chloroform); $\tilde{\nu}_{max}$ (neat/ cm^{-1}) 3659 (N-H, w), 3296 (N-H, w), 2980 (C-H, s), 1738 (C=O, m), 1690 (C=O, w), 1651 (C=O, m), 1593 (C=C, m), 1379 (C-H, m), 1235 (C-N, m), 1216 (C-O, m), 1075 (C-N, m), 908 (C-H, m) 753 (C-H, m) 693 (C-H, w); ^{1}H NMR (400 MHz, CDCl3) δ 8.77 (1H, d, *J* 2.3, H - 6), 8.36 (1H, s, H - 13), 7.49–7.44 (2H, m, H - 17), 7.43–7.37 (2H, m, H - 18), 7.35–7.30 (1H, m, H - 19), 7.13 (1H, d, *J* 2.3, H - 4), 4.75 (2H, s, H - 7), 4.21 (2H t, *J* 6.8, H - 9), 2.22 (3H, s, H - 15), 1.71–1.60 (2H, m, H - 10), 1.44–1.30 (2H, m, H - 11), 0.93 (3H, t, *J* 7.4, H - 12); ^{13}C NMR (101 MHz, $CDCl_3$) δ 169.6 (C-14), 167.7 (C-8), 157.2 (C-2), 137.0 (C-3), 129.7 (C-5), 129.4 (C-18), 128.0 (C-19), 127.7 (C-4), 126.8 (C-17), 122.9 (C-6), 121.9 (C-16), 66.4 (C-9), 51.81 (C-7), 30.9 (C-10), 25.3 (C-15), 19.5 (C-11), 14.1 (C-12); HRMS *m/z* (ESI^+) [Found: 365.14720, $C_{19}H_{22}N_2O_4Na$ requires $[M+Na]^+$ 365.14718]; LRMS *m/z* (ESI^+) 365 ($[M+Na]^+$, 60%), 493, (100%); HPLC retention time 9.7 min (method 1, 254 nm only), >99%.

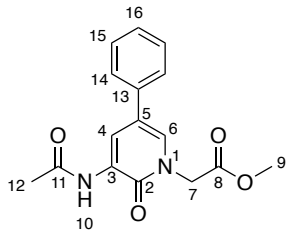
Methyl [3-acetamido-5-(4,4,5,5-tetramethyl-1,3,2-dioxaborolan-2-yl)-2-oxopyridin-1-yl] acetate, 93



A solution of 1,10-phenanthroline (3.2 mg, 0.020 mmol, 0.040 eq), and (1,5-cyclooctadiene)(methoxy)iridium(I) dimer (1.8 mg, 0.020 mmol, 0.040 eq) in tetrahydrofuran (0.5 mL) was stirred for 5 min, and then added to a solution of methyl

(3-acetamido-2-oxopyridin-1-yl)acetate (100 mg, 0.45 mmol, 1.0 eq) and bis(pinacolato)diboron (170 mg, 0.67 mmol, 1.5 eq) in THF (0.9 mL) under nitrogen. The resulting mixture was heated to 80 °C and stirred. Complete consumption of the starting material was observed after 22.5 h following analysis by TLC. The mixture was diluted with ethyl acetate (10 mL), filtered through a pad of deactivated alumina, dried with sodium sulfate and concentrated *in vacuo*. The crude mixture was purified by flash column chromatography on silica (30% toluene in acetone) to afford the title compound (101 mg, 64%): R_f 0.27 (30% toluene in acetone); m.p. 237–238 °C (toluene); $\tilde{\nu}_{max}$ (neat/ cm^{-1}) 2965 (N-H, w), 1760 (C=O, m), 1664 (C=O, m), 1610 (C=O, m), 1583 (C=C, s), 1556 (C=C, s), 1527 (C=C, s), 1211 (C-N, s), 1180 (C-O, s) 1153 (C-O, s), 1113 (C-O, s), 986 (C=C, s), 915 (C=C, m), 767 (C-H, m), 699 (C-H, s); ^{1}H NMR (400 MHz, MeOD) 9.59 (1H, s, H - 10), 7.03 (1H, d, *J* 6.8, H - 6), 6.54 (1H, d, *J* 6.8, H - 4), 4.66 (2H, s, H - 7), 3.75 (3H, s, H - 9), 2.37 (3H, s, H - 12), 1.59 (12H, s, H - 6',7'). ^{13}C NMR (126 MHz, $CDCl_3$) 170.4 (C-11), 167.5 (C-8), 155.2 (C-2), 141.0 (C-3), 133.0 (C-6), 127.7 (C-5), 110.5 (C-4), 81.2 (C-4', 5'), 52.9 (C-9), 50.7 (C-7), 26.1 (C-6',7'), 22.6 (C-12); HRMS *m/z* (ESI^+) [Found: 351.17252, $C_{16}H_{23}BN_2O_6$ requires $[M+H]^+$ 351.17220]; LRMS *m/z* (ESI^-) 373 ($[M+H]^+$, 100%); HPLC (method 1) retention time 4.2 min, >99.9%.

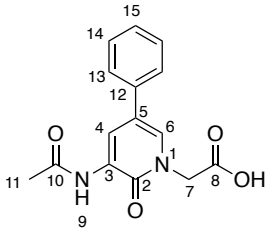
Methyl (3-acetamido-2-oxo-5-phenylpyridin-1-yl)acetate, 78



A mixture of methyl (3-acetamido-5-bromo-2-oxopyridin-1-yl)acetate (110 mg, 0.36 mmol, 1.0 eq.), phenyl boronic acid (66 mg, 0.54 mmol, 1.5 eq.), palladium diacetate (9.0 mg, 0.040 mmol, 0.1 eq.), XPhos (19 mg, 0.040 mmol, 0.10 eq.) and potassium phosphate tribasic hydrate (170 mg, 0.72 mmol, 2.0 eq.) in *tert*-butanol (3.6 mL) was heated to 100 °C in a sealed tube under argon. Complete consumption of the starting material was observed after 21 h following analysis by TLC. The reaction mixture was washed through a pad of Celite® with chloroform and concentrated *in vacuo* to afford the crude product. The crude residue was purified by flash column chromatography on silica (chloroform) to afford the title compound (75 mg, 69%) as a colourless solid: R_f 0.61 (2% ethanol in chloroform); m.p. 166–167 °C (from chloroform); $\tilde{\nu}_{max}$ (neat/ cm^{-1}) 3659 (N-H, w), 3297 (N-H, m), 2980 (C-H, s), 1742 (C=O, m), 1683 (C=O, w), 1653 (C=O, m), 1591 (C=C, m), 1534 (C=C, s) 1499 (C=C, s), 1223 (C-O, m), 1178 (C-N, m), 753 (C-H, m) 702 (C-H, m), 684 (C-H, m); ^{1}H NMR (400 MHz, $CDCl_3$) δ 8.77 (1H d, *J* 2.4, H - 6), 8.37 (1H, s, N-H), 7.48–7.43 (2H, m, H - 15), 7.42–7.37 (2H, m, 1.3, H - 14), 7.35–7.29 (1H, m, H - 16), 7.14 (1H, d, *J* 2.4, H - 4), 4.75 (2H, s, H - 7), 3.80 (3H, s, H - 9), 2.21 (3H, s, H - 12); ^{13}C NMR (101 MHz, $CDCl_3$) δ 169.3 (C-11), 167.8 (C-8), 156.8 (C-2), 136.6 (C-3), 129.3 (C-5), 129.1 (C-14), 127.7 (C-16), 127.3 (C-4), 126.4 (C-15), 122.7 (C-6), 121.6 (C-13), 53.0 (C-9), 51.4 (C-7), 24.9 (C-12); HRMS *m/z* (ESI^+) [Found: 323.09946, $C_{16}H_{16}N_2O_4Na$ requires

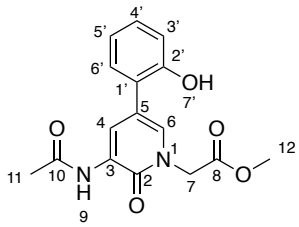
[M+Na]$^+$ 323.10023]; LRMS *m/z* (ESI$^+$) 323 ([M+Na]$^+$, 19%); HPLC retention time 7.9 min (method 3), 95.8%.

3-Acetamido-2-oxo-5-phenylpyridin-1-yl)acetic acid, 71



Lithium hydroxide (38 mg, 1.6 mmol, 10 eq.) was added to a suspension of methyl (3-acetamido-2-oxo-5-phenylpyridin-1-yl)acetate (48 mg, 0.16 mmol, 1.0 eq.) in tetrahydrofuran/methanol/water, 3:2:1 (1.6 mL). The resulting solution was stirred at RT, complete consumption of the starting material was observed after 6 h following analysis by TLC. The solution was concentrated *in vacuo* to afford the title compound (40 mg, 87% yield) as a colourless solid: R_f 0.39 (1% acetic acid, 5% ethanol in ethyl acetate); m.p. 242–244 °C (decomposed, methanol); $\tilde{\nu}_{max}$ (neat/ cm^{-1}) 3230 (N-H, w), 2722 (C-H, s), 1735 (C=O, m), 1642 (C=O, m), 1592 (C=O, m), 1524 (C=C, s) 1495 (C=C, s), 1456 (C=C, m), 1411 (O-H, m), 1215 (C-N, s), 1195 (C-O, s), 768 (C-H, m), 698 (C-H, m); ^{1}H NMR (400 MHz, D_6-DMSO) δ 9.43 (1H, s, H - NH), 8.65 (1H, d, *J* 2.5, H - 6), 7.84 (1H, d, *J* 2.5, H - 4), 7.52–7.41 (4H, m, H - 13, 14), 7.36–7.29 (1H, m, H - 15), 4.75 (2H, s, H - 7), 2.15 (3H, s, H - 11); ^{13}C NMR (126 MHz, D_6-DMSO) δ 169.7 (C-10), 169.2 (C-8), 156.1 (C-2), 136.5 (C-3), 129.7 (C-4), 129.1 (C-14), 128.8 (C-5), 127.1 (C-15), 125.4 (C-13), 122.0 (C-6), 117.7 (C-12), 51.0 (C-7), 24.1 (C-11); HRMS *m/z* (ESI$^+$) [Found: 287.10268, $C_{15}H_{15}N_2O_4$ requires [M+H]$^+$ 287.10263]; LRMS *m/z* (ESI$^-$) 285 ([M–H]$^-$, 100%) 241 ([M–COOH]$^-$, 14%); HPLC (method 3) retention time 7.0 min, 97.2%.

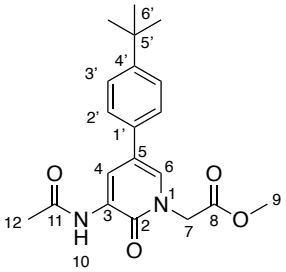
Methyl (3-acetamido-2-oxo-5-(2'-hydroxyphenyl)-pyridin-1-yl)acetate, 95



A mixture of methyl (3-acetamido-5-bromo-2-oxopyridin-1-yl)acetate (100 mg, 0.33 mmol, 1.0 eq.), 2-hydroxyphenyl boronic acid (81 mg, 0.50 mmol, 1.5 eq.), palladium diacetate (3.7 mg, 0.020 mmol, 0.05 eq.), XPhos (15.8 mg, 0.030 mmol, 0.10 eq.) and potassium phosphate tribasic hydrate (153 mg, 0.66 mmol, 2.0 eq.) in *tert*-butanol (3.9 mL) was heated to 80 °C in a sealed tube under argon. Complete consumption of the starting material was observed after 2 h following analysis by TLC, and the reaction mixture was washed through a pad of Celite® with chloroform and concentrated *in vacuo* to afford the crude product. The crude residue was purified by flash column chromatography on silica (20% acetone in toluene) to afford the title compound (79.2 mg, 76%) as a colourless solid: R_f 0.11 (1% ethanol in chloroform); m.p. 168–169 °C (from ethanol); $\tilde{\nu}_{max}$ (neat/ cm^{-1}) 3300(O-H, w), 2921 (C-H, s), 2851 (C-H), 1748 (C=O, s), 1650 (C=O, m), 1597 (C=O, s), 1531 (C=C, m), 1509 (C=C, m), 1231 (C-O, m), 1212 (C-O, m), 747(C-H, m); ^{1}H NMR (500 MHz, $CDCl_3$) δ 8.64 (1H, d, *J* 2.0, H - 6), 8.33 (1H, s, H - 9), 7.25–7.19 (2H, m, H - 3', 6'), 7.17 (1H, d, *J* 2.0, H - 4), 6.98–6.88 (2H, m, H - 5', 4'), 4.73 (2H, s, H - 7), 3.81 (3H, s, H - 12), 2.19 (3H, s, H - 11); ^{13}C NMR (126 MHz, $CDCl_3$) δ 169.2 (C-10), 167.9 (C-8), 156.6 (C-2), 152.9 (C-2'), 130.1 (C-6), 129.6 (C-4), 129.4 (C-16), 128.9 (C-5), 124.5 (C-6'), 123.5 (C-1'), 121.0 (C-4'), 117.4 (C-3), 116.4 (C-5'), 52.9 (C-12), 51.1 (C-7), 24.7 (C-11); HRMS *m/z* (ESI^+) [Found: 339.09513, $C_{16}H_{16}N_2O_5Na$ requires $[M+Na]^+$

339.09514]; LRMS *m/z* (ESI$^+$) 339 ([M+Na]$^+$, 100%); HPLC retention time 6.9 min (method 3), 98.4%.

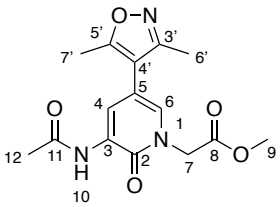
Methyl [3-acetamido-5-(4'-*tert*-butylphenyl)-2-oxopyridin-1-yl]acetate, 96



A mixture of methyl (3-acetamido-5-bromo-2-oxopyridin-1-yl)acetate (100 mg, 0.33 mmol, 1.0 eq), 4-*tert*-butylphenylboronic acid (62 mg, 0.35 mmol, 1.5 eq), palladium diacetate (7.4 mg, 0.030 mmol, 0.10 eq), XPhos (31.6 mg, 0.060 mmol, 0.20 eq.) and potassium phosphate tribasic hydrate (150 mg, 0.66 mmol, 2.0 eq) in *tert*-butanol (3.3 mL) was heated to 100 °C in a sealed tube under argon. Complete consumption of the starting material was observed after 6 h following analysis by TLC, the reaction mixture and was washed through a pad of Celite® with chloroform and concentrated *in vacuo* to afford the crude product. The crude residue was purified by flash column chromatography on silica (20% acetone in toluene) to afford the title compound (21.6 mg, 18%) as an off-white solid: R_f 0.39 (20% acetone in toluene); m.p. 134–136 °C (from toluene); $\tilde{\nu}_{max}$ (neat/ cm^{-1}) 3296 (N-H, w), 2954 (C-H, w), 2926 (C-H, w), 1752 (C=O, m), 1653 (C=C, m), 1600 (C=C, m), 1514 (C=C, m), 1208 (C-O, s), 1178 (C-O, m), 821 (C=C, m); ^{1}H NMR (400 MHz, $CDCl_3$) 8.77 (1H, d, *J* 2.3, H - 6), 8.35 (1H, s, H - 10), 7.47–7.36 (4H, m, H - 2'–3'), 7.11 (1H, d, *J* 2.3, H - 4), 4.75 (2H, s, H - 7), 3.81 (3H, s, H - 9), 2.21 (3H, s, H - 12), 1.34 (9H, s, H - 6'); ^{13}C NMR (101 MHz, $CDCl_3$) δ 169.2 (C-11), 167.7 (C-8), 156.8 (C-2), 150.9 (C-4'), 133.7 (C-1'), 129.3 (C-3), 127.0 (C-4), 126.1 (C-2'–3'), 126.0 (C-2'–3'),

122.7 (C-6), 121.5 (C-5), 53.0 (C-9), 51.4 (C-7), 34.7 (C-5'), 31.5 (C-6'), 24.9 (C-12); HRMS *m/*z (ESI$^+$) [Found: 357.18073, $C_{20}H_{25}N_2O_4$ requires $[M+H]^+$ 357.18088]; LRMS *m/z* (ESI$^+$) 357 ($[M+H]^+$, 6%, 493 (100%)); HPLC retention time 10.0 min (method 3), 98.2%.

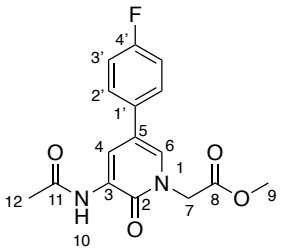
Methyl [3-acetamido-5-(3',5'-dimethyl-1',2'-oxazol-4'-yl)-2-oxopyridin-1-yl]acetate, 97



A mixture of methyl (3-acetamido-5-bromo-2-oxopyridin-1-yl)acetate 50 mg, 0.17 mmol, 1.0 eq), 3,5-dimethylisoxazole-4-boronic acid pinacol ester (56 mg, 0.25 mmol, 1.5 eq), palladium diacetate (2.2 mg, 0.01 mmol, 0.050 eq), XPhos (9.6 mg, 0.02 mmol, 0.10 eq.) and potassium phosphate tribasic hydrate (76 mg, 0.33 mmol, 2.0 eq) in *tert*-butanol (1.7 mL) was heated to 80 °C in a sealed tube under argon. Complete consumption of the starting material was observed after 24 h following analysis by TLC. The mixture was washed through a syringe filter with ethanol and concentrated *in vacuo* to afford the crude product. The crude residue was purified by flash column chromatography on silica (6:4 → 1:1 ethyl acetate in toluene) to afford the title compound (25.6 mg, 47%) as an off-white solid: R_f 0.25 (40% ethyl acetate in toluene); m.p. 143–144 °C (chloroform); $\tilde{\nu}$ max (neat/ cm^{-1}) 3294 (N-H, m), 1751 (C=O, m), 1658 (C=O, m), 1628 (C=O, s), 1601 (C=C, s), 1521 (N-O, s), 1438 (C-H, m), 1417 (C-H, w), 1374 (C-O, m), 1221 (C-O, s) , 1198 (C-O, s), 730 (C-H, m), 618 (C-H, m); ^{1}H NMR (500 MHz, $CDCl_3$) 8.37 (1H, d, *J* 2.2, H - 6), 8.35 (1H, s, H - 10), 6.83 (1H, d, *J* 2.2, H - 4), 4.74 (2H, s, H - 7), 3.80 (3H, s, H - 9), 2.39 (3H, s, H - 12), 2.25 (3H, s, H - 6'), 2.19 (3H, s, H - 7'); ^{13}C NMR (126 MHz, $CDCl_3$) 169.1 (C-11), 167.5 (C-8), 165.7 (C-5'), 158.5 (C-2), 156.4 (C-3), 129.24 (C-3'), 129.17 (C-4), 123.4 (C-6),

112.2 (C-4'), 109.9 (C-5), 52.7 (C-9), 50.6 (C-7), 24.6 (C-12), 11.4 (C-7'), 10.5 (C-6'); HRMS *m/z* (ESI$^+$) [Found: 320.12421, $C_{15}H_{18}N_3O_5$ requires $[M–H]^-$ 320.12410]; LRMS *m/z* (ESI$^+$) 342 ($[M+Na]^+$, 100%); HPLC retention time 5.3 min (method 3), 97.2%.

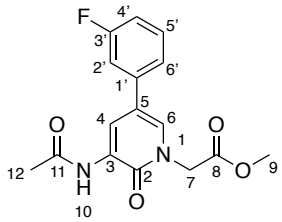
Methyl [3-acetamido-5-(4'-fluorophenyl)-2-oxopyridin-1-yl]acetate, 98



A mixture of methyl (3-acetamido-5-bromo-2-oxopyridin-1-yl)acetate (50 mg, 0.17 mmol, 1.0 eq), 4-fluorophenylboronic acid (35 mg, 0.25 mmol, 1.5 eq), palladium diacetate (2.2 mg, 0.010 mmol, 0.050 eq), XPhos (9.6 mg, 0.020 mmol, 0.10 eq.) and potassium phosphate tribasic hydrate (76 mg, 0.33 mmol, 2.0 eq) in *tert*-butanol (1.7 mL) was heated to 80 °C in a sealed tube under argon. Complete consumption of the starting material was observed after 18 h following analysis by TLC. The mixture was washed through a syringe filter with ethanol, and concentrated *in vacuo* to afford the crude product. The crude residue was purified by flash column chromatography on silica (40% ethyl acetate in toluene) to afford the title compound (13 mg, 24%) as an off-white solid: R_f 0.57 (20% acetone in toluene); m.p. 164–168 °C (decomposed, chloroform); $\tilde{\nu}_{max}$ (neat/ cm^{-1}) 3304 (N-H, m), 2954 (C-H, w), 1746 (C=O, s), 1689 (C=O, m), 1655 (C=O, s), 1603 (C=C, s), 1508 (C=C, s), 1232 (C-F, s), 826 (C-H, m) 775 (C-H, m), 747 (C-H, w); ^{1}H NMR (500 MHz, $CDCl_3$) 8.71 (1H, d, J 2.4, H - 6), 8.35 (1H, s, H - 10), 7.44–7.39 (2H, m, H - 2'), 7.12–7.06 (3H, m, H - 4 and 3'), 4.75 (2H, s, H - 7), 3.81 (3H, s, H - 9), 2.22 (3H, s, H - 12); ^{13}C NMR (126 MHz, $CDCl_3$) 169.1 (C-11), 167.5 (C-8), 162.4 (d, C-4', *J* 248.2), 156.5

(C-2), 132.6 (C-1'), 132.6 (C-3), 129.1 (C-3), 127.9 (d, C-2', *J* 7.6), 126.9 (C-4), 122.3 (C-6), 120.5 (C-5), 115.8 (d, C-3', *J* 21.4), 52.8 (C-9), 51.1 (C-7), 24.7 (C-12); ^{19}F NMR (471 MHz, $CDCl_3$, ^{1}H decoupled) –141.7 (1F, s, F - 4'); HRMS *m/z* (ESI$^+$) [Found: 341.09075, $C_{16}H_{15}N_2O_4F$ requires $[M+Na]^+$ 341.09081]; LRMS *m/z* (ESI$^+$) 341 ($[M+H]^+$, 100%; HPLC retention time 7.1 min (method 3), 95.4%.

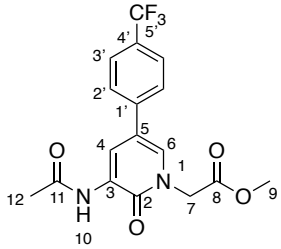
Methyl [3-acetamido-5-(3'-fluorophenyl)-2-oxopyridin-1-yl]acetate, 99



A mixture of methyl (3-acetamido-5-bromo-2-oxopyridin-1-yl)acetate (50 mg, 0.17 mmol, 1.0 eq), 3-fluorophenylboronic acid (35 mg, 0.25 mmol, 1.5 eq), palladium diacetate (2.2 mg, 0.01 mmol, 0.050 eq), XPhos (9.6 mg, 0.020 mmol, 0.10 eq.) and potassium phosphate tribasic hydrate (76 mg, 0.33 mmol, 2.0 eq) in *tert*-butanol (1.7 mL) was heated to 80 °C in a sealed tube under argon. Complete consumption of the starting material was observed after 24 h following analysis by TLC. The mixture was washed through a syringe filter with ethanol and concentrated *in vacuo* to afford the crude product. The crude residue was purified by flash column chromatography on silica (20% acetone in toluene) to afford the title compound (2.4 mg, 8%) as an off-white solid: R_f 0.35 (40% acetone in toluene); m.p. 189–190 °C (decomposed, chloroform); $\tilde{\nu}_{max}$ (neat/ cm^{-1}) 3295 (N-H, m), 1750 (C=O, m), 1686 (C=O, m), 1652 (C=O, s), 1601 (C=C, s) 1526 (C=C, m), 1489 (C=C, m), 1414 (C-N, m), 1379 (C-O, m) 1224 (C-F, s) 781 (C-H, m), 731 (C-H, w); ^{1}H NMR (500 MHz, $CDCl_3$) 8.73 (1H, d, H - 6, *J* 2.3), 8.35 (1H, s, H - 10), 7.36 (1H,

ddd, *J* 8.0, 6.0, 9.0 H - 5'), 7.26–7.24 (1H, ddd, *J* 8.0, 0.95, 1.6, H - 6'), 7.17–7.14 (2H, m, H - 2', 4), 7.01 (1H, ddd, *J* 8.0, 2.4, 0.7, H - 4'), 4.75 (2H, s, H - 7), 3.81 (3H, s, H - 9), 2.21 (3H, s, H - 12); ^{13}C NMR (126 MHz, $CDCl_3$) 169.6 (C-11), 168.0 (C-8), 163.6 (d, C-3', *J* 240.3), 157.1 (C-2), 139.1 (d, C-1', *J* 28.3), 130.9 (d, C-5', *J* 28.3), 129.7 (C-3), 127.9 (C-4), 122.5 (C-6), 122.3 (d, C-6', *J* 9.4), 120.7 (d, C-5, *J* 9.4), 114.9 (d, C-4', *J* 80.1), 113.6 (d, C-2', *J* 80.1), 53.3 (C-9), 51.7 (C-7), 25.1 (C-12); ^{19}F NMR (471 MHz, $CDCl_3$, ^{1}H decoupled) –112.4 (1F, s, F - 3'); HRMS *m/z* (ESI$^+$) [Found: 341.09084, $C_{16}H_{15}N_2O_4F$ requires $[M+Na]^+$ 341.09081]; LRMS *m/z* (ESI$^+$) 341 ($[M+H]^+$, 100%; HPLC retention time 7.0 min (method 3), 98.0%.

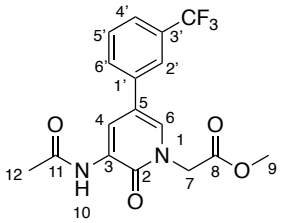
Methyl {3-acetamido-2-oxo-5-[4'-(trifluoromethyl)phenyl]pyridin-1-yl}acetate, 100



A mixture of methyl (3-acetamido-5-bromo-2-oxopyridin-1-yl)acetate (50 mg, 0.20 mmol, 1.0 eq), 4-trifluoromethylphenylboronic acid (57 mg, 0.30 mmol, 1.5 eq), palladium diacetate (2.2 mg, 0.010 mmol, 0.050 eq), XPhos (9.2 mg, 0.020 mmol, 0.10 eq.) and potassium phosphate tribasic hydrate (76 mg, 0.40 mmol, 2.0 eq) in *tert*-butanol (1.7 mL) was heated to 80 °C in a sealed tube under argon. Complete consumption of the starting material was observed after 18 h following analysis by TLC, the mixture was washed through a syringe filter with ethanol, and concentrated *in vacuo* to afford the crude product. The crude residue was purified by flash column chromatography on silica (2:8 → 3:7 ethyl acetate in toluene) to afford the title

compound (37 mg, 50%) as an off-white solid: R_f 0.48 (20% acetone in toluene); m.p. 202–204 °C (from chloroform); $\tilde{\nu}_{max}$ (neat/ cm^{-1}) 3302 (N-H, w), 1753 (C=O, m), 1693 (C-O, m), 1654 (C=O, s), 1605 (C=C, s), 1515 (C=C, m), 1403 (C=C, m), 1327 (C-F, s), 1120 (C-O, m) 836 (C-H, m), 669 (C-H, m); ^{1}H NMR (500 MHz, $CDCl_3$) 8.78 (1H, d, *J* 2.4, H - 6), 8.36 (1H, s, H - 10), 7.67 (2H, d, *J* 8.3, H - 2'), 7.58 (2H, d, *J* 8.3, H - 3'), 7.19 (1H, d, *J* 2.4, H - 4), 4.77 (2H, s, H - 7), 3.82 (3H, s, H - 9), 2.23 (3H, s, H - 12); ^{13}C NMR (101 MHz, $CDCl_3$) δ 169.7 (C-11), 167.9 (C-8), 157.2 (C-2), 140.4 (C-1'), 134.4 (C-2), 130.1 (q, C-4', *J* 26.3), 128.2 (C-4), 126.9 (C-2'), 126.4 (q, C-3', *J* 3.0), 124.5 (q, C-5', *J* 219.2), 122.2 (C-6), 120.4 (C-5), 53.3 (C-9), 51.7 (C-7), 25.2 (C-12); ^{19}F NMR (471 MHz, $CDCl_3$, ^{1}H decoupled) –62.5(3F, s, F - 5'); (HRMS *m/z* (ESI^+) [Found: 391.08627, $C_{17}H_{15}N_2O_4F_3$ requires $[M+Na]^+$ 391.08761]; LRMS *m/z* (ESI^+) 391 ($[M+Na]^+$, 100%; HPLC retention time 8.1 min (method 3), 94.8%.

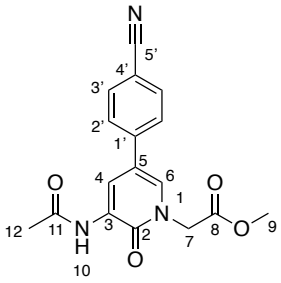
Methyl {3-acetamido-2-oxo-5-[3'-(trifluoromethyl)phenyl]pyridin-1-yl}acetate, 101



A mixture of methyl (3-acetamido-5-bromo-2-oxopyridin-1-yl)acetate (50 mg, 0.20 mmol, 1.0 eq), 3-trifluoromethylphenylboronic acid (57 mg, 0.30 mmol, 1.5 eq), palladium diacetate (2.2 mg, 0.010 mmol, 0.050 eq), XPhos (9.2 mg, 0.020 mmol, 0.10 eq.) and potassium phosphate tribasic hydrate (76 mg, 0.40 mmol, 2.0 eq) in *tert*-butanol (1.7 mL) was heated to 80 °C in a sealed tube under argon. Complete consumption of the starting material was observed after 18 h following analysis by TLC.

The mixture was washed through a syringe filter with ethanol and concentrated *in vacuo* to afford the crude product. The crude residue was purified by flash column chromatography on silica (2:8 → 3:7 ethyl acetate in toluene) to afford the title compound (37 mg, 50%) as an off-white solid: R_f 0.28 (40% ethyl acetate in toluene); m.p. 153°C (decomposed, chloroform); $\tilde{\nu}_{max}$ (neat/ cm^{-1}) 3302 (N-H, m), 1742 (C=O, m), 1655 (C=O, s), 1600 (C=O, s), 1533 (C=C, s), 1337 (C-F, s), 1231 (C-N, m), 1164 (C-N, m) 1115 (C-O, s) 669 (C-H, w); ^{1}H NMR (500 MHz, $CDCl_3$) 8.76 (1H, d, H - 6, *J* 2.5), 8.36 (1H, s, H - 10), 7.69–7.65 (2H, m, H - 4'/5'), 7.61–7.57 (1H, m, H - 2'), 7.56–7.52 (1H, m, H - 6'), 7.17 (1H, d, *J* 2.5, H - 4), 4.78 (2H, s, H - 7), 3.82 (3H, s, H - 9), 2.22 (3H, s, H - 12);^{13}C NMR (126 MHz, $CDCl_3$) 169.7 (C-11), 167.9 (C-8), 157.2 (C-2), 138.3 (C-1'), 131.8 (q, C-3', *J* 32.8), 130.1 (C-5'), 130.0 (C-6'), 129.9 (C-3), 129.0 (q, *J* 162.5, C-7'), 128.1 (C-4), 124.7 (q, C-2', *J* 3.8), 123.3 (q, C-4', *J* 3.8), 122.3 (C-6), 120.5 (C-5), 53.3 (C-9), 51.7 (C-7), 25.2 (C-12); ^{19}F NMR (471 MHz, $CDCl_3$, ^{1}H decoupled) –62.6 (1F, s, F - 3'); HRMS *m/z* (ESI^+) [Found: 369.10538, $C_{17}H_{16}N_2O_4F_3$ requires $[M+H]^+$ 369.10567]; LRMS *m/z* (ESI^+) 369 ($[M+H]^+$, 57%), 760 (100%); HPLC retention time 8.1 min (method 3), 98.9%.

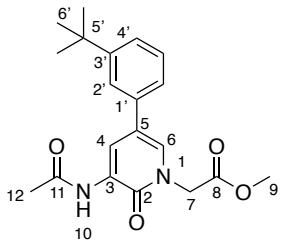
Methyl [3-acetamido-5-(4'-cyanophenyl)-2-oxopyridin-1-yl]acetate, 102



A mixture of methyl (3-acetamido-5-bromo-2-oxopyridin-1-yl)acetate (50 mg, 0.17 mmol, 1.0 eq), 4-cyanophenylboronic acid (57 mg, 0.25 mmol, 1.5 eq), palladium diacetate (2.2 mg, 0.010 mmol, 0.050 eq), XPhos (9.6 mg, 0.020 mmol, 0.10 eq.) and

potassium phosphate tribasic hydrate (76 mg, 0.34 mmol, 2.0 eq) in *tert*-butanol (1.7 mL) was heated to 80 °C in a sealed tube under argon. Complete consumption of the starting material was observed after 18 h following analysis by TLC. The mixture was washed through a syringe filter with ethanol and concentrated *in vacuo* to afford the crude product. The crude residue was purified by flash column chromatography on silica (20% acetone in toluene) to afford the title compound (7.7 mg, 14%) as an off-white solid: R_f 0.52 (20% acetone in toluene); m.p. 152–154 °C (chloroform); $\tilde{\nu}_{max}$ (neat/ cm^{-1}) 3301 (N-H, w), 2226 (CN, w), 1741 (C=O, m), 1689 (C=O, m), 1648 (C=O, s), 1593 (C=C, s) 1245 (C-N, m) 837 (C-H, w), 826 (C-H, w), 777 (C-H); ^{1}H NMR (500 MHz, $CDCl_3$) 8.80 (2H, d, *J* 2.4, H - 6), 8.38 (1H, s, H - 10), 7.74–7.72 (2H, m, H - 2'), 7.62–7.60 (2H, m, H - 3'), 7.24 (1H, d, *J* 2.4, H - 4), 4.81 (2H, s, H - 7), 3.86 (3H, s, H - 9), 2.26 (3H, s, H - 12); ^{13}C NMR (126 MHz, $CDCl_3$) 169.5 (C-11), 167.6 (C-8), 156.9 (C-2), 141.2 (C-3), 133.0 (C-2'), 129.8 (C-5), 128.2 (C-4), 126.9 (C-3'), 121.4 (C-6), 119.6 (C-1'), 118.8 (C-4'), 111.4 (C-5'), 53.1 (C-9), 51.4 (C-7), 25.0 (C-12); HRMS *m/z* (ESI^+) [Found: 348.09552, $C_{17}H_{15}N_3O_4$ requires $[M+Na]^+$ 348.09548]; LRMS *m/z* (ESI^+) 348 ($[M+Na]^+$, 100%; HPLC retention time 6.3 min (method 3), 98.4%.

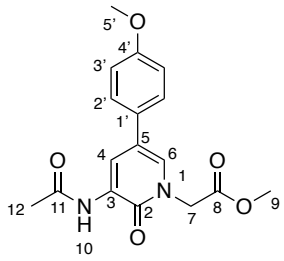
Methyl [3-acetamido-5-(3'-*tert*-butylphenyl)-2-oxopyridin-1-yl]acetate, 103



A mixture of methyl (3-acetamido-5-bromo-2-oxopyridin-1-yl)acetate (50 mg, 0.20 mmol, 1.0 eq), 3-*tert*-butylphenylboronic acid (45 mg, 0.30 mmol, 1.5 eq), palladium

diacetate (2.2 mg, 0.010 mmol, 0.050 eq), XPhos (9.2 mg, 0.020 mmol, 0.10 eq.), and potassium phosphate tribasic hydrate (76 mg, 0.40 mmol, 2.0 eq) in *tert*-butanol (1.7 mL) was heated to 80 °C in a sealed tube under argon. Complete consumption of the starting material was observed after 18 h following analysis by TLC. The mixture was washed through a syringe filter with ethanol and concentrated *in vacuo* to afford the crude product. The crude residue was purified by flash column chromatography on silica (2:8 → 3:7 ethyl acetate in toluene) to afford the title compound (47 mg, 78%) as a colourless solid: R_f 0.37 (40% ethyl acetate in toluene); m.p. 78–80 °C (chloroform); $\tilde{\nu}_{max}$ (neat/ cm^{-1}) 3293 (N-H, w), 2958 (C-H, w), 1752 (C=O, m), 1686 (C=O, m), 1650 (C=O, s), 1594 (C=C, s), 1520 (C=C, s), 1489 (C=C, m), 1410 (C-H, m), 1375 (C-H, m), 1199 (C-O, s), 795 (C-H, w), 782 (C-H, w), 732 (C-H, m), 705 (C-H, m); ^{1}H NMR (500 MHz, $CDCl_3$) 8.76 (1H, d, H - 6, *J* 2.4), 8.40 (1H, s, H - 10), 7.44–7.43 (1H, m, H- 6'), 7.37–7.31 (2H, m, H - 2'/ 5'), 7.27–7.25 (1H, m, H - 4'), 7.13 (1H, d, *J* 2.4, H - 4), 4.75 (2H, s, H - 7), 3.79 (3H, s, H - 9), 2.20 (3H, s, H - 12), 1.34 (9H, s, H - 8'); ^{13}C NMR (126 MHz, $CDCl_3$) 169.3 (C-11), 167.8 (C-8), 156.8 (C-2), 152.0 (C-1'), 136.4 (C-3), 129.2 (C-5'), 128.8 (C-1'), 127.4 (C-4), 124.8 (C-2'), 123.7 (C-4'), 123.4 (C-6'), 123.0 (C-6), 122.1 (C-3'), 52.9 (C-9), 51.4 (C-7), 34.9 (C-7'), 31.4 (C-8'), 24.8 (C-12); HRMS *m/z* (ESI^+) [Found: 379.16277, $C_{20}H_{24}N_2O_4$ requires $[M+Na]^+$ 379.16283]; LRMS *m/z* (ESI^+) 379 ($[M+Na]^+$, 92%) 315 ($[M–H_3CO +H_2]^+$ 100%); HPLC retention time 9.2 min (method 3), 97.3%.

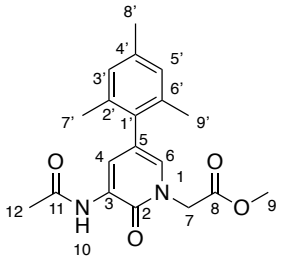
Methyl [3-acetamido-5-(4'-methoxyphenyl)-2-oxopyridin-1-yl]acetate, 104



A mixture of methyl (3-acetamido-5-bromo-2-oxopyridin-1-yl)acetate (50 mg, 0.17 mmol, 1.0 eq), 4-methoxyphenylboronic acid (21 mg, 0.25 mmol, 1.5 eq), palladium diacetate (2.2 mg, 0.010 mmol, 0.050 eq), XPhos (9.6 mg, 0.020 mmol, 0.10 eq.), and potassium phosphate tribasic hydrate (76 mg, 0.33 mmol, 2.0 eq) in *tert*-butanol (1.7 mL) was heated to 80 °C in a sealed tube under argon. Complete consumption of the starting material was observed after 18 h following analysis by TLC, the reaction mixture was washed through a syringe filter with ethanol and concentrated *in vacuo* to afford the crude product. The crude residue was purified by flash column chromatography on silica (20% acetone in toluene) to afford the title compound (19.8 mg, 35%) as an off-white solid: R_f 0.48 (20% acetone in toluene); m.p. 162–165 °C (decomposed, chloroform); $\tilde{\nu}_{max}$ (neat/ cm^{-1}) 3296 (N-H, w), 1752 (C=O, m), 1684 (C=O, m), 1651 (C=O, s), 1611 (C=C, s), 1600 (C=C, s), 1510 (C=C, s), 1438 (C-H, m), 1405 (C-H, m), 1377 (C-H, m), 1248 (C-O, m), 1181 (C-O, m), 828 (C-H, m), 780 (C-H, m), 732 (C-H, m); ^{1}H NMR (400 MHz, $CDCl_3$) 8.78 (1H, d, *J* 2.4, H - 6), 8.35 (1H, s, H - 10), 7.39–7.37 (2H, m, H - 2'), 7.07 (1H, d, *J* 2.4, H - 4), 6.94–6.92 (2H, m, H - 3'), 4.74 (2H, s, H - 7), 3.83 (3H, s, H - 5'), 3.80 (3H, s, H - 9), 2.21 (3H, s, H - 12); ^{13}C NMR (101 MHz, $CDCl_3$) δ 169.5 (C-11), 168.1 (C-8), 159.7 (C-2), 157.0 (C-3), 129.5 (C-1' or 5), 129.4 (C-1' or 5), 127.8 (C-2'), 126.9 (C-4), 123.0 (C-6), 121.6 (C-4'), 114.8 (C-3'), 55.8 (C-5), 53.2 (C-9), 51.7 (C-7), 25.2 (C-12); HRMS *m/z* (ESI^+) [Found:

353.11084, $C_{17}H_{18}N_2O_5$ requires $[M+Na]^+$ 353.11079]; LRMS *m/z* (ESI^+) 353 ($[M+Na]^+$, 100%); HPLC retention time 6.9 min (method 3), 96.3%.

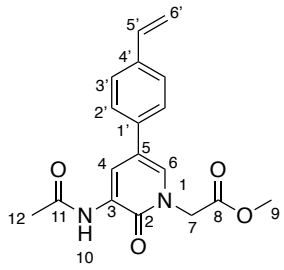
Methyl [3-acetamido-5-(2',4',6'-trimethylphenyl)-2-oxopyridin-1-yl]acetate, 105



A mixture of methyl (3-acetamido-5-bromo-2-oxopyridin-1-yl)acetate (50 mg, 0.20 mmol, 1.0 eq), 2,4,6-trimethylphenylboronic acid (41 mg, 0.25 mmol, 1.5 eq), palladium diacetate (2.2 mg, 0.010 mmol, 0.050 eq), XPhos (9.2 mg, 0.020 mmol, 0.10 eq.) and potassium phosphate tribasic hydrate (76 mg, 0.40 mmol, 2.0 eq) in *tert*-butanol (1.7 mL) was heated to 80 °C in a sealed tube under argon. Complete consumption of the starting material was observed after 19 h following analysis by TLC. The reaction mixture was washed through a syringe filter with ethanol and concentrated *in vacuo* to afford the crude product. The crude residue was purified by flash column chromatography on silica (2:8 → 3:7 ethyl acetate in toluene) to afford the title compound (37 mg, 62%) as a colourless solid: R_f 0.25 (30% ethyl acetate in toluene); m.p. 80–84 °C (chloroform); $\tilde{\nu}_{max}$ (neat/ cm^{-1}) 3284 (N-H, w), 2955 (C-H, w), 1751 (C=O, m), 1687 (C=O, m), 1651 (C=O, s), 1595 (C=C, s), 1519 (C-H, s), 1486 (C=C, m), 1437 (C-H, m), 1406 (C-H, m), 1373 (C-H, m), 1216 (C-O, s), 1196 (C-N, s), 851 (C-H, m), 781 (C-H, m), 648 (C-H, m); ^{1}H NMR (500 MHz, $CDCl_3$) 8.39 (1H, s, H - 10), 8.27 (1H, d, *J* 2.2, H - 6), 6.91 (2H, s, H - 3', 5'), 6.71 (1H, d, *J* 2.2, H - 4), 4.72 (2H, s, H - 7), 3.79 (3H, s, H - 9), 2.30 (3H, s, H - 8'), 2.18 (3H, s, H - 12), 2.12 (6H, s, H - 7', 9'); ^{13}C NMR (126 MHz, $CDCl_3$) 169.4 (C-11),

168.2 (C-8), 157.0 (C-2), 137.9 (C-4'), 137.2 (C-2', 6'), 133.8 (C-1'), 129.4 (C-3), 129.3 (C-4), 128.7 (C-3', 5'), 125.4 (C-6), 120.3 (C-5), 53.1 (C-9), 51.1 (C-7), 25.1 (C-12), 21.4 (C-8'), 21.0 (C-7', 9'); HRMS *m/z* (ESI^+) [Found: 365.14743, $C_{19}H_{22}N_2O_4$ requires $[M+Na]^+$ 365.14718]; LRMS *m/z* (ESI^+) 493 (100%), 365 ($[M+Na]^+$, 28%); HPLC (method 3) retention time 8.2 min, 99.5%.

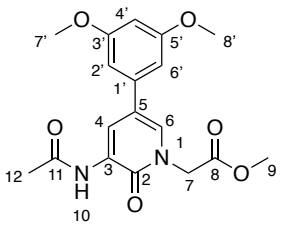
Methyl [3-acetamido-5-(4'-ethenylphenyl)-2-oxopyridin-1-yl]acetate, 106



A mixture of methyl (3-acetamido-5-bromo-2-oxopyridin-1-yl)acetate (50 mg, 0.20 mmol, 1.0 eq), 4-vinyl phenylboronic acid (37 mg, 0.25 mmol, 1.5 eq), palladium diacetate (2.2 mg, 0.010 mmol, 0.050 eq), XPhos (9.2 mg, 0.020 mmol, 0.10 eq.) and potassium phosphate tribasic hydrate (76 mg, 0.40 mmol, 2.0 eq) in *tert*-butanol (1.7 mL) was heated to 80 °C in a sealed tube under argon. Complete consumption of the starting material was observed after 19 h following analysis by TLC. The reaction mixture was washed through a syringe filter with ethanol and concentrated *in vacuo* to afford the crude product. The crude residue was purified by flash column chromatography on silica (3:7 ethyl acetate in toluene) to afford the title compound (8.8 mg, 16%) as a colourless solid: R_f 0.19 (30% ethyl acetate in toluene); m.p. 170–172°C (chloroform); ῡmax (neat/ cm^{-1}) 3303 (N-H, w), 1740 (C=O, s), 1695 (C=O, m), 1651 (C=O, s), 1598 (C=C, s), 1527 (C=C, m), 1509 (C=C, m), 1233 (C-O, m), 1195 (C-N, m), 839 (C-H, m), 776 (C-H, m); 1H NMR (500 MHz, $CDCl_3$) 8.77 (1H, d, *J* 2.4, H - 6), 8.35 (1H, s, H - 10), 7.54–7.37 (4H, m,

H - 2',3'), 7.15 (1H, d, *J* 2.4, H - 4), 6.72 (1H, dd, *J* 17.6, 10.9, H - 5'), 5.78 (1H, dd, *J* 17.6, 0.8, H - 6' trans), 5.28 (1H, dd, J 10.9, 0.8, H - 6' cis), 4.75 (2H, s, H - 7), 3.81 (3H, s, H - 9), 2.22 (3H, s, H - 12); ^{13}C NMR (126 MHz, $CDCl_3$) 169.6 (C-11), 168.0 (C-8), 157.1 (C-2), 137.3 (C-5'), 136.5 (C-1'), 136.2 (C-4'), 129.6 (C-3), 127.4 (C-4), 127.2 (C-2'/3'), 126.7 (C-2'/3'), 122.7 (C-6), 121.4 (C-5), 114.6 (C-6'), 53.2 (C-9), 51.7 (C-7), 25.2 (C-12); HRMS *m/z* (ESI^+) [Found: 349.11600, $C_{18}H_{18}N_2O_4$ requires $[M+Na]^+$ 349.11588]; LRMS *m/z* (ESI^+) 493 (100%), 349 ($[M+Na]^+$, 19%); HPLC (method 3) retention time 7.4 min, 94.8%.

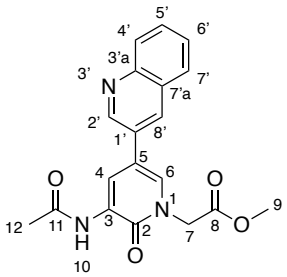
Methyl [3-acetamido-5-(3',5'-dimethoxyphenyl)-2-oxopyridin-1-yl]acetate, 107



A mixture of methyl (3-acetamido-5-bromo-2-oxopyridin-1-yl)acetate (50 mg, 0.20 mmol, 1.0 eq), 3,5-dimethoxyphenylboronic acid (47 mg, 0.25 mmol, 1.5 eq), palladium diacetate (2.2 mg, 0.010 mmol, 0.050 eq), XPhos (9.2 mg, 0.020 mmol, 0.10 eq.) and potassium phosphate tribasic hydrate (76 mg, 0.40 mmol, 2.0 eq) in *tert*-butanol (1.7 mL) was heated to 80 °C in a sealed tube under argon. Complete consumption of the starting material was observed after 19 h following analysis by TLC. The reaction mixture was washed through a syringe filter with ethanol and concentrated *in vacuo* to afford the crude product. The crude residue was purified by flash column chromatography on silica (3:7 ethyl acetate in toluene) to afford the title compound (9.6 mg, 15%) as a colourless solid: R_f 0.23 (30% ethyl acetate in toluene); m.p. 171–174°C (chloroform); $\tilde{\nu}_{max}$ (neat/ cm^{-1}) 3304 (N-H, w), 1736 (C=O, s), 1689 (C=O, m), 1651 (C=O,

s), 1586 (C=C, s), 1524 (C=C, m), 1478 (C=C, m), 1404 (C=C, m), 1376 (C=C, m), 1264 (C-N, m), 1232 (C-O, m), 1197 (C-O, s), 1158 (C-O, s), 1058 (C-O, m), 834 (C-H, m), 776 (C-H, m); ^{1}H NMR (500 MHz, $CDCl_3$) 8.74 (1H, d, *J* 2.4, H - 6), 8.34 (1H, s, H - 10), 7.12 (1H, d, *J* 2.4, H - 4), 6.58 (2H, d, *J* 2.3, H - 2', 6'), 6.44 (1H, t, *J* 2.3, H - 4'), 4.74 (2H, s, H - 7), 3.82 (6H, s, H - 7', 8'), 3.81 (3H, s, H - 9), 2.21 (3H, s, H - 12); ^{13}C NMR (126 MHz, $CDCl_3$) 169.0 (C-11), 167.5 (C-8), 161.1 (C-3', 5'), 156.7 (C-2), 138.6 (C-1'), 129.0 (C-3), 127.3 (C-4), 122.4 (C-6), 121.4 (C-5), 104.5 (C-2', 6'), 99.5 (C-4'), 55.4 (C-7'/8'), 52.7 (C-9), 51.2 (C-7), 24.7 (C-12); HRMS *m/z* (ESI^+) [Found: 383.12140, $C_{18}H_{20}N_2O_6$ requires $[M+Na]^+$ 383.12136]; LRMS *m/z* (ESI^+) 493 (100%), 391 ($[M–COO^–+H^+$, 33%), 383 ($[M+Na]^+$, 29%); HPLC (method 3) retention time 7.1 min, 94.6%.

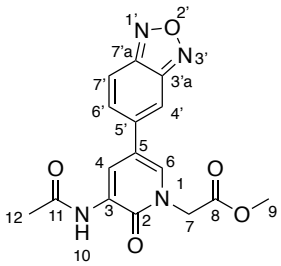
Methyl [3-acetamido-2-oxo-5-(quinolin-3-yl)pyridin-1-yl]acetate, 108



A mixture of methyl (3-acetamido-5-bromo-2-oxopyridin-1-yl)acetate (100 mg, 0.33 mmol, 1.0 eq.), 3-quinoline boronic acid (60 mg, 0.35 mmol, 1.5 eq.), palladium diacetate (7.4 mg, 0.030 mmol, 0.10 eq.), XPhos (31.6 mg, 0.060 mmol, 0.20 eq.), and potassium phosphate tribasic hydrate (150 mg, 0.66 mmol, 2.0 eq.) in *tert*-butanol (3.3 mL) was heated to 100 °C in a sealed tube under argon. Complete consumption of the starting material was observed after 6 h following analysis by TLC, the reaction mixture was washed through a pad of Celite® with chloroform and concentrated *in vacuo* to afford the crude product. The crude residue was purified by flash column

chromatography on silica (1% ethanol in chloroform) to afford the title compound (16.3 mg, 14%) as a colourless solid: R_f 0.18 (20% acetone in toluene); m.p. 210–212 °C (chloroform, decomposed); $\tilde{\nu}_{max}$ (neat/ cm^{-1}) 3300 (N-H, w), 2922 (C-H, m), 2851 (C-H, w), 1751 (C=O, s), 1687 (C=O, m), 1650 (C=O, s), 1605 (C=C, s), 1591 (C=C, m), 1527 (C=C, m), 1442 (C-N, m), 1416 (C-N, m), 1384 (C-N, m), 1209 (C-O, m), 775 (C-H, m), 751 (C-H, m) 624 (C-H, m); ^{1}H NMR (500 MHz, $CDCl_3$) 9.03 (1H, d, *J* 2.4, H - 6), 8.89 (1H, d, *J* 2.5, H - 4), 8.40 (1H, s, H - 10), 8.24 (1H, d, *J* 2.4, H- 2'), 8.12 (1H, d, *J* 8.4, H - 4'), 7.86 (1H, d, *J* 8.2, H - 7'), 7.76–7.69 (1H, m, H - 5'), 7.63–7.55 (1H, m, H - 6'), 7.30 (1H, d, *J* 2.5, H - 8'), 4.82 (2H, s, H - 7), 3.84 (3H, s, H - 9), 2.25 (3H, s, H - 12); ^{13}C NMR (126 MHz, $CDCl_3$) δ 169.5 (C-11), 167.7 (C-8), 156.9 (C-2), 148.6 (C-4), 147.5 (C-3a), 132.8 (C-2'), 129.9 (C-3/1'), 129.8 (C-5'), 129.5 (C-1'/3), 129.4 (C-4'), 128.1 (C-7'), 127.9 (C-7'a), 127.9 (C-8'), 127.5 (C-6'), 121.9 (C-6), 118.4 (C-5), 53.1 (C-9), 51.5 (C-7), 25.0 (C-12); HRMS *m/z* (ESI^+) [Found: 339.09513, $C_{16}H_{16}N_2O_5Na$ requires $[M+Na]^+$ 339.09514]; LRMS *m/z* (ESI^+) 339 ($[M+Na]^+$, 100%); HPLC retention time 6.9 min (method 1), 98.4%.

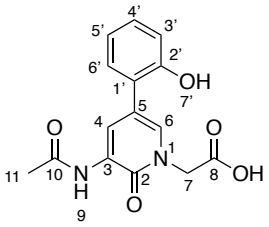
Methyl [3-acetamido-5-(2',1',3'-benzoxadiazol-5'-yl)2-oxopyridin-1-yl]acetate, 109



A mixture of methyl (3-acetamido-5-bromo-2-oxopyridin-1-yl)acetate (50 mg, 0.20 mmol, 1.0 eq), 4,4-benzodioxan-6-boronic acid (62 mg, 0.25 mmol, 1.5 eq), palladium diacetate (2.2 mg, 0.010 mmol, 0.050 eq), XPhos (9.2 mg, 0.020 mmol, 0.10 eq.) and potassium phosphate tribasic hydrate (76 mg, 0.40 mmol, 2.0 eq) in

tert-butanol (1.7 mL) was heated to 80 °C in a sealed tube under argon. Complete consumption of the starting material was observed after 19 h following analysis by TLC, the reaction mixture was washed through a syringe filter with ethanol, and concentrated *in vacuo* to afford the crude product. The crude residue was purified by flash column chromatography on silica (3:7 ethyl acetate in toluene) to afford the title compound (5.7 mg, 10%) as a yellow-brown solid: R_f 0.26 (30% ethyl acetate in toluene); m.p. 211–214°C (chloroform); $\tilde{\nu}_{max}$ (neat/ cm^{-1}) 3296 (N-H, w), 1748 (C=O, m), 1736 (C=O, m), 1687 (C=O, m), 1651 (C=C, m), 1599 (C=N, s), 1528 (N-O, s), 1470 (C=C, m), 1409 (C-N, m), 1374 (C-N, s), 1230 (C-O, m), 776 (C-H, m), 754 (C-H, m), 645 (C-H, m); ^{1}H NMR (500 MHz, $CDCl_3$) 8.83 (1H, d, *J* 2.5, H - 6), 8.36 (1H, s, H - 10), 7.91 (1H, dd, *J* 9.4, 1.3, H - 7'), 7.88 (1H, s, H - 4'), 7.58 (1H, dd, *J* 9.4, 1.3, H - 6'), 7.29 (1H, d, *J* 2.5, H - 4), 4.80 (2H, s, H - 7), 3.84 (3H, s, H - 9), 2.24 (3H, s, H - 12); ^{13}C NMR (126 MHz, $CDCl_3$) 169.2 (C-11), 167.3 (C-8), 156.7 (C-2), 149.4 (C-7'a), 148.3 (C-3'a), 139.6 (C-5'), 131.4 (C-6'), 129.6 (C-3), 128.3 (C-4), 120.8 (C-6), 119.0 (C-5), 117.2 (C-7'), 111.8 (C-4'), 52.9 (C-7), 51.1 (C-9), 24.7(C-12); HRMS *m/z* (ESI^+) [Found: 341.08924, $C_{16}H_{13}N_4O_5$ requires $M–H]^-$ 341.08914]; LRMS *m/z* (ESI^+) 493 ($[M–H]^-$, 100%); HPLC (method 3) retention time 6.7 min, 97.8%.

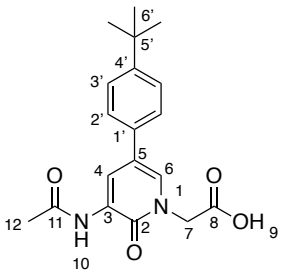
[3-Acetamido-5-(2'-hydroxyphenyl)-2-oxopyridin-1-yl]acetic acid, 117



Lithium hydroxide (23 mg, 1.0 mmol, 10 eq.) was added to a solution of methyl (3-acetamido-2-oxo-5-(2-hydroxyphenyl)-pyridin-1-yl)acetate (30 mg, 0.10 mmol,

1.0 eq.) in tetrahydrofuran/methanol/water, 3:2:1 (1.0 mL) and 1 drop of DMSO. The resulting solution was stirred at RT. Complete consumption of the starting material was observed after 40 min following analysis by TLC. The solution was concentrated *in vacuo* to afford a crude residue, that was purified by flash column chromatography on silica (toluene/acetone, 1:1 and 1% acetic acid → acetone and 1% acetic acid) to afford the title compound as an off white solid (9.6 mg, 33 %): R_f 0.36 (1% acetic acid, acetone); m.p. 139–142 °C (acetone); $\tilde{\nu}_{max}$ (neat/ cm^{-1}) 3248 (C-H, br), 2031 (C-H, s), 1977 (C-H, s) 1733 (C=O, m), 1649 (C=O, s), 1587 (C=O, s), 1529 (C=C, m), 1417 (O-H, m), 1377 (O-H, m), 1285 (C-O, m), 1229 (C-O, m), 756 (C-H, m); ^{1}H NMR (400 MHz, MeOD) 8.66 (1H, d, *J* 2.3, H - 6), 7.55 (1H, d, *J* 2.3, H - 4), 7.25 (1H, dd, *J* 7.9, 1.7, H - 3'), 7.17–7.13 (1H, m, H - 6'), 6.94–6.83 (2H, m, H - 4', 5'), 4.80 (2H, s, H - 7), 2.20 (3H, s, H - 11); ^{13}C NMR (126 MHz, MeOD) 172.1 (C-10), 171.4 (C-8), 158.2 (C-5), 155.7 (C-2'), 132.9 (C-4), 130.7 (C-3'), 129.9 (C-6'), 128.9 (C-2), 128.4 (C-6), 125.0 (C-3), 121.0 (C-4' or 5'), 119.5 (C-1'), 117.0 (C-4' or 5'), 52.7 (C-7), 24.1 (C-11); HRMS *m/z* (ESI^+) [Found: 301.08330, $C_{15}H_{13}N_2O_5$ requires $[M–H]^-$ 301.08299]; LRMS *m/z* (ESI^-) 301 ($[M–H]^-$, 74%) 198 (100%); HPLC (method 3) retention time 6.0 min, 98.2%.

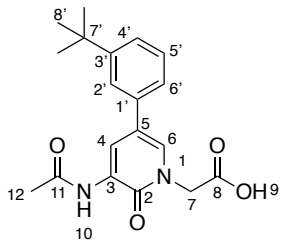
[3-Acetamido-5-(4'-*tert*-butylphenyl)-2-oxopyridin-1-yl]acetic acid, 118



Lithium hydroxide (15 mg, 0.6 mmol, 10 eq.) was added to a solution of methyl (3-acetamido-2-oxo-5-(4'-*tert*butylphenyl)-pyridin-1-yl)acetate (22 mg, 0.06 mmol,

1.0 eq.) in tetrahydrofuran/methanol/water, 3:2:1 (0.6 mL) and 1 drop of DMSO. The resulting solution was stirred at RT. Complete consumption of the starting material was observed after 40 min following analysis by TLC. The solution was concentrated *in vacuo* to afford a crude residue, that was purified by flash column chromatography on silica (toluene/acetone, 1:1 and 1% acetic acid → acetone and 1% acetic acid) to afford the title compound (11.7 mg, 57%): R_f 0.46 (1% acetic acid, acetone); m.p. 166–168 °C (toluene); $\tilde{\nu}_{max}$ (neat/ cm^{-1}) 3247 (O-H, br), 2032 (C-H, m), 1976 (C-H, m), 1740 (C=O, m), 1723 (C=O, m), 1644 (C=O, s), 1593 (C=C, s), 1516 (C=C, s), 1456 (C=C, m), 1417 (O-H, m), 1399 (O-H, m), 1195 (C-O, m), 826 (C-H, m), 779 (C-H, m); ^{1}H NMR (400 MHz, MeOD) 8.70 (1H, d, *J* 2.4, H - 6), 7.60 (1H, d, *J* 2.4, H - 4), 7.46 (4H, s, H - 2', 3'), 4.78 (2H, s, H - 7), 2.22 (3H, s, H - 12), 1.34 (9H, s, H - 16'); ^{13}C NMR (126 MHz, MeOD) 172.3 (C-11), 171.9 (C-8), 158.3 (C-2), 151.6 (C-4'), 135.1 (C-3), 130.6 (C-4), 129.8 (C-5), 126.9 (C-2' or 3'), 126.7 (C-2' or 3'), 125.2 (C-6), 121.6 (C-1'), 53.0 (C-7) 35.4 (C-5'), 31.7 (C-6'), 24.1 (C-12); HRMS *m/z* (ESI^+) [Found: 343.16532, $C_{19}H_{23}N_2O_4$ requires $[M+H]^+$ 343.16523]; LRMS *m/z* (ESI^-) 341 ($[M–H]^-$, 100%); HPLC (method 3) retention time 9.0 min, 97.3%.

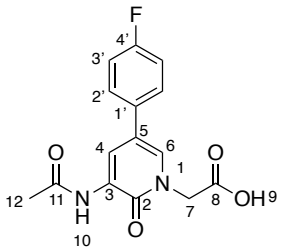
[3-Acetamido-5-(3'-*tert*-butylphenyl)-2-oxopyridin-1-yl]acetic acid, 119



Lithium hydroxide (32 mg, 1.3 mmol, 10 eq.) was added to a solution of methyl (3-acetamido-2-oxo-5-(3'-*tert*butylphenyl)-pyridin-1-yl)acetate (47 mg, 0.13 mmol, 1.0 eq.) in tetrahydrofuran/methanol/water, 3:2:1 (1.3 mL). Complete consumption of

the starting material was observed after 4.5 h following analysis by TLC. The solution was concentrated *in vacuo* to afford a crude residue, that was purified by flash column chromatography on silica (acetone and 1% acetic acid) to afford the title compound (11.7 mg, 57%): R_f 0.24 (10% ethanol in DCM, 1% acetic acid); too hygroscopic to obtain an accurate melting point; $\tilde{\nu}_{max}$ (neat/cm^{-1}) 3372 (O-H, br), 1647 (C=O, m), 1592 (C=O, s), 1415 (C=C, m), 1047 (C-O, m), 1024 (C-O, s), 990 (C=C, s), 828 (C-H, m) 766 (C-H, m); ^{1}H NMR (500 MHz, D_6-DMSO) 9.16 (1H, s, H - 9), 8.45 (1H, d, *J* 2.6, (H - 6), 7.53 (1H, d, *J* 2.6, H - 4), 7.37 (1H, s, H - 2'), 7.24–7.22 (2H, m, H, 5', 4' or 6'), 7.17–7.15 (1H, m, H - 4' or 6'), 4.33 (2H, s, H - 7), 2.03 (3H, s, H - 12), 1.20 (9H, s, H - 8'); ^{13}C NMR (126 MHz, D_6-DMSO) 169.6 (C-8/11), 169.5 (C-8/11), 156.0 (C-2), 151.3 (1'), 136.8 (C-4), 130.7 (C-5'), 128.7 (C-3), 128.5 (C-4'/6'), 123.7 (C-4'/6'), 122.7 (C-2'), 122.2 (C-6), 121.5 (C-5), 117.1 C-7), 53.2(C-7), 34.5 (C-7'), 31.2 (C-8'), 24.2 (C-12); HRMS *m/z* (ESI$^-$) [Found: 341.15063, $C_{19}H_{21}N_2O_4$ requires [M–H]$^-$ 341.15068]; LRMS *m/z* (ESI$^-$) 341 ([M–H]$^-$, 100%); HPLC (method 3) retention time 7.5 min, 97.6%.

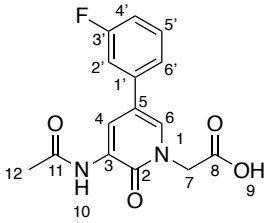
[3-Acetamido-5-(4'-fluorophenyl)-2-oxopyridin-1-yl]acetic acid, 120



Lithium hydroxide (49 mg, 2.1 mmol, 10 eq.) was added to a solution of methyl (3-acetamido-2-oxo-5-(4'-fluorophenyl)-pyridin-1-yl)acetate (65 mg, 0.21 mmol, 1.0 eq.) in tetrahydrofuran/methanol/water, 3:2:1 (2.0 mL), and the resulting solution was stirred at RT. Complete consumption of the starting material was observed after 2.5 h following

analysis by TLC. The solution was neutralised to pH 7, diluted with water (1 mL), and extracted with ethyl acetate (3 × 1 mL) to afford the title compound as a pale grey solid (13 mg, 21%): R_f 38 (ethanol and 1% acetic acid); m.p. 260 °C (decomposed, chloroform); $\tilde{\nu}_{max}$ (neat/ cm^{-1}) 3304 (O-H, m), 1746 (C=O, s), 1689 (C=O, m), 1655 (C=O, s), 1603 (C=C, m), 1535 (C=C, m), 1508 (C-F, s), 1231 (C-O, m), 1203 (C-O, m), 826 (C-H, s), 775 (C-H, m), 747 (C-H, m); ^{1}H NMR (500 MHz, MeOD) 8.64 (1H, d, *J* 2.4, H - 6), 7.56–7.52 (3H, m, H - 4, 2'), 7.14 (2H, t, *J* 8.8, H - 3'), 4.64 (2H, s, H - 7), 2.21 (3H, s, H - 12); ^{13}C NMR (126 MHz, MeOD) 174.1 (C-8), 172.2 (C-11), 163.7 (d, *J* 975.0, C-4'), 158.2 (C-2), 134.8 (d, *J* 15, C-1'), 131.3 (C-4), 129.9 (C-3), 129.0 (d, *J* 35, C-2'), 124.6 (C-6), 120.4 (C-5), 116.7 (d, *J* 90, C-3'), 54.7 (C-7), 24.1 (C-12); ^{19}F NMR (471 MHz, $CDCl_3$, ^{1}H decoupled) –117.9 (1F, s, F - 4'); HRMS *m/z* (ESI^-) [Found: 303.0791, $C_{15}H_{13}N_2O_4F$ requires $[M–H]^-$ 34303.0787]; LRMS *m/z* a LR spectrum could not be obtained for this compound; HPLC (method 5) retention time 7.37 min, 98.8%.

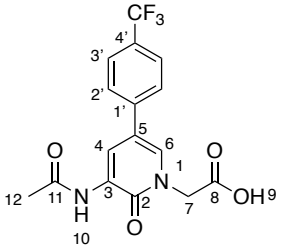
[3-Acetamido-5-(3'-fluorophenyl)-2-oxopyridin-1-yl]acetic acid, 121



Lithium hydroxide (9.4 mg, 0.40 mmol, 10 eq.) was added to a solution of methyl (3-acetamido-2-oxo-5-(3'-fluorophenyl)-pyridin-1-yl)acetate (13 mg, 0.040 mmol, 1.0 eq.) in tetrahydrofuran/methanol/water, 3:2:1 (0.40 mL), and the resulting solution was stirred at RT. Complete consumption of the starting material was observed after 2 h following analysis by TLC. The solution was neutralised to pH 7 with aqueous hydrochloric acid (1.0 M), diluted with water (1 mL), and extracted with ethyl acetate (3 × 1 mL) to

afford the title compound (12 mg, >99%): R_f 0.43 (10% ethanol in DCM, 1% acetic acid); m.p. 208–212°C (chloroform); $\tilde{\nu}_{max}$ (neat/ cm^{-1}) 3375 (O-H, s), 1720 (C=O, m), 1681 (C=O, m), 1650 (C=O, s), 1596 (C=C, s), 1530 (C-H, m), 1490 (C-H, m), 1415 (C-F, m), 1225 (C-N, m), 1197 (C-N, m), 1023 (C-O, s), 988 (C-O, s), (C-H, 774, m), 713 (C-H, m), 634 (C-H, m); ^{1}H NMR (500 MHz, D6-DMSO) 9.43 (1H, s, H - 9), 8.62 (1H, d, J 2.5, H - 6), 7.97 (1H, d, J 2.5, H - 4), 7.49 (1H, d, *J* 8.1, 6.3, 8.1, H - 5'), 7.37–7.27 (2H, m, H - 2', 6'), 7.15 (1H, ddd, J 8.4, 8.5, 2.5, H - 4'), 4.75 (2H, s, H - 7), 2.15 (3H, s, H - 12); ^{13}C NMR (126 MHz, $CDCl_3$) 169.8 (C-8), 169.1 (C-11), 162.7 (d, *J* 243.2, C-3), 156.2 (C-2), 139.0 (d, *J* 7.6, C-1'), 131.2 (d, *J* 8.9, C-5'), 130.6 (C-4), 128.8 (C-3), 121.7 (C-6), 121.4 (d, *J* 2.5, C-6'), 116.3 (d, *J* 3.8, C-5), 113.8 (d, *J* 20.2, C-4'), 112.0 (d, *J* 22.7, C-2'), 51.1 (C-7), 24.1 (C-12); ^{19}F NMR (471 MHz, $CDCl_3$, ^{1}H decoupled) –112.8 (1F, s, F - 3'); HRMS *m/z* (ESI^-) [Found: 341.15063, $C_{19}H_{21}N_2O_4$ requires $[M–H]^-$ 341.15068]; LRMS *m/z* (ESI^-) 341 ($[M–H]^-$, 100%); HPLC (method 3) retention time 7.5 min, 97.6%.

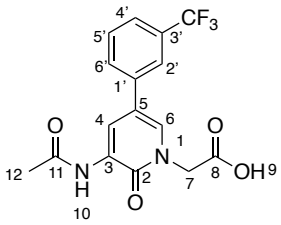
[3-Acetamido-5-(4'-trifluoromethylphenyl)-2-oxopyridin-1-yl]acetic acid, 122



Lithium hydroxide (55 mg, 2.3 mmol, 10 eq.) was added to a solution of methyl (3-acetamido-2-oxo-5-(4'-trifluoromethylphenyl)-pyridin-1-yl)acetate (85 mg, 0.23 mmol, 1.0 eq.) in tetrahydrofuran/methanol/water, 3:2:1 (2.3 mL), and the resulting solution was stirred at RT. Complete consumption of the starting material was observed after 2.5 h following analysis by TLC. The solution was neutralised to pH 7, diluted with

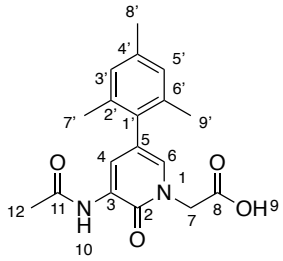
water (1 mL), and extracted with ethyl acetate (3 × 1 mL) to afford the title compound as a brown solid (49 mg, 61%): R_f 0.43 (1:1 toluene/acetone, 1% acetic acid); too hygroscopic to obtain an accurate melting point; $\tilde{\nu}_{max}$ (neat/ cm^{-1}) 3300 (O-H, br), 1647 (C=O, m), 1599 (C=O, s), 1400 (O-H, m), 1326 (C-F, s), 1112 (C-O, s), 1068 (C-O), 832 (C-H, m); ^{1}H NMR (500 MHz, MeOD) 8.72 (1H, d, *J* 2.4, H - 6), 7.79–7.65 (5H, m, H - 2'–3', 4), 4.66 (2H, s, H - 7), 2.22 (3H, s, H - 12); ^{13}C NMR (126 MHz, MeOD) 174.0 (C-8), 172.2 (C-11), 158.4 (C-2), 142.3 (C-1), 132.3 (C-4), 130.1 (C-3), 130.0 (q, *J* 32.8, C-4'), 127.4 (C-2'), 126.9 (q, *J* 3.8, C-3'), 126.0 (q, *J* 270.9, C-5'), 124.7 (C-6), 119.5 (C-5), 54.7 (C-7), 24.14 (C-12); ^{19}F NMR (471 MHz, $CDCl_3$, ^{1}H decoupled) –63.9 (1F, s, F - 4'); HRMS *m/z* (ESI^-) [Found: 353.0756, $C_{16}H_{13}N_2O_4F$ requires $[M–H]^-$ 353.0755]; LRMS *m/z*, a LRMS could not be obtained for this compound; HPLC (method 5) retention time 8.2 min, 97.4%.

[3-Acetamido-2-oxo-5-(3-[trifluoromethyl]phenyl)pyridin-1-yl]acetic acid, 123



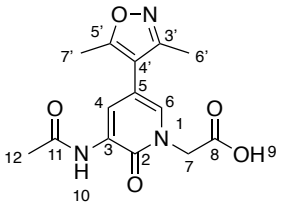
Lithium hydroxide (24 mg, 1.0 mmol, 10 eq.) was added to a solution of methyl (3-acetamido-2-oxo-5-(3'-trifluoromethylphenyl)pyridin-1-yl)acetate (37 mg, 0.10 mmol, 1.0 eq.) in tetrahydrofuran/methanol/water, 3:2:1 (1.0 mL), and the resulting solution was stirred at RT. Complete consumption of the starting material was observed after 5 h following analysis by TLC. The solution was neutralised with aqueous hydrochloric acid (1.0 M), then extracted with ethyl acetate (3 × 2 mL) and the combined organic components concentrated *in vacuo* to afford the title compound as an off-white solid (10 mg, 28%): R_f 0.36 (acetone and 1% acetic acid); m.p. 100–120 °C (decomposed, acetone); $\tilde{\nu}_{max}$ (neat/ cm^{-1}) 3300 (O-H, br s), 1647 (C=O, m), 1599 (C=C, s), 1537 (C=C, m), 1517 (C=C, m), 1400 (O-H, m), 1326 (C-F, s), 1165 (C-O, s), 1069 (C-O, s), 833 (C-H, m), 785 (C-H, m); ^{1}H NMR (500 MHz, D_6-DMSO) 9.47 (1H, s, H - 9), 8.67 (1H, d, *J* 2.5, H - 6), 8.03 (1H, d, *J* 2.5, H - 4), 7.85–7.78 (2H, m, H - 2', 5'), 7.73–7.67 (2H, m, H - 4', 6'), 4.74 (2H, s, H - 7), 2.16 (3H, s, H - 12); ^{13}C NMR (126 MHz, D_6-DMSO) 170.3 (C-8), 169.5 (C-11), 156.6 (C-2), 138.1 (C-1'), 131.3 (C-4), 130.8 (C-6'), 130.31 (q, *J* 31.5, C-3'), 129.8 (C-5'), 129.4 (C-3), 124.7 (q, *J* 273.4, C-7'), 124.0 (q, *J* 3.8, C-4'), 122.1 (q, *J* 3.8, C-2'), 121.9 (C-6), 116.4 (C-5), 51.6 (C-7), 24.5 (C-12); ^{19}F NMR (471 MHz, $CDCl_3$, ^{1}H decoupled) –61.1 (3F, s, F - 7'); HRMS *m/z* (ESI^+) [Found: 353.0751, $C_{16}H_{13}N_2O_4F_3$ requires $[M–H]^–$ 353.0755]; LRMS *m/z* (ESI^+) 353 ($[M–H]^–$, 100%); HPLC (method 3) retention time 8.3 min, 94.5%.

[3-Acetamido-5-(2',4',6'-trimethylphenyl)-2-oxopyridin-1-yl]acetic acid, 124



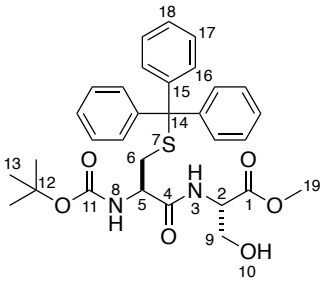
Lithium hydroxide (24 mg, 1.0 mmol, 10 eq.) was added to a solution of methyl (3-acetamido-2-oxo-5-(2',4',6'-trimethylphenyl)-pyridin-1-yl)acetate (36 mg, 0.10 mmol, 1.0 eq.) in tetrahydrofuran/methanol/water, 3:2:1 (1.0 mL), and the resulting solution was stirred at RT. Complete consumption of the starting material was observed after 1 h following analysis by TLC. The solution was concentrated to afford the crude residue, and then re-dissolved in ethyl acetate (1 mL) and water (1 mL), and the aqueous components extracted with ethyl acetate (1 mL) to afford the title compound as an off-white solid (10 mg, 32%): R_f 0.41 (1% acetic acid in acetone); m.p. 200°C (decomposed, ethyl acetate); $\tilde{\nu}_{max}$ (neat/ cm^{-1}) 3296 (O-H, m), 1737 (C=O, m), 1677 (C=O, s), 1649 (C=O, s), 1582 (C=C, s), 1572 (C=C, s), 1559 (C=C, s), 1539 (C=C, s), 1523 (C-H, s), 1376 (C-H), 1411 (O-H, s), 1249 (C-N, m), 1213 (C-O, s), 1194 (C-O, s), 778 (C-H, m), 733 (C-H); ^{1}H NMR (500 MHz, D_6-DMSO) 9.3 (1H, s, H - 9), 8.0 (1H, d, *J* 2.3, H - 6), 7.2 (1H, d, *J* 2.3, H - 4), 6.9 (2H, s, H - 3'/5'), 4.6 (2H, s, H - 7), 2.2 (3H, s, H - 12), 2.1 (3H, s, H - 8'), 2.1 (6 H, s, H - 7'/9'); ^{13}C NMR (126 MHz, D_6-DMSO) 169.5 (C-11), 169.2 (C-8), 155.9 (C-2), 136.5 (C-4'), 136.2 (C-2'/6'), 134.0 (C-1'), 131.2 (C-4), 128.4 (C-3), 128.1 (C-3'/5'), 124.8 (C-5), 116.2 (C-6), 51.0 (C-7), 24.0 (C-8), 20.6 (C-12), 20.3 (C-7'/9'); HRMS *m/z* (ESI^+) [Found: 329.14966, $C_{18}H_{21}N_2O_4$ requires $[M+H]^+$ 329.14958]; LRMS *m/z* (ESI^+) 351 ($[M+Na]^+$, 100%); HPLC (method 3) retention time 6.5 min, 97.4%.

[3-Acetamido-5-(3',5'-dimethyl-1',2'-oxazol-4'-yl)-2-oxopyridin-1-yl]acetic acid, 125



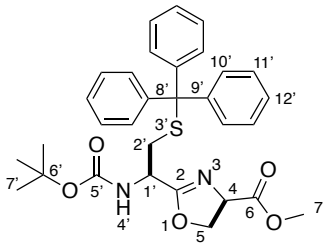
Lithium hydroxide (15 mg, 0.6 mmol, 10 eq.) was added to a solution of methyl (3-acetamido-2-oxo-5-(4'-*tert*butylphenyl)-pyridin-1-yl)acetate (22 mg, 0.06 mmol, 1.0 eq.) in tetrahydrofuran/methanol/water, 3:2:1 (0.6 mL) and 1 drop of DMSO, and the resulting solution was stirred at RT. Complete consumption of the starting material was observed after 40 min following analysis by TLC. The solution was concentrated *in vacuo* to afford a crude residue, that was purified by flash column chromatography on silica (toluene/acetone 1:1 and 1% acetic acid → acetone and 1% acetic acid) to afford the title compound (12 mg, 57%): R_f 0.46 (1% acetic acid, acetone); m.p. 122–23 °C (methanol); $\tilde{\nu}_{max}$ (neat/ cm^{-1}) 3372 (O-H, br s), 3292 (N-H, w), 1714 (C=O, m), 1652 (C=O), 1607 (C=C, s), 1592 (C=C, s), 1528 (N-O, m), 1420 (C-H, m), 1401 (O-H, m), 1377 (C-H, m), 1248 (C-O, m), 1199 (C-O, m), 669 (C-H, m); ^{1}H NMR (400 MHz, MeOD) 8.34 (1H, d, *J* 2.3, H - 6), 7.35 (1H, d, *J* 2.3, H - 4), 4.76 (2H, s, H - 7), 2.42 (3H, s, H - 12), 2.26 (3H, s, H -7'), 2.20 (3H, s, H - 6');^{13}C NMR (126 MHz, MeOD) 172.3 (C-11), 171.9 (C-8), 167.6 (C-3'), 160.2 (C-5'), 158.2 (C-2), 133.4 (C-3), 130.1 (C-4), 126.3 (C-6), 113.9 (C-4'), 110.1 (C-5), 24.0 (C-7'), 11.3 (C-4'), 10.5 (C-5); HRMS *m/z* (ESI^+) [Found: 328.09033, $C_{14}H_{15}N_3O_5$ requires $[M+Na]^+$ 328.09039]; LRMS *m/z* (ESI^+) 328 ($[M+Na]^+$, 100%); HPLC (method 3) retention time 4.2 min, 99.7%.

Methyl *N*-(*tert*-butoxycarbonyl)-(*R*)-(triphenylmethyl)cysteinyl-(*S*)-serinate, 150,[282]



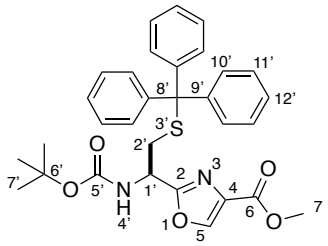
A solution of methyl-(*S*)-serinate hydrochloride (250 mg, 1.6 mmol, 1.1 eq.) and *N*-(*tert*-butoxycarbonyl)-(*R*)-(triphenylmethyl)cysteine (680 mg, 1.5 mmol, 1.0 eq.) in *N,N*-dimethylformamide (9 mL) was cooled to 0 °C, followed by addition of diphenyl phosphorazidate (0.39 mL, 1.8 mmol, 1.2 eq.) and triethylamine (0.48 mL, 3.1 mmol, 2.1 eq.). Complete consumption of the starting material was observed after 17 h following analysis by TLC, the reaction mixture was diluted with ethyl acetate (50 mL), and washed with lithium chloride solution (0.5 M, 5 × 60 mL). The combined aqueous components were extracted with ethyl acetate (80 mL), and the combined organic components dried with anhydrous sodium sulfate, diluted with hexane and toluene, and concentrated *in vacuo*. The crude residue was purified by flash column chromatography on silica (petroleum ether/ethyl acetate, 1:1), to afford the title compound (700 mg, 85%) as a colourless solid: R_f 0.35 (petroleum ether/ethyl acetate, 1:1); $[\alpha]_D^{25}$ = +33.9 (*c* 1.0, chloroform); m.p. 155–156 °C (from ethyl acetate); ^{1}H NMR (500 MHz, $CDCl_3$) δ 7.46–7.39 (m, 6H, H - 17), 7.34–7.30 (6H, m, H - 18) 7.30–7.20 (3H, m, H - 15), 6.75 (1H, s, H - 8), 4.83 (1H, s, H - 3), 4.60–4.52 (1H, m, H - 5), 4.04–3.94 (1H, m, H - 6), 3.92–3.84 (1H, m, H - 6), 3.76 (3H, s, H - 19), 3.52 (1H, s, H - 13), 2.86 (1H, s, H - 2), 2.78 (1H, dd, *J* 13.3, 6.3, H - 12), 2.57 (1H, dd, *J* 13.3, 6.3, H - 12), 1.42 (9H, s, 11); LRMS *m/z* (ESI$^+$) 564 $[M+H]^+$ 17%). ^{1}H NMR is in agreement with the literature, (^{13}C, IR).[282]

Methyl 2-{(1'*R*)-1'-[(*tert*-butoxycarbonyl)amino]-2'-[(triphenylmethyl)sulfanyl]ethyl}-4,5-dihydro-1,3-oxazole-(4*S*)-carboxylate, 151,[230,282,283]



A solution of methyl *N*-(*tert*-butoxycarbonyl)-(*R*)-(triphenylmethyl)cysteinyl-(*S*)-serinate (1.9 g, 3.4 mmol, 1.0 eq.) in anhydrous tetrahydrofuran (34 mL) was added to triphenyl phosphine (1.4 g, 5.1 mmol, 1.5 eq.), followed by addition of diethyl azodicarboxylate (DEAD, 0.80 mL, 5.1 mmol, 1.5 eq.). The solution was stirred at 0 °C. Complete consumption of the starting material was observed after 20 h following analysis by TLC, and so the solution was concentrated *in vacuo*. The crude residue was purified by column chromatography on silica (petroleum ether/ ethyl acetate, 6:4) and concentrated *in vacuo*. The isolated material was dissolved in toluene (20 mL), washed with water (5 × 20 mL), and the combined organic components were concentrated to afford the title compound (71% yield by NMR): R_f 0.51 (petroleum ether/ethyl acetate, 6:4); $[\alpha]_D^{25}$ = +22.4 (*c* 1.0, chloroform) [lit[283] +13.4 (*c* 1.0, chloroform); m.p. 56–57 °C (from hexane); ^{1}H NMR (400 MHz, $CDCl_3$) δ 7.42–7.37 (6H, m, 10'–12'), 7.31–7.18 (9H, m, 10'–12'), 5.14 (1H, d, *J* 6.6, H -1'), 4.74 (1H, ddd, *J* 9.6, 9.6, 1.5, H - 4), 4.53 (1H, dd, *J* 9.6, 9.6, H - 5), 4.49–4.38 (2H, m, H - 5, 4'), 3.76 (3H, s, H - 7), 2.59 (2H, d, *J* 6.6, H - 2'), 1.42 (9H, s, 3 × H - 7'); LRMS *m/z* (ESI$^+$) 547 ([M+H]$^+$, 14%). The data are in agreement with the literature.[282,283]

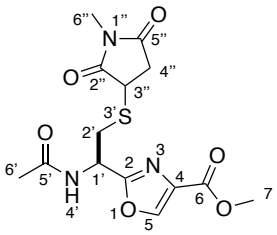
Methyl 2-{(1'*R*)-1'-[(*tert*-butoxycarbonyl)amino]-2'-[(triphenylmethyl)sulfanyl]ethyl}-1,3-oxazole-4-carboxylate, 152



Bromotrichloromethane (0.010 mL, 0.10 mmol, 1.1 eq.) was added to a solution of methyl 2-{(1'*R*)-1-[(*tert*-butoxycarbonyl)amino]-2-[(triphenylmethyl)sulfanyl]ethyl}-4,5-dihydro-1,3-oxazole-4-carboxylate (42 mg, 0.090 mmol, 1.0 eq.) in DCM (0.45 mL) at 0 °C, followed by addition of 1,8-diazabicyclo[5.4.0]undec-7-ene (DBU, 1.0 mL, 1.1 mmol, 1.1 eq.). Complete consumption of the starting material was observed after 2 h following analysis by TLC. The reaction was diluted with DCM (10 mL) and washed with aqueous hydrochloric acid (1 M, 15 mL), water (15 mL) and brine (15 mL). The combined aqueous components were extracted with DCM (2 × 15 mL), the combined organic components dried with anhydrous sodium sulfate and concentrated *in vacuo*. The crude residue was purified by flash column chromatography on silica (petroleum ether/ethyl acetate, 7:3) to afford the title compound (35 mg, 71%) as a colourless solid: R_f 0.23 (petroleum ether/ethyl acetate, 8:2); $[\alpha]_D^{25}$ = –2.1 (*c* 1.0, chloroform); m.p. 92–94 °C (from hexane); $\tilde{\nu}_{max}$ (thin film/ cm^{-1}) 3344 (N-H, w), 1717 (C=O, s), 1166 (C-O, m), 1582 (C=C, m), 1166 (C-O, m), 1111 (C-O, m), 745 (C=C, m), 701 (C-H, m); ^{1}H NMR (400 MHz, $CDCl_3$) δ 8.12 (1H, s, H - 5), 7.40–7.33 (6H, m, H - 10'–12'), 7.31–7.24 (6H, m, H - 10'–12'), 7.24–7.18 (3H, m, H - 10'–12'), 5.17 (1H, s, H - 4'), 4.83 (1H, s, H - 1'), 3.91 (3H, s, H - 7), 2.77–2.73 (2H, m, H - 2'), 1.42 (9H, s, 3 × H - 7'); ^{13}C NMR (151 MHz, $CDCl_3$) δ 163.9 (C-2), 161.5

(C-5'), 154.7 (C-6), 144.3 (C-Ar), 144.1 (C-5), 133.3 (C-4), 129.5 (C-Ar), 128.0 (C-Ar), 127.0 (C-Ar), 80.32 (C-6'), 67.1 (C-8'), 52.2 (C-7), 48.2 (C-1'), 35.7 (C-2'), 28.3 (C-7'); HRMS *m/z* (ESI$^+$) [Found: 567.1918, $C_{31}H_{32}N_2O_5SNa$ requires $[M+Na]^+$ 567.1924.]; LRMS *m/z* (ESI$^+$) 567 ($[M+H]^+$, 8%); HPLC retention time 12.3 min (method 3), 98.7%.

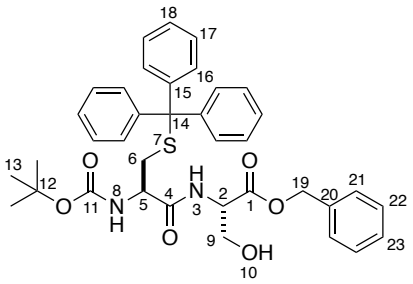
Methyl 2-{(1'*R*)-1'-acetamido-2'-[(1''-methyl-2'',5''-dioxopyrrolidin-3''-yl)sulfanyl]ethyl}-1,3-oxazole-4-carboxylate, 148



Triethylsilane (0.74 mL, 47 mmol, 30 eq.) was added to a solution of methyl 2-{(1'*R*)-1-[(*tert*-butoxycarbonyl)amino]-2-[(triphenylmethyl)sulfanyl]ethyl}-1,3-oxazole-4-carboxylate (85 mg, 0.16 mmol, 1.0 eq.) in DCM (2.3 mL) and trifluoroacetic acid (20% *v/v*), and the solution was stirred for 1 h before removal of the DCM *in vacuo*. The residue was re-dissolved in methanol (1.4 mL), *N*-methylmaleimide added (18 mg, 0.16 mmol, 1.0 eq.), and the resulting solution was stirred. Complete consumption of the starting material was observed after 24 h following analysis by TLC. The solution was concentrated *in vacuo* and dissolved in tetrahydrofuran (1.6 mL), followed by addition of acetyl chloride (12 µL, 0.17 mmol, 1.1 eq.) and triethylamine (0.050 mL, 0.32 mmol, 2.0 eq.). Complete consumption of the starting material was observed after 4.5 h following analysis by TLC, the reaction mixture was concentrated *in vacuo* and purified by flash column chromatography on silica (ethyl acetate) to afford the title compound (19 mg, 34% yield) as a colourless oil: R_f 0.31 (ethyl acetate); $[\alpha]_D^{25}$ = −20.4 (*c* 1.0,

chloroform); $\tilde{\nu}_{max}$ (thin film/ cm^{-1}) 3468 (N-H, w), 2954 (C-H, w), 2925 (C-H, w), 1776 (C=O, m), 1697 (C-O, s), 1582 (C=C, w), 1537 (C=C, w), 1438 (N-H, m), 1282 (C-O, m), 1115 (C-O, m), 755 (C-H, m), 692 (C-H, m); ^{1}H NMR (400 MHz, $CDCl_3$) (diastereomer A) δ 8.21 (1H, s, H - 5), 6.66 (1H, d, *J* 8.5, H – 4'), 5.67–5.52 (1H, m, H - 1'$_x$), 3.98 (0.5H, dd, J_{AX} 9.2, J_{BX} 4.0, H_x – 3''), 3.91 or 3.90 (1.5, s, H - 7), 3.61 (1H, dd, J_{AB} 14.2, J_{AX} 5.2, H_a - 2'), 3.18–3.07 (3H, m, H_b - 2', H_aH_b - 4''), 3.00 or 2.99 (1.5, s, H - 6''), 2.43 (1H, dd, J_{AB} 15.2, J_{BX} 4.0, H_b - 4''), 2.08 or 2.07 (1.5, s, H - 6'); ^{1}H NMR (400 MHz, $CDCl_3$) (diastereomer B) δ 8.21(1H, s, H - 5), 7.10 (1H, d, *J* 8.3, H – 4'), 5.67–5.52 (1H, m, H_aH_b - 1'$_x$), 3.91 or 3.90 (1.5, s, H - 7), 3.74 (0.5H, dd, J_{AX} 9.2, J_{BX} 4.0, H_x - 3''), 3.65 (1H, dd, J_{AB} 14.4, J_{BX} 5.3, H_b - 2'), 3.24 (0.5H, dd, J_{AB} 14.4, J_{AX} 5.7, H_a - 2'), 3.18–3.07 (1.5H, m, H_b - 2', H_aH_b - 4''), 3.00 or 2.99 (1.5, s, H - 6''), 2.48 (1H, dd, J_{AB} 15.1, J_{BX} 4.0, H_b - 4''), 2.08 or 2.07 (1.5H, s, H - 6'); ^{13}C NMR (101 MHz, $CDCl_3$) (Diastereomers A and B) δ 177.4 (C-2'' A or C-2'' B), 177.2 (C-2'' A or C-2'' B), 174.8 (C-5'' A or C-5'' B), 174.5 (C-5'' A or C-5'' B), 170.6 (C-5' A or C-5' B), 170.4 (C-5' A or C-5' B), 163.8 (C-6 A or C-6 B), 163.7 (C-6 A or C-6 B), 161.7 (C-4), 144.9 (C-5 A or C-5 B), 144.9 (C-5 A or C-5 B), 133.8 (C-2 A or C-2 B) , 133.7 (C-2 A or C-2 B), 52.8 (C-7), 48.10 (C-1'), 46.9 (C-1'), 40.2 (C-3''), 39.2 (C-3''), 36.6 (C-4''), 36.3 (C-2''), 36.1 (C-2' or C-4''), 36.1 (C-2' or C-4''), 25.7 (C-2 or C-6''), 25.6 (C-2 or C-6''), 23.1 (C-6'); HRMS *m/z* (ESI^+) [Found: 378.07229, $C_{14}H_{17}N_3O_6S$ requires $[M+Na]^+$ 378.07358]; LRMS *m/z* (ESI^+) 378 ($[M+Na]^+$, 100%); HPLC retention time 5.8 min (method 3), 96.3%.

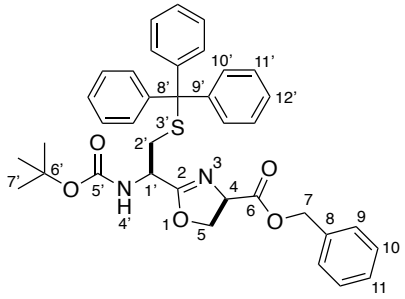
Benzyl *N*-(*tert*-butoxycarbonyl)-(*R*)-(triphenylmethyl)cysteinyl-(*S*)-serinate, 161,[282]



A solution of benzyl-(*S*)-serinate hydrochloride (200 mg, 0.86 mmol, 1.1 eq.) and *N*-(*tert*-butoxycarbonyl)-(*R*)-(triphenylmethyl)cysteine (360 mg, 0.78 mmol, 1.0 eq.) was dissolved in *N,N*-dimethylformamide (4.6 mL), followed by addition of diphenyl phosphorazidate (0.40 mL, 1.9 mmol, 1.2 eq.) and triethylamine (0.46 mL, 3.3 mmol, 2.1 eq.), and the solution was stirred at RT. Complete consumption of the starting material was observed after 25 h following analysis by TLC. The solution was diluted with ethyl acetate (20 mL) and washed with lithium chloride solution (0.5 M, 5 × 25 mL). The combined aqueous components were extracted with ethyl acetate (80 mL), the combined organic components were dried with anhydrous sodium sulfate, diluted with chloroform and hexane, and concentrated *in vacuo*. The crude residue was purified by flash column chromatography on silica (petroleum ether/ethyl acetate, 7:3), to afford the title compound (355 mg, 71%) as a colourless solid: R_f 0.17 (petroleum ether/ethyl acetate, 7:3). $[\alpha]_D^{25}$ = 31.4 (*c* 1.0, chloroform); m.p. 55–57 °C (ethyl acetate); $\tilde{\nu}_{max}$ (thin film/cm^{-1}) 3392 (O-H, w), 2977 (N-H, w), 1742 (C=O, m), 1671 (C=O, s), 1493 (C=C, s), 1445 (C=C, m), 1395 (O-H, m), 1167 (C-N, s), 745 (C-H, s), 700 (C-H, s); ^{1}H NMR (500 MHz, $CDCl_3$) δ 7.45–7.39 (6H, m, H - 16–18, 21–23), 7.37–7.18 (14H, m, H - 16–18, 21–23), 6.77 (1H, s, H - 8), 5.20 (2H, s, H - 19), 4.83 (1H, s, H - 3), 4.59–4.53 (1H, m, H - 5), 3.98 (1H, d, *J* 11.7, H - 6), 3.87 (1H, d, *J* 11.7, H - 6), 3.54–3.44 (1H, m, H - 2), 2.88 (1H, s, H - 10), 2.77 (1H, dd, *J* 13.2, 7.8, H - 9), 2.57 (1H, dd, *J* 13.2, 5.0, H - 9), 1.40 (9H, s, H - 13). ^{13}C NMR

(126 MHz, $CDCl_3$) δ 170.7 (C-4), 170.0 (C-1), 155.7 (C-11), 144.4 (C-15), 135.2 (C-20), 129.7, 128.8, 128.7, 128.30, 128.27, 127.1 (C-16–18, 21–23), 80.9 (C-12), 67.6 (C-19), 67.5 (C-14), 62.7 (C-6), 55.4 (C-5), 54.1 (C-2), 33.4 (C-9), 28.4 (C-13). HRMS *m/;* (ESI^+) [Found: 663.24908, $C_{37}H_{40}N_2O_6SNa$ requires $[M+Na]^+$ 663.24993]; LRMS *m/z* (ESI^-) 639 ($[M-H]^-$, 52%) 565 (100%); HPLC (method 1) retention time 12.1 min, 100.0%.

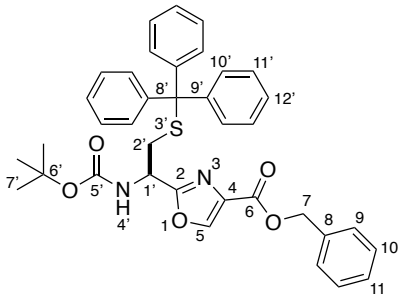
Benzyl 2-{(1R)-1'-[(*tert*-butoxycarbonyl)amino]-2'-[(triphenylmethyl)sulfanyl]ethyl}-4,5-dihydro-1,3-oxazole-(4*S*)-carboxylate, 162,[230,282,283]



A solution of benzyl *N*-(*tert*-butoxycarbonyl)-(*R*)-(triphenylmethyl)cysteinyl-(*S*)-serinate (300 mg, 0.48 mmol, 1.0 eq.) in anhydrous tetrahydrofuran (4.8 mL) was added to triphenyl phosphine (PPh_3, 190 mg, 0.72 mmol, 1.5 eq.), followed by addition of diethyl azodicarboxylate (DEAD, 0.11 mL, 0.72 mmol, 1.5 eq.), and the solution was stirred at RT. Complete consumption of the starting material was observed after 2.5 h, following analysis by TLC, and the solution was concentrated *in vacuo*. The crude residue was purified by column chromatography on silica (cyclohexane/ ethyl acetate, 8:2) to afford the title compound (160 mg, 54% yield) as a colourless foam: R_f 0.24 (cyclohexane/ ethyl acetate, 8:2). $[\alpha]_D^{25}$ = 36.9 (*c* 1.0, chloroform); $\tilde{\nu}_{max}$ (thin film/ cm^{-1}) 2975 (N-H, w), 2929 (N-H, w), 1742 (C=O, m), 1716 (C=O, s), 1662 (C=C, m), 1494 (C=C, m), 1367 (C-N, m), 1250 (C-O, m), 1170 (C-O, s), 744 (C-H, s), 700 (C-H, s); ^1H NMR (400 MHz, $CDCl_3$) 7.43–7.37 (6H, m, H - 3''), 7.37–7.23 (11H, m, H - 9–11, 2'',4''), 7.23–7.18 (3H, m, H - 5''),

5.23–5.11 (2H, m, H - 7), 4.80–4.71 (1H, m, H - 4), 4.54–4.37 (3H, m, H - 5, 1'), 2.66–2.55 (2H, m, H - 2'), 1.43 (9H, s, H - 7'); ^{13}C NMR (126 MHz, $CDCl_3$) δ 170.7 (C-4), 170.0 (C-1), 155.7 (C-11), 144.4 (C-15), 135.2 (C-20), 129.7, 128.8, 128.7, 128.3, 128.3, 127.1 (Cs-16–18, 21–23), 80.9 (C-12), 67.6 (C-19), 67.5 (C-14), 62.7 (C-6), 55.4 (C-5), 54.1 (C-2), 33.4 (C-9), 28.4 (C-13). HRMS *m/z* (ESI^+) [Found: 621.24289, $C_{37}H_{37}N_2O_5S$ requires $[M-H]^-$ 621.24287]; LRMS *m/z* (ESI^-) 621 ($[M-H]^-$, 21%) 113 (100%); HPLC (method 1) retention time 13.0 min, 94.8%.

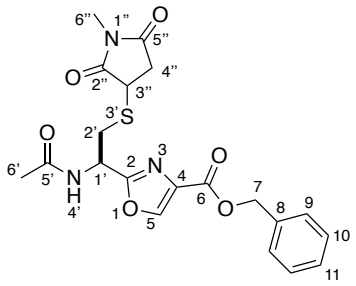
Benzyl 2-{(1'*R*)-1'-[(*tert*-butoxycarbonyl)amino]-2'-[(triphenylmethyl)sulfanyl]ethyl}-1,3-oxazole-4-carboxylate, 163



Bromotrichloromethane (7.0 µL, 0.071 mmol, 1.1 eq.) was added to a solution of benzyl 2-{(1'*R*)-1-[(*tert*-butoxycarbonyl)amino]-2-[(triphenylmethyl)sulfanyl]ethyl}-4,5-dihydro-1,3-oxazole-4-carboxylate (42 mg, 0.067 mmol, 1.0 eq.) in DCM (0.34 mL) at 0 °C, followed by addition of DBU (20 µL, 0.13 mmol, 1.1 eq.). Complete consumption of the starting material was observed after 17 h, and the solution was concentrated *in vacuo*. The crude residue was purified by flash column chromatography on silica (petroleum ether/ethyl acetate, 7:3) to afford the title compound (3.7 mg, 9%) as a colourless solid: R_f 0.31 (diethyl ether/hexane, 2:3); $[\alpha]_D^{25}$ = –4.8 (*c* 1.0, chloroform); m.p. 55–57 °C (from hexane); $\tilde{\nu}_{max}$ (thin film/ cm^{-1}) 2980 (N-H, w), 1717 (C=O, s), 1580 (C=C, m), 1493 (C-H, m), 1367 (C-H, m), 1250 (C-N, m), 1164 (C-O, m), 1109 (C-O, m), 745 (C=C, m), 699 (C-H,

m); ^{1}H NMR (500 MHz, $CDCl_3$) 8.10 (1H, s, H-5), 7.46–7.16 (20 H, m, H 9–11, 3''–5''), 5.35 (1H, s, H - 7), 5.16 (1H, d, *J* 8.5, H - 4'), 4.83 (1H, s, H - 1'), 2.77–2.68 (2H, m, H-2'), 1.41 (9H, s, H - 7').^{13}C NMR (101 MHz, $CDCl_3$) δ 163.9 (C-2), 160.8 (C-6), 154.8 (C-5') 144.3 (C-4), 144.2 (C-5), 135.4 (C-8), 133.4 (C-2'') 129.5 (C-4''), 128.76 (C-10), 128.72 (C-9), 128.5 (C-11), 128.0 (C-3''), 126.9 (C-5''), 80.5 (C-6') 66.8 (C-1''), 48.3 (C-1'), 35.7 (C-2'), 28.3 (C-7'); HRMS *m/z* (ESI^+) [Found: 643.22435, $C_{37}H_{36}N_2O_5SNa$ requires $[M+Na]^+$ 643.22371]; LRMS could not be obtained for this compound; HPLC retention time 13.1 min (method 3), 97.6%.

Benzyl 2'-{(1'*R*)-1'-acetamido-2'-[(1''-methyl-2'',5''-dioxopyrrolidin-3''-yl)sulfanyl]ethyl}-1,3-oxazole-4-carboxylate, 164

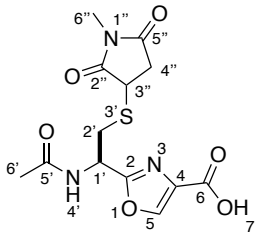


Triethylsilane (0.090 mL, 0.56 mmol, 3.0 eq.) was added to a solution of benzyl 2-{(1'*R*)-1-[(*tert*-butoxycarbonyl)amino]-2-[(triphenylmethyl)sulfanyl]ethyl}-1,3-oxazole-4-carboxylate (118 mg, 0.19 mmol, 1.0 eq.) in DCM (2.6 mL) and trifluoroacetic acid (20% *v/v*), and the solution was stirred for 1 h before removal of the DCM *in vacuo*. The residue was re-dissolved in methanol (1.9 mL) and *N*-methylmaleimide added (21 mg, 0.19 mmol, 1.0 eq.). The solution was stirred at RT. Complete consumption of the starting material was observed after 3.5 h following analysis by TLC. The solution was concentrated *in vacuo* and dissolved in tetrahydrofuran (1.9 mL), followed by addition of acetyl chloride (20 µL, 0.21 mmol, 1.1 eq.) and triethylamine (0.030 mL, 0.38 mmol,

2.0 eq.). Complete consumption of the intermediate was observed after 4.5 h following analysis by TLC. The solution was concentrated *in vacuo* and purified by flash column chromatography on silica (20% acetone in toluene) to afford the title compound (34 mg, 41% yield) as a colourless oil: R_f 0.40 (ethyl acetate); $[\alpha]_D^{25}$ = −17.9 (*c* 1.0, chloroform); $\tilde{\nu}_{max}$ (thin film/ cm^{-1}) 3341 (N-H, w), 1776 (C=O, m), 1699 (C=O, s), 1580 (C=C, m), 1540 (C=C, m), 1455 (O-H, w), 1383 (C-N, m), 1282 (C-O, m), 1139 (C-O, m), 697 (C-H, w), 697 (C-H, m); ^{1}H NMR (400 MHz, $CDCl_3$) (diastereomer A) δ 8.20 or 8.19 (0.5H, s, H - 5), 7.43–7.31 (5H, m, H - 9–11), 6.70 (0.5H, d, *J* 8.4, H - 4'), 5.60–5.54 (1H, m, H_x - 1'), 5.34 (2H, s, H - 7), 3.98 (0.5H, dd, J_{AX} 9.1, J_{BX} 3.9, H_x - 3''), 3.60 (0.5H, dd, J_{AB} 14.1, J_{BX} 4.0, H_b - 2'), 3.18–3.07 (1.5H, m, H_a - 2', H_aH_b - 4''), 2.99 or 2.98 (3H, s, H - 6''), 2.42 (0.5H, dd, J_{AB} 16.8, J_{BX} 3.9, H_a - 4''), 2.07 or 2.06 (3H, s, H - 6'); (diastereomer B) δ 8.20 (0.5H, s, H_aH_b - 5), 8.20 or 8.19 (0.5H, s, H - 5), 7.43–7.31 (5H, m, H - 9–11), 7.09 (0.5H, d, *J* 8.4, H - 4'), 5.60–5.54 (1H, m, H_x - 1'), 5.34 (2H, s, H - 7), 3.75 (0.5H, dd, J_{AX} 9.2, J_{BX} 4.1, H_x - 3''), 3.64 (0.5H, dd, J_{AB} 14.4, J_{BX} 5,3, H_b - 2'), 3.24 (0.5H, dd, J_{AB} 14.4, J_{AX} 5.9, H_b - 2'), 3.18–3.07 (1.5H, m, H_a - 2', H_aH_b - 4''), 2.99 or 2.98 (3H, s, H - 6''), 2.46 (0.5H, dd, J_{AB} 16.9, J_{BX} 4.1, H_b - 4''), 2.07 or 2.06 (3H, s, H_aH_b - 6'); ^{13}C NMR (101 MHz, $CDCl_3$) (Diastereomers A and B) δ 177.1 (C-2'' A or C-2'' B), 176.9 (C-2''A or C-2'' B), 174.5 (C-5'' A or C-5'' B), 174.2 (C-5'' A or C-5'' B), 170.2 (C-5' A or C-5' B), 170.1 (C-5' A or C-5' B), 163.5 (C-6' A or C-6' B), 163.4 (C-6' A or C-6' B), 160.8 (C-4), 144.7 (C-5' A or C-5' B), 144.6 (C-5 'A or C-5' B), 135.34 (C-8 A or C-8 B), 135.33 (C-8 A or C-8 B), 133.4 (C-2 A or C-2 B), 133.3 (C-2 A or C-2 B), 128.8 (C-9–11), 128.7 (C-9–11), 128.7 (C-9–11), 67.14 (C-7 A or C-7 B), 67.12 (C-7 A or C-7 B), 47.8 (C-1' B), 46.6 (C-1' A), 39.8 (C-3'' B), 38.8 (C-3'' A), 36.2 (C-2', 4'' A or C-2', 4'' B), 36.0 (C-2', 4'' A or C-2', 4'' B), 35.8 (C-2', 4'' A or C-2', 4'' B), 35.7 (C-2', 4'' A or C-2', 4'' B), 25.4 (C-6'' A or C-6'' B), 25.3 (C-6'' A or C-6'' B), 23.2 (C-6'). HRMS *m/z* (ESI^+) [Found: 432.12298,

$C_{20}H_{22}N_3O_6S$ requires $[M+H]^+$ 432.12238]; LRMS *m/z* (ESI$^+$) 455 ($[M+Na]^+$, 100%); HPLC retention time 7.8 min (method 3), 97.8%.

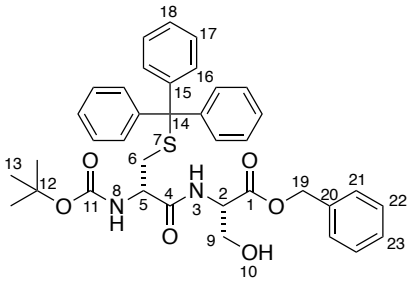
2-{(1'*R*)-1'-Acetamido-2'-[(1''-methyl-2'',5''-dioxopyrrolidin-3''-yl)sulfanyl]ethyl}-1,3-oxazole-4-carboxylic acid, 72



To a solution of benzyl 2-{(1'*R*)-1-acetamido-2-[(1-methyl-2,5-dioxopyrrolidin-3-yl)sulfan yl]ethyl}-1,3-oxazole-4-carboxylate (36 mg, 0.080 mmol, 1.0 eq) in DCM (0.8 mL) was added iodotrimethylsilane (0.18 mL, 1.25 mmol, 15.0 eq) and stirred under argon at RT. Complete consumption of the starting material was observed after 15 h following analysis by TLC, the reaction was quenched with methanol (1 mL) and concentrated *in vacuo*. The crude mixture was purified by column chromatography on silica (ethyl acetate) to afford the title compound as a pale yellow oil (16 mg, 60%): R_f 0.16 (ethyl acetate); $[\alpha]_D^{25}$ = −31.1 (*c* 1.0, methanol); $\tilde{\nu}_{max}$ (thin film/ cm^{-1}) 3268 (O-H, w), 1775 (C=O, m), 1696 (C=O, s), 1579 (C=C, m), 1541 (C=C, w), 1439 (O-H, w, bend), 1385 (C-N, m), 1285 (C-O, m), 1120 (C-O, m), 958 (C=C, m), 760 (C-H, m), 693 (C-H, m); ^{1}H NMR (400 MHz, $CDCl_3$) (diastereomer A) δ H (400 MHz, MeOD) 8.38 (1H, s, H - 5), 5.45 (0.5H, dd, J_{AX} 10.0, J_{BX} 7.6, H_x - 1'), 4.03 (0.5H, dd, J_{AX} 12.0, J_{BX} 4.6 H_x - 3''), 3.62 (0.5H, dd, J_{AB} 17.5, J_{BX} 7.6, H_b - 2'), 3.25–3.07 (1.5H, m, H_aH_b - 4', H_a - 2'), 2.96 or 2.95 (1.5, s, H- 6''), 2.45 (0.5H, dd, J_{AB} 16.3, J_{BX} 4.7, H_b - 4''), 2.02 or 2.01 (1.5H, s, H - 6'); (diastereomer B) δ H (400 MHz, MeOD) 8.38 (1H, s, H - 5), 5.53–5.31 (1H, m, H_x - 1'), 4.00 (0.5H, dd, J_{AX} 11.5, J_{BX} 4.7, H_x - 3''), 3.43

(0.5H, dd, J_{AB} 17.6, J_{BX} 8.9, H_b - 2'), 3.38–3.32 (0.5H, m, H_b - 2'), 3.25–3.07 (1.5H, m, H - 4', H_a - 2'), 2.96 or 2.95 (1.5, s, H - 6''), 2.49 (0.5H, dd, J_{AB} 16.5, J_{BX} 4.7, H_b - 4''), 2.02 or 2.01 (1.5H, s, H - 6'); ^{13}C NMR (101 MHz, $CDCl_3$) (Diastereomers A and B) δ 178.1 (C-5'' A B, or C-2'' A or B), 176.9 (C-5' A or C-5' B), 176.8 (C-5' A or C-5' B), 173.2 (C-6 A or C-6 B), 165.1 (C-2 A or C-2 B), 145.4 (C-5), 136.3 (C-4), 48.1 (C-1), 41.1 (C-3' A or C-3' B), 40.4 (C-3' A or C-3' B), 36.9 (C-4' A or C-4' B), 36.8 (C-4' A or C-4' B), 35.4 (C-4' A or C-4' B), 35.2 (C-2' A or C-2' B), 35.2 (C-2' A or C-2' B), 25.3 (C-6'' A or C-6'' B), 25.2 (C-6'' A or C-6'' B), 22.4 (C-6'); HRMS *m/z* (ESI$^+$) [Found: 364.05732, $C_{13}H_{15}N_3O_6SNa$ requires $[M+Na]^+$ 364.05738]; LRMS *m/z* (ESI$^+$) 364 ($[M+Na]^+$, 98%, 379 $(M+K)^+$; HPLC retention time 4.2 min (method 3), >99.9%.

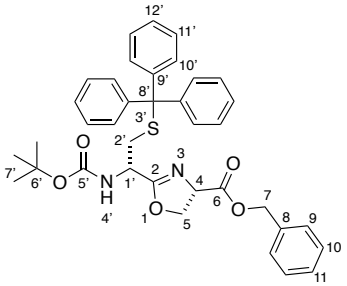
Benzyl *N*-(*tert*-butoxycarbonyl)-(*S*)-(triphenylmethyl)cysteinyl-(*S*)-serinate,[282] 167



A solution of (*S*)-serine benzyl ester hydrochloride (400 mg, 1.71 mmol, 1.1 eq.) and *N*-(*tert*-butoxycarbonyl)-(*S*)-(triphenylmethyl)cysteine (720 mg, 1.55 mmol, 1.0 eq.) was dissolved in *N,N*-dimethylformamide (9.2 mL), followed by addition of diphenyl phosphorazidate (0.40 mL, 1.9 mmol, 1.2 eq.) and triethylamine (0.46 mL, 3.3 mmol, 2.1 eq.). The solution was stirred at RT. Complete consumption of the starting material was observed after 25 h following analysis by TLC, the mixture was diluted with ethyl acetate (40 mL) and washed with lithium chloride solution (0.5 M, 5 × 40 mL). The combined aqueous components were extracted with ethyl acetate (40 mL), and the

combined organic components dried with anhydrous sodium sulfate. The residue was diluted with chloroform and hexane and concentrated *in vacuo*. The crude residue was purified by flash column chromatography on silica (petroleum ether/ethyl acetate, 7:3), to afford the title compound (840 mg, 85%) as a colourless foam: R_f 0.17 (petroleum ether/ethyl acetate, 7:3); $[\alpha]_D^{25}$ = 18.7 (*c* 1.0, chloroform); m.p. 56–58 °C (ethyl acetate); $\tilde{\nu}_{max}$ (thin film/ cm^{-1}) 2980 (N-H, w), 1740 (C=O, m), 1670 (C=O, s), 1490 (C=C, s), 1445 (C=C, m), 1367 (O-H, m), 1163 (C-O, s), 742 (C-H, s), 698 (C-H, s); ^{1}H NMR (400 MHz, $CDCl_3$) 7.39–7.32 (6 H, m, H-16–18/21–23), 7.28–7.11 (14H, m, H-16–18/21–23), 6.75 (1H, d, *J* 7.0, H - 8), 5.17–5.08 (2H, m, H - 19), 4.72 (1H, s, H - 3), 4.60–4.54 (1H, m, H - 5), 3.92 (1H, s, H - 6), 3.80 (1H, td, *J* 8.2, 3.9, H - 6), 3.71 (1H, s, H - 2), 2.61–2.47 (3H, m, H - 9, 10), 1.34 (9H, s, H - 13); ^{13}C NMR (101 MHz, $CDCl_3$) 170 (C-1/4), 169.9 (C-1/4), 144.2 (C-15), 135.1 (C-20), 129.5 (C-17), 128.7 (C-22), 128.5 (C-23), 128.18 (C-16), 128.16 (C-21), 127.0 (C-18), 80.8 (C-12), 67.5 (C-19), 67.4 (C-14), 62.5 (C-6), 55.1 (C-5), 54.0 (C-2), 33.5 (C-9), 28.2 (C-13); HRMS *m/z* (ESI^+) [Found: 663.24988, $C_{37}H_{40}N_2O_6SNa$ requires $[M+Na]^+$ 663.24993]; LRMS *m/z* (ESI^+) 663 ($[M+Na]^+$, 33%) 243 (100%); HPLC (method 3) retention time 10.2 min, 97.9%.

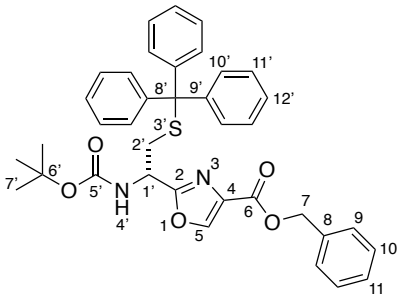
Benzyl 2-{(1'*S*)-1'-[(*tert*-butoxycarbonyl)amino]-2'-[(triphenylmethyl)sulfanyl]ethyl}-4,5-dihydro-1,3-oxazole-4-carboxylate, 168



A solution of benzyl *N*-(*tert*-butoxycarbonyl)-(*S*)-(triphenylmethyl)cysteinyl-(*S*)-serinate (1.5 g, 2.3 mmol, 1.0 eq.) in anhydrous tetrahydrofuran (23 mL) was added to triphenyl phosphine (1.0 g, 3.5 mmol, 1.5 eq.), followed by addition of diethyl azodicarboxylate (DEAD, 0.54 mL, 3.5 mmol, 1.5 eq.) and the solution was stirred at RT. Complete consumption of the starting material was observed after 19 h following analysis by TLC, and the solution was concentrated *in vacuo*. The crude residue was purified by column chromatography on silica (cyclohexane/ ethyl acetate, 8:2) concentrated *in vacuo* to afford the title compound as a colourless foam (1.3 g, 92%): R_f 0.24 (cyclohexane /ethyl acetate, 8:2); $[\alpha]_D^{25}$ = 23.9 (*c* 1.0, chloroform); $\tilde{\nu}_{max}$ (thin film/ cm^{-1}) 3658 (N-H, w), 2981 (N-H, m), 1741 (C=O, m), 1716 (C=O, m), 1661 (C=O, m), 1491 (C-H, m), 1382 (C-N, m), 1367 (C-N, m), 1367 (C-N, m), 1250 (C-O, m), 1165 (C-O, s), 955 (C=C, m), 743 (C-H, s), 699 (C-H, s); ^{1}H NMR (400 MHz, $CDCl_3$) 7.45–7.11 (20 H, m, H - 3''–5'', 9–11), 5.23–5.06 (3H, m, H - 7, 4'), 4.74 (1H, ddd, *J* 10.6, 8.3, 0.9, H - 4), 4.54–4.43 (2H, m, H - 5, 1'), 4.38 (1H, dd, *J* 10.6, 8.3, H - 5), 2.66–2.58 (1H, m, H - 2'), 2.51 (1H, dd, *J* 12.2, 5.6, H - 2'), 1.40 (9H, d, *J* 1.6, H - 7'); ^{13}C NMR (126 MHz, $CDCl_3$) δ 170.5 (C-6), 168.7 (C-2), 154.9 (C-5'), 144.6 (C-2''), 135.4 (C-8), 129.7 , 128.7, 128.6, 128.4, 128.1, 126.9 (C3''–5'', 9–11), 80.0 (C-6'), 70.4 (C-5), 68.1 (C-4), 67.4 (C-7), 66.8 (C-1''), 48.1 (C-1'), 35.0 (C-2'), 28.4 (C-7'); HRMS *m/z* (ESI^+) [Found: 623.25774, $C_{37}H_{39}N_2O_5S$ requires $[M+H]^+$ 623.25742]; LRMS *m/z*

(ESI⁻) 645 ([M+Na]⁺, 13%), 243 (trityl 100%); HPLC (method 3) retention time 10.0 min, 97.4%.

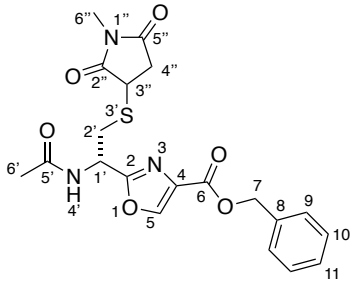
Benzyl 2-{(1'*S*)-1'-[(*tert*-butoxycarbonyl)amino]-2'-[(triphenylmethyl)sulfanyl]ethyl}-1,3-oxazole-(4*S*)-carboxylate, 169



Bromotrichloromethane (50 µL, 0.27 mmol, 1.1 eq.) was added to a solution of benzyl 2-{(1'*S*)-1-[(*tert*-butoxycarbonyl)amino]-2-[(triphenylmethyl)sulfanyl]ethyl}-4,5-dihydro-1,3-oxazole-4-carboxylate (160 mg, 0.26 mmol, 1.0 eq.) in DCM (1.3 mL) at 0 °C, followed by addition of DBU (80 µL, 0.51 mmol, 1.1 eq.). Complete consumption of the starting material was observed after 7 h following analysis by TLC, and the solution was concentrated *in vacuo*. The crude residue was purified by flash column chromatography on silica (petroleum ether/ethyl acetate, 8:2), and then dried at 60 °C under a high vacuum for 24 h to afford the title compound (59 mg, 36%) as a colourless oil: R_f 0.48 (cyclohexane/ethyl acetate, 8:2); $[\alpha]_D^{25}$ = 5.5 (*c* 1.0, chloroform); m.p. 53–56 °C (from hexane); $\tilde{\nu}_{max}$ (thin film/ cm^{-1}) 2978 (N-H, w), 1716 (C=O, s), 1716 (C=O, s), 1581 (C=C, m), 1493 (C-H, m), 1446 (C-H, m), 1367 (C-N, m), 1317 (C-N, m), 1250 (C-O, m), 1166 (C-O, s), 1110 (C-O, s), 745 (C=C, s), 699 (C-H, s); ^{1}H NMR (400 MHz, $CDCl_3$) 8.10 (1H, s, H - 5), 7.45–7.33 (11H, m, H - 4, 9, 10, 11), 7.30–7.15 (9H, m, H - 3'', 5''), 5.35 (2H, s, H - 7), 5.23–5.08 (1H, m, H - 4'), 4.83 (1H, s, H - 1'), 2.80–2.66 (2H, m, H - 2'), 1.42 (9H, s, 7'); ^{13}C NMR (101 MHz, $CDCl_3$) δ 164.1 (C-2), 161.0 (C-6), 154.8 (C-5'), 144.4 (C-4), 144.3 (C-5), 135.5

(C-8), 133.4 (C-2''), 129.6, 128.8, 128.7, 128.6, 128.2, 127.0 (C-3''–5'', 9–11), 80.4 (C-6'), 67.2 (C-1''), 67.0 (C-7), 48.3 (C-1'), 35.8 (C-2'), 28.4 (C-7'); HRMS *m/z* (ESI^+) [Found: 643.22351, $C_{37}H_{36}N_2O_5S$ requires $[M+Na]^+$ 643.22481]; LRMS *m/z* (ESI^+) 643 ($[M+Na]^+$, 100%); HPLC retention time 12.9 min (method 3), >99%.

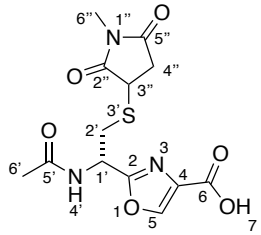
Benzyl 2'-{(1'*S*)-1'-acetamido-2'-[(1''-methyl-2'',5''-dioxopyrrolidin-3''-yl)sulfanyl]ethyl}-1,3-oxazole-4-carboxylate, 170



Triethylsilane (0.27 mL, 1.7 mmol, 3.0 eq.) was added to a solution of benzyl 2-{(1'*S*)-1-[(*tert*-butoxycarbonyl)amino]-2-[(triphenylmethyl)sulfanyl]ethyl}-1,3-oxazole-4-carboxylate (360 mg, 0.57 mmol, 1.0 eq.) in DCM (9.5 mL) and trifluoroacetic acid (20% *v/v*), and the solution was stirred for 1 h before removal of the DCM *in vacuo*. The residue was re-dissolved in methanol (5.7 mL) and *N*-methylmaleimide added (63 mg, 0.57 mmol, 1.0 eq.), and the solution stirred for 5 h after which another equivalent of maleimide was added. Complete consumption of the intermediate thiol was observed after 15 h following analysis by TLC. The solution was concentrated *in vacuo* and dissolved in tetrahydrofuran (5.7 mL), followed by addition of acetyl chloride (50 µL, 0.63 mmol, 1.1 eq.) and triethylamine (0.16 mL, 1.1 mmol, 2.0 eq.). Complete consumption of the second intermediate amine was observed after 6.5 h following analysis by TLC, the solution was concentrated *in vacuo* and purified by flash column chromatography on silica (20% → 50% acetone in toluene) to afford the title compound (190 mg, 79% yield)

as a colourless oil: R_f 0.14 (20% acetone in toluene); $[\alpha]_D^{25}$ = 29.5 (*c* 1.0, methanol); $\tilde{\nu}_{max}$ (thin film/ cm^{-1}) 3292 (N-H, w), 1777 (C=O, w), 1697 (C=O, s), 1580 (C=C, m), 1532 (C=C, m), 1436 (C-H, m), 1382 (C-H, m), 1281 (C-O, m), 1110 (C-O, s), 911 (C=C, m), 729 (C-H, s), 695 (C-H, m); ^{1}H NMR (500 MHz, MeOD) (diastereomer A) 8.18 or 8.17 (1H, s, H - 5), 7.41–7.28 (5H, m, H - 9–11), 6.92 (0.5H, d, *J* 8.6, H - 4'), 5.64–5.46 (0.5H, m, H_x - 1'), 5.31 (2H, s, H - 7) 3.96 (1H, dd, J_{AX} 9.1, J_{BX} 3.8, H_X - 3''), 3.62–3.55 (1H, m, H_aH_b - 2'), 3.16–3.06 (1.5H, m, H_aH_b - 2', H_a - 4''), 2.96 or 2.95 (1.5H, s, H - 6''), 2.40 (1H, dd, J_{AB} 18.0, J_{BX} 3.8, H_a - 4''), 2.04 or 2.03 (3H, s, H - 6'); (diastereomer B) 8.18 or 8.17 (1H, s, H - 5), 7.41–7.28 (5H, m, H - 9–11), 7.24 (0.5H, d, *J* 8.6, H - 4'), 5.64–5.46 (0.5H, m, H_aH_b - 1'), 5.31 (2H, s, H - 7), 3.77 (1H, dd, J_{AX} 9.2, J_{BX} 4.1, H_x - 3''), 3.62–3.55 (1H, m, H_aH_b - 2'), 3.23 (0.5H, dd, *J* 14.3, 6.0, H_b - 2') 3.16–3.05 (1.5H, m, H_aH_b - 2', H_a - 4''), 2.96 or 2.95 (1.5H, s, H - 6''), 2.44 (1H, dd, J_{AB} 18.4, J_{BX} 4.1 H_b - 4''), 2.04 or 2.03 (3.0H, s, H_aH_b - 6'), 2.03 (1.5H, s, H - 6'); ^{13}C NMR (126 MHz, $CDCl_3$) (Diastereomers A and B) 177.3 (C-2'' A or C-2'' B), 177.1 (C-2'' A or C-2'' B), 174.7 (C-5'' A or C-5'' B), 174.6 (C-5'' A or C-5'' B), 170.6 (C-5' A or C-5' B), 170.4 (C-5' A or C-5' B), 163.76 (C-6 A or C-6 B), 163.66 (C-6 A or C-6 B), 161.0 (C-4), 144.9 (C-5 A or C-5 B), 144.8 (C-5 A or C-5 B), 135.54 (C-8 A or C-8 B), 135.52 (C-8 A or C-8 B), 133.6 (C-2 A or C-2 B), 133.5 (C-2 A or C-2 B), 128.97 (C-9/10 A or C-9/10 B), 128.96 (C-9/10 A or C-9/10 B), 128.91 (C-11 A or C-11 B), 128.90 (C-11 A or C-11 B), 128.88 (C-9/10 A or C-9/10 B), 128.87 (C-9/10 A or C-9/10 B), 67.29 (C-7 A or C-7 B), 67.28 (C-7 A or C-7 B), 47.9 (C-1' B), 46.8 (C-1' A), 40.0 (C-3'' B), 39.0 (C-3'' A), 36.4 (C-4'' A or C-4'' B), 36.00 (C-2' A or C-2' B), 35.92 (C-4'' A or C-4'' B), 35.8 (C-2' A or C-2' B), 25.6 (C-6'' A or C-6'' B), 25.5 (C-6'' A or C-6'' B), 23.3 (C-6'); HRMS *m/z* (ESI^+) [Found: 454.10463, $C_{20}H_{12}N_3O_6S$ requires $[M+Na]^+$ 454.10433]; LRMS *m/z* (ESI^+) 454 ($[M+Na]^+$, 100%); HPLC retention time 6.9 min (method 3), 99.6%.

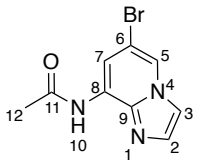
2-{(1'*S*)-1'-Acetamido-2'-[(1''-methyl-2'',5''-dioxopyrrolidin-3''-yl)sulfanyl]ethyl}-1,3-oxazole-4-carboxylic acid, 165



To a solution of benzyl 2-{(1'*S*)-1-acetamido-2-[(1-methyl-2,5-dioxopyrrolidin-3-yl)sulfanyl]ethyl}-1,3-oxazole-4-carboxylate (128 mg, 0.30 mmol, 1.0 eq) in DCM (3.0 mL) was added iodotrimethylsilane (0.63 mL, 4.45 mmol, 15.0 eq) and stirred under argon at RT. Complete consumption of the starting material was observed after 21 h following analysis by TLC, the reaction was quenched with water (1 mL), and concentrated *in vacuo*. The crude mixture was purified by column chromatography on silica (ethyl acetate and 1% acetic acid → acetone and 1% acetic acid) to afford the title compound (22 mg, 22%): R_f 0.41 (acetone and 1% acetic acid); $[\alpha]_D^{25}$ = 17.2 (*c* 1.0, methanol); $\tilde{\nu}_{max}$ (thin film/ cm^{-1}) 3287 (O-H, m br), 1775 (C=O, w), 1698 (C=O, s), 1542 (C=C, m), 1438 (O-H, m), 1386 (C-H, m), 1286 (C-O, m), 1121 (C-N, m), 692 (C-H, w); ^{1}H NMR (500 MHz, MeOD) (diastereomer A) 8.38 (1H, s, H - 5), 5.46 (0.5H, s, H_x - 1'), 4.08–3.95 (1H, m, H_x - 3''), 3.61 (0.5H, d, J_{AB} 13.9, H_b - 2'), 3.46–3.30 (1H, m, H_aH_b - 2'), 3.25–3.06 (1.5H, m, H_a - 2', H_aH_b - 4'), 2.95 or 2.94 (1.5H, s, H - 6''), 2.45 (1H, d, J_{AB} 17.6, H_b - 4''), 2.02 or 2.01 (1.5, s, H - 6'); (diastereomer B) 8.38 (1H, s, H_aH_b, H - 5), 5.41 (0.5H, s, H_x - 1'), 4.08-3.95 (1H, m, H_x - 3''), 3.46–3.30 (1H, m, H_aH_b - 2'), 3.25–3.06 (1.5H, m, H_a - 2', H_aH_b - 4'), 2.95 or 2.94 (1.5H, s, H - 6''), 2.47 (1H, d, J_{AB} 16.8, H_b - 4''), 2.02 or 2.01 (1.5H, s, H - 6'); ^{13}C NMR (101 MHz, $CDCl_3$) (Diastereomers A and B) δ 178.8 (C-2''/5'' A or C-2''/5'' B), 178.7 (C-2''/5'' A or C-2''/5'' B) 176.9 (C-5' A or C-5' B), 176.8 (C-5' A or C-5' B), 173.2 (C-6 A or C-6 B), 173.0

(C-6 A or C-6 B), 165.3 (C-2 A or C-2 B), 164.3 (C-2 A or C-2 B), 145.4 (C-5), 136.3 (C-4), 48.1 (C-1), 41.0 (C-3' A or C-3' B), 40.4 (C-3' A or C-3' B), 36.9 (C-4' A or C-4' B), 36.7 (C-4' A or C-4' B), 35.2 (C-2' A or C-2' B), 35.2 (C-2' A or C-2' B), 25.3 (C-6'' A or C-6'' B), 25.2 (C-6'' A or C-6'' B), 22.4 (C-6'); HRMS *m/z* (ESI^+) [Found: 364.05767, $C_{13}H_{15}N_3O_6S$ requires $[M+Na]^+$ 364.05738]; LRMS *m/z* (ESI^+) 364 ($[M+Na]^+$, 100%; HPLC retention time 2.44 min (method 3), 97.9%.

N-(6-Bromoimidazo[1,2-*a*]pyridin-8-yl)acetamide, 179

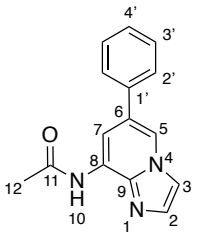


Hydrochloric acid (0.3 mL conc., 2% *v/v*) was added to a solution of bromoacetaldehyde diethyl acetal (2.4 mL, 15 mmol, 1.9 eq) in dioxane/water (2:1, 15 mL) and heated to 88 °C for 40 min. The solution was cooled to RT, after which sodium hydrogen carbonate (2.6 g) was added, followed by the dropwise addition of a mixture of 2,3-diamino-5-bromopyridine (1.5 g, 8.0 mmol, 1.0 eq) in dioxane/water (2:1, 15 mL). The resulting mixture was heated to 88 °C, complete consumption of the starting material was observed after 23.5 h following analysis by TLC. The mixture was diluted with aqueous sodium hydroxide (1 M, 100 mL), shaken with DCM (100 mL), and the resulting emulsion filtered through a pad of celite under reduced pressure. The aqueous components were extracted and filtered again with DCM (100 mL), the combined organic components washed with sat. brine solution (100 mL) and filtered. The combined organic components were dried with sodium sulfate, concentrated *in vacuo*, to afford the crude

intermediate 6-bromoimidazo[1,2-*a*]pyridin-8-amine which was used without further purification.

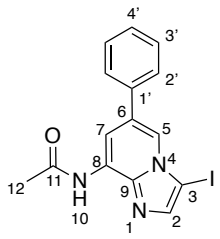
Acetic anhydride (0.45 mL, 4.8 mmol, 1.5 eq), pyridine (0.28 mL, 3.5 mmol, 1.1 eq), and DMAP (39 mg, 0.32 mmol, 0.1 eq) were added to a solution of the intermediate 6-bromoimidazo[1,2-*a*]pyridin-8-amine in DCM (3.2 mL) and the resulting mixture stirred at RT for 6 h after which acetic anhydride (0.30mL, 3.2 mmol, 1.0 eq) was added. The mixture was stirred for an additional 16 h, after which acetic anhydride (0.45 mL, 4.8 mmol, 1.5 eq) and triethylamine (0.66 mL, 4.8 mmol, 1.5 eq) was added. The mixture was warmed to 30 °C and stirred for 6 h before a final addition of acetic anhydride (0.45 mL, 4.8 mmol, 1.5 eq), and the resulting mixture was stirred for 18.5 h, before being concentrated *in vacuo*. The crude residue was purified by flash column chromatography on silica (20% acetone in toluene) to afford the title compound as a brown solid (420 mg, 52%): R_f 0.31 (30% acetone in toluene); m.p. 130–135 °C (decomposed, chloroform); ṽmax (neat/ cm^{-1}) 3143 (N-H, w), 1688 (C=O, s), 1542 (C=C, s), 1487 (N-H, m), 1415 (C-H, m), 1290 (C-N, m), 1260 (C-N, m), 1229 (N-C, m), 1145 (C-N, m), 747 (C-H, s), 710 (C-H, m); ^{1}H NMR (500 MHz, $CDCl_3$) 8.68 (1H, s, H - 10), 8.28 (1H, d, *J* 1.7, H - 5), 8.00 (1H, d, *J* 1.7, H - 7), 7.53 (1H, d, *J* 1.2, H - 2 or H - 3), 7.50 (1H, d, *J* 1.2, H - 2 or H - 3), 2.27 (3H, s, H -12); ^{13}C NMR (126 MHz, $CDCl_3$) 169.7 (C-11), 138.1 (C-9), 132.7 (C-3 and C-2), 127.8 (C-8), 120.6 (C-7), 114.2 (C-5), 108.5(C-6), 25.1 (C-12); HRMS *m/z* (ESI^+) [Found: 253.99248, 255.99032 $C_9H_9N_3OBr$ requires $[M+H]^+$ 253.99235, 255.99030]; LRMS *m/z* (ESI^+) 254 ($[M+H]^+$, 100%), 256 (97%); HPLC (method 4) retention time 9.3 min, 98.5%.

N-(6-Phenylimidazo[1,2-*a*]pyridin-8-yl)acetamide, 180



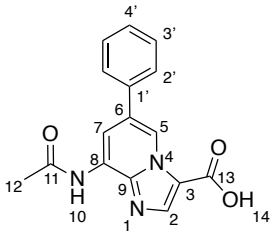
Caesium chloride (1.6 g, 5.0 mmol, 2.5 eq) was added to a solution of *N*-(6-bromoimidazo[1,2-*a*]pyridin-8-yl)acetamide (0.50 g, 2.0 mmol, 1.0 eq) in de-gassed toluene (5.2 mL) followed by phenylboronic acid (290 mg, 2.4 mmol, 1.2 eq) and [1,1′-bis(diphenylphosphino)ferrocene]dichloropalladium(II) (48 mg, 0.060 mmol, 0.030 eq). The resulting mixture was stirred at 90 °C. Complete consumption of the starting material was observed after 6 h following analysis by TLC. The reaction mixture was washed through a pad of celite with ethanol and concentrated *in vacuo* to afford the crude product. The crude residue was purified by flash column chromatography on silica (ethyl acetate) to afford the desired compound as an off-white solid (480 mg, 97%): R_f 0.39 (ethyl acetate) m.p. 162–164 °C (chloroform); ṽmax (neat/ cm^{-1}) 1691 (C=O, m), 1556 (C=C, s), 1503 (N-H, m), 1485 (N-H, m), 1420 (C-H, m), 1368 (C-H, m), 1316 (C-H, m), 1254 (C-N, m), 764 (C-H, m), 698 (C-H, m); ^{1}H NMR (500 MHz, $CDCl_3$) 8.74 (1H, s, H - 10), 8.47 (1H, d, *J* 1.7, H - 5), 8.03 (1H, d, *J* 1.7, H - 7), 7.62 (1H, d, *J* 1.0, H - 2), 7.60–7.56 (4H, m, H - 3'), 7.54 (1H, d, *J* 1.0, H - 3), 7.47–7.42 (2H, m, H - 2'), 7.40–7.36 (1H, m, H - 4'), 2.30 (3H, s, H - 12); ^{13}C NMR (126 MHz, $CDCl_3$) 169.2 (C-11), 138.4 (C-9), 137.3 (C-1'), 132.1 (C-3), 128.8 (C-2' or C-3'), 127.8 (C-4'), 127.1 (C-6), 127.0 (C-2' or C-3'), 117.5 (C-7), 114.0 (C-2), 111.1 (C-5), 24.7 (C-12); HRMS *m/z* (ESI^+) [Found: 252.11316, $C_{15}H_{14}N_3O$ requires $[M+H]^+$ 252.11314; LRMS *m/z* (ESI^+) 252.0 ($[M+H]^+$, 100%); HPLC (method 3) retention time 3.3 min, 97.2%.

N-(3-Iodo-6-phenylimidazo[1,2-*a*]pyridin-8-yl)acetamide, 181



N-Iodosuccinimide (37 mg, 0.16 mmol, 1.2 eq) was added to a solution of *N*-(6-phenylimidazo[1,2-*a*]pyridin-8-yl)acetamide (34 mg, 0.14 mmol, 1.0 eq) in DCM (1.4 mL) in a foil covered flask at 0 °C dropwise under argon. Complete consumption of the starting material was observed after 3 h following analysis by TLC. The solution was diluted with ethyl acetate (10 mL), washed with sat. sodium thiosulfate (10 mL), dried with sodium sulfate, and concentrated *in vacuo*. The crude residue was purified by flash column chromatography on silica (ethyl acetate), and the resulting product dissolved in DCM (2 mL) and washed with sat. sodium bicarbonate (4 mL), water (2 mL), brine (2 mL). The organic components were dried with sodium sulfate and concentrated *in vacuo* to afford the title compound as a light brown solid (35.8 mg, 68%): R_f 0.31 (6:4 petroleum ether/ethyl acetate); m.p. 146–148 °C (chloroform); ṽmax (neat/ cm^{-1}) 3284 (N-H, w), 3233 (N-H, w), 1698 (C=O, s), 1562 (C=C, s), 1503 (C-H, m), 1481 (C-H, m), 1411 (C-H, m), 1262 (C-N, s), 1005 (C-N, m), 742 (C-H, m), 691 (C-I, s); ^{1}H (500 MHz, $CDCl_3$, 34 mg mL^{-1}) 8.60–8.51 (2H, m, H - 5, 10), 8.00 (1H, d, *J* 1.5, H - 7), 7.66–7.60 (3H, m, H - 2, 2'/3'), 7.51–7.46 (2H, m, H - 2'/3'), 7.44–7.39 (1H, m, H - 4'), 2.32 (3H, s, H - 12); ^{13}C NMR (126 MHz, $CDCl_3$) 169.4 (C-11), 140.6 (C-9), 139.0 (C-2), 137.5 (C-1'), 129.2 (C-2'/3'), 129.1 (C-8), 128.3 (C-4'), 127.5 (C-2'/3'), 127.2 (C-6), 118.0 (C-5), 111.8 (C-7), 62.7 (C-3), 25.0 (C-12); HRMS *m/z* (ESI^+) [Found: 378.0099 $C_{15}H_{12}N_3O$ requires $[M+H]^+$ 378.0098; LRMS *m/z* (ESI^+) 378 ($[M+H]^+$, 100%); HPLC (method 3) retention time 5.1 min, 99.5%.

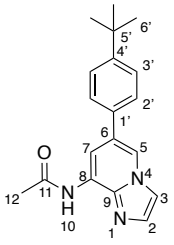
8-Acetamido-6-phenylimidazo[1,2-*a*]pyridine-3-carboxylic acid, 73



A solution of sodium formate (36 mg, 0.53 mmol, 2.5 eq), DIPEA (0.073 mL, 0.42 mmol, 2.0 eq), and acetic anhydride (0.040 mL, 0.42 mmol, 2.0 eq) in DMF (0.6 mL) was stirred at RT for 30 min under argon. Following this a solution of *N*-(3-iodo-6-phenylimidazo[1,2-*a*]pyridin-8-yl)acetamide (80 mg, 0.21 mmol, 1.0 eq), lithium chloride (28 mg, 0.65 mmol, 3.1 eq), and palladium acetate (9.0 mg, 0.040 mmol, 0.20 eq) in DMF (1.0 mL) under argon was added, and the resulting mixture heated to 80 °C. Complete consumption of the starting material was observed after 5 h following analysis by TLC. The mixture was filtered through a syringe filter with water (20 mL) and ethyl acetate (20 mL). The aqueous components were acidified to approximately pH 2 with HCl (2 M) and extracted with ethyl acetate (2 × 20 mL), and the organic components dried with sodium sulfate, and concentrated *in vacuo*. The resulting crude residue was purified by flash column chromatography on silica (9:1 DCM/MeOH → 9:1 DCM/MeOH and 1% acetic acid) to afford the title compound as a colourless solid (44 mg, 71%): R_f 0.19 (9:1 DCM/MeOH); m.p. 194–197°C (decomposed, methanol); $\tilde{\nu}_{max}$ (neat/ cm^{-1}) 3234 (O-H, w), 1677 (C=O, m), 1631 (C=N, m), 1561 (C=C, s), 1544 (C=C, m), 1469 (C-H, m), 1404 (O-H, s), 1374 (O-H, s), 1243 (C-N, s), 1214 (C-N, s), 1147 (C-O, s), 754 (C-H, s), 690 (C-H, s), 658 (C-H, s); ^{1}H NMR (400 MHz, D_6-DMSO) 10.25 (1H, s, H - 14), 9.27 (1H, s, H - 5), 8.51 (1H, s, H - 7), 8.18 (1H, s, H - 2), 7.65–7.62 (2H, m, H - 3'), 7.56–7.51 (2H, m, H - 2'), 7.47–7.43 (1H, m, H - 4'), 2.25 (3H, s, H - 12); ^{13}C NMR (126 MHz, D_6-DMSO) 170.3 (C-11),

162.0 (C-13), 140.2 (C-9), 139.0 (C-2), 137.2 (C-1'), 129.4 (C-2'), 128.2 (C-4'), 127.8 (C-6), 127.6 (C-3), 126.9 (C-3'), 119.3 (C-8), 119.2 (C-5), 113.6 (C-7), 24.1 (C-12); HRMS *m/z* (ESI$^-$) [Found: 294.0889, $C_{16}H_{13}N_3O_3$ requires [M–H]$^-$ 294.0884]; LRMS *m/z* a LR spectrum could not be obtained for this compound; HPLC (method 3) retention time 7.4 min, 98.8%.

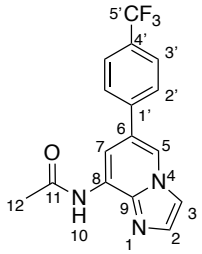
N-[6-(4'-*Tert*-butylphenyl)imidazo[1,2-*a*]pyridin-8-yl]acetamide, 186



Caesium chloride (1600 mg, 4.9 mmol, 2.5 eq) was added to a solution of *N*-(6-bromoimidazo[1,2-*a*]pyridin-8-yl)acetamide (500 mg, 2.0 mmol, 1.0 eq) in de-gassed toluene (5.2 mL) followed by (4-*tert*-butyl)phenylboronic acid (420 mg, 2.4 mmol, 1.2 eq) and [1,1′-Bis(diphenylphosphino)ferrocene]dichloropalladium(II) (48 mg, 0.060 mmol, 0.030 eq). The resulting mixture was stirred at 90 °C for 3 h until the starting material showed complete consumption by TLC to give the desired compound as an off-white solid (180 mg, 28%): R_f 0.37 (ethyl acetate); m.p. 52–56 °C (chloroform); ṽmax (neat/ cm^{-1}) 1683 (C=O, s), 1558 (C=C, s), 1509 (C=C, m), 1485 (C=C, m), 1428 (C-H, m), 1365 (C-H, m), 1316 (C-H, m), 1247 (C-N, m), 828 (C-H, s), 733 (C-H, s), 695 (C-H, m); ^{1}H NMR (500 MHz, Chloroform-d) 8.78 (1 H, s, H - 10), 8.47 (1 H, d, *J* 1.6, H - 5), 8.02 (1 H, d, *J* 1.6, H - 7), 7.60 (1 H, d, *J* 1.3, H - 3), 7.56–7.50 (3 H, m, H - 2, 2'), 7.49–7.45 (2 H, m, H - 3'), 2.28 (3 H, s, H -12), 1.36 (10 H, s, H -6'); ^{13}C NMR (126 MHz, $CDCl_3$) 169.4 (C-11), 151.2 (C-4'), 138.6 (C-3), 134.6 (C-8), 132.2 (C-2), 127.9 (C-6), 127.2

(C-1'), 126.9 (C-2'), 126.1 (C-3'), 117.5 (C-7), 114.2 (C-3), 111.5 (C-5), 34.7 (C-5'), 31.4 (C-6'), 24.9 (C-12); HRMS m/z (ESI$^+$) [Found: 308.1759, $C_{19}H_{22}N_3O$ requires $[M+H]^+$ 308.1757; LRMS m/z (ESI$^+$) 308 ($[M+H]^+$, 100%); HPLC (method 3) retention time 8.1 min, 95.4%.

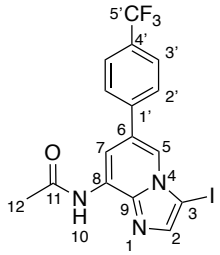
N-[6-(4'-Trifluoromethylphenyl)imidazo[1,2-*a*]pyridin-8-yl]acetamide, 185



Caesium chloride (1600 mg, 4.9 mmol, 2.5 eq) was added to a solution of *N*-(6-bromoimidazo[1,2-*a*]pyridin-8-yl)acetamide (500 mg, 2.0 mmol, 1.0 eq) in degassed toluene (5.2 mL) followed by (4-trifluoromethyl)phenylboronic acid (450 mg, 2.4 mmol, 1.2 eq) and [1,1′-bis(diphenylphosphino)ferrocene]dichloropalladium(II) (48 mg, 0.060 mmol, 0.030 eq). The resulting mixture was stirred at 90 °C. Complete consumption of the starting material was observed after 3 h following analysis by TLC. The reaction mixture was washed through a pad of celite with ethanol and concentrated *in vacuo* to afford the crude product. The crude residue was purified by flash column chromatography on silica (ethyl acetate) to afford the desired compound as an off-white solid (350 mg, 55%): R_f 0.30 (ethyl acetate); m.p. 154 °C (ethyl acetate); ῡmax (neat/ cm^{-1}) 1708 (C=O, m), 1681 (C=N, m), 1556 (C=C, s), 1485 (C-H, m), 1407 (C-H, m), 1320 (C-F, s), 1235 (C-N, m), 1166 (C-N, m), 1112 (C-N, s), 1070 (C=C, s), 821 (C-H, m), 736 (C-H, m); ^{1}H NMR (500 MHz, $CDCl_3$) 8.69 (1H, s, H - 10), 8.47 (1H, d, *J* 1.7, H - 5), 8.07 (1H, d, *J* 1.7, H - 7), 7.70 (4H, s, H - 2', 3'), 7.65 (1H, d, *J* 1.3, H - 3), 7.58 (1H, d, *J* 1.3, H - 2), 2.31

(3H, s, H - 12); ^{13}C NMR (126 MHz, $CDCl_3$) 169.6 (C-11), 141.2 (C-1'), 138.7 (C-9), 132.8 (C-2), 130.2 (q, *J* 32.8, C-4'), 127.7 (C-8), 127.6 (C-2'), 126.7 (C-6), 126.1 (q, *J* 2.52, 10, C-3'), 124.3 (q, *J* 272.2, C-5'), 118.2 (C-7), 114.5 (C-3), 110.6 (C-5), 24.9 (C-12); ^{19}F NMR (471 MHz, CDCl3, ^{1}H decoupled) –62.5 (3F, s, F - 5'); HRMS *m/z* (ESI^+) [Found: 320.1004, $C_{16}H_{13}N_3OF_3$ requires $[M+H]^+$ 320.1005; LRMS *m/z* (ESI^+) 320 ($[M+H]^+$, 100%); HPLC (method 5) retention time 8.2 min, 97.3%.

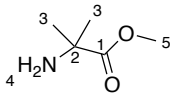
N-[3-Iodo-6-(4'-trifluoromethylphenyl)imidazo[1,2-*a*]pyridin-8-yl]acetamide, 187



N-Iodosuccinimide (300 mg, 1.3 mmol, 1.2 eq) was added to a solution of *N*-(3-iodo-6-[4-(trifluoromethyl)phenyl]imidazo[1,2-*a*]pyridin-8-yl)acetamide (350 mg, 1.1 mmol, 1.0 eq) in DCM (7.2 mL) in a foil covered flask at 0 °C dropwise under argon, and the resulting solution was stirred. Complete consumption of the starting material was observed after 6 h following analysis by TLC. The crude residue was purified by flash column chromatography on silica (20% acetone in toluene), and the resulting product dissolved in DCM (40 mL) and washed with sat. sodium thiosulfate (40 mL), sat. sodium bicarbonate (40 mL), water (40 mL), and brine (40 mL). The organic components were dried with sodium sulfate and concentrated *in vacuo* to afford the title compound as a light brown solid (170 mg, 35%): R_f 0.49 (20% acetone in toluene); m.p. 104–125 °C (decomposed, chloroform); $\tilde{\nu}$max (neat/cm^{-1}) 1693 (C=O, m), 1677 (C=O, m), 1558 (C=C, m), 1487 (C-H, m), 1403 (C-H, m), 1326 (C-F, s), 1167 (C-N, m), 1112 (C-N, s), 1072 (C-N,

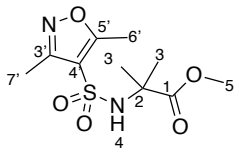
m), 1016 (C-N, m), 846 (C-H, m), 810 (C-H, m); ^{1}H (500 MHz, $CDCl_3$, 34 mg mL^{-1}) 8.70 (1H, s, H - 10), 8.56 (1H, d, *J* 1.6, H - 5), 8.02 (1H, d, *J* 1.6, H - 7), 7.74 (4H, s, H - 2'/3'), 2.33 (3H, s, H - 12); ^{13}C NMR (126 MHz, $CDCl_3$) 169.6 (C-11), 141.0 (C-1'), 140.5 (C-9), 139.0 (C-2), 130.6 (q, *J* 32.8, C-4'), 127.81 (C-2'), 127.79 (C-8), 127.5 (C-6), 126.2 (q, *J* 3.8, C-3'), 124.2 (q, *J* 272.2, C-5') 118.4 (C-7), 111.5 (C-5), 63.17 (C-3), 25.0 (C-12); ^{19}F NMR (471 MHz, $CDCl_3$, ^{1}H decoupled) –62.5 (3F, s, F - 5'); HRMS *m/z* (ESI^+) [Found: 445.9976 $C_{16}H_{12}N_3OF_3I$ requires $[M+H]^+$ 445.9972; LRMS *m/z* (ESI^+) 446.0 ($[M+H]^+$, 95%), 502 (100%); HPLC (method 3) retention time 9.2 min, 87.2%.

Methyl 2-methylalaninate, 194[284,285]



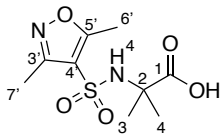
Trimethylsilyl chloride (2.5 mL, 19 mmol, 2.0 eq) was added to 2-aminoisobutyric acid (1000 mg, 9.7 mmol, 1.0 eq) dropwise under stirring. Methanol (10 mL) was then added and the solution stirred at RT. Complete consumption of the starting material was observed after 18 h following analysis by TLC, and the mixture was concentrated *in vacuo*. The residue was suspended in hexane (20 mL), isolated by Büchner filtration and washed with hexane. The residue was dried *in* v*acuo* to afford the title compound (1400 mg, 94%) as a colourless solid: R_f 0.32 (methanol); m.p. 152–154 °C (from methanol, compound is hygroscopic) [lit.[284] 180–182 °C from ethanol/ether, lit.[285] 181 °C from methanol/ether]; ^{1}H NMR (400 MHz, MeOD) δ 3.85 (3H, s, H - 5), 1.57 (6H, s, 2 × H - 3); *m/z* (ESI^+) 118 ($[M+H]^+$, 100%). Spectroscopic data are in agreement with literature.[284,285]

Methyl *N*-((3',5'-dimethyl-1',2'-oxazole-4'-sulfonyl)amino)-2-methylalaninate, 195



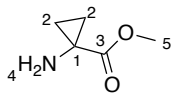
Triethylamine (0.43 mL, 3.1 mmol, 3.0 eq) was added to a solution of methyl 2-amino-2-methylpropanoate (240 mg, 1.5 mmol, 1.5 eq) in THF (5.0 mL) at RT, and stirred for 1 h. 3,5-Dimethylisoxazole-4-sulfonyl chloride (200 mg, 1.0 mmol, 1.0 eq) was then added and the mixture stirred at RT. Complete consumption of the starting material was observed after 18 h following analysis by TLC, and the reaction mixture was diluted with DCM (20 mL) washed with water (3 × 20 mL) and brine (2 × 20 mL). The organic component was dried over magnesium sulfate, filtered, and concentrated *in vacuo*, purification by flash column chromatography on silica (7:3 petroleum ether/ethyl acetate) to afford the title compound (72 mg, 26 %) as a colourless solid: R_f 0.37 (petroleum ether/ ethyl acetate 7:3); m.p. 98–100 °C (from ethyl acetate); $\tilde{\nu}_{max}$ (neat/ cm^{-1}) 3288 (N-H, m), 1737 (C=O, m), 1596 (C=C, m), 1321 (S=O, m), 1321 (C-H, m), 1278 (C-H, m), 1168 (S=O, m), 1152 (S=O, m), 1118 (C-O, m), 1010 (C-N, m), 988 (C-N, m), 641 (C-H, s); ^{1}H NMR (400 MHz, $CDCl_3$) δ 5.40 (1H, s, H - 4), 3.71 (3H, s, H - 5), 2.62 (3H, s, H - 6'), 2.42 (3H, s, H - 7'), 1.48 (6H, s, H - 3) ^{13}C NMR (101 MHz, $CDCl_3$) δ 174.2 (C-1), 172.4 (C-5'), 157.5 (C-3'), 118.1 (C-4'), 59.1 (C-2), 53.1 (C-5), 25.5 (C-3), 12.7 (C-6'), 10.7 (C-7'); HRMS *m/z* (ESI^-) [Found: 275.0710, $C_{10}H_{16}N_2O_5S$ requires $[M–H]^-$ 275.0707]; LRMS *m/z* (ESI^-) 311 (100%), 275 ($[M–H]^-$, 38%); HPLC retention time 7.8 min (method 3), 99%.

N-(3',5'-dimethyl-1',2'-oxazole-4'-sulfonyl)-2-methylalanine, 74



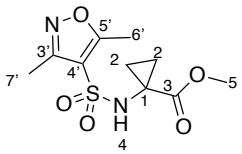
Methyl *N*-((3',5'-dimethyl-1',2'-oxazole-4'-sulfonyl)amino)-2-methylalaninate (10 mg, 0.36 mmol, 1.0 eq) in THF (1.8 mL) was added to a solution of lithium hydroxide (88 mg, 3.6 mmol, 10 eq) in water (0.60 mL) followed by methanol (1.2 mL) at RT. Complete consumption of the starting material was observed after 24 h following analysis by TLC, and the reaction mixture was acidified with HCl (aq, 1 M) until pH 2–3. The mixture was extracted with ethyl acetate (3 × 35 mL), dried over magnesium sulfate, filtered, and concentrated *in vacuo*, to afford the title compound (90 mg, 95%) as a colourless solid: R_f 0.69 (ethyl acetate, 1% acetic acid); m.p. 182–184 °C (from ethyl acetate); $\tilde{\nu}_{max}$ (neat/ cm^{-1}) 3156 (N-H, w), 2981 (O-H, w br), 1738 (C=O, m), 1600 (C=C, m), 1325 (S=O, m), 1259 (C-O, m), 1150 (S=O, m), 1122 (S=O, s), 1009 (C-O, m), 863 (C-H, m), 633 (C-H, s); ^{1}H NMR (400 MHz, MeOD) δ 2.60 (3H, s, H - 6'), 2.40 (3H, s, H - 7'), 1.38 (6H, s, H - 3,4); ^{13}C NMR (126 MHz, MeOD) δ 180.1 (C-1), 172.6 (C-5'), 158.9 (C-3'), 121.0 (C-4'), 61.7 (C-2), 25.1 (C-3,4), 12.5 (C-6'), 10.7 (C-7'); HRMS *m/z* (ESI^+) [Found: 263.0699, $C_9H_{15}N_2O_5S$ requires $[M+H]^+$ 263.0696]; LRMS *m/z* (ESI^-) 261 ($[M-H]^-$, 100%), 175 ($[M-(C(CH_3)_2COOH)]^-$, 38%), 160 ($[M-NC(CH_3)_2COOCH_3]^-$, 22%); HPLC retention time 6.6 min (method 3), 99.0%.

Methyl 1-aminocyclopropane-1-carboxylate, 197,[285,286]



Trimethylsilyl chloride (TMSCl, 0.50 mL, 4.0 mmol, 2.0 eq) was added to 1-aminocyclopropane-1-carboxylic acid (200 mg, 2.0 mmol, 1.0 eq) dropwise with stirring. Methanol (5.0 mL) was then added, and the solution stirred at RT. An additional equivalent of TMSCl was added (0.25 mL) after TLC analysis showed incomplete consumption of the acid after 4 days. The reaction was still incomplete after 7 days and the mixture was concentrated *in vacuo*. The title compound was obtained (1500 mg, 68% estimated yield from ^{1}H NMR) as a colourless solid: R_f 0.14 (EtOH); m.p. 144–148 °C (from methanol, impure material) [lit.[285] 184–184.5 °C from methanol/ether]; ^{1}H NMR (400 MHz, MeOD) δ 3.81 (3H, s, H - 5), 1.62–1.54 (2H, m, H - 2, 2'), 1.37 (2H, s, H - 2, 2'); HRMS *m/z* (ESI^{+}) [116.0707, $C_5H_9NO_2$ requires $[M+H]^{+}$ 116.0707]. A LRMS spectrum could not be obtained for this compound. Spectroscopic data are in good agreement with the literature.[285,286]

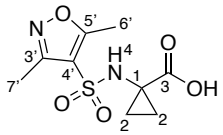
Methyl 1-((3',5'-dimethyl-1',2'-oxazole-4'-sulfonyl)amino)cyclopropane-1-carboxylate, 198



Triethylamine (0.40 mL, 2.7 mmol, 3.0 eq) was added to a solution of methyl-1-aminocyclopropane-1-carboxylate hydrochloride (210 mg, 1.4 mmol, 1.5 eq) in THF (4.0 mL) at RT and stirred for 1 h. Then 3,5-dimethylisoxazole-4-sulfonyl chloride (180 mg, 0.90 mmol, 1.0 eq) was added and the mixture stirred at RT. Complete

consumption of the starting material was observed after 18 h following analysis by TLC. The reaction mixture was diluted with DCM (20 mL), washed with water (3 × 20 mL) and brine (2 × 20 mL). The organic component was dried over magnesium sulfate, filtered, and concentrated *in vacuo*, purified by flash column chromatography on silica (petroleum ether → 7:3 petroleum ether/ethyl acetate) to afford the title compound (60 mg, 24%) as an orange solid: R_f 0.36 (petroleum ether/ ethyl acetate, 7:3); m.p. 182–184 °C (from ethyl acetate); $\tilde{\nu}_{max}$ (neat/ cm^{-1}) 3254 (N-H, m), 1736 (C=O, m), 1712 (C=N, s), 1596 (C=C, m), 1440 (C-H, m), 1412 (C-H, m), 1319 (S=O, s), 1182 (S=O, s) 1155 (C-N, m), 1124 (C-O, s), 638 (C-H, s); ^{1}H NMR (400 MHz, Methanol- D_4) δ 2.59 (3H, s, H - 5), 2.40 (3H, s, H - 6'), 1.41 (6H, s, H - 2); ^{13}C NMR (101 MHz, $CDCl_3$) δ 173.5 (C-3), 171.8 (C-5'), 158.0 (C-3'), 115.8 (C-4'), 52.8 (C-5), 35.6 (C-1), 16.7 (C-2), 12.6 (C-6'), 10.9 (C-7'); HRMS *m/*z (ESI^-) [Found: 273.0549, $C_{10}H_{14}N_2O_5S$ requires $[M–H]^-$ 273.0550]; LRMS *m/z* (ESI^-) 273 ($[M–H]^-$, 100%), 113 ($[NC(CH_2)_2COOCH_3]^-$ 66%); HPLC retention time 10.6 min (method 2), >99.9%.

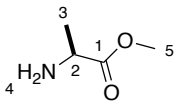
1-((3’,5’-Dimethyl-1’,2’-oxazole)-4’-sulfonylamino)cyclopropane-1-carboxylic acid, 199



Methyl 1-((3’,5’-dimethyl-1’,2’-oxazole-4’-sulfonyl)amino)cyclopropane-1-carboxylate (39 mg, 0.15 mmol) in THF (0.73 mL) was added to a solution of lithium hydroxide (35 mg, 1.5 mmol, 10 eq) in water (0.24 mL) followed by methanol (0.49 mL) at RT. Complete consumption of the starting material was observed after 23 h following analysis by TLC, and the mixture was acidified with HCl (aq, 1 M) until pH 2–3. The mixture was extracted with ethyl acetate (10 mL), washed with water (3 × 6 mL), dried over magnesium sulfate,

filtered, and concentrated *in vacuo* to afford the title compound (27 mg, 65%) as an off-white solid: R_f 0.72 (ethyl acetate, 1% acetic acid); m.p. 156–158 °C (from ethyl acetate); $\tilde{\nu}_{max}$ (neat/ cm^{-1}) 3156 (N-H, w), 2981 (O-H, w br), 1698 (C=O, m), 1600 (C=C, m), 1439 (C-H, m), 1413 (C-H, m), 1348 (C=O, s), 1298 (C-N, m), 1262 (C-N, m), 1205 (S=O, s), 1187 (C-O, s), 1105 (C-N, m), 854 (C-H, s), 689 (C-H, m), 636 (C-H, s), 621 (C-H, s); ^{1}H NMR (400 MHz, MeOD) δ 2.59 (3H, s, H - 16'), 2.40 (3H, s, H - 7'), 1.41 (4H, s, H - 2); ^{13}C NMR (101 MHz, MeOD) δ 175.1 (C-3), 174.0 (C-5'), 160.0 (C-3'), 118.4 (C-4'), 35.8 (C-1), 17.2 (C-2), 12.5 (C-16'), 11.0 (C-7'); HRMS *m/z* (ESI$^+$) [Found: 261.0537, $C_8H_{12}N_2O_5S$ requires $[M+H]^+$ 260.0467]; LRMS *m/z* (ESI$^-$) 259 ($[M-H]^-$, 100%), ($[M-NC(CH_2)_2COOH]^-$, 7%); HPLC retention time 6.5 min (method 3), 99.0%.

Methyl (*S*)-alaninate hydrochloride, 201,[287,288]

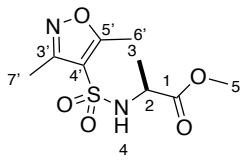


Trimethylsilyl chloride (2.8 mL, 23 mmol, 2.0 eq) was added to (*S*)-alanine (1000 mg, 11 mmol, 1.0 eq) dropwise with stirring. Methanol (10 mL) was then added, and the solution stirred at RT. Complete consumption of the starting material was observed after 23 h following analysis by TLC, and the mixture was concentrated *in vacuo*. The residue was suspended in hexane (20 mL), isolated by Büchner filtration and washed with hexane. The residue was dried *in vacuo* to afford the title compound (1500 mg, 96 %) as a colourless solid: R_f 0.21 (ethyl acetate/ethanol/ triethyl amine 97:2:1); $[\alpha]_D^{25}$ = +8.3 (*c* 1.0, methanol) [lit. +7.0 from methanol];[†] compound is too hygroscopic to gain an accurate

[†] Sigma Aldrich 330639
https://www.sigmaaldrich.com/catalog/product/aldrich/330639?lang=en&region=GB accessed 10Aug18.

melting point [lit.[287] 180 °C (from ethyl acetate), lit.[288] 180 °C (from ether)]; ^{1}H NMR (400 MHz, Methanol- D_4) δ 4.10 (1H, q, *J* 7.2, H - 2), 3.84 (3H, s, H - 5), 1.53 (3H, d, *J* 7.2, H - 3). HRMS *m/*z (ESI$^+$) [104.0708, $C_4H_9NO_2$ requires $[M+H]^+$ 104.0706]. A LRMS could not be obtained for this compound, otherwise the spectroscopic data are in good agreement with the literature.[287,288]

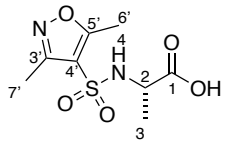
Methyl *N*-((3',5'-dimethyl-1',2'-oxazole-4'-)sulfonyl)-(*S*)-alaninate, 202



Triethylamine (0.86 mL, 6.1 mmol, 3.0 eq) was added to a solution of methyl (*S*)-alaninate hydrochloride (430 mg, 1.5 mmol, 1.5 eq) in THF (8.0 mL) at RT, and stirred for 45 min. Then 3,5-dimethylisoxazole-4-sulfonyl chloride (400 mg, 2.1 mmol, 1.0 eq) was added and the mixture stirred at RT. Complete consumption of the starting material was observed after 18 h following analysis by TLC, and the reaction mixture was diluted with DCM (20 mL) washed with water (3 × 20 mL), and brine (2 × 20 mL). The organic component was dried over magnesium sulfate, filtered, and concentrated *in vacuo*. The residue was purified by flash column chromatography on silica (petroleum ether → 7:3 petroleum ether/ethyl acetate) to afford the title compound (190 mg, 73%) as a colourless solid: R_f 0.35 in (petroleum ether/ethyl acetate 7:3); $[\alpha]_D^{25}$ = –58.4 (*c* 1.0, methanol); Mp = 76–78 °C (from ethyl acetate); $\tilde{\nu}_{max}$ (neat/ cm^{-1}) 3146 (N-H, m), 1748 (C=O, m), 1591 (C=C, m), 1411 (C-H, m), 1340 (S=O, s), 1325 (S=O, m), 1205 (C-N, m), 1178 (S-O, s), 1120 (C-O, s), 706 (C-H, m), 688 (C-H, m), 637 (C-H); ^{1}H NMR (400 MHz, $CDCl_3$) δ 3.92 (1H, q, *J* 7.2, H - 2), 3.64 (3H, s, H - 5), 2.62 (3H, s, H - 6'), 2.41 (3H, s, H - 7'),

1.43 (3H, d, *J* 7.2, H - 3); ^{13}C NMR (101 MHz, $CDCl_3$) δ 173.4 (C-1), 172.5 (C-5'), 157.7 (C-3'), 115.6 (C-4'), 53.0 (C-5), 51.3 (C-2), 19.6 (C-3), 12.6 (C-6'), 10.7 (C-7'); HRMS *m/z* (ESI$^+$) [Found: 263.0692, $C_9H_{14}N_2O_5S$ requires $[M+H]^+$ 263.0700]; LRMS *m/z* (ESI$^-$) 201 (100%), 261 ($[M-H]^-$, 24%) 160 ($[M-NCH(CH_3)COOCH_3]^-$, 18%); HPLC retention time 10.3 min (method 2), >99.9%.

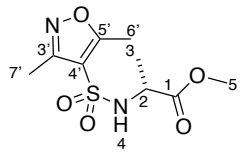
N-(3',5'-Dimethyl-1',2'-oxazole-4'-sulfonyl)-(*S*)-alanine, 203



Methyl *N*-((3',5'-dimethyl-1',2'-oxazole-4'-)sulfonyl)-(*S*)-alaninate (100 mg, 0.38 mmol) in THF (1.9 mL) was added to a solution of lithium hydroxide (91 mg, 3.8 mmol, 10 eq) in water (0.64 mL) followed by methanol (1.3 mL) at RT. Complete consumption of the starting material was observed after 23 h following analysis by TLC, the mixture was acidified with HCl (aq, 1 M) until pH 2–3. The mixture was extracted with ethyl acetate (10 mL), washed with water (3 × 6 mL), dried over magnesium sulfate, filtered, and concentrated *in vacuo*, to afford the title compound (69 mg, 69%) as a colourless solid: R_f 0.72 (ethyl acetate, 1% acetic acid); $[\alpha]_D^{25}$ = –36.8 (*c* 1.0, methanol); m.p. 121–123 °C (from ethyl acetate); $\tilde{\nu}_{max}$ (neat/ cm^{-1}) 3283 (N-H, w), 3064 (O-H, vw br), 1736 (C=O, m), 1595 (C=C, m), 1412 (C-H, m), 1372 (O-H, m), 1344 (S=O, s), 1187 (C-N, s), 1124 (S=O, m), 1059 (C-O, m), 853 (C-H, m), 658 (C-H, s), 632 (C-H, s); ^{1}H NMR (400 MHz, MeOD) δ 3.90 (1H, q, *J* 7.2, H - 1), 2.58 (3H, s, H - 6'), 2.38 (3H, s, H - 7'), 1.39 (3H, d, *J* 7.2, H - 3); ^{13}C NMR (101 MHz, MeOD) δ 175.2 (C-1), 174.1 (C-5'), 159.3 (C-3'), 118.0 (C-4'), 52.5 (C-2), 19.3 (C-3), 12.5 (C-6'), 10.8 (C-7'); HRMS *m/z* (ESI$^+$) [Found: 249.0538, $C_8H_{12}N_2O_5S$ requires

[M+H]$^+$ 249.0539.]; LRMS *m/z* (ESI$^-$) 495 (100%), 247 ([M−H]$^-$, 43%); HPLC retention time 6.3 min (method 3), >99.9%.

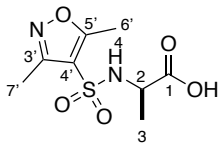
Methyl *N*-((3',5'-dimethyl-1',2'-oxazole-4'-)sulfonyl)-(*R*)-alaninate, 205



Triethylamine (4.2 mL, 30 mmol, 3.0 eq) was added to a solution of methyl (*R*)-alaninate hydrochloride (2100 mg, 15 mmol, 1.5 eq) in THF (40 mL) at RT and stirred for 18 h. Then 3,5-dimethylisoxazole-4-sulfonyl chloride (2000 mg, 10 mmol, 1.0 eq) was added and the mixture stirred at RT. Complete consumption of the starting material was observed after 3 h following analysis by TLC, and the reaction mixture was diluted with DCM (150 mL), washed with water (1 × 150 mL, 2 × 100 mL) and brine (2 × 100 mL). The organic component was dried over magnesium sulfate, filtered, and concentrated *in vacuo*. The residue was purified using flash column chromatography on silica (petroleum ether → 7:3 petroleum ether/ethyl acetate) to afford the title compound (1600 mg, 59%) as a colourless solid: R_f 0.47 in (petroleum ether/ethyl acetate 7:3); $[\alpha]_D^{25}$ = +59.4 (*c* 1.0, methanol); m.p. = 62–64 °C (ethyl acetate); $\tilde{\nu}_{max}$ (neat/ cm^{-1}) 3145 (N-H, m), 1748 (C=O, m), 1591 (C=C, m), 1412 (C-H, m), 1339 (S=O, s), 1325 (S=O, m), 1205 (C-N, s), 1178 (S=O, s), 1120 (C-O, s), 705 (C-H, m), 636 (C-H, s); ^{1}H NMR (400 MHz, $CDCl_3$) δ 3.92 (1H, q, *J* 7.2, H - 2), 3.64 (3H, s, H - 5), 2.62 (3H, s, H - 6'), 2.41 (3H, s, H - 7'), 1.43 (3H, d, *J* 7.2, H - 3); ^{13}C NMR (101 MHz, $CDCl_3$) δ 173.4 (C-1), 172.6 (C-5'), 157.7 (C-3'), 115.7 (C-4'), 53.0 (C-5), 51.3 (C-2), 19.6 (C-3), 12.6 (C-6'), 10.7 (C-7'); HRMS *m/*z (ESI$^+$) [Found: 263.0700,

$C_9H_{14}N_2O_5S$ requires $[M+H]^+$ 263.0700]; LRMS *m/z* (ESI^-) 201 (100%), 261 ($[M-H]^-$, 47%), 160 ($[M-NCH(CH_3)COOCH_3]^-$, 19%); HPLC retention time 7.4 min (method), >99.9%.

N-(3',5'-Dimethyl-1',2'-oxazole-4'-sulfonyl)-(*R*)-alanine, 206



Methyl *N*-((3',5'-dimethyl-1',2'-oxazole-4'-)sulfonyl)-(*R*)-alaninate (37 mg, 0.15 mmol) in THF (0.76 mL) was added to a solution of lithium hydroxide (37 mg, 1.5 mmol, 10 eq) in water (0.25 mL) followed by methanol (0.51 mL) at RT. Complete consumption of the starting material was observed after 23 h following analysis by TLC, and the mixture was acidified with HCl (aq, 1M) until pH 2–3. The mixture was extracted with ethyl acetate (10 mL), washed with water (3 × 6 mL), dried over magnesium sulfate, filtered, and concentrated *in vacuo*, to afford the title compound (24 mg, 60%) as a colourless solid: R_f 0.72 (ethyl acetate, 1% acetic acid); $[\alpha]_D^{25}$ = +38.4 (*c* 1.0, methanol); m.p. 122–124 °C (from ethyl acetate); $\tilde{\nu}_{max}$ neat/ cm^{-1}) 3278 (N-H, m), 3064 (O-H, w br), 1736 (C=O, m), 1595 (C=C, m), 1382 (C-H, m), 1370 (O-H, m), 1343 (S=O, m), 1186 (C-N, s), 1128 (S=O, m), 1040 (C-O, m), 878 (C-H, m), 632 (C-H, s), 621 (C-H, m); ^{1}H NMR (400 MHz, MeOD) δ 3.90 (1H, q, *J* 7.2, H - 12), 2.58 (3H, s, H - 6'), 2.39 (3H, s, H - 7'), 1.39 (3H, d, *J* 7.2, H - 3); ^{13}C NMR (101 MHz, MeOD) δ 175.2 (C-1), 174.1 (C-5'), 159.3 (C-3'), 118.0 (C-4'), 19.3 (C-13), 12.5 (C-6'), 10.8 (C-7'); HRMS *m/z* (ESI^+) [Found: 249.0537, $C_8H_{12}N_2O_5S$ requires $[M+H]^+$ 249.0539]; LRMS *m/z* (ESI^-) 495 (100%), 247 ($[M-H]^-$, 98%); HPLC retention time 6.3 min (method 3), >99.9%.

7.3 Biology Experimental

7.3.1 General biology experimental

Biological materials were obtained from the following suppliers:

Material	Supplier
β-Mercaptoethanol	Sigma Aldrich
96-Well PCR plates	Perkin Elmer
Bacto Agar	Fisher Scientific
Coomassie Blue	Fisher Scientific
DMSO (Dimethylsulfoxide) and D_2O	Sigma Aldrich
IPTG and Ampicillin	Apollo Scientific
Organic Solvents (Ethanol, Methanol)	Fisher Scientific and Sigma Aldrich
SDS-PAGE Reagents (Sodium dodecyl sulfate, poly acrylamide gel electrophoresis)	Bio-Rad and Sigma
SYPRO® Orange 5000x Stock	Merck
Thermowell Sealing Tape	Corning

Purified (Milli-Q) water was obtained from a Millipore Elix® Reverse Osmosis system which was further purified by a Millipore Milli-Q® Synthesis system with a 0.22 µm filter on the outlet.

Reagent quantities given as weight per volume (*w/v*) correspond to g/mL unless otherwise stated.

pH measurements were performed using a Jenway pH Meter 3305, with an Aldrich glass/calomel combination electrode. Calibration was carried out at pH 4.0, 7.0, and 10.0 immediately before use, with buffer solutions of phthalate (pH 4.0), phosphate (pH 7.0)

and borate (pH 10.0) from Fischer Scientific. Electrodes were stored in a 4 M aqueous potassium chloride solution.

Centrifugation protein samples of up to 2.0 mL were centrifuged in a Beckman Microfuge 22R Centrifuge (14,000 rpm) at 4 °C. Cell growth media and cell lysates were centrifuged in a Beckman Avanti J-25 (8500 rpm: JA-10 rotor; 15,000 rpm: JA-16.250 rotor and 24,000 rpm: JA-25.50 rotor, respectively).

Incubation of cells was performed in a New Brunswick G-25 Shaker Incubator at 37 °C and 180 rpm. Optical density at 600 nm was measured with a Novaspec III visible spectrophotometer.

7.3.2 Protein expression and purification

E. coli BL21DE3 (supplied by Dr Catherine Haslam) cells transformed with the plasmid containing the protein of interest (*Sd*KefQCTD) were grown as a starter culture overnight at 37 °C in 2xTy media with 0.1 gmL^{-1} of ampicillin. 10 mL of this starter culture was added to each 1 L of 2xTy autoclaved media containing 0.1 μgmL^{-1} of ampicillin. The cultures were grown to an OD_{600} of 1.0 after approximately 4 h at 30 °C, 180 rpm, after which IPTG was added to a final concentration of 0.5 mM. The cultures were grown for 4.5 h before being spun down at 8000 rpm for 10 min at 4 °C, from which the cell pellet could be isolated and then frozen at –80 °C until needed.

Cell pellets were resuspended in extraction buffer (100 mL per 20 g cell mass), 25 Units (U) of Benzonase was added, then the cells were lysed by sonication for thirty minutes of 5 sec bursts interrupted by 5 sec pauses. Polyethyleneimine (PEI, 0.15% *v/v*) was added, and the cells were incubated on ice for 15 mins. The lysate was clarified by centrifugation and the supernatant decanted, filtered through a 0.45 µm filter, and applied to a purification column.

Buffers:	Binding	Extraction	Wash	Elution	Strip	SEC
pH:	7.4	7.4	7.4	7.4	7.6	7.4
HEPES	–	–	–	–	50 mM	–
NaH_2PO_4 / Na_2HPO_4	50 mM	50 mM	50 mM	50 mM	–	50 mM
NaCl	500 mM	500 mM	500 mM	500 mM	500 mM	150 mM
Glycerol	10% *v/v*	10% *v/v*	10% *v/v*	10% *v/v*	–	–
Imidazole	5 mM	–	45 to 90 mM	500 mM	–	–
EDTA	–	–	–	–	50 mM	–
Sigma tablet	–	1 / 100 mL	–	–	–	–

Immobilised metal affinity chromatography (IMAC) was performed with a HisTrap™ (6 mL) column (GE Healthcare) charged with 4 CV of 100 mM $NiSO_4$ and washed with 10 CV of binding buffer prior to loading the cell lysate at 1 mL/min. The column was then washed with approximately 20 CV binding buffer. When all residual products of bacterial fermentation were eluted from the column by binding buffer, the protein of interest was batch-eluted with 15 CV elution buffer. Eluted protein was collected and fractionated; fractions containing the highest levels of pure protein (as determined by SDS-PAGE gels and UV trace) were concentrated using 5k or 10k concentrators (GE Healthcare) in a Beckmann Allegra™ 21R centrifuge.

Further purification was achieved by gel filtration chromatography. Concentrated fractions (<2 mL) were loaded on a 120 mL Superdex 75 size exclusion chromatography column (Amersham). Eluted protein was collected and fractionated; fractions containing the highest levels of pure protein (as determined by SDS-PAGE gels) were concentrated (to 50–500 µM) as described before.

Protein concentration was estimated by measuring the absorbance at 280 nm using a Nanodrop® ND-1000 spectrophotometer (Nanodrop® Technologies Inc.) with the 'Protein A280' program module according to the manufacturer's instructions. Protein molecular weight and molar extinction coefficient were calculated using ProtParam on the ExPASy Bioinformatics Resource Portal.

7.3.3 SDS-PAGE

Polyacrylamide gel electrophoresis (PAGE) was used to determine protein purity. Gels were prepared using 70 mm × 100 mm glass plates, with 0.75 mm spacers. When possible gels were cast, and run in duplicates. Gel composition (quantities for two gels):

Reagent	16% Resolving gel	4% Stacking gel
Milli-Q water	2.1 mL	2.9 mL
1.5 M Tris-HCL, pH 8.8	2.5 mL	–
0.5 M Tris-HCL, pH 6.8	–	1.3 mL
30% Acrylamide/bis	5.3 mL	0.7 mL
10% *w/v* SDS	100 µL	50 µL
TEMED	8 µL	5 µL
10% *w/v* APS	100 µL	50 µL

TEMED (tetramethylethylenediamine) and ammonium persulfate (APS) were added just prior to pouring the gels. The resolving gel was cast, then covered with a thin layer of methanol to ensure a level surface, which was removed before casting the stacking gel. Gels were run on a mini-PROTEAN Tetra Electrophoresis System (BioRad) at constant potential. Typically, the gel was run at 100 V for 10 to 15 mins, then at 200 V for the remaining of the run to ensure neat stacking. For denaturing PAGE analysis, samples were prepared by mixing with sample loading buffer (2 × or 4 ×, containing 10% ß-ME) and incubated at 100 °C for 10 mins. All gels were loaded with a molecular weight ladder: colour protein standard, broad range (NEB). Following electrophoresis, gels were stained for 15 mins with InstantBlue™ Coomasie® stain.

Buffer	Reagent	Amount / L
SDS-PAGE running buffer	Tris-HCl	30 g
	Glycine	144 g
	SDS	10 g
SDS-PAGE stain	Coomassie® brilliant blue	5 g
	Acetic acid	100 mL
	Methanol	500 mL
SDS-PAGE destaining solution	Methanol	500 mL
	Acetic acid	100 mL

7.3.4 Water-ligand observed via gradient spectroscopy (WaterLOGSY) NMR

For each compound, a water-suppressed ^{1}H NMR spectrum was recorded as a reference, followed by a WaterLOGSY spectrum of the compound in the absence of protein as a negative control, and then another waterLOGSY spectrum in the presence of the specified protein. Samples were prepared to a total volume of 160 µL in Kef SEC PBS (NaH_2PO_4/Na_2HPO_4 50 mM, NaCl 150 mM, pH 7.4 in filtered milli Q), with 500 µM compound from 50 mM *d*-DMSO stock solutions, 10% D_2O for signal locking, and 20 µM

protein for samples with protein. Where compounds formed soluble aggregates the compound and protein concentration were decreased. After loading into 3 mm Hilgenberg NMR tubes for Bruker Match^{TM} system, samples were briefly centrifuged in a manual benchtop rotor. Spectra were recorded on a Bruker AVIII 700 MHz spectrometer with inverse TCI cryoprobe, or a Bruker Biospin 750 MHz Avance spectrometer with III HD console and a 5 mm TCI cryoprobe, using a standard WaterLOGSY pulse sequence.[216]

7.3.5 DSF

Experiments were performed using a Stratagene Mx3005P real-time polymerase chain reaction (qPCR) system (Biochemistry Department, University of Oxford), using SYPRO® Orange dye with filters set at 465 nm (excitation) and 590 nm (emission). The temperature was increased from 25 °C to 85 °C, in increments of 1 °C per 30 s, and fluorescence measurements taken at each interval. The melting temperature (T_m) was identified by fitting to the Boltzmann equation, using Prism 9.[220] The thermal shift (ΔT_m) was calculated as the difference in melting temperatures of the protein in the absence/presence of ligand. Stock solutions of the ligand (50/100 mM) in D_6-DMSO were diluted ten-fold with PBS buffer (KH_2PO_4 2 mM, NaH_2PO_4 8 mM, NaCl 150 mM, pH 7.6, in milli Q). A protein master mix containing *Sd*KefQCTD (13.3 µM) and SYPRO® Orange dye (11.1 x, from 5000 x stock) was prepared in PBS. 96-well PCR plates (Axygen) were prepared using the diluted ligand solutions (5/10 mM, 2.5 µL) and the protein master mix (22.5 µL) to give a final concentration in each well of 500 µM/1 mM ligand, 12 µM *Sd*KefQCTD, 10x SYPRO® Orange in PBS. The 96-well PCR plates were sealed and centrifuged (1000 rpm, 1 min, 25 °C) before measurement.

7.3.6 Kirby-Bauer disc assay

MJF645 *E. coli* (supplied by Dr Anthony Chan) were inoculated onto 2× TY agar plates [16 g/L Tryptone (Oxoid Ltd.), 10 g/L yeast extract (Oxoid Ltd.), 5 g/L NaCl, 1.5% (*w/v*) Oxoid™ Bacto Agar (Thermo Fisher Scientific Inc.)] and incubated for 18–24 h at 37 °C before selection of well-isolated colonies. The full-length pTrc*Sd*KefH_6,[289] and pKc11[290] plasmids were transformed into the *E. coli* hosts. For each isolate, three morphologically similar colonies were selected from the agar plate from the above step, transferred into a sterile Falcon™ 50 mL conical centrifuge tube (Thermo Fisher Scientific Inc.) containing 5 mL of sterile 2× TY media [16 g/L Tryptone (Oxoid Ltd), 10 g/L yeast extract (Oxoid Ltd), 5 g/L NaCl], using an inoculation loop. The bacterial culture was grown aerobically to 0.5 McFarland turbidity standard[291] at 37 °C with an agitation speed of 200 rpm. During this incubation period, test discs were prepared by impregnating 20 µL of 15 mM test compounds (in milli-Q water) onto Whatman® antibiotic assay discs of 6 mm diameter (Sigma-Aldrich Co.). After the cell culture reached the cell density of 0.5 McFarland turbidity standard, the cell isolate was inoculated onto 2× TY agar plates (prepared as described above), using a sterile cotton swab. Subsequently the compound discs were aseptically placed onto the bacterial plates. After 24 h of incubation at 37 °C, inhibition zone diameters associated with the inhibition effect of the compounds were recorded by averaging both the vertical and horizontal diameters of each zone, and are given to the nearest whole mm. All experimental procedures were performed according to the standards set by the Clinical and Laboratory Standards Institute.[292]

References

(1) O'Neill, J. *Tackling Drug-Resistant Infections Globally - Final Report and Recommendations*; 2016; Vol. 136.

(2) Wilcox, M. H. Tigecycline and the Need for a New Broad-Spectrum Antibiotic Class. *Surg. Infect. (Larchmt).* 2006, **7**, 69–80.

(3) Hutchings, M.; Truman, A.; Wilkinson, B. Antibiotics: Past, Present and Future. *Curr. Opin. Microbiol.* 2019, **51**, 72–80.

(4) Piddock, L. J. V. The Crisis of No New Antibiotics-What Is the Way Forward? *Lancet Infect. Dis.* 2012, **12**, 249–253.

(5) Projan, S. J. Why Is Big Pharma Getting out of Antibacterial Drug Discovery? *Curr. Opin. Microbiol.* 2003, **6**, 427–430.

(6) Livermore, D. M. Discovery Research: The Scientific Challenge of Finding New Antibiotics. *J. Antimicrob. Chemother.* 2011, **66**, 1941–1944.

(7) Payne, D. J.; Gwynn, M. N.; Holmes, D. J.; Pompliano, D. L. Drugs for Bad Bugs: Confronting the Challenges of Antibacterial Discovery. *Nat. Rev. Drug Discov.* 2007, **6**, 29–40.

(8) Peleg, A. Y.; Hooper, D. C. Hospital-Acquired Infections Due to Gram-Negative Bacteria. *N. Engl. J. Med.* 2010, **362**, 1804–1813.

(9) Brogan, D. M.; Mossialos, E. A Critical Analysis of the Review on Antimicrobial Resistance Report and the Infectious Disease Financing Facility. *Global. Health* 2016, **12**, 1–7.

(10) Levy, S. B. Antibiotic Resistance - The Problem Intensifies. *Adv. Drug Deliv. Rev.*

2005, **57**, 1446–1450.

(11) Davies, J. A.; Anderson, G. K.; Beveridge, T. J.; Clark, H. C. Chemical Mechanism of the Gram Stain and Synthesis of a New Electron-Opaque Marker for Electron Microscopy Which Replaces the Iodine Mordant of the Stain. *J. Bacteriol.* 1983, **156**, 837–845.

(12) Coico, R. Gram Staining BASIC PROTOCOL Commonly Used Techniques. *Curr. Protoc. Microbiol.* 2005, 3–4.

(13) Figures created in BioRender, https://biorender.com.

(14) Allegranzi, B.; Nejad, S. B.; Combescure, C.; Graafmans, W.; Attar, H.; Donaldson, L.; Pittet, D. Burden of Endemic Health-Care-Associated Infection in Developing Countries: Systematic Review and Meta-Analysis. *Lancet* 2011, **377**, 228–241.

(15) Pendleton, J. N.; Gorman, S. P.; Gilmore, B. F. Clinical Relevance of the ESKAPE Pathogens. *Expert Rev. Anti. Infect. Ther.* 2013, **11**, 297–308.

(16) Pagès, J. M.; Amaral, L. Mechanisms of Drug Efflux and Strategies to Combat Them: Challenging the Efflux Pump of Gram-Negative Bacteria. *Biochim. Biophys. Acta - Proteins Proteomics* 2009, **1794**, 826–833.

(17) Zhao, S.; Adamiak, J. W.; Bonifay, V.; Mehla, J.; Zgurskaya, H. I.; Tan, D. S. Defining New Chemical Space for Drug Penetration into Gram-Negative Bacteria. *Nat. Chem. Biol.* 2020, **16**, 1293–1302.

(18) Lloyd, N. C.; Morgan, H. W.; Nicholson, B. K.; Ronimus, R. S. The Composition of Ehrlich's Salvarsan: Resolution of a Century-Old Debate. *Angew. Chemie - Int. Ed.* 2005, **44**, 941–944.

(19) Voegtlin, C. The Pharmacology of Arsphenamine (Salvarsan) and Related Arsenicals. *Physiol. Rev.* 1925, **5**, 63–94.

(20) Fleming, A. On the Antibacterial Action of Cultures of a Penicillium, with Special Reference to Their Use in the Isolation of B. Influenzae. *Br. J. Exp. Pharmacol.* 1929, **10**, 226–236.

(21) Peláez, F. The Historical Delivery of Antibiotics from Microbial Natural Products - Can History Repeat? *Biochem. Pharmacol.* 2006, **71**, 981–990.

(22) Overbye, K. M.; Barrett, J. F. Antibiotics: Where Did We Go Wrong? *Drug Discov. Today* 2005, **10**, 45–52.

(23) Travis, J. Reviving the Antibiotic Miracle? *Science* 1994, **264**, 360–362.

(24) Levy, S. B. *The Antibiotic Paradox: How Miracle Drugs Are Destroying the Miracle*; Springer, 2013.

(25) Fischbach, M. A.; Walsh, C. T. Antibiotics for Emerging Pathogens. *Science* 2009, **325**, 1089–1093.

(26) Fair, R. J.; Tor, Y. Perspectives in Medicinal Chemistry Antibiotics and Bacterial Resistance in the 21st Century. *Perspect. Medicin. Chem.* 2014, 25–64.

(27) Lewis, K. Platforms for Antibiotic Discovery. *Nat. Rev. Drug Discov.* 2013, **12**, 371–387.

(28) Hamilton-Miller, J. M. T. Sir Edward Abraham's Contribution to the Development of the Cephalosporins: A Reassessment. *Int. J. Antimicrob. Agents* 2000, **15**, 179–184.

(29) Miyadera, T.; Sugimura, Y.; Hashimoto, T.; Tanaka, T.; Iino, K.; Shibata, T.; Sugawara, S. Synthesis and in Vitro Activity of a New Carbapenem, RS-533. *J. Antibiot. (Tokyo).* 1983, **36**, 15–18.

(30) Jana, S.; Deb, J. K. Molecular Understanding of Aminoglycoside Action and Resistance. *Appl. Microbiol. Biotechnol.* 2006, **70**, 140–150.

(31) Bunch, R. L.; McGuire, J. M. Erythromycin, Its Salts, and Method of Preparation. US2653899A, 1953.

(32) Jukes, T. H. Some Historical Notes on Chlortetracycline. *Rev. Infect. Dis.* 1985, **7**, 702–707.

(33) Sensi, P. History of the Development of Rifampin. *Rev. Infect. Dis.* 1983, **5**, S402–S406.

(34) Griffith, R. S. Introduction to Vancomycin. *Rev. Infect. Dis.* 1981, **3**, S200–S204.

(35) Lesher, G. Y.; Froelich, E. J.; Gruett, M. D.; Bailey, J. H.; Brundage, R. P. 1,8-Naphthyridine Derivatives. A New Class of Chemotherapeutic Agents. *J. Med. Pharm. Chem.* 1962, **5**, 1063–1065.

(36) Vazquez, D. Studies on the Mode of Action of the Streptogramin Antibiotics. *J. Gen. Microbiol.* 1966, **113**, 273–290.

(37) Fugitt, R. B.; Luckenbaugh, R. W. 5-Halomethyl-3-Phenyl-2-Oxazolidinones. US4128654, 1978.

(38) Brickner, S. J.; Hutchinson, D. K.; Barbachyn, M. R.; Manninen, P. R.; Ulanowicz, D. A.; Garmon, S. A.; Grega, K. C.; Hendges, S. K.; Toops, D. S.; Ford, C. W.; Zurenko, G. E. Synthesis and Antibacterial Activity of U-100592 and U-100766, Two Oxazolidinone Antibacterial Agents for the Potential Treatment of Multidrug-Resistant Gram-Positive Bacterial Infections. *J. Med. Chem.* 1996, **39**, 673–679.

(39) Eliopoulos, G. M.; Willey, S.; Reiszner, E.; Spitzer, P. G.; Caputo, G.; Moellering, R. C. In Vitro and in Vivo Activity of LY 146032, a New Cyclic Lipopeptide Antibiotic. *Antimicrob. Agents Chemother.* 1986, **30**, 532–535.

(40) Bassetti, M.; Merelli, M.; Temperoni, C.; Astilean, A. New Antibiotics for Bad Bugs: Where Are We? *Ann. Clin. Microbiol. Antimicrob.* 2013, **12**, 1–15.

(41) MacGowan, A.; Albur, M. Frontline Antibiotic Therapy. *Clin. Med. J. R. Coll. Physicians London* 2013, **13**, 263–268.

(42) Dolk, F. C. K.; Pouwels, K. B.; Smith, D. R. M.; Robotham, J. V.; Smieszek, T. Antibiotics in Primary Care in England: Which Antibiotics Are Prescribed and for Which Conditions? *J. Antimicrob. Chemother.* 2018, **73**, ii2–ii10.

(43) The National Institute for Health and Care Excellence (NICE) and Public Health England (PHE). *Summary of Antimicrobial Prescribing Guidance - Managing Common Infections*; 2020.

(44) Organisation, W. H. *Report of the 21st WHO Expert Committee on the Selection and Use of Essential Medicines*; 2017.

(45) Seifert, R. Drugs for the Treatment of Bacterial Infections. In *Basic Knowledge of Pharmacology*; Springer, Cham, 2019; pp 392–409.

(46) Yılmaz; Özcengiz, G. Antibiotics: Pharmacokinetics, Toxicity, Resistance and Multidrug Efflux Pumps. *Biochem. Pharmacol.* 2017, **133**, 43–62.

(47) Rice, L. B. Progress and Challenges in Implementing the Research on ESKAPE Pathogens. *Infect. Control Hosp. Epidemiol.* 2010, **31**, S7–S10.

(48) Coates, A. R.; Halls, G.; Hu, Y. Novel Classes of Antibiotics or More of the Same? *Br. J. Pharmacol.* 2011, **163**, 184–194.

(49) Nikaido, H. Bacterial Resistance to Antibiotics as a Function of Outer Membrane Permeability. *J. Antimicrob. Chemother.* 1988, **22**, 17–22.

(50) Webber, M. A.; Piddock, L. J. V. The Importance of Efflux Pumps in Bacterial Antibiotic Resistance. *J. Antimicrob. Chemother.* 2003, **51**, 9–11.

(51) Douafer, H.; Andrieu, V.; Phanstiel IV, O.; Brunel, J. M. Antibiotic Adjuvants: Make Antibiotics Great Again! *J. Med. Chem.* 2019, **62**, 8665–8681.

(52) Andam, C. P.; Fournier, G. P.; Gogarten, J. P. Multilevel Populations and the Evolution of Antibiotic Resistance through Horizontal Gene Transfer. *FEMS Microbiol. Rev.* 2011, **35**, 756–767.

(53) Santajit, S.; Indrawattana, N. Mechanisms of Antimicrobial Resistance in ESKAPE Pathogens. *Biomed Res. Int.* 2016, **2016**, 1–8.

(54) Courvalin, P. Transfer of Antibiotic Resistance Genes between Gram-Positive and Gram-Negative Bacteria. *Antimicrob. Agents Chemother.* 1994, **38**, 1447–1451.

(55) Brown, N. M. *Bacterial Resistance to Antibiotics – From Molecules to Man*, First.; Bonev, B. B., Brown, N. M., Eds.; John Wiley & Sons Ltd, 2019.

(56) Song, M.; Liu, Y.; Huang, X.; Ding, S.; Wang, Y. A Broad-Spectrum Antibiotic Adjuvant Reverses Multidrug-Resistant Gram-Negative Pathogens. *Nat. Microbiol.*

(57) Waley, S. G. SS-Lactamase: Mechanism of Action. In *The Chemistry of β-Lactams*; 1992; pp 198–228.

(58) Park, J. T.; Strominger, J. L. Mode of Action of Penicillin. Biochemical Basis for the Mechanism of Action of Penicillin and for Its Selective Toxicity. *Science* 1957, **125**, 99–101.

(59) Yocum, R. R.; Waxman, D. J.; Rasmussen, J. R.; Strominger, J. L. Mechanism of Penicillin Action: Penicillin and Substrate Bind Covalently to the Same Active Site Serine in Two Bacterial D-Alanine Carboxypeptidases. *Proc. Natl. Acad. Sci. U. S. A.* 1979, **76**, 2730–2734.

(60) Drawz, S. M.; Bonomo, R. A. Three Decades of β-Lactamase Inhibitors. *Clin. Microbiol. Rev.* 2010, **23**, 160–201.

(61) Giedraitienė, A.; Vitkauskienė, A.; Naginienė, R.; Pavilonis, A. Correspondence to Antibiotic Resistance Mechanisms of Clinically Important Bacteria. *Rev. Med.* 2011,

47, 137–183.

(62) Krause, K. M.; Serio, A. W.; Kane, T. R.; Connolly, L. E. Aminoglycosides: An Overview. *Cold Spring Harb. Perspect. Med.* 2016, **6**, 1–18.

(63) Wong, K.; Ma, J.; Rothnie, A.; Biggin, P. C.; Kerr, I. D. Towards Understanding Promiscuity in Multidrug Efflux Pumps. *Trends Biochem. Sci.* 2014, **39**, 8–16.

(64) Piddock, L. J. V. Multidrug-Resistance Efflux Pumps – Not Just for Resistance. *Nat. Rev. Microbiol.* 2006, **4**, 629–636.

(65) Garvey, M. I.; Baylay, A. J.; Wong, R. L.; Piddock, L. J. V. Overexpression of PatA and PatB, Which Encode ABC Transporters, Is Associated with Fluoroquinolone Resistance in Clinical Isolates of Streptococcus Pneumoniae. *Antimicrob. Agents Chemother.* 2011, **55**, 190–196.

(66) Mulani, M. S.; Kamble, E. E.; Kumkar, S. N.; Tawre, M. S.; Pardesi, K. R. Emerging Strategies to Combat ESKAPE Pathogens in the Era of Antimicrobial Resistance: A Review. *Front. Microbiol.* 2019, **10**.

(67) De Oliveira, D. M. P.; Forde, B. M.; Kidd, T. J.; Harris, P. N. A.; Schembri, M. A.; Beatson, S. A.; Paterson, D. L.; Walker, M. J. Antimicrobial Resistance in ESKAPE Pathogens. *Clin. Microbiol. Rev.* 2020, **33**, 1–49.

(68) Di, L.; Kerns, E.; Carter, G. Drug-Like Property Concepts in Pharmaceutical Design. *Curr. Pharm. Des.* 2009, **15**, 2184–2194.

(69) Mugumbate, G.; Overington, J. P. The Relationship between Target-Class and the Physicochemical Properties of Antibacterial Drugs. *Bioorganic Med. Chem.* 2015, **23**, 5218–5224.

(70) Dougherty, T. J.; Pucci, M. J. *Antibiotic Discovery and Development*; Springer, 2012.

(71) Lipinski, C. A.; Lombardo, F.; Dominy, B. W.; Feeney, P. J. Experimental and

Computational Approaches to Estimate Solubility and Permeability in Drug Discovery and Development Settings. *Adv. Drug Deliv. Rev.* 1996, **23**, 3–25.

(72) Lipinski, C. A. Lead- and Drug-like Compounds: The Rule-of-Five Revolution. *Drug Discov. Today Technol.* 2004, **1**, 337–341.

(73) Costantino, L.; Barlocco, D. Privileged Structures as Leads in Medicinal Chemistry. *Curr. Med. Chem.* 2005, **13**, 65–85.

(74) Yet, L. *Privileged Structures in Drug Discovery: Medicinal Chemistry and Synthesis*; 2018.

(75) Schneider, P.; Schneider, G. Privileged Structures Revisited. *Angew. Chemie - Int. Ed.* 2017, **56**, 7971–7974.

(76) Leeson, P. D.; Davis, A. M.; Steele, J. Drug-like Properties: Guiding Principles for Design - Or Chemical Prejudice? *Drug Discov. Today Technol.* 2004, **1**, 189–195.

(77) Boström, J.; Brown, D. G.; Young, R. J.; Keserü, G. M. Expanding the Medicinal Chemistry Synthetic Toolbox. *Nat. Rev. Drug Discov.* 2018, **17**, 709–727.

(78) Blaskovich, M. A. T.; Zuegg, J.; Elliott, A. G.; Cooper, M. A. Helping Chemists Discover New Antibiotics. *ACS Infect. Dis.* 2016, **1**, 285–287.

(79) Moloney, M. G. Natural Products as a Source for Novel Antibiotics. *Trends Pharmacol. Sci.* 2016, **37**, 689–701.

(80) Wright, G. D. Solving the Antibiotic Crisis. *ACS Infect. Dis.* 2016, **1**, 80–84.

(81) Irwin, J. J.; Shoichet, B. K. ZINC – A Free Database of Commercially Available Compounds for Virtual Screening. *J. Chem. Inf. Model.* 2005, **45**, 177–182.

(82) Morrison, C. N.; Prosser, K. E.; Stokes, R. W.; Cordes, A.; Metzler-Nolte, N.; Cohen, S. M. Expanding Medicinal Chemistry into 3D Space: Metallofragments as 3D Scaffolds for Fragment-Based Drug Discovery. *Chem. Sci.* 2020, **11**, 1216–1225.

(83) Durand, G. A.; Raoult, D.; Dubourg, G. Antibiotic Discovery: History, Methods and Perspectives. *Int. J. Antimicrob. Agents* 2019, **53**, 371–382.

(84) Provenzani, A.; Hospodar, A. R.; Meyer, A. L.; Leonardi Vinci, D.; Hwang, E. Y.; Butrus, C. M.; Polidori, P. Multidrug-Resistant Gram-Negative Organisms: A Review of Recently Approved Antibiotics and Novel Pipeline Agents. *Int. J. Clin. Pharm.* 2020, **42**, 1016–1025.

(85) Hughes, D.; Karlén, A. Discovery and Preclinical Development of New Antibiotics. *Ups. J. Med. Sci.* 2014, **119**, 162–169.

(86) Singh, S. B. Confronting the Challenges of Discovery of Novel Antibacterial Agents. *Bioorganic Med. Chem. Lett.* 2014, **24**, 3683–3689.

(87) Jones, S. Permeability Rules for Antibiotic Design. *Nat. Biotechnol.* 2017, **35**, 639.

(88) Richter, M. F.; Drown, B. S.; Riley, A. P.; Garcia, A.; Shirai, T.; Svec, R. L.; Hergenrother, P. J. Predictive Compound Accumulation Rules Yield a Broad-Spectrum Antibiotic. *Nature* 2017, **545**, 299–304.

(89) Van Bambeke, F.; Glupczynski, Y.; Plésiat, P.; Pechère, J. C.; Tulkens, P. M. Antibiotic Efflux Pumps in Prokaryotic Cells: Occurence, Impact on Resistance and Strategies for the Future of Antimicrobial Therapy. *J. Antimicrob. Chemother.* 2003, **51**, 1055–1065.

(90) Schneider, T.; Sahl, H. G. An Oldie but a Goodie - Cell Wall Biosynthesis as Antibiotic Target Pathway. *Int. J. Med. Microbiol.* 2010, **300**, 161–169.

(91) Li, G.; Lou, H. X. Strategies to Diversify Natural Products for Drug Discovery. *Med. Res. Rev.* 2018, **38**, 1255–1294.

(92) Mwangi, J.; Hao, X.; Lai, R.; Zhang, Z. Antimicrobial Peptides : New Hope in the War against Multidrug Resistance. *Zool. Res.* 2019, **40**, 488–505.

(93) Matthews, T.; Salgo, M.; Greenberg, M.; Chung, J.; DeMasi, R.; Bolognesi, D. Enfuvirtide: The First Therapy to Inhibit the Entry of HIV-1 into Host CD4 Lymphocytes. *Nature Reviews Drug Discovery*. 2004.

(94) Li, S.; Schöneich, C.; Borchardt, R. T. Chemical Instability of Protein Pharmaceuticals: Mechanisms of Oxidation and Strategies for Stabilization. *Biotechnol. Bioeng.* 1995.

(95) Manning, M. C.; Patel, K.; Borchardt, R. T. Stability of Protein Pharmaceuticals. *Pharm. Res.* 1989, **6**, 903.

(96) Mezo, G. Peptide and Protein Based Pharmaceuticals. *Amin. Acids, Pept. Proteins* 2013, **38**, 203–252.

(97) Craik, D. J.; Fairlie, D. P.; Liras, S.; Price, D. The Future of Peptide-Based Drugs. *Chem. Biol. Drug Des.* 2013.

(98) Manning, M. C.; Chou, D. K.; Murphy, B. M.; Payne, R. W.; Katayama, D. S. Stability of Protein Pharmaceuticals: An Update. *Pharm. Res.* 2010, **27**, 544.

(99) Chu, W.; Prodromou, R.; Day, K. N.; Schneible, J. D.; Bacon, K. B.; Bowen, J. D.; Kilgore, R. E.; Catella, C. M.; Moore, B. D.; Mabe, M. D.; Alashoor, K.; Xu, Y.; Xiao, Y.; Menegatti, S. Peptides and Pseudopeptide Ligands: A Powerful Toolbox for the Affinity Purification of Current and next-Generation Biotherapeutics. *J. Chromatogr. A* 2021, **1635**, 461632.

(100) Tsomaia, N. Peptide Therapeutics: Targeting the Undruggable Space. *Eur. J. Med. Chem.* 2015, **94**, 459–470.

(101) Hamman, J. H.; Enslin, G. M.; Kotzé, A. F. Oral Delivery of Peptide Drugs: Barriers and Developments. *BioDrugs* 2005, **19**, 165–177.

(102) Fosgerau, K.; Hoffmann, T. Peptide Therapeutics: Current Status and Future

Directions. *Drug Discov. Today* 2015, **20**, 122–128.

(103) Pirtskhalava, M.; Amstrong, A. A.; Grigolava, M.; Chubinidze, M.; Alimbarashvili, E.; Vishnepolsky, B.; Gabrielian, A.; Rosenthal, A.; Hurt, D. E.; Tartakovsky, M. DBAASP v3: Database of Antimicrobial/Cytotoxic Activity and Structure of Peptides as a Resource for Development of New Therapeutics. *Nucleic Acids Res.* 2021, **49**, D288–D297.

(104) Brayden, D. J.; Hill, T. A.; Fairlie, D. P.; Maher, S.; Mrsny, R. J. Systemic Delivery of Peptides by the Oral Route: Formulation and Medicinal Chemistry Approaches. *Adv. Drug Deliv. Rev.* 2020, **157**, 2–36.

(105) Yap, P. G.; Gan, C. Y. In Vivo Challenges of Anti-Diabetic Peptide Therapeutics: Gastrointestinal Stability, Toxicity and Allergenicity. *Trends Food Sci. Technol.* 2020, **105**, 161–175.

(106) Adessi, C.; Soto, C. Converting a Peptide into a Drug: Strategies to Improve Stability and Bioavailability. *Curr. Med. Chem.* 2005, **9**, 963–978.

(107) Hughes, J.; Smith, T. W.; Kosterlitz, H. W.; Fothergill, L. A.; Morgan, B. A.; Morris, H. R. Identification of Two Related Pentapeptides from the Brain with Potent Opiate Agonist Activity. *Nature* 1975, **258**, 577–579.

(108) Langmuir, I. Isomorphism, Isosterism and Covalence. *J. Am. Chem. Soc.* 1919, **41**, 1543–1559.

(109) Meanwell, N. A. Synopsis of Some Recent Tactical Application of Bioisosteres in Drug Design. *J. Med. Chem.* 2011, **54**, 2529–2591.

(110) Wagener, M.; Lommerse, J. P. M. The Quest for Bioisosteric Replacements. *J. Chem. Inf. Model.* 2006, **46**, 677–685.

(111) Lassalas, P.; Oukoloff, K.; Makani, V.; James, M.; Tran, V.; Yao, Y.; Huang, L.;

Vijayendran, K.; Monti, L.; Trojanowski, J. Q.; Lee, V. M. Y.; Kozlowski, M. C.; Smith, A. B.; Brunden, K. R.; Ballatore, C. Evaluation of Oxetan-3-Ol, Thietan-3-Ol, and Derivatives Thereof as Bioisosteres of the Carboxylic Acid Functional Group. *ACS Med. Chem. Lett.* 2017, **8**, 864–868.

(112) Sanderson, P. E. J.; Lyle, T. A.; Cutrona, K. J.; Dyer, D. L.; Dorsey, B. D.; McDonough, C. M.; Naylor-Olsen, A. M.; Chen, I. W.; Chen, Z.; Cook, J. J.; Cooper, C. M.; Gardell, S. J.; Hare, T. R.; Krueger, J. A.; Lewis, S. D.; Lin, J. H.; Lucas, B. J.; Lyle, E. A.; Lynch, J. J.; Stranieri, M. T.; Vastag, K.; Yan, Y.; Shafer, J. A.; Vacca, J. P. Efficacious, Orally Bioavailable Thrombin Inhibitors Based on 3- Aminopyridinone or 3-Aminopyrazinone Acetamide Peptidomimetic Templates. *J. Med. Chem.* 1998, **41**, 4466–4474.

(113) Böhm, H. J.; Banner, D.; Bendels, S.; Kansy, M.; Kuhn, B.; Müller, K.; Obst-Sander, U.; Stahl, M. Fluorine in Medicinal Chemistry. *ChemBioChem* 2004, **5**, 637–643.

(114) Barreiro, E. J.; Kümmerle, A. E.; Fraga, C. A. M. The Methylation Effect in Medicinal Chemistry. *Chem. Rev.* 2011, **111**, 5215–5246.

(115) Spatola, A. F. *Synthesis of Pseudopeptides*; ACADEMIC PRESS, INC., 1993; Vol. 13.

(116) Estiarte, M. A.; Diez, A.; Rubiralta, M.; Jackson, R. F. W. Synthesis of a 3-Aminopiperidin-2,5-Dione as a Conformationally Constrained Surrogate of the Ala-Gly Dipeptide. *Tetrahedron* 2001, **57**, 157–161.

(117) Kumari, S.; Carmona, A.; Tiwari, A. K.; Trippier, P. C. Amide Bond Bioisosteres : Strategies , Synthesis and Successes. *J. Med. Chem.* 2020, 0–194.

(118) Kamiya, K.; Boero, M.; Shiraishi, K.; Oshiyama, A. Enol-to-Keto Tautomerism of Peptide Groups. *J. Phys. Chem. B* 2006, **110**, 4443–4450.

(119) Hu, X.; Zhang, W.; Carmichael, I.; Serianni, A. S. Amide Cis-Trans Isomerization in

Aqueous Solutions of Methyl N-Formyl-d-Glucosaminides and Methyl N-Acetyl-d -Glucosaminides: Chemical Equilibria and Exchange Kinetics. *J. Am. Chem. Soc.* 2010, **132**, 4641–4652.

(120) Ahrens, V. M.; Bellmann-Sickert, K.; Beck-Sickinger, A. G. Peptides and Peptide Conjugates: Therapeutics on the Upward Path. *Future Med. Chem.* 2012, **4**, 1567–1586.

(121) Kumari, S.; Carmona, A. V.; Tiwari, A. K.; Trippier, P. C. Amide Bond Bioisosteres: Strategies, Synthesis, and Successes. *J. Med. Chem.* 2020, **63**, 12290–12358.

(122) Thota, C. K.; Berger, A. A.; Harms, B.; Seidel, M.; Böttcher, C.; von Berlepsch, H.; Xie, C.; Süssmuth, R.; Roth, C.; Koksch, B. Short Self-Assembling Cationic Antimicrobial Peptide Mimetics Based on a 3,5-Diaminobenzoic Acid Scaffold. *Pept. Sci.* 2020, **112**.

(123) Mankoci, S.; Kaiser, R. L.; Sahai, N.; Barton, H. A.; Joy, A. Bactericidal Peptidomimetic Polyurethanes with Remarkable Selectivity against Escherichia Coli. *ACS Biomater. Sci. Eng.* 2017, **3**, 2588–2597.

(124) Zhou, M.; Qian, Y.; Xie, J.; Zhang, W.; Jiang, W.; Xiao, X.; Chen, S.; Dai, C.; Cong, Z.; Ji, Z.; Shao, N.; Liu, L.; Wu, Y.; Liu, R. Poly(2-Oxazoline)-Based Functional Peptide Mimics: Eradicating MRSA Infections and Persisters While Alleviating Antimicrobial Resistance. *Angew. Chemie - Int. Ed.* 2020, **59**, 6412–6419.

(125) Lin, S.; Wade, J. D.; Liu, S. De Novo Design of Flavonoid-Based Mimetics of Cationic Antimicrobial Peptides: Discovery, Development, and Applications. *Acc. Chem. Res.* 2021, **54**, 104–119.

(126) Bann, S. J.; Ballantine, R. D.; Cochrane, S. A. The Tridecaptins: Non-Ribosomal Peptides That Selectively Target Gram-Negative Bacteria. *RSC Med. Chem.* 2021,

12, 538–551

(127) Fujisawa, M.; Ito, M.; Krulwich, T. A. Three Two-Component Transporters with Channel-like Properties Have Monovalent Cation/Proton Antiport Activity. *Proc. Natl. Acad. Sci. U. S. A.* 2007, **104**, 13289–13294.

(128) Roosild, T. P.; Castronovo, S.; Healy, J.; Miller, S.; Pliotas, C.; Rasmussen, T.; Bartlett, W.; Conway, S. J.; Booth, I. R. Mechanism of Ligand-Gated Potassium Efflux in Bacterial Pathogens. *Proc. Natl. Acad. Sci.* 2010, **107**, 19784–19789.

(129) Roosild, T. P.; Miller, S.; Booth, I. R.; Choe, S. A Mechanism of Regulating Transmembrane Potassium Flux through a Ligand-Mediated Conformational Switch. *Cell* 2002, **109**, 781–791.

(130) Lyngberg, L.; Healy, J.; Bartlett, W.; Miller, S.; Conway, S. J.; Booth, I. R.; Rasmussen, T. KefF, the Regulatory Subunit of the Potassium Efflux System KefC, Shows Quinone Oxidoreductase Activity. *J. Bacteriol.* 2011, **193**, 4925–4932.

(131) Bakker, E. P.; Booth, I. R.; Dinnbier, U.; Epstein, W.; Gajewska, A. Evidence for Multiple K+ Export Systems in Escherichia Coli. *J. Bacteriol.* 1987, **169**, 3743–3749.

(132) Munro, A. W.; Ritchie, G. Y.; Lamb, A. J.; Douglas, R. M.; Booth, I. R. The Cloning and DNA Sequence of the Gene for the Glutathione-regulated Potassium-efflux System KefC of Escherichia Coli. *Mol. Microbiol.* 1991, **5**, 607–616.

(133) Ferguson, G. P.; Munro, A. W.; Douglas, R. M.; McLaggan, D.; Booth, I. R. Activation of Potassium Channels during Metabolite Detoxification in Escherichia Coli. *Mol. Microbiol.* 1993, **9**, 1297–1303.

(134) Brey, R. N.; Beck, J. C.; Rosen, B. P. Cation/Proton Antiport Systems in Escheriehia Coli. *Biochem. Biophys. Res. Commun.* 1978, **83**, 1588–1594.

(135) Bossemeyer, D.; Borchard, A.; Dosch, D. C.; Helmer, G. C.; Epstein, W.; Booth, I. R.;

Bakker, E. P. K+-Transport Protein TrkA of Escherichia Coli Is a Peripheral Membrane Protein That Requires Other Trk Gene Products for Attachment to the Cytoplasmic Membrane. *J. Biol. Chem.* 1989, **264**, 16403–16410.

(136) Ferguson, G. P.; Mclaggan, D.; Booth, I. R. Potassium Channel Activation by Glutathione-S- Conjugates in Escherichia Coil: Protection against Methylglyoxal Is Mediated by Cytoplasmic Acidification. *Mol. Microbiol.* 1995, **17**, 1025–1033.

(137) McLaggan, D.; Rufino, H.; Jaspars, M.; Booth, I. R. Glutathione-Dependent Conversion of N-Ethylmaleimide to the Maleamic Acid by Escherichia Coli: An Intracellular Detoxification Process. *Appl. Environ. Microbiol.* 2000, **66**, 1393–1399.

(138) Ferguson, G. P.; Nikolaev, Y.; McLaggan, D.; Maclean, M.; Booth, I. R. Survival during Exposure to the Electrophilic Reagent N-Ethylmaleimide in Escherichia Coli: Role of KefB and KefC Potassium Channels. *J. Bacteriol.* 1997, **179**, 1007–1012.

(139) Roosild, T. P.; Castronovo, S.; Miller, S.; Li, C.; Rasmussen, T.; Bartlett, W.; Gunasekera, B.; Choe, S.; Booth, I. R. KTN (RCK) Domains Regulate K+ Channels and Transporters by Controlling the Dimer-Hinge Conformation. *Structure* 2009, **17**, 893–903.

(140) Pliotas, C.; Grayer, S. C.; Ekkerman, S.; Chan, A. K. N.; Healy, J.; Marius, P.; Bartlett, W.; Khan, A.; Cortopassi, W. A.; Chandler, S. A.; Rasmussen, T.; Benesch, J. L. P.; Paton, R. S.; Claridge, T. D. W.; Miller, S.; Booth, I. R.; Naismith, J. H.; Conway, S. J. Adenosine Monophosphate Binding Stabilizes the KTN Domain of the Shewanella Denitrificans Kef Potassium Efflux System. *Biochemistry* 2017, **56**, 4219–4234.

(141) Buehner, M.; Ford, G. C.; Moras, D.; Olsen, K. W.; Rossmann, M. G. Three-Dimensional Structure of D-Glyceraldehyde-3-Phosphate Dehydrogenase. *J. Mol. Biol.* 1974, **90**, 25–49.

(142) Miller, S.; Ness, L. S.; Wood, C. M.; Fox, B. C.; Booth, I. R. Identification of an Ancillary Protein, YabF, Required for Activity of the KefC Glutathione-Gated Potassium Efflux System in Escherichia Coli. *J. Bacteriol.* 2000, **182**, 6536–6540.

(143) Bennett, B. D.; Kimball, E. H.; Gao, M.; Osterhout, R.; Van Dien, S. J.; Rabinowitz, J. D. Absolute Metabolite Concentrations and Implied Enzyme Active Site Occupancy in Escherichia Coli. *Nat. Chem. Biol.* 2009, **5**, 593–599.

(144) Serrano, L.; Fersht, A. R. Capping and A-Helix Stability. *Nature* 1989, **342**, 296–299.

(145) Healy, J.; Ekkerman, S.; Pliotas, C.; Richard, M.; Bartlett, W.; Grayer, S. C.; Morris, G. M.; Miller, S.; Booth, I. R.; Conway, S. J.; Rasmussen, T. Understanding the Structural Requirements for Activators of the Kef Bacterial Potassium Efflux System. *Biochemistry* 2014, **53**, 1982–1992.

(146) Booth, I. R.; Ferguson, G. P.; Miller, S.; Li, C.; Gunasekera, B.; Kinghorn, S. Bacterial Production of Methylglyoxal: A Survival Strategy or Death by Misadventure? *Biochem. Soc. Trans.* 2003, **31**, 1406–1408.

(147) Ferguson, G. P.; Tötemeyer, S.; MacLean, M. J.; Booth, I. R. Methylglyoxal Production in Bacteria: Suicide or Survival? *Arch. Microbiol.* 1998, **170**, 209–218.

(148) Ferguson, G. P.; Munro, A. W.; Douglas, R. M.; McLaggan, D.; Booth, I. R. Activation of Potassium Channels during Metabolite Detoxification in Escherichia Coli. *Mol. Microbiol.* 1993.

(149) Haslam, C. A. Analysis of Potassium (K^+) Efflux Systems (Kef) as an Antibiotic Target in Pathogenic Bacteria, University of Oxford, 2019.

(150) Walderhaug, M. O.; Dosch, D. C.; Epstein, W. *Potassium Transport in Bacteria*; ACADEMIC PRESS, INC., 1987.

(151) Epstein, W. The Roles and Regulation of Potassium in Bacteria. *Prog. Nucleic Acid*

Res. Mol. Biol. 2003, **75**, 293–320.

(152) Ferguson, G. P.; Creighton, R. I.; Nikolaev, Y.; Booth, I. R. Importance of RpoS and Dps in Survival of Exposure of Both Exponential- and Stationary-Phase Escherichia Coli Cells to the Electrophile N- Ethylmaleimide. *J. Bacteriol.* 1998, **180**, 1030–1036.

(153) Grayer, S. C. Studies on the Bacterial Potassium Efflux System Kef in Shewanella Denitrificans SdKef, University of Oxford, 2015.

(154) Boratyn, G. M.; Schäffer, A. A.; Agarwala, R.; Altschul, S. F.; Lipman, D. J.; Madden, T. L. Domain Enhanced Lookup Time Accelerated BLAST. *Biol. Direct* 2012, **7**, 1–14.

(155) Newton, G. L.; Rawat, M.; La Clair, J. J.; Jothivasan, V. K.; Budiarto, T.; Hamilton, C. J.; Claiborne, A.; Helmann, J. D.; Fahey, R. C. Bacillithiol Is an Antioxidant Thiol Produced in Bacilli. *Nat. Chem. Biol.* 2009, **5**, 625–627.

(156) Chandrangsu, P.; Dusi, R.; Hamilton, C. J.; Helmann, J. D. Methylglyoxal Resistance in Bacillus Subtilis: Contributions of Bacillithiol-Dependent and Independent Pathways. *Mol. Microbiol.* 2014, **91**, 706–715.

(157) Brettar, I.; Christen, R.; Hölfe, M. G. Shewanella Denitrificans Sp. Nov., a Vigorously Denitrifying Bacterium Isolated from the Oxic-Anoxic Interface of the Gotland Deep in the Central Baltic Sea. *Int. J. Syst. Evol. Microbiol.* 2002, **52**, 2211–2217.

(158) Healy, J. Studies on the Bacterial Potassium Efflux System KefC , and Its Ancillary Protein KefF, University of Aberdeen, 2010.

(159) Healy, J.; Rasmussen, T.; Miller, S.; Booth, I. R.; Conway, S. J. The Photochemical Thiol–Ene Reaction as a Versatile Method for the Synthesis of Glutathione S-Conjugates Targeting the Bacterial Potassium Efflux System Kef. *Org. Chem. Front.* 2016, **3**, 439.

(160) Jafari, R.; Almqvist, H.; Axelsson, H.; Ignatushchenko, M.; Lundbäck, T.; Nordlund, P.; Molina, D. M. The Cellular Thermal Shift Assay for Evaluating Drug Target Interactions in Cells. *Nat. Protoc.* 2014, **9**, 2100–2122.

(161) Axer, A. Master's Thesis: Development of Molecular Probes for the Potassium Efflux System Kef, University of Münster, 2015.

(162) Tucker, J. Probing the Effects of Ester Exchange in Novel Activators of the Kef Potassium Ion Efflux System, University of Oxford, 2016.

(163) Hudzicki, J. Kirby-Bauer Disk Diffusion Susceptibility Test Protocol Created : Tuesday , 08 December 2009 Last Update : Monday , 01 April 2013 Author Jan Hudzicki. *ASM MicrobeLibrary* 2009, No. April 2013, 1–22.

(164) Cougnon, F. B. L.; Sanders, J. K. M. Evolution of Dynamic Combinatorial Chemistry. *Acc. Chem. Res.* 2011, **45**, 2211–2221.

(165) Wilson, M. The Use of Dynamic Combinatorial Chemistry for the Identification of Novel Activators of the Kef Potassium Efflux System, University of Oxford, 2018.

(166) Warner, P.; Green, R. C.; Games, B.; Strimpled, A. M. Non-Peptidic Inhibitors of Human Leukocyte Elastase. 1. The Design and Synthesis of Pyridone-Containing Inhibitors. *J Med Chem* 1994, **37**, 3090–3099.

(167) Rittle, K. E.; Barrow, J. C.; Cutrona, K. J.; Glass, K. L.; Krueger, J. A.; Kuo, L. C.; Lewis, S. D.; Lucas, B. J.; McMasters, D. R.; Morrissette, M. M.; Nantermet, P. G.; Newton, C. L.; Sanders, W. M.; Yan, Y.; Vacca, J. P.; Selnick, H. G. Unexpected Enhancement of Thrombin Inhibitor Potency with O-Aminoalkylbenzylamides in the P1 Position. *Bioorganic Med. Chem. Lett.* 2003, **13**, 3477–3482.

(168) Brown, F. J.; Andisik, D. W.; Bernstein, P. R.; Bryant, C. B.; Ceccarelli, C.; Damewood, J. R.; Edwards, P. D.; Earley, R. A.; Feeney, S.; Green, R. C.; Gomes, B.; Kosmider, B.

J.; Krell, R. D.; Shaw, A.; Steelman, G. B.; Thomas, R. M.; Vacek, E. P.; Veale, C. A.; Tuthill, P. A.; Warner, P.; Williams, J. C.; Wolanin, D. J.; Woolson, S. A. Design of Orally Active, Non-Peptidic Inhibitors of Human Leukocyte Elastase. *J. Med. Chem.* 1994, **37**, 1259–1261.

(169) Sanderson, P. E. J.; Dyer, D. L.; Naylor-Olsen, A. M.; Vacca, J. P.; Gardell, S. J.; Lewis, S. D.; Lucas Jr., B. J.; Lyle, E. A.; Lynch, J. J.; Mulichak, A. M. L-373,890, An Achiral, Noncovalent, Subnanomolar Thrombin Inhibitor. *Bioorganic Med. Chem. Lett.* 1997, **7**, 1497–1500.

(170) Plant, A.; Stieber, F.; Scherkenbeck, J.; Lösel, P.; Dyker, H. Syntheses of Analogues of the Insect Neuropeptide Proctolin Containing an Oxazole Ring as an Amide Bond Replacement. *Org. Lett.* 2001, **3**, 3427–3430.

(171) Liskamp, R. M. J. Conformationally Restricted Amino Acids and Dipeptides, (Non)Peptidomimetics and Secondary Structure Mimetics. *Recl. des Trav. Chim. des Pays-Bas* 1994, **113**, 1–19.

(172) Gordon, T.; Hansen, P.; Morgan, B.; Singh, J.; Baizman, E.; Ward, S. Peptide Azoles: A New Class Of Biologically-Active Dipeptide Mimetics. *Bioorganic Med. Chem. Lett.* 1993, **3**, 915–920.

(173) Falorni, M.; Dettori, G.; Giacomelli, G. Synthesis of New Oxazole-Containing Peptidomimetics. *Tetrahedron Asymmetry* 1998, **9**, 1419–1426.

(174) Videnov, G.; Kaiser, D.; Kempter, C.; Jung, G. Synthesis of Naturally Occurring, Conformationally Restricted Oxazole- And Thiazole-Containing Di- And Tripeptide Mimetics. *Angew. Chemie (International Ed. English)* 1996, **35**, 1503–1506.

(175) Liang, J.; Van Abbema, A.; Balazs, M.; Barrett, K.; Berezhkovsky, L.; Blair, W. S.; Chang, C.; Delarosa, D.; DeVoss, J.; Driscoll, J.; Eigenbrot, C.; Goodacre, S.; Ghilardi,

N.; MacLeod, C.; Johnson, A.; Bir Kohli, P.; Lai, Y.; Lin, Z.; Mantik, P.; Menghrajani, K.; Nguyen, H.; Peng, I.; Sambrone, A.; Shia, S.; Smith, J.; Sohn, S.; Tsui, V.; Ultsch, M.; Williams, K.; Wu, L. C.; Yang, W.; Zhang, B.; Magnuson, S. Identification of an Imidazopyridine Scaffold to Generate Potent and Selective TYK2 Inhibitors That Demonstrate Activity in an in Vivo Psoriasis Model. *Bioorganic Med. Chem. Lett.* 2017, **27**, 4370–4376.

(176) Kim, Y. B.; Kang, C. W.; Ranatunga, S.; Yang, H.; Sebti, S. M.; Del Valle, J. R. Imidazo[1,2-a]Pyridine-Based Peptidomimetics as Inhibitors of Akt. *Bioorganic Med. Chem. Lett.* 2014, **24**, 4650–4653.

(177) Hejazi, S. A.; Osman, O. I.; Alyoubi, A. O.; Aziz, S. G.; Hilal, R. H. The Thermodynamic and Kinetic Properties of 2-Hydroxypyridine/2-Pyridone Tautomerization: A Theoretical and Computational Revisit. *Int. J. Mol. Sci.* 2016, **17**.

(178) Hatherley, L. D.; Brown, R. D.; Godfrey, P. D.; Pierlot, A. P.; Caminati, W.; Damiani, D.; Melandri, S.; Favero, L. B. Gas-Phase Tautomeric Equilibrium of 2-Pyridinone and 2-Hydroxypyridine by Microwave Spectroscopy. *J. Phys. Chem.* 1993, **97**, 46–51.

(179) Purcell, W. P.; Singer, J. A. Electronic and Molecular Structure of Selected Unsubstituted and Dimethyl Amides from Measurements of Electric Moments and Nuclear Magnetic Resonance. *J. Phys. Chem.* 1967, **71**, 4316–4319.

(180) Dewar, M. J. S.; Turchi, I. J. Ground States of Molecules. Part XXXII. A MINDO/3 Study of Mesoionic Oxazoles and Imidazoles. *J. Chem. Soc. Perkin Trans. 2* 1976, 548.

(181) Kumar, A.; Sheridan, J.; Stiefvater, O. L. The Microwave Spectrum of Oxazole II. Dipole Moment and Quadrupole Coupling Constants. *Zeitschrift fur Naturforsch. -*

Sect. A J. Phys. Sci. 1978, **33**, 549–558.

(182) Broughton, H. B.; Watson, I. A. Selection of Heterocycles for Drug Design. *J. Mol. Graph. Model.* 2004, **23**, 51–58.

(183) Bhagavan, N. V.; Ha, C.-E. Three-Dimensional Structure of Proteins and Disorders of Protein Misfolding. *Essentials Med. Biochem.* 2015, 31–51.

(184) Shaffer, A. A.; Wierschke, S. G. Comparison of Computational Methods Applied to Oxazole, Thiazole, and Other Heterocyclic Compounds. *J. Comput. Chem.* 1993, **14**, 75–88.

(185) O'Sullivan, P. S.; De la Vega, J.; F. Hameka, H. Calculations of Bond Angles in Five-Membered Conjugated Ring Systems. *Chem. Phys. Lett.* 1970, **5**, 576–578.

(186) Pettus, L.; Tasker, A.; Xu, S.; Wurz, R. Pyrazolo-Pyridinone Compounds, Process for Their Preparation, and Their Pharmaceutical Use. CA2685674A1, 2008.

(187) Borzilleri, R. M.; Schroeder, G. M.; Cai, Z. Pyridinone Compounds. US7851489B2, 2007.

(188) Cilibrizzi, A.; Abbate, V.; Chen, Y. L.; Ma, Y.; Zhou, T.; Hider, R. C. Hydroxypyridinone Journey into Metal Chelation. *Chem. Rev.* 2018, **118**, 7657–7701.

(189) Abdelrazek, F. M.; Gomha, S. M.; Abdelrahman, A. H.; Metz, P.; Sayed, M. A. A Facile Synthesis and Drug Design of Some New Heterocyclic Compounds Incorporating Pyridine Moiety and Their Antimicrobial Evaluation. *Lett. Drug Des. Discov.* 2017, **14**, 752–762.

(190) Sanderson, P. E. J.; Cutrona, K. J.; Dorsey, B. D.; Dyer, D. L.; McDonough, C. M.; Naylor-Olsen, A. M.; Chen, I. W.; Chen, Z.; Cook, J. J.; Gardell, S. J.; Krueger, J. A.; Lewis, S. D.; Lin, J. H.; Lucas, B. J.; Lyle, E. A.; Lynch, J. J.; Stranieri, M. T.; Vastag, K.; Shafer, J. A.; Vacca, J. P. L-374,087, an Efficacious, Orally Bioavailable, Pyridinone

Acetamide Thrombin Inhibitor. *Bioorganic Med. Chem. Lett.* 1998, **8**, 817–822.

(191) Haack, M.; Enck, S.; Seger, H.; Geyer, A.; Beck-Sickinger, A. G. Pyridone Dipeptide Backbone Scan to Elucidate Structural Properties of a Flexible Peptide Segment. *J. Am. Chem. Soc.* 2008, **130**, 8326–8336.

(192) Williams, J. C.; Falcone, R. C.; Knee, C.; Stein, R. L.; Strimpler, A. M.; Reaves, B.; Giles, R. E.; Krell, R. D. Biologic Characterization of ICI 200,880 and ICI 200,355, Novel Inhibitors of Human Neutrophil Elastase. *Am. Rev. Respir. Dis.* 1991, **144**, 875–883.

(193) Lyle, T. A.; Chen, Z.; Appleby, S. D.; Freidinger, R. M.; Gardell, S. J.; Lewis, S. D.; Li, Y.; Lyle, E. A.; Lynch, J. J.; Mulichak, A. M.; Ng, A. S.; Naylor-Olsen, A. M.; Sanders, W. M. Synthesis, Evaluation, and Crystallographic Analysis of L-371,912: A Potent and Selective Active-Site Thrombin Inhibitor. *Bioorganic Med. Chem. Lett.* 1997, **7**, 67–72.

(194) Advanced Chemistry Development, I. (ACD/Labs). Physical Sciences Data-science Service.

(195) Hill, A. P.; Young, R. J. Getting Physical in Drug Discovery: A Contemporary Perspective on Solubility and Hydrophobicity. *Drug Discov. Today* 2010, **15**, 648–655.

(196) Clark, D. E. Rapid Calculation of Polar Molecular Surface Area and Its Application to the Prediction of Transport Phenomena. 2. Prediction of Blood-Brain Barrier Penetration. *J. Pharm. Sci.* 1999, **88**, 815–821.

(197) Clark, D. What Has Polar Surface Area Ever Done for Drug Discovery? *Future Med. Chem.* 2008, **3**, 469–484.

(198) Palm, K.; Stenberg, P.; Luthman, K.; Artursson, P. Polar Molecular Surface

Properties Predict the Intestinal Absorption of Drugs in Humans. *Pharmaceutical Research*. 1997, pp 568–571.

(199) Vankar, Y. D.; Kumaravel, G. N-Chlorosuccinimide/Sodium Iodide: A Convenient Source of N-Iodosuccinimide. Synthesis of α-Iodo Carbonyl Compounds and Trans-1,2-Iodoacetates. *Tetrahedron Lett.* 1984, **25**, 233–236.

(200) Racys, D. T.; Warrilow, C. E.; Pimlott, S. L.; Sutherland, A. Highly Regioselective Iodination of Arenes via Iron(III)-Catalyzed Activation of N-Iodosuccinimide. *Org. Lett.* 2015, **17**, 4782–4785.

(201) Incremona, J. H.; Martin, J. C. N-Bromosuccinimide. Mechanisms of Allylic Bromination and Related Reactions. *J. Am. Chem. Soc.* 1970, **92**, 627–634.

(202) Cid, J. M.; Tresadern, G.; Duvey, G.; Lütjens, R.; Finn, T.; Rocher, J. P.; Poli, S.; Vega, J. A.; De Lucas, A. I.; Matesanz, E.; Linares, M. L.; Andrés, J. I.; Alcazar, J.; Alonso, J. M.; Macdonald, G. J.; Oehlrich, D.; Lavreysen, H.; Ahnaou, A.; Drinkenburg, W.; Mackie, C.; Pype, S.; Gallacher, D.; Trabanco, A. A. Discovery of 1-Butyl-3-Chloro-4-(4-Phenyl-1-Piperidinyl)-(1 H)-Pyridone (JNJ-40411813): A Novel Positive Allosteric Modulator of the Metabotropic Glutamate 2 Receptor. *J. Med. Chem.* 2014, **57**, 6495–6512.

(203) Hansen, P.; Lawitz, K.; Lönn, H.; Nikitidis, A. 2-Pyridine Derivatives as Inhibitors of Neutrophile Elastase. WO2006098683A1, 2006.

(204) Chen, Y.; Wang, F.; Jia, A.; Li, X. Palladium-Catalyzed Selective Oxidative Olefination and Arylation of 2-Pyridones. *Chem. Sci.* 2012, **3**, 3231–3236.

(205) Sherwood, J.; Clark, J. H.; Fairlamb, I. J. S.; Slattery, J. M. Solvent Effects in Palladium Catalysed Cross-Coupling Reactions. *Green Chem.* 2019, **21**, 2164–2213.

(206) Miura, W.; Hirano, K.; Miura, M. Iridium-Catalyzed Site-Selective C-H Borylation of

2-Pyridones. *Synth.* 2017, **49**, 4745–4752.

(207) Jiang, X.; Hao, X.; Jing, L.; Wu, G.; Kang, D.; Liu, X.; Zhan, P. Recent Applications of Click Chemistry in Drug Discovery. *Expert Opin. Drug Discov.* 2019, **14**, 779–789.

(208) Kumar, G. S.; Lin, Q. Light-Triggered Click Chemistry. *Chem. Rev.* 2020. DOI:10.1021/acs.chemrev.0c00799

(209) Nguyen, S. S.; Prescher, J. A. Developing Bioorthogonal Probes to Span a Spectrum of Reactivities. *Nat. Rev. Chem.* 2020, **4**, 476–489.

(210) Nolan, M. D.; Scanlan, E. M. Applications of Thiol-Ene Chemistry for Peptide Science. *Front. Chem.* 2020, **8**, 1–21.

(211) Kolb, H. C.; Sharpless, K. B. The Growing Impact of Click Chemistry on Drug Discovery. *Drug Discov. Today* 2003, **8**, 401–422.

(212) Walker, S. E.; Lamb, C. J. C.; Beattie, N. A.; Nikodemiak, P.; Lee, A. L. Oxidative Heck Desymmetrisation of 2,2-Disubstituted Cyclopentene-1,3-Diones. *Chem. Commun.* 2015, **51**, 4089–4092.

(213) Lamb, C. J. C.; Nderitu, B. G.; McMurdo, G.; Tobin, J. M.; Vilela, F.; Lee, A. L. Auto-Tandem Catalysis: PdII-Catalysed Dehydrogenation/Oxidative Heck Reaction of Cyclopentane-1,3-Diones. *Chem. - A Eur. J.* 2017, **23**, 18282–18288.

(214) Brun, O.; Agramunt, J.; Raich, L.; Rovira, C.; Pedroso, E.; Grandas, A. Selective Derivatization of N-Terminal Cysteines Using Cyclopentenediones. *Org. Lett.* 2016, **18**, 4836–4839.

(215) Dalvit, C.; Pevarello, P.; Tato, M.; Veronesi, M.; Vulpetti, A.; Sundström, M. Identification of Compounds with Binding Affinity to Proteins via Magnetization Transfer from Bulk Water. *J. Biomol. NMR* 2000, **18**, 65–68.

(216) Dalvit, C.; Fogliatto, G.; Stewart, A.; Veronesi, M.; Stockman, B. WaterLOGSY as a

Method for Primary NMR Screening: Practical Aspects and Range of Applicability. *J. Biomol. NMR* 2001, **21**, 349–359.

(217) Fielding, L. NMR Methods for the Determination of Protein-Ligand Dissociation Constants. *Prog. Nucl. Magn. Reson. Spectrosc.* 2007, **51**, 219–242.

(218) Claridge, T. D. W. *High-Resolution NMR Techniques in Organic Chemistry 3rd Edition*; 2016.

(219) Claridge, T. D. W. Protein–Ligand Screening by NMR. In *High-Resolution NMR Techniques in Organic Chemistry (Third Edition)*; Elsevier, 2016; pp 421–455.

(220) Niesen, F. H.; Berglund, H.; Vedadi, M. The Use of Differential Scanning Fluorimetry to Detect Ligand Interactions That Promote Protein Stability. *Nat. Protoc.* 2007, **2**, 2212–2221.

(221) Zhao, Y.; Ren, J.; Harlos, K.; Jones, D. M.; Zeltina, A.; Bowden, T. A.; Padilla-Parra, S.; Fry, E. E.; Stuart, D. I. Toremifene Interacts with and Destabilizes the Ebola Virus Glycoprotein. *Nature* 2016, **535**, 169–172.

(222) Laurin, C. Chemical Tools To Probe The Role Of Bromodomains In The Parasite Trypanosoma Cruzi, University of Oxford, 2019.

(223) Fielding, L. NMR Methods for the Determination of Protein- Ligand Dissociation Constants. *Curr. Top. Med. Chem.* 2003, **3**, 39–53.

(224) Furukawa, A.; Konuma, T.; Yanaka, S.; Sugase, K. Quantitative Analysis of Protein-Ligand Interactions by NMR. *Prog. Nucl. Magn. Reson. Spectrosc.* 2016, **96**, 47–57.

(225) Dalvit, C. Ligand- and Substrate-Based 19F NMR Screening: Principles and Applications to Drug Discovery. *Prog. Nucl. Magn. Reson. Spectrosc.* 2007, **51**, 243–271.

(226) Willcott, M. R. MestRe Nova *J. Am. Chem. Soc.* 2009, **131**, 13180–13180.

(227) Sekirnik (née Measures), A. R.; Hewings, D. S.; Theodoulou, N. H.; Jursins, L.; Lewendon, K. R.; Jennings, L. E.; Rooney, T. P. C.; Heightman, T. D.; Conway, S. J. Isoxazole-Derived Amino Acids Are Bromodomain-Binding Acetyl-Lysine Mimics: Incorporation into Histone H4 Peptides and Histone H3. *Angew. Chemie - Int. Ed.* 2016, **55**, 8353–8357.

(228) Schröder, D. C.; Kracker, O.; Fröhr, T.; Góra, J.; Jewginski, M.; Nieß, A.; Antes, I.; Latajka, R.; Marion, A.; Sewald, N. 1,4-Disubstituted 1H-1,2,3-Triazole Containing Peptidotriazolamers: A New Class of Peptidomimetics with Interesting Foldamer Properties. *Front. Chem.* 2019, **7**, 1–19.

(229) Brill, Z. G.; Condakes, M. L.; Ting, C. P.; Maimone, T. J. Navigating the Chiral Pool in the Total Synthesis of Complex Terpene Natural Products. *Chem. Rev.* 2017, **117**, 11753–11795.

(230) Nakamura, M.; Shibata, T.; Nakane, K.; Nemoto, T.; Ojika, M.; Yamada, K. Stereochemistry and Total Synthesis of Dolastatin E. *Tetrahedron Lett.* 1995, **36**, 5059–5062.

(231) Evans, D. A.; Gage, J. R.; Leighton, J. L. Total Synthesis of (+)-Calyculin A. *J. Am. Chem. Soc.* 1992, **114**, 9434–9453.

(232) Clayden, J.; Clayton, J.; Harvey, R. A.; Karlubíková, O. A One-Pot Synthesis of 2-Aryl-4,5-Anti-Diphenyloxazolines. *Synlett* 2009, No. 17, 2836–2838.

(233) Benito, J. M.; Christensen, C. A.; Meldal, M. Versatile Solid-Phase Synthesis of Peptide-Derived 2-Oxazolines. Application in the Synthesis of Ligands for Asymmetric Catalysis. *Org. Lett.* 2005, **7**, 581–584.

(234) Knerr, P. J.; Van Der Donk, W. A. Chemical Synthesis and Biological Activity of Analogues of the Lantibiotic Epilancin 15X. *J. Am. Chem. Soc.* 2012, **134**, 7648–

7651.

(235) Williams, D. R.; Lowder, P. D.; Gu, Y. G.; Brooks, D. A. Studies of Mild Dehydrogenations in Heterocyclic Systems. *Tetrahedron Lett.* 1997, **38**, 331–334.

(236) Chen, G.; Cushing, T. D.; Fisher, B.; He, X.; Li, K.; Li, Z.; McGee, L. R.; Pattaropong, V.; Faulder, P.; Seganish, J. L.; Shin, Y. Alkynyl Alcohols as Kinase Inhibitors. WO2009158011A1, 2009.

(237) Mattsson, S.; Dahlström, M.; Karlsson, S. A Mild Hydrolysis of Esters Mediated by Lithium Salts. *Tetrahedron Lett.* 2007, **48**, 2497–2499.

(238) Delinck, D. L.; Margolin, A. L. Synthesis of Chiral Building Blocks for Selective Adenosine Receptor Agents. Lipase-Catalyzed Resolution of 2-Benzylpropanol and 2-Benzylpropionic Acid. *Tetrahedron Lett.* 1990, **31**, 6797–6798.

(239) Schmid, R. D.; Verger, R. Lipases: Interfacial Enzymes with Attractive Applications. *Angew. Chemie - Int. Ed.* 1998, **37**, 1608–1633.

(240) Caroff, E.; Keller, M.; Kimmer-Lin, T.; Meyer, E. 4-(Benzoimidazol-2-yl)-Thiazole Compounds and Related Aza Derivatives. WO2013114332A1, 2013.

(241) Cai, T. B.; Tang, X.; Nagorski, J.; Brauschweiger, P. G.; Wang, P. G. Synthesis and Cytotoxicity of 5-Fluorouracil/Diazeniumdiolate Conjugates. *Bioorganic Med. Chem.* 2003, **11**, 4971–4975.

(242) Joffrin, A. The Synthesis Of Enantiomerically Pure Inositol Derivatives: From Resolution To Enzymatic Desymmetrisation – Volume 1, University of Oxford, 2017.

(243) Dymińska, L. Imidazopyridines as a Source of Biological Activity and Their Pharmacological Potentials - Infrared and Raman Spectroscopic Evidence of Their Content in Pharmaceuticals and Plant Materials. *Bioorganic Med. Chem.* 2015, **23**,

6087–6099.

(244) Blakeney, J. S.; Reid, R. C.; Le, G. T.; Fairlie, D. P. Nonpeptidic Ligands for Peptide-Activated G Protein-Coupled Receptors. *Chem. Rev.* 2007, **107**, 2960–3041.

(245) Dwyer, M. P.; Guzi, T. J.; Paruch, K.; Doll, R. J.; Keertikar, K. M.; Girijavallabhan, V. M. Novel Imidazopyridines As Cyclin Dependent Kinase Inhibitors. WO 2004/026867, 2004.

(246) Salvà, P.; Costa, J. Clinical Pharmacokinetics and Pharmacodynamics of Zolpidem. *Clin. Pharmacokinet.* 1995, **29**, 142–153.

(247) Hill, R. J.; Lou, Y.; Dewdney, N.; Sarma, K.; Gabriel, T.; McIntosh, J.; Davis, D.; Hong, J.; Goldstein, D. M.; Owens, T. D.; Kuglstatter, A.; Soth, M.; Han, X.; Frauchiger, S.; Park, J.; Kondru, R. K.; Taygerly, J. P.; Zecic, H.; Kocer, B.; Suh, J.; Sweeney, Z. K.; Litman, R. Structure-Based Drug Design of RN486, a Potent and Selective Bruton's Tyrosine Kinase (BTK) Inhibitor, for the Treatment of Rheumatoid Arthritis. *J. Med. Chem.* 2015, **58**, 512–516.

(248) Hand, E. S.; Paudler, W. W. Teleamination of the Imidazo[l,2-a]Pyridine System. *J. Org. Chem.* 1978, **43**, 2900–2906.

(249) Dwyer, M. P.; Paruch, K.; Alvarez, C.; Doll, R. J.; Keertikar, K.; Duca, J.; Fischmann, T. O.; Hruza, A.; Madison, V.; Lees, E.; Parry, D.; Seghezzi, W.; Sgambellone, N.; Shanahan, F.; Wiswell, D.; Guzi, T. J. Versatile Templates for the Development of Novel Kinase Inhibitors: Discovery of Novel CDK Inhibitors. *Bioorganic Med. Chem. Lett.* 2007, **17**, 6216–6219.

(250) Montgomery, J. A.; Secrist, J. A. Other Imidazoles with Fused Six-Membered Rings. In *Comprehensive Heterocyclic Chemistry*; 1984; Vol. 5–7, 607–668.

(251) Tan, E. S. W.; Tai, S. J.; Yeap, Y. S.; Sangthongpitag, K.; Joy, J. K.; Choong, M. L.;

Jeyaraj, D. A.; Chuah, C.; Kannan, S.; Lee, M. A.; Ho, M. W. T.; Low, C. B.; Liu, B.; Ong, E. H.; Ong, T. S.; Poulsen, A.; Yang, H.; Kwek, P.; Matter, A.; Lim, S.; Pendharkar, V.; Retna, P.; Verma, C. S.; Manoharan, V.; Ang, S. H.; Vuddagiri, S.; Nacro, K.; Chew, Y. S.; Hill, J.; Wee, J. L. K.; Chennamaneni, L. R.; Nguyen, T. T. H.; Dinie, N. Optimization of Selective Mitogen-Activated Protein Kinase Interacting Kinases 1 and 2 Inhibitors for the Treatment of Blast Crisis Leukemia. *J. Med. Chem.* 2018, **61**, 4348–4369.

(252) Yoshido, I.; Yoneda, N.; Ohashi, Y.; Suzuki, S.; Miyamoto, M.; Miyazaki, F.; Seshimo, H.; Kamata, J.; Takase, Y.; Shirato, M.; Shimokubo, D.; Sakuma, Y.; Yokohama, H. Nitrogenous Fused-Ring Compound Having Pyrazolyl Group as Substituent and Medicinal Composition Thereof. EP 1 382 603 B1, 2008.

(253) Castanedo, G. M.; Blaquiere, N.; Beresini, M.; Bravo, B.; Brightbill, H.; Chen, J.; Cui, H. F.; Eigenbrot, C.; Everett, C.; Feng, J.; Godemann, R.; Gogol, E.; Hymowitz, S.; Johnson, A.; Kayagaki, N.; Kohli, P. B.; Knüppel, K.; Kraemer, J.; Krüger, S.; Loke, P.; McEwan, P.; Montalbetti, C.; Roberts, D. A.; Smith, M.; Steinbacher, S.; Sujatha-Bhaskar, S.; Takahashi, R.; Wang, X.; Wu, L. C.; Zhang, Y.; Staben, S. T. Structure-Based Design of Tricyclic NF-KB Inducing Kinase (NIK) Inhibitors That Have High Selectivity over Phosphoinositide-3-Kinase (PI3K). *J. Med. Chem.* 2017, **60**, 627–640.

(254) Somers, M.; Bartolomé-Nebreda, J. M.; Tong, H. M.; Martínez-Viturro, C. M.; Martín-Martín, M. L.; Fontana, A.; Pena, M. Á.; Alonso, J. M.; Alonso de Diego, S. A.; Megens, A.; Vanhoof, G.; Delgado, Ó.; Delgado, F.; Artola, M.; Langlois, X.; Macdonald, G. J.; Conde-Ceide, S.; Van Gool, M. Identification of a Novel Orally Bioavailable Phosphodiesterase 10A (PDE10A) Inhibitor with Efficacy in Animal

Models of Schizophrenia. *J. Med. Chem.* 2015, **58**, 978–993.

(255) Golec, J. M. C.; Mullican, M. D.; Murcko, M. A.; Wilson, K. P.; Kay, D. P.; Jones, S. D.; Murdoch, R.; Bemis, G. W.; Raybuck, S. A.; Luong, Y. P.; Livingston, D. J. Structure-Based Design of Non-Peptidic Pyridone Aldehydes as Inhibitors of Interleukin-1β Converting Enzyme. *Bioorganic Med. Chem. Lett.* 1997, **7**, 2181–2186.

(256) Latli, B.; Hrapchak, M.; Li, G.; Lorenz, J.; Horan, J.; Busacca, C. A.; Senanayake, C. H. Synthesis of Highly Potent Lymphocyte Function-Associated Antigen-1 Antagonists Labeled with Carbon-14 and with Stable Isotopes, Part 3. *J. Label. Compd. Radiopharm. 2019* 2019, **62**, 77–85.

(257) Cacchi, S.; Fabrizi, G.; Goggiamani, A. Palladium-Catalyzed Hydroxycarbonylation of Aryl and Vinyl Halides or Triflates by Acetic Anhydride and Formate Anions. *Org. Lett.* 2003, **5**, 4269.

(258) Berger, P.; Bessmernykh, A.; Caille, J. C.; Mignonac, S. Palladium-Catalyzed Hydroxycarbonylation of Aryl and Vinyl Bromides by Mixed Acetic Formic Anhydride. *Synthesis (Stuttg).* 2006, No. 18, 3106–3110.

(259) Böhm, H. J.; Flohr, A.; Stahl, M. Scaffold Hopping. *Drug Discov. Today Technol.* 2004, **1**, 217–224.

(260) Schneider, G.; Schneider, P.; Renner, S. Scaffold-Hopping: How Far Can You Jump? *QSAR Comb. Sci.* 2006, **25**, 1162–1171.

(261) Schneider, G.; Neidhart, W.; Giller, T.; Schmid, G. "Scaffold-Hopping" by Topological Pharmacophore Search: A Contribution to Virtual Screening. *Angew. Chemie - Int. Ed.* 1999, **38**, 2894–2896.

(262) Hessler, G.; Baringhaus, K. H. The Scaffold Hopping Potential of Pharmacophores.

Drug Discov. Today Technol. 2010, **7**, 263–269.

(263) Kearsley, S. K.; Smith, G. M. An Alternative Method for the Alignment of Molecular Structures: Maximizing Electrostatic and Steric Overlap. *Tetrahedron Comput. Methodol.* 1990, **3**, 615–633.

(264) Cheeseright, T.; Mackey, M.; Rose, S.; Vinter, A. SparkTM, Version 10.4, 2016, Cresset, Litlington, Cambridgeshire, UK; *J. Chem. Inf. Model.* 2006, **46**, 665.

(265) Hawkins, P. C. D.; Skillman, A. G.; Nicholls, A. Comparison of Shape-Matching and Docking as Virtual Screening Tools. *J. Med. Chem.* 2007, **50**, 74.

(266) Cheeseright, T. .; Mackey, M. D.; Melville, J. L.; Vinter, J. G. BlazeTM, Version 10.2, 2014, Cresset, Litlington, Cambridgeshire, UK; *J. Chem. Inf. Model.* 2008, **48**, 2108.

(267) Molecular Operating Environment (MOE), 2013.08. Molecular Operating Environment (MOE), 2013.08; Chemical Computing Group Inc., 1010 Sherbooke St. West, Suite #910, Montreal, QC, Canada, H3A 2R7. *Mol. Oper. Environ. (MOE), 2013.08; Chem. Comput. Gr. Inc., 1010 Sherbooke St. West, Suite #910, Montr. QC, Canada, H3A 2R7, 2013.* 2016.

(268) Maass, P.; Schulz-Gasch, T.; Stahl, M.; Rarey, M. Recore: A Fast and Versatile Method for Scaffold Hopping Based on Small Molecule Crystal Structure Conformations. *J. Chem. Inf. Model.* 2007, **47**, 390.

(269) Mason, J.; Good, A.; Martin, E. 3-D Pharmacophores in Drug Discovery. *Curr. Pharm. Des.* 2005, **7**, 567–597.

(270) Yang, S. Y. Pharmacophore Modeling and Applications in Drug Discovery: Challenges and Recent Advances. *Drug Discov. Today* 2010, **15**, 444–450.

(271) Choudhury, C.; Narahari Sastry, G. Pharmacophore Modelling and Screening: Concepts, Recent Developments and Applications in Rational Drug Design.

Challenges Adv. Comput. Chem. Phys. 2019, **27**, 25–53.

(272) Schaller, D.; Šribar, D.; Noonan, T.; Deng, L.; Nguyen, T. N.; Pach, S.; Machalz, D.; Bermudez, M.; Wolber, G. Next Generation 3D Pharmacophore Modeling. *Wiley Interdiscip. Rev. Comput. Mol. Sci.* 2020, No. February, 1–20.

(273) Cox, J. M.; Chu, H. D.; Yang, C.; Shen, H. C.; Wu, Z.; Balsells, J.; Crespo, A.; Brown, P.; Zamlynny, B.; Wiltsie, J.; Clemas, J.; Gibson, J.; Contino, L.; Lisnock, J.; Zhou, G.; Garcia-Calvo, M.; Bateman, T.; Xu, L.; Tong, X.; Crook, M.; Sinclair, P. Mineralocorticoid Receptor Antagonists: Identification of Heterocyclic Amide Replacements in the Oxazolidinedione Series. *Bioorganic Med. Chem. Lett.* 2014, **24**, 1681–1684.

(274) Jiang, B.; Guo, B.; Cui, J.; Dong, Y.; Cui, L.; Zhang, L.; Yang, Q.; Yang, X. New Lead Discovery of Insect Growth Regulators Based on the Scaffold Hopping Strategy. *Bioorganic Med. Chem. Lett.* 2020, **30**, 127500.

(275) Radchenko, T.; Brink, A.; Siegrist, Y.; Kochansky, C.; Bateman, A.; Fontaine, F.; Morettoni, L.; Zamora, I. Correction: Software-Aided Approach to Investigate Peptide Structure and Metabolic Susceptibility of Amide Bonds in Peptide Drugs Based on High Resolution Mass Spectrometry (PLoS ONE (2017) 12: 11 (E0186461) DOI: 10.1371/Journal.Pone.0186461). *PLoS One* 2018, **13**, 1–23.

(276) Hyldtoft, L.; Madsen, R. Carbohydrate Carbocyclization by a Novel Zinc-Mediated Domino Reaction and Ring-Closing Olefin Metathesis. *J. Am. Chem. Soc.* 2000, **122**, 8444–8452.

(277) Li, J.; Sha, Y. A Convenient Synthesis of Amino Acid Methyl Esters. *Molecules* 2008, **13**, 1111–1119.

(278) Melancon, B. J.; Utley, T. J.; Sevel, C.; Mattmann, M. E.; Cheung, Y. Y.; Bridges, T.

M.; Morrison, R. D.; Sheffler, D. J.; Niswender, C. M.; Scott Daniels, J.; Jeffrey Conn, P.; Lindsley, C. W.; Wood, M. R. Development of Novel M 1 Antagonist Scaffolds through the Continued Optimization of the MLPCN Probe ML012. *Bioorganic Med. Chem. Lett.* 2012, **22**, 5035–5040.

(279) McIver, E. G.; Bryans, J.; Birchall, K.; Chugh, J.; Drake, T.; Lewis, S. J.; Osborne, J.; Smiljanic-Hurley, E.; Tsang, W.; Kamal, A.; Levy, A.; Newman, M.; Taylor, D.; Arthur, J. S. C.; Clark, K.; Cohen, P. Synthesis and Structure-Activity Relationships of a Novel Series of Pyrimidines as Potent Inhibitors of TBK1/IKKε Kinases. *Bioorganic Med. Chem. Lett.* 2012, **22**, 7169–7173.

(280) Lei, H.; Yang, Y.; Li, C.; Jia, F.; Jiang, N.; Gong, P.; Zhai, X. Catalyst-Free Cyclization-And Curtius Rearrangement-Induced Functional Group Transformation: An Improved Synthetic Strategy of First-in-Class ATX Inhibitor Ziritaxestat (GLPG-1690). *Org. Process Res. Dev.* 2020, **24**, 997–1005.

(281) Fulmer, G. R.; M Miller, A. J.; Sherden, N. H.; Gottlieb, H. E.; Nudelman, A.; Stoltz, B. M.; Bercaw, J. E.; Goldberg, K. I.; Beckman, M. NMR Chemical Shifts of Trace Impurities: Common Laboratory Solvents, Organics, and Gases in Deuterated Solvents Relevant to the Organometallic Chemist. *Organometallics* 2010, **29**, 2176.

(282) Brandstätter, M.; Roth, F.; Luedtke, N. W. Synthesis of 2-Oxazolines by in Situ Desilylation and Cyclodehydration of β-Hydroxyamides. *J. Org. Chem.* 2015, **80**, 40–51.

(283) Loos, P.; Ronco, C.; Riedrich, M.; Arndt, H. D. Unified Azoline and Azole Syntheses by Optimized Aza-Wittig Chemistry. *European J. Org. Chem.* 2013, No. 16, 3290–3315.

(284) Solá, J.; Fletcher, S. P.; Castellanos, A.; Clayden, J. Nanometer-Range

Communication of Stereochemical Information by Reversible Switching of Molecular Helicity. *Angew. Chemie - Int. Ed.* 2010, **49**, 6836–6839.

(285) Yoshioka, M.; Narisada, M. Peptide Sweeteners. 6. Structural Studies on the C-Terminal Amino Acid of L-Aspartyl Dipeptide Sweeteners. *J. Med. Chem.* 1984, No. 1, 1663–1668.

(286) Isogai, K.; Sakai, J.; Yamauchi, K.; Watanabe, K. Regioselectivity in the Catalytic Hydrolysis of 1-Amino-1-Cyclopropanecarboxylic Acid and It's Methyl Ester. *Bull. Chem. Soc. Jpn.* 1986, **59**, 2849–2842.

(287) Aitali, M.; Allaoud, S.; Karim, A.; Meliet, C. file:///Users/HP/Documents/!!Holly'. D. C. Y. L. C. D. ref1. pd.; Mortreux, A. Enantioselective Reduction of Aromatic Ketones Catalysed by Chiral Ruthenium(II) Complexes. *Tetrahedron Asymmetry* 2000, **11**, 1367–1374.

(288) Rehm, T.; Stepanenko, V.; Zhang, X.; Würthner, F.; Gröhn, F.; Klein, K.; Schmuck, C. A New Type of Soft Vesicle-Forming Molecule: An Amino Acid Derived Guanidiniocarbonyl Pyrrole Carboxylate Zwitterion. *Org. Lett.* 2008, **10**, 1469–1472.

(289) Miller, S.; Douglas, R. M.; Carter, P.; Booth, I. R. Mutations in the Glutathione-Gated KefC K+ Efflux System of Escherichia Coli That Cause Constitutive Activation. *J. Biol. Chem.* 1997, **272**, 24942–24947.

(290) Miller, S.; Ness, L. S.; Wood, C. M.; Fox, B. C.; Booth, I. R. Identification of an Ancillary Protein, YabF, Required for Activity of the KefC Glutathione-Gated Potassium Efflux System in Escherichia Coli. *J. Bacteriol.* 2000, **182**, 6536–6540.

(291) McFarland, J. The Nephelometer: An Instrument for Estimating the Number of Bacteria in Suspensions Used for Calculating the Opsonic Index and for Vaccines.

JAMA J. Am. Med. Assoc. 1907, XLIX, 1176.

(292) *Clinical and Laboratory Standards Institute*; 2012; Vol. 32.

Appendices

A: Supplementary Figures

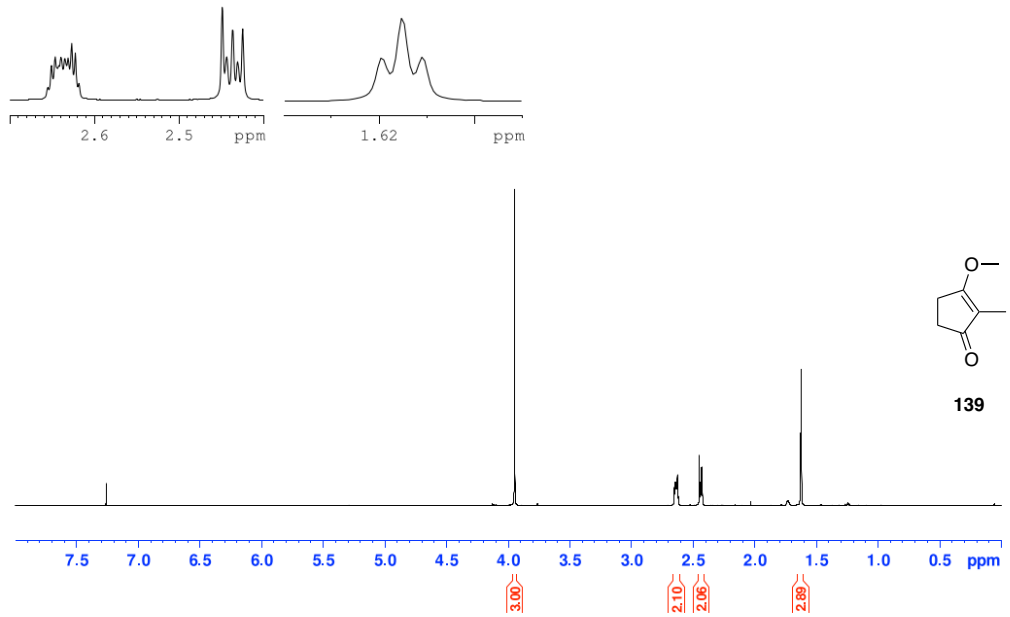


Figure S.1. ^{1}H NMR of only isolated compound 139 from Scheme 2.11 a, b and c. The attempted alkylation only occurred on oxygen, for all conditions investigated. Inset shows two expanded regions of the spectrum.

B: *Sd*KefQCTD Protein Characterisation

***Sd*KefQCTD**

Kef System: *Sd*KefQCTD (*Shewanella denitrificans* C-terminal domain)

Plasmid: pTrc*Sd*KefQCTDH_6 (pTrc99A)

DNA:
ATGGGCCACGAGTTAGAAGTGGATATCGAACCGAAGAAAACCCCAGAAAATCCG
GAATACGATAATGAAATTGAGGCAACTAATAGCGTTATCATTGCCGGTTATGGTC
GCTTTGGCCAAGTTGTTGGTCGTCTGCTGTCTGCGCAGGGCTACCACCTGAGCAT
CTTGGACCATAGCCCGTCTCAAATTGACATGCTGCGCCGTTTCGGTAATAAGGTTT
TCTATGGCGATGCGGCGCGTAAAGATCTGCTGGAGGCGGCAGGCGCGAAGGAC
GCCCAACTGCTGGTGATTGCGATCGACGCCCCTGACAAGGCGCTGGAGATCGTT
GAGCTGGCTCATAAACACTACCCGCAATTGAAAATCGTGGCCCGTGCGATTGATC
GCCGCCACGCGTACCAGTACCTGCGTCTGGGCGTGACTTCTTTCAAACGTGAAAC
CTTCGACTCCGCGGTGAATCTGGGCATTGAAGCGCTGACCCTGCTGGGTAACAGC
TCCACCGTGGCAGAGCGCGCTGGCGACCTGTTCTCCCAGCACGATAATGCAAGCC
TGCACGAGTTGGCAGCCCTGTGGGGTGATGACCACACGTATGGCGTCGCGGTCC
GCCAGCGTATGGAAGATCTGAAGCAAGTTCTGGCAAAAGATAAGGCAGCACAGG
AACGCCTGAATACGTGTAAAGGTGGTGACTGTCTCGAGCACCACCACCACCACCA
CTGATAA

Amino acid sequence:
MGHELEVDIEPKKTPENPEYDNEIEATNSVIIAGYGRFGQVVGRLLSAQGYHLSILDHS
PSQIDMLRRFGNKVFYGDAARKDLLEAAGAKDAQLLVIAIDAPDKALEIVELAHKHYP
QLKIVARAIDRRHAYQYLRLGVTSFKRETFDSAVNLGIEALTLLGNSSTVAERAGDLFSQ

HDNASLHELAALWGDDHTYGVAVRQRMEDLKQVLAKDKAAQERLNTCKGGDCLEH

HHHHH

Molecular weight (Da): 26402.7

Other: ε = 34840

*Sd*KefH$_6$

Kef System: *Sd*KefH$_6$ (*Shewanella denitrificans* full length Kef system)

Plasmid: pTrc*Sd*KefH$_6$ (pTrc99A)

DNA:

ATGGTGCTGGAAATGGCTGTTATCTATCTGGCGGCTGCAATCGTGGCAGTTCCGG
TGGCGAAACGTCTGGGTCTGGGTAGCGTCCTGGGCTACTTGCTGGCAGGTATTCT
GATCGGCCCGTTTTTGCTGGGCCTGGTCGGCGAGCAAACCGACGTGATGCACTTT
GCGGAGTTCGGTGTCGTGATGATGTTGTTTCTGGTGGGCCTGGAACTGCAACCGT
CCCGTCTGTGGAAACTGCGTCATAGCATCATCGGTCTGGGTGGTTTGCAGGTTCT
GCTGAGCGCAGGCCTGATTTTCGCTATCGGCTTCTACCTGTTTGAACTGCAATGGC
AAACGGCTCTGGCCATCGGTTTGATGCTGTCGCTGAGCTCTACCGCAATTGTGCT
GCAAACTCTGACGGAAAAAGGCTGGATTAAGCAGGACGCTGGTCAGAACGCGTT
TTCGGTCCTGCTGTTCCAGGACATCGCTGTCATTCCGATCCTGGCGCTGATCCCGT
TGCTGGCTTTTACGGACATCAATGCGGCCCAAGCAGACCACGGTAATATGATCGC
GCATCTGCCTAGCTATTTGCAGGTCATGATCAGCCTGGGTGTGATTGGTACCATTA
TCCTGGCAGGTCGTTACGTGTCTGCACCGCTGTTTCGTTATATCGCGGAAACCCAT
CTGCGTGAAATTTTCACCATTTCGGCGCTGTTCCTGGTCGTCGCAATTGCAGTCAT
CATGCAGAAGATCGGCCTGTCGCCGGCCTTGGGCACGTTTCTGGCAGGTGTCGT
GCTGGCGGAGAGCGAATTTCGTCATGAACTGGAGGTTGATATTGAGCCGTTTAA
GGGTCTGCTGCTGGGTCTGTTCTTCATCACCGTGGGTGCGTCGATTGACTTTCCG
CTGCTGTTGGAGCAGTCTCTGTTGGTTCTGGGTTTGGTCCTGGGTTTGCTGTTGGT
CAAAGCCCTGGTTCTGTTTGTCCTGGCGCAAGGCTTTAAGATGCAAGGTGAGCAA
AAGCTGCTGTTCACTCTGGCCCTGGCACAGGGCGGTGAATTTGCGTTCGTCCTGC
TGAGCTTGACCCAAAATCTGGAAATCCTGACGCTGGAGCAAACGAAGGTCGTCAC

CCTGGTCGTGACCATCTCTATGCTGTGTGCGCCACTGCTGCTGATGTTCTACGAGC

GTCTGCTGGTTAAGAAAACCCCAGAAAATCCGGAATACGATAATGAAATTGAGGC

AACTAATAGCGTTATCATTGCCGGTTATGGTCGCTTTGGCCAAGTTGTTGGTCGTC

TGCTGTCTGCGCAGGGCTACCACCTGAGCATCTTGGACCATAGCCCGTCTCAAAT

TGACATGCTGCGCCGTTTCGGTAATAAGGTTTTCTATGGCGATGCGGCGCGTAAA

GATCTGCTGGAGGCGGCAGGCGCGAAGGACGCCCAACTGCTGGTGATTGCGATC

GACGCCCCTGACAAGGCGCTGGAGATCGTTGAGCTGGCTCATAAACACTACCCGC

AATTGAAAATCGTGGCCCGTGCGATTGATCGCCGCCACGCGTACCAGTACCTGCG

TCTGGGCGTGACTTCTTTCAAACGTGAAACCTTCGACTCCGCGGTGAATCTGGGC

ATTGAAGCGCTGACCCTGCTGGGTAACAGCTCCACCGTGGCAGAGCGCGCTGGC

GACCTGTTCTCCCAGCACGATAATGCAAGCCTGCACGAGTTGGCAGCCCTGTGGG

GTGATGACCACACGTATGGCGTCGCGGTCCGCCAGCGTATGGAAGATCTGAAGC

AAGTTCTGGCAAAAGATAAGGCAGCACAGGAACGCCTGAATACGTGTAAAGGTG

GTGACTGTCTCGAGCACCACCACCACCACCACTGATAA

Amino acid sequence: MVLEMAVIYLAAAIVAVPVAKRLGLGSVLGYLLAGILIGPFLLGLVGEQTDVMHFAEF

GVVMMLFLVGLELQPSRLWKLRHSIIGLGGLQVLLSAGLIFAIGFYLFELQWQTALAIG

LMLSLSSTAIVLQTLTEKGWIKQDAGQNAFSVLLFQDIAVIPILALIPLLAFTDINAAQAD

HGNMIAHLPSYLQVMISLGVIGTIILAGRYVSAPLFRYIAETHLREIFTISALFLVVAIAVI

MQKIGLSPALGTFLAGVVLAESEFRHELEVDIEPFKGLLLGLFFITVGASIDFPLLLEQSLL

VLGLVLGLLLVKALVLFVLAQGFKMQGEQKLLFTLALAQGGEFAFVLLSLTQNLEILTLE

QTKVVTLVVTISMLCAPLLLMFYERLLVKKTPENPEYDNEIEATNSVIIAGYGRFGQVV

GRLLSAQGYHLSILDHSPSQIDMLRRFGNKVFYGDAARKDLLEAAGAKDAQLLVIAIDA

PDKALEIVELAHKHYPQLKIVARAIDRRHAYQYLRLGVTSFKRETFDSAVNLGIEALTLL

GNSSTVAERAGDLFSQHDNASLHELAALWGDDHTYGVAVRQRMEDLKQVLAKDKA

AQERLNTCKGGDCLEHHHHHH

Molecular weight (Da):	67347.3 (Predicted using the ProtParam Tool from Expasy in Daltons, Da)
Other:	Codon optimised. GenBank ID of *Sd*Kef: ABE53663.1.

*Ec*KefFC

Kef System: *Ec*KefFC (Full length *E. coli* Kef expressed under own promoter)

Plasmid: pKc11

DNA:

ATGATTCTTATAATTTATGCGCATCCGTATCCGCATCATTCCCATGCGAATAAACG
GATGCTTGAACAGGCAAGGACGCTGGAAGGCGTCGAAATTCGCTCTCTTTATCAA
CTCTATCCTGACTTCAATATCGATATTGCCGCCGAGCAGGAGGCGCTGTCTCGCG
CCGATCTGATCGTCTGGCAGCATCCGATGCAGTGGTACAGCATTCCTCCGCTCCTC
AAACTTTGGATCGATAAAGTTTTCTCCCACGGCTGGGCTTACGGTCATGGCGGCA
CGGCGCTGCATGGCAAACATTTGCTGTGGGCGGTGACGACCGGCGGCGGGGAA
AGCCATTTTGAAATTGGTGCGCATCCGGGCTTTGATGTGCTGTCGCAGCCGCTAC
AGGCGACGGCAATCTACTGCGGGCTGAACTGGCTGCCACCGTTTGCCATGCACTG
CACCTTTATTTGTGACGACGAAACCCTCGAAGGGCAGGCGCGTCACTATAAGCAA
CGTCTGCTGGAATGGCAGGAGGCCCATCATGGATAGCCATACGCTGATTCAGGC
GCTGATTTATCTCGGTTCGGCAGCGCTGATTGTACCCATTGCGGTACGTCTTGGTC
TGGGATCGGTACTTGGCTACCTGATCGCCGGCTGCATTATTGGCCCGTGGGGGCT
GCGACTGGTGACCGATGCCGAATCTATTCTGCACTTTGCCGAGATTGGGGTGGTG
CTGATGCTGTTTATTATCGGCCTCGAACTCGATCCACAAAGGCTGTGGAAGCTGC
GTGCGGCAGTGTTCGGCTGTGGCGCATTGCAGATGGTGATTTGCGGCGGCCTGC
TGGGGCTGTTCTGCATGTTACTTGGGCTGCGCTGGCAGGTCGCGGAATTGATCG
GCATGACGCTGGCGCTCTCCTCTACGGCGATTGCCATGCAGGCGATGAATGAAC
GCAATCTGATGGTGACGCAAATGGGTCGCAGTGCCTTTGCGGTGCTGCTGTTCCA
GGATATCGCGGCGATCCCGCTGGTGGCGATGATTCCGCTACTGGCAACGAGCAG
TGCCTCGACGACGATGGGCGCATTTGCTCTCTCGGCGTTAAAAGTGGCGGGTGC

GCTGGTGCTGGTGGTATTGCTGGGGCGCTATGTCACGCGTCCGGCGCTGCGTTTT

GTAGCCCGCTCTGGCTTGCGGGAAGTGTTTAGTGCCGTGGCGTTATTCCTCGTGT

TTGGCTTTGGTTTGCTGCTGGAAGAGGTCGGCTTGTCGATGGCGATGGGCGCGT

TTCTGGCGGGCGTACTGCTGGCAAGCTCGGAATACCGTCATGCGCTGGAGAGCG

ATATCGAACCATTTAAAGGTTTGCTGTTGGGGCTGTTTTTCATCGGTGTTGGCATG

TCGATAGACTTTGGCACGCTGCTTGAAAACCCATTGCGCATTGTCATTTTGCTGCT

CGGTTTCCTCATCATCAAAATCGCCATGCTGTGGCTGATTGCCCGACCGTTGCAAG

TGCCAAATAAACAGCGTCGTTGGTTTGCGGTGTTGTTAGGGCAGGGCAGTGAGT

TTGCCTTTGTGGTATTTGGCGCGGCGCAGATGGCGAATGTGCTGGAGCCGGAGT

GGGCGAAATCGCTGACCCTGGCGGTGGCGCTGTCGATGGCAGCAACGCCGATTC

TGCTGGTGATCCTCAATCGCCTTGAGCAATCTTCTACTGAGGAAGCGCGTGAAGC

CGATGAGATCGACGAAGAACAGCCGCGCGTGATTATCGCCGGATTCGGTCGTTTT

GGGCAGATTACCGGACGTTTACTGCTCTCCAGCGGGGTGAAAATGGTGGTACTC

GATCACGATCCGGACCATATCGAAACCTTGCGTAAATTTGGTATGAAAGTGTTTTA

TGGCGATGCCACGCGGATGGATTTACTGGAATCTGCCGGAGCGGCGAAAGCGGA

AGTGCTGATTAACGCCATCGACGATCCGCAAACCAACCTGCAACTGACAGAGATG

GTGAAAGAACATTTCCCGCATTTGCAGATTATTGCCCGCGCCCGCGATGTCGACC

ACTACATTCGTTTGCGTCAGGCAGGCGTTGAAAAGCCGGAGCGTGAAACCTTCGA

AGGTGCGCTGAAAACCGGGCGTCTGGCACTGGAAAGTTTAGGTCTGGGGCCGTA

TGAAGCGCGAGAACGTGCCGATGTGTTCCGCCGCTTTAATATTCAGATGGTGGAA

GAGATGGCAATGGTTGAGAACGACACCAAAGCCCGCGCGGCGGTCTATAAACGC

ACCAGCGCGATGTTAAGTGAGATCATTACCGAGGACCGCGAACATCTGTCATTAA

TTCAACGACATGGCTGGCAGGGAACCGAAGAAGGTAAACATACCGGCAACATGG

CGGATGAACCGGAAACGAAACCCTCATCCTAA

Amino acid sequence:

Kef F: MILIIYAHPYPHHSHANKRMLEQARTLEGVEIRSLYQLYPDFNIDIAAEQEALSR

ADLIVWQHPMQWYSIPPLLKLWIDKVFSHGWAYGHGGTALHGKHLLWAVTTGGG

ESHFEIGAHPGFDVLSQPLQATAIYCGLNWLPPFAMHCTFICDDETLEGQARHYKQR

LLEWQEAHHG

Kef C: MDSHTLIQALIYLGSAALIVPIAVRLGLGSVLGYLIAGCIIGPWGLRLVTDAESIL

HFAEIGVVLMLFIIGLELDPQRLWKLRAAVFGCGALQMVICGGLLGLFCMLLGLRWQ

VAELIGMTLALSSTAIAMQAMNERNLMVTQMGRSAFAVLLFQDIAAIPLVAMIPLLA

TSSASTTMGAFALSALKVAGALVLVVLLGRYVTRPALRFVARSGLREVFSAVALFLVFG

FGLLLEEVGLSMAMGAFLAGVLLASSEYRHALESDIEPFKGLLLGLFFIGVGMSIDFGTL

LENPLRIVILLLGFLIIKIAMLWLIARPLQVPNKQRRWFAVLLGQGSEFAFVVFGAAQM

ANVLEPEWAKSLTLAVALSMAATPILLVILNRLEQSSTEEAREADEIDEEQPRVIIAGFG

RFGQITGRLLLSSGVKMVVLDHDPDHIETLRKFGMKVFYGDATRMDLLESAGAAKAE

VLINAIDDPQTNLQLTEMVKEHFPHLQIIARARDVDHYIRLRQAGVEKPERETFEGALK

TGRLALESLGLGPYEARERADVFRRFNIQMVEEMAMVENDTKARAAVYKRTSAMLS

EIITEDREHLSLIQRHGWQGTEEGKHTGNMADEPETKPSS

Molecular weight (Da):

Kef F: 20170.0, Kef C: 67795.8

(Predicted using the ProtParam Tool from Expasy in Daltons, Da)

C: WaterLOGSY Full Spectra

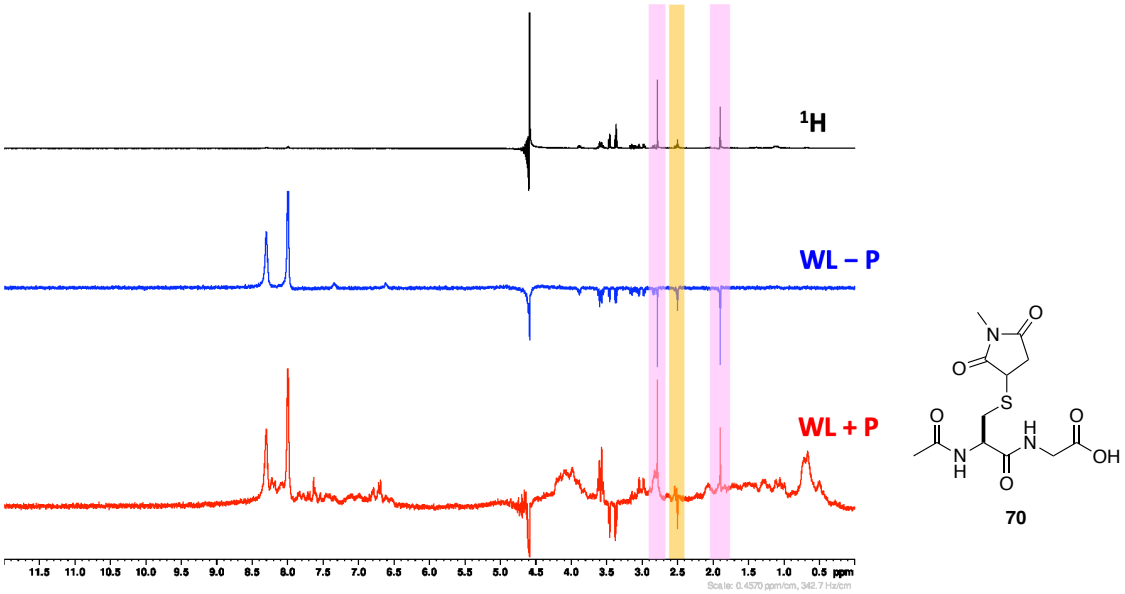


Figure S.2. Full waterLOGSY spectrum of positive control dipeptide 70. Stack top to bottom: black, water-supressed ^{1}H NMR of **70**; blue, waterLOGSY spectrum without protein; red, waterLOGSY spectrum with *Sd*KefQCTD protein. DMSO is highlighted at 2.50 ppm in yellow and is the sample reference. Compound peaks of interest are highlighted in pink.

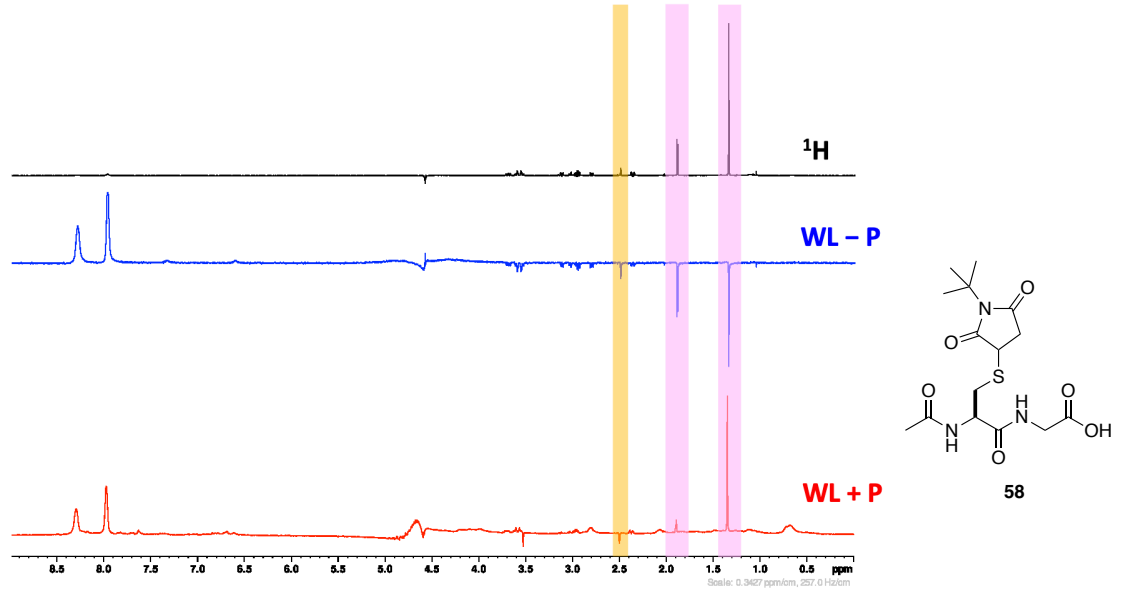


Figure S.3. Full waterLOGSY spectrum of positive control dipeptide 58. Stack top to bottom: black, water-supressed ^{1}H NMR of **58**; blue, waterLOGSY spectrum without protein; red, waterLOGSY spectrum with *Sd*KefQCTD protein. DMSO is highlighted at 2.50 ppm in yellow and is the sample reference. Compound peaks of interest are highlighted in pink.

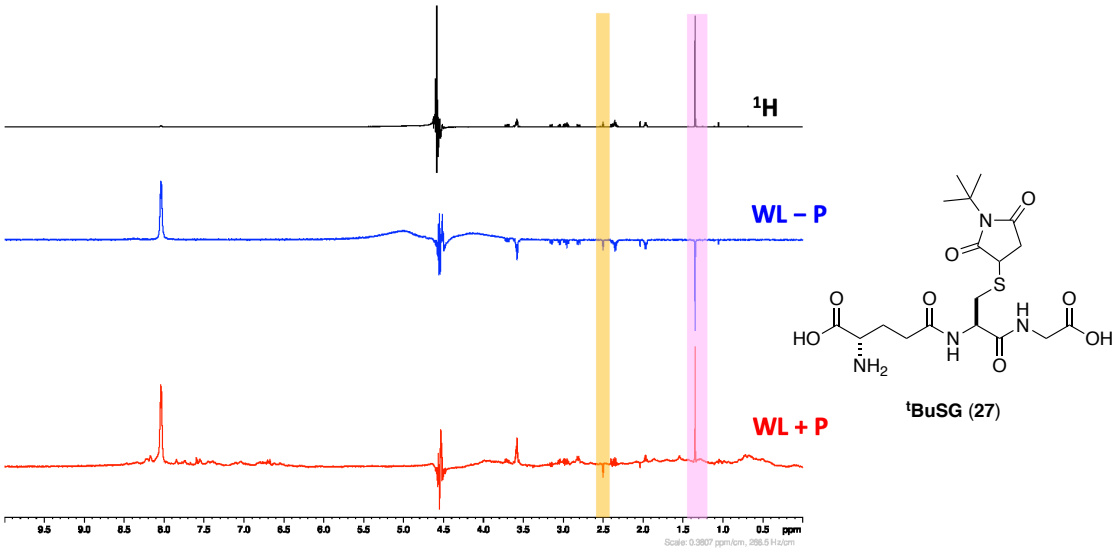


Figure S.4. Full waterLOGSY spectrum of positive control GSX adduct ^{t}BuSG. Stack top to bottom: black, water-supressed ^{1}H NMR of **^{t}BuSG**; blue, waterLOGSY spectrum without protein; red, waterLOGSY spectrum with *Sd*KefQCTD protein. DMSO is highlighted at 2.50 ppm in yellow and is the sample reference. Compound peaks of interest are highlighted in pink.

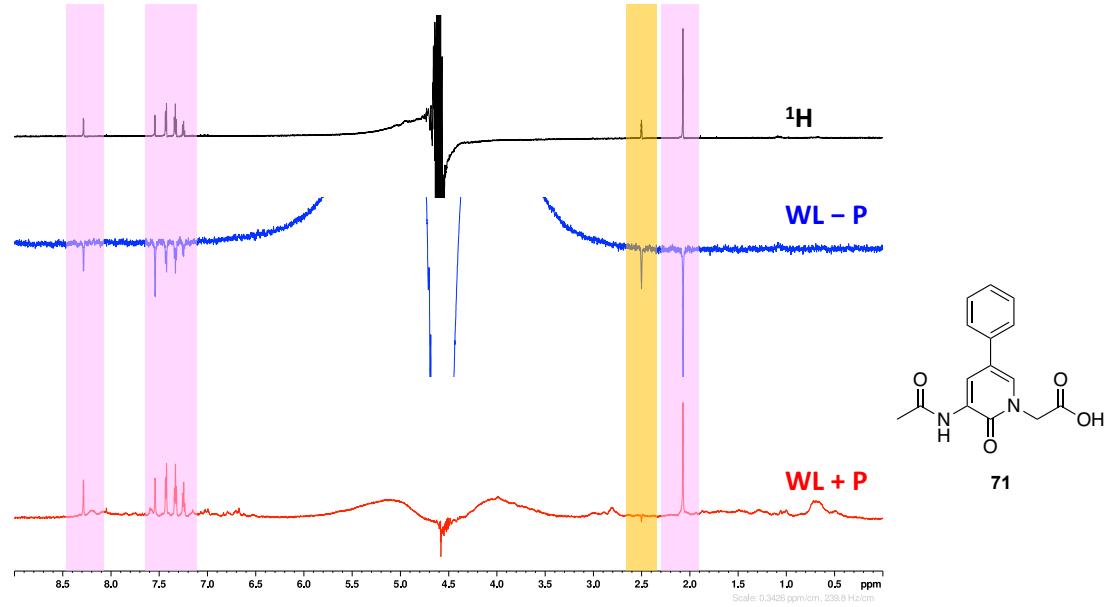


Figure S.5. Full waterLOGSY spectrum of 71. Stack top to bottom: black, water-supressed ^{1}H NMR of **71**; blue, waterLOGSY spectrum without protein; red, waterLOGSY spectrum with *Sd*KefQCTD protein. DMSO is highlighted at 2.50 ppm in yellow and is the sample reference. Compound peaks of interest are highlighted in pink.

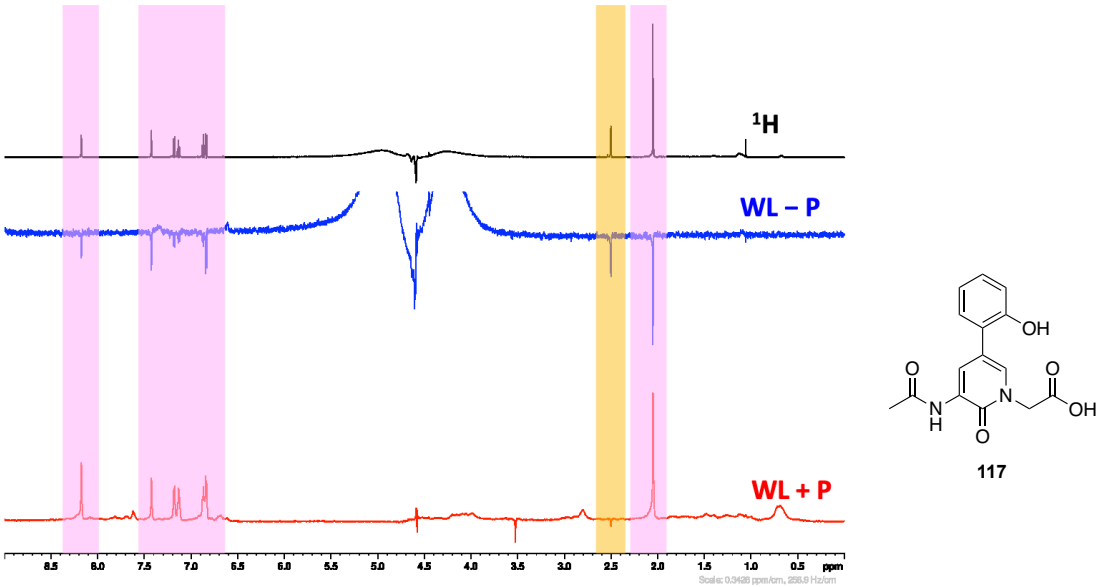


Figure S.6. Full waterLOGSY spectrum of 117. Stack top to bottom: black, water-supressed ^{1}H NMR of **117**; blue, waterLOGSY spectrum without protein; red, waterLOGSY spectrum with *Sd*KefQCTD protein. DMSO is highlighted at 2.50 ppm in yellow and is the sample reference. Compound peaks of interest are highlighted in pink.

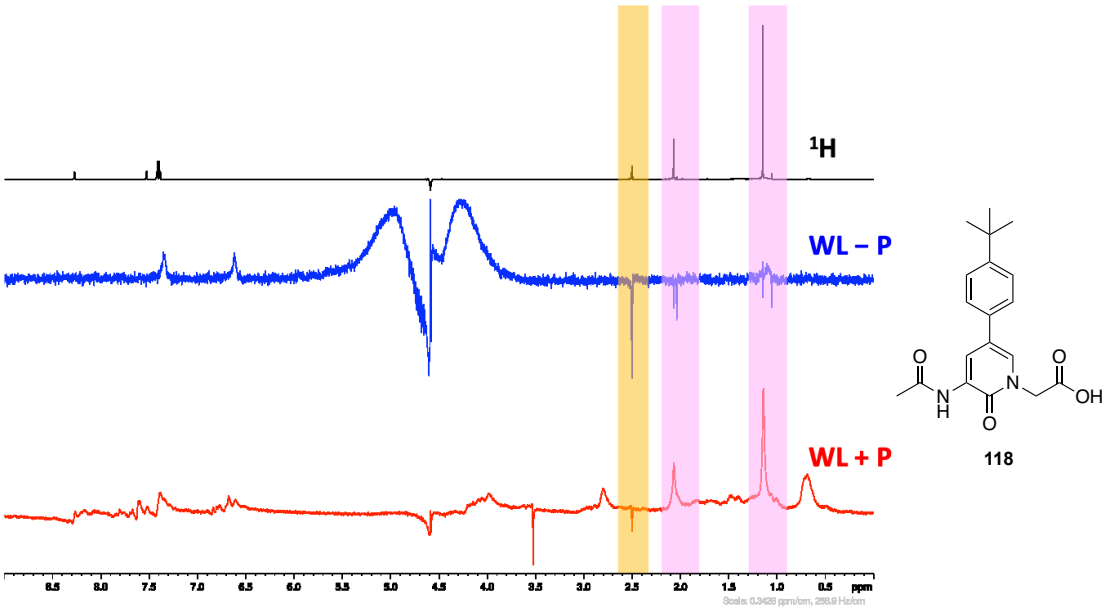


Figure S.7. Full waterLOGSY spectrum of 119. Stack top to bottom: black, water-supressed ^{1}H NMR of **119**; blue, waterLOGSY spectrum without protein; red, waterLOGSY spectrum with *Sd*KefQCTD protein. DMSO is highlighted at 2.50 ppm in yellow and is the sample reference. Compound peaks of interest are highlighted in pink.

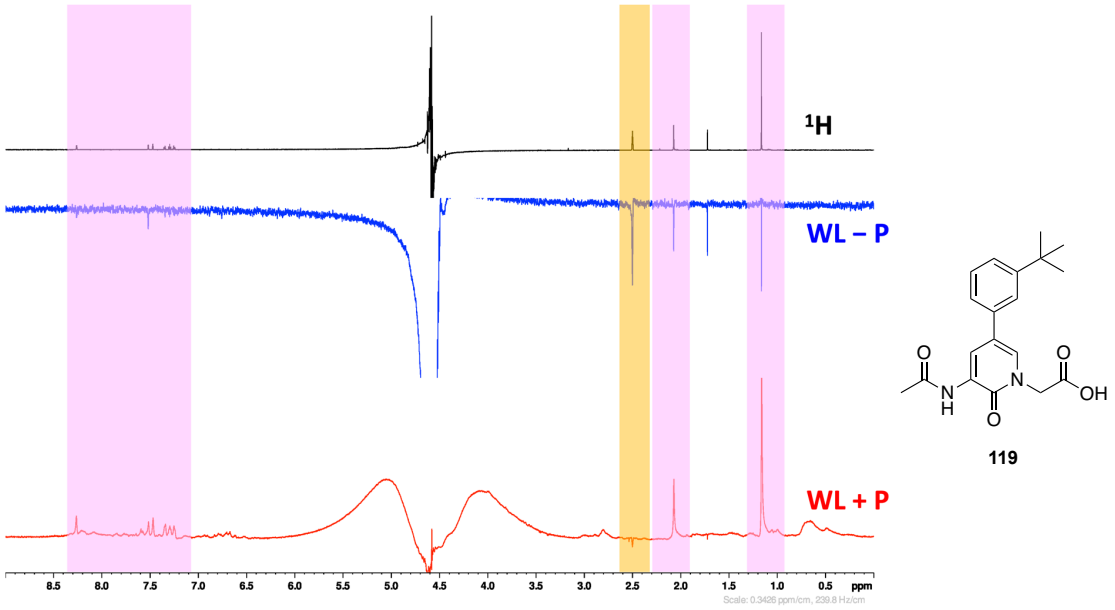


Figure S.8. Full waterLOGSY spectrum of 119. Stack top to bottom: black, water-supressed ^{1}H NMR of **119**; blue, waterLOGSY spectrum without protein; red, waterLOGSY spectrum with *Sd*KefQCTD protein. DMSO is highlighted at 2.50 ppm in yellow and is the sample reference. Compound peaks of interest are highlighted in pink.

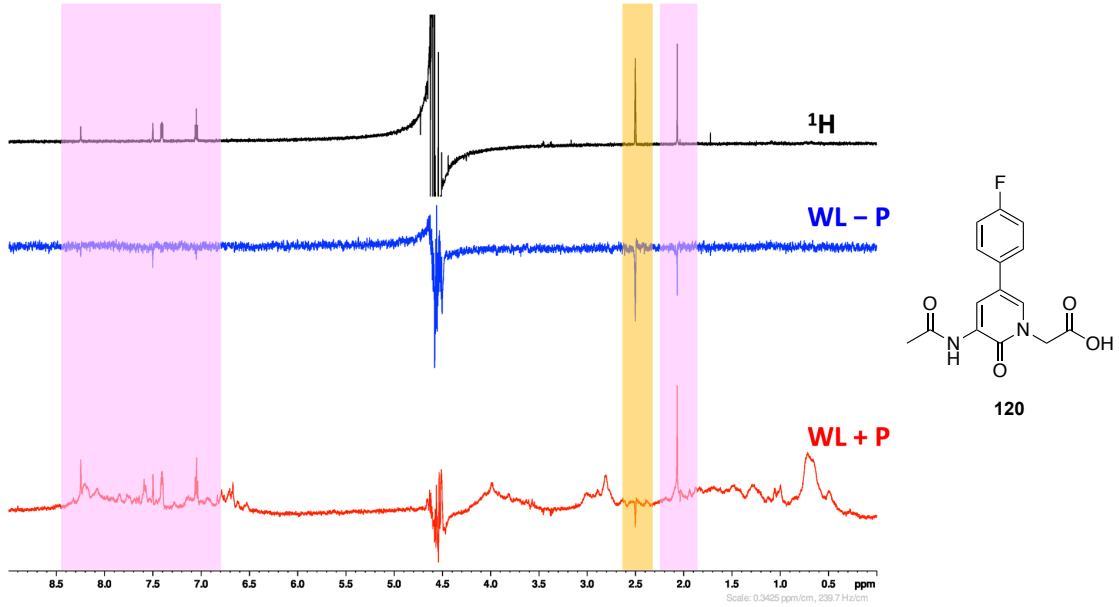


Figure S.9. Full waterLOGSY spectrum of 120. Stack top to bottom: black, water-supressed ^{1}H NMR of **120**; blue, waterLOGSY spectrum without protein; red, waterLOGSY spectrum with *Sd*KefQCTD protein. DMSO is highlighted at 2.50 ppm in yellow and is the sample reference. Compound peaks of interest are highlighted in pink.

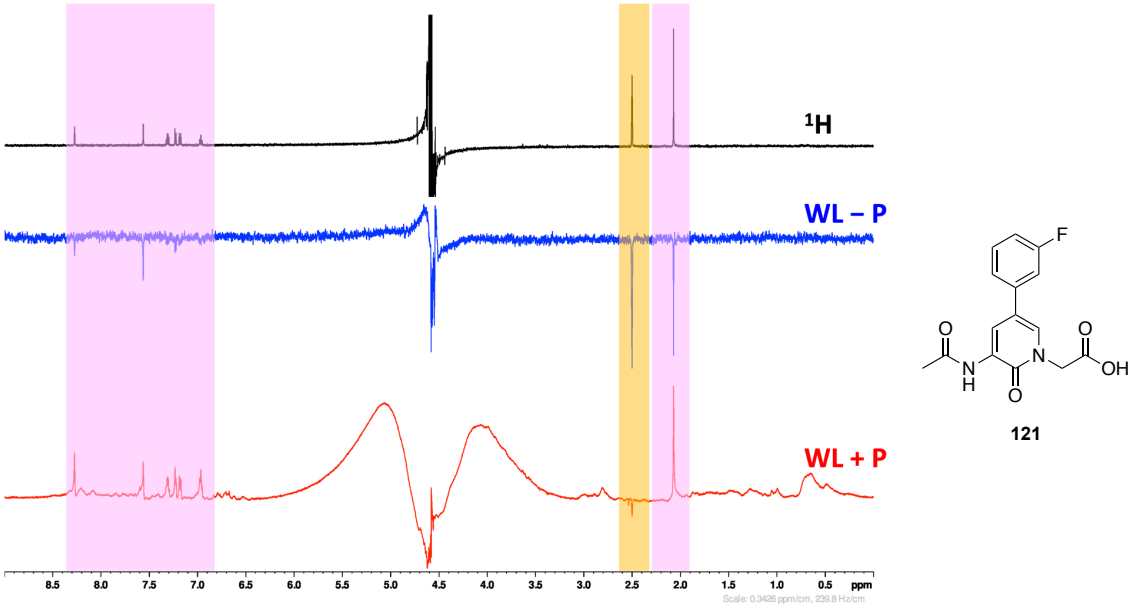


Figure S.10. Full waterLOGSY spectrum of 121. Stack top to bottom: black, water-supressed ^{1}H NMR of **121**; blue, waterLOGSY spectrum without protein; red, waterLOGSY spectrum with *Sd*KefQCTD protein. DMSO is highlighted at 2.50 ppm in yellow and is the sample reference. Compound peaks of interest are highlighted in pink.

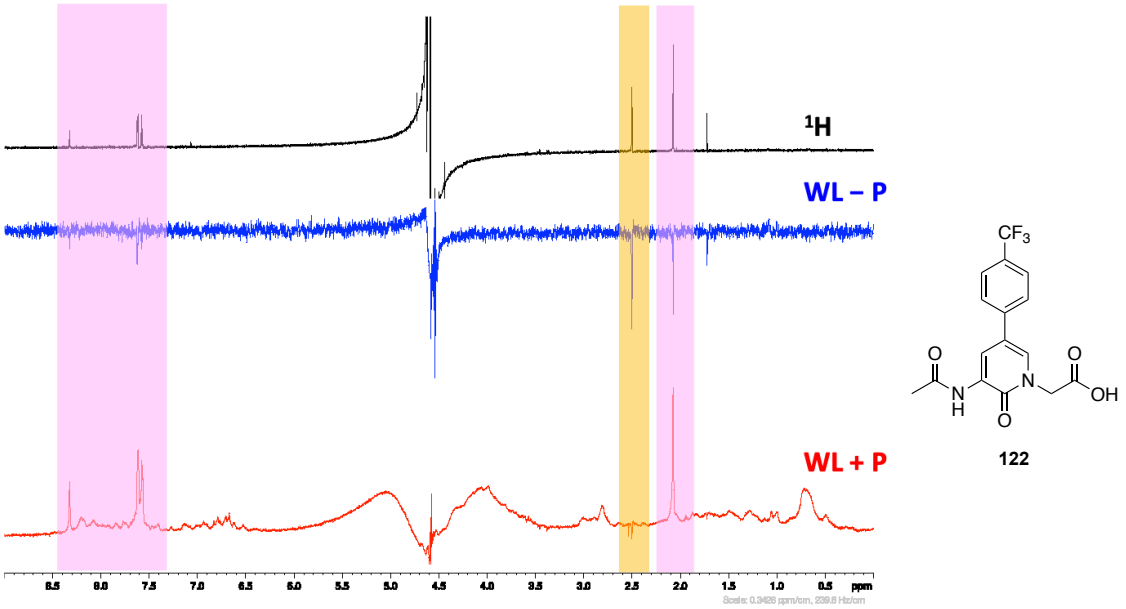


Figure S.11. Full waterLOGSY spectrum of 122. Stack top to bottom: black, water-supressed ^{1}H NMR of **122**; blue, waterLOGSY spectrum without protein; red, waterLOGSY spectrum with *Sd*KefQCTD protein. DMSO is highlighted at 2.50 ppm in yellow and is the sample reference. Compound peaks of interest are highlighted in pink.

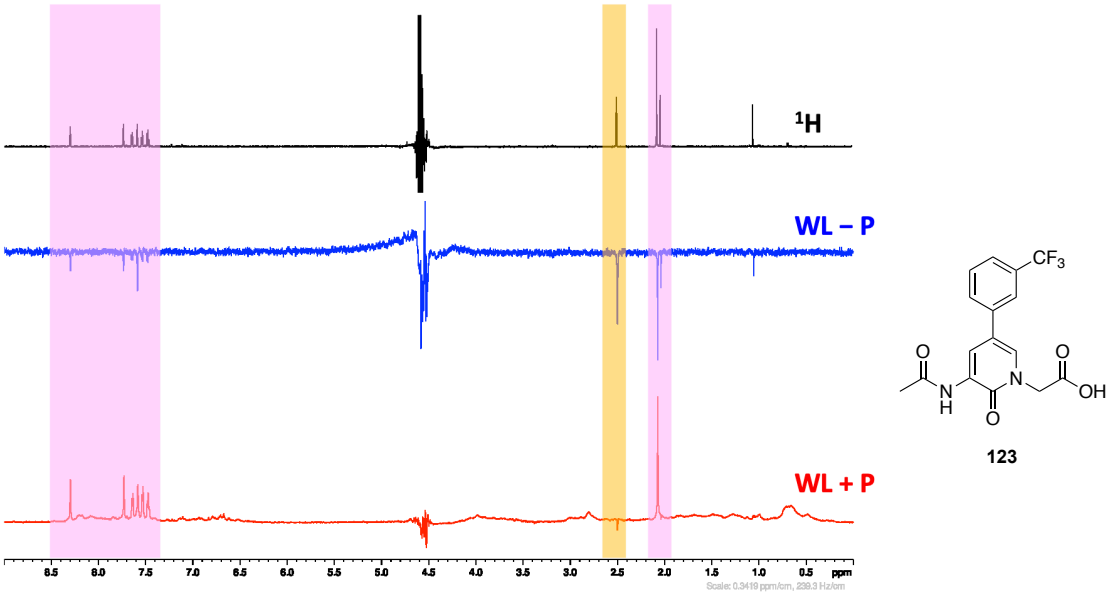


Figure S.12. Full waterLOGSY spectrum of 123. Stack top to bottom: black, water-supressed ^{1}H NMR of **123**; blue, waterLOGSY spectrum without protein; red, waterLOGSY spectrum with *Sd*KefQCTD protein. DMSO is highlighted at 2.50 ppm in yellow and is the sample reference. Compound peaks of interest are highlighted in pink.

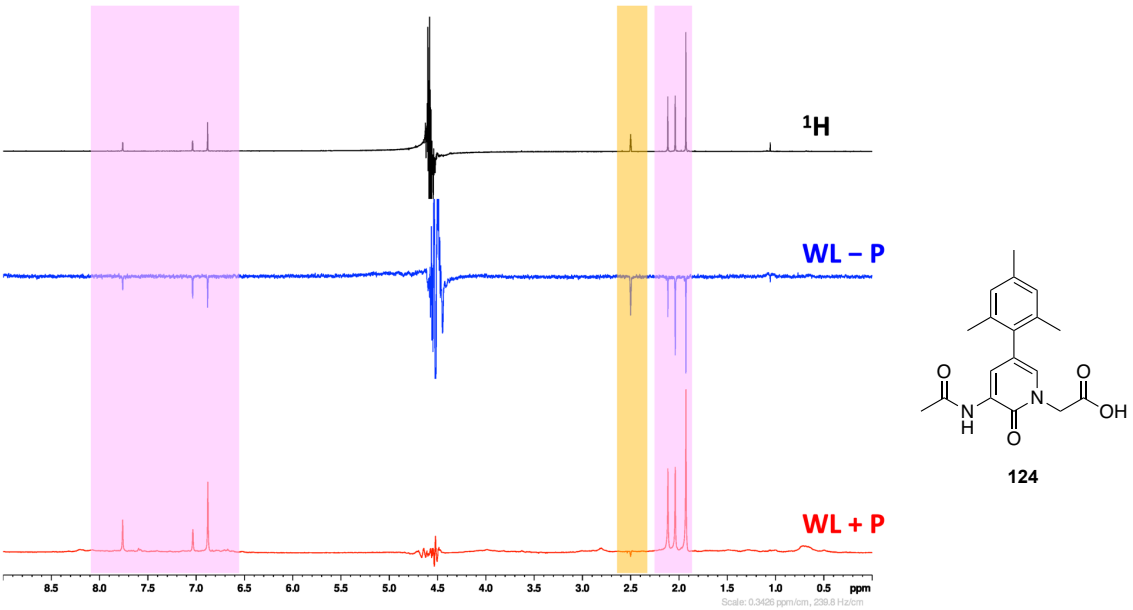


Figure S.13. Full waterLOGSY spectrum of 124. Stack top to bottom: black, water-supressed ^{1}H NMR of **124**; blue, waterLOGSY spectrum without protein; red, waterLOGSY spectrum with *Sd*KefQCTD protein. DMSO is highlighted at 2.50 ppm in yellow and is the sample reference. Compound peaks of interest are highlighted in pink.

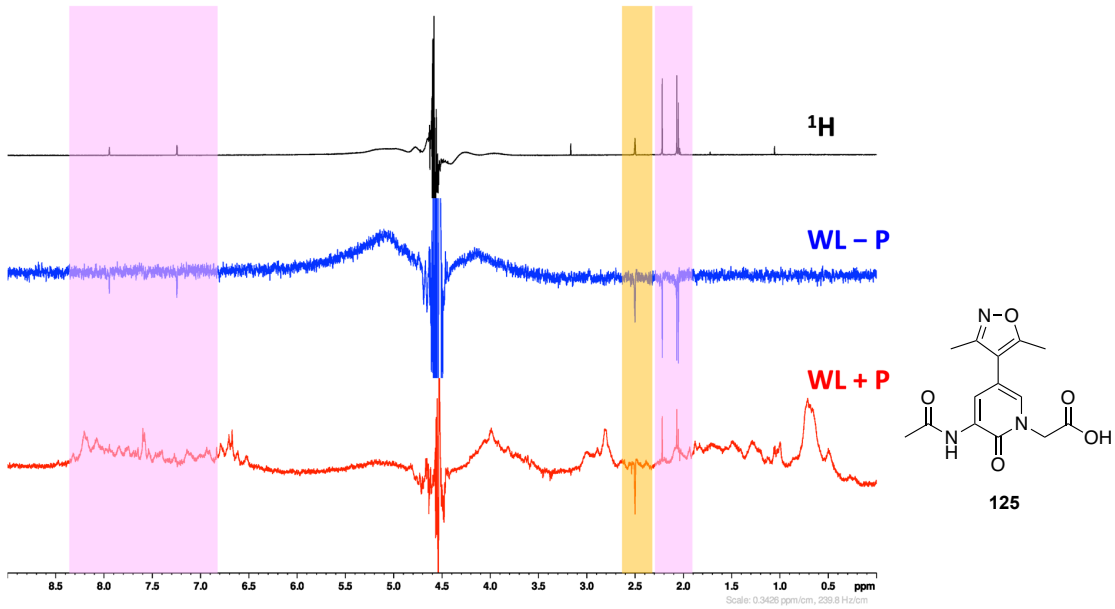


Figure S.14. Full waterLOGSY spectrum of 125. Stack top to bottom: black, water-supressed ^{1}H NMR of **125**; blue, waterLOGSY spectrum without protein; red, waterLOGSY spectrum with *Sd*KefQCTD protein. DMSO is highlighted at 2.50 ppm in yellow and is the sample reference. Compound peaks of interest are highlighted in pink.

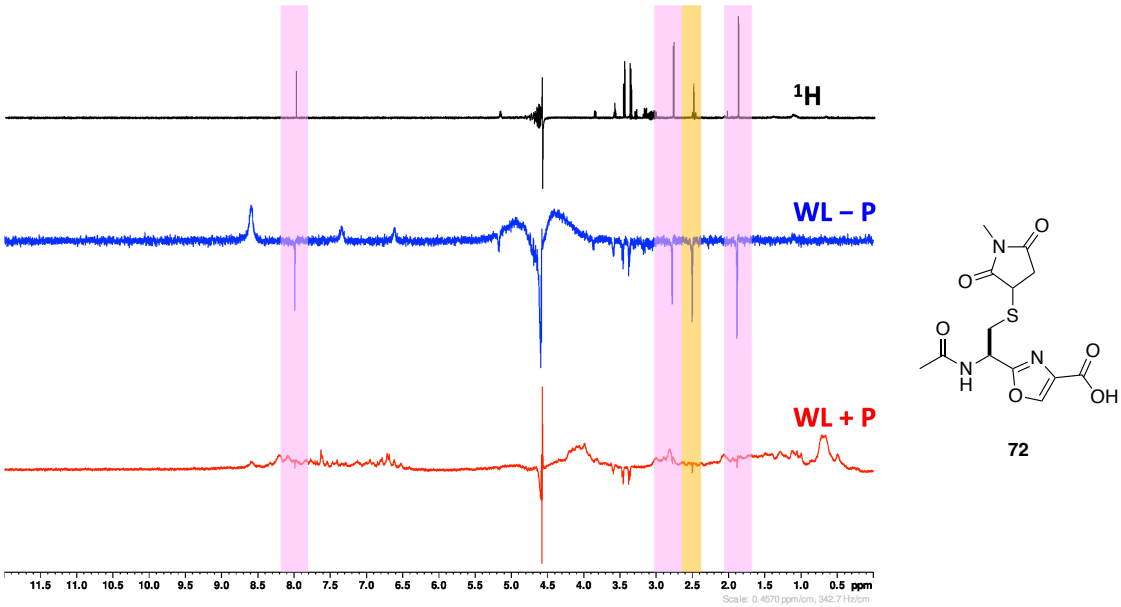


Figure S.15. Full waterLOGSY spectrum of 72. Stack top to bottom: black, water-supressed ^{1}H NMR of **72**; blue, waterLOGSY spectrum without protein; red, waterLOGSY spectrum with *Sd*KefQCTD protein. DMSO is highlighted at 2.50 ppm in yellow and is the sample reference. Compound peaks of interest are highlighted in pink.

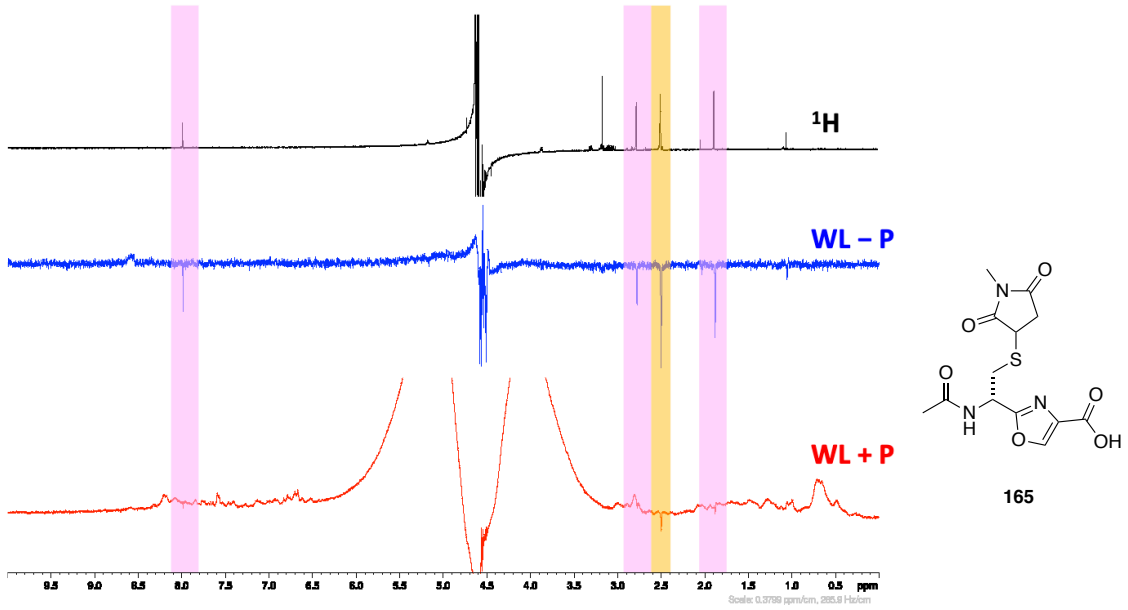


Figure S.16. Full waterLOGSY spectrum of 165. Stack top to bottom: black, water-supressed ^{1}H NMR of **165**; blue, waterLOGSY spectrum without protein; red, waterLOGSY spectrum with *Sd*KefQCTD protein. DMSO is highlighted at 2.50 ppm in yellow and is the sample reference. Compound peaks of interest are highlighted in pink.

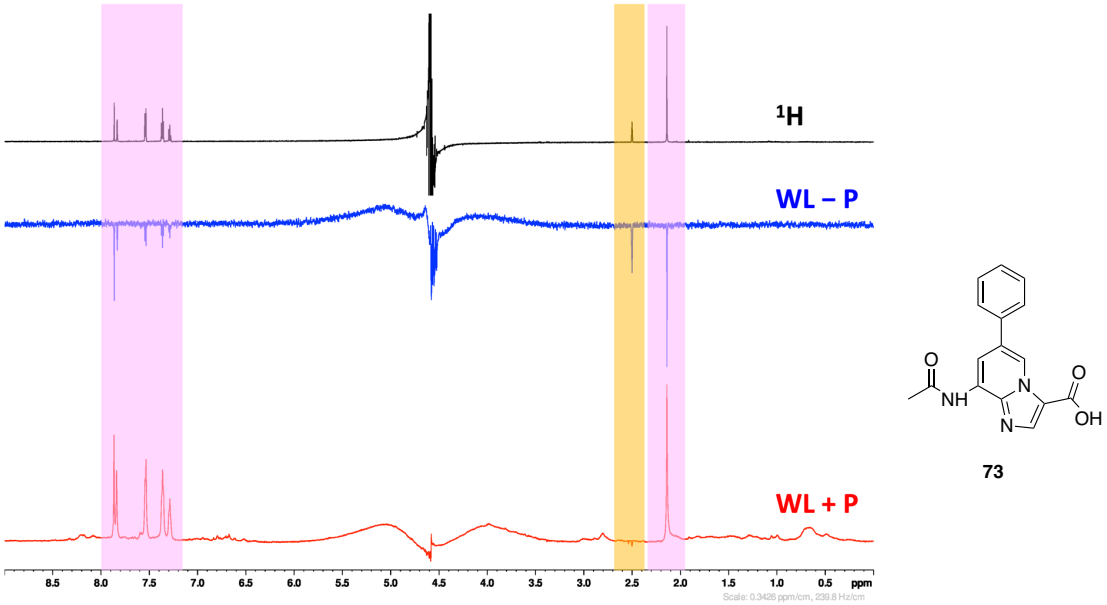


Figure S.17. Full waterLOGSY spectrum of 73. Stack top to bottom: black, water-supressed ^{1}H NMR of **73**; blue, waterLOGSY spectrum without protein; red, waterLOGSY spectrum with *Sd*KefQCTD protein. DMSO is highlighted at 2.50 ppm in yellow and is the sample reference. Compound peaks of interest are highlighted in pink.

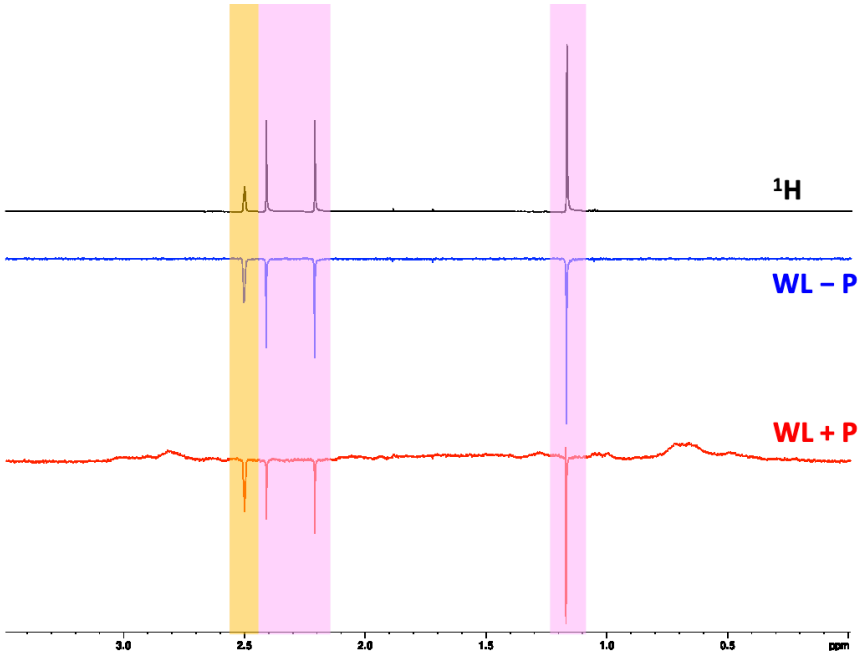


Figure S.18. Full waterLOGSY spectrum of 74. Stack top to bottom: black, water-supressed ^{1}H NMR of **74**; blue, waterLOGSY spectrum without protein; red, waterLOGSY spectrum with *Sd*KefQCTD protein. DMSO is highlighted at 2.50 ppm in yellow and is the sample reference. Compound peaks of interest are highlighted in pink.

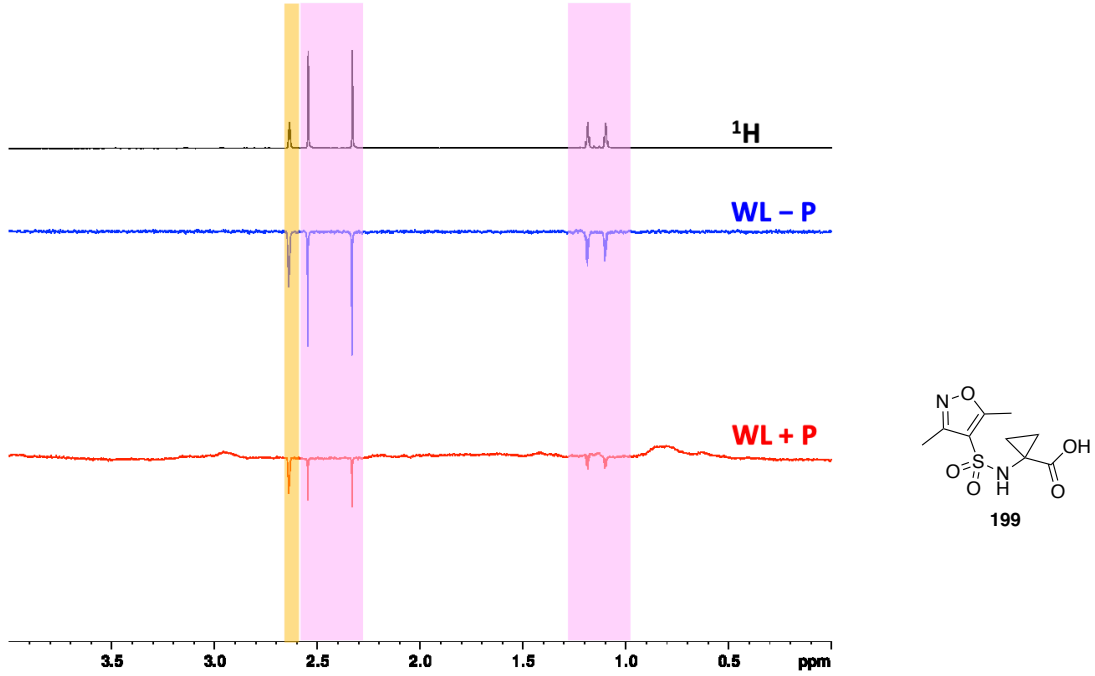
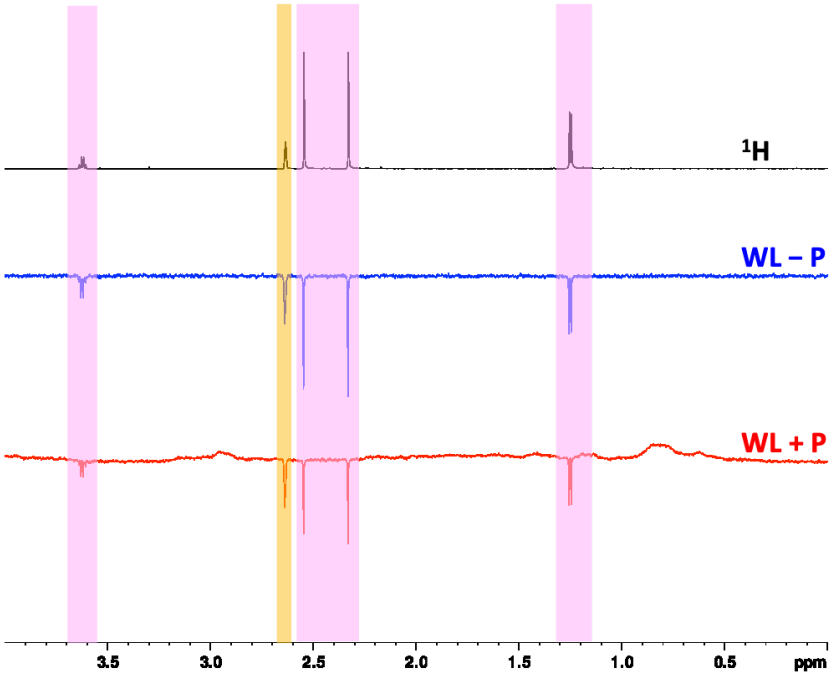
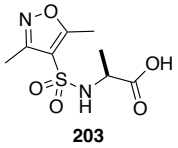


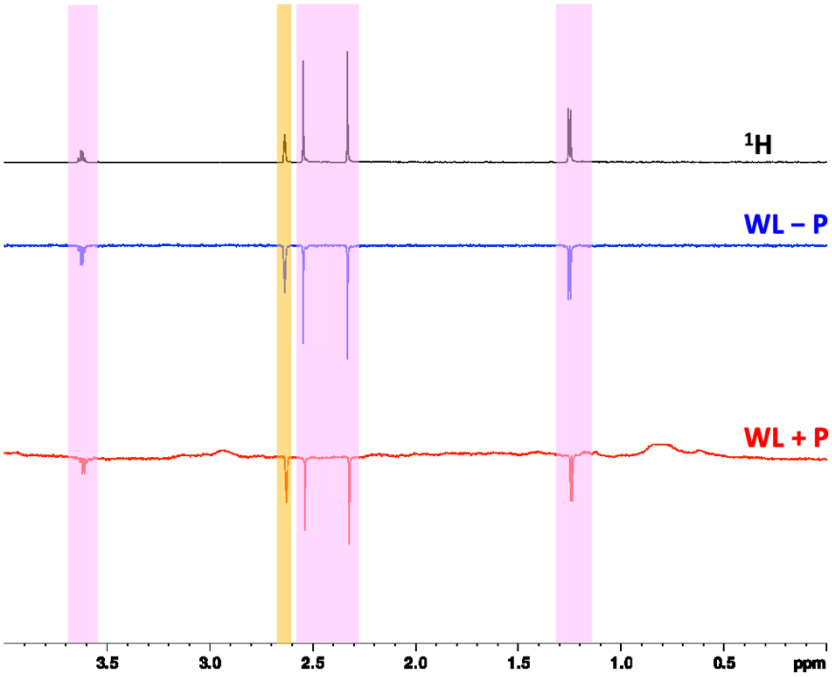
Figure S.19. Full waterLOGSY spectrum of 199. Stack top to bottom: black, water-supressed ^{1}H NMR of **199**; blue, waterLOGSY spectrum without protein; red, waterLOGSY spectrum with *Sd*KefQCTD protein. DMSO is highlighted at 2.50 ppm in yellow and is the sample reference. Compound peaks of interest are highlighted in pink.

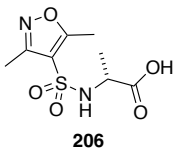




203

Figure S.20. Full waterLOGSY spectrum of 203. Stack top to bottom: black, water-supressed ^{1}H NMR of **203**; blue, waterLOGSY spectrum without protein; red, waterLOGSY spectrum with *Sd*KefQCTD protein. DMSO is highlighted at 2.50 ppm in yellow and is the sample reference. Compound peaks of interest are highlighted in pink.





206

Figure S.21. Full waterLOGSY spectrum of 206. Stack top to bottom: black, water-supressed ^{1}H NMR of **206**; blue, waterLOGSY spectrum without protein; red, waterLOGSY spectrum with *Sd*KefQCTD protein. DMSO is highlighted at 2.50 ppm in yellow and is the sample reference. Compound peaks of interest are highlighted in pink.

D: Thermal Shift Data

Table A.1. Experiment 1: DSF melting temperatures of *Sd*KefQCTD calculated from Boltzmann fitting of fluorescence in Prism 9. The protein with no ligand (DMSO) was used as a reference for the thermal shift, with 1 mM ligand. Each set of conditions were run in triplicate on the same plate and used to calculate the mean.

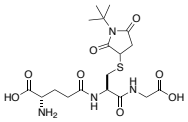
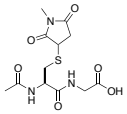
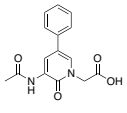
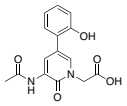
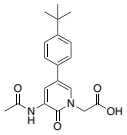
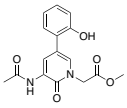
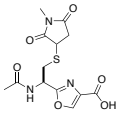
Identity	Structure	Melting Temperature/ °C			Average/ °C
		1	2	3	
DMSO	-	42.32	41.68	42.39	42.13
^{t}BuSG (**27**)		50.96	51.33	51.26	51.18
70		43.34	43.69	44.11	43.71
71		42.30	41.54	43.01	42.28
117		42.34	42.33	43.23	42.63
119		43.36	43.86	43.03	43.42
95		42.63	42.87	42.45	42.65
72		41.96	42.99	42.44	42.46

Table A.2. Experiment 2: DSF melting temperatures of *Sd*KefQCTD calculated from Boltzmann fitting of fluorescence in Prism 9. The protein with no ligand (DMSO) was used as a reference for the thermal shift, with 1 mM ligand. Each set of conditions were run in triplicate on the same plate and used to calculate the mean. Blank values are displayed when the melting temperature could not be estimated due to an irregular transition.

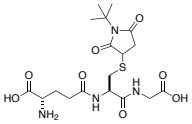
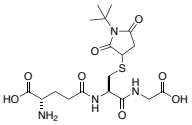
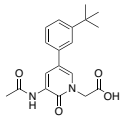
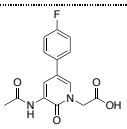
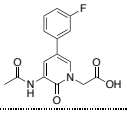
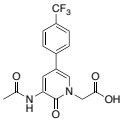
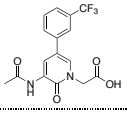
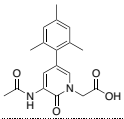
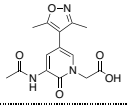
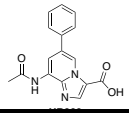
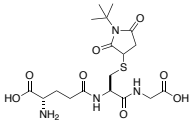
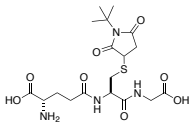
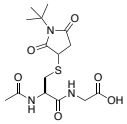
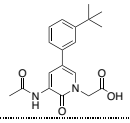
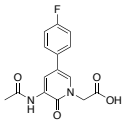
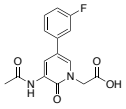
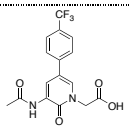
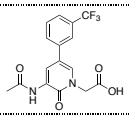
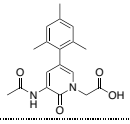
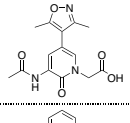
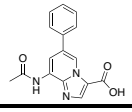
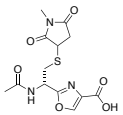
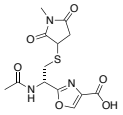
Identity	Structure	Melting Temperature/ °C			Average/ °C
		1	2	3	
DMSO	-	41.39	-	43.37	42.38
^{t}BuSG (**27**)		43.87	-	53.81	48.84
^{t}BuSG (**27**) (Repeat)		51.62	49.24	49.44	50.10
119		39.81	40.88	40.36	40.35
120		41.06	38.90	46.83	42.26
121		40.56	37.20	41.20	39.65
122		42.60	49.54	41.78	44.64
123		50.58	43.19	41.33	45.03
124		39.15	44.50	39.14	40.93
125		38.62	39.25	38.65	38.84
73		43.73	53.12	41.13	45.99

Table A.3. Experiment 1: DSF melting temperatures of *Sd*KefQCTD calculated from Boltzmann fitting of fluorescence in Prism 9. The protein with no ligand (DMSO) was used as a reference for the thermal shift, with 500 µM ligand (except **165** where indicated). Each set of conditions were run in triplicate on the same plate and used to calculate the mean. Blank values are displayed when the melting temperature could not be estimated due to an irregular transition.

Identity	Structure	Melting Temperature/ °C			Average/ °C
		1	2	3	
DMSO	-	38.89	38.70	44.99	40.86
DMSO (Repeat)	-	39.44	41.77	39.93	40.38
^{t}BuSG (**27**)		46.47	45.54	47.35	46.45
^{t}BuSG (**27**) (Repeat)		46.87	48.00	50.26	48.38
70		41.36	41.00	41.65	41.34
119		40.34	40.42	41.16	40.64
120		39.49	39.41	40.52	39.81
121		-	42.48	41.39	41.94
122		45.74	41.07	45.43	44.08
123		40.02	40.06	37.6	39.23
124		39.01	39.37	39.99	39.46
125		39.31	38.99	40.01	39.44
73		41.76	-	40.76	41.26

165		45.17	37.49	40.17	40.94
165 (1mM)		39.12	38.94	43.51	40.52

E: Kirby-Bauer Disc Assay

Table A.4. Results from Kirby-Bauer Disc assay testing scaffold hopping compounds. The compounds **74**, **199**, **203**, and **206** were tested in *E. coli* strain MJF645 expressing *Sd*Kef or *Ec*KefFC systems. pTrc*Sd*Kef required IPTG as a promoter, whereas pkC11 was expressed under its own promoter. Diameter measurements of the growth inhibition zones are recorded as an average of two perpendicular diameter measurements in mm. The disc impregnated with compound measures 6 mm, therefore zones larger than this show inhibition of cell growth. MJF645 expressing no Kef is used as a negative control to check for non-specific compound toxicity. There was no positive control for this assay. Symbol meanings: + included in these conditions, – not included.

Entry	1	2	3	4	5	6
Host	MJF645	MJF645	MJF645	MJF645	MJF645	MJF645
Plasmid	pTrc*Sd*KefH_6	pTrc*Sd*KefH_6	pkC11	pkC11	none	none
IPTG	+	+	-	-	-	-
Amp	+	+	+	+	-	-
MQ	6	6	6	6	6	6
74 /mm	6	6	6	6	6	6
199/mm	6	6	6	6	6	6
203 /mm	6	6	6	6	6	6
206/mm	6	6	6	6	6	6
Remark	No effect	No effect	No effect	No effect	Negative Control	Negative Control

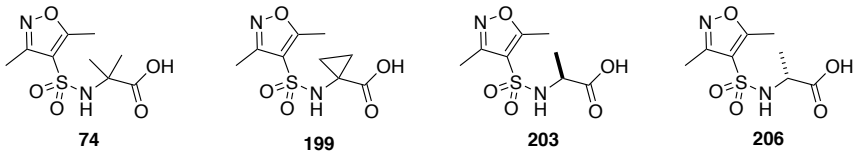


Figure S.22. Structures of compounds (74, 199, 203, and 206) tested in the Kirby-Bauer disc assay generated from scaffold hopping experiments.

Table A.5. *E. coli* cell strains employed in the Kirby-Bauer disc diffusion assay. These were received from Dr Samantha Miller (University of Aberdeen).

E. coli Strain	Genotype	Reference
MJF5645	MG1655, kefF, kefC, kefG, kefB, gshA	Healy, J.; Ekkerman, S.; Pliotas, C.; Richard, M.; Bartlett, W.; Grayer, S. C.; Morris, G. M.; Miller, S.; Booth, I. R.; Conway, S. J.; Rasmussen, T. *Biochemistry* **2014**, 53, 1982–1992.

Table A.6. Plasmids used for the Kirby-Bauer disc diffusion assay. pTrc*Sd*KefH_6, and pKc11 were obtained from Dr Anthony Chan.

Entry	Plasmid	Description	Reference
1	pTrc*Sd*KefH_6	C-terminal hex-His (LEH_6) full-length *Sd*Kef (codon-optimised) expressed under the trc promoter. GenBank ID of SdKef: ABE53663.1	Miller, S.; Douglas, R. M.; Carter, P.; Booth, I. R. *J. Biol. Chem*. **1997**, 272, 24942–24947.
2	pKc11	Full-length *Ec*KefFC expressed under own promoter	Miller, S.; Ness, L. S.; Wood, C. M.; Fox, B. C.; Booth, I. R. *J. Bacteriol*. **2000**, 182, 6536–6540.

F: Computational Chemistry

Native GSH ligand created from protein structure PDB ID = 3L9X (*Ec*Kef) with the binding pose maintained. The dipeptide or ESG backbone query was used in the following programmes (see Table A.1) to create and view hits, using default libraries (Table A.2) and settings to search for suitable mimetics.

Table A.7. Summary of programmes used for scaffold hopping experiments.

Programme	Role	Reference
ROCS	3D-shape screening of compounds	Hawkins, P.C.D.; Skillman, A.G.; Nicholls, A., *Journal of Medicinal Chemistry* 2007, *50*, 74.
Spark	Scaffold hopping	Spark™, version 10.4, 2016, Cresset, Litlington, Cambridgeshire, UK; Cheeseright, T.; Mackey, M.; Rose, S.; Vinter, A.*; J. Chem. Inf. Model.* 2006, 46, 665.
Blaze	3D-shape and electrostatic screening of compounds	Blaze™, version 10.2, 2014, Cresset, Litlington, Cambridgeshire, UK; Cheeseright, T.J.; Mackey, M.D., Melville, J.L.; Vinter, J.G.; *J. Chem. Inf. Model*. 2008, 48, 2108.
MOE	Pharmacophore query set-up, and results filtering and visualisation.	*Molecular Operating Environment (MOE),* 2013.08; Chemical Computing Group Inc., 1010 Sherbooke St. West, Suite #910, Montreal, QC, Canada, H3A 2R7, 2017.

Table A.8. Summary of libraries used for scaffold hopping experiments.

Library	Reference
ZINC	Irwin, J. J.; Shoichet, B. K. *J. Chem. Inf. Model.* 2005, *45*, 177–182
OMEGA	Hawkins, P. C. D.; Skillman, A. G.; Warren, G. L.; Ellingson, B. A.; Stahl, M. T. *J. Chem. Inf. Model.* 2010, *50*, 572–584

The following parameters were used to generate a pharmacophore to filter results and select hits (table A.3) within MOE.

Table A.9. Pharmacophore query parameters used to prioritise results and screen hits.

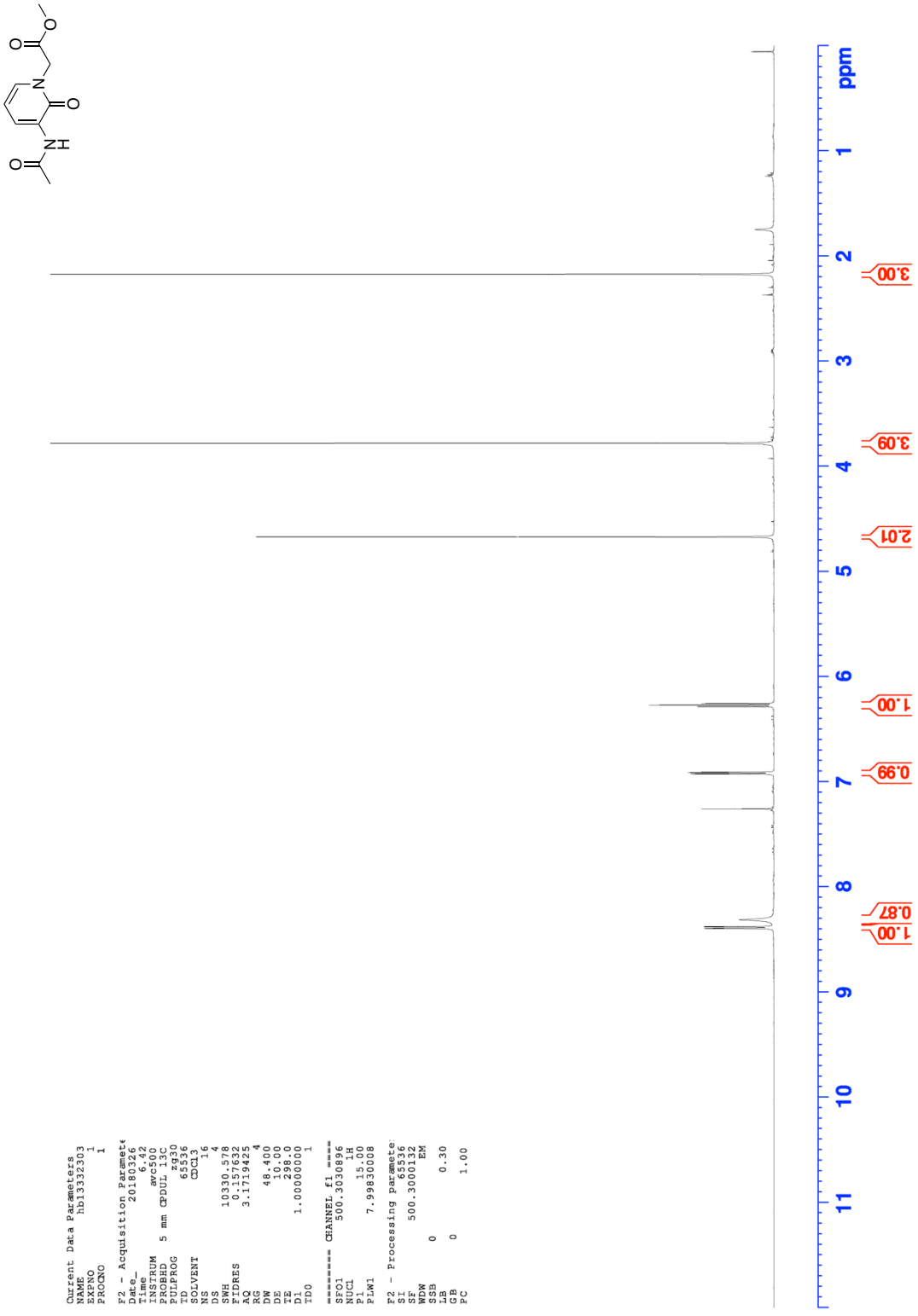
Filtering Parameter	Results
Amide bonds	None within area ligand will bind to receptor
Hydrogen bond donor/acceptors	≥3/5 satisfied of original native ligand interactions
Excluded volume	No clashes with receptor

To prioritise the results, the list was ranked by the Tanimoto coefficient in MOE, and one candidate was selected by visual inspection based on the binding pose, and the synthetic viability of the ligand (by H. Bunce and S. J. Conway) to arrive at the target.

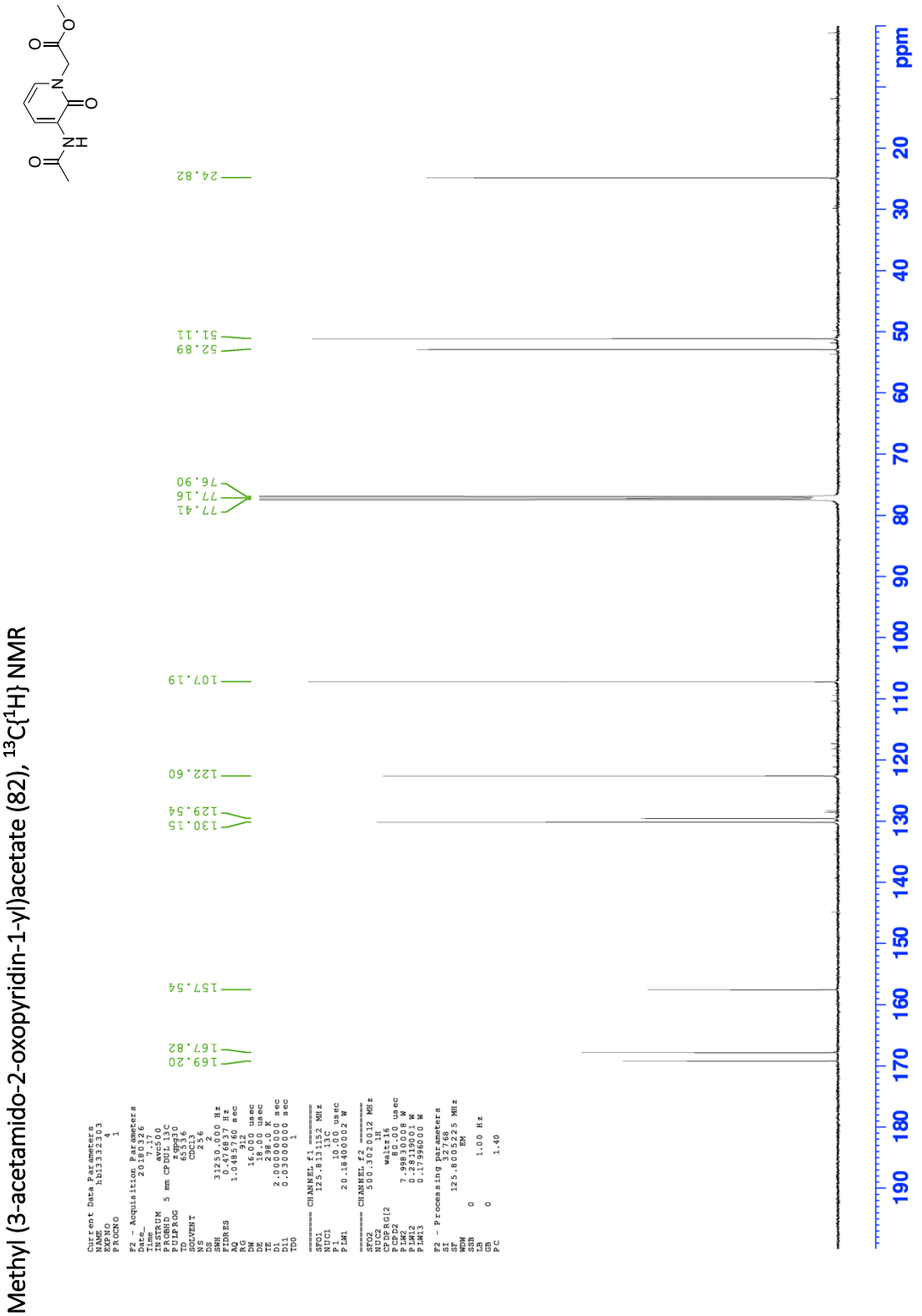
G: NMR Spectra of Novel Compounds

^{1}H, ^{13}C, ^{11}B, and ^{19}F NMR (where appropriate) spectra for all novel compounds. Spectra are presented in numerical order according to compound number.

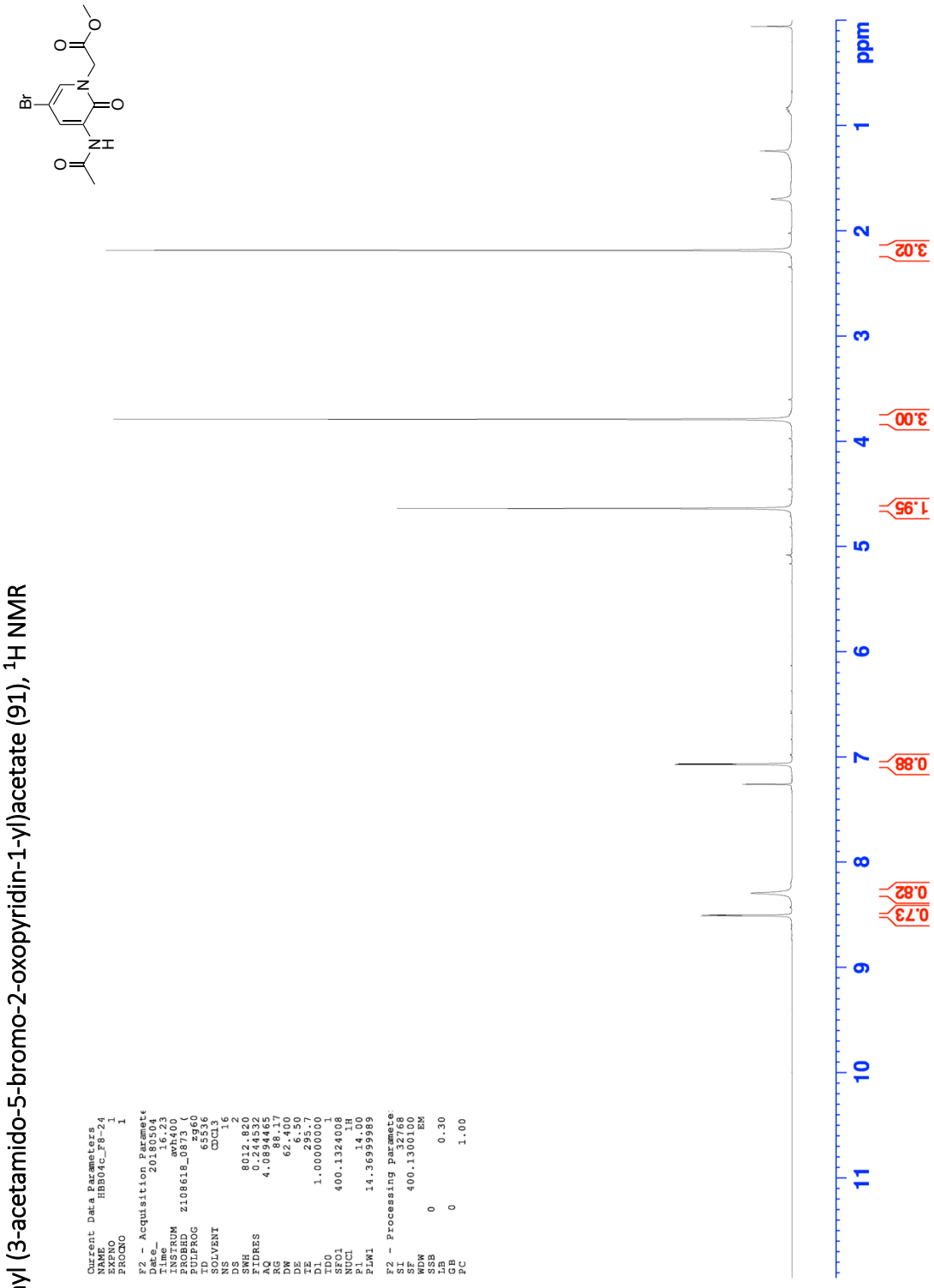
NMR Spectra of Methyl (3-acetamido-2-oxopyridin-1-yl)acetate (82), ^{1}H NMR



Methyl (3-acetamido-2-oxopyridin-1-yl)acetate (82), $^{13}C\{^{1}H\}$ NMR



Methyl (3-acetamido-5-bromo-2-oxopyridin-1-yl)acetate (91), ^{1}H NMR

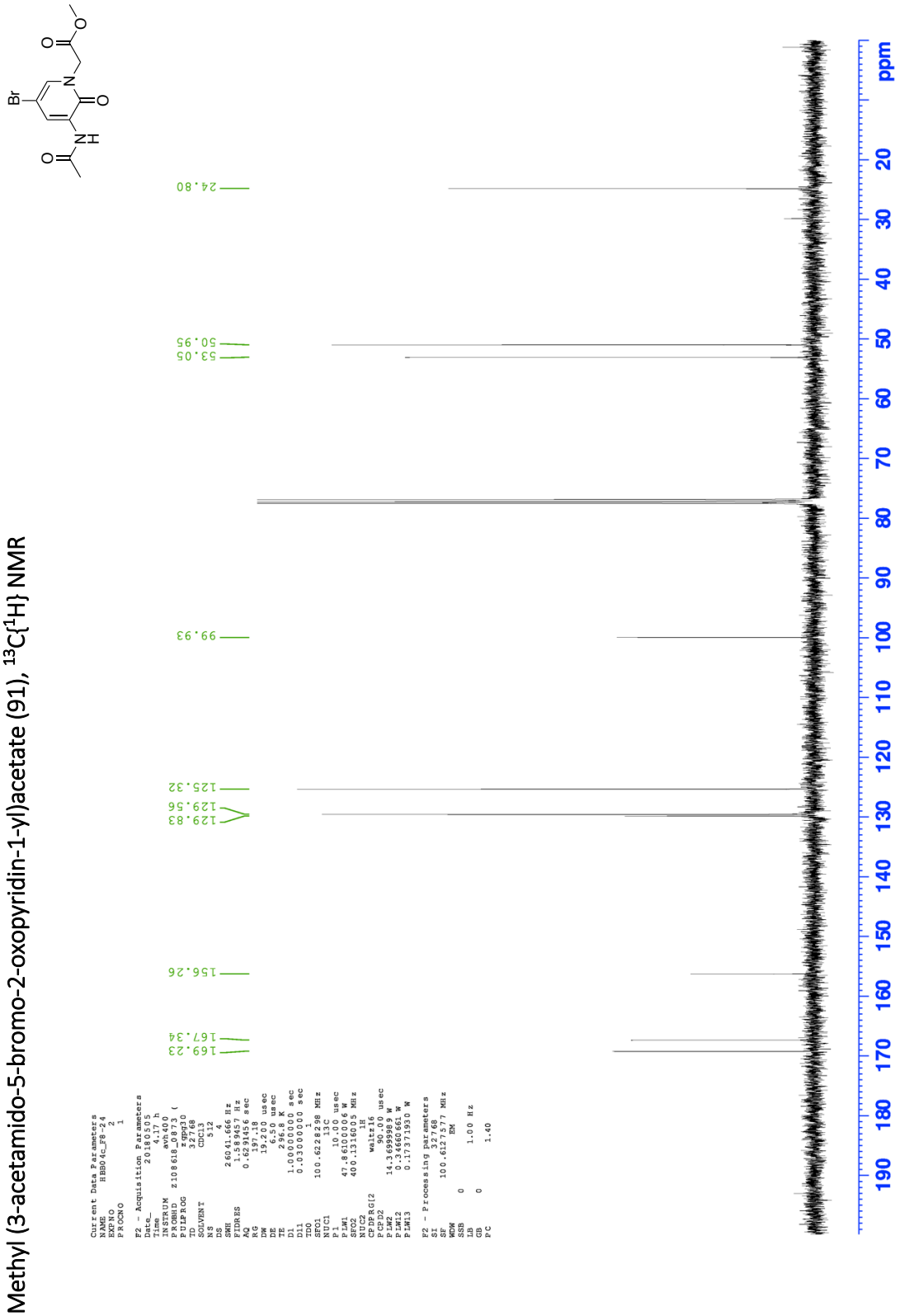


Current Data Parameters
NAME HBB04c_F8-24
EXPNO 1
PROCNO 1

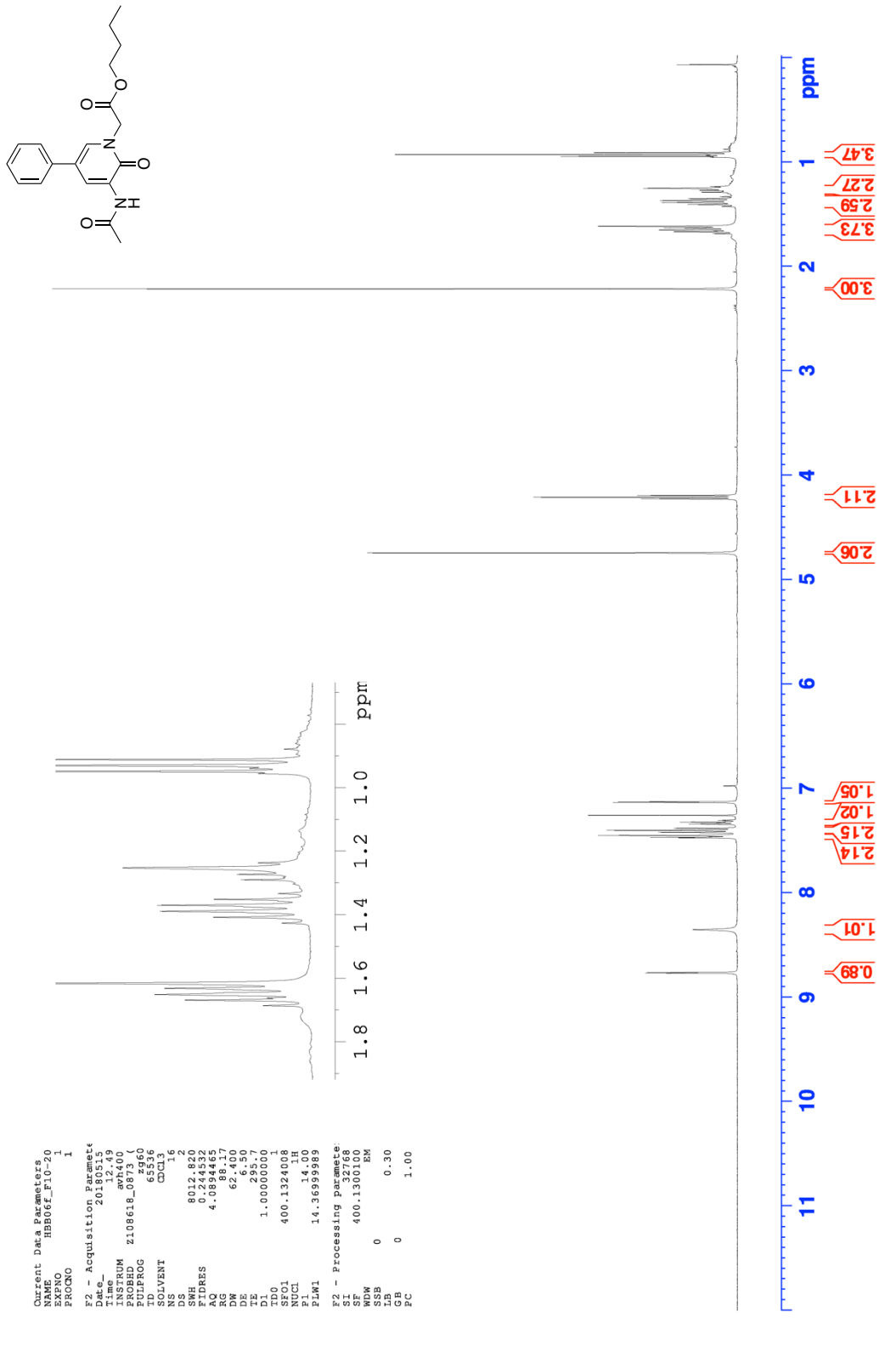
F2 - Acquisition Parameters
Date_ 20180504
Time 16.23
INSTRUM avh400
PROBHD Z108618_0873 (
PULPROG zg60
TD 65536
SOLVENT CDCl3
NS 16
DS 2
SWH 8012.820
FIDRES 0.244532
AQ 4.0894465
RG 88.17
DW 62.400
DE 6.50
TE 295.7
D1 1.00000000
TD0 1
SFO1 400.1324008
NUC1 1H
P1 14.00
PLW1 14.36999989

F2 - Processing parameters
SI 32768
SF 400.1300100
WDW EM
SSB 0
LB 0.30
GB 0
PC 1.00

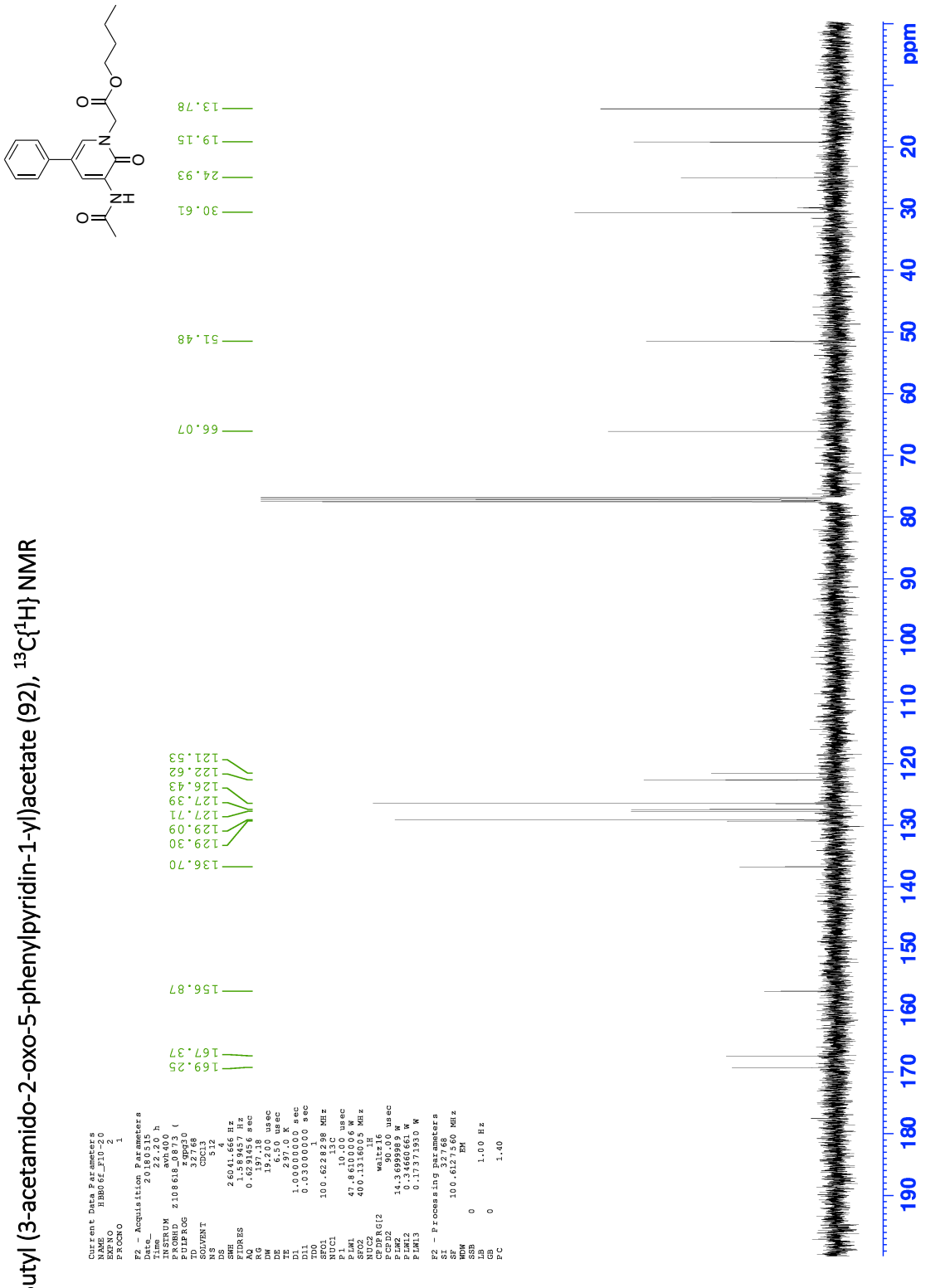
Methyl (3-acetamido-5-bromo-2-oxopyridin-1-yl)acetate (91), $^{13}C\{^{1}H\}$ NMR



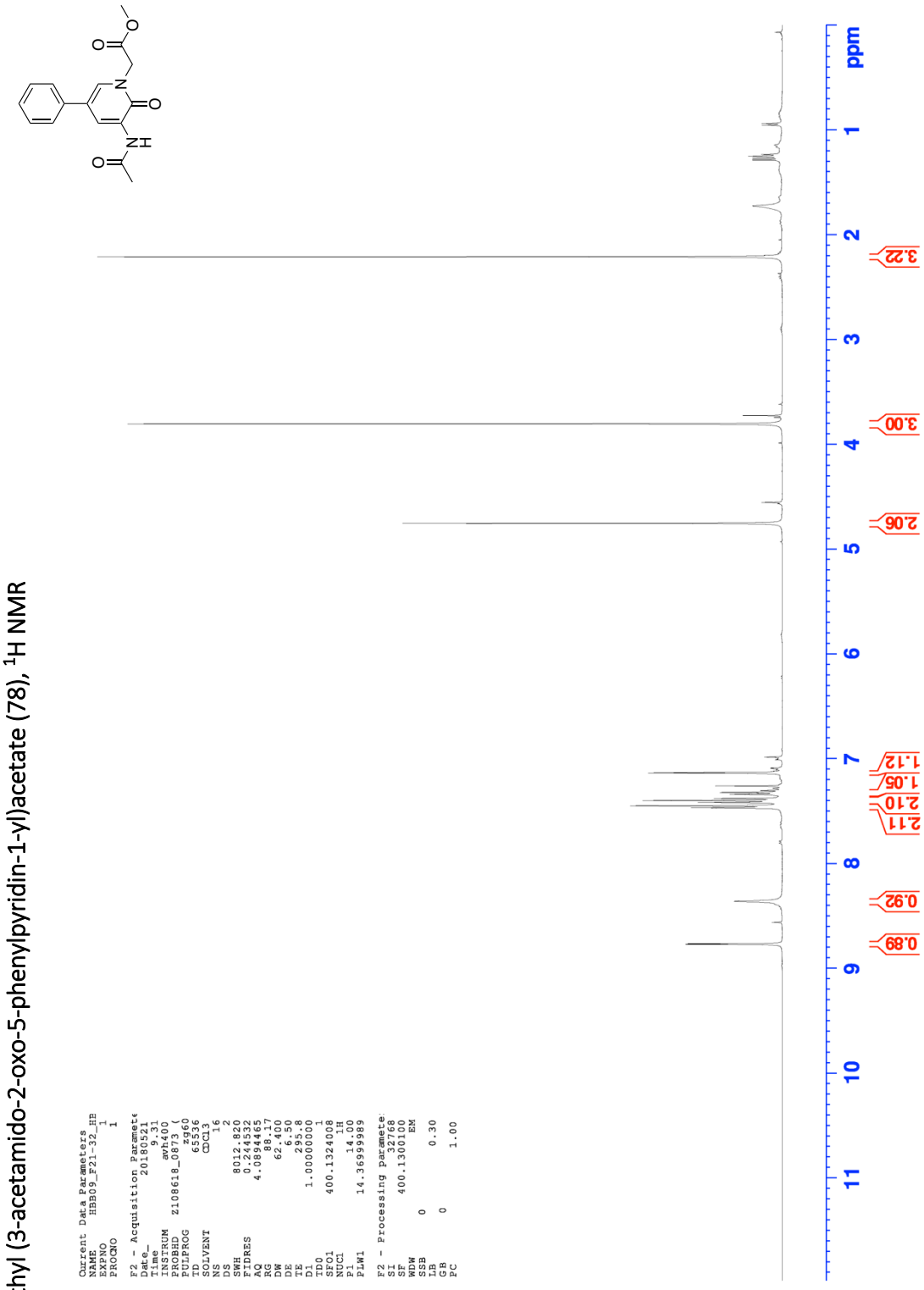
Butyl (3-acetamido-2-oxo-5-phenylpyridin-1-yl)acetate (92), ^{1}H NMR



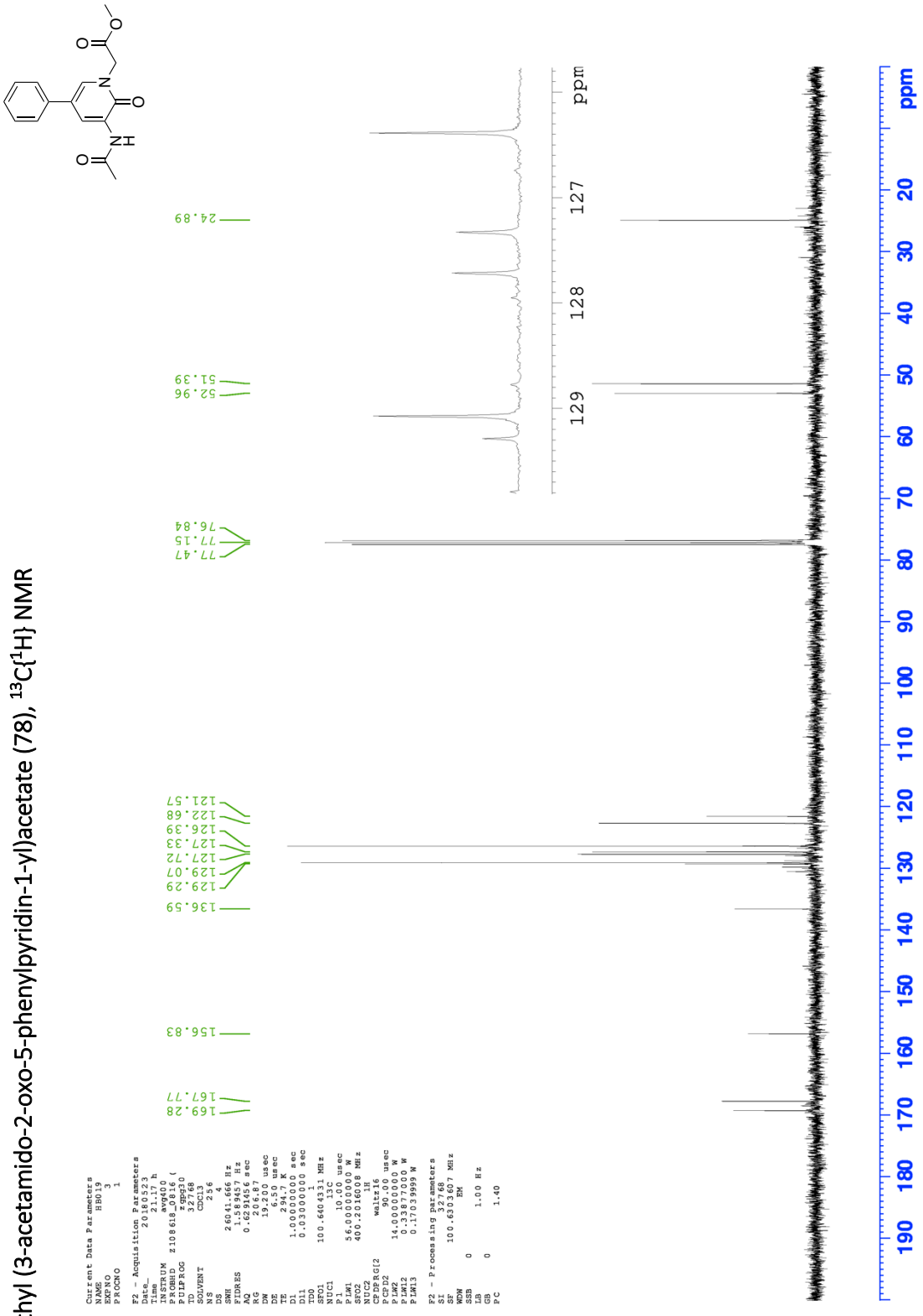
Butyl (3-acetamido-2-oxo-5-phenylpyridin-1-yl)acetate (92), $^{13}C\{^{1}H\}$ NMR



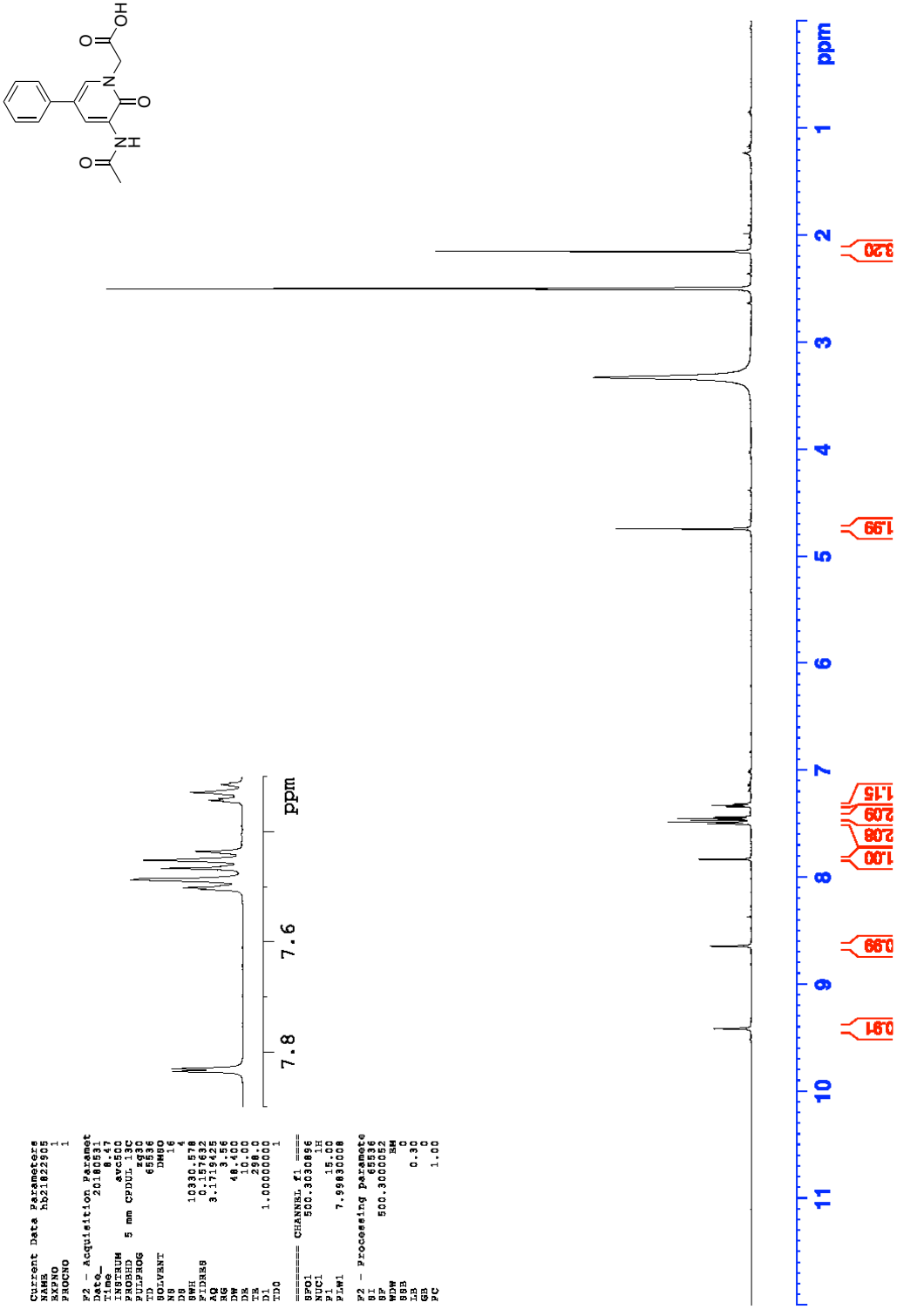
Methyl (3-acetamido-2-oxo-5-phenylpyridin-1-yl)acetate (78), ^{1}H NMR



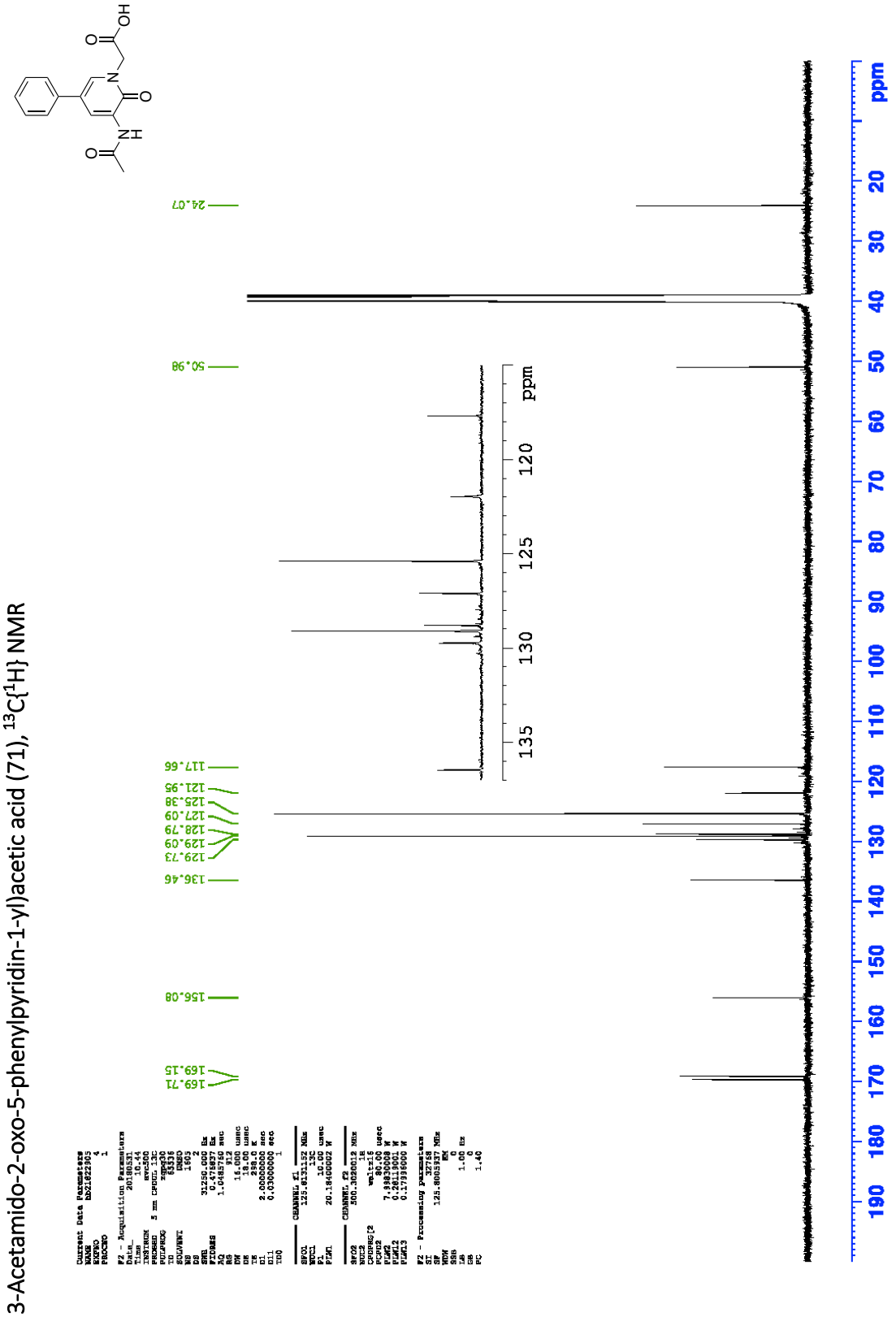
Methyl (3-acetamido-2-oxo-5-phenylpyridin-1-yl)acetate (78), $^{13}C\{^{1}H\}$ NMR



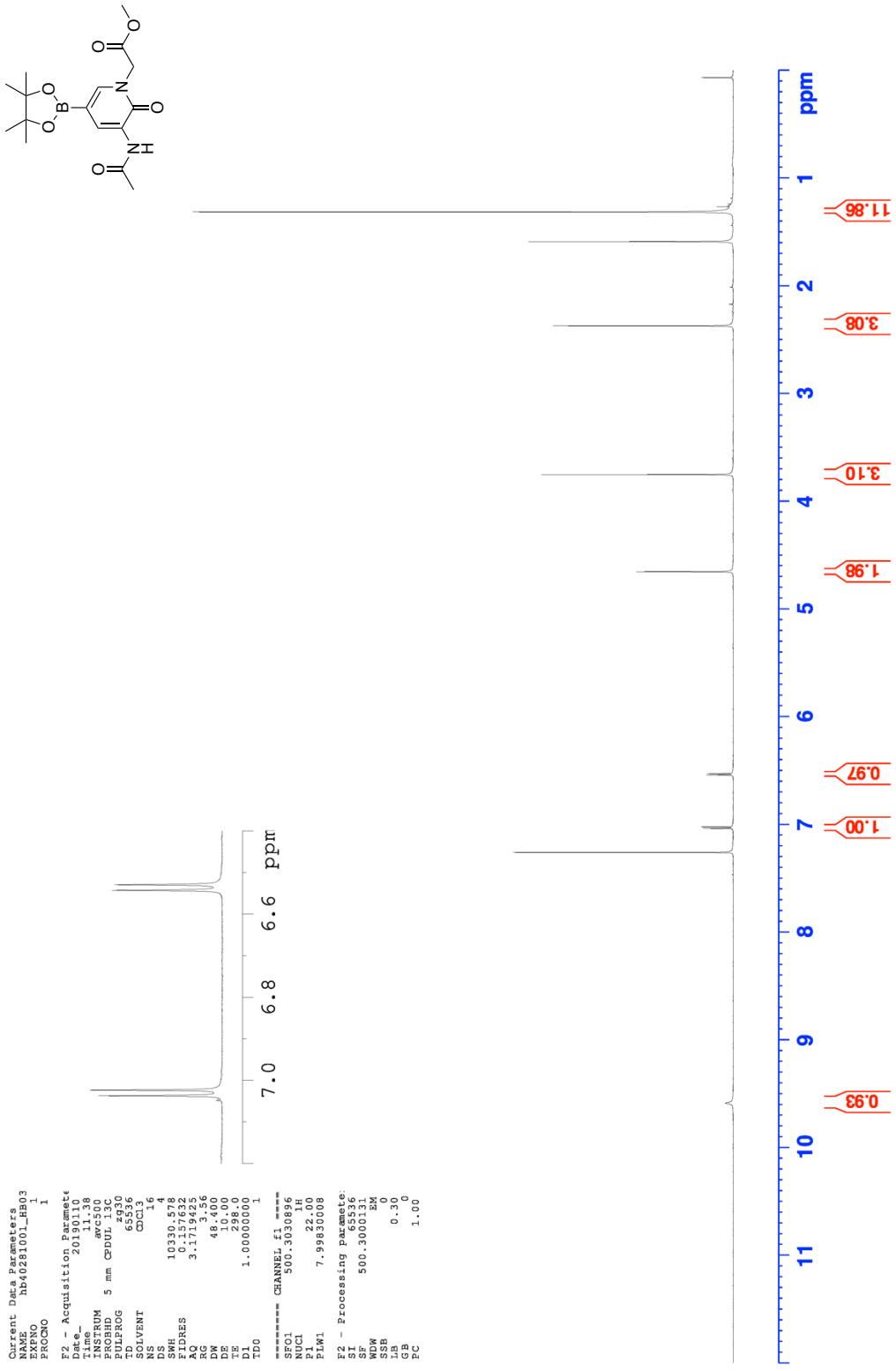
3-Acetamido-2-oxo-5-phenylpyridin-1-yl)acetic acid (71), ^{1}H NMR



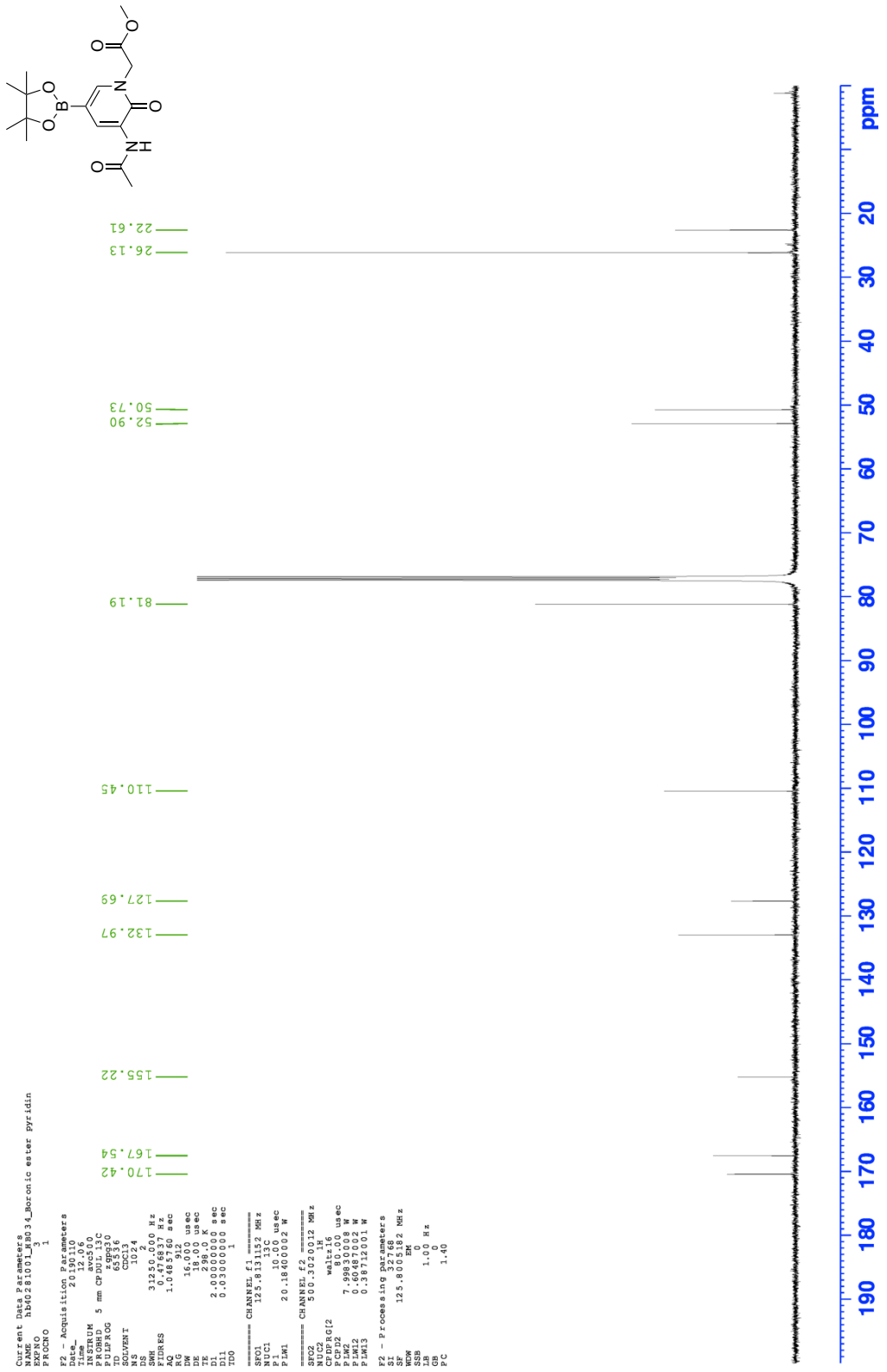
3-Acetamido-2-oxo-5-phenylpyridin-1-yl)acetic acid (71), $^{13}C\{^{1}H\}$ NMR



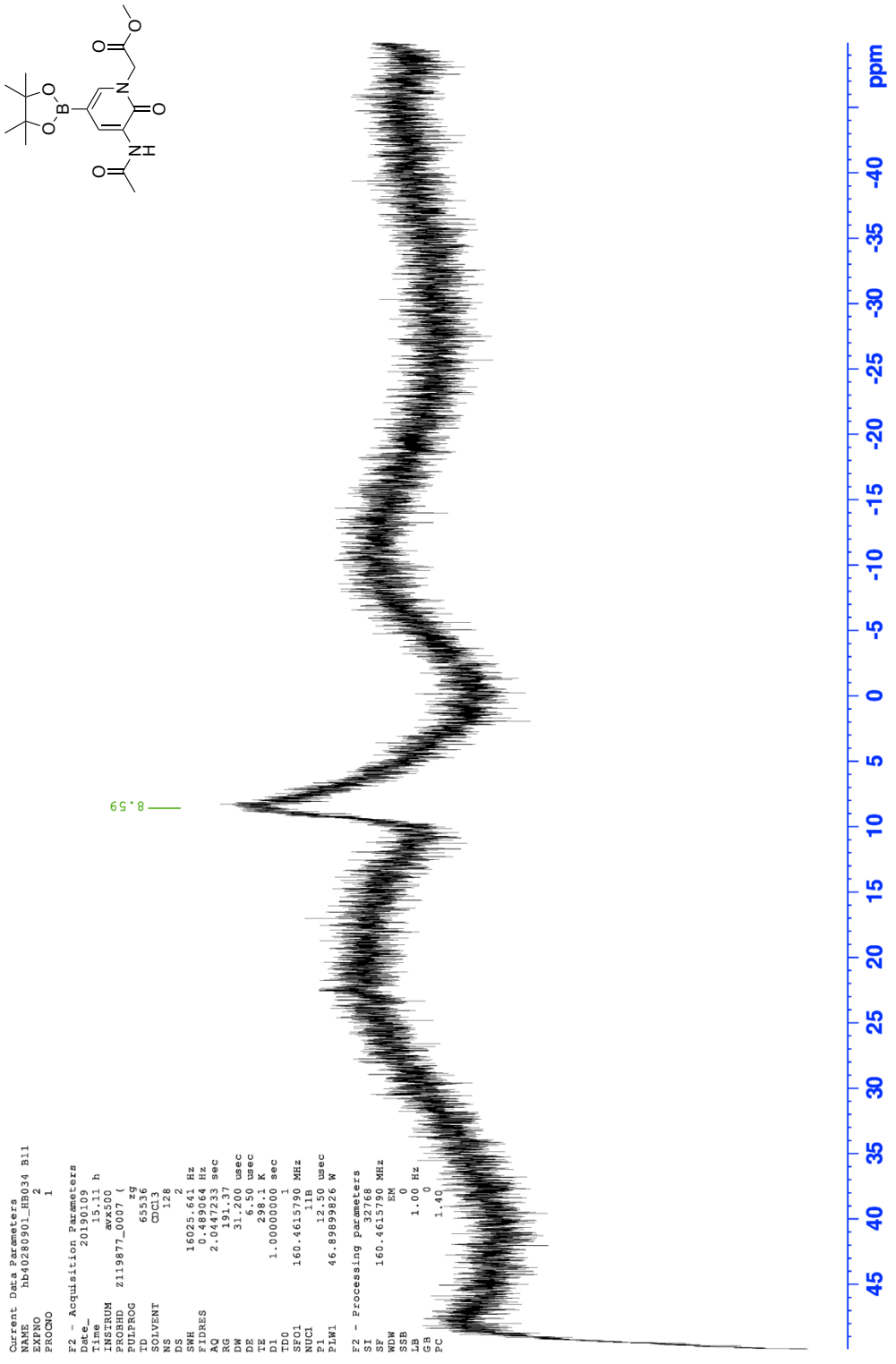
Methyl [3-acetamido-5-(4,4,5,5-tetramethyl-1,3,2-dioxaborolan-2-yl)-2-oxopyridin-1-yl]acetate (93), ^{1}H NMR



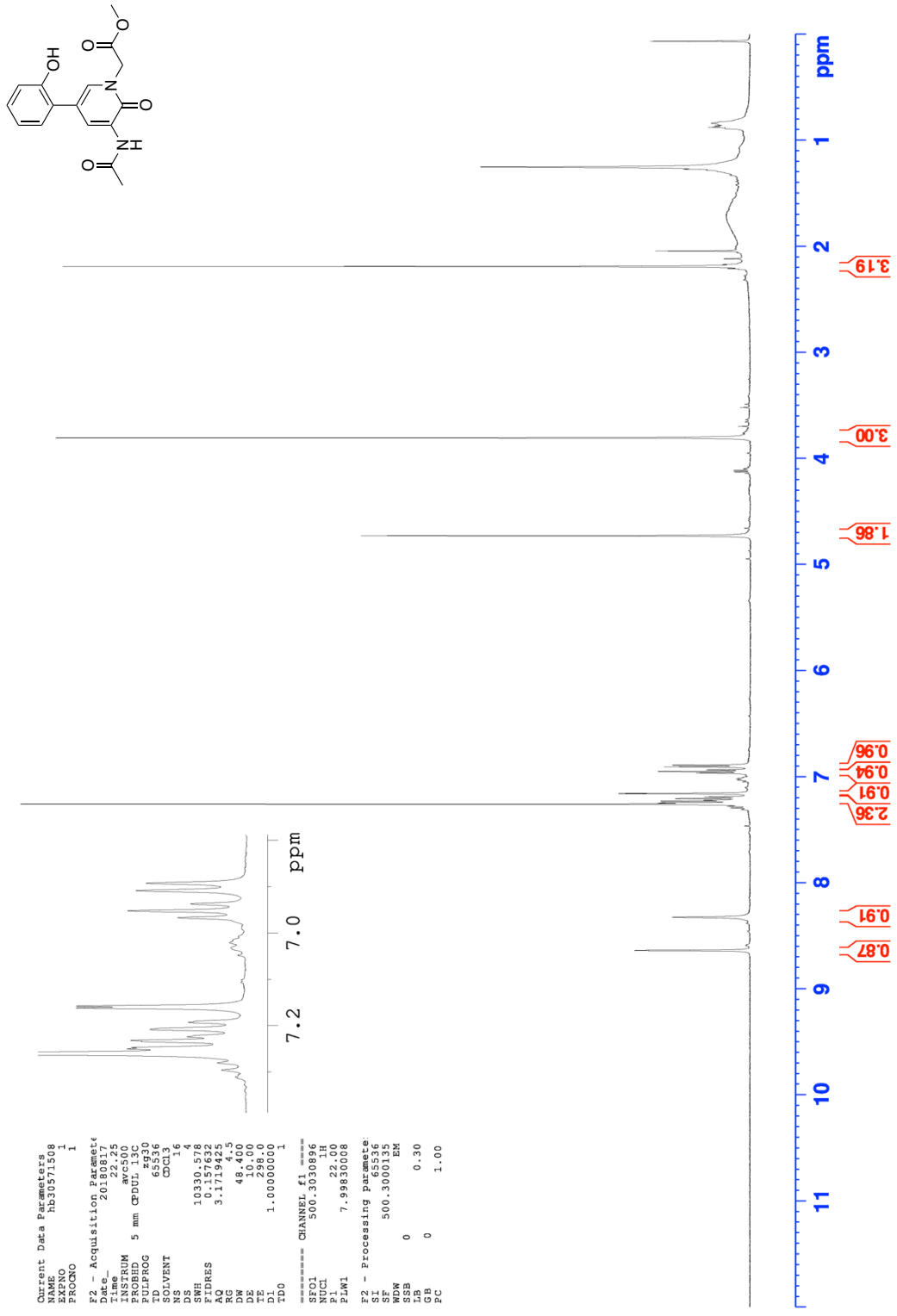
Methyl [3-acetamido-5-(4,4,5,5-tetramethyl-1,3,2-dioxaborolan-2-yl)-2-oxopyridin-1-yl]acetate (93), $^{13}C\{^{1}H\}$ NMR



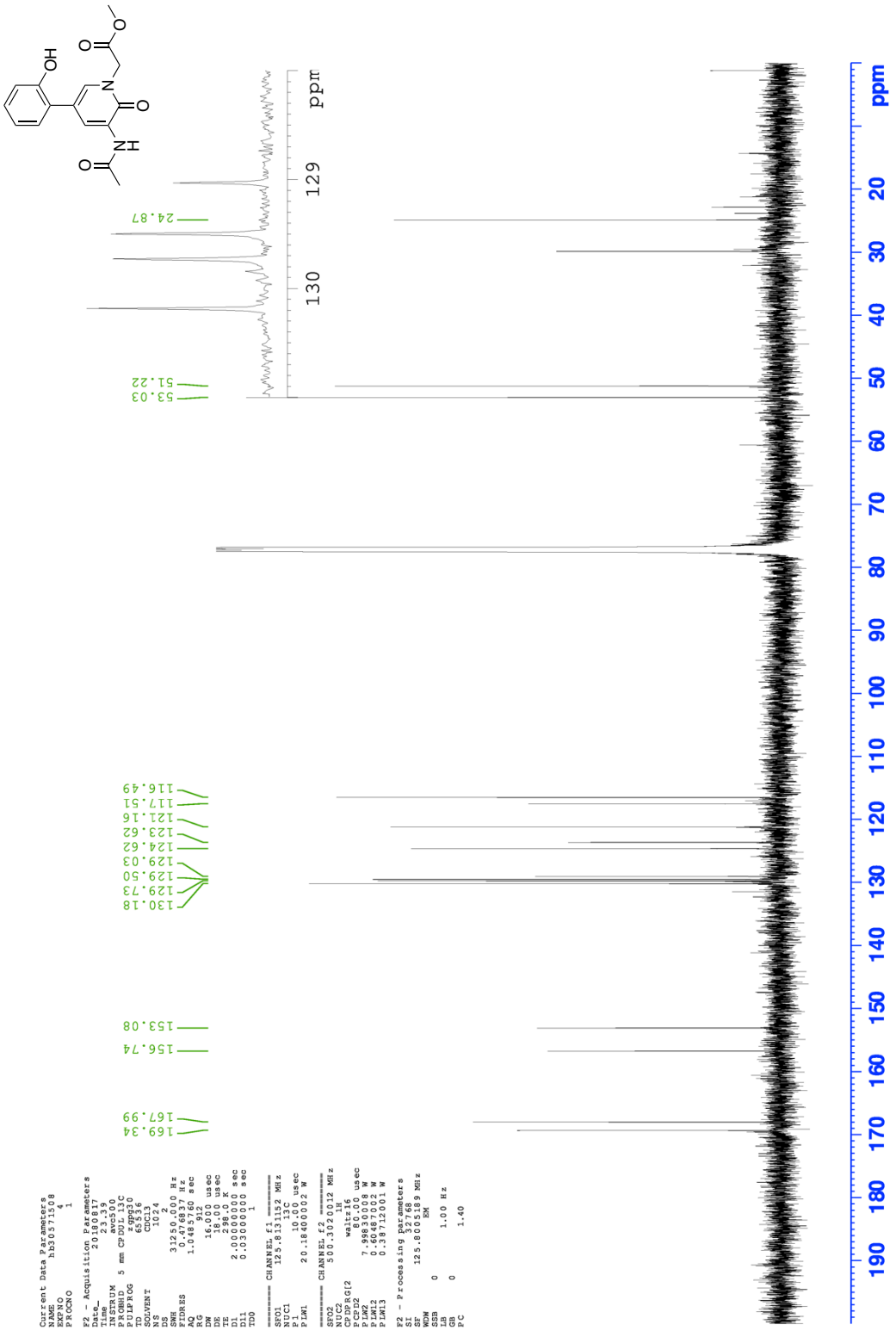
Methyl [3-acetamido-5-(4,4,5,5-tetramethyl-1,3,2-dioxaborolan-2-yl)-2-oxopyridin-1-yl]acetate (93), ^{11}B NMR



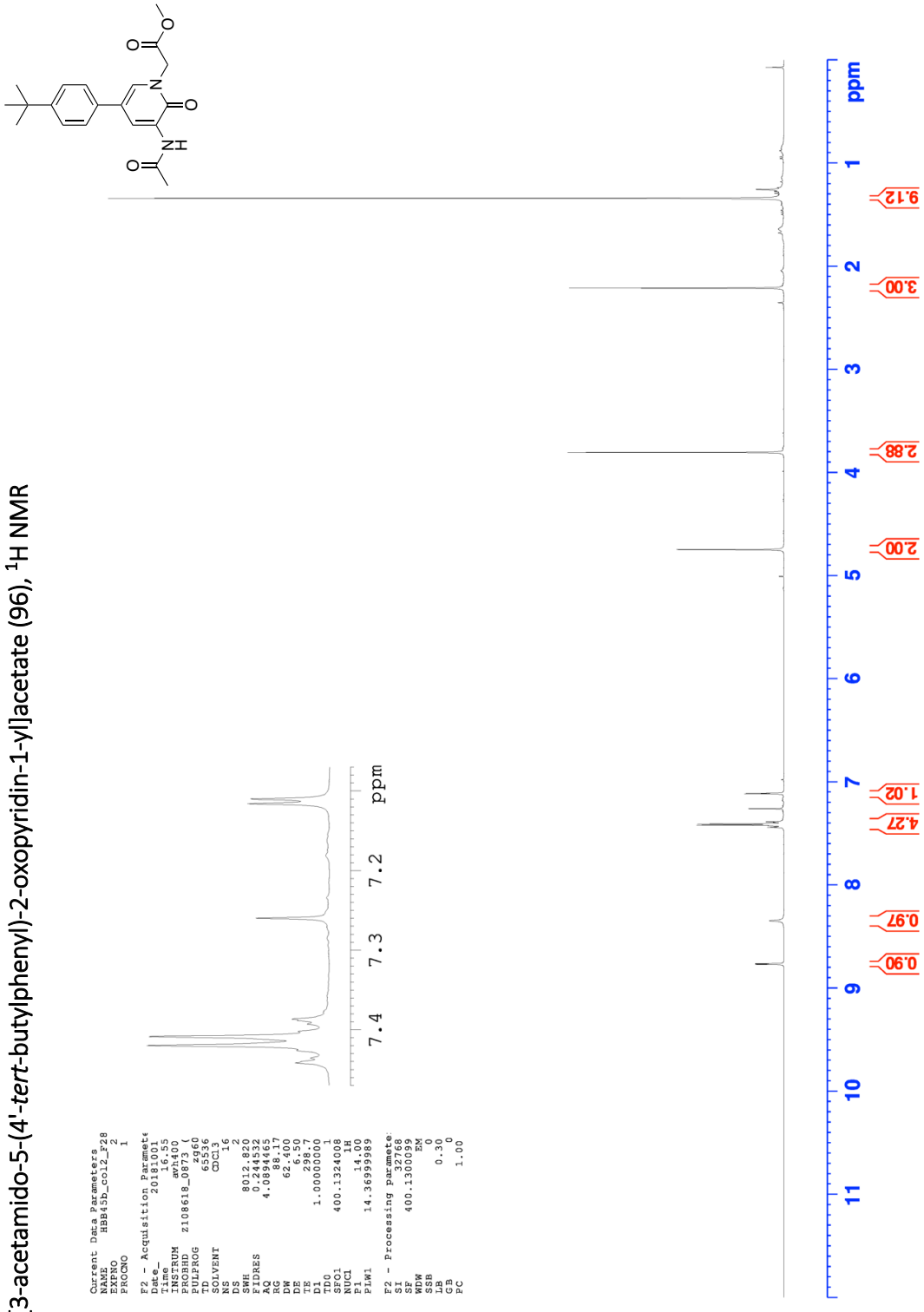
Methyl (3-acetamido-2-oxo-5-(2'-hydroxyphenyl)-pyridin-1-yl)acetate (95), ^{1}H NMR



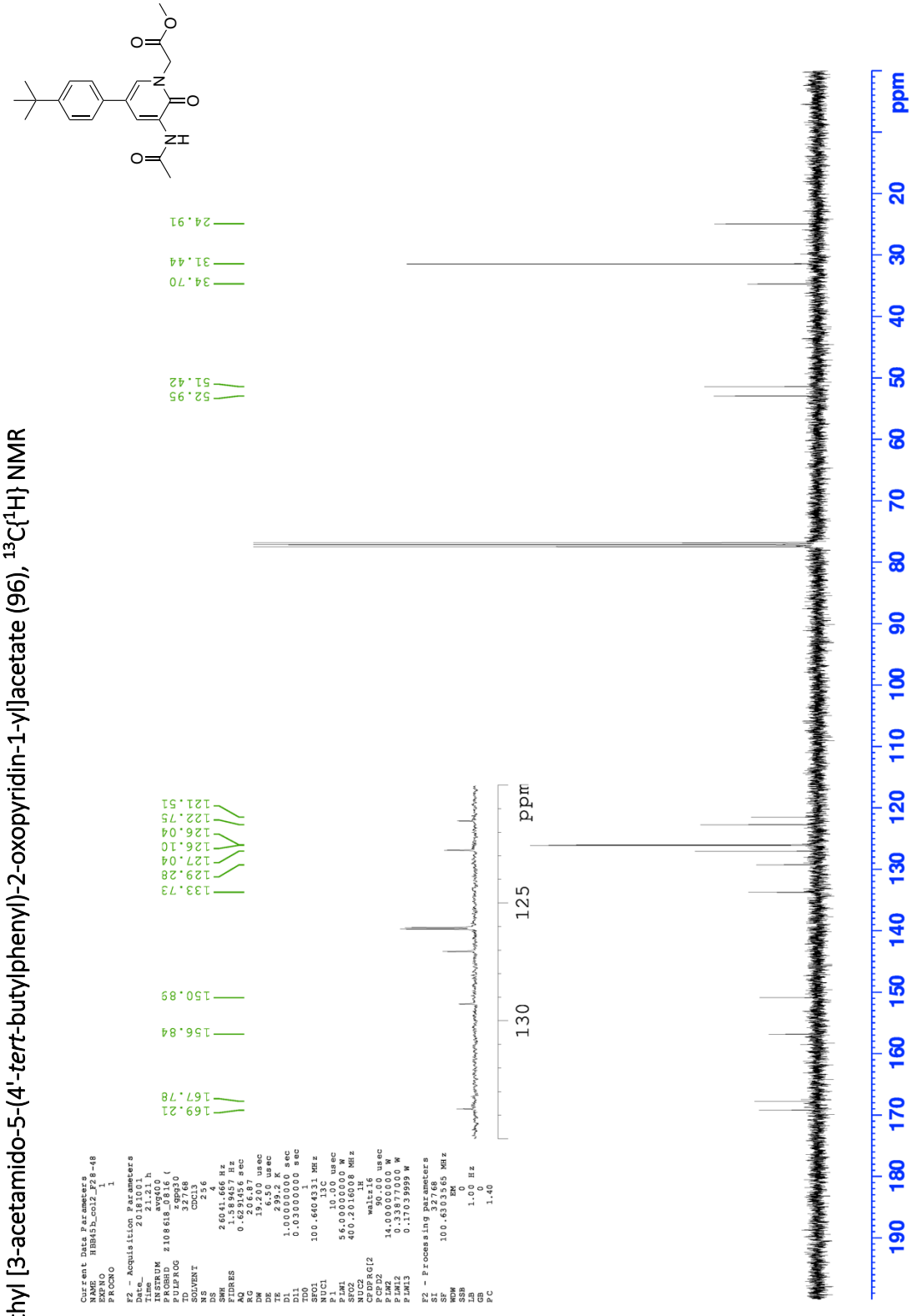
Methyl (3-acetamido-2-oxo-5-(2'-hydroxyphenyl)-pyridin-1-yl)acetate (95), $^{13}C\{^{1}H\}$ NMR



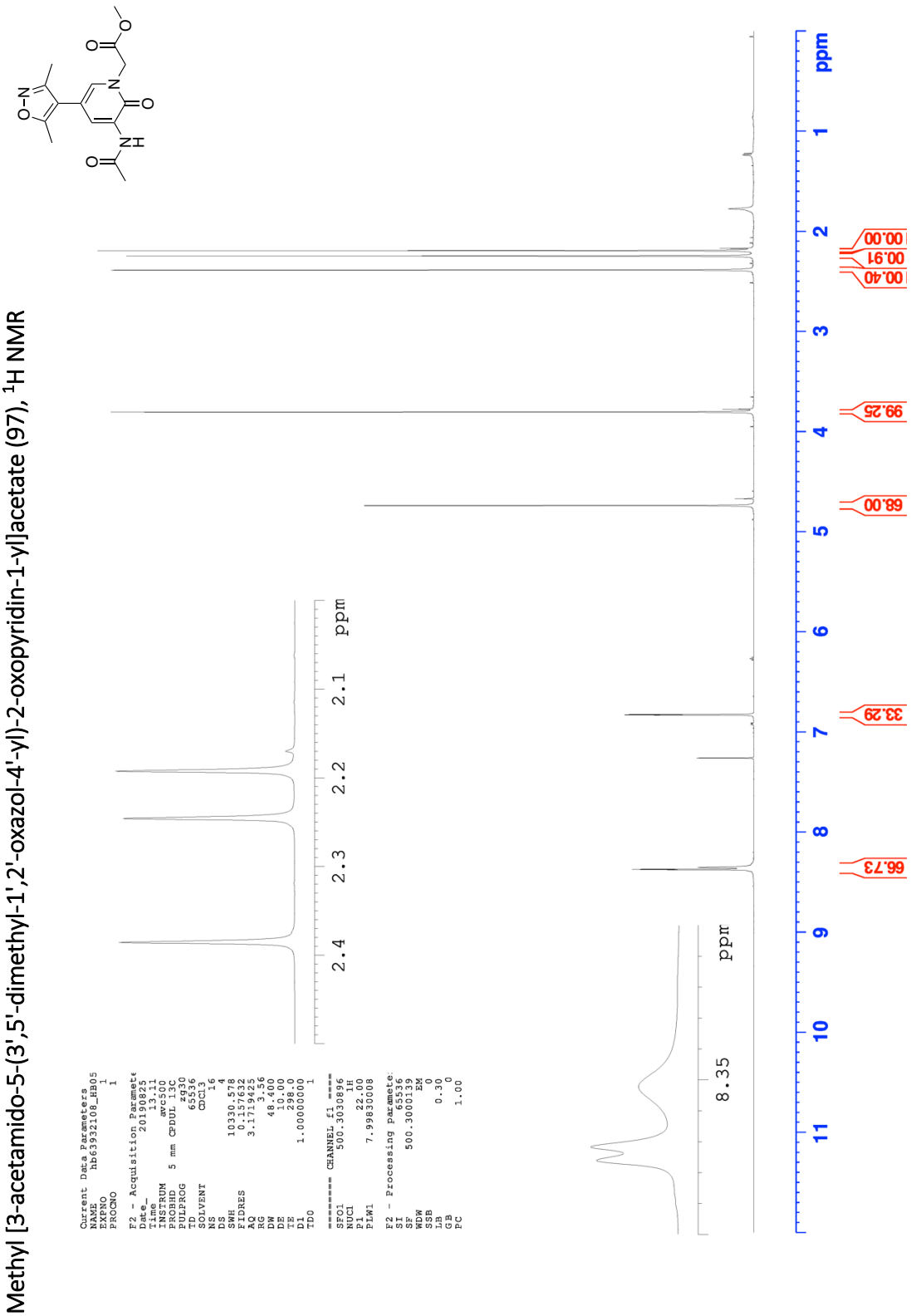
Methyl [3-acetamido-5-(4'-*tert*-butylphenyl)-2-oxopyridin-1-yl]acetate (96), ^{1}H NMR



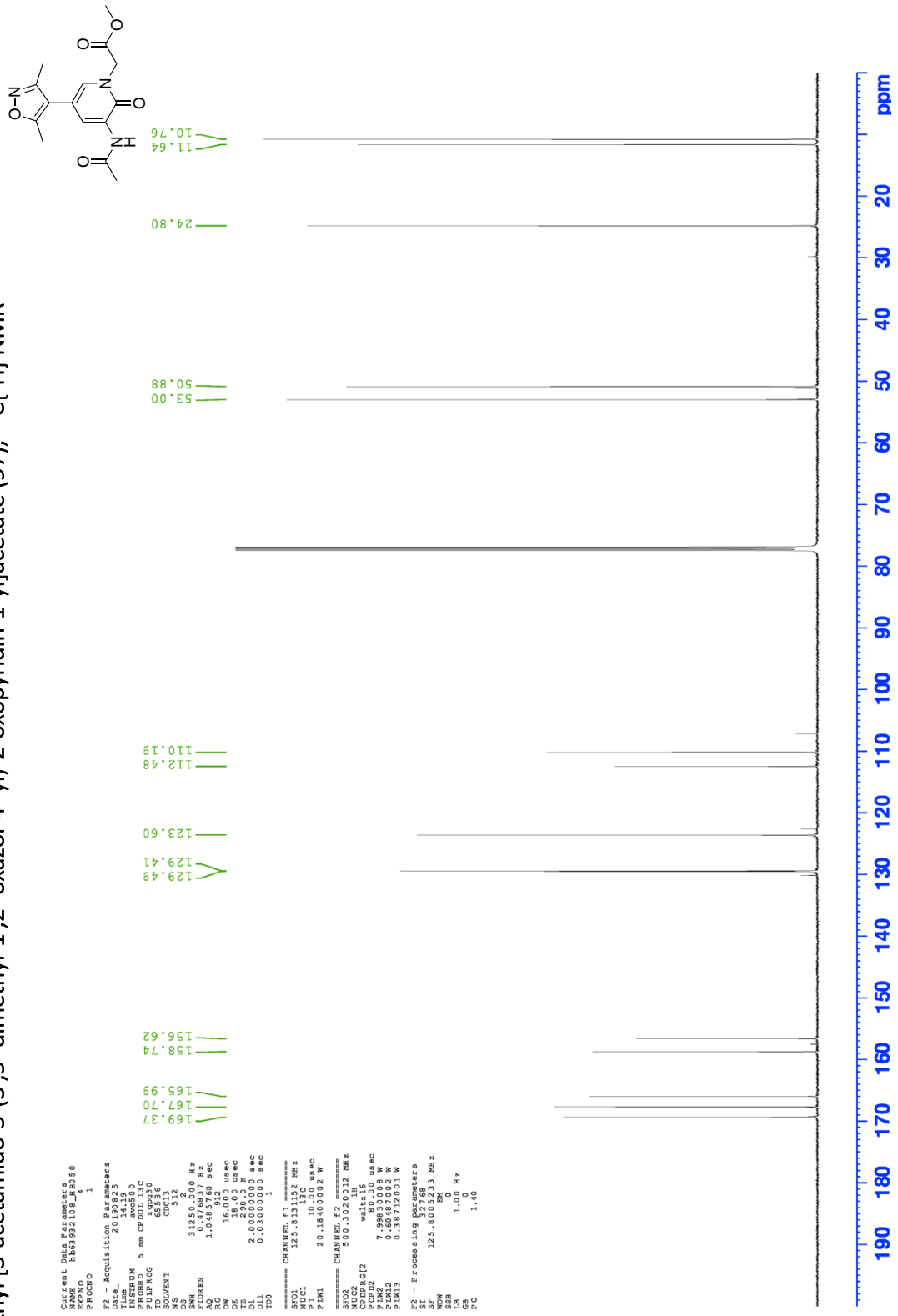
Methyl [3-acetamido-5-(4'-*tert*-butylphenyl)-2-oxopyridin-1-yl]acetate (96), $^{13}C\{^{1}H\}$ NMR



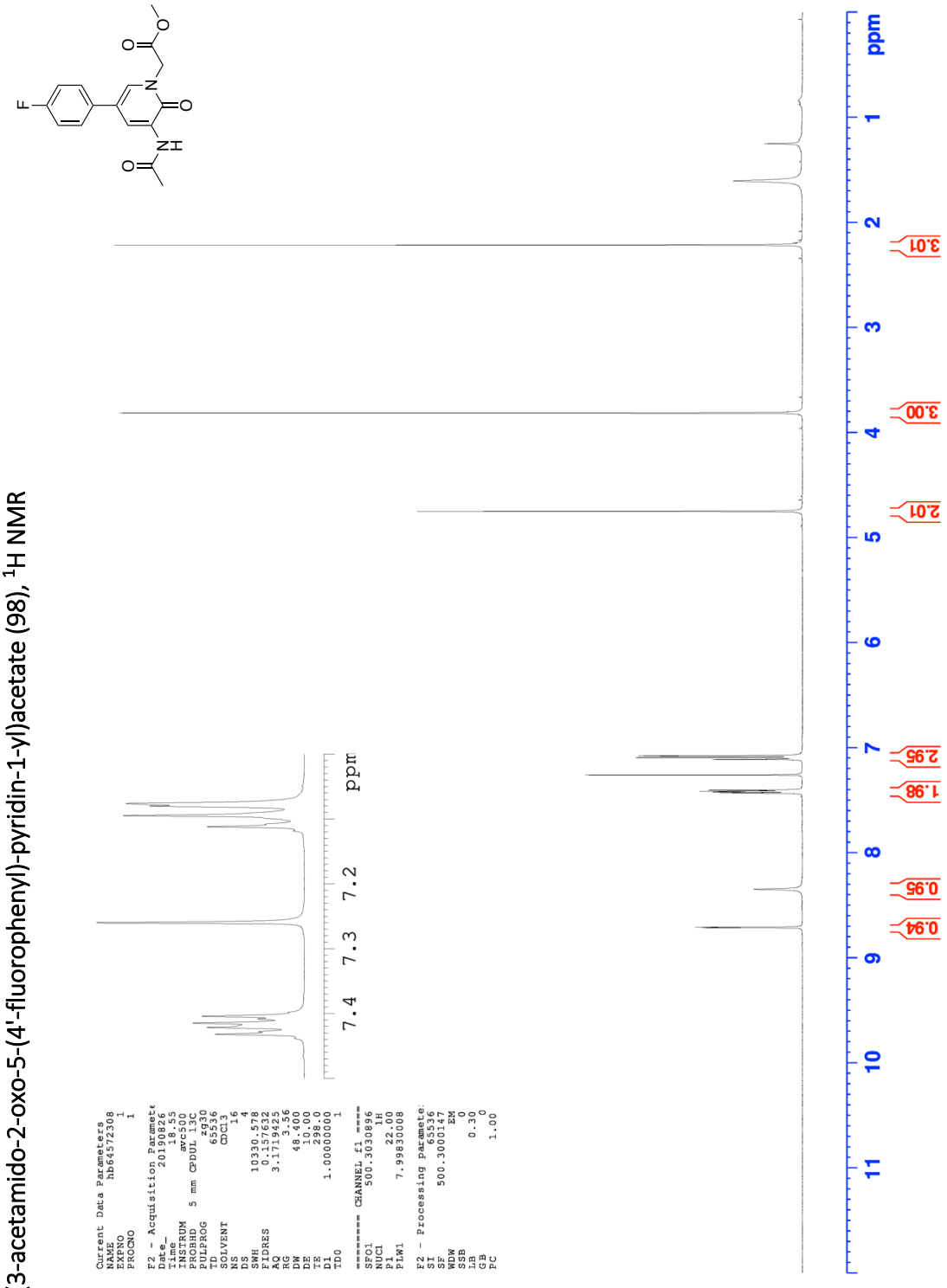
Methyl [3-acetamido-5-(3',5'-dimethyl-1',2'-oxazol-4'-yl)-2-oxopyridin-1-yl]acetate (97), ^{1}H NMR



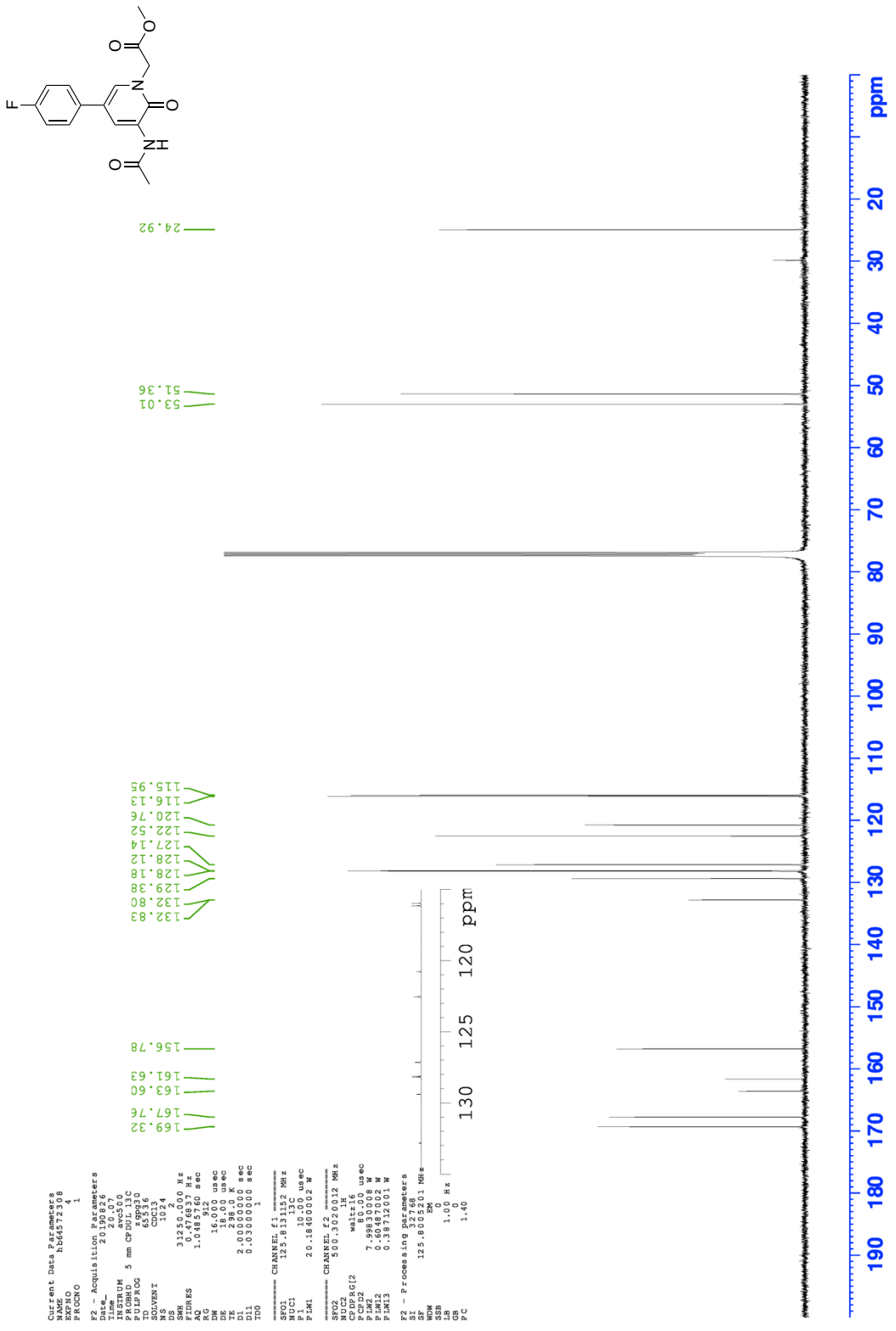
Methyl [3-acetamido-5-(3',5'-dimethyl-1',2'-oxazol-4'-yl)-2-oxopyridin-1-yl]acetate (97), $^{13}C\{^{1}H\}$ NMR



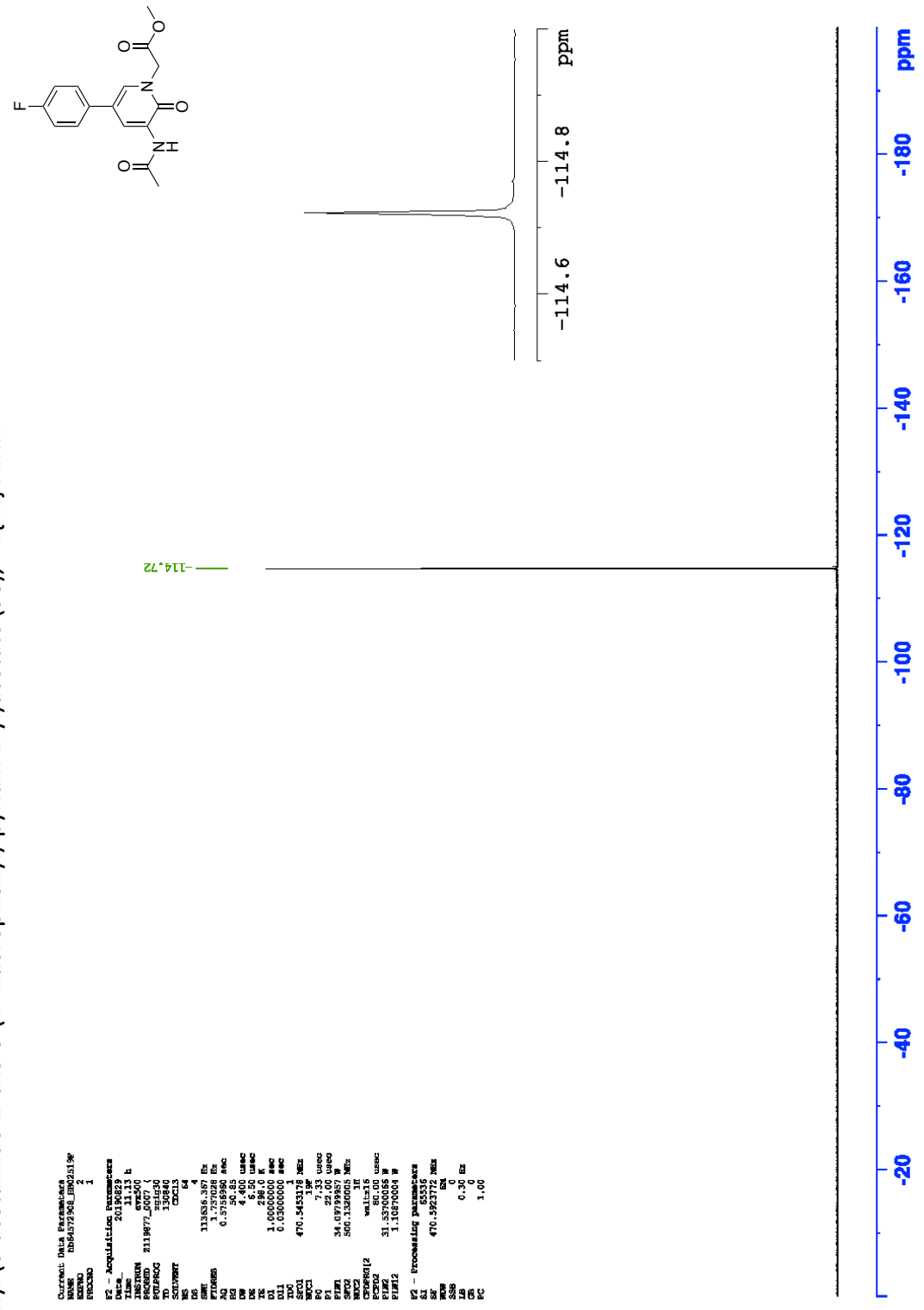
Methyl (3-acetamido-2-oxo-5-(4'-fluorophenyl)-pyridin-1-yl)acetate (98), ^{1}H NMR



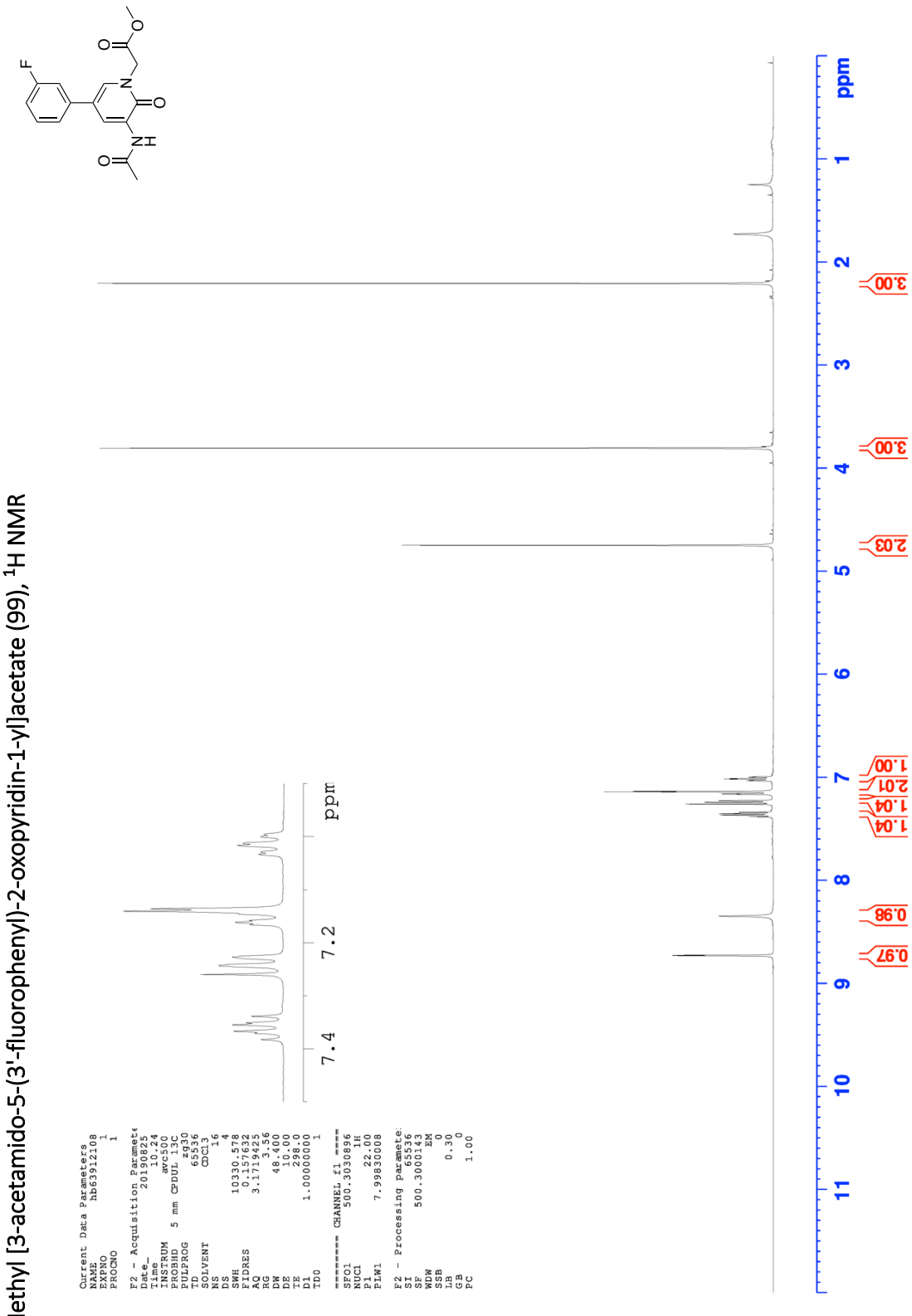
Methyl (3-acetamido-2-oxo-5-(4'-fluorophenyl)-pyridin-1-yl)acetate (98), $^{13}C\{^{1}H\}$ NMR



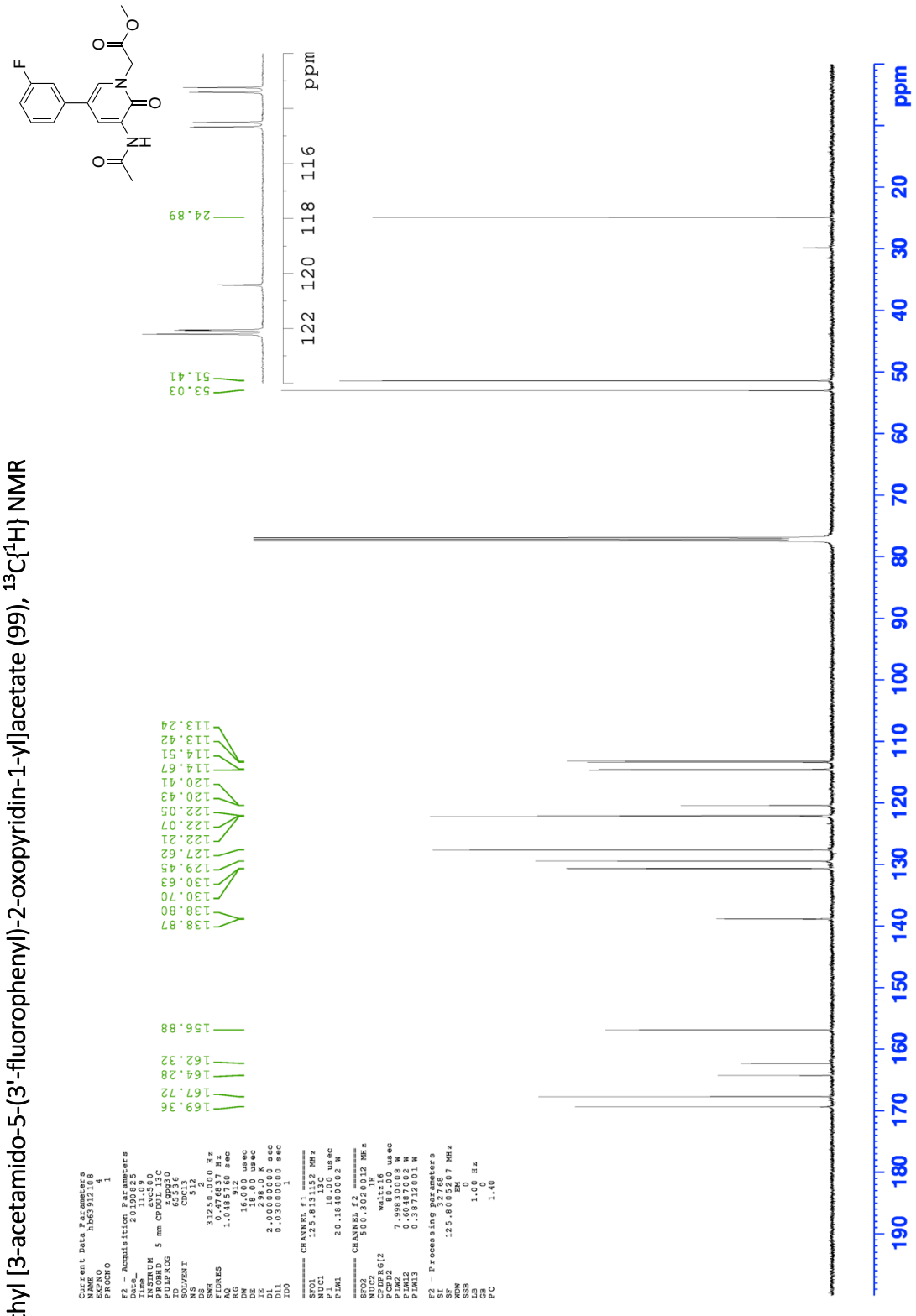
Methyl (3-acetamido-2-oxo-5-(4'-fluorophenyl)-pyridin-1-yl)acetate (98), $^{19}F\{^{1}H\}$ NMR



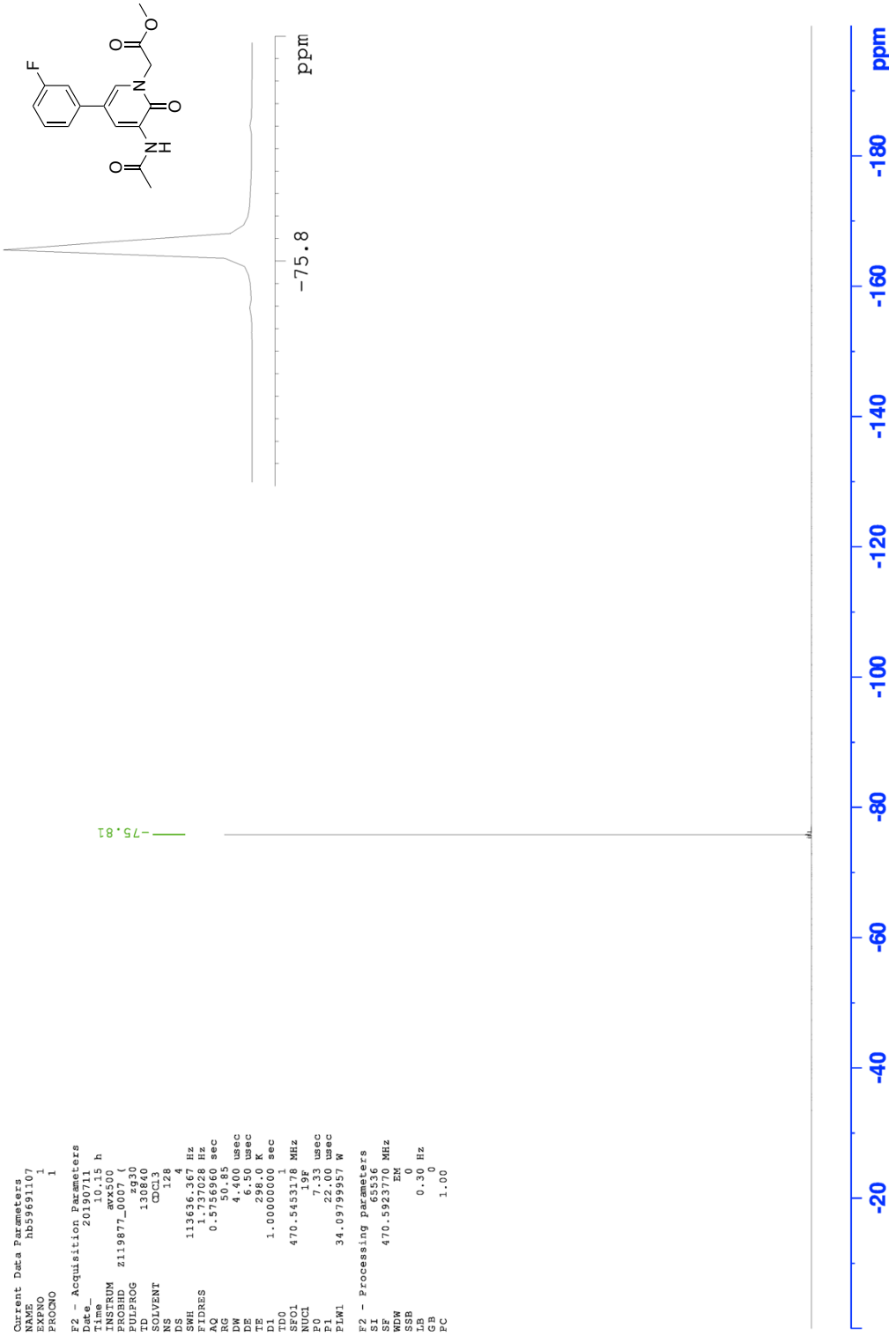
Methyl [3-acetamido-5-(3'-fluorophenyl)-2-oxopyridin-1-yl]acetate (99), ^{1}H NMR



Methyl [3-acetamido-5-(3'-fluorophenyl)-2-oxopyridin-1-yl]acetate (99), $^{13}C\{^{1}H\}$ NMR



Methyl [3-acetamido-5-(3'-fluorophenyl)-2-oxopyridin-1-yl]acetate (99), $^{19}F\{^{1}H\}$ NMR

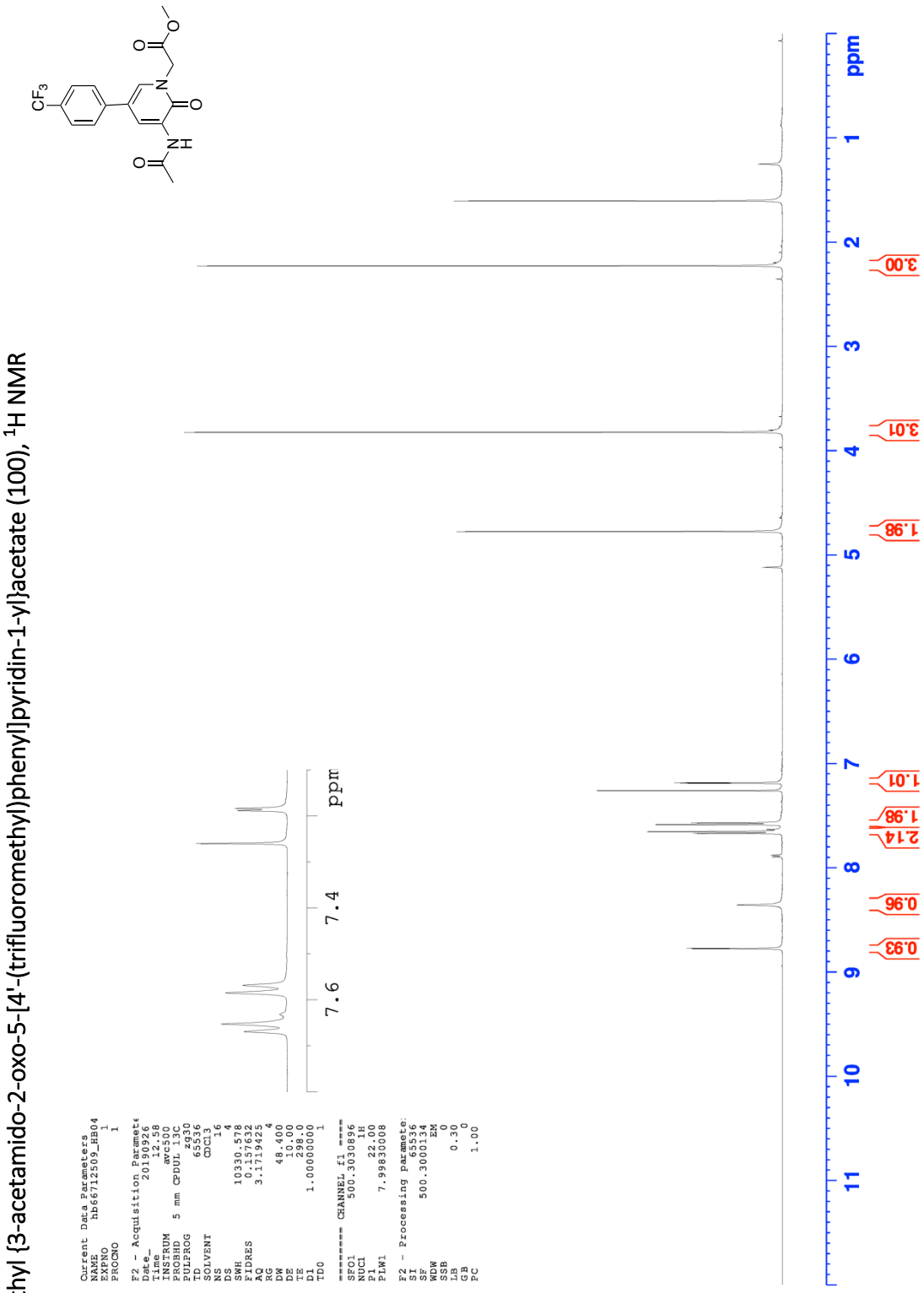



```
Current Data Parameters
NAME                  hb59691107
EXPNO                          1
PROCNO                         1

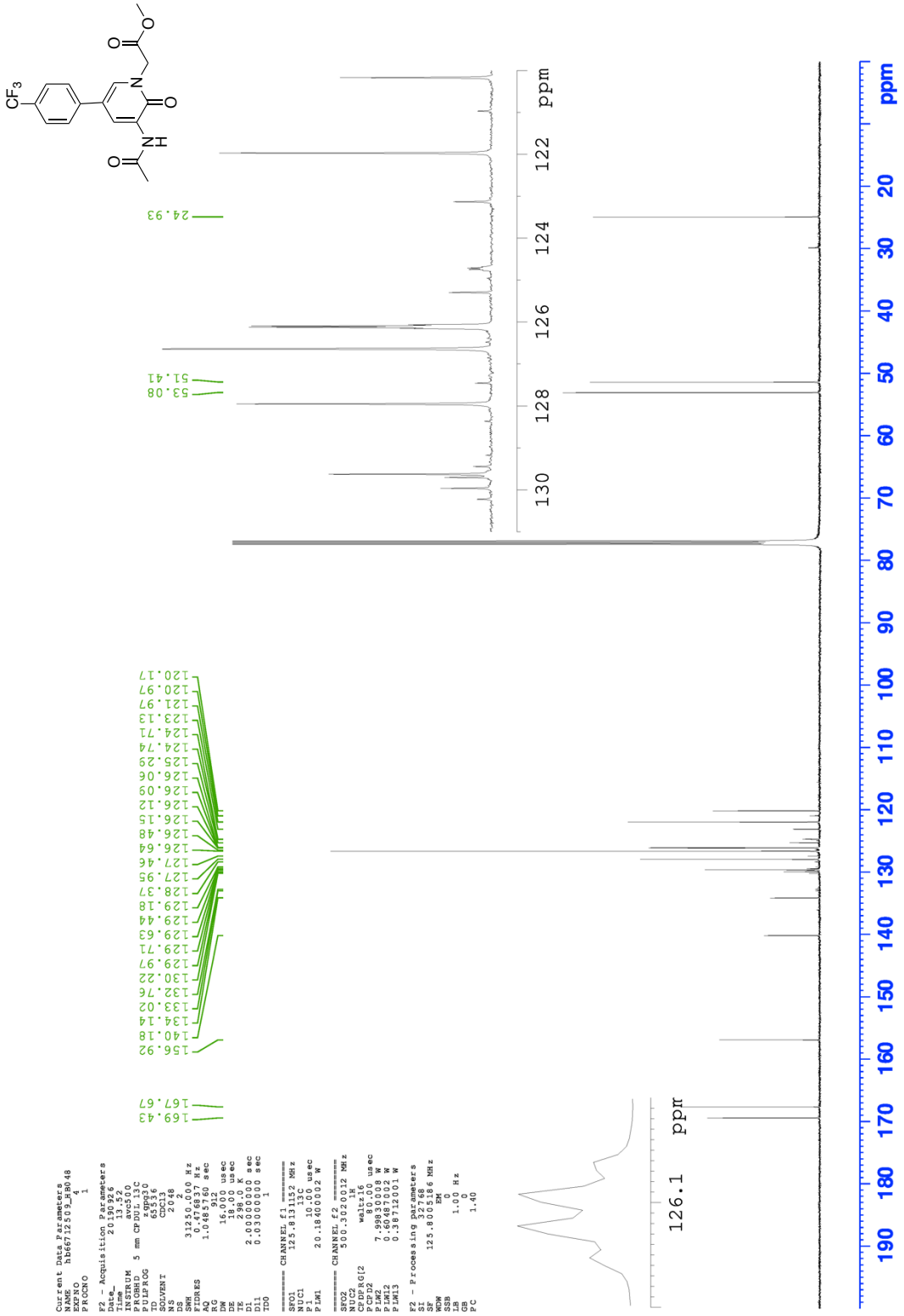
F2 - Acquisition Parameters
Date_                   20190711
Time                      10.15 h
INSTRUM                  av500
PROBHD                 z119877_0007 (
PULPROG                zg30
TD                        130840
SOLVENT                   CDCl3
NS                              128
DS                                4
SWH                     113636.367 Hz
FIDRES                    1.737028 Hz
AQ                        0.5756960 sec
RG                             50.85
DW                            4.400 usec
DE                            6.50 usec
TE                           298.0 K
D1                        1.00000000 sec
TD0                               1
SFO1                    470.5453178 MHz
NUC1                          19F
P0                            7.33 usec
P1                           22.00 usec
PLW1                   34.09799957 W

F2 - Processing parameters
SI                            65536
SF                      470.5923770 MHz
WDW                             EM
SSB                              0
LB                            0.30 Hz
GB                               0
PC                            1.00
```

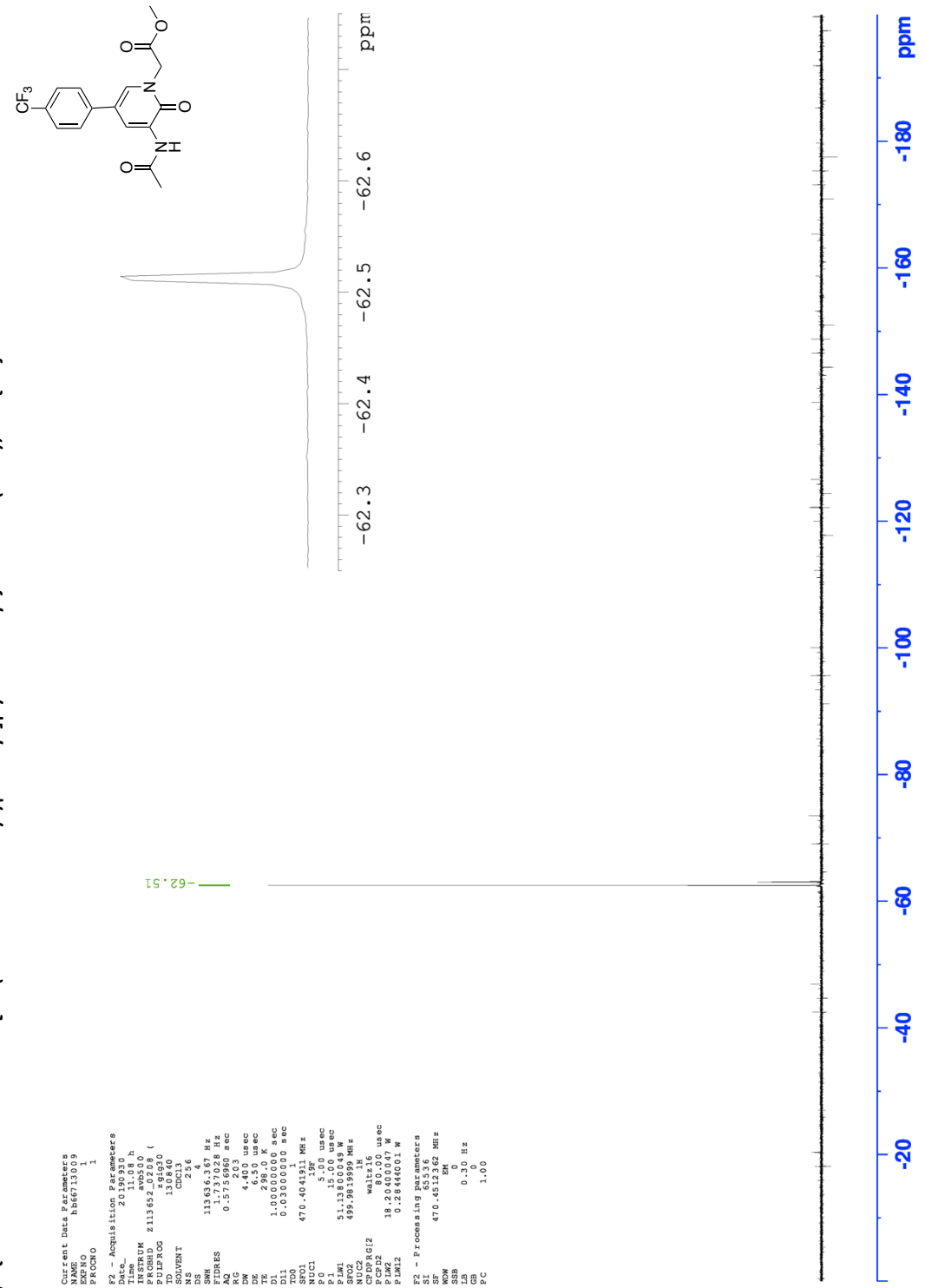
Methyl {3-acetamido-2-oxo-5-[4'-(trifluoromethyl)phenyl]pyridin-1-yl}acetate (100), ^{1}H NMR



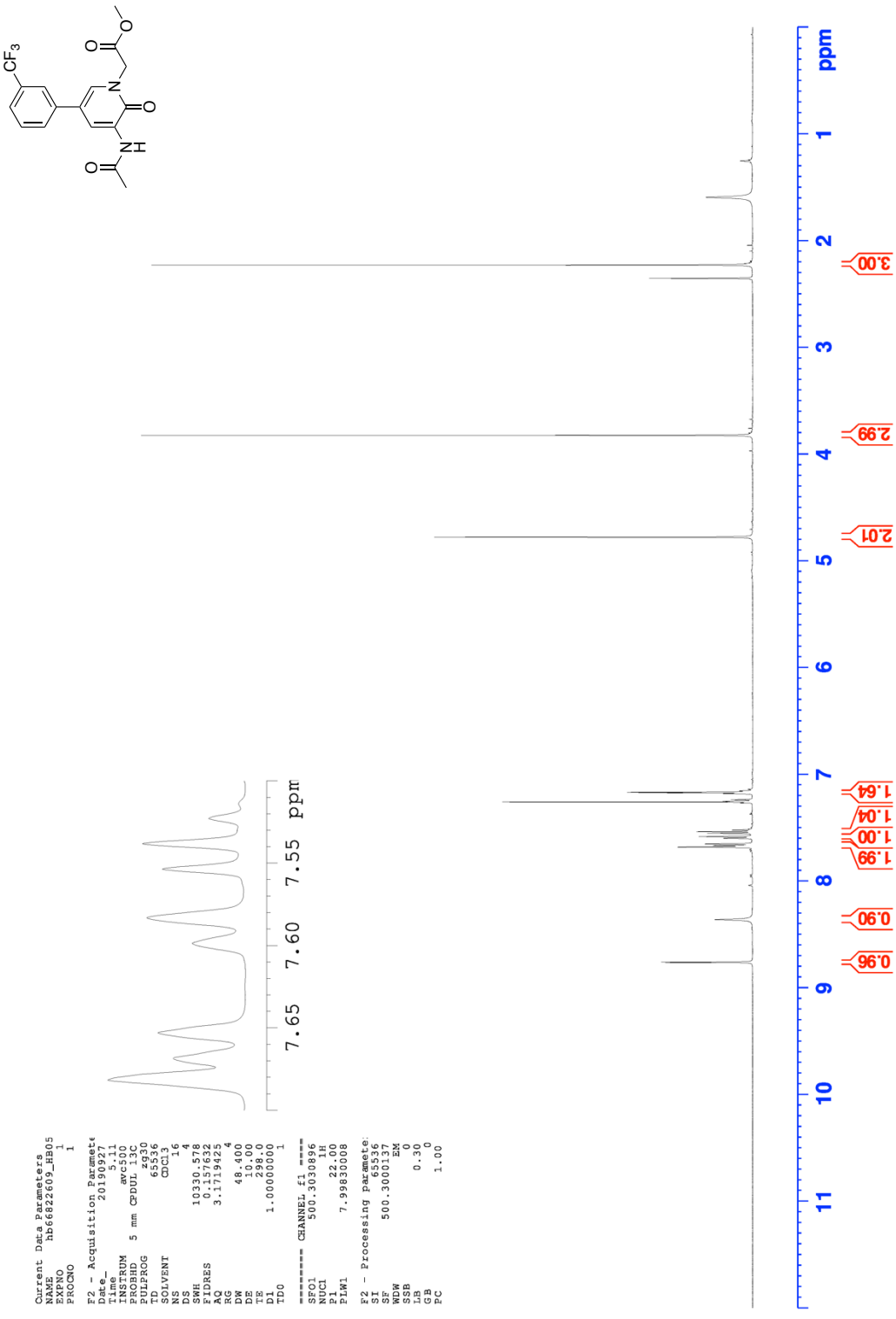
Methyl {3-acetamido-2-oxo-5-[4'-(trifluoromethyl)phenyl]pyridin-1-yl}acetate (100), $^{13}C\{^{1}H\}$ NMR



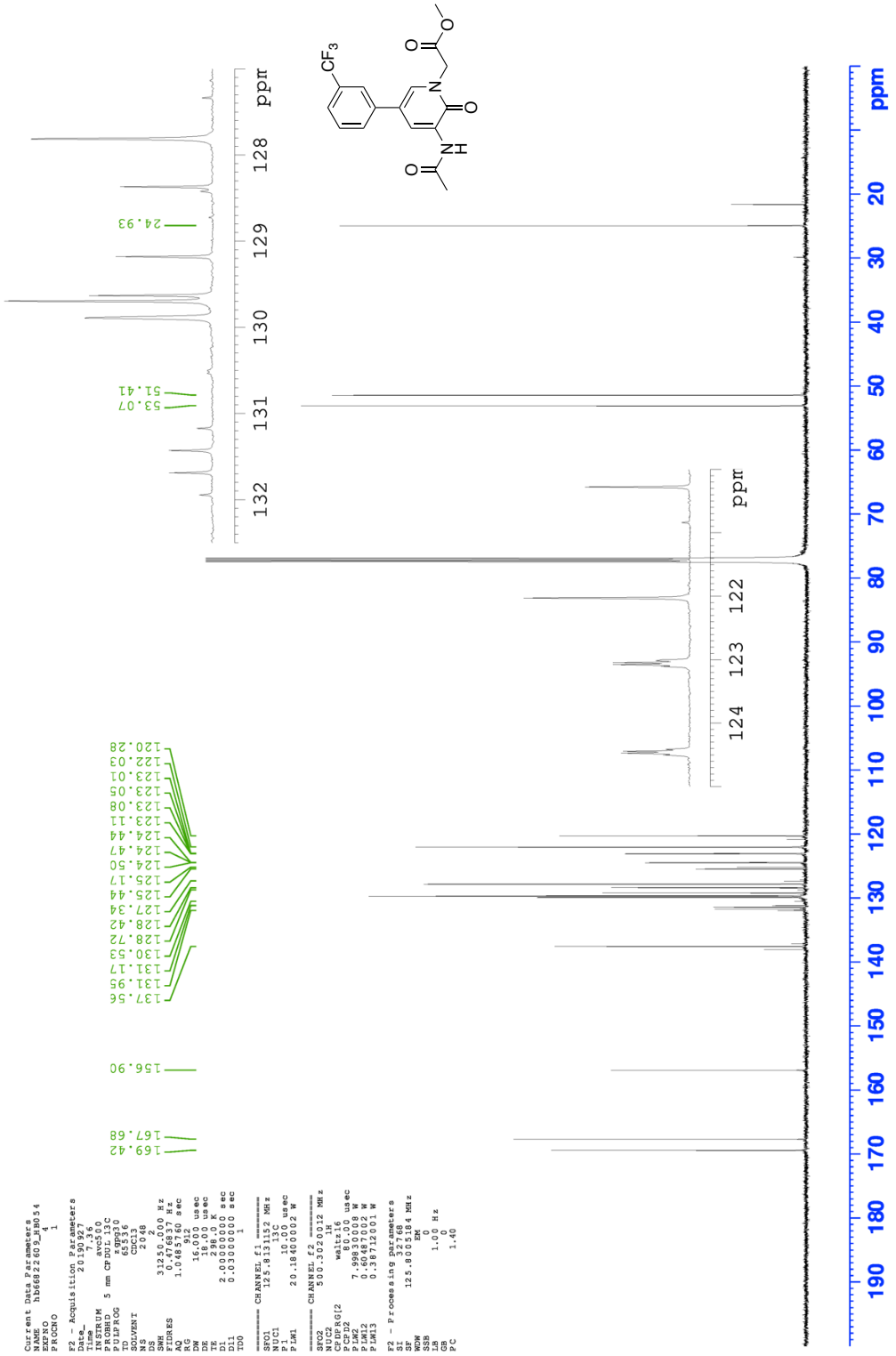
Methyl {3-acetamido-2-oxo-5-[4'-(trifluoromethyl)phenyl]pyridin-1-yl}acetate (100), $^{19}F\{^{1}H\}$ NMR



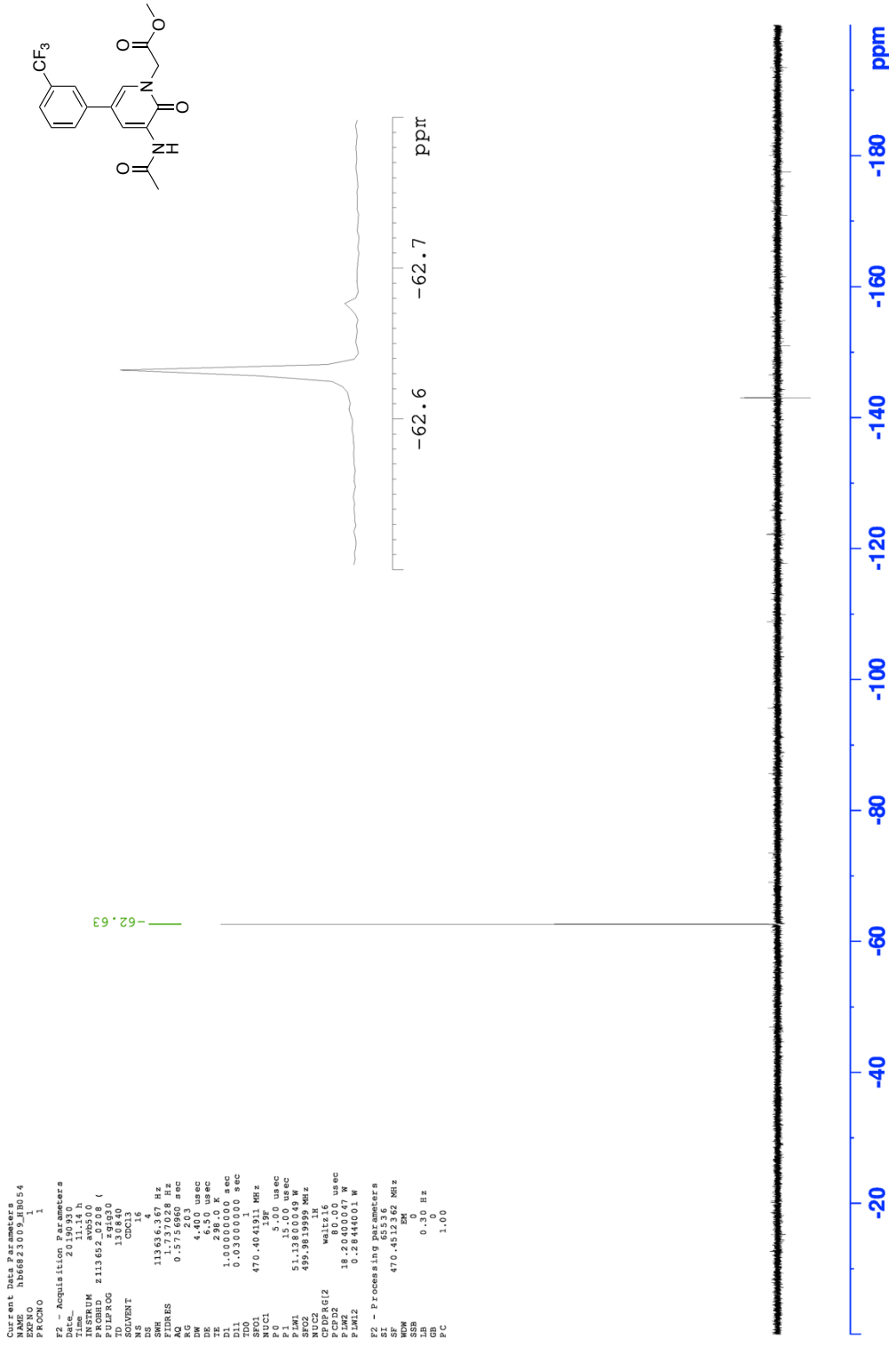
Methyl {3-acetamido-2-oxo-5-[3'-(trifluoromethyl)phenyl]pyridin-1-yl}acetate (101), ^{1}H NMR



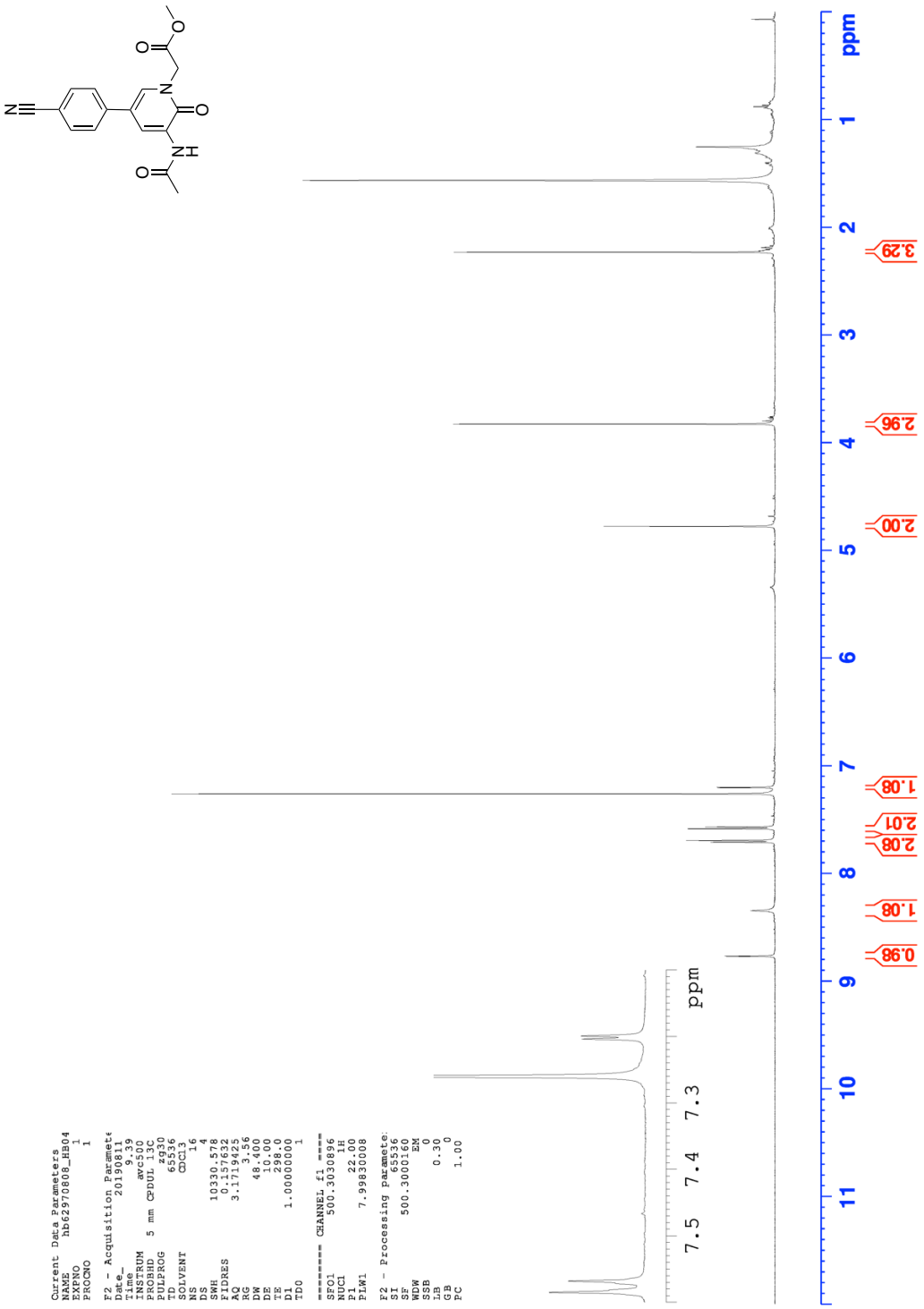
Methyl {3-acetamido-2-oxo-5-[3'-(trifluoromethyl)phenyl]pyridin-1-yl}acetate (101), $^{13}C\{^{1}H\}$ NMR



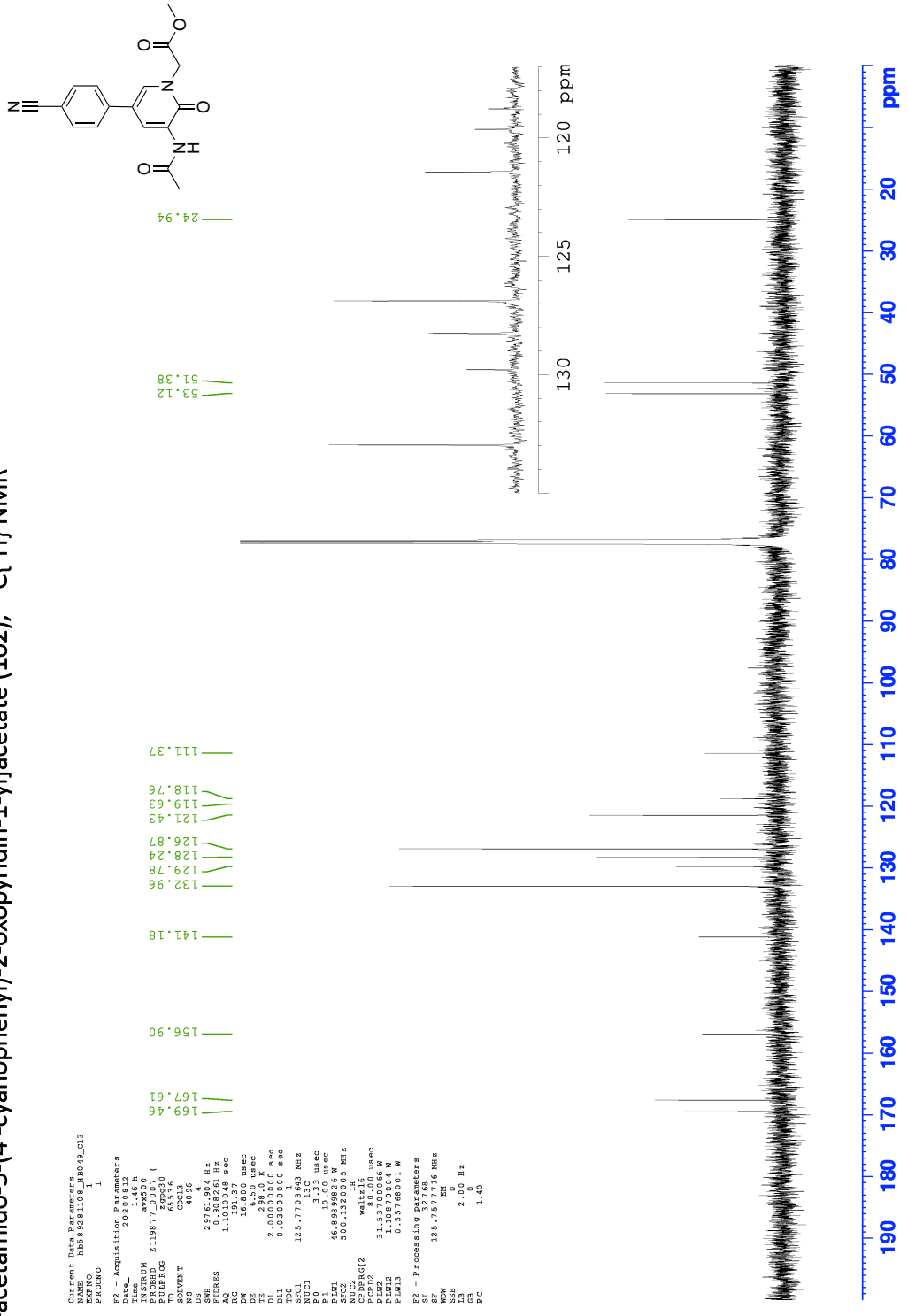
Methyl {3-acetamido-2-oxo-5-[3'-(trifluoromethyl)phenyl]pyridin-1-yl}acetate (101), $^{19}F\{^{1}H\}$ NMR



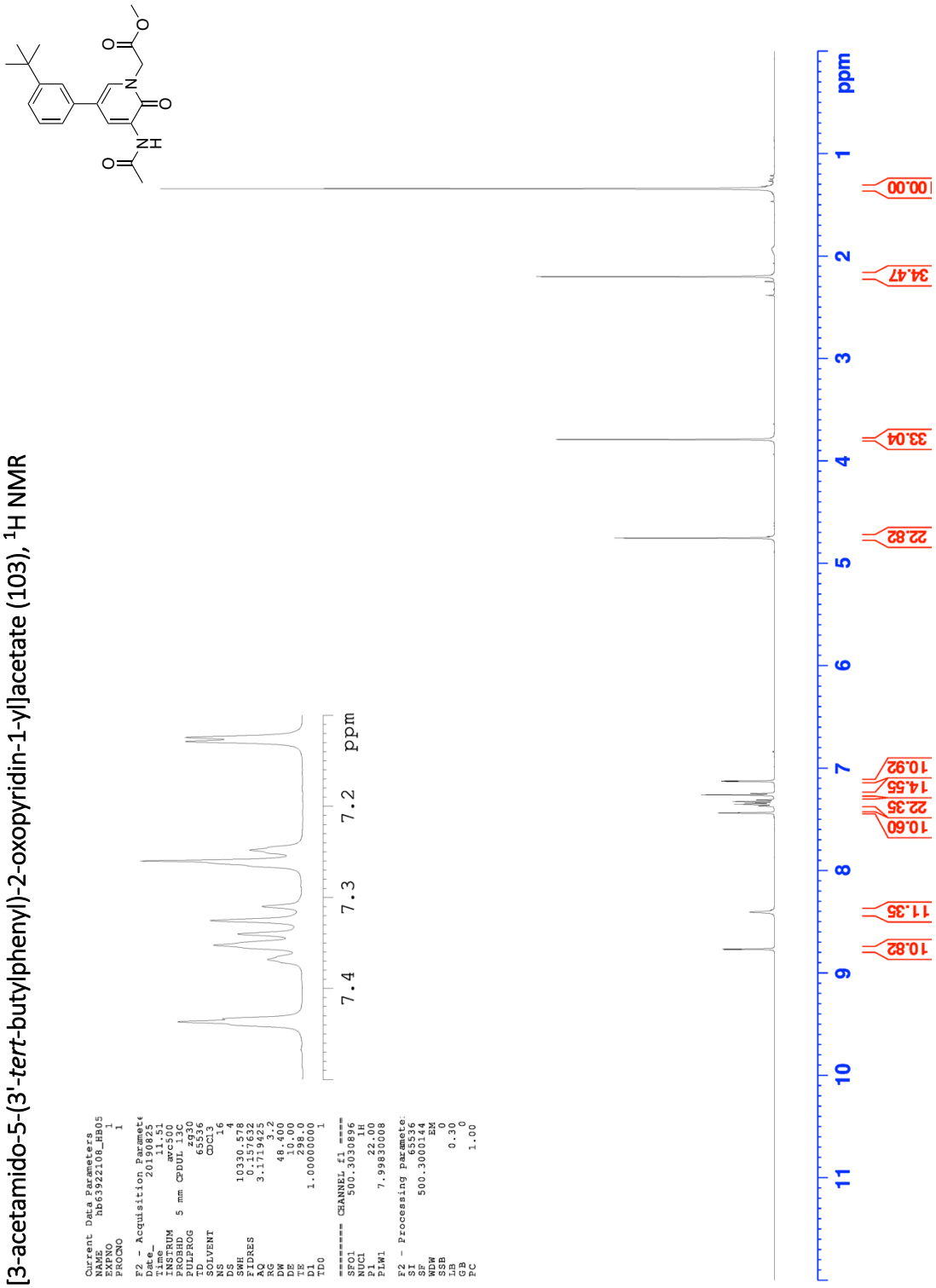
Methyl [3-acetamido-5-(4'-cyanophenyl)-2-oxopyridin-1-yl]acetate (102), ^{1}H NMR



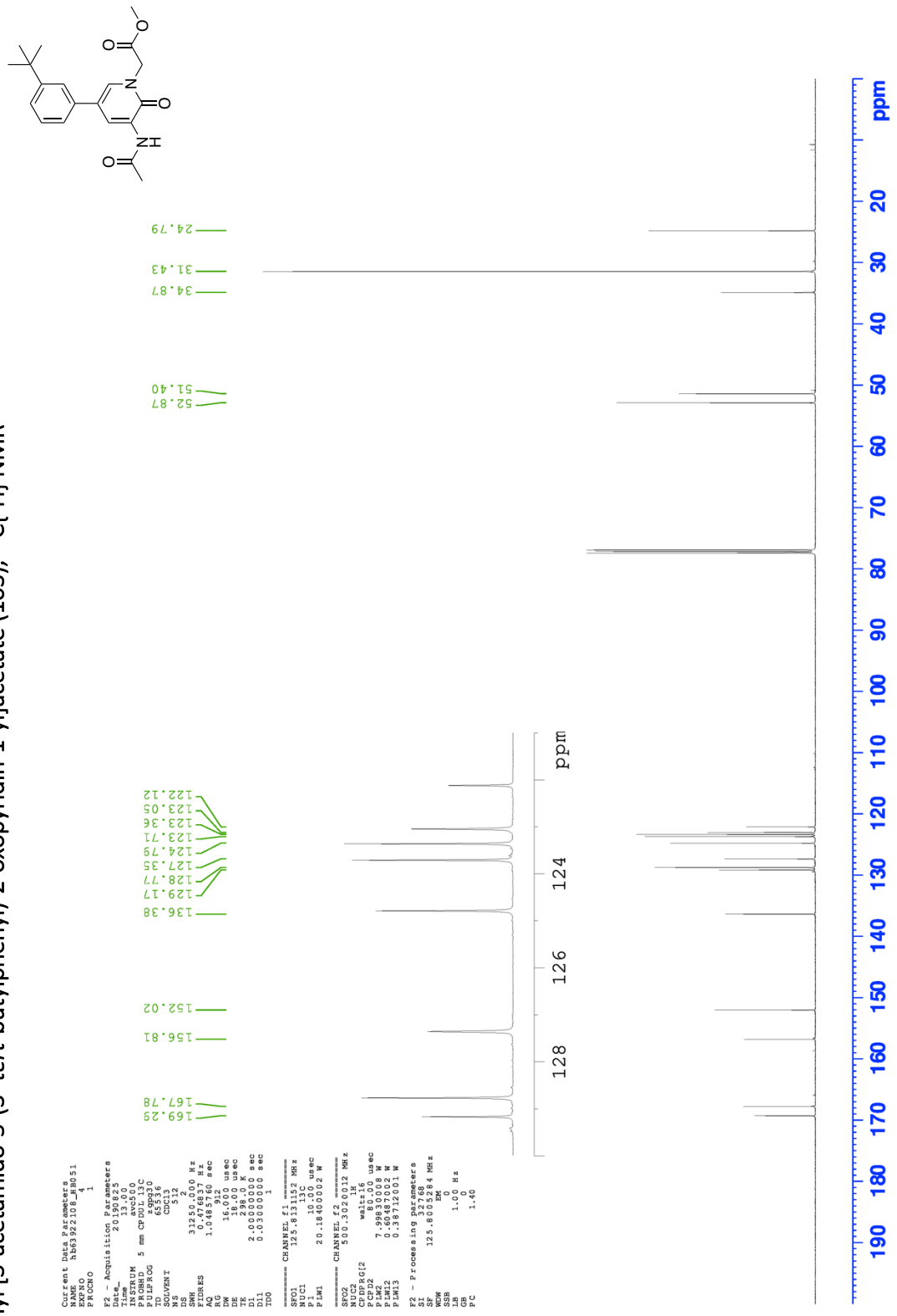
Methyl [3-acetamido-5-(4'-cyanophenyl)-2-oxopyridin-1-yl]acetate (102), $^{13}C\{^{1}H\}$ NMR



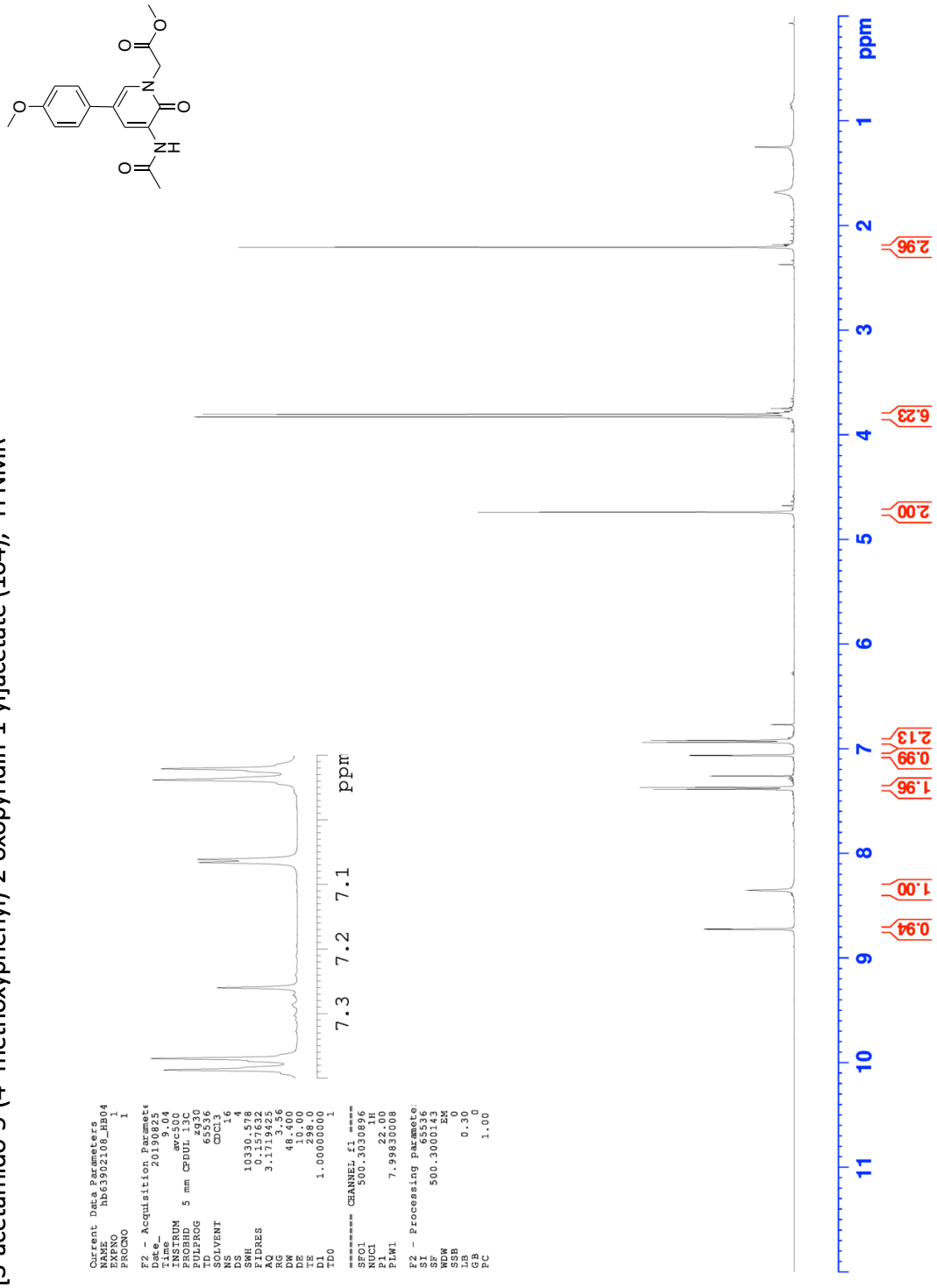
Methyl [3-acetamido-5-(3'-*tert*-butylphenyl)-2-oxopyridin-1-yl]acetate (103), ^{1}H NMR



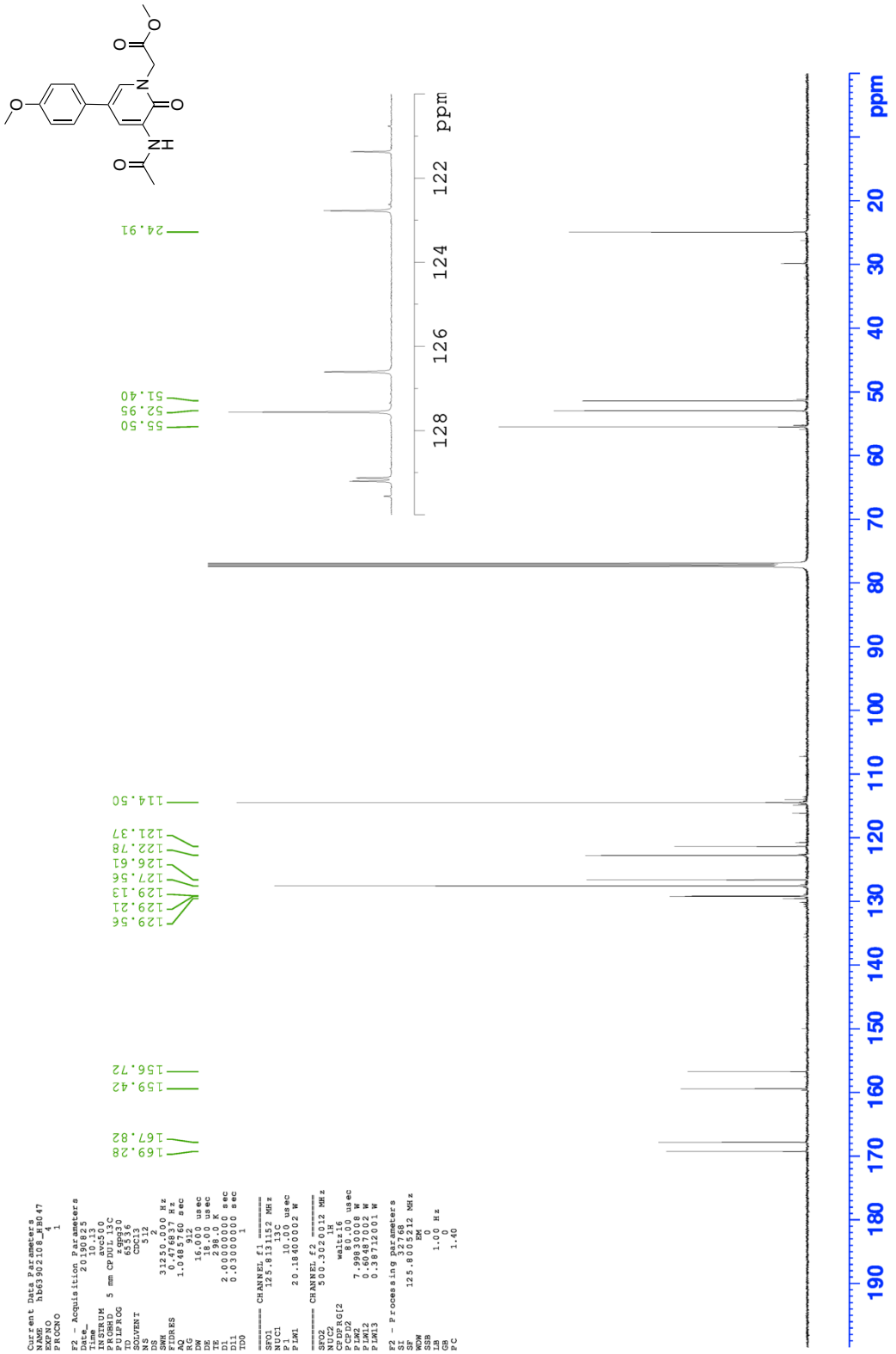
Methyl [3-acetamido-5-(3'-*tert*-butylphenyl)-2-oxopyridin-1-yl]acetate (103), $^{13}C\{^{1}H\}$ NMR



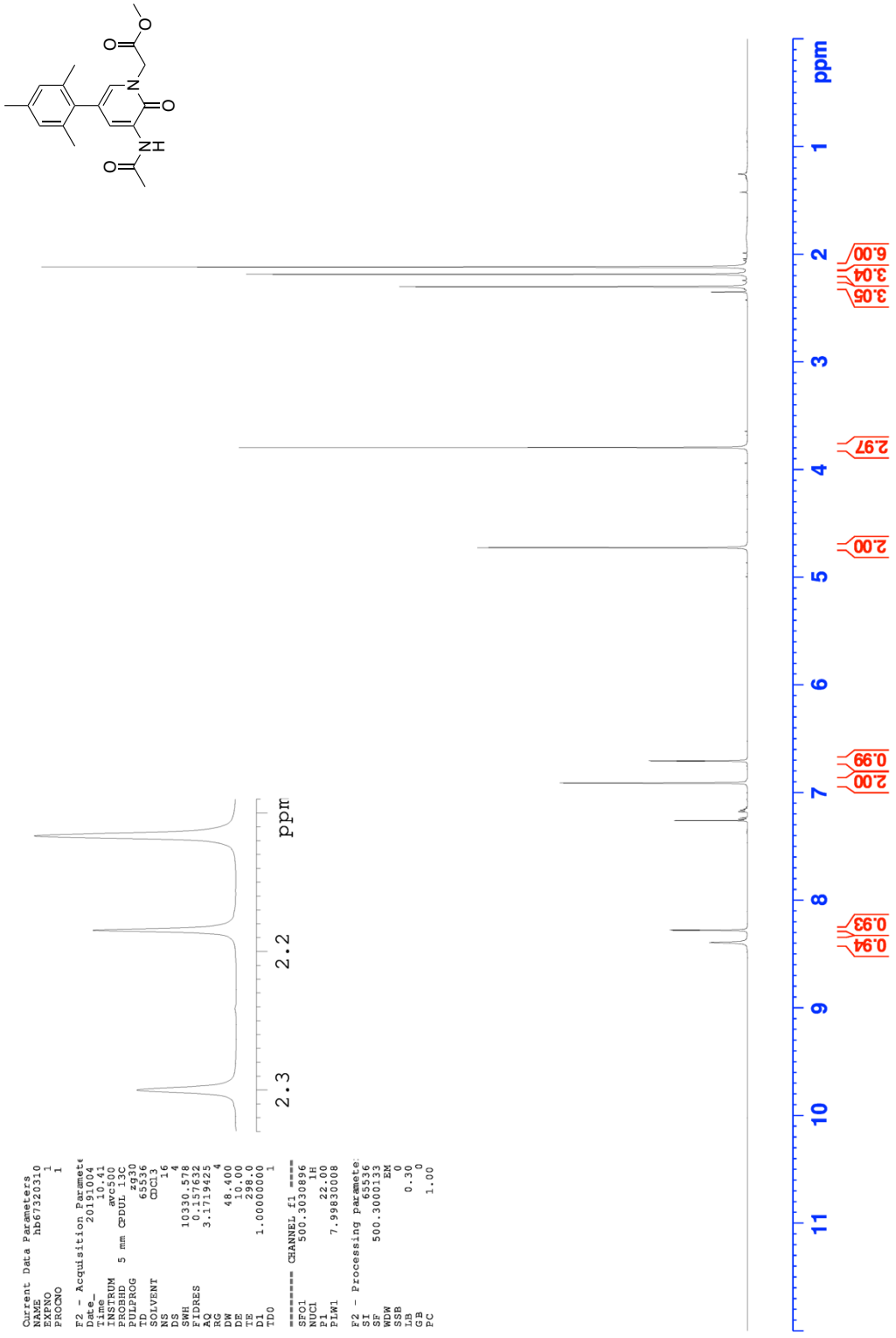
Methyl [3-acetamido-5-(4'-methoxyphenyl)-2-oxopyridin-1-yl]acetate (104), ^{1}H NMR



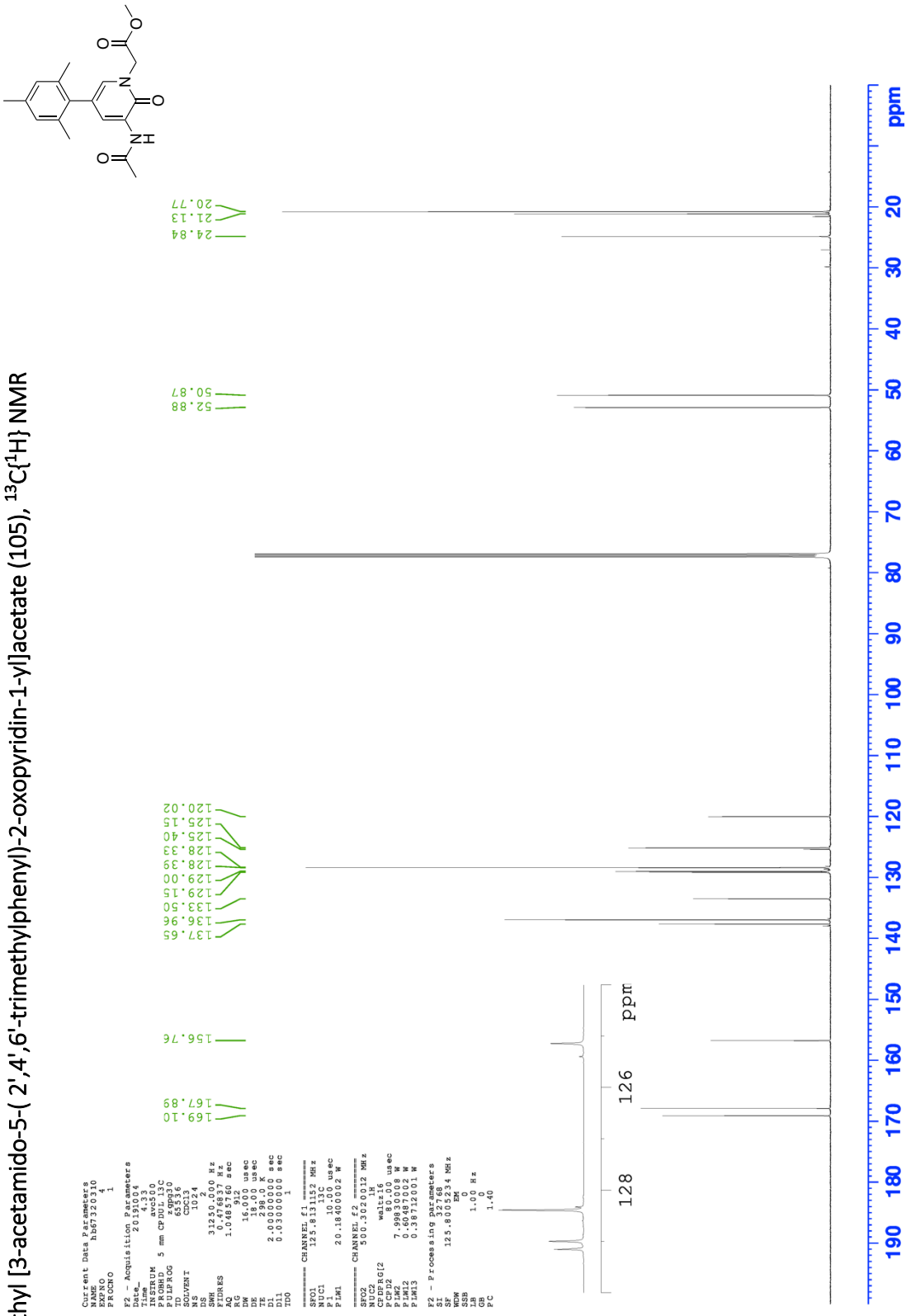
Methyl [3-acetamido-5-(4'-methoxyphenyl)-2-oxopyridin-1-yl]acetate (104), $^{13}C\{^{1}H\}$ NMR



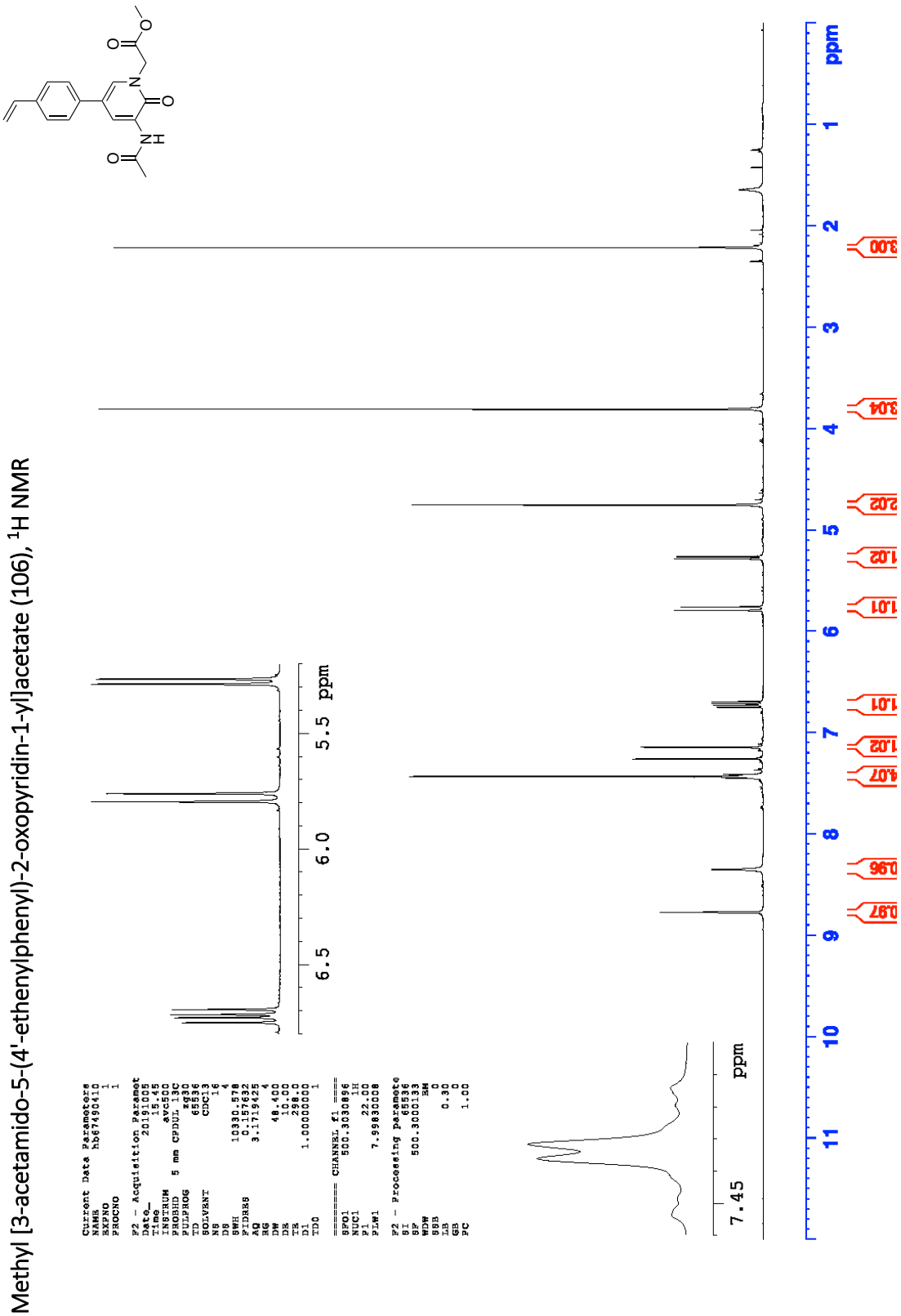
Methyl [3-acetamido-5-(2',4',6'-trimethylphenyl)-2-oxopyridin-1-yl]acetate (105), ^{1}H NMR



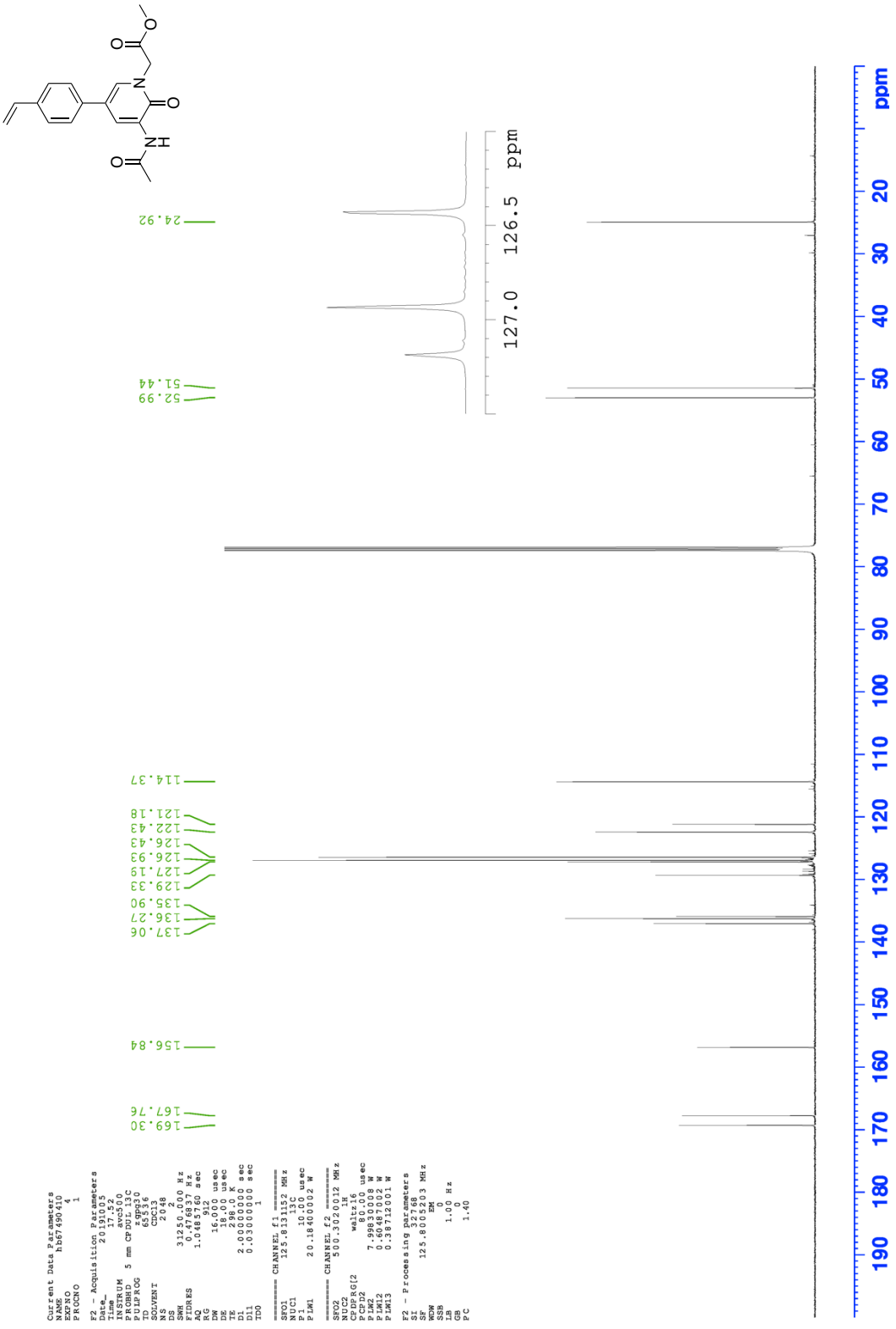
Methyl [3-acetamido-5-(2',4',6'-trimethylphenyl)-2-oxopyridin-1-yl]acetate (105), $^{13}C\{^{1}H\}$ NMR



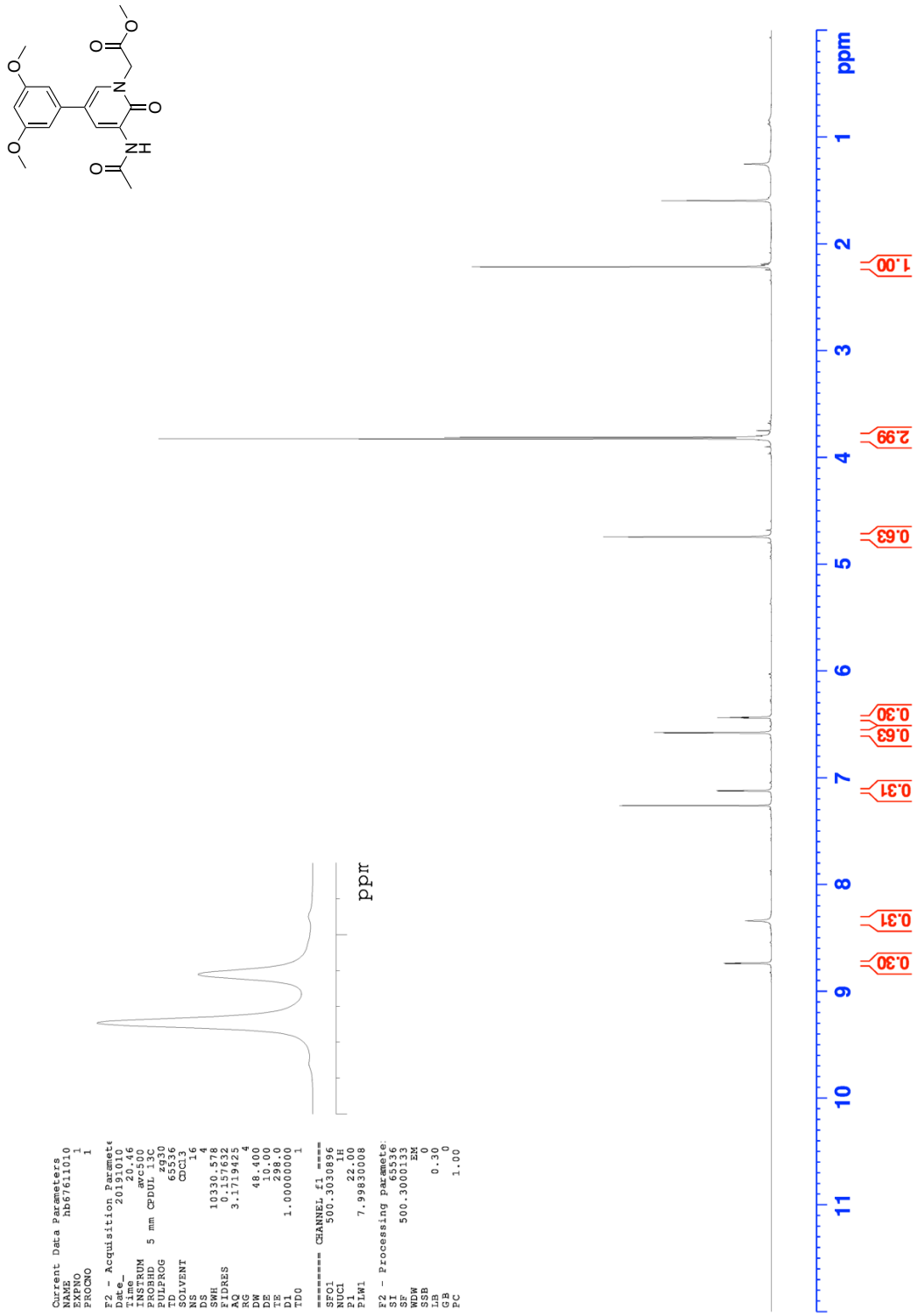
Methyl [3-acetamido-5-(4'-ethenylphenyl)-2-oxopyridin-1-yl]acetate (106), ^{1}H NMR



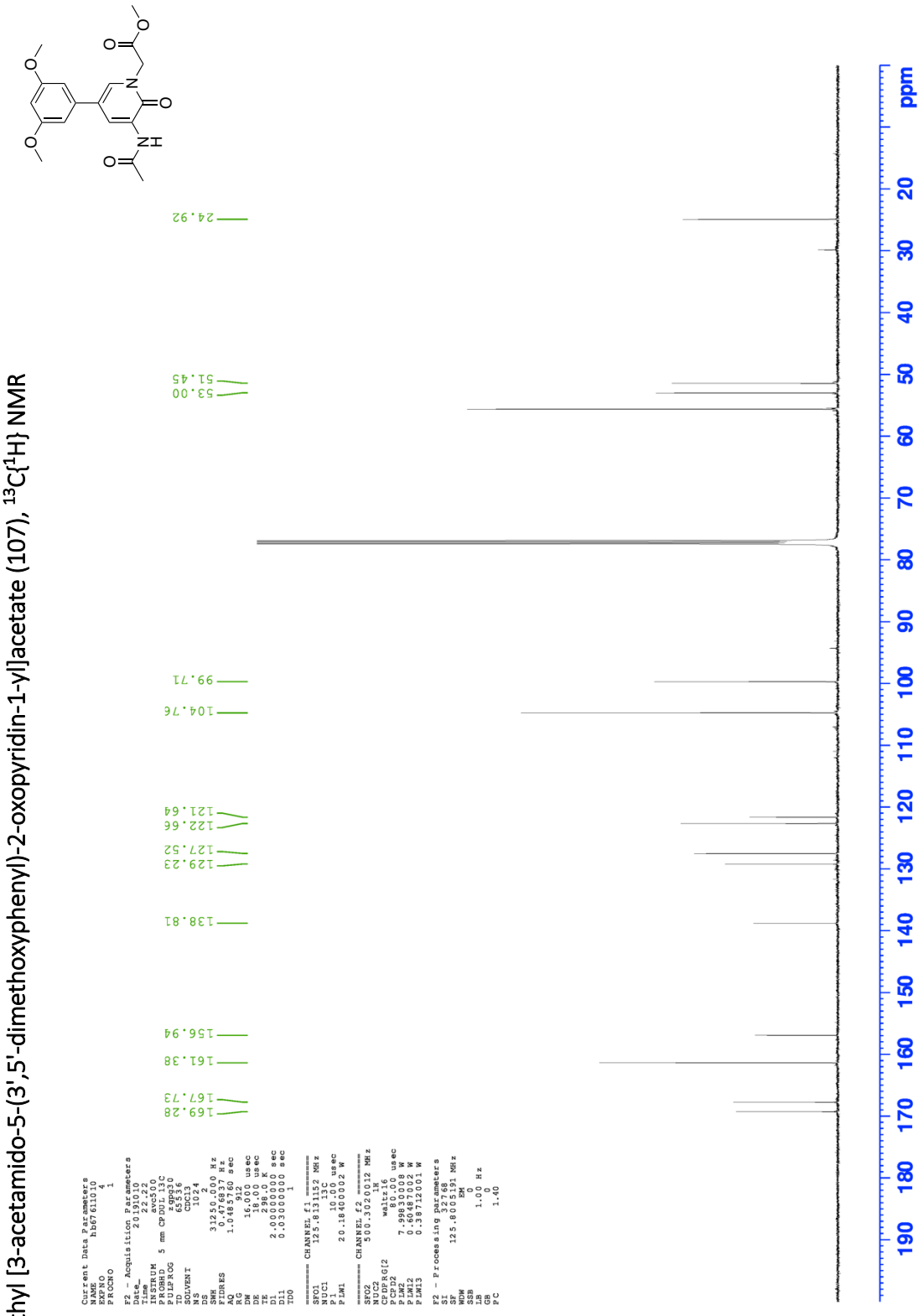
Methyl [3-acetamido-5-(4'-ethenylphenyl)-2-oxopyridin-1-yl]acetate (106), $^{13}C\{^{1}H\}$ NMR



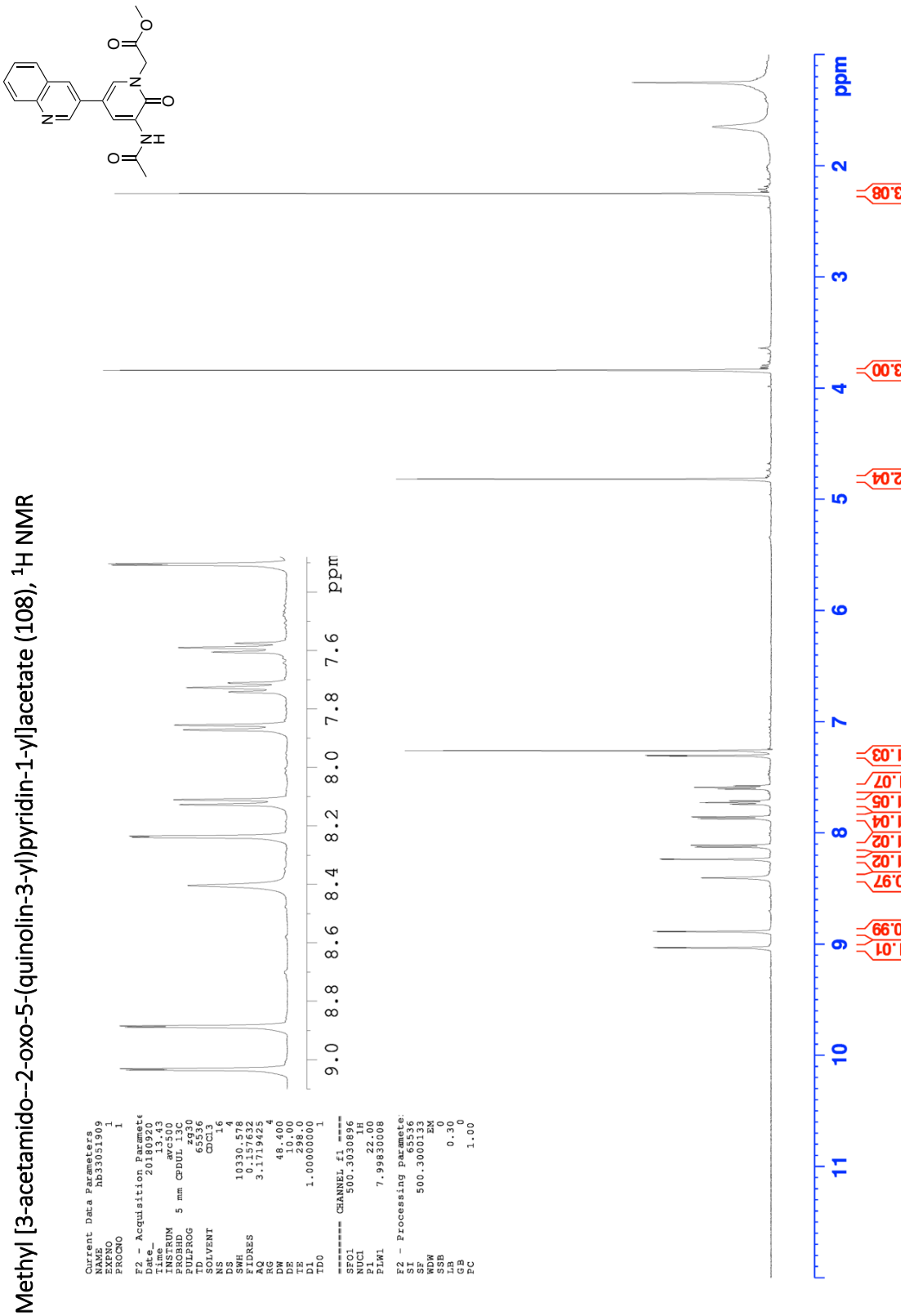
Methyl [3-acetamido-5-(3',5'-dimethoxyphenyl)-2-oxopyridin-1-yl]acetate (107), ^{1}H NMR



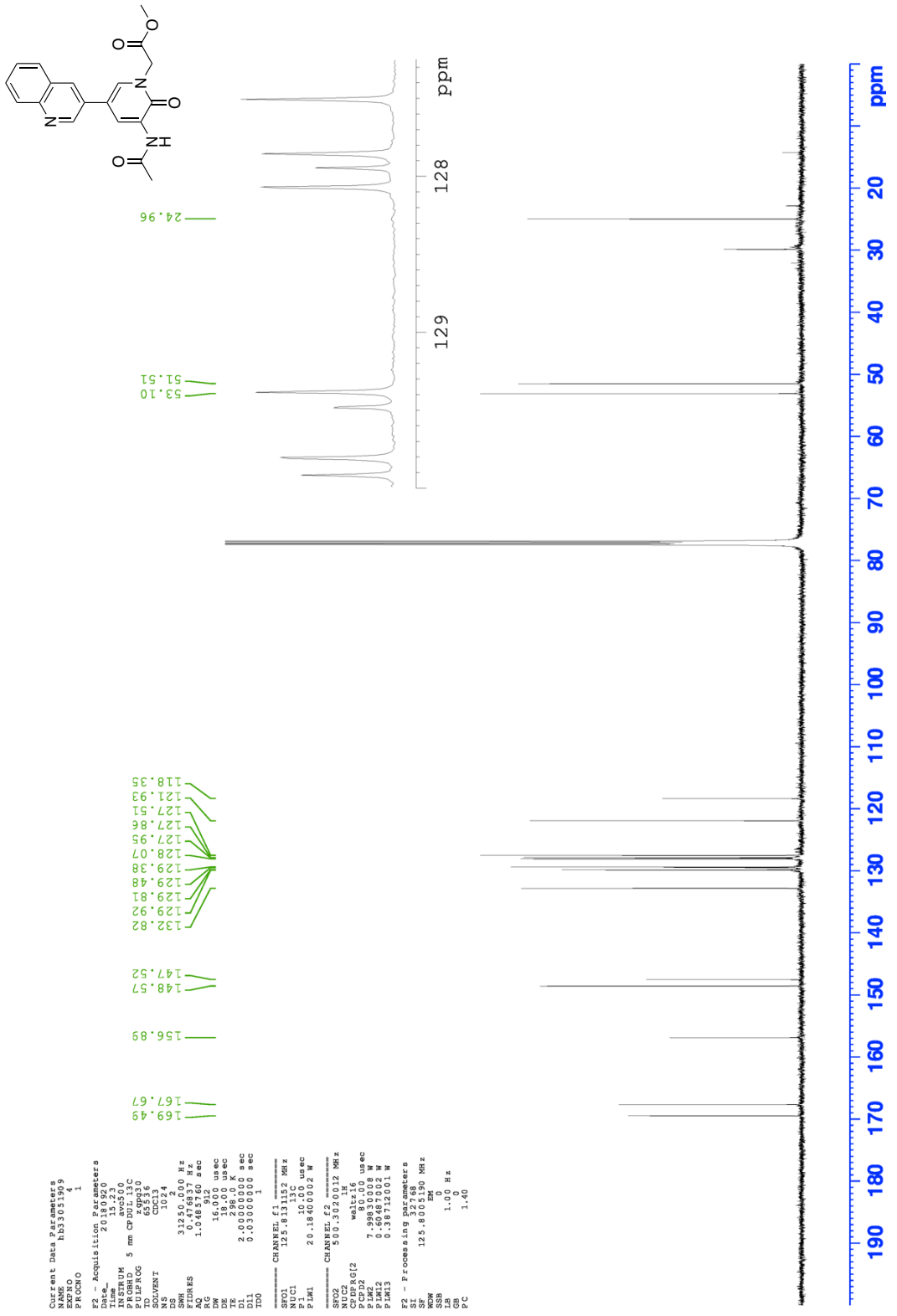
Methyl [3-acetamido-5-(3',5'-dimethoxyphenyl)-2-oxopyridin-1-yl]acetate (107), $^{13}C\{^{1}H\}$ NMR



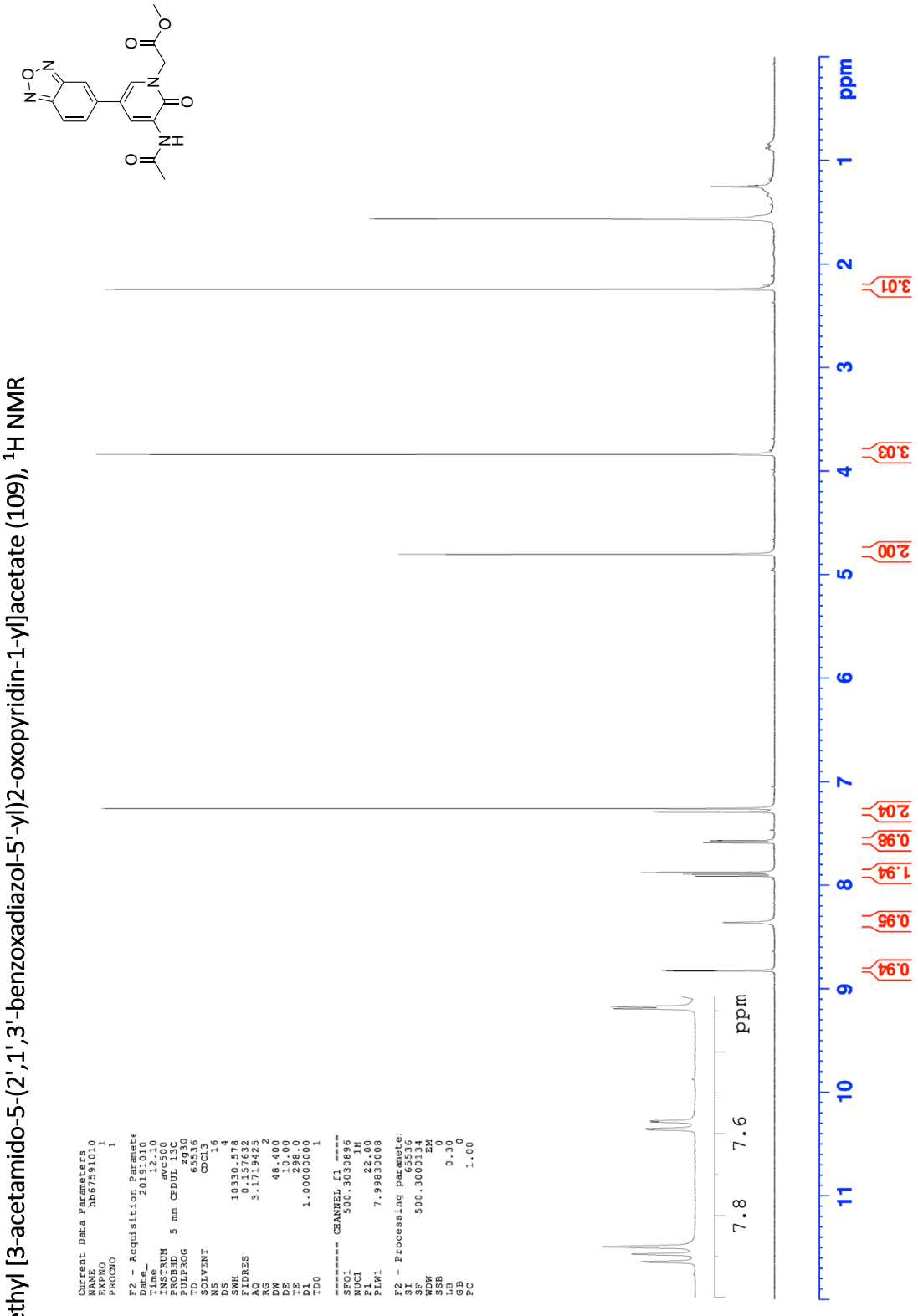
Methyl [3-acetamido−2-oxo-5-(quinolin-3-yl)pyridin-1-yl]acetate (108), ^{1}H NMR



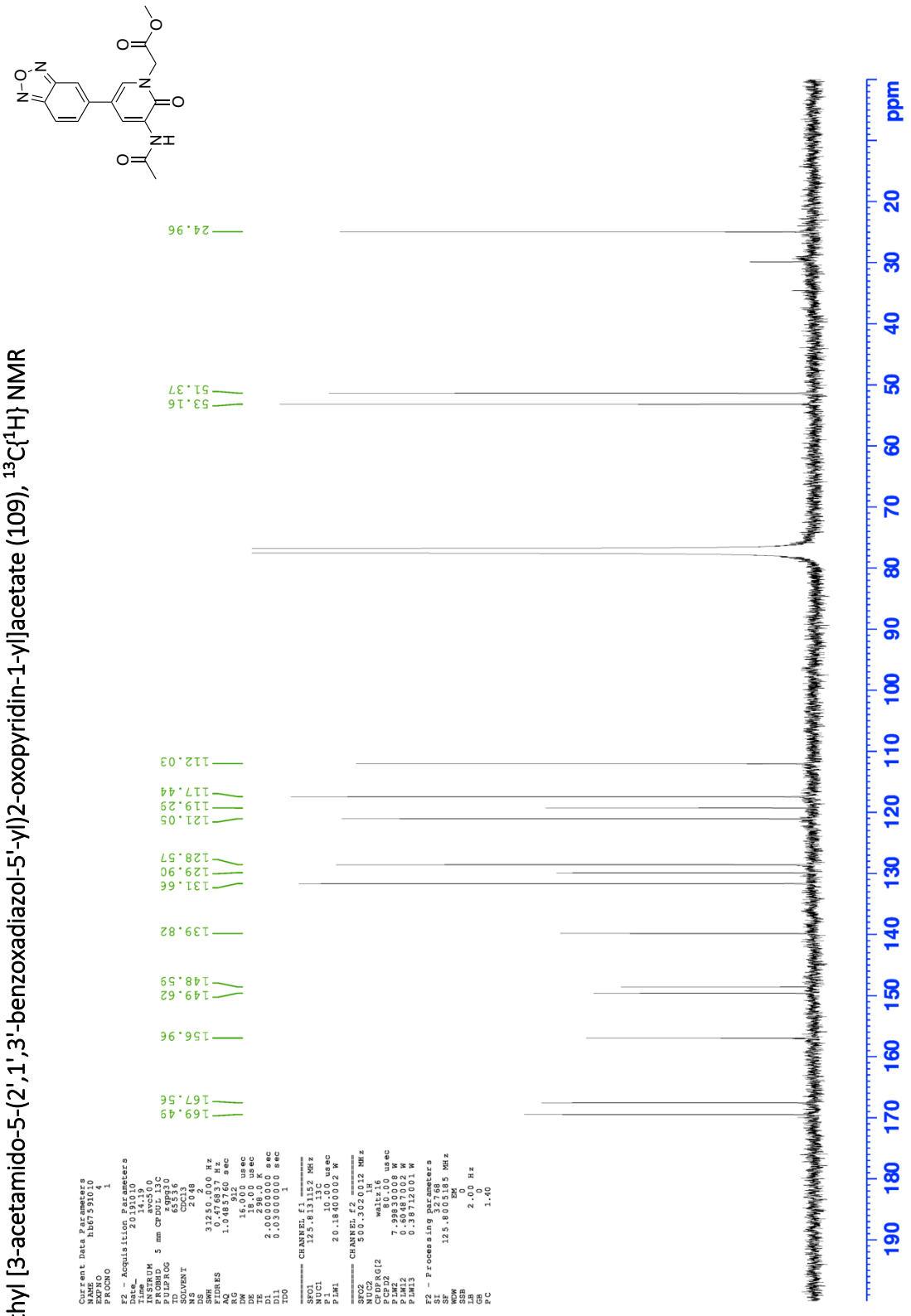
Methyl [3-acetamido-2-oxo-5-(quinolin-3-yl)pyridin-1-yl]acetate (108), $^{13}C\{^{1}H\}$ NMR



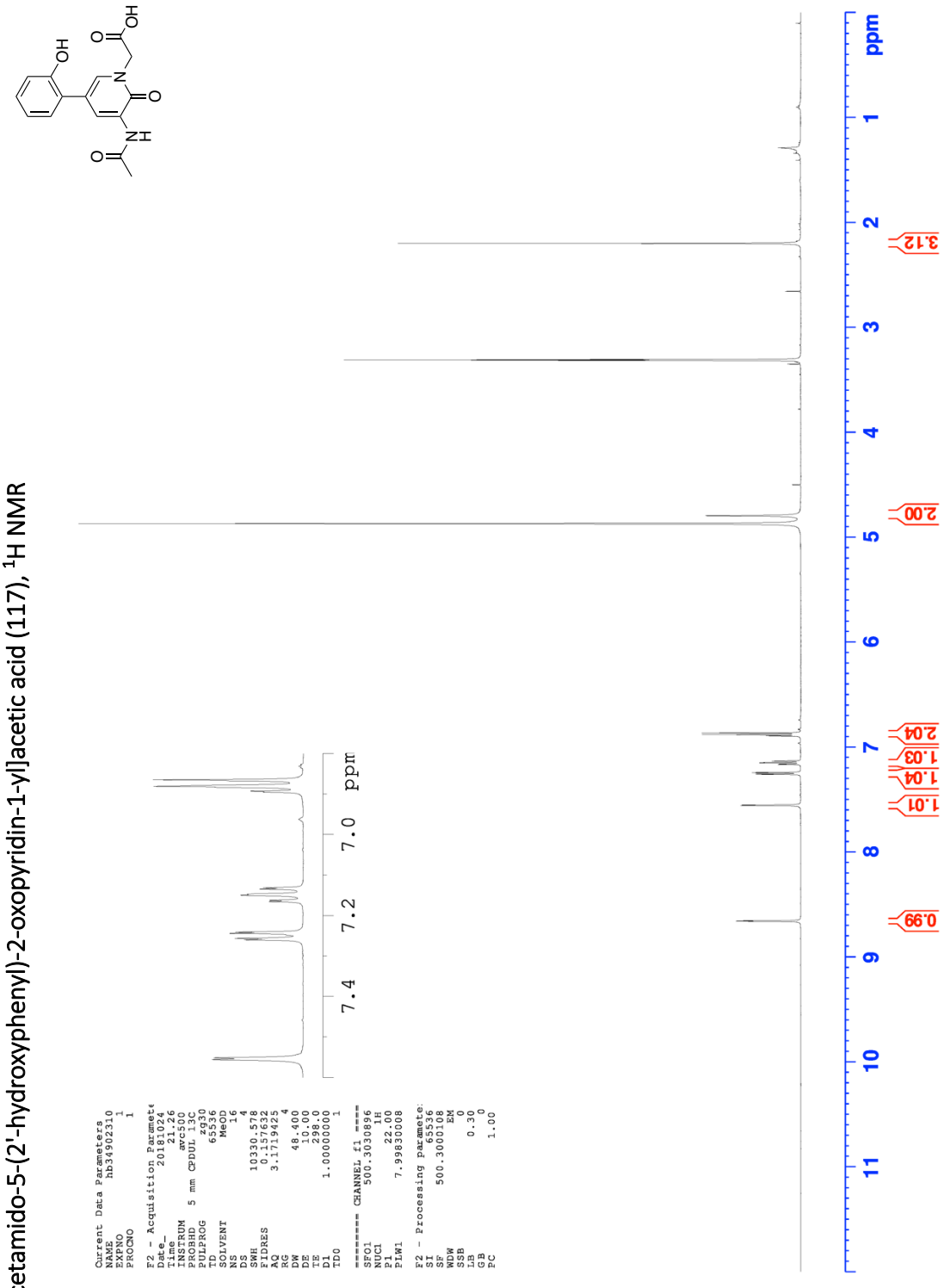
Methyl [3-acetamido-5-(2',1',3'-benzoxadiazol-5'-yl)2-oxopyridin-1-yl]acetate (109), ^{1}H NMR



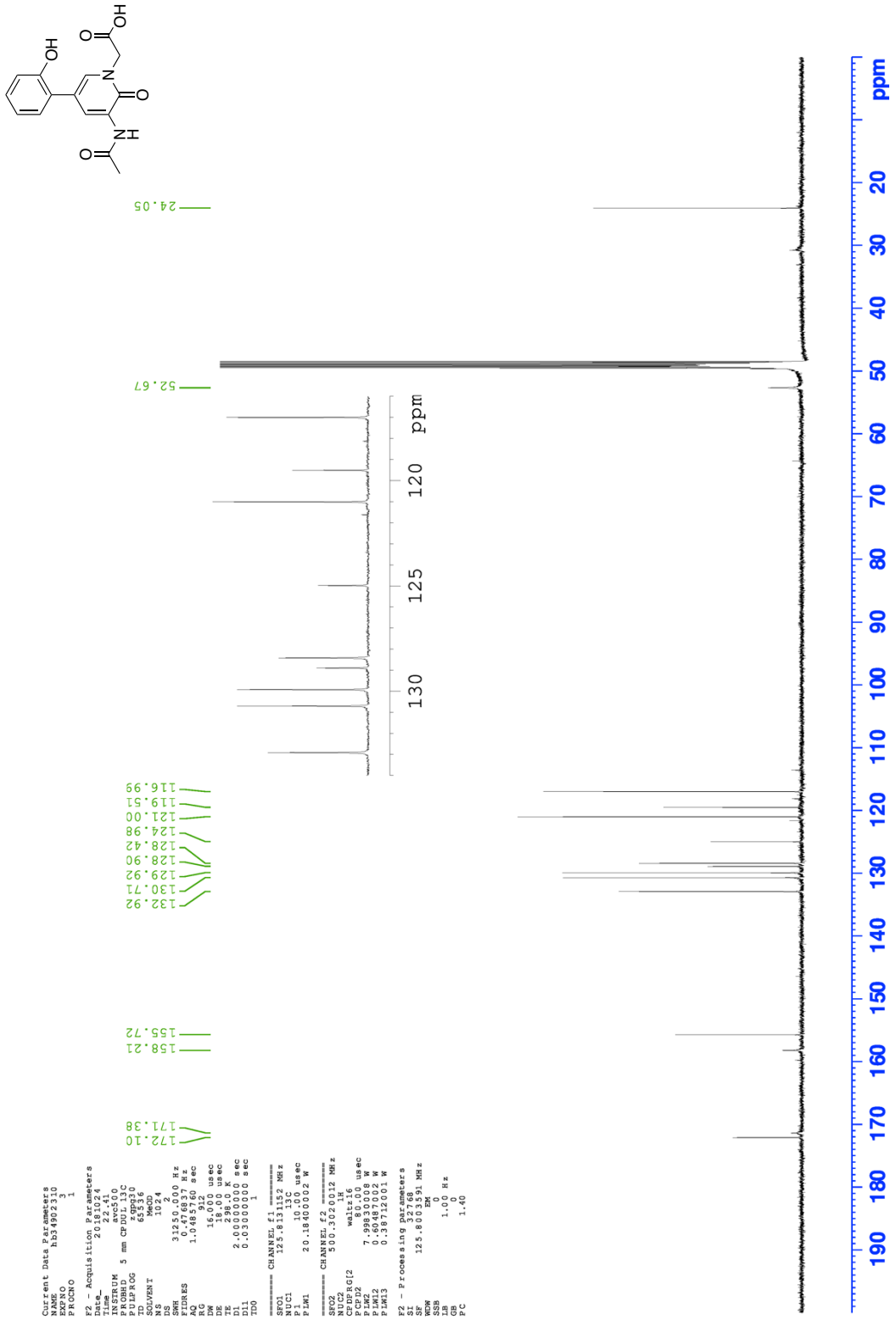
Methyl [3-acetamido-5-(2',1',3'-benzoxadiazol-5'-yl)2-oxopyridin-1-yl]acetate (109), $^{13}C\{^{1}H\}$ NMR



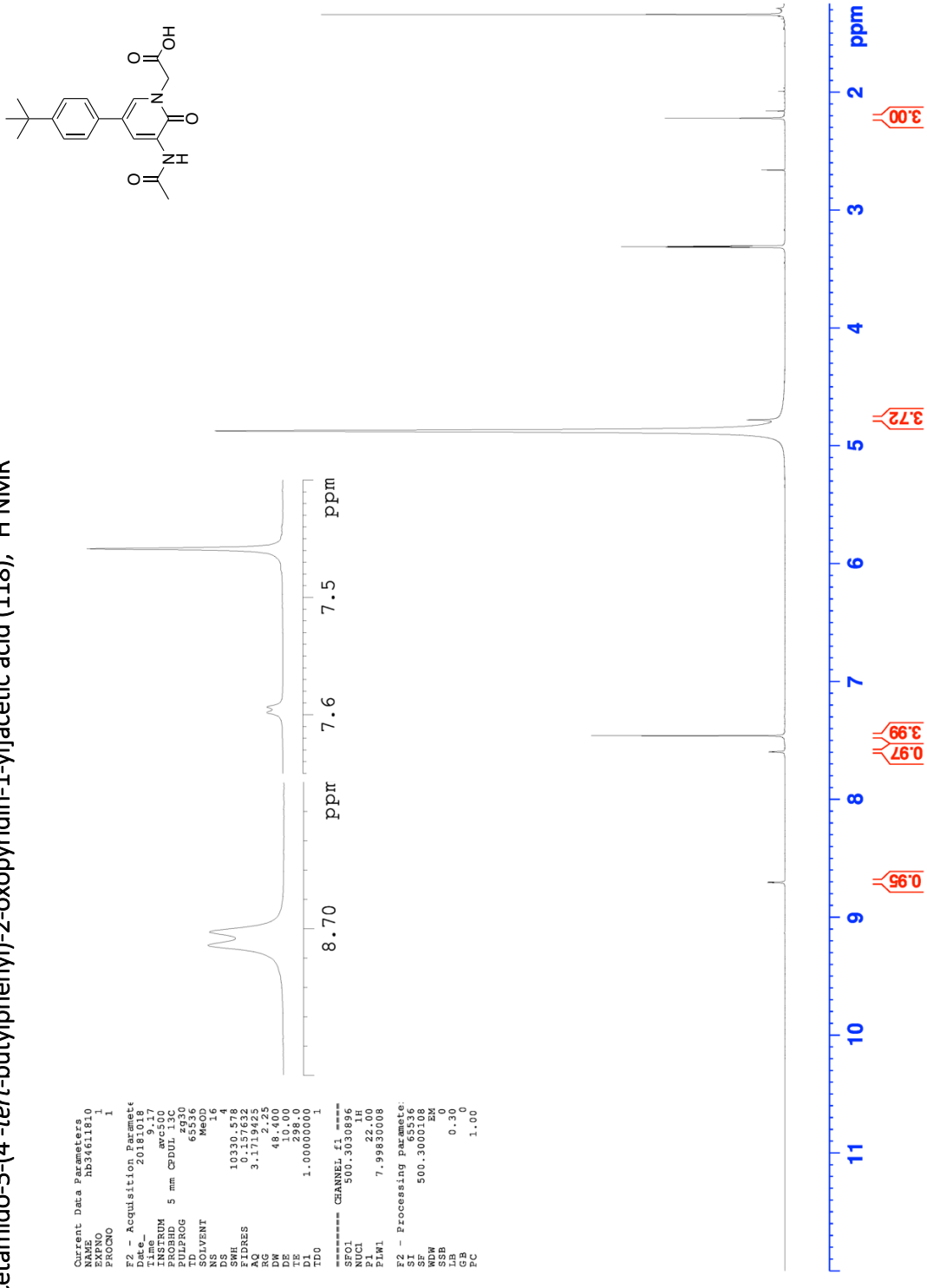
[3-Acetamido-5-(2'-hydroxyphenyl)-2-oxopyridin-1-yl]acetic acid (117), ^{1}H NMR



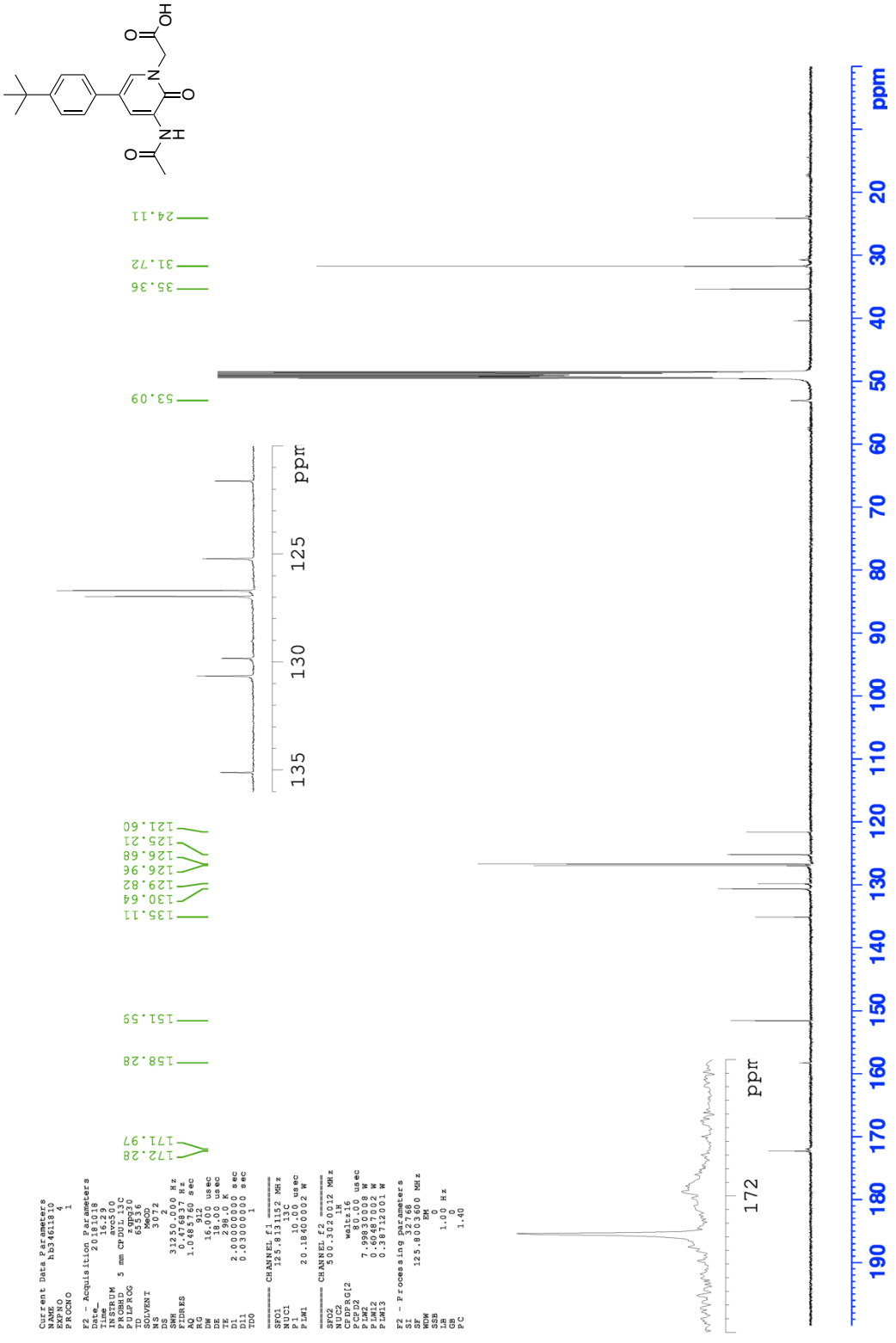
[3-Acetamido-5-(2'-hydroxyphenyl)-2-oxopyridin-1-yl]acetic acid (117), $^{13}C\{^{1}H\}$ NMR



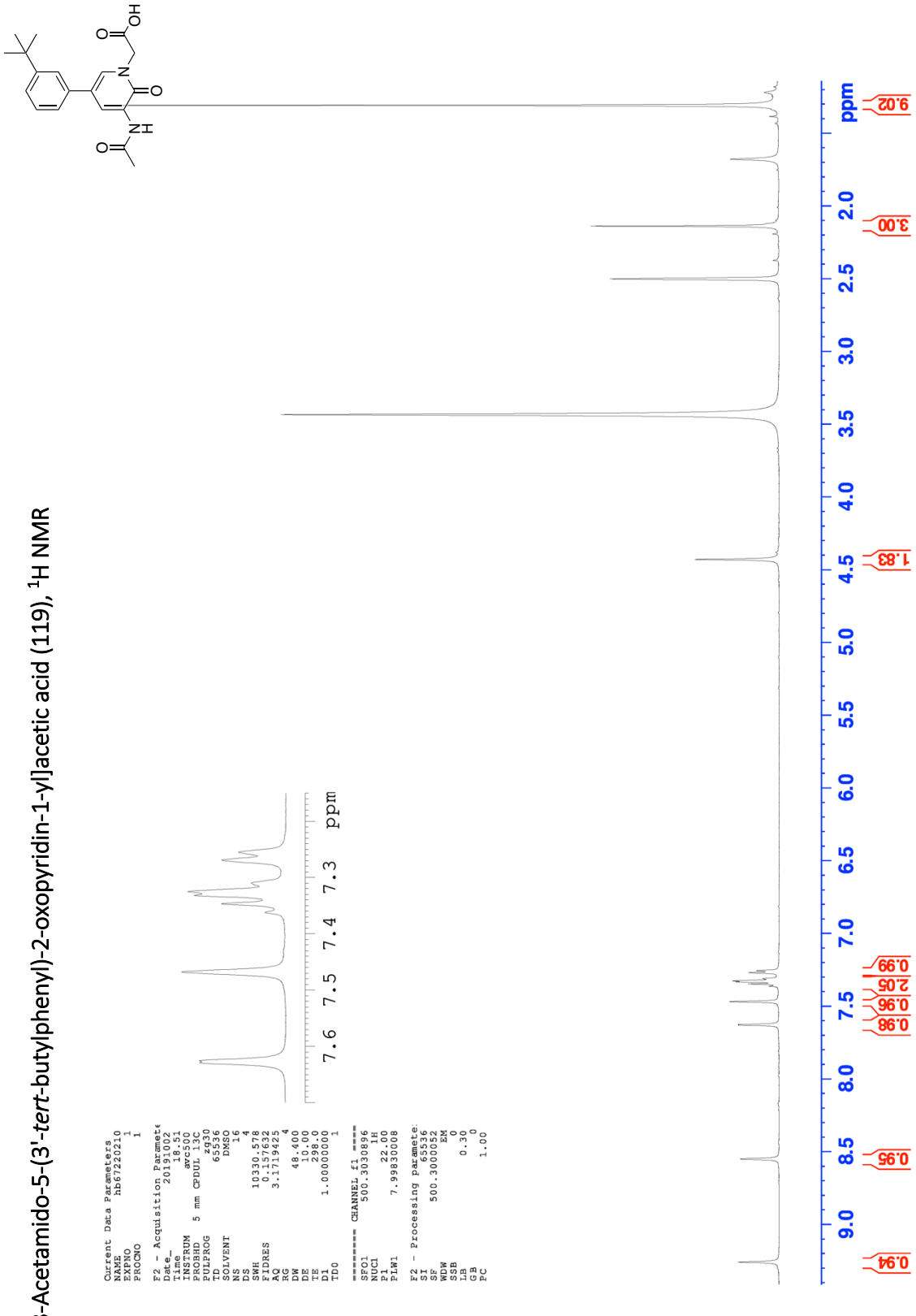
[3-Acetamido-5-(4'-*tert*-butylphenyl)-2-oxopyridin-1-yl]acetic acid (118), ^{1}H NMR



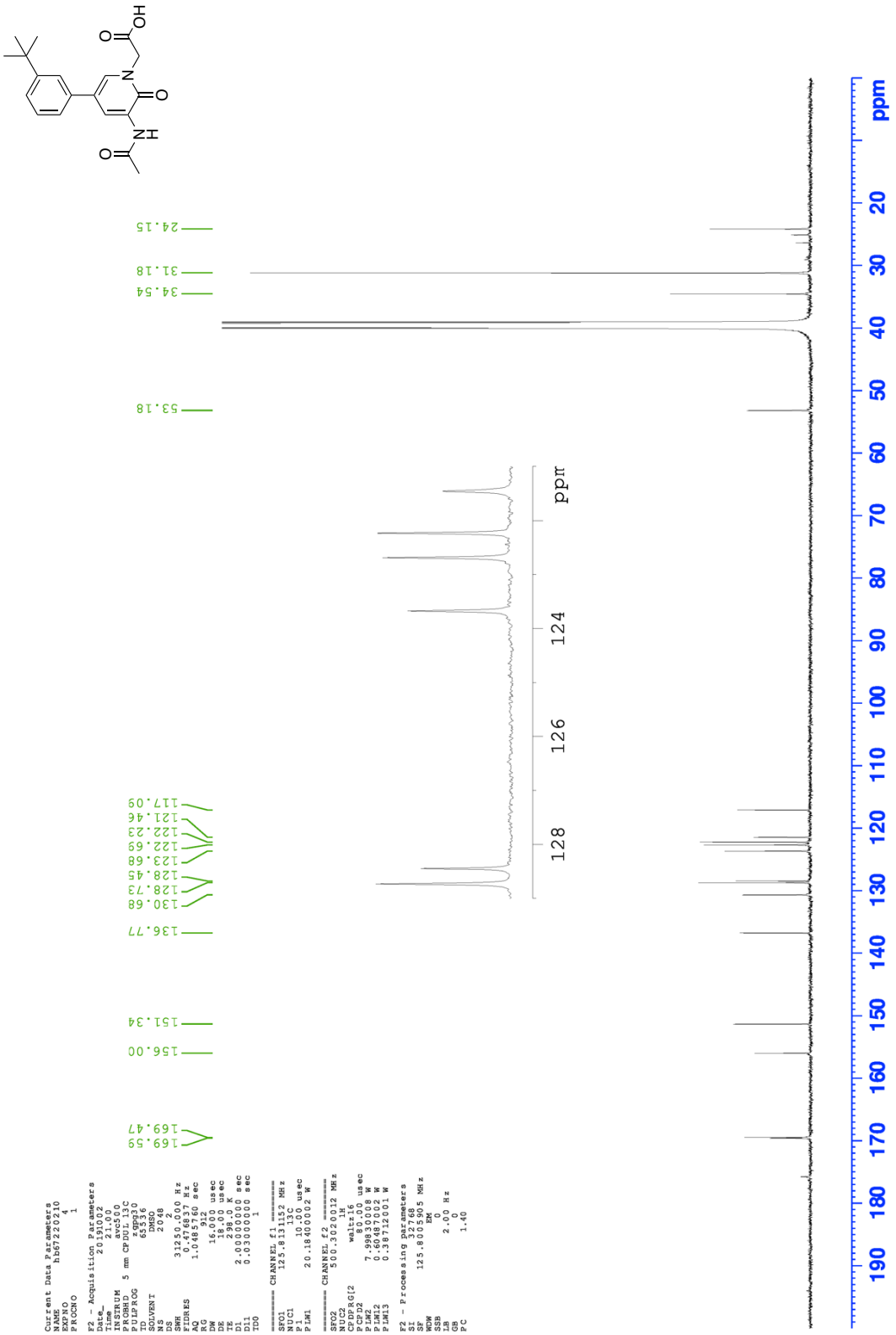
[3-Acetamido-5-(4'-*tert*-butylphenyl)-2-oxopyridin-1-yl]acetic acid (118), $^{13}C\{^{1}H\}$ NMR



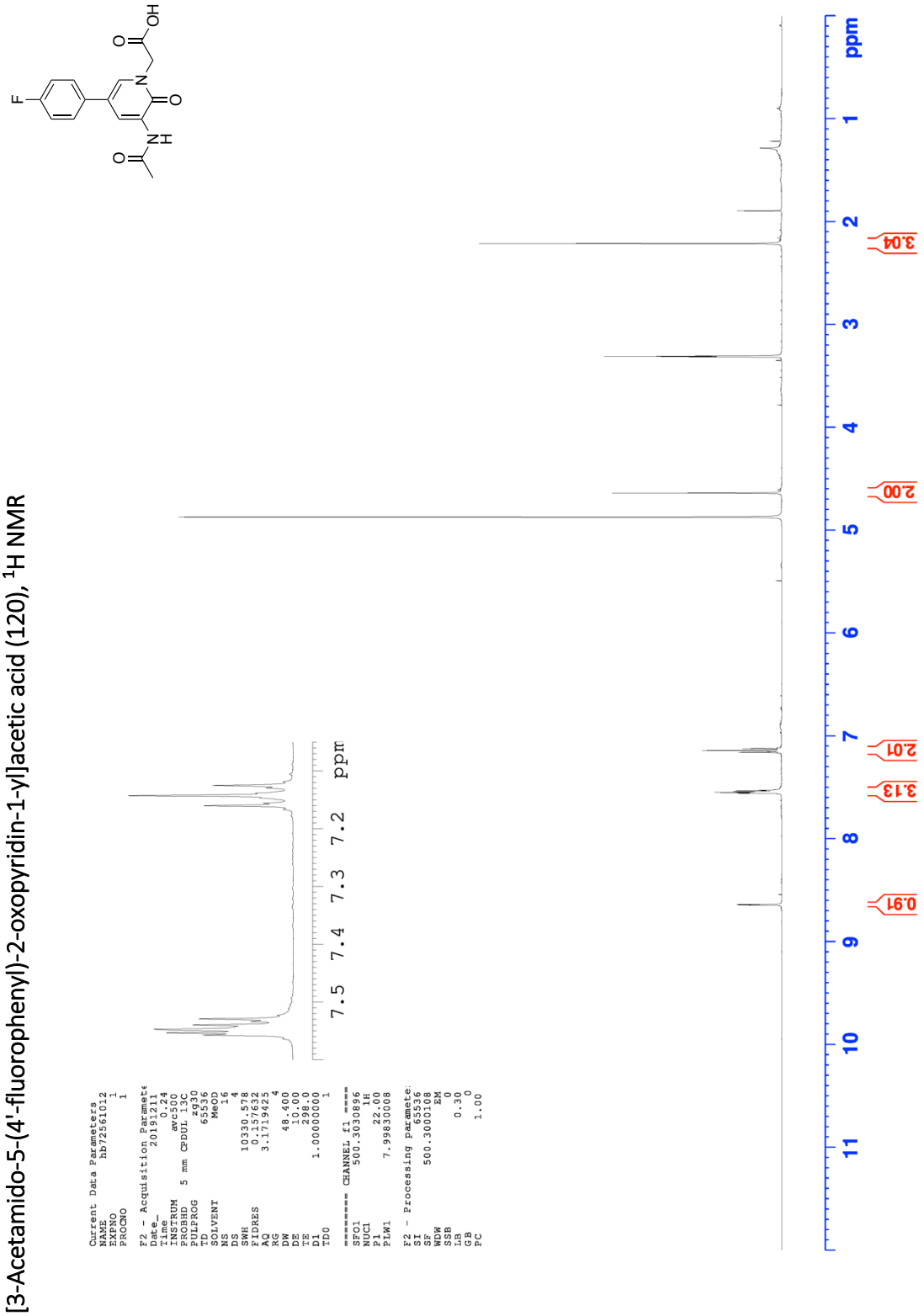
[3-Acetamido-5-(3'-*tert*-butylphenyl)-2-oxopyridin-1-yl]acetic acid (119), ^{1}H NMR



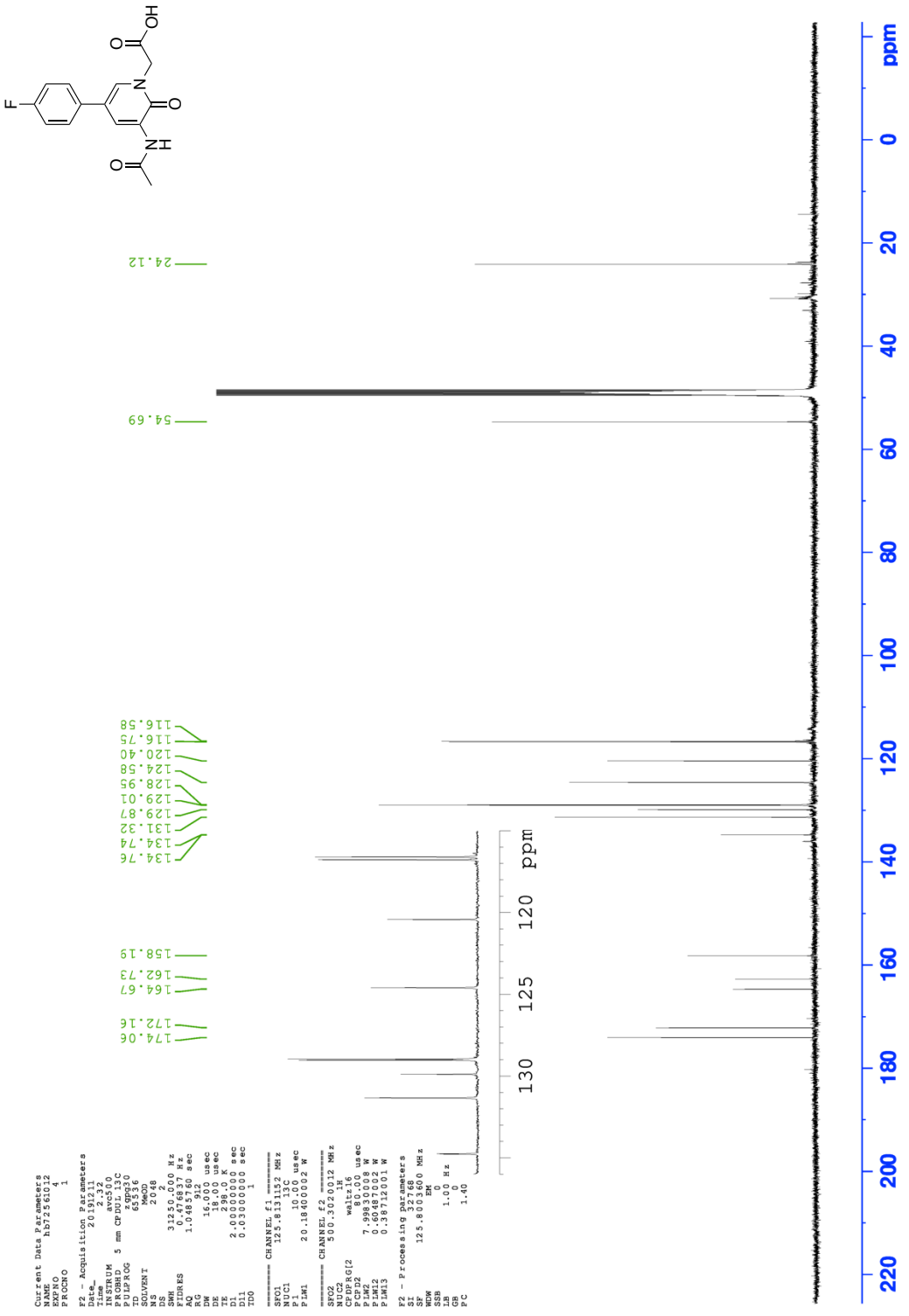
[3-Acetamido-5-(3'-*tert*-butylphenyl)-2-oxopyridin-1-yl]acetic acid (119), $^{13}C\{^{1}H\}$ NMR



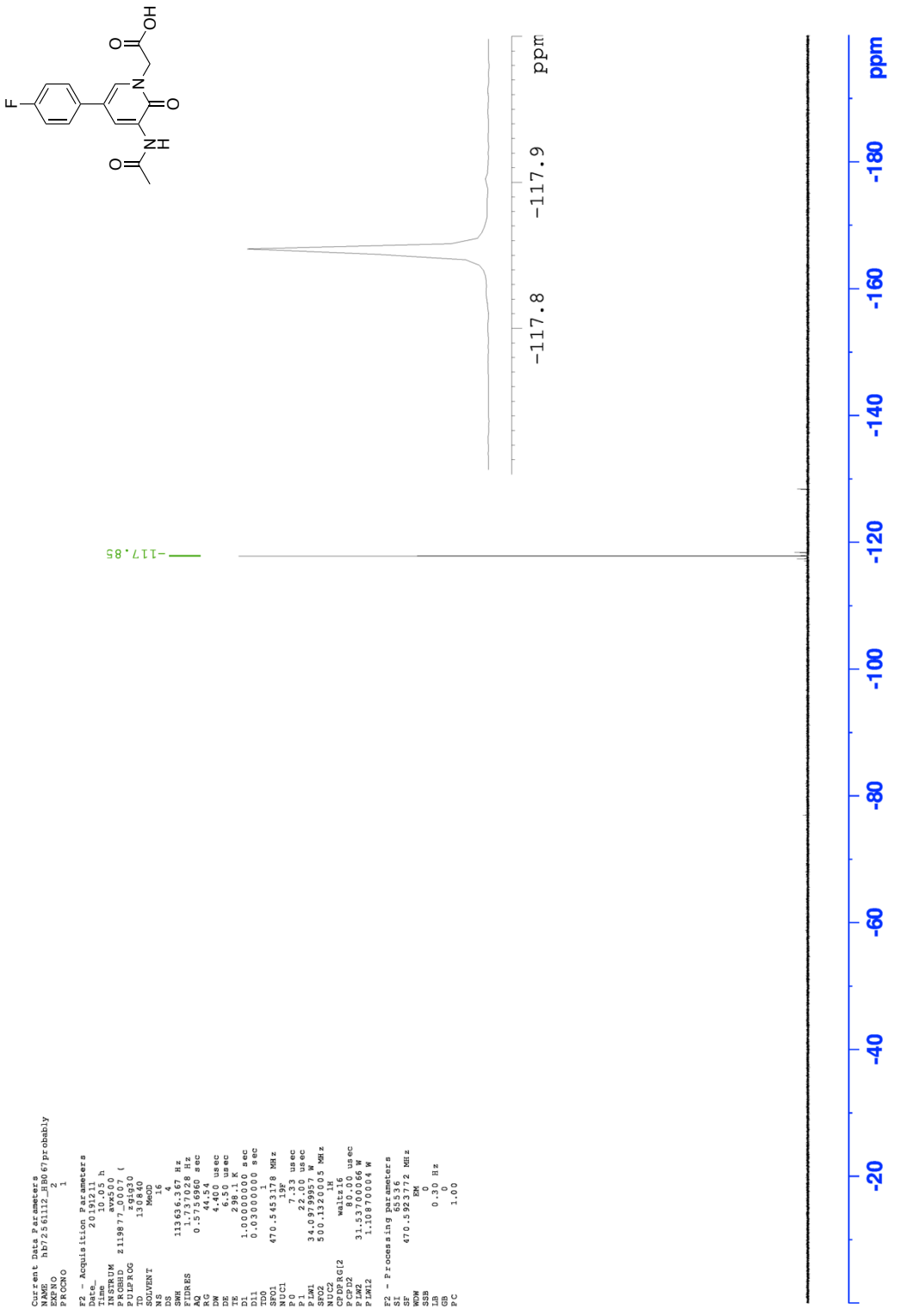
[3-Acetamido-5-(4'-fluorophenyl)-2-oxopyridin-1-yl]acetic acid (120), ^{1}H NMR



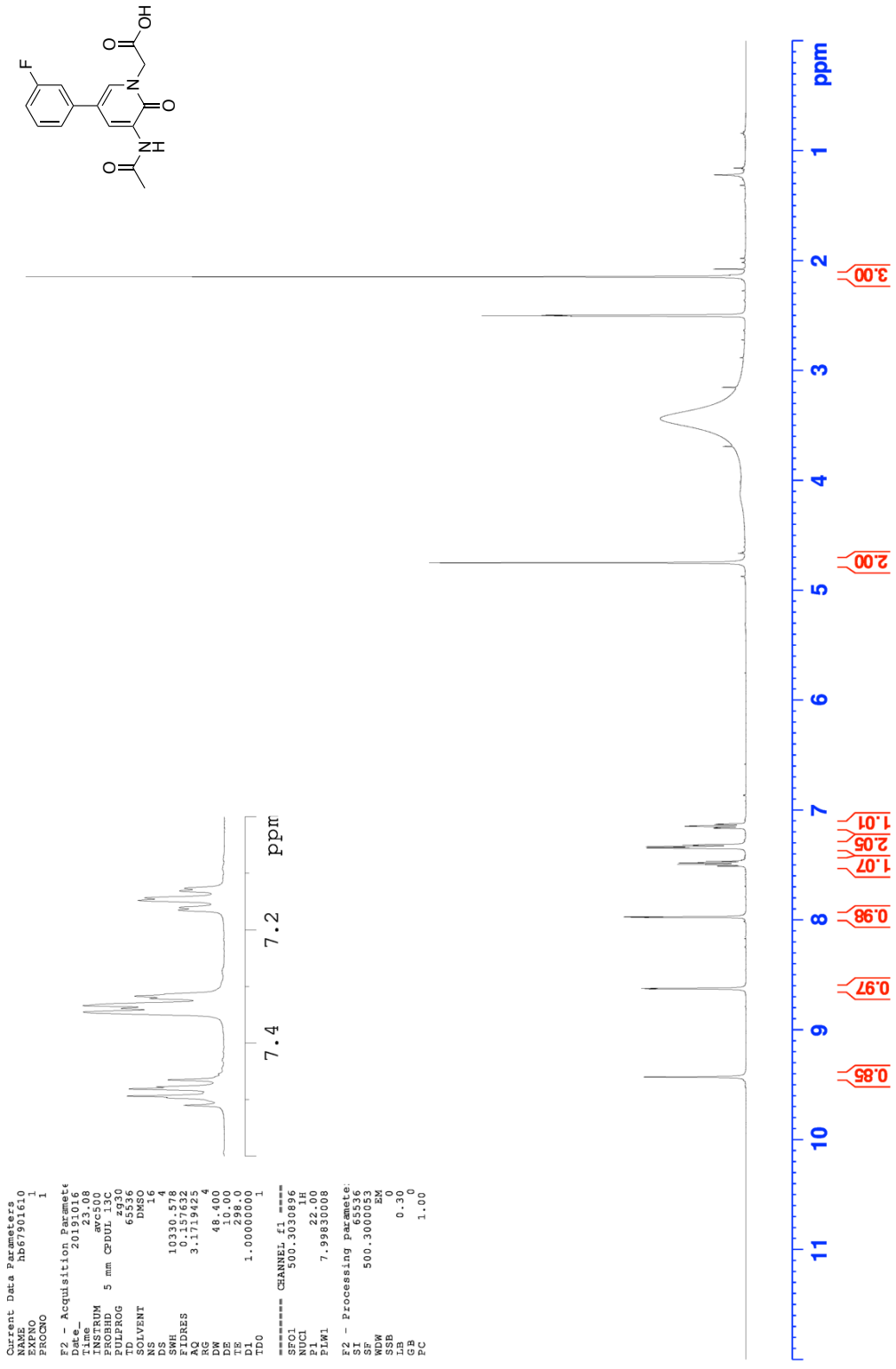
[3-Acetamido-5-(4'-fluorophenyl)-2-oxopyridin-1-yl]acetic acid (120), $^{13}C\{^{1}H\}$ NMR



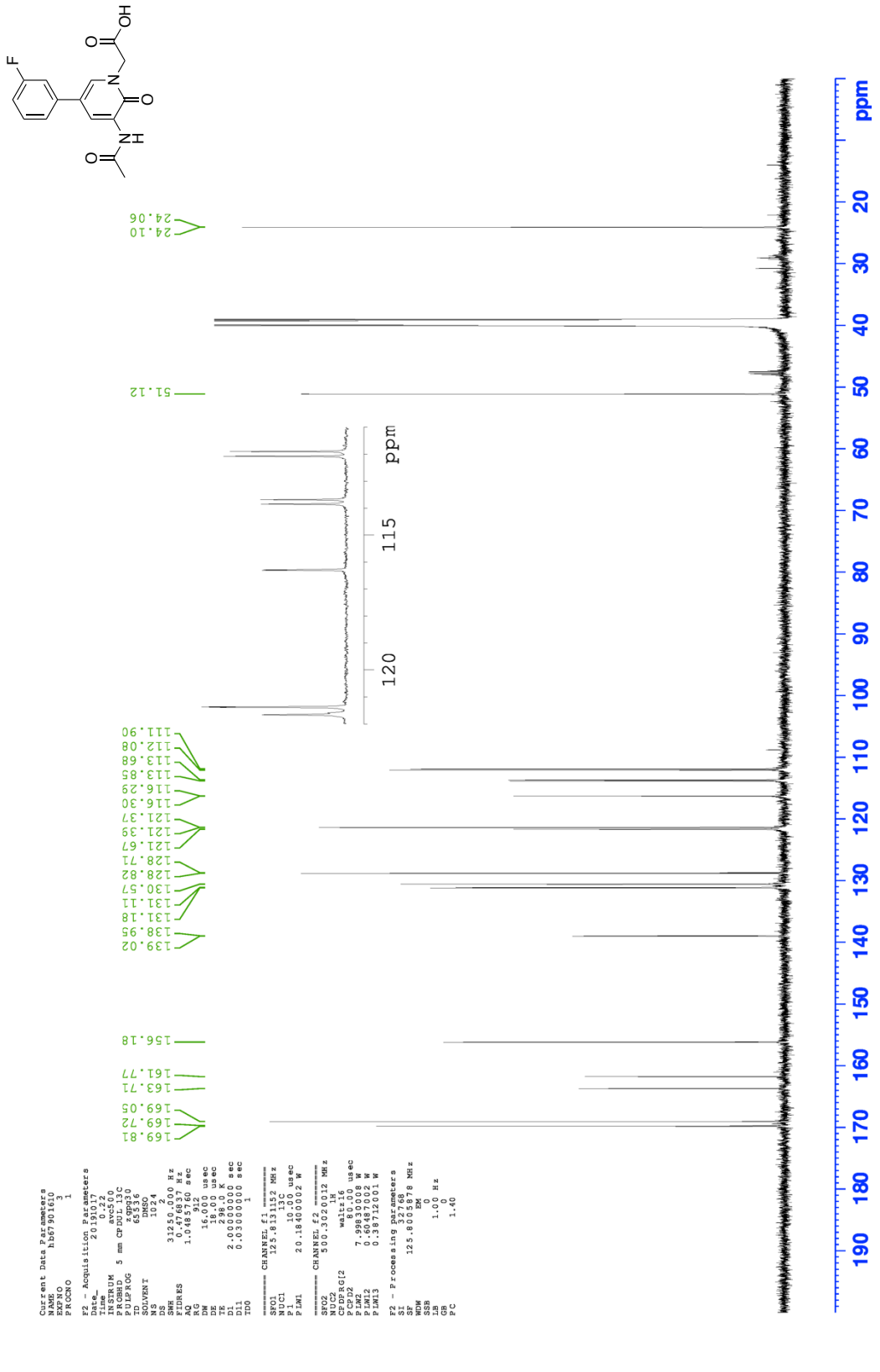
[3-Acetamido-5-(4'-fluorophenyl)-2-oxopyridin-1-yl]acetic acid (120), $^{19}F\{^{1}H\}$ NMR



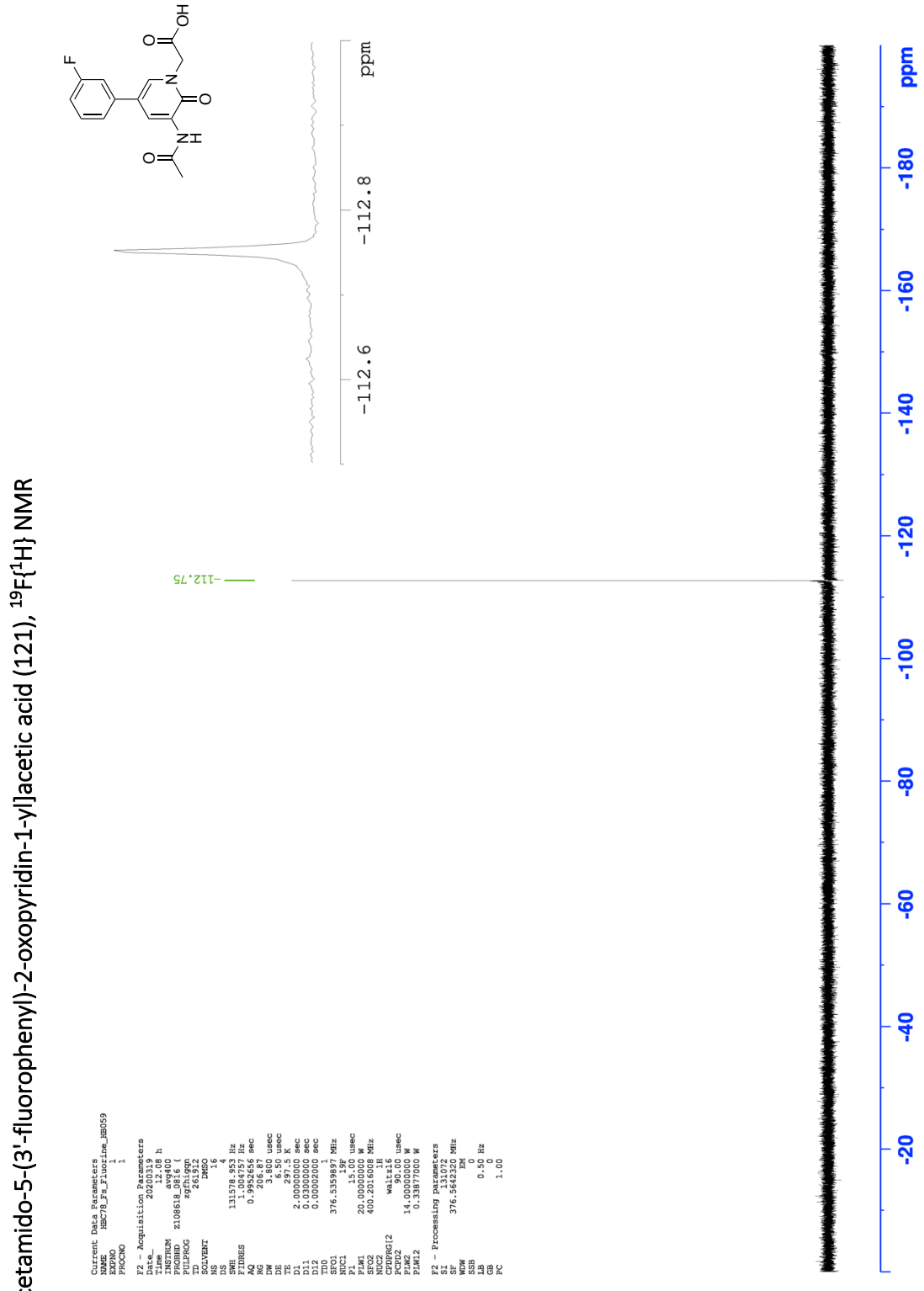
[3-Acetamido-5-(3'-fluorophenyl)-2-oxopyridin-1-yl]acetic acid (121), ^{1}H NMR



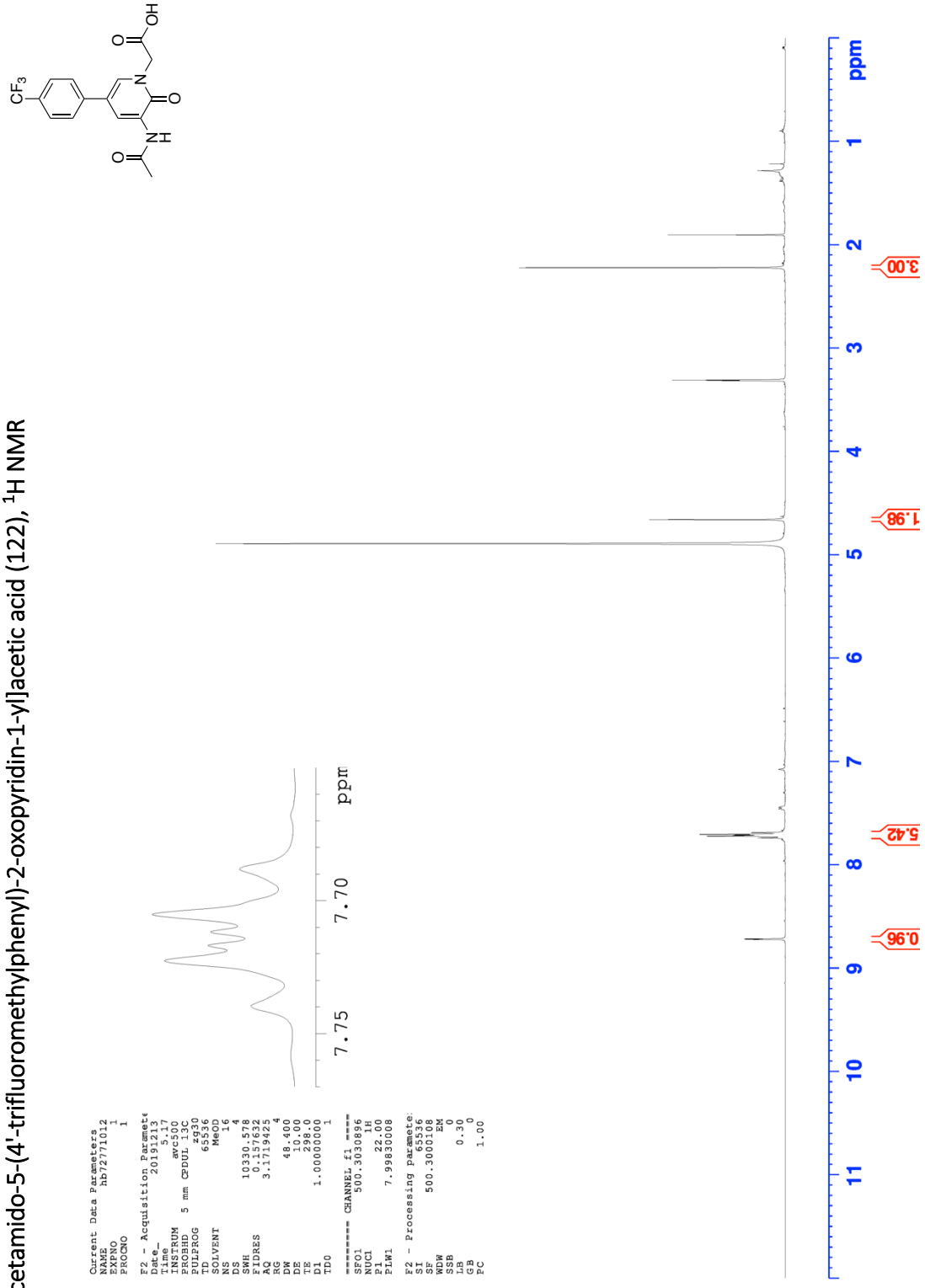
[3-Acetamido-5-(3'-fluorophenyl)-2-oxopyridin-1-yl]acetic acid (121), $^{13}C\{^{1}H\}$ NMR



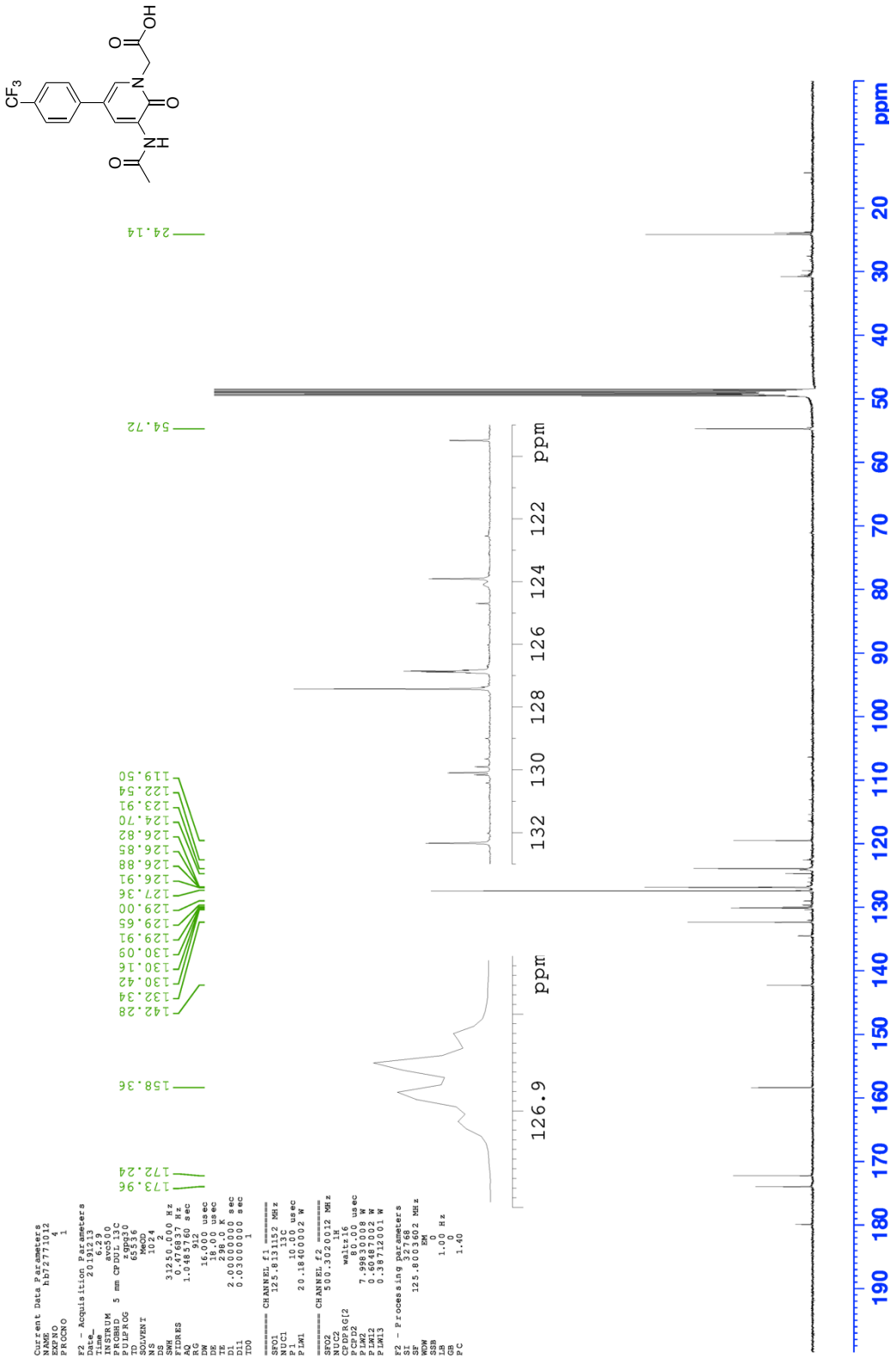
[3-Acetamido-5-(3'-fluorophenyl)-2-oxopyridin-1-yl]acetic acid (121), $^{19}F\{^{1}H\}$ NMR



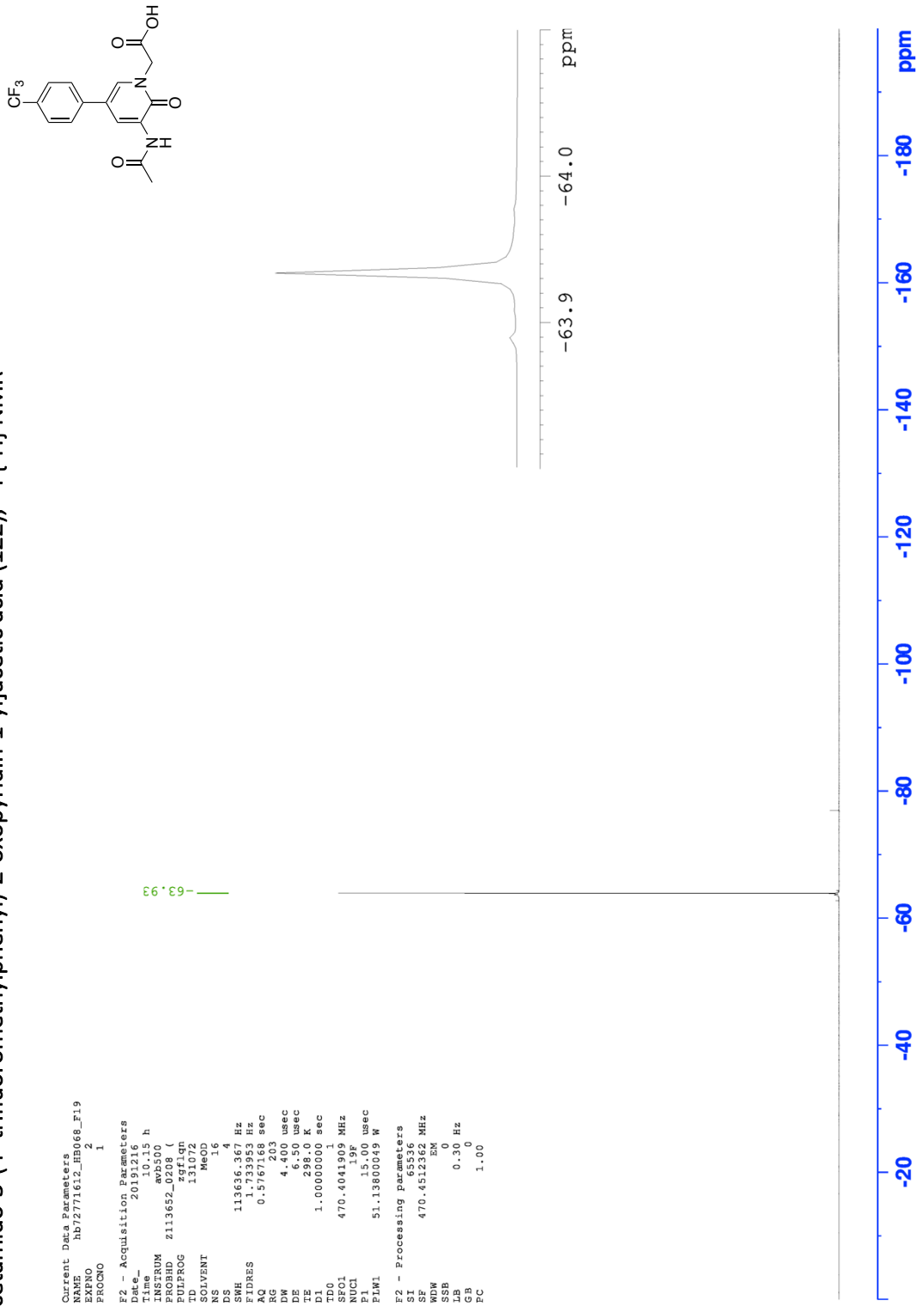
[3-Acetamido-5-(4'-trifluoromethylphenyl)-2-oxopyridin-1-yl]acetic acid (122), ^{1}H NMR



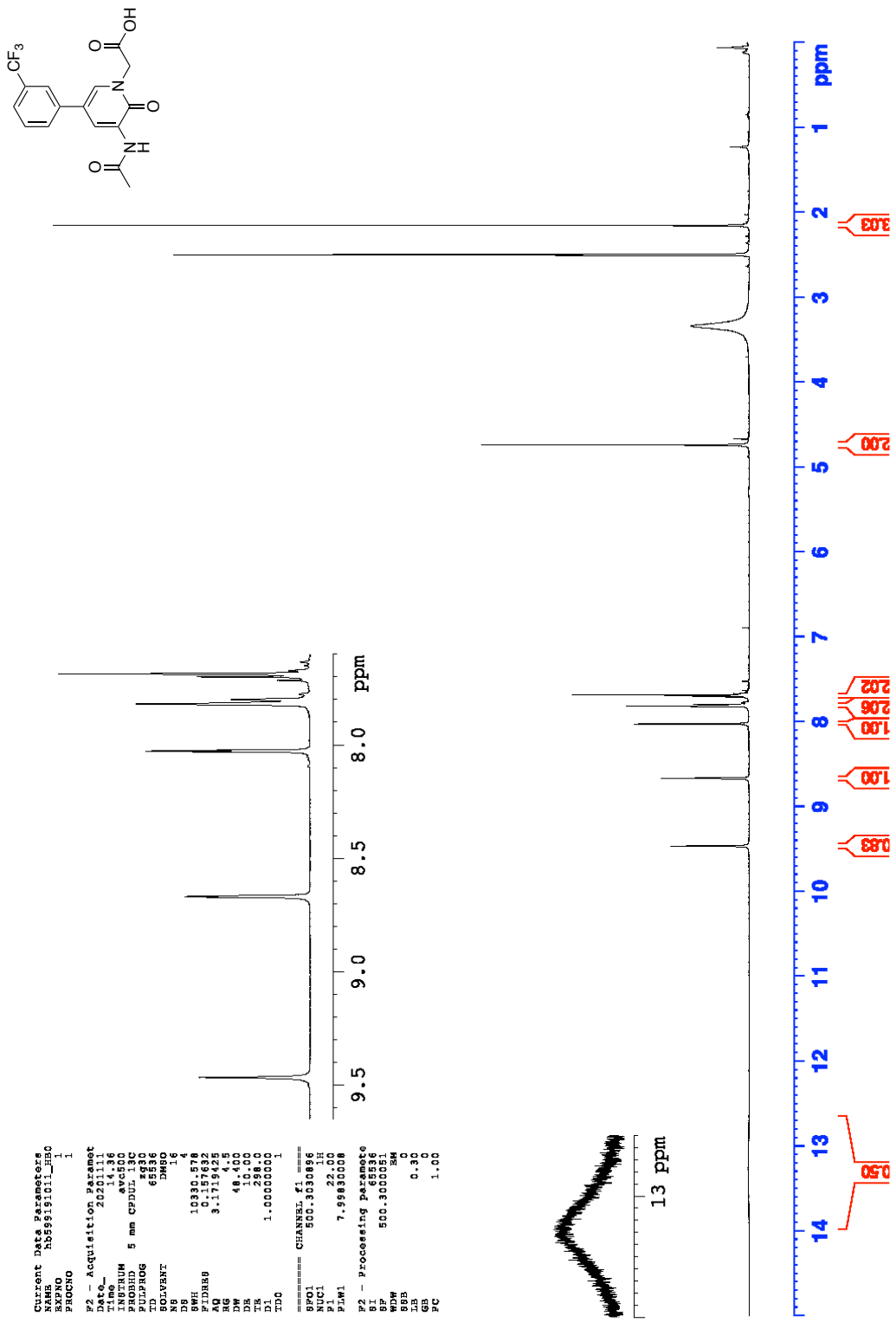
[3-Acetamido-5-(4'-trifluoromethylphenyl)-2-oxopyridin-1-yl]acetic acid (122), $^{13}C\{^{1}H\}$ NMR



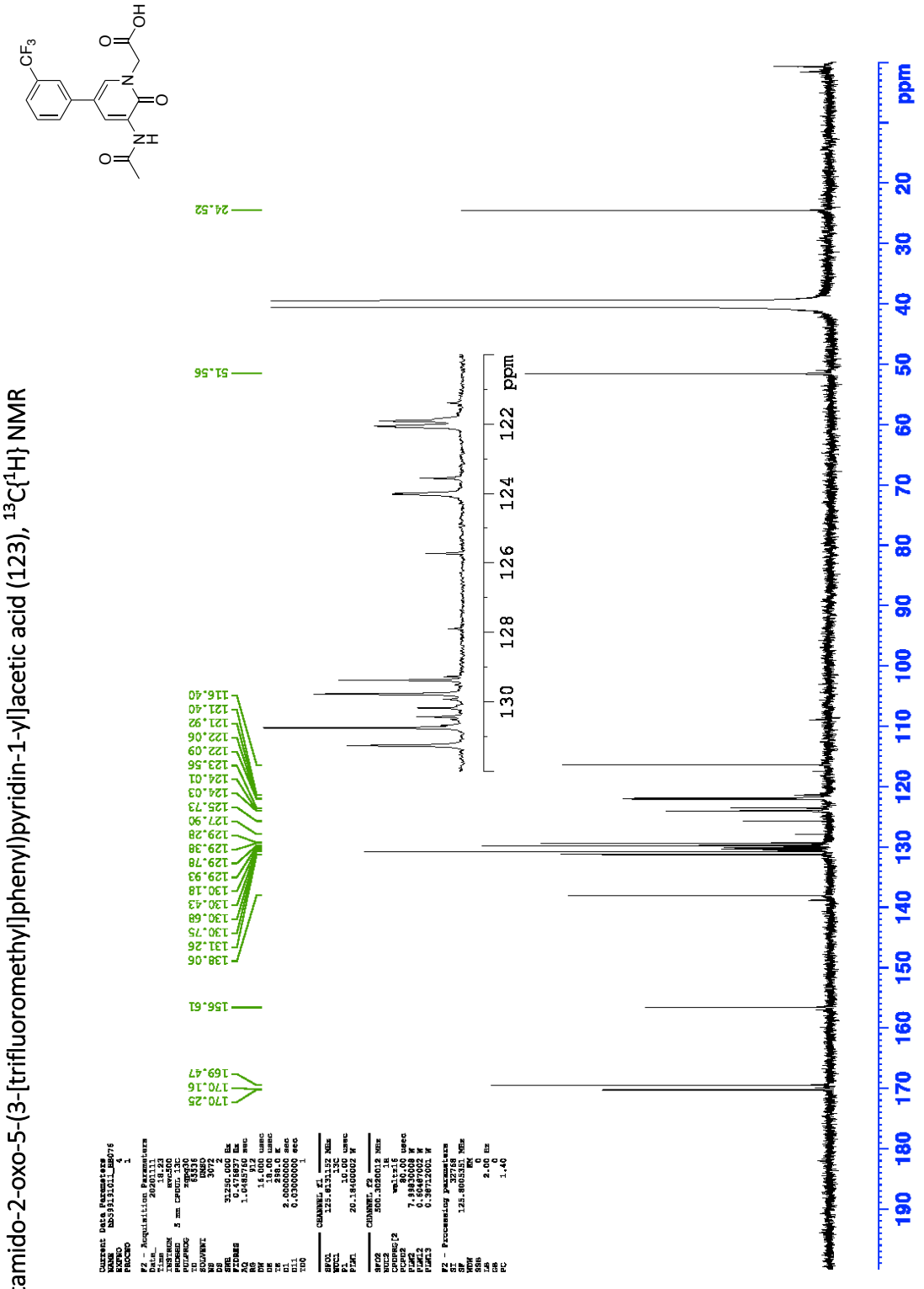
[3-Acetamido-5-(4'-trifluoromethylphenyl)-2-oxopyridin-1-yl]acetic acid (122), $^{19}F\{^{1}H\}$ NMR



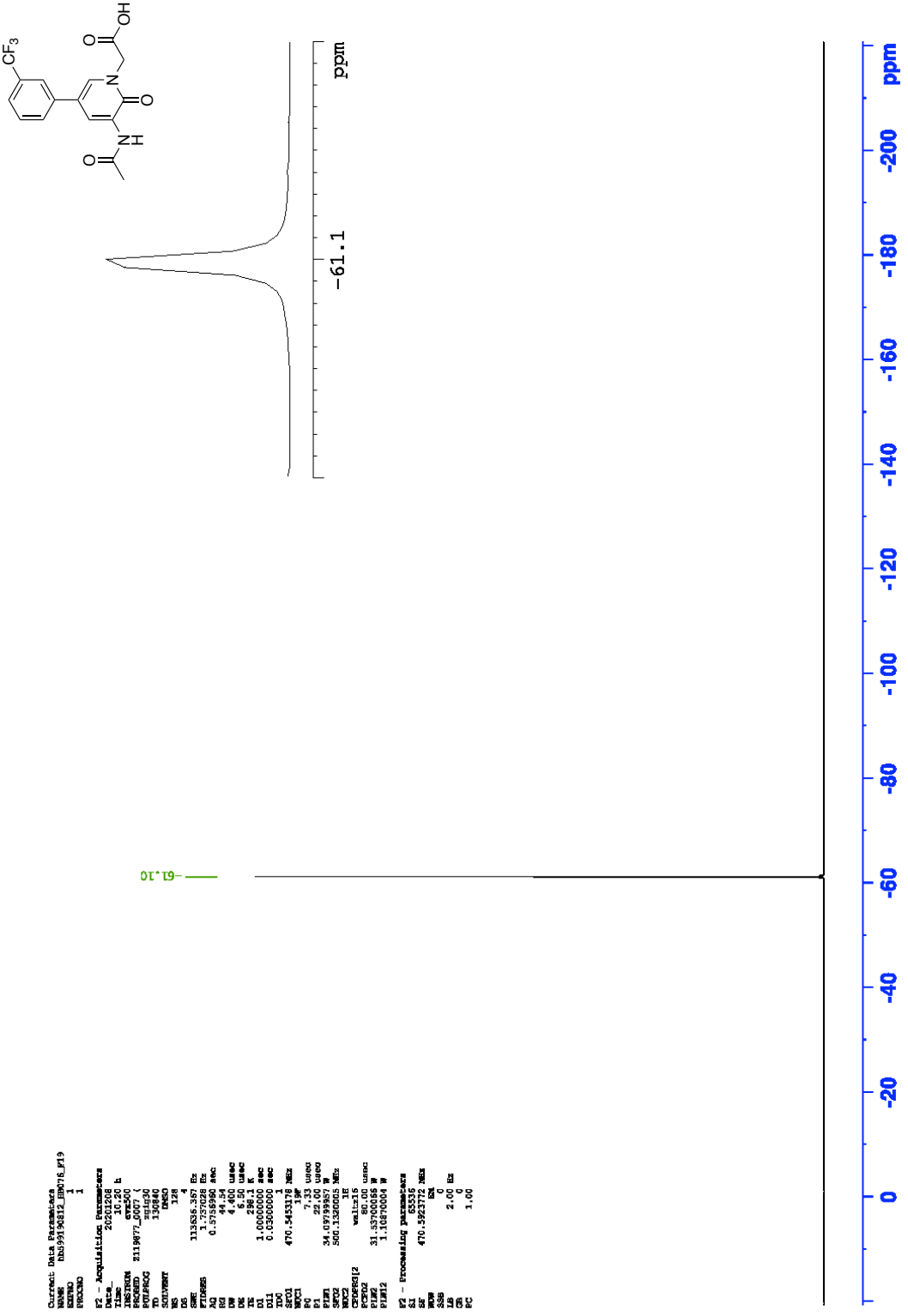
[3-Acetamido-2-oxo-5-(3-[trifluoromethyl]phenyl)pyridin-1-yl]acetic acid (123), ^{1}H NMR



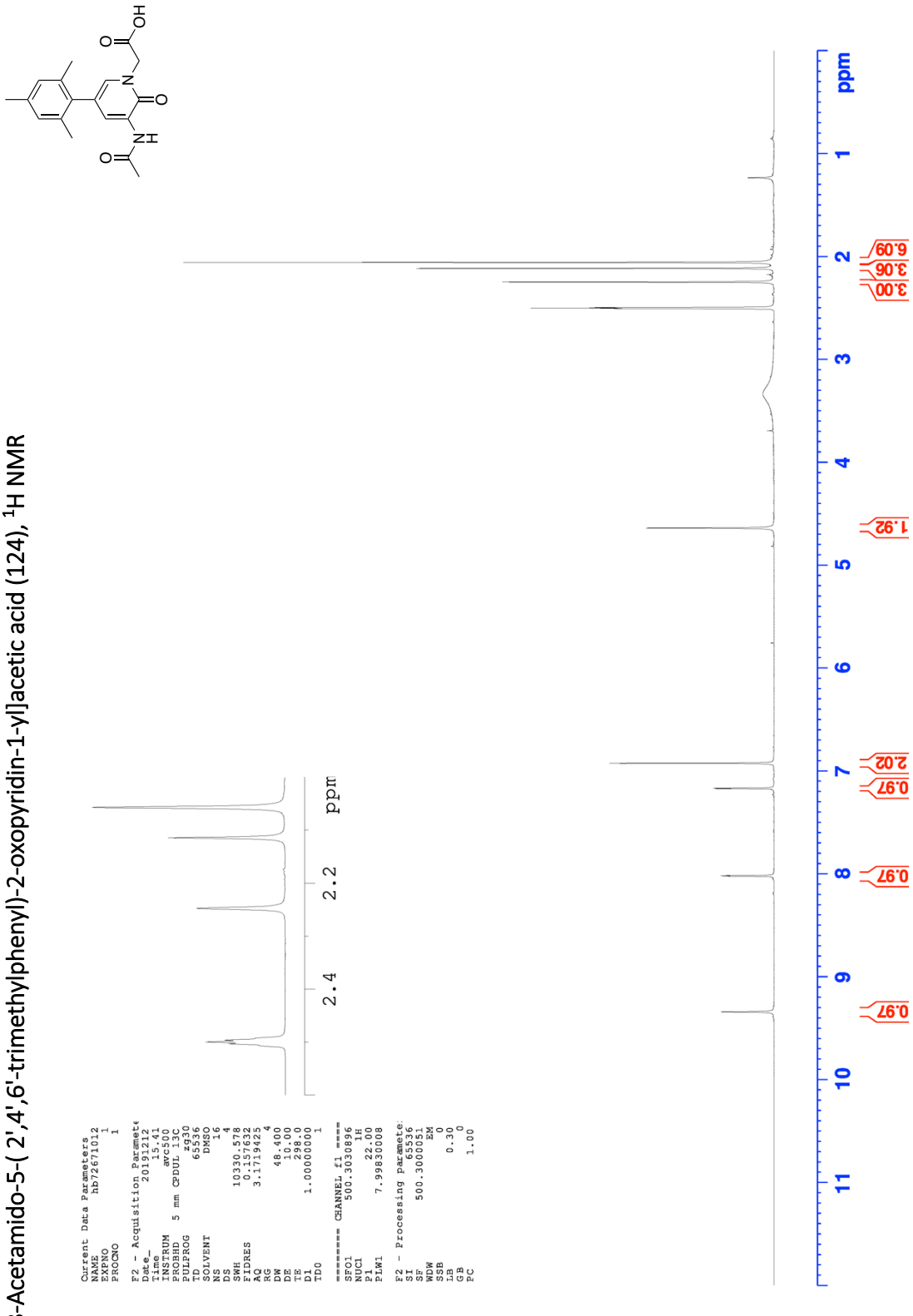
[3-Acetamido-2-oxo-5-(3-[trifluoromethyl]phenyl)pyridin-1-yl]acetic acid (123), $^{13}C\{^{1}H\}$ NMR



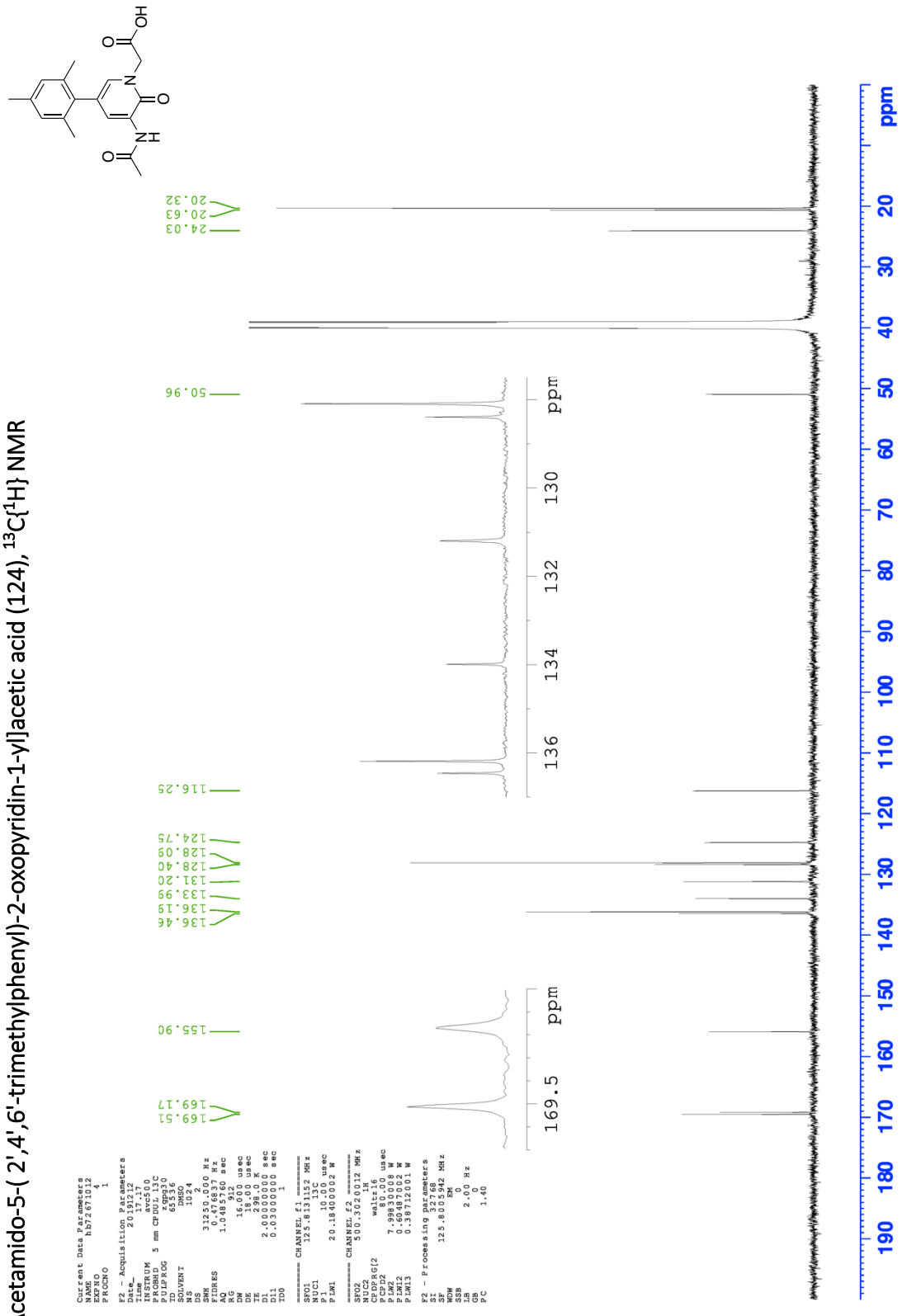
[3-Acetamido-2-oxo-5-(3-[trifluoromethyl]phenyl)pyridin-1-yl]acetic acid (123), $^{19}F\{^{1}H\}$ NMR



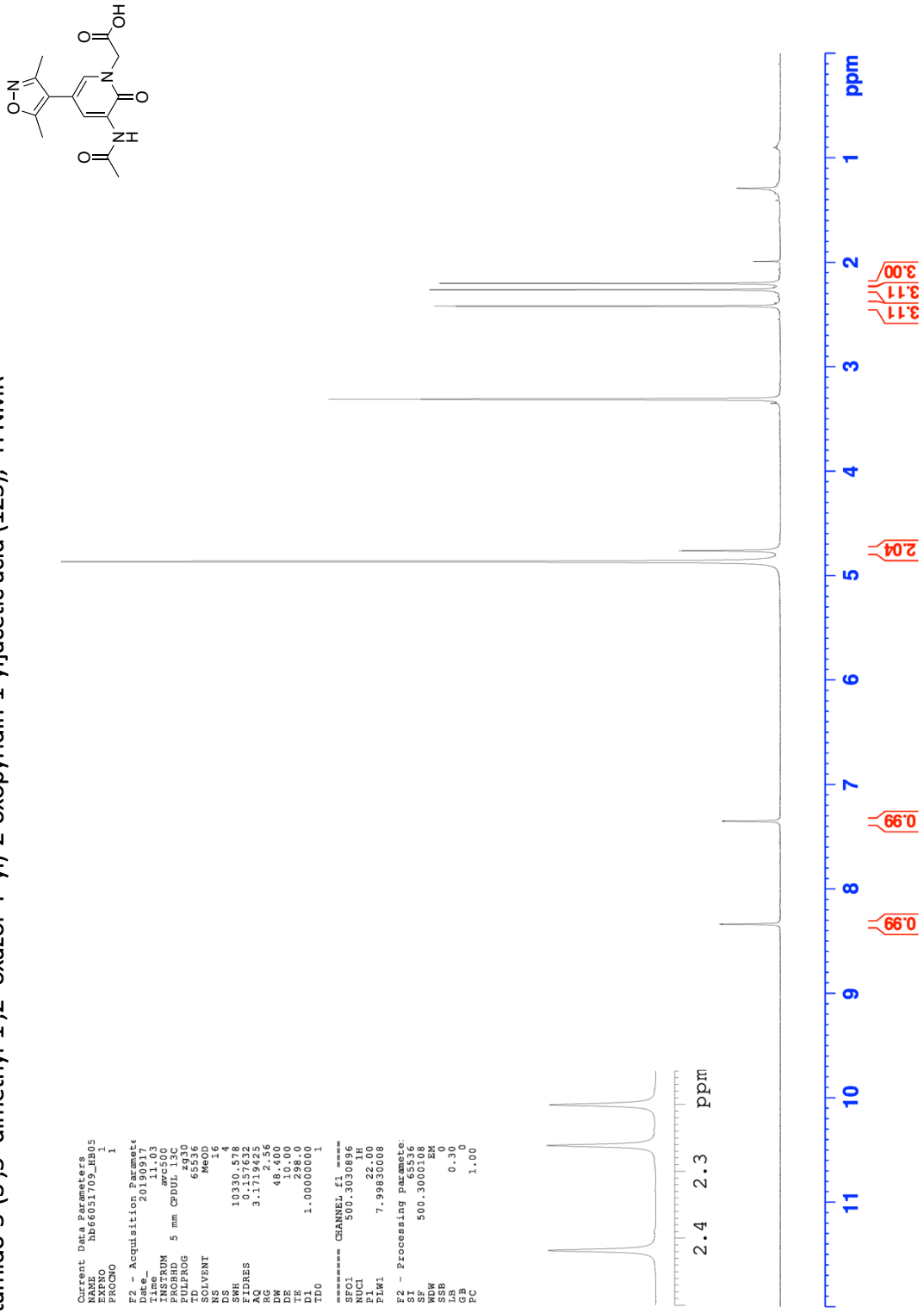
[3-Acetamido-5-(2',4',6'-trimethylphenyl)-2-oxopyridin-1-yl]acetic acid (124), ^{1}H NMR



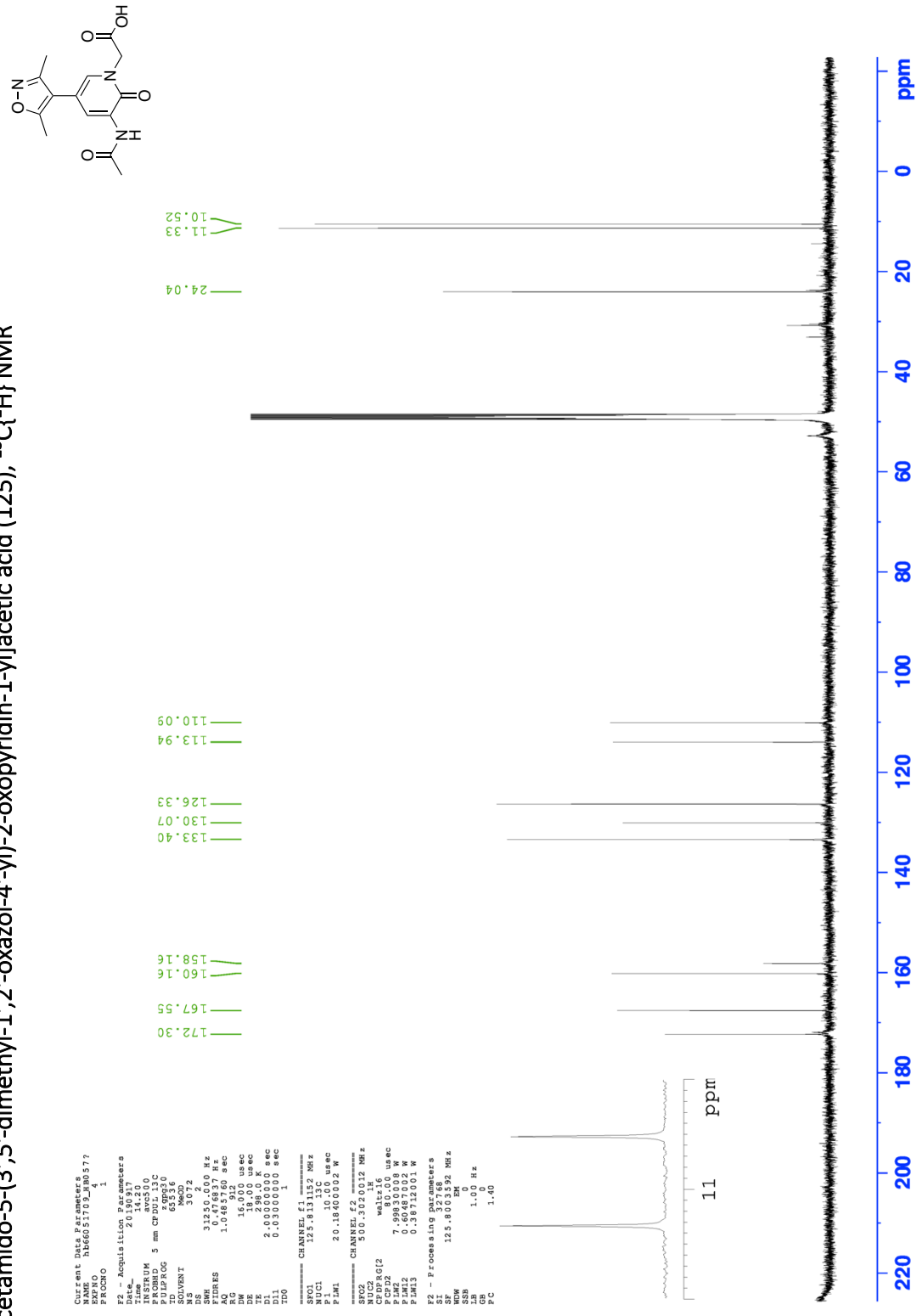
[3-Acetamido-5-(2',4',6'-trimethylphenyl)-2-oxopyridin-1-yl]acetic acid (124), $^{13}C\{^{1}H\}$ NMR



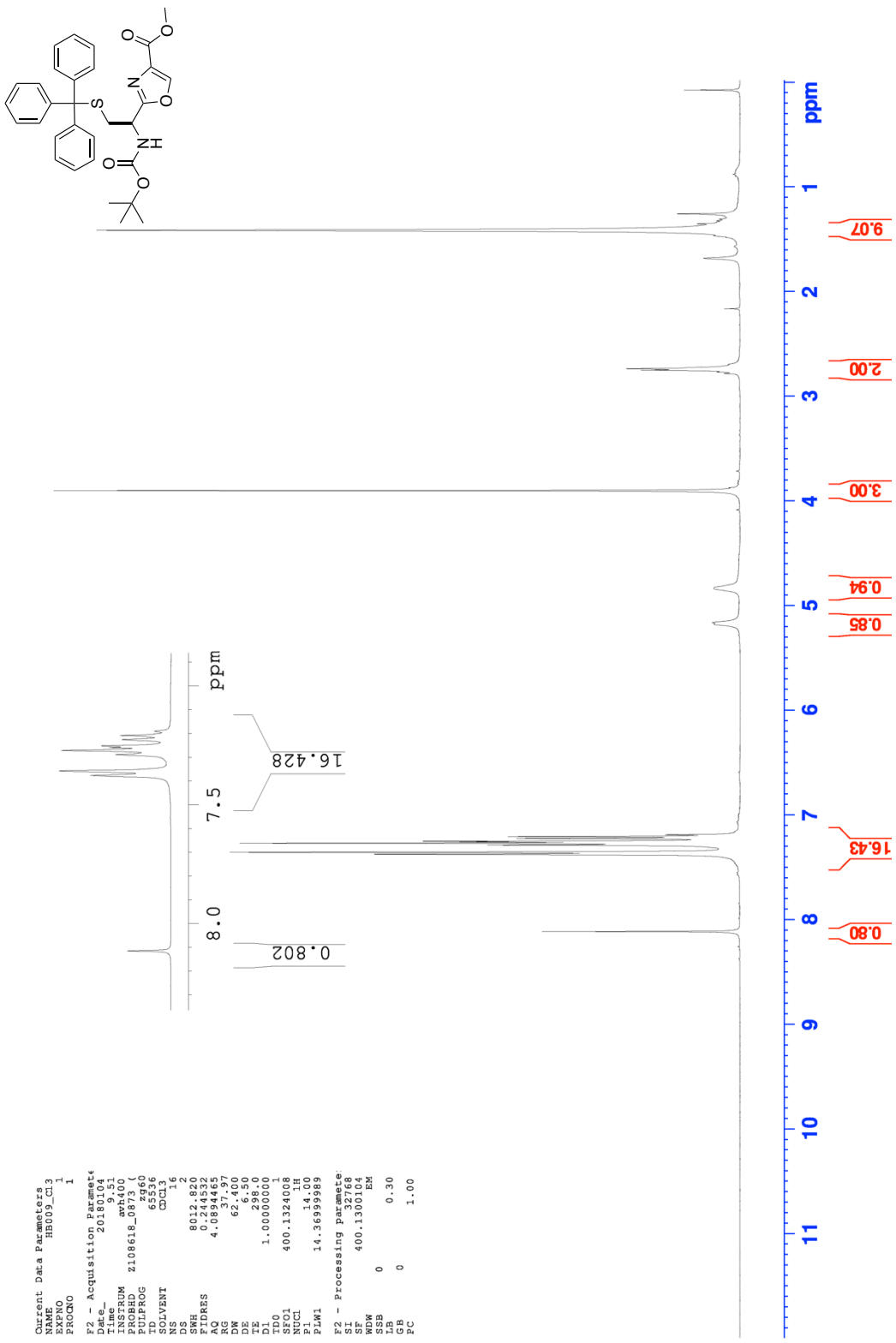
[3-Acetamido-5-(3',5'-dimethyl-1',2'-oxazol-4'-yl)-2-oxopyridin-1-yl]acetic acid (125), ^{1}H NMR



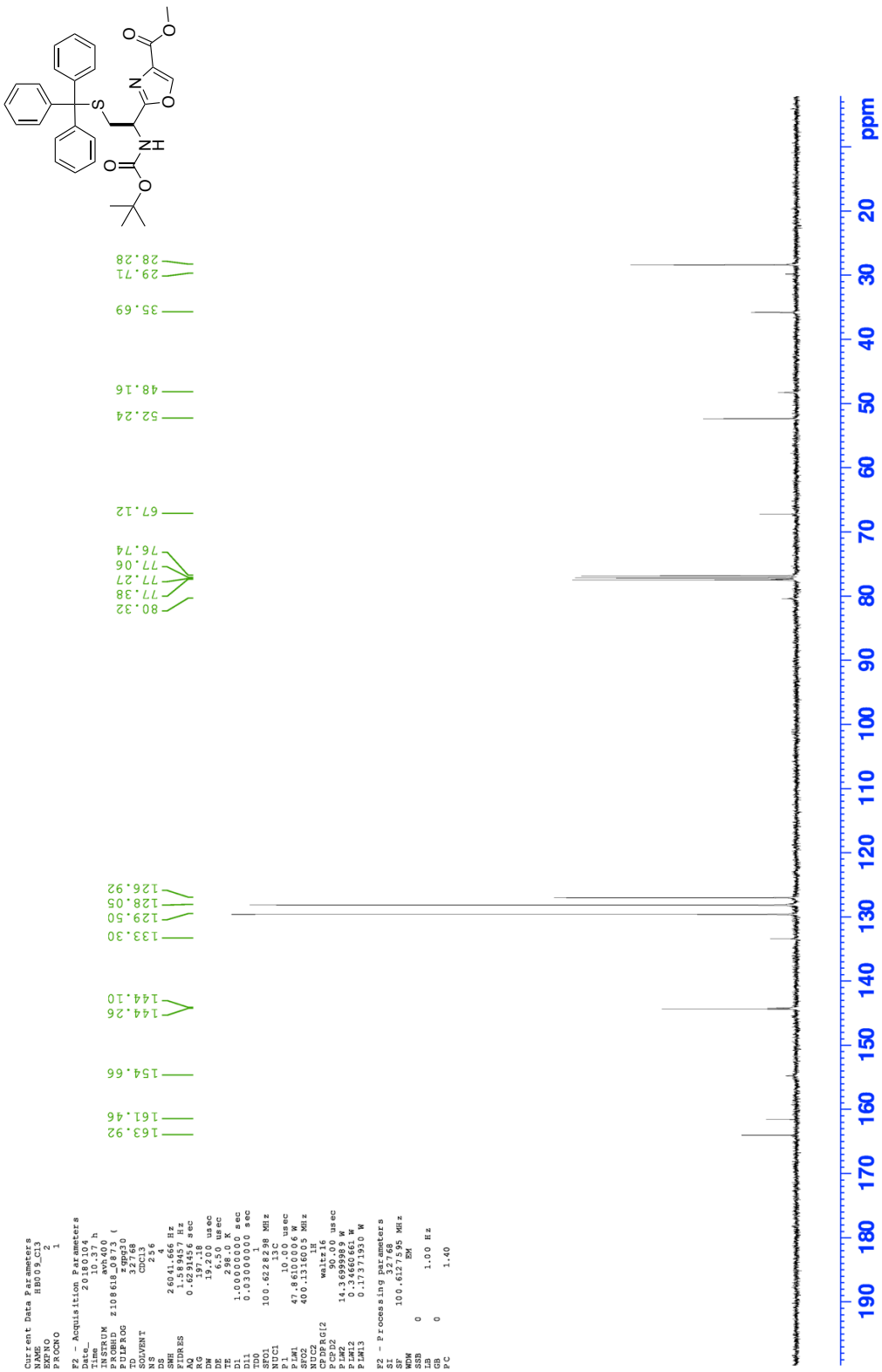
[3-Acetamido-5-(3',5'-dimethyl-1',2'-oxazol-4'-yl)-2-oxopyridin-1-yl]acetic acid (125), $^{13}C\{^{1}H\}$ NMR



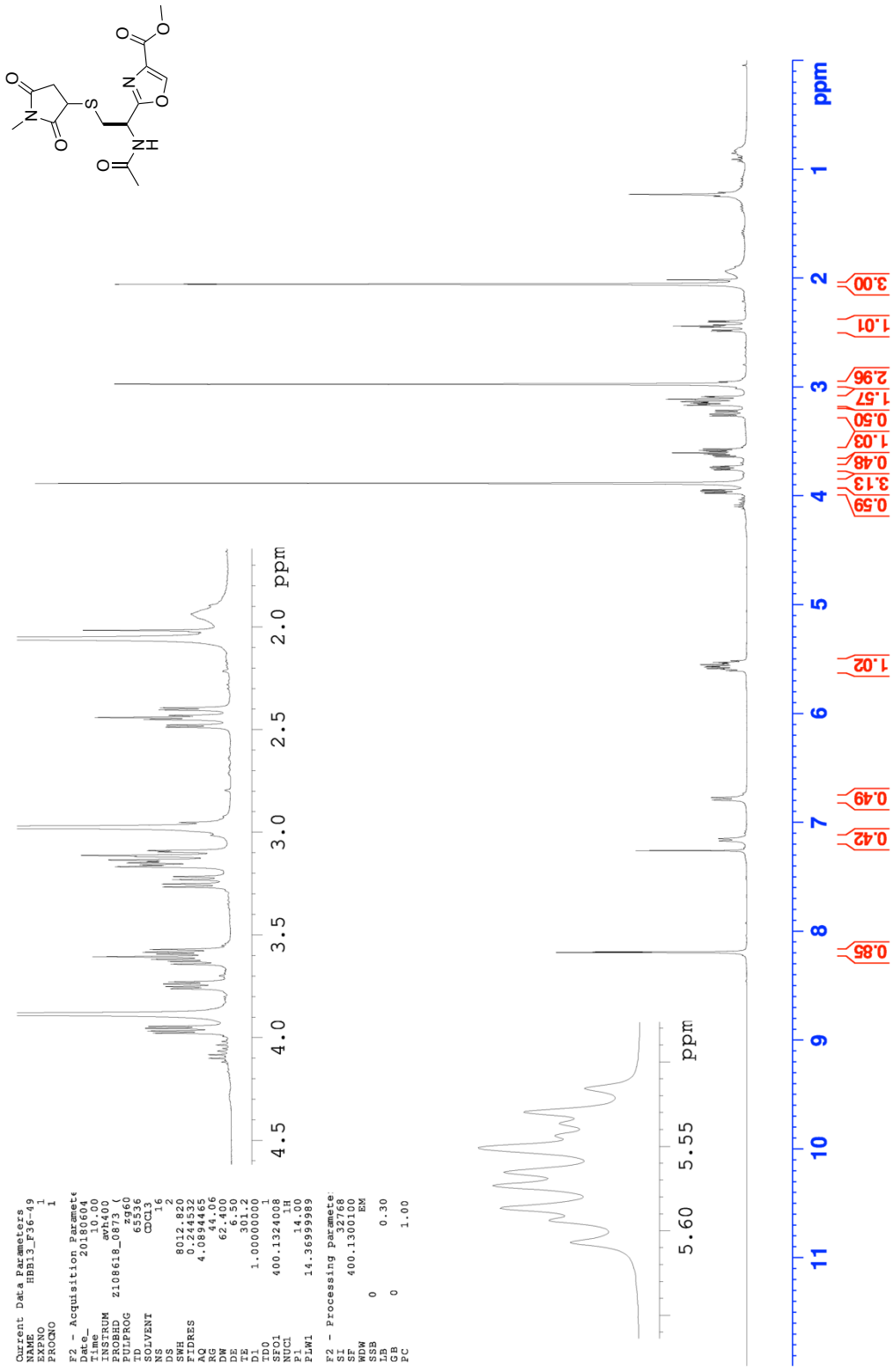
Methyl 2-{(1'*R*)-1'-[(*tert*-butoxycarbonyl)amino]-2'-[(triphenylmethyl)sulfanyl]ethyl}-1,3-oxazole-4-carboxylate (152), ^{1}H NMR



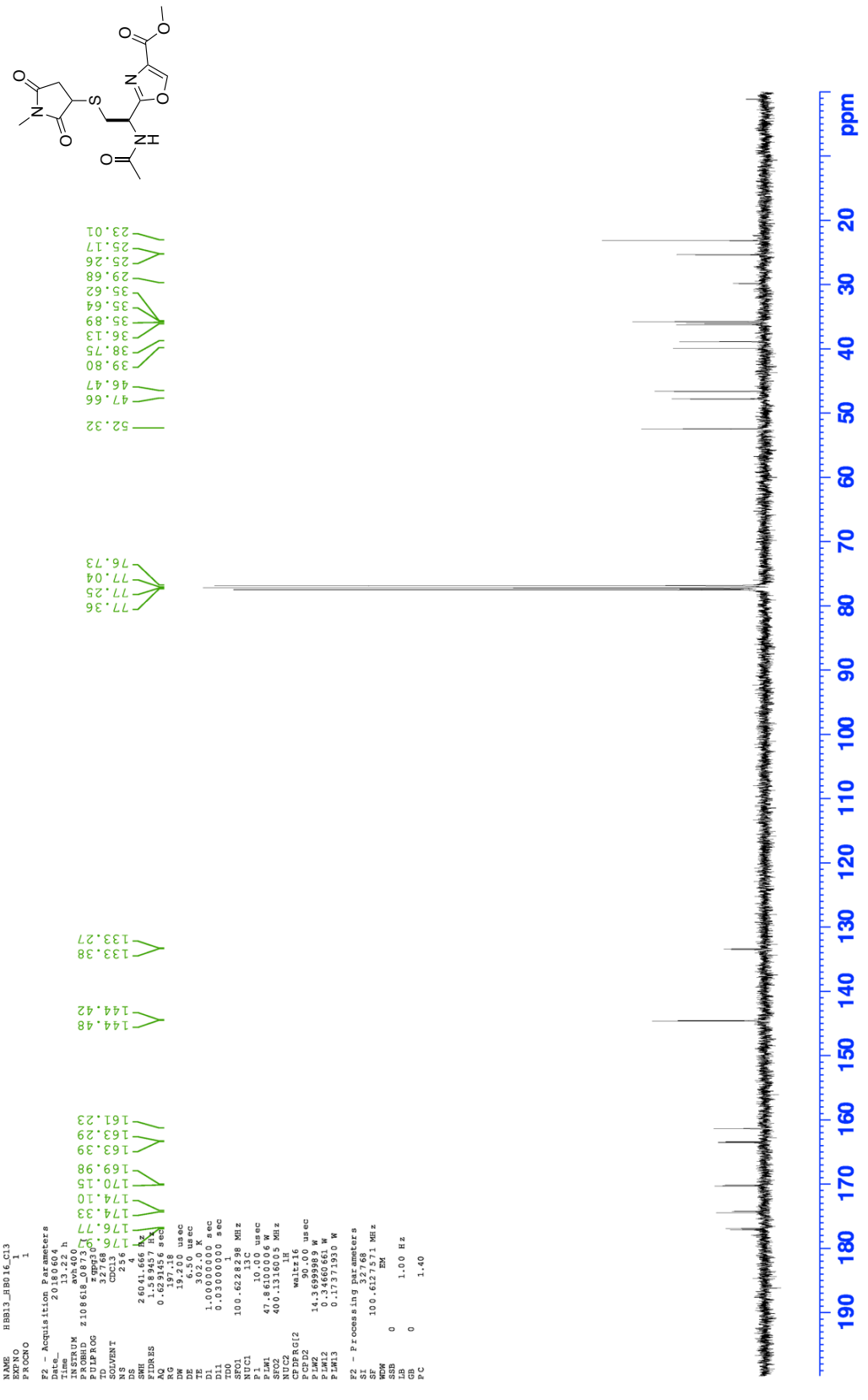
Methyl 2-{(1*R*)-1'-[(*tert*-butoxycarbonyl)amino]-2'-[(triphenylmethyl)sulfanyl]ethyl}-1,3-oxazole-4-carboxylate (152), $^{13}C\{^{1}H\}$ NMR



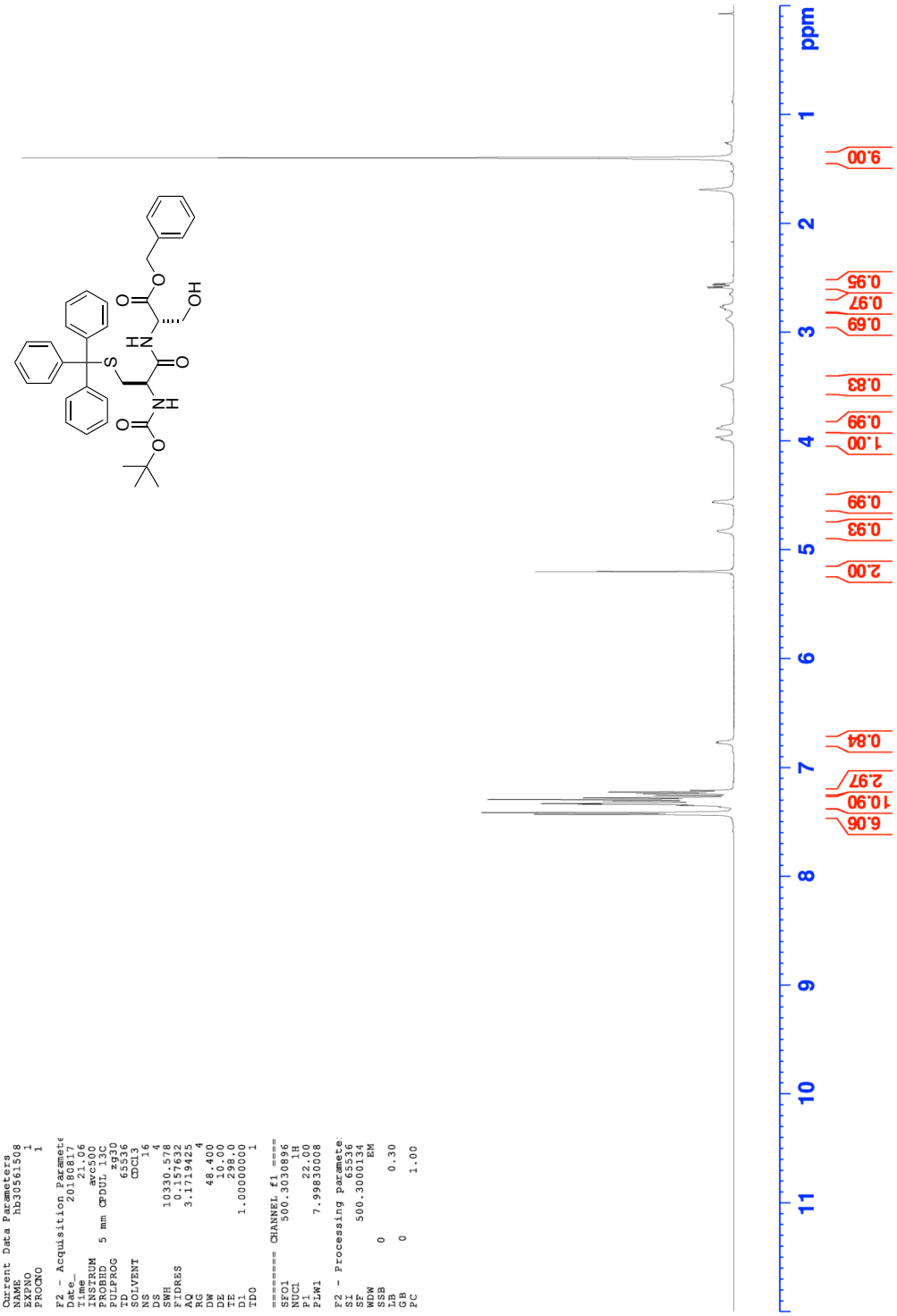
Methyl 2-{(1'*R*)-1'-acetamido-2'-[(1''-methyl-2'',5''-dioxopyrrolidin-3''-yl)sulfanyl]ethyl}-1,3-oxazole-4-carboxylate (148), ^{1}H NMR



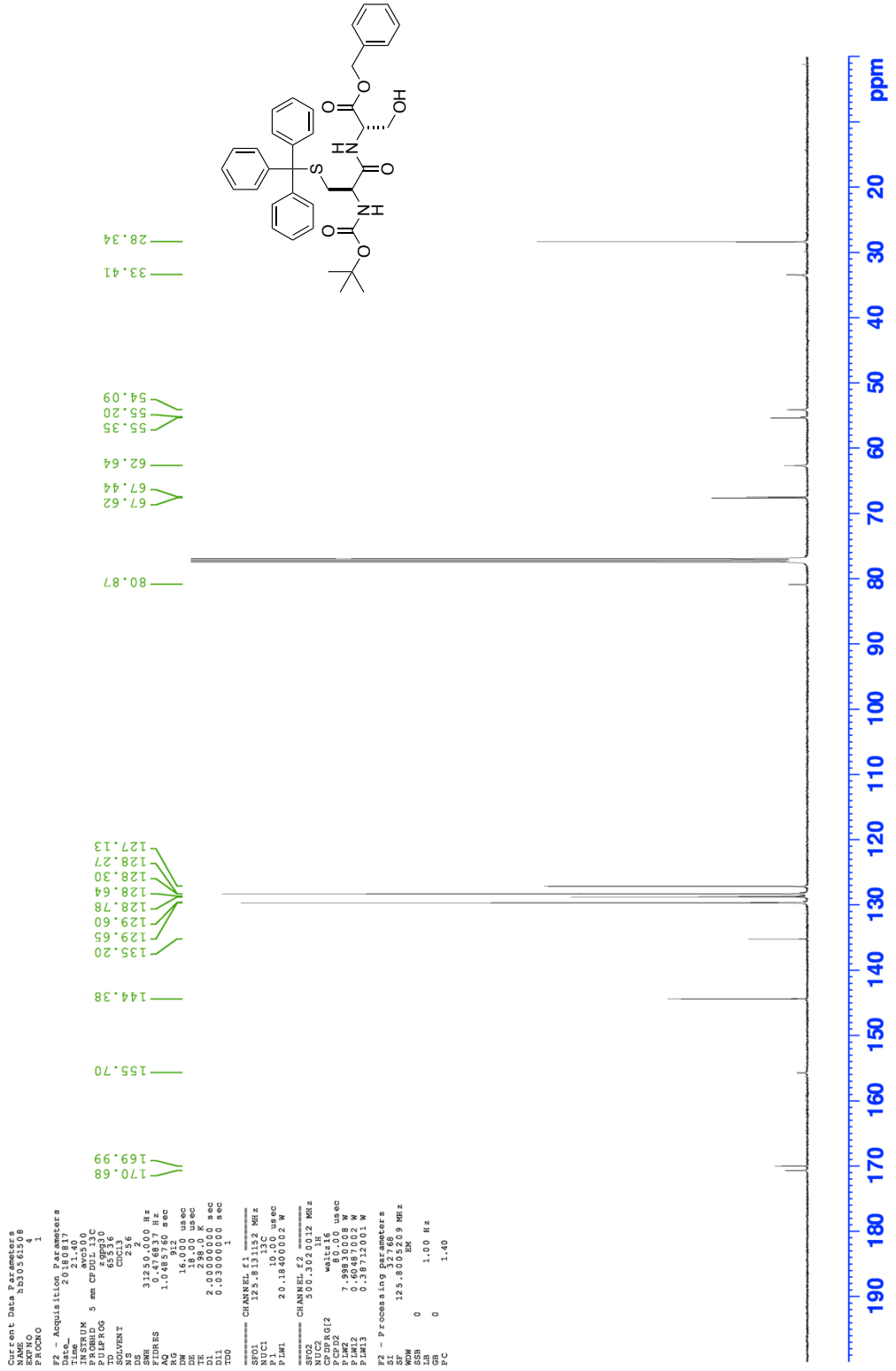
Methyl 2-{(1'*R*)-1'-acetamido-2'-[(1''-methyl-2'',5''-dioxopyrrolidin-3''-yl)sulfanyl]ethyl}-1,3-oxazole-4-carboxylate (148), $^{13}C\{^{1}H\}$ NMR



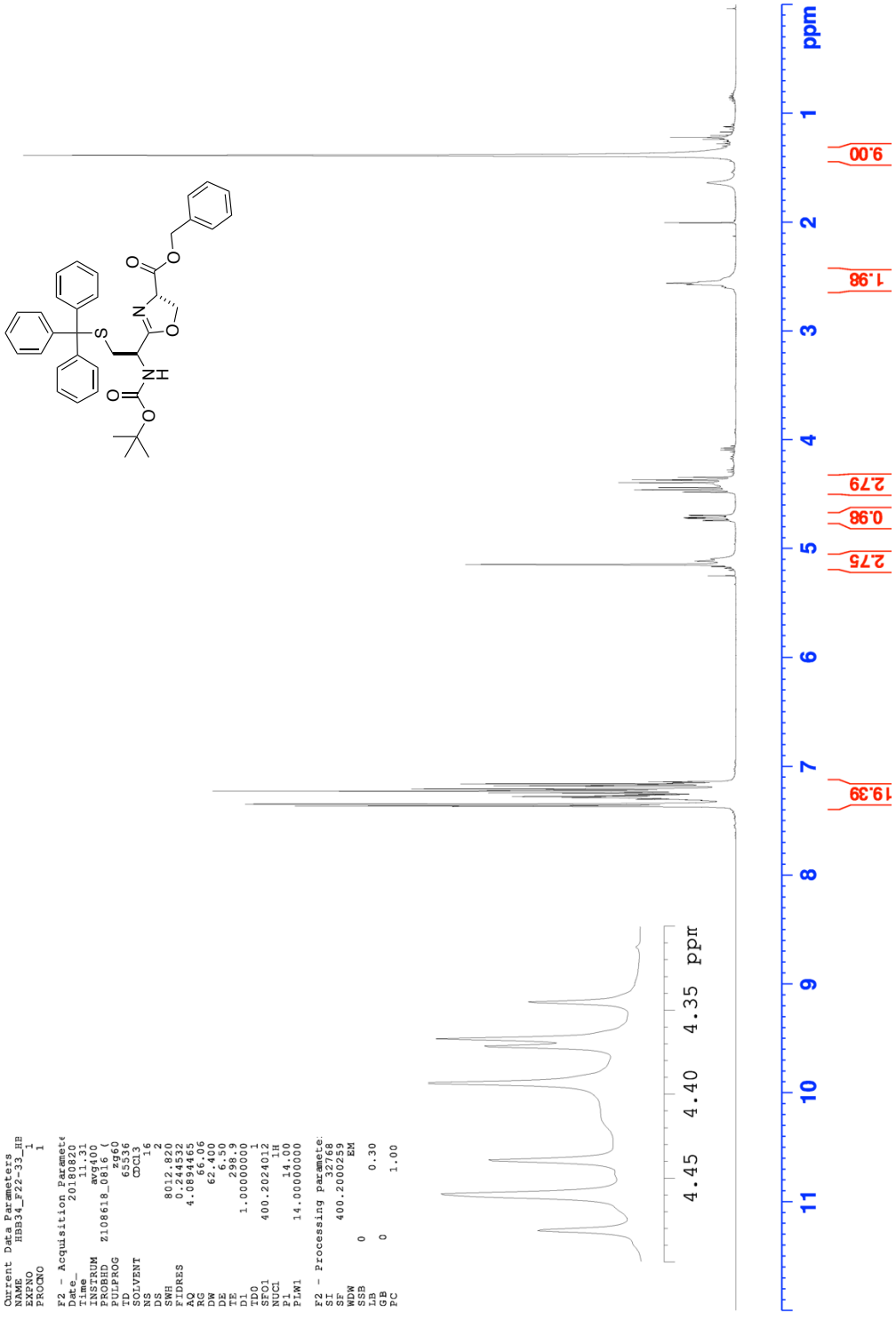
Benzyl *N*-(*tert*-butoxycarbonyl)-(*R*)-(triphenylmethyl)cysteinyl-(*S*)-serinate (161), ^{1}H NMR



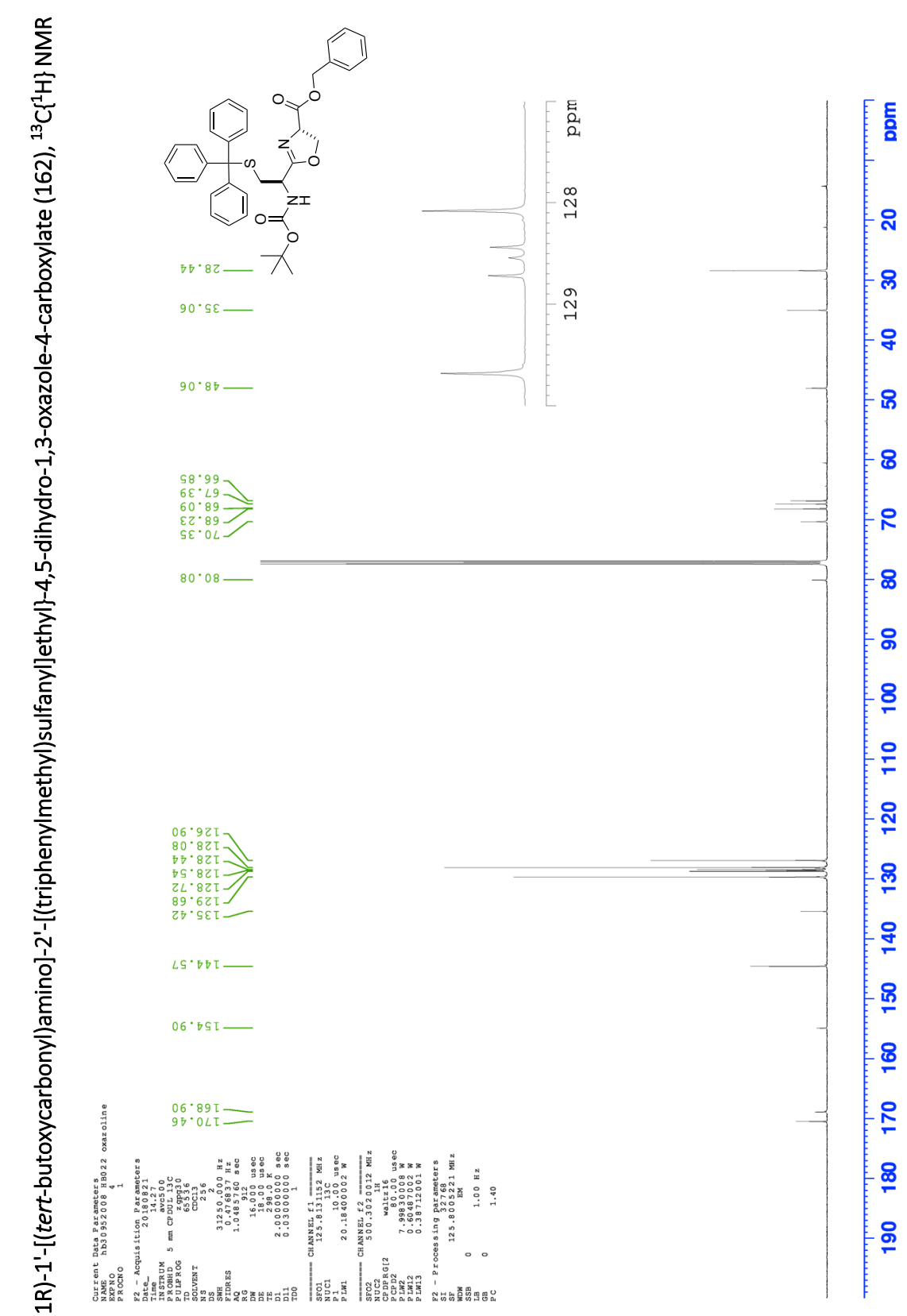
Benzyl *N*-(*tert*-butoxycarbonyl)-(*R*)-(triphenylmethyl)cysteinyl-(*S*)-serinate (161), $^{13}C\{^{1}H\}$ NMR



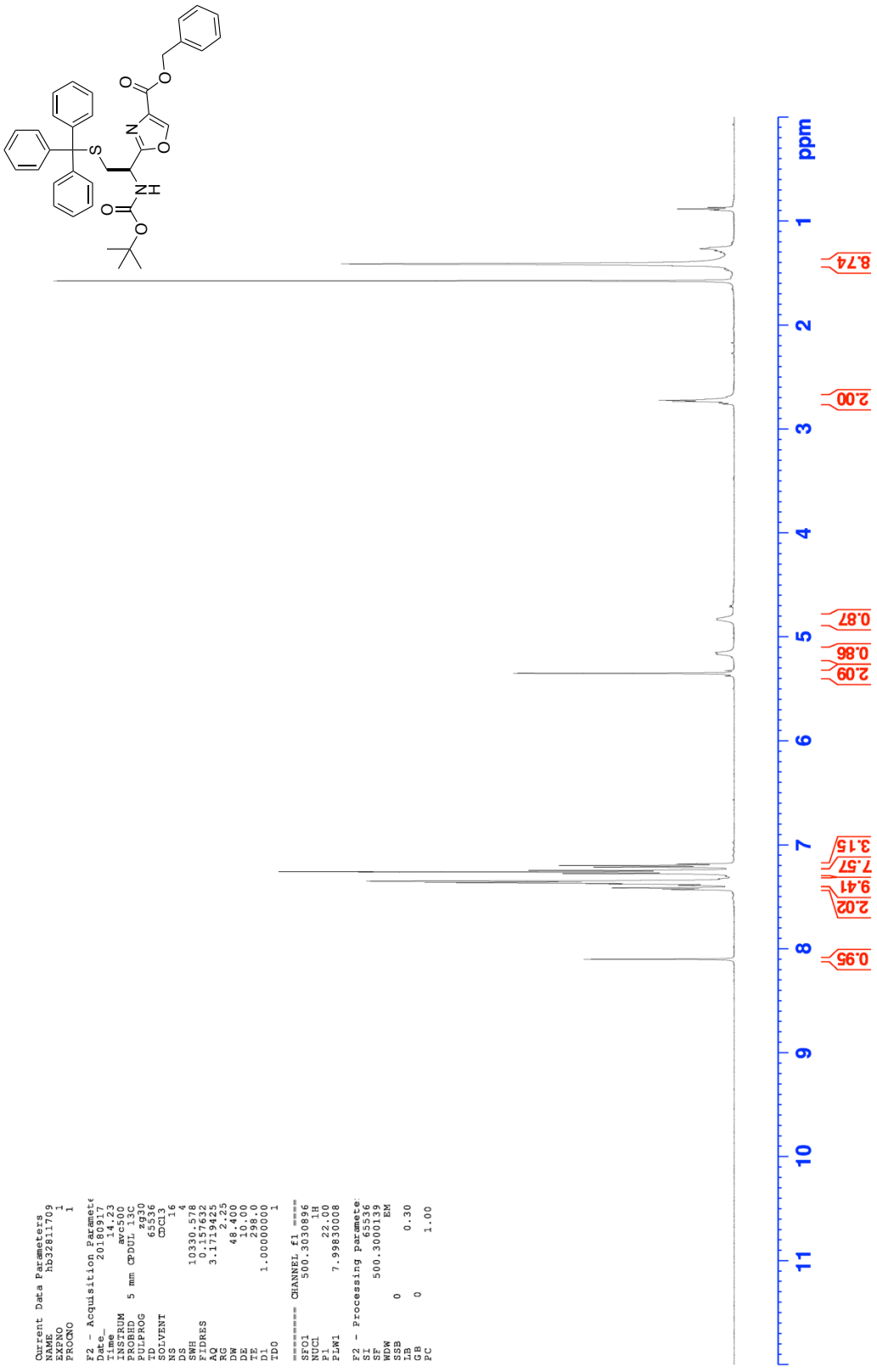
Benzyl 2-{(1'R)-1'-[(*tert*-butoxycarbonyl)amino]-2'-[(triphenylmethyl)sulfanyl]ethyl}-4,5-dihydro-1,3-oxazole-4-carboxylate (162), ^{1}H NMR



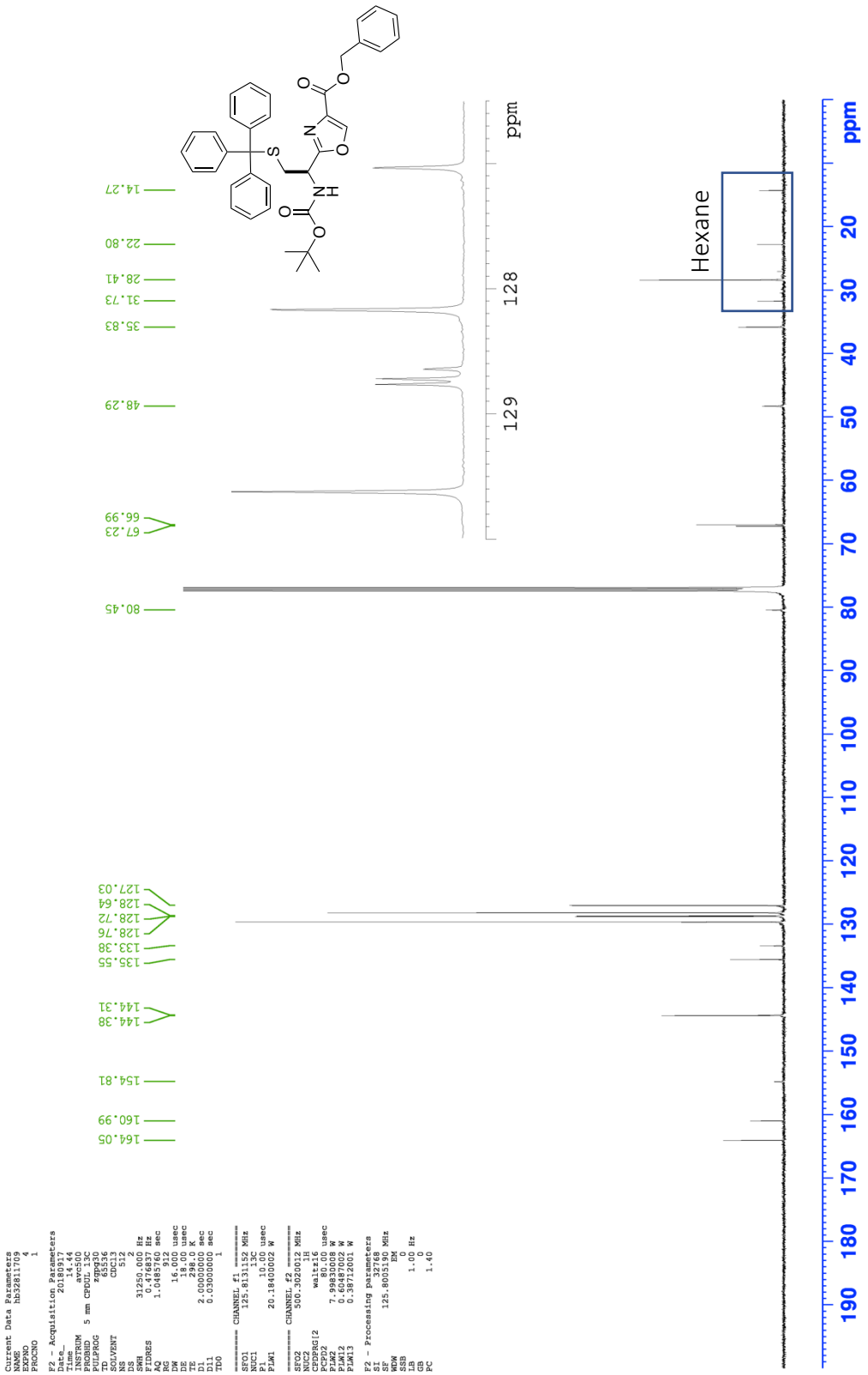
Benzyl 2-{(1R)-1'-[(*tert*-butoxycarbonyl)amino]-2'-[(triphenylmethyl)sulfanyl]ethyl}-4,5-dihydro-1,3-oxazole-4-carboxylate (162), $^{13}C\{^{1}H\}$ NMR



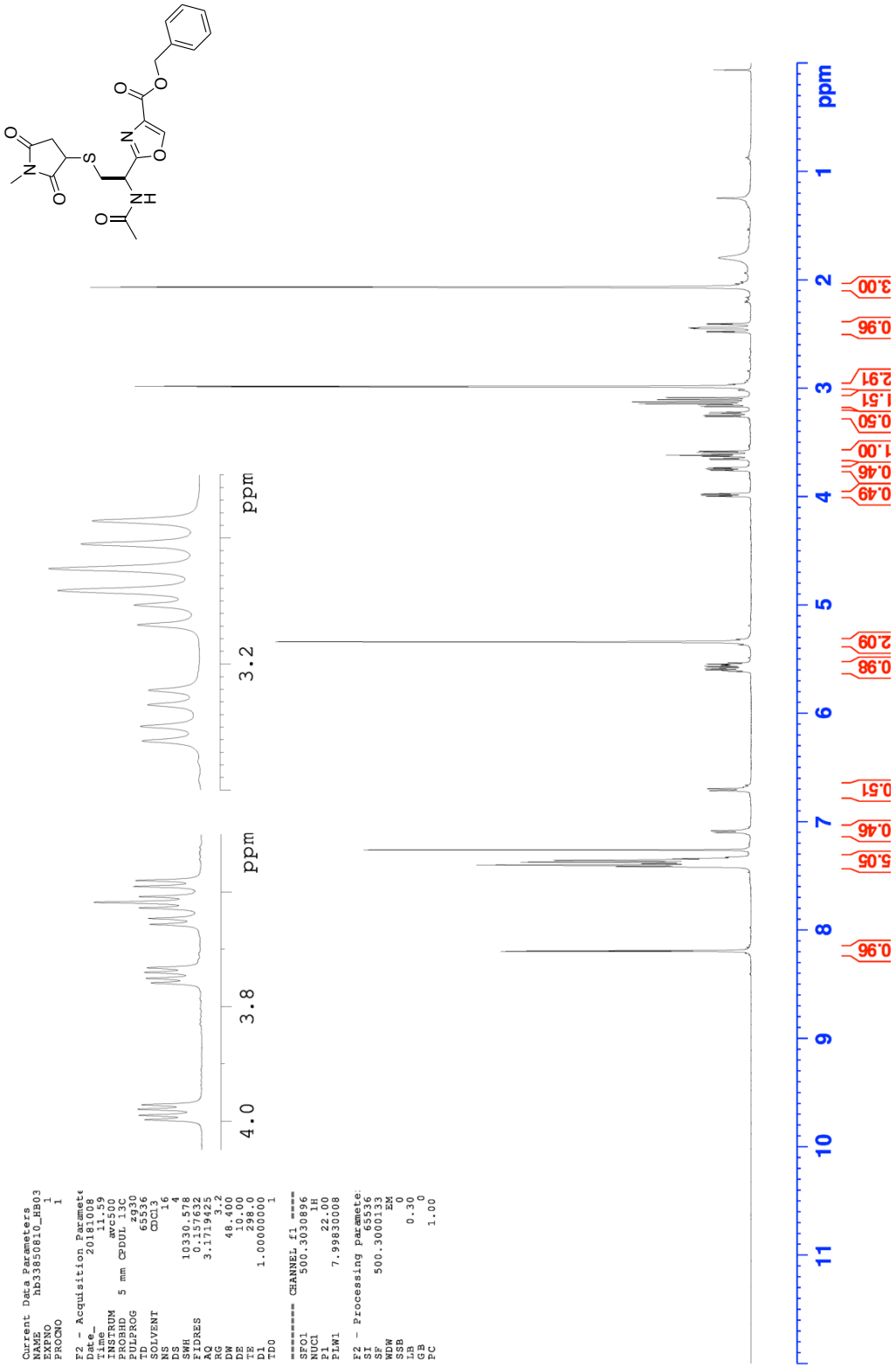
Benzyl 2-{(1'R)-1'-[(*tert*-butoxycarbonyl)amino]-2'-[(triphenylmethyl)sulfanyl]ethyl}-1,3-oxazole-4-carboxylate (163), ^{1}H NMR



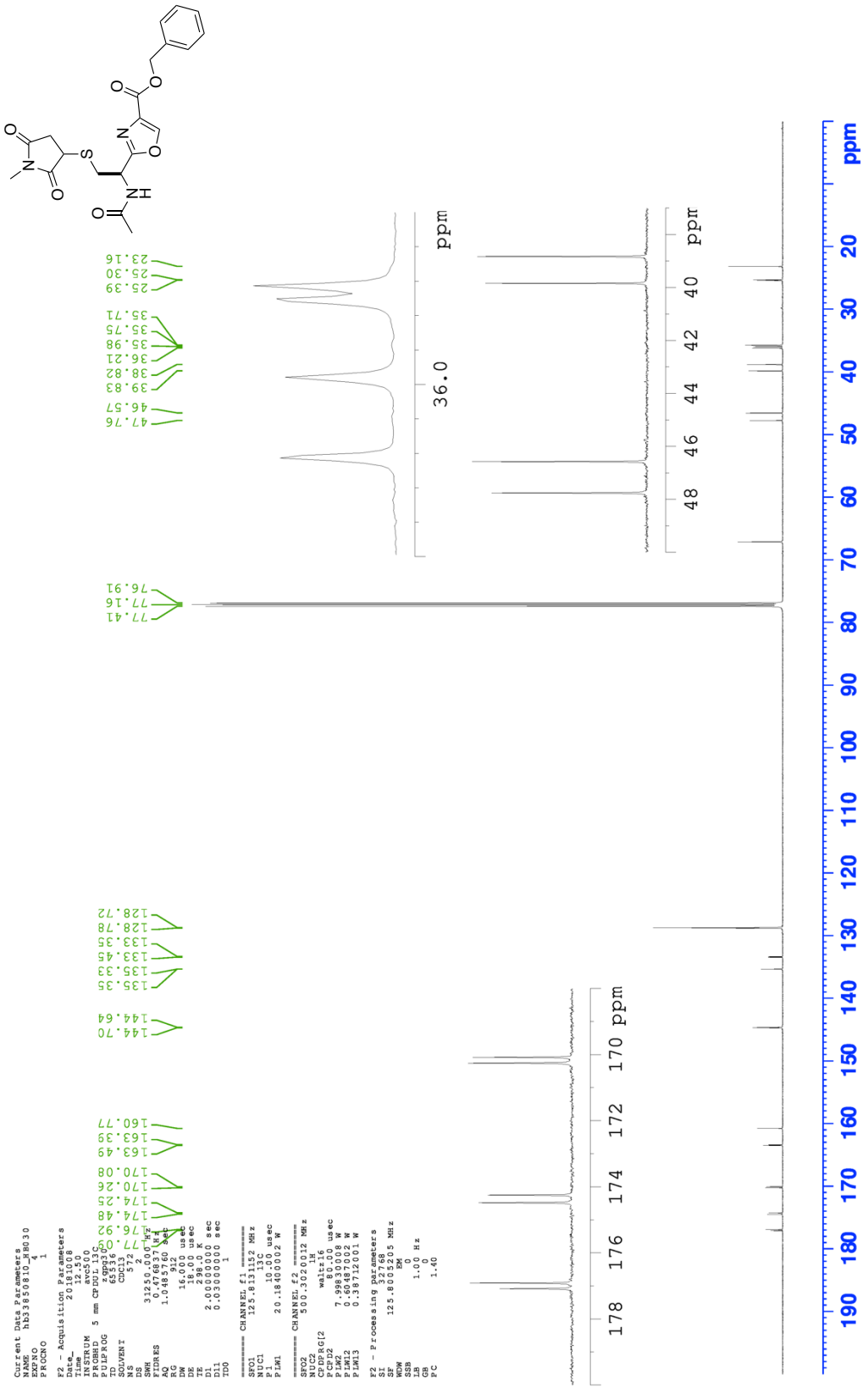
Benzyl 2-{(1'R)-1'-[(*tert*-butoxycarbonyl)amino]-2'-[(triphenylmethyl)sulfanyl]ethyl}-1,3-oxazole-4-carboxylate (163), $^{13}C\{^{1}H\}$ NMR



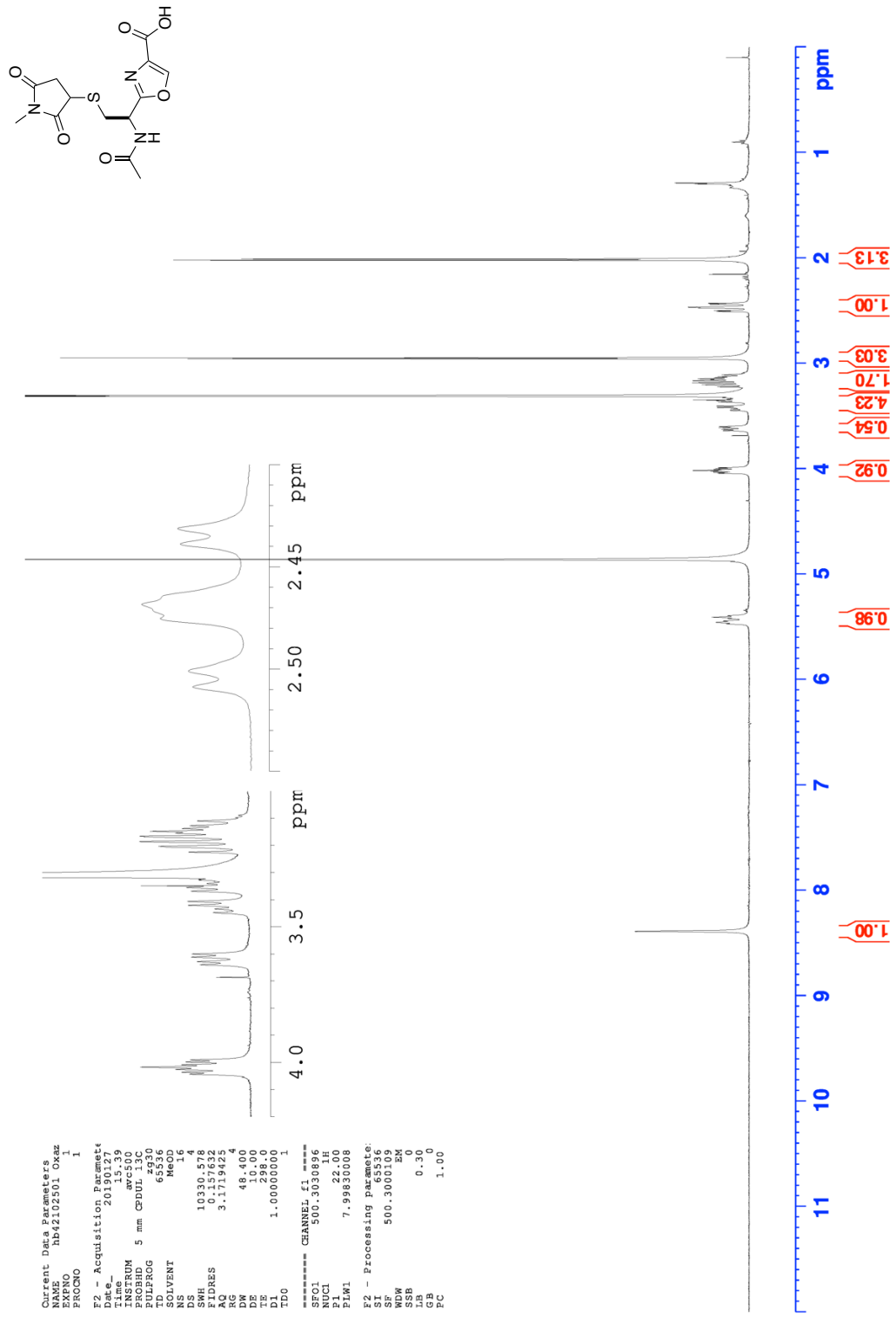
Benzyl 2'-{(1'*R*)-1'-acetamido-2'-[(1''-methyl-2'',5''-dioxopyrrolidin-3''-yl)sulfanyl]ethyl}-1,3-oxazole-4-carboxylate (164), ^{1}H NMR



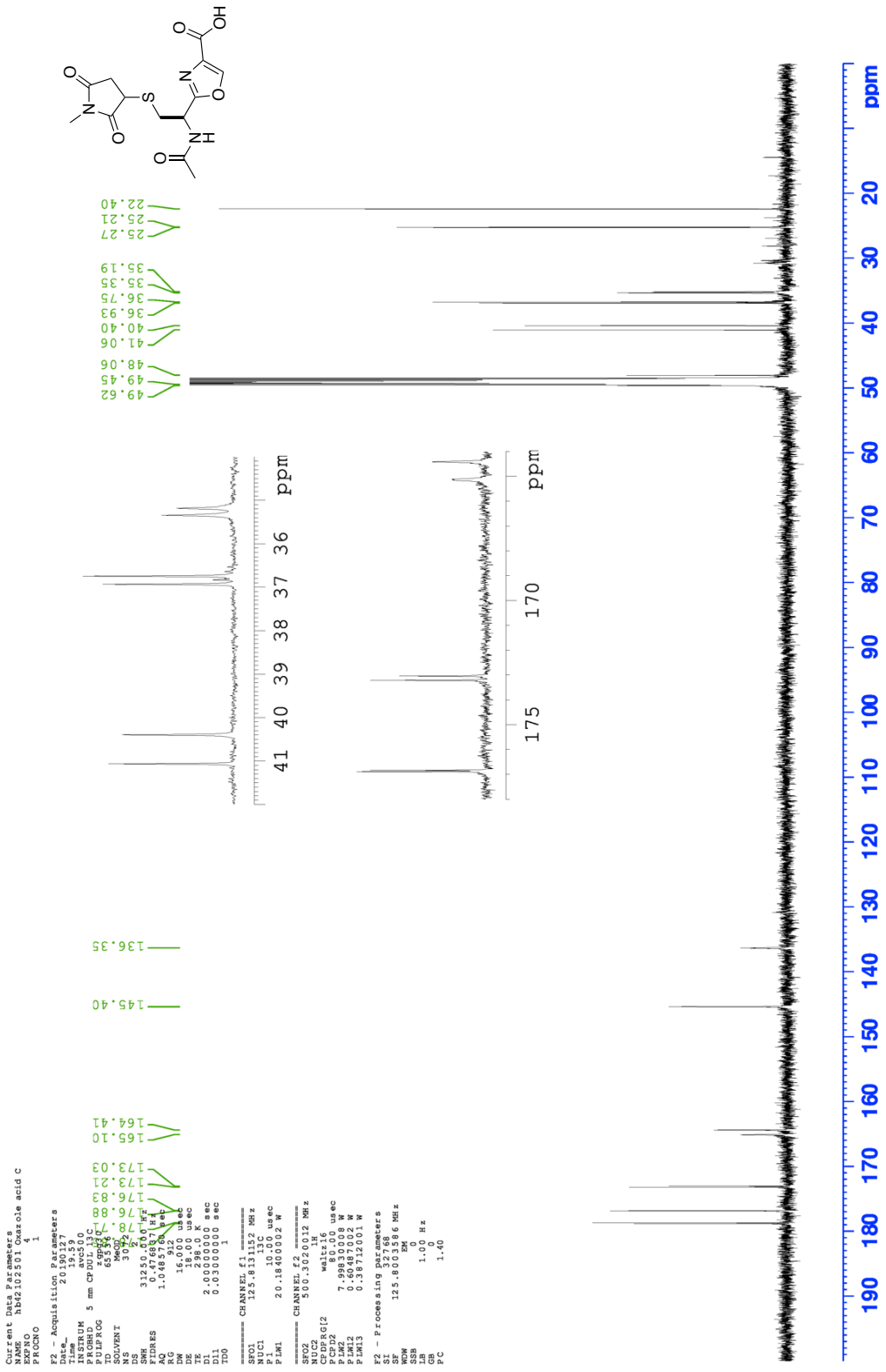
Benzyl 2'-[(1'*R*)-1'-acetamido-2'-[(1''-methyl-2'',5''-dioxopyrrolidin-3''-yl)sulfanyl]ethyl]-1,3-oxazole-4-carboxylate (164), $^{13}C\{^{1}H\}$ NMR



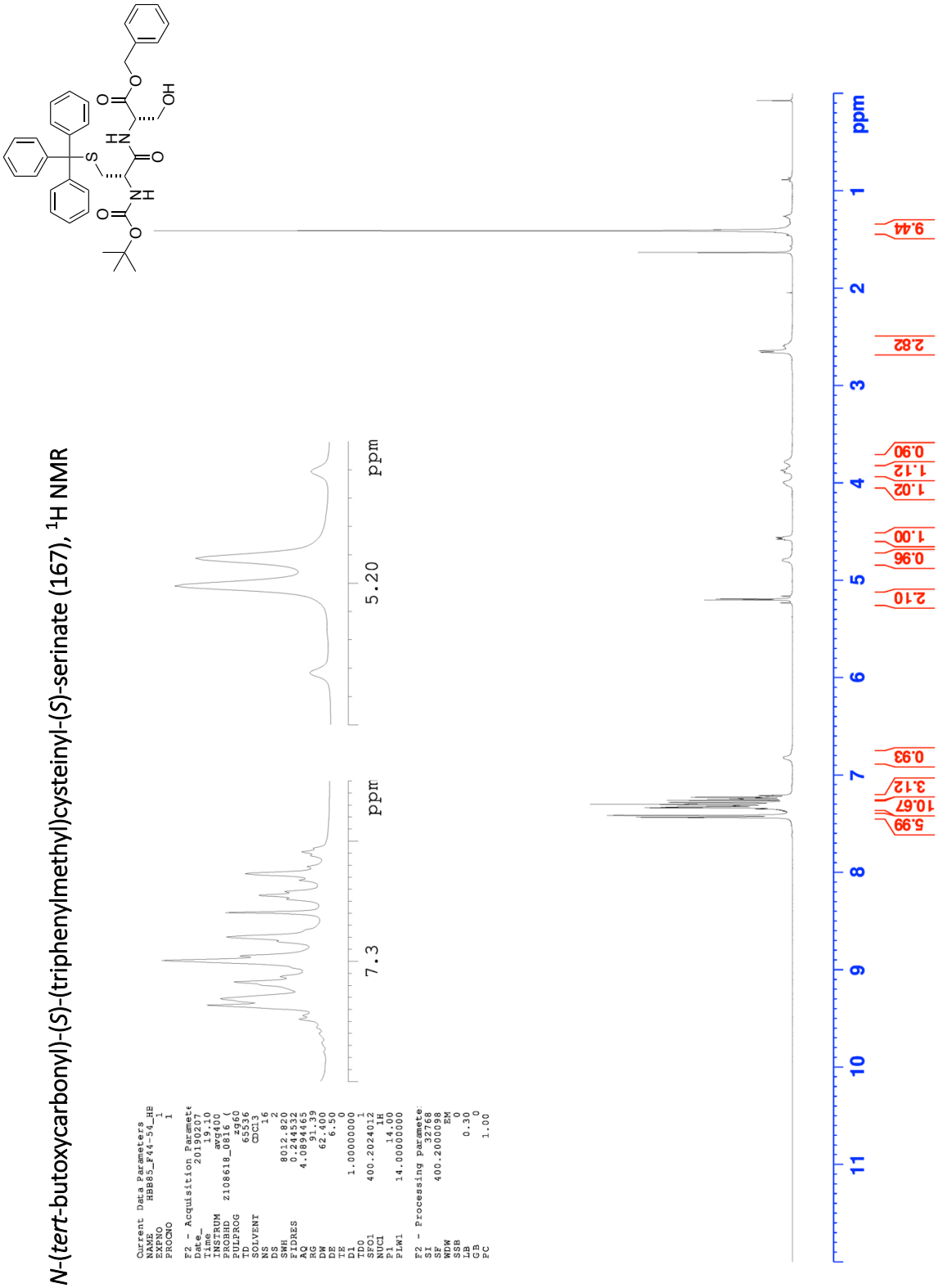
2-{(1'*R*)-1'-Acetamido-2'-[(1''-methyl-2'' ,5''-dioxopyrrolidin-3''-yl)sulfanyl]ethyl}-1,3-oxazole-4-carboxylic acid (72), ^{1}H NMR



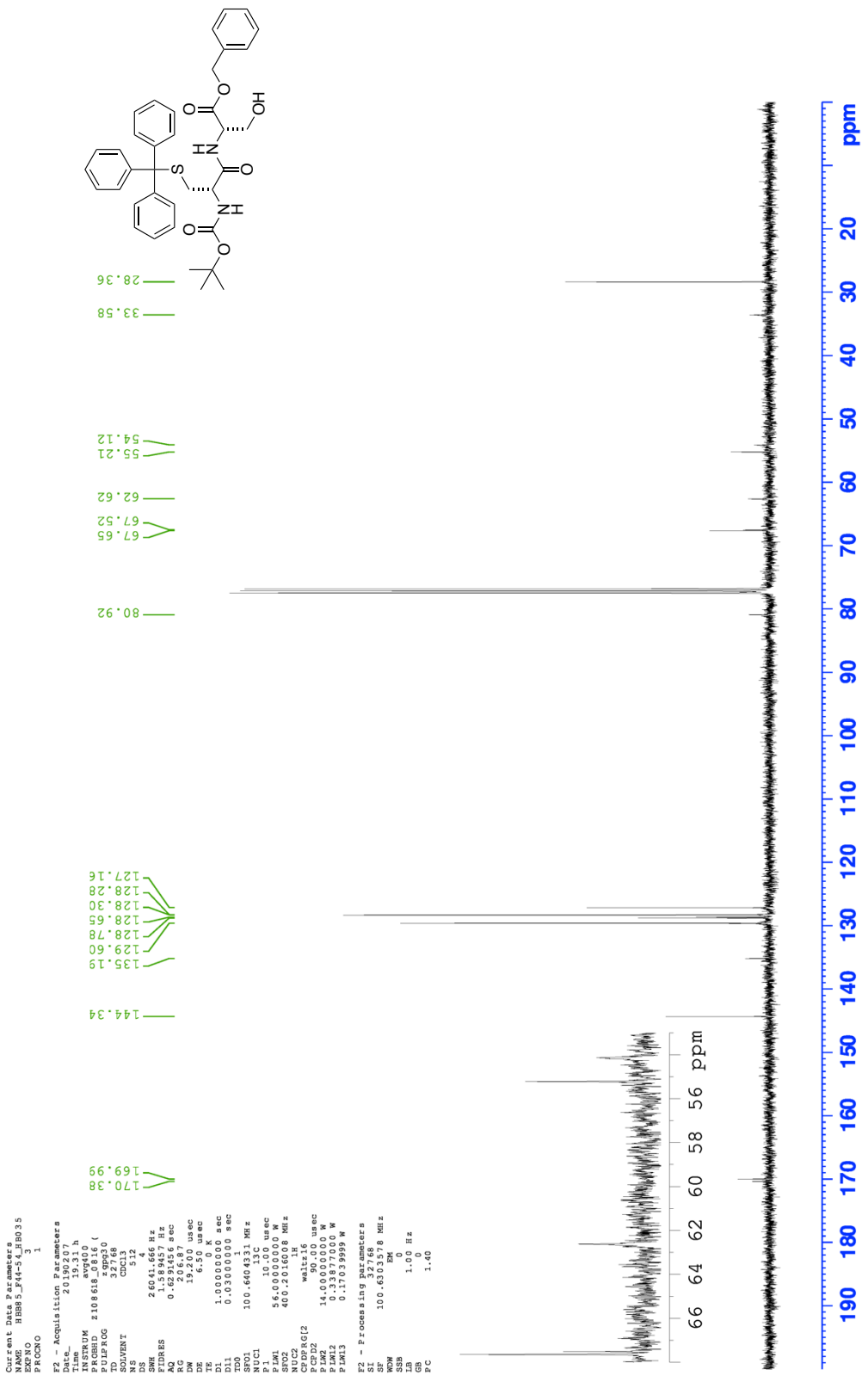
2-{(1'*R*)-1'-Acetamido-2'-[(1''-methyl-2'',5''-dioxopyrrolidin-3''-yl)sulfanyl]ethyl}-1,3-oxazole-4-carboxylic acid (72), $^{13}C\{^{1}H\}$ NMR



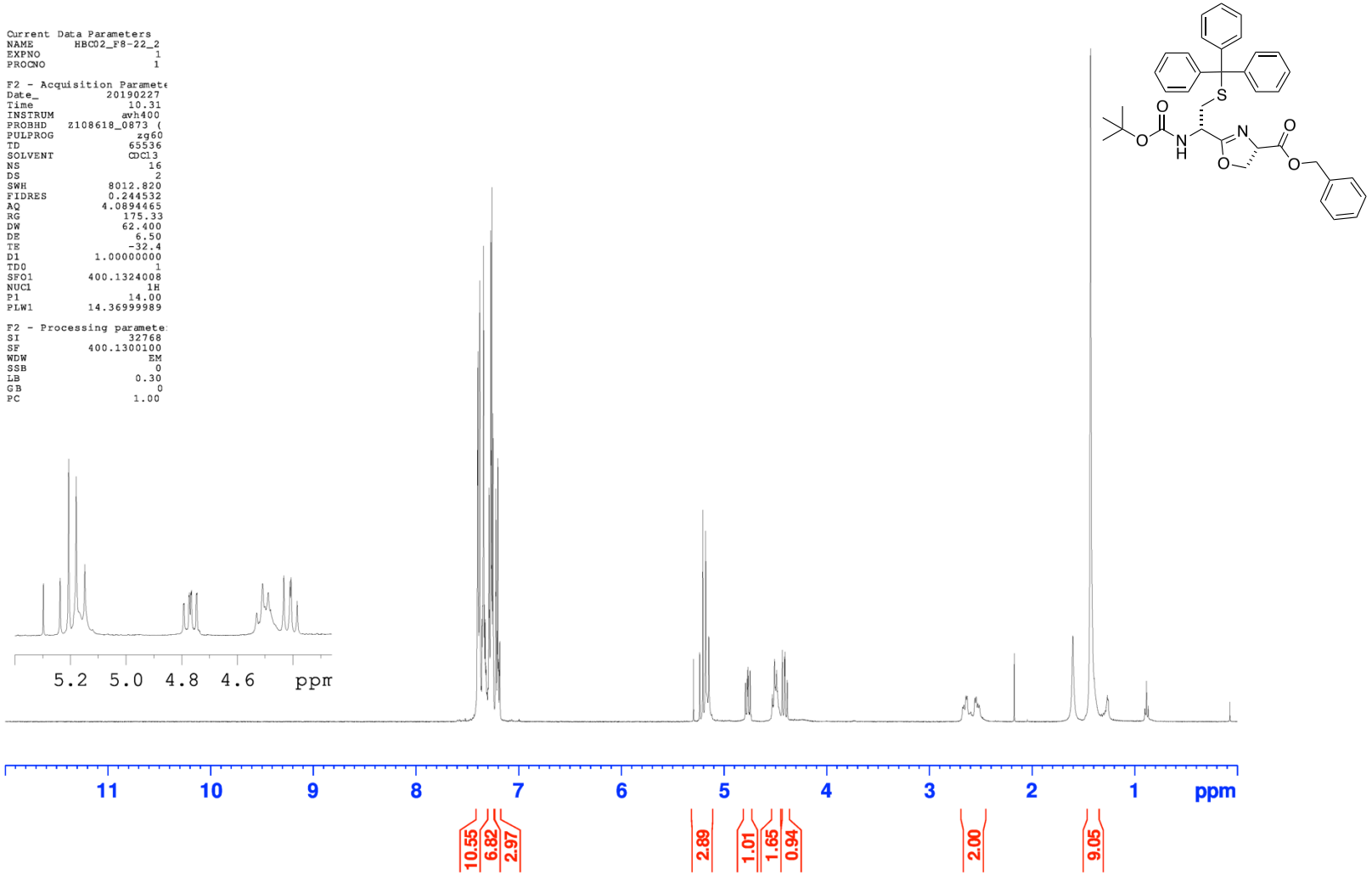
Benzyl *N*-(*tert*-butoxycarbonyl)-(*S*)-(triphenylmethyl)cysteinyl-(*S*)-serinate (167), ^{1}H NMR



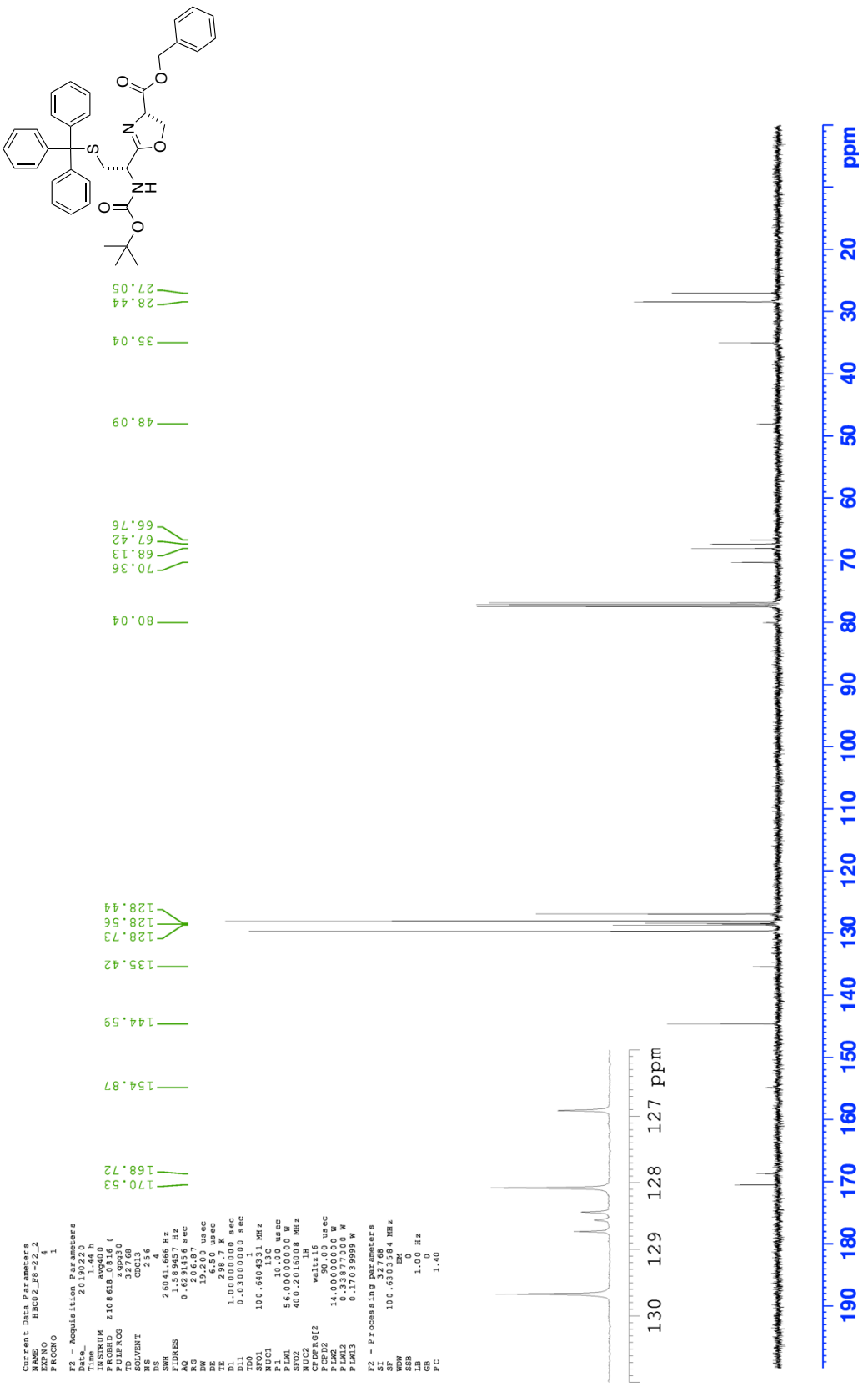
Benzyl *N*-(*tert*-butoxycarbonyl)-(*S*)-(triphenylmethyl)cysteinyl-(*S*)-serinate (167), $^{13}C\{^{1}H\}$ NMR



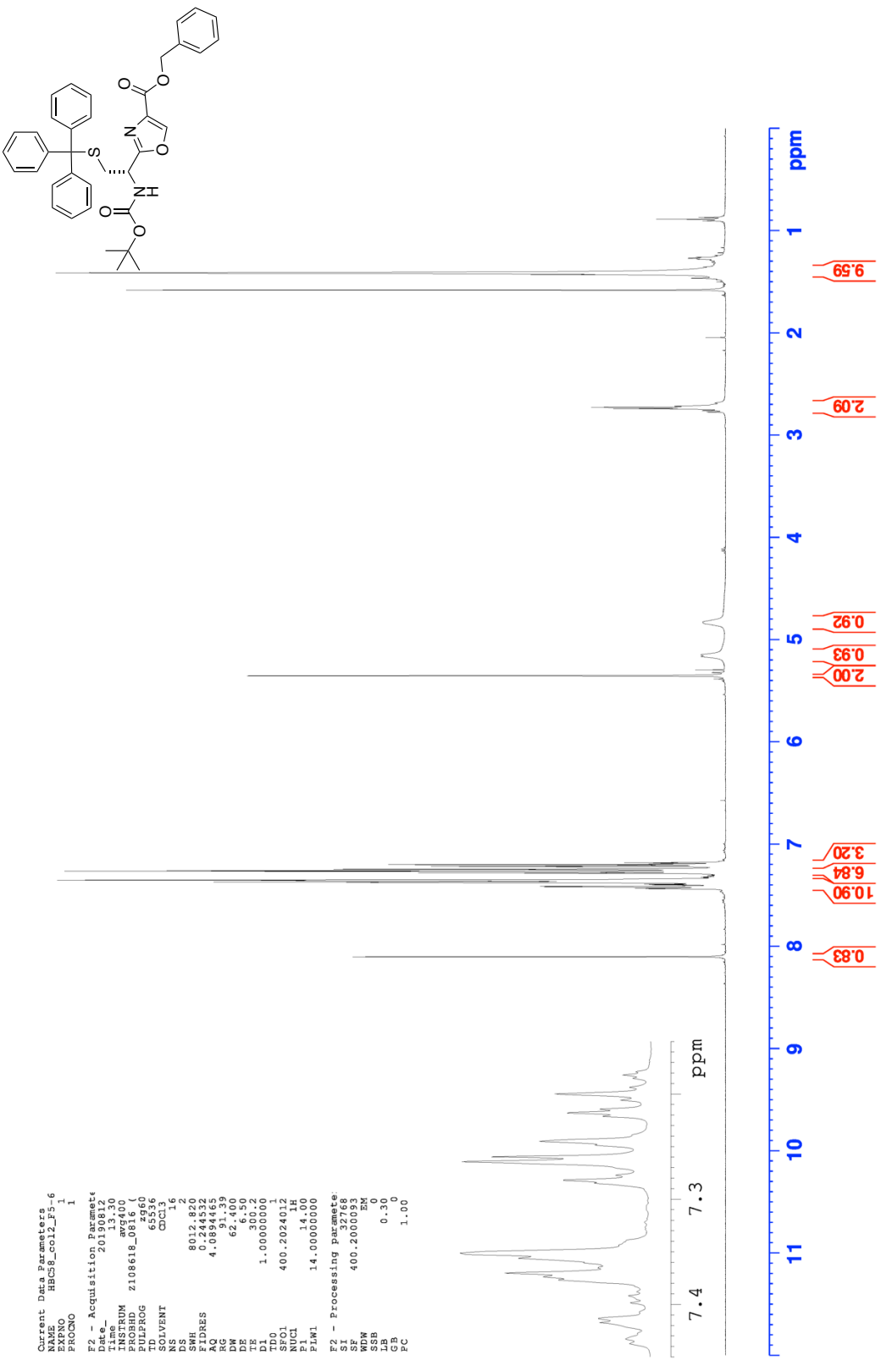
Benzyl 2-{(1'S)-1'-[(*tert*-butoxycarbonyl)amino]-2'-[(triphenylmethyl)sulfanyl]ethyl}-4,5-dihydro-1,3-oxazole-4-carboxylate (168), ^{1}H NMR



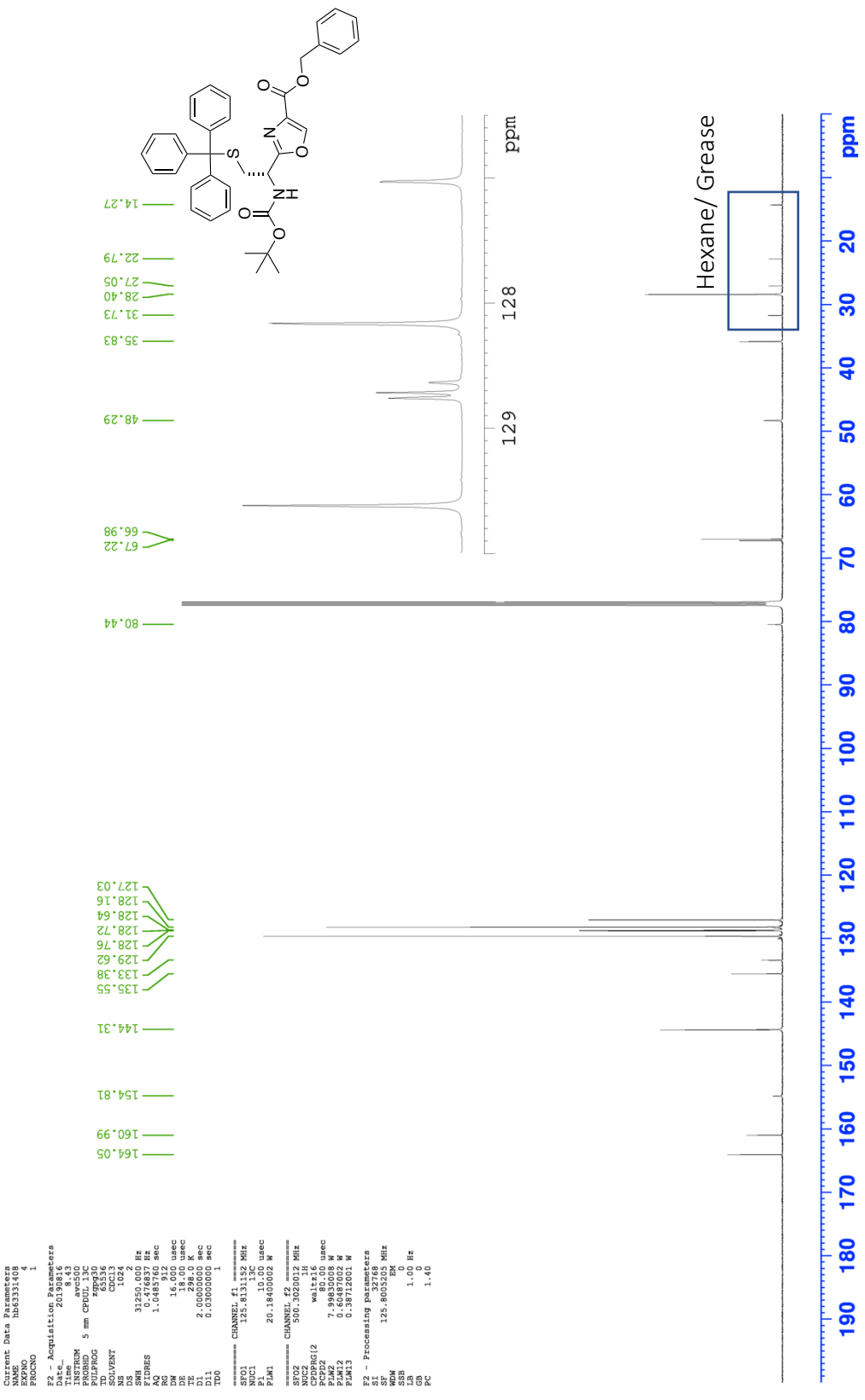
Benzyl 2-{(1'S)-1'-[(*tert*-butoxycarbonyl)amino]-2'-[(triphenylmethyl)sulfanyl]ethyl}-4,5-dihydro-1,3-oxazole-4-carboxylate (168), $^{13}C\{^{1}H\}$ NMR



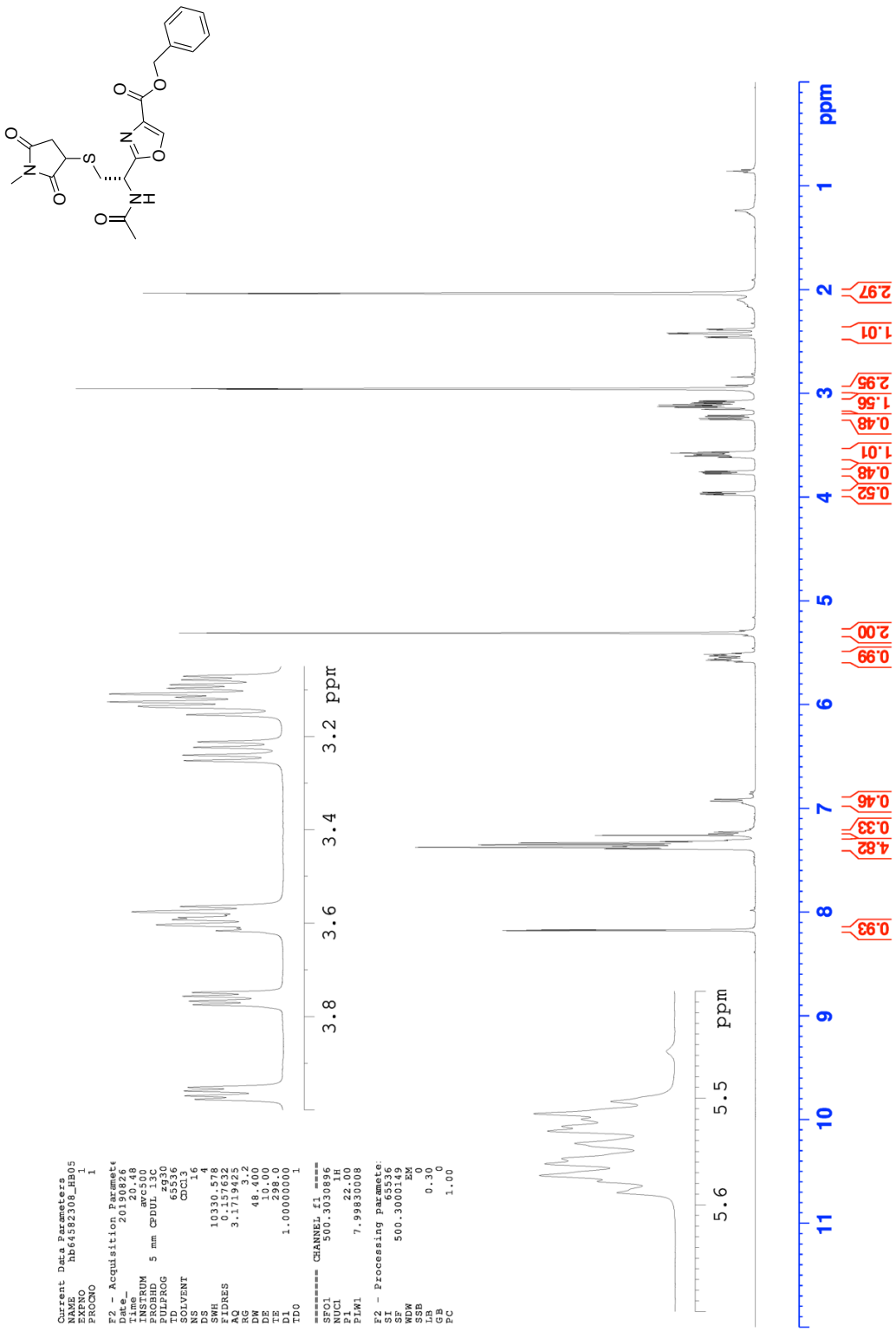
Benzyl 2-{(1'S)-1'-[(*tert*-butoxycarbonyl)amino]-2'-[(triphenylmethyl)sulfanyl]ethyl}-1,3-oxazole-4-carboxylate (169), ^{1}H NMR



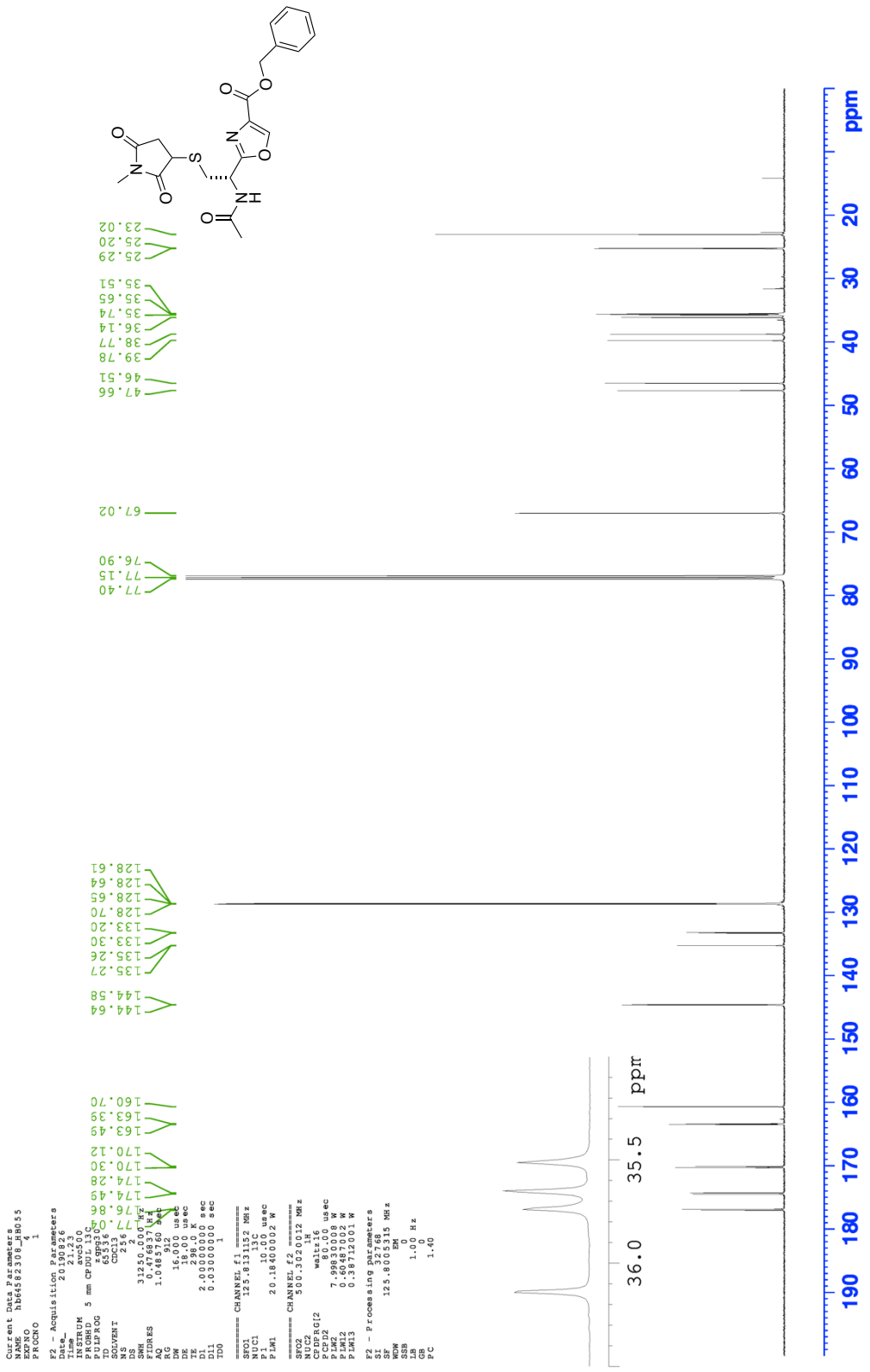
Benzyl 2-{(1'S)-1'-[(*tert*-butoxycarbonyl)amino]-2'-[(triphenylmethyl)sulfanyl]ethyl}-1,3-oxazole-4-carboxylate (169), $^{13}C\{^{1}H\}$ NMR



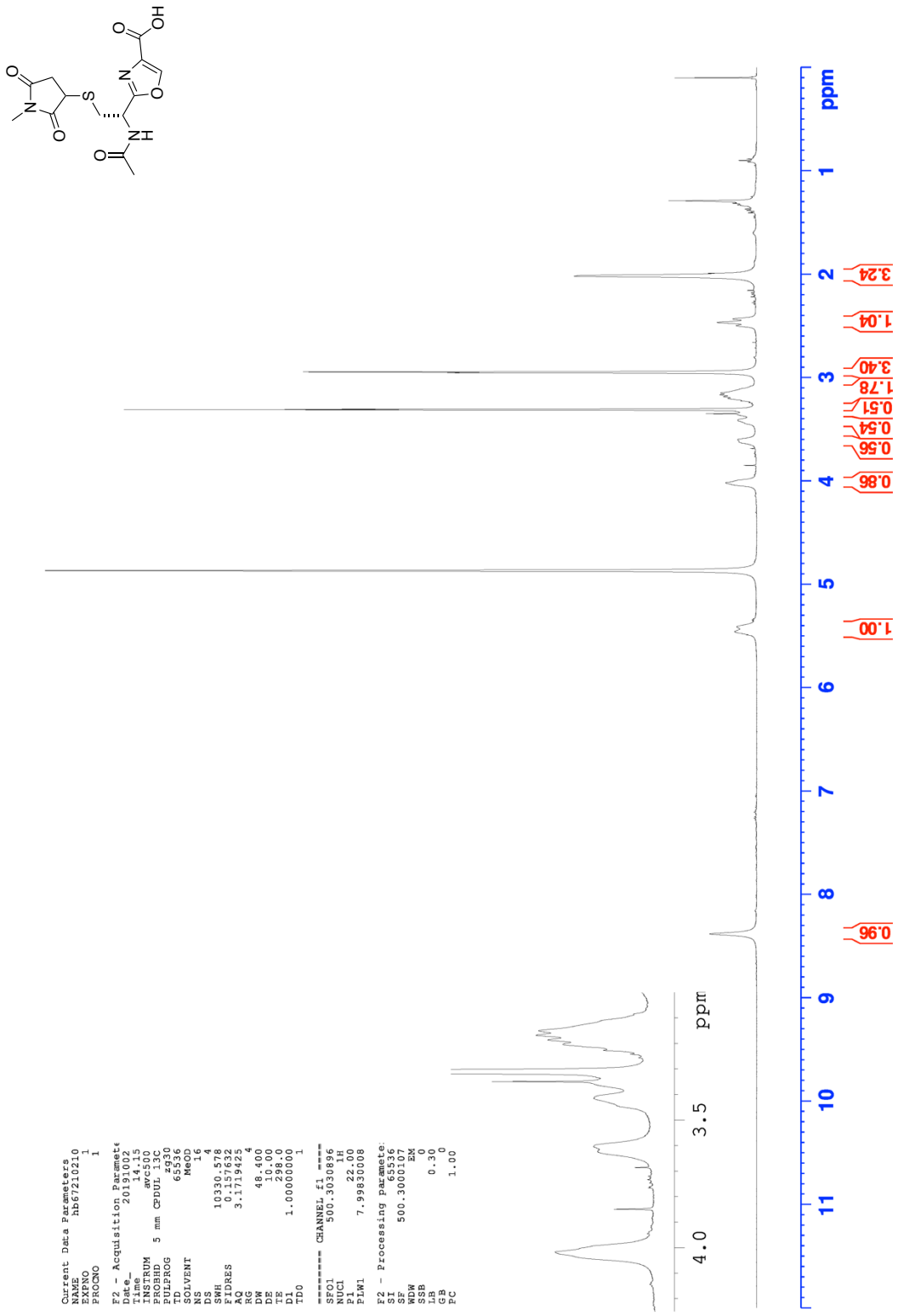
Benzyl 2'-{(1'S)-1'-acetamido-2'-[(1''-methyl-2'' ,5''-dioxopyrrolidin-3''-yl)sulfanyl]ethyl}-1,3-oxazole-4-carboxylate (170), ^{1}H NMR



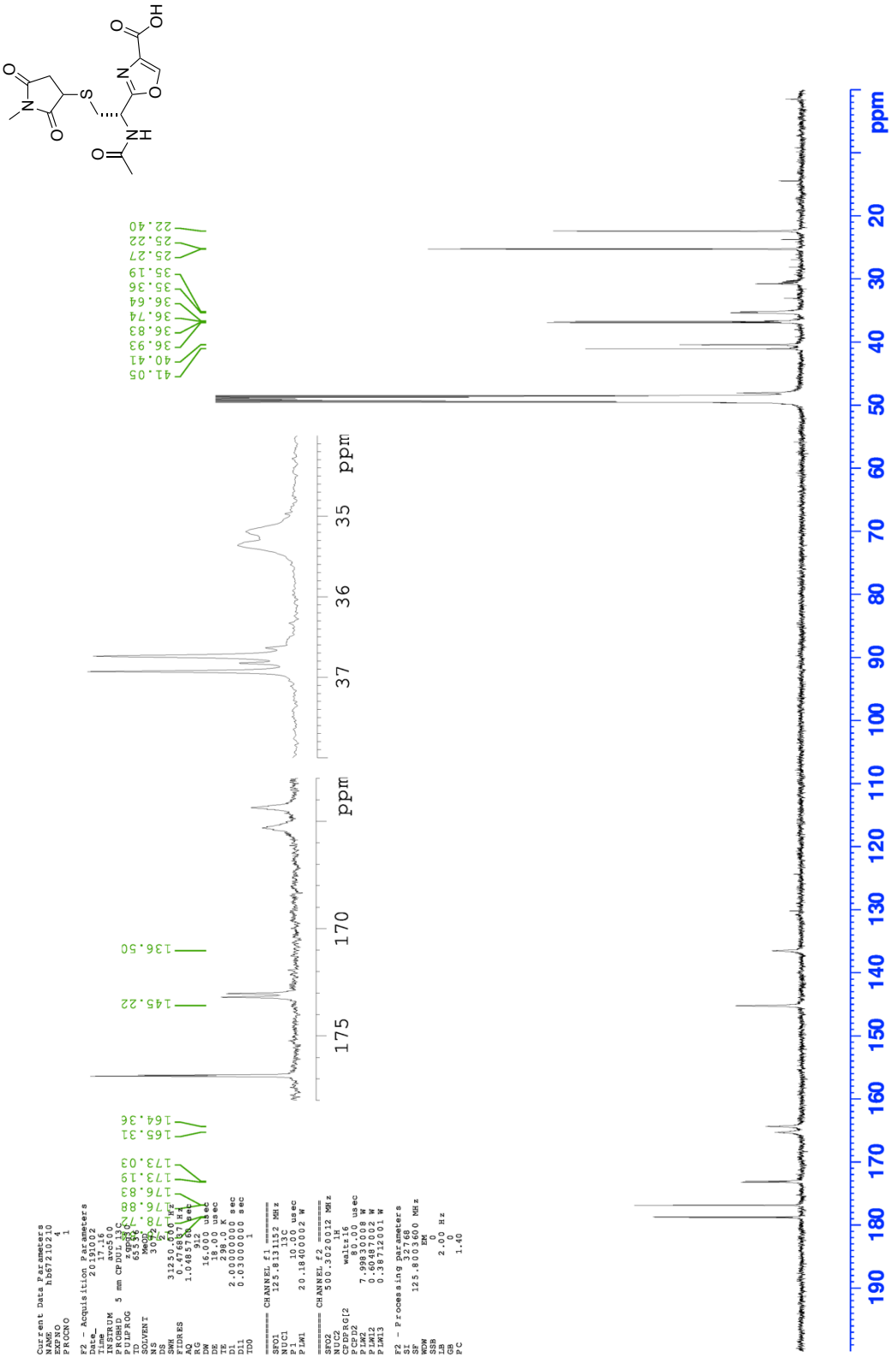
Benzyl 2'-{(1'S)-1'-acetamido-2'-[(1''-methyl-2'',5''-dioxopyrrolidin-3''-yl)sulfanyl]ethyl}-1,3-oxazole-4-carboxylate (170), $^{13}C\{^{1}H\}$ NMR



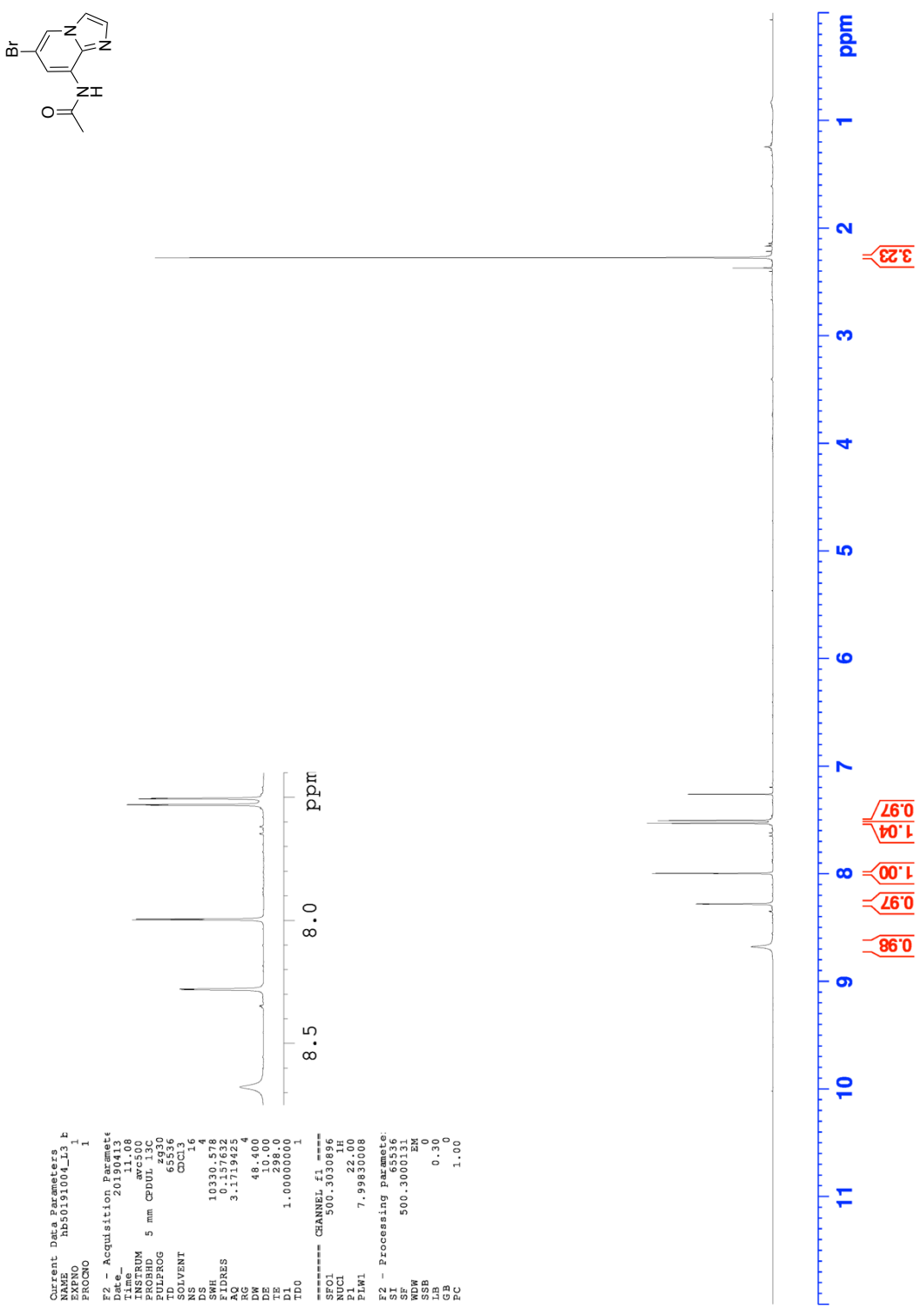
2'-{(1'S)-1'-Acetamido-2'-[(1''-methyl-2'',5''-dioxopyrrolidin-3''-yl)sulfanyl]ethyl}-1,3-oxazole-4-carboxylic acid (165), ^{1}H NMR



2'-{(1'S)-1'-Acetamido-2'-[(1''-methyl-2'',5''-dioxopyrrolidin-3''-yl)sulfanyl]ethyl}-1,3-oxazole-4-carboxylic acid (165), $^{13}C\{^{1}H\}$ NMR



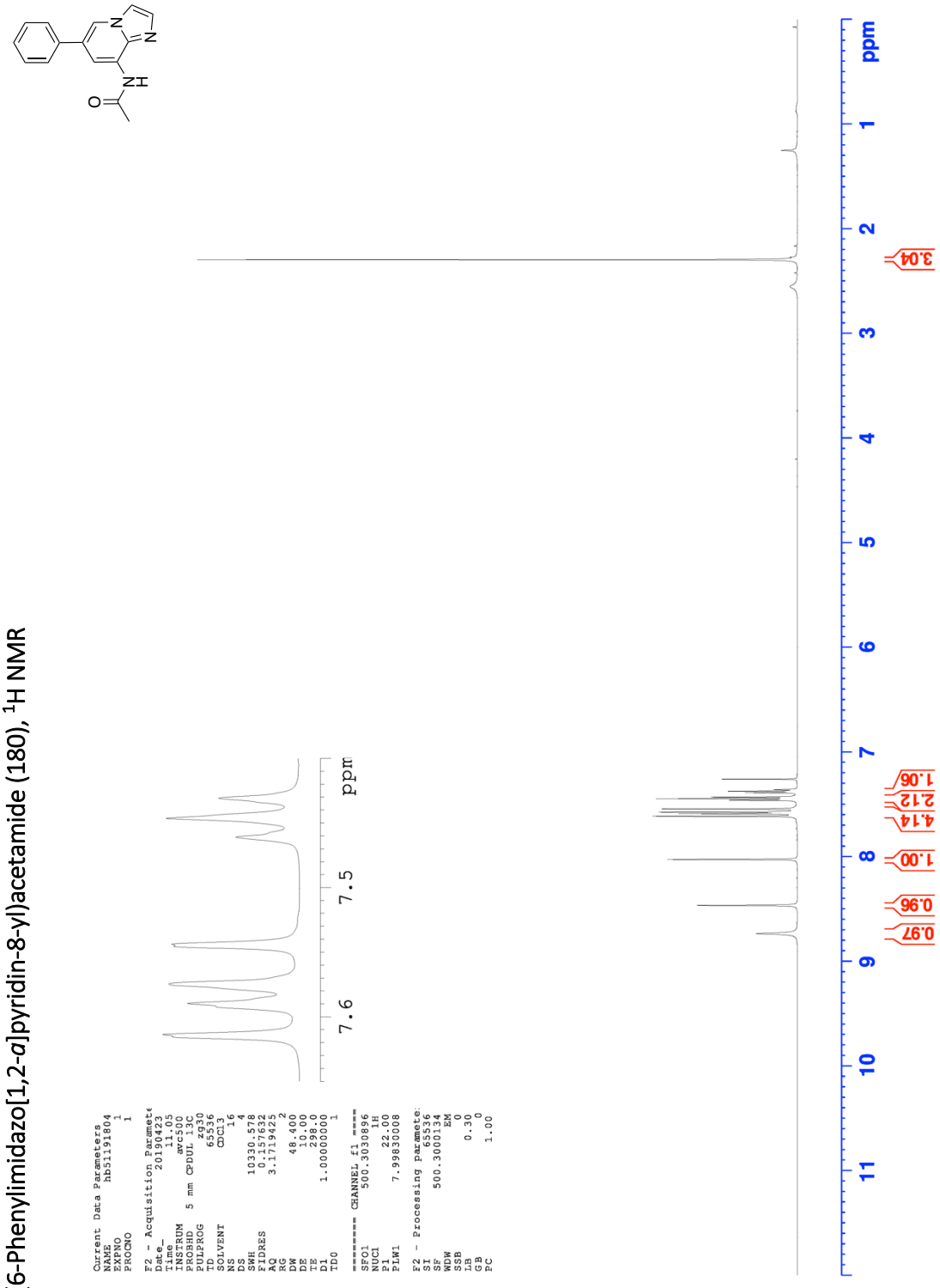
N-(6-Bromoimidazo[1,2-*a*]pyridin-8-yl)acetamide (179), ^{1}H NMR



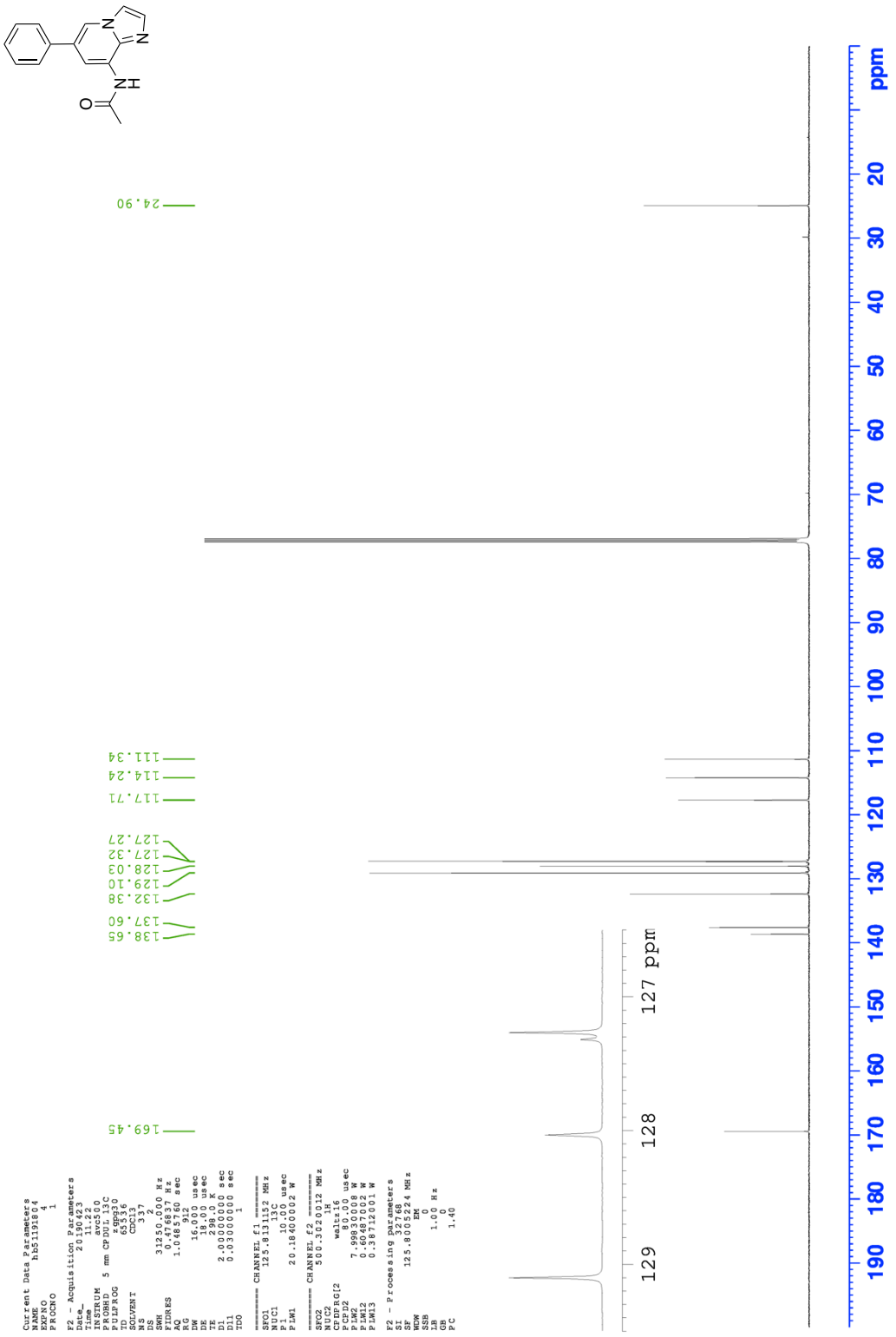
N-(6-Bromoimidazo[1,2-*a*]pyridin-8-yl)acetamide (179), $^{13}C\{^{1}H\}$ NMR



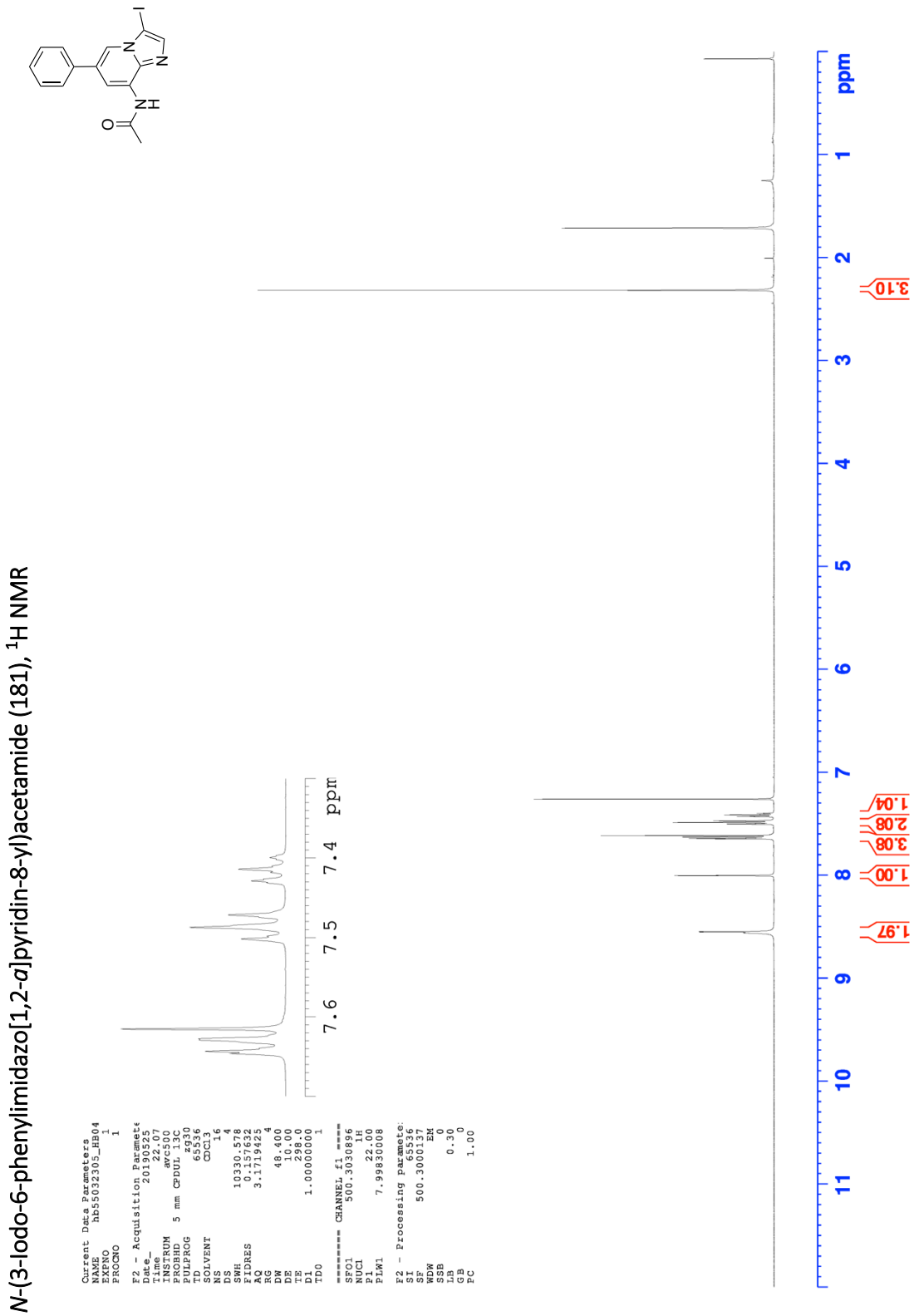
N-(6-Phenylimidazo[1,2-*a*]pyridin-8-yl)acetamide (180), ^{1}H NMR



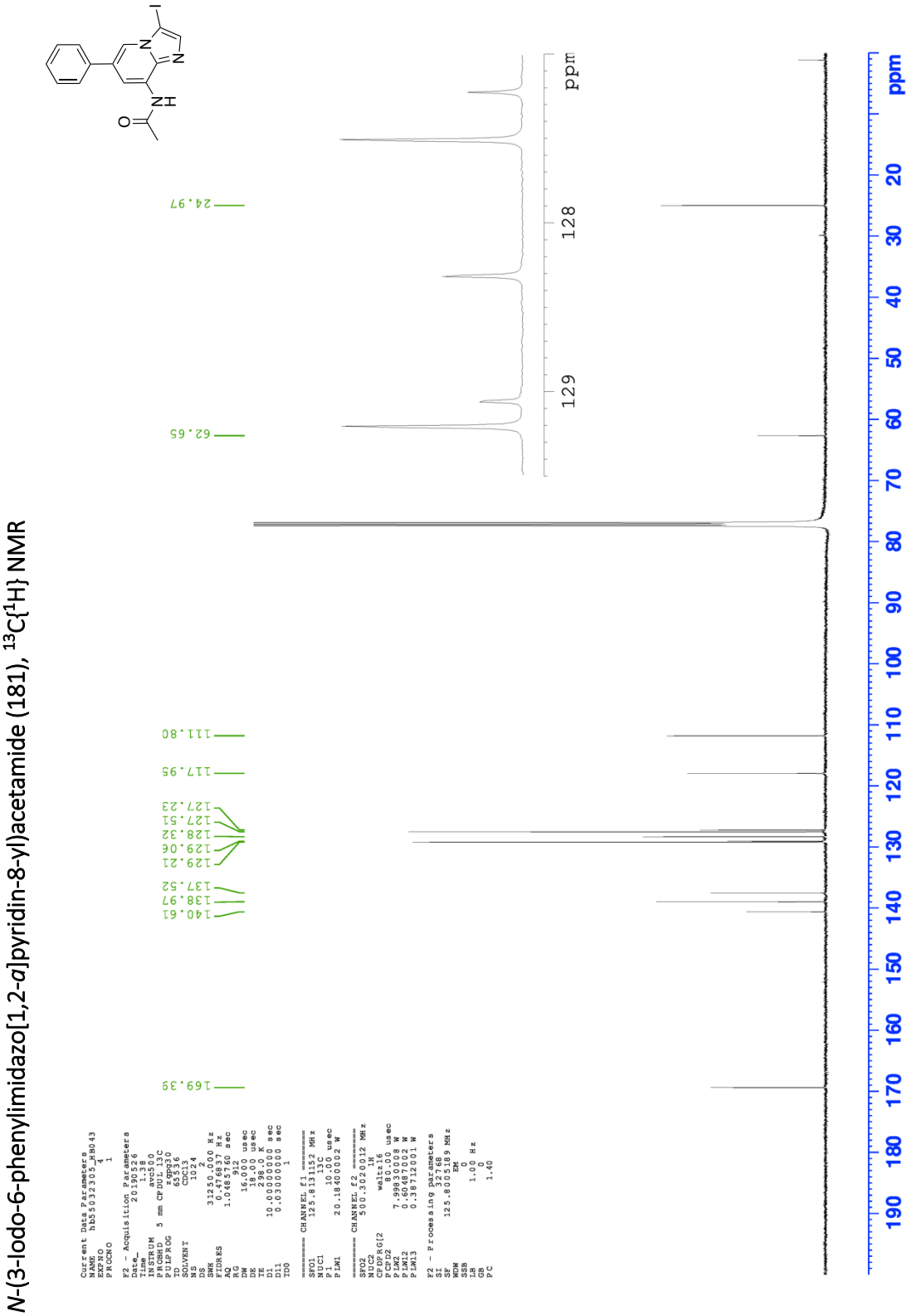
N-(6-Phenylimidazo[1,2-*a*]pyridin-8-yl)acetamide (180), $^{13}C\{^{1}H\}$ NMR



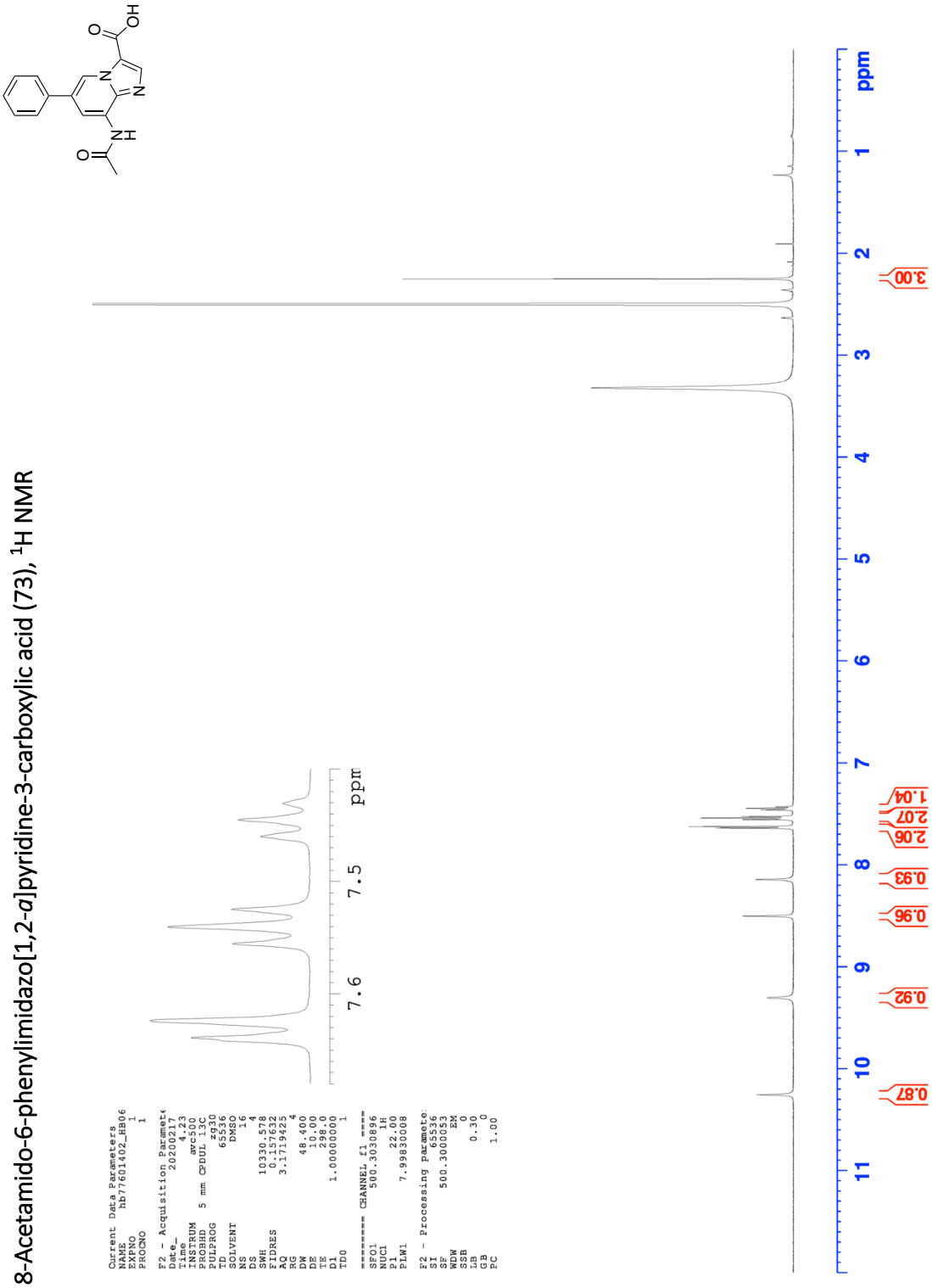
N-(3-Iodo-6-phenylimidazo[1,2-*a*]pyridin-8-yl)acetamide (181), ^{1}H NMR



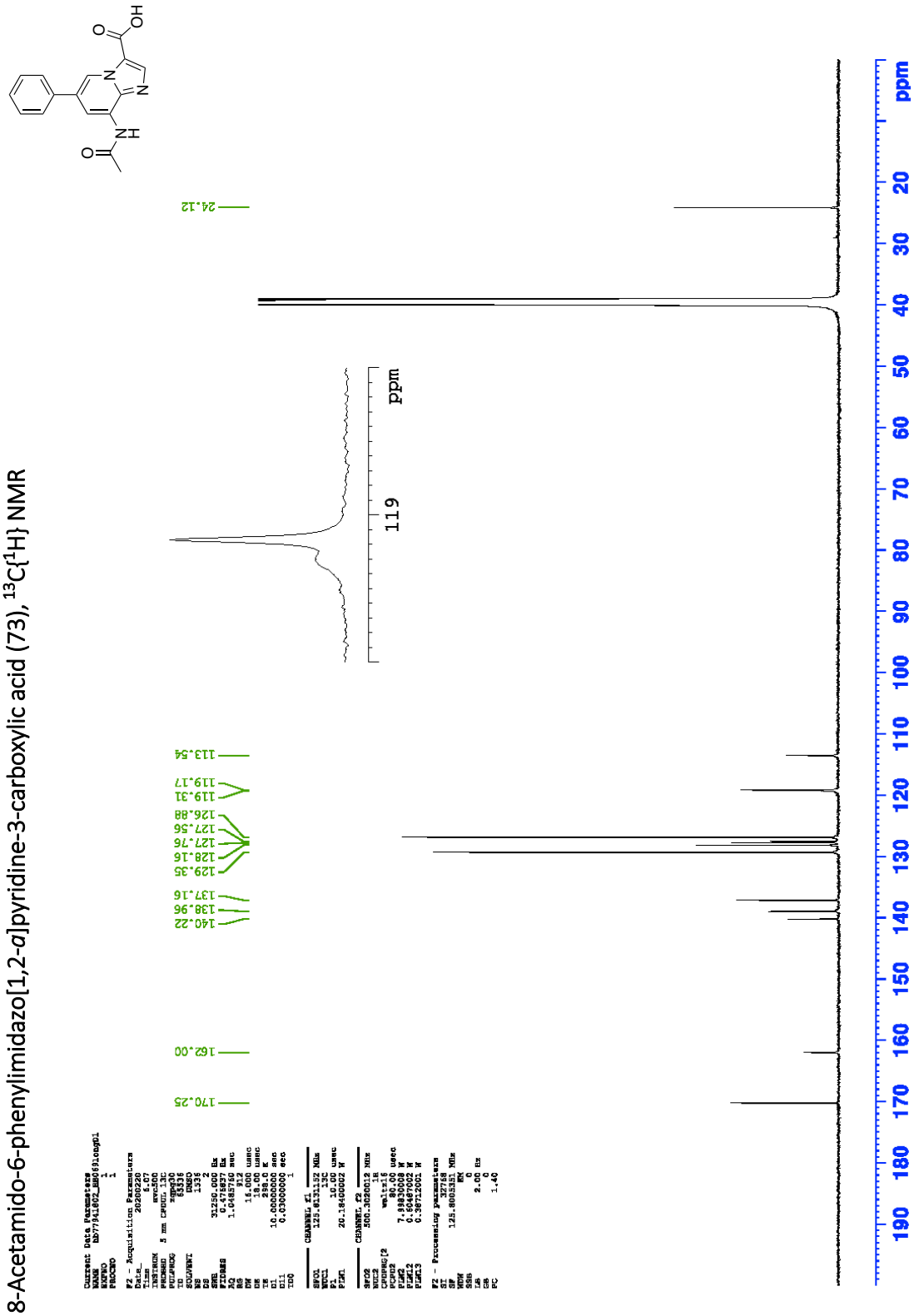
N-(3-Iodo-6-phenylimidazo[1,2-*a*]pyridin-8-yl)acetamide (181), $^{13}C\{^{1}H\}$ NMR



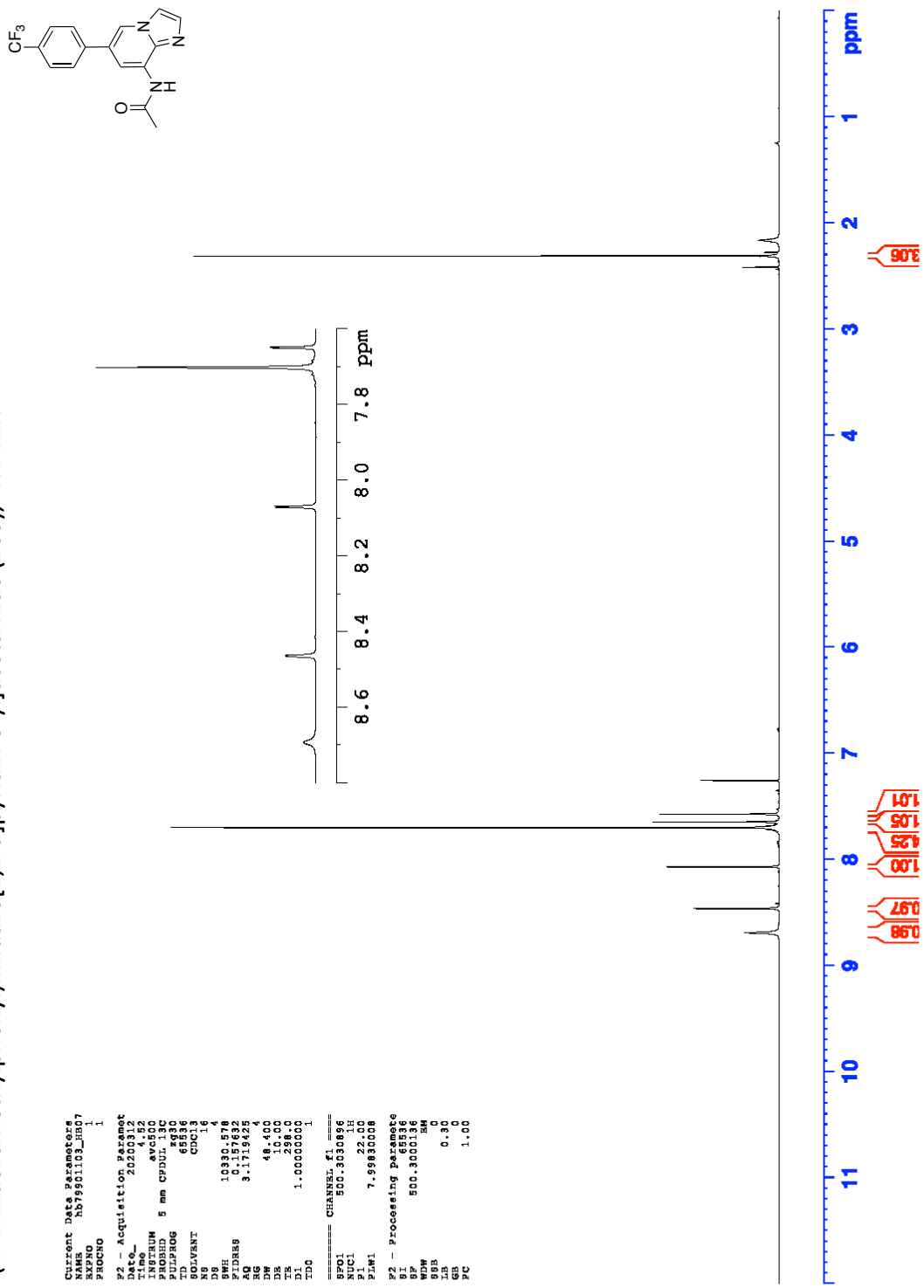
8-Acetamido-6-phenylimidazo[1,2-*a*]pyridine-3-carboxylic acid (73), ^{1}H NMR



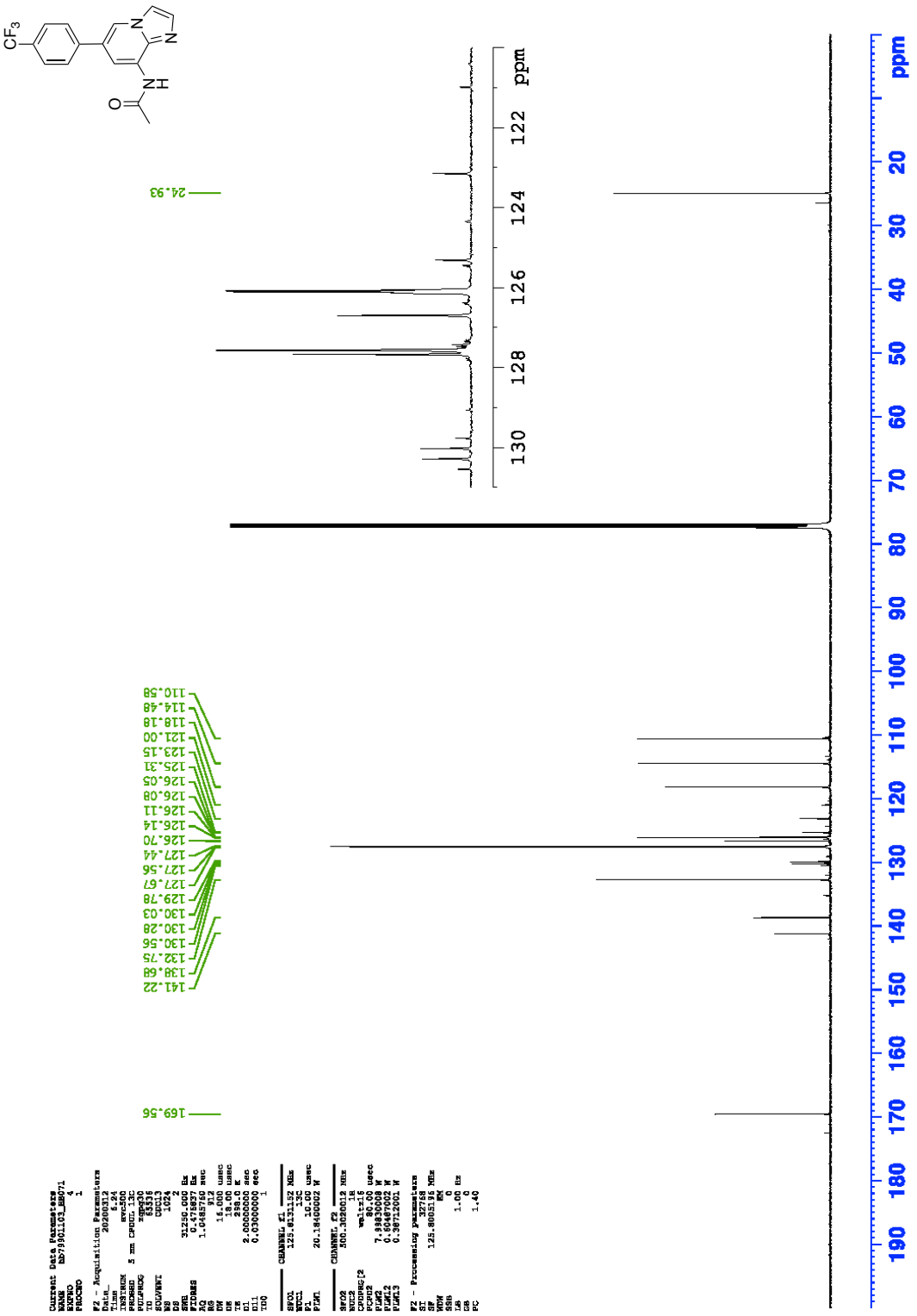
8-Acetamido-6-phenylimidazo[1,2-*a*]pyridine-3-carboxylic acid (73), $^{13}C\{^{1}H\}$ NMR



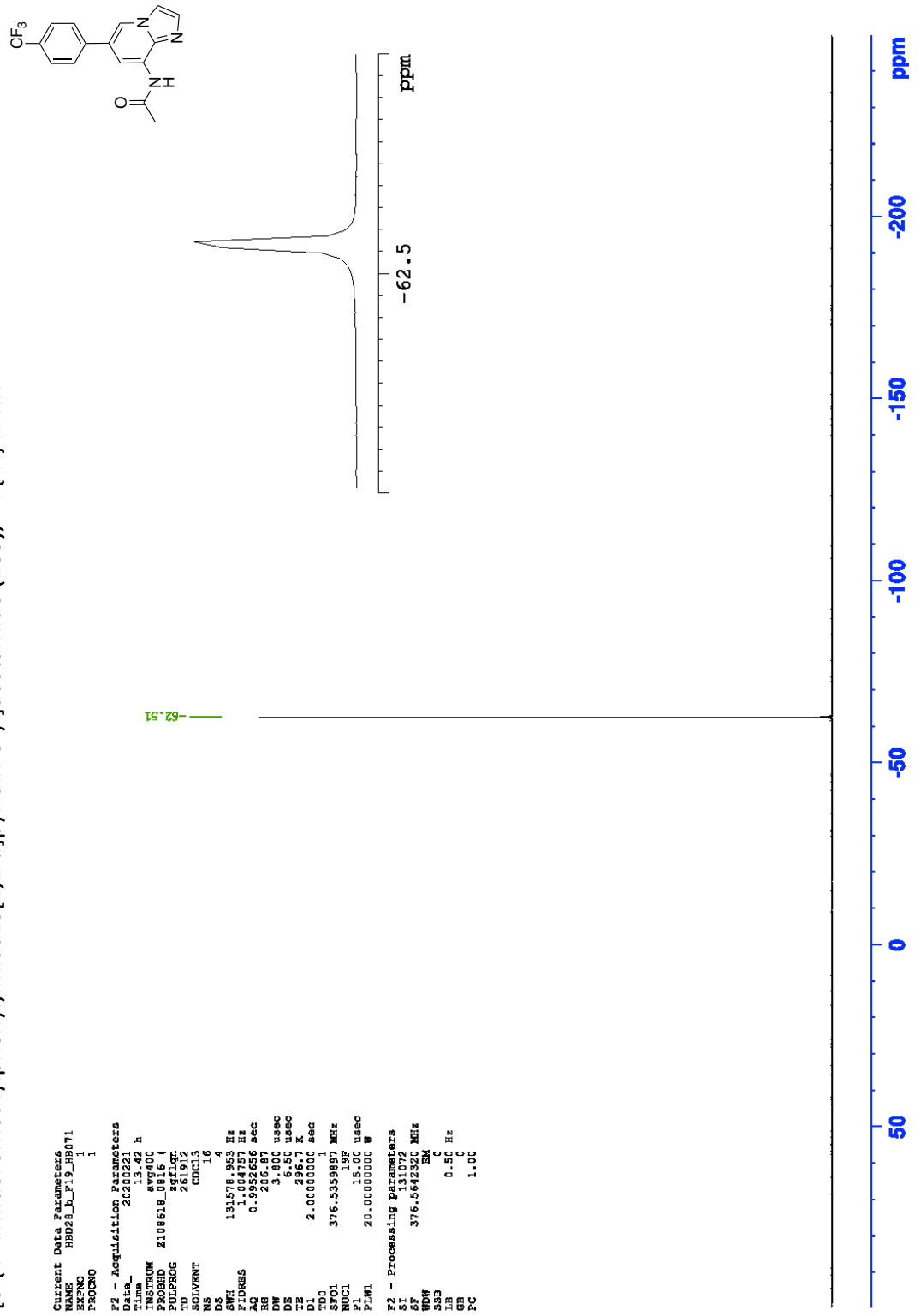
N-[6-(4'-Trifluoromethylphenyl)imidazo[1,2-*a*]pyridin-8-yl]acetamide (185), ^{1}H NMR



N-[6-(4'-Trifluoromethylphenyl)imidazo[1,2-*a*]pyridin-8-yl]acetamide (185), $^{13}C\{^{1}H\}$ NMR



N-[6-(4'-Trifluoromethylphenyl)imidazo[1,2-*a*]pyridin-8-yl]acetamide (185), $^{19}F\{^{1}H\}$ NMR

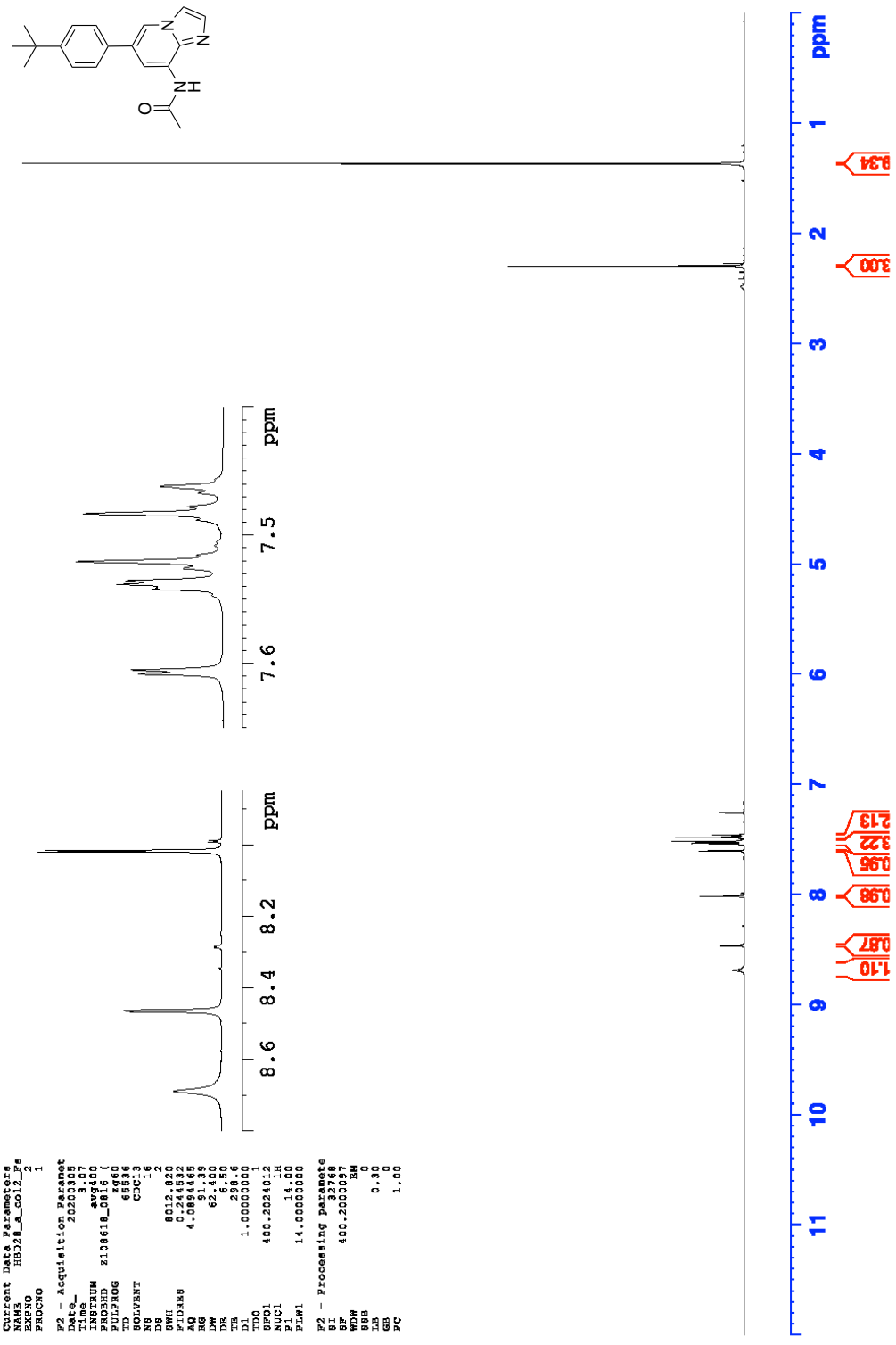



```
Current Data Parameters
NAME      H8D28_b_P19_H8071
EXPNO              1
PROCNO             1

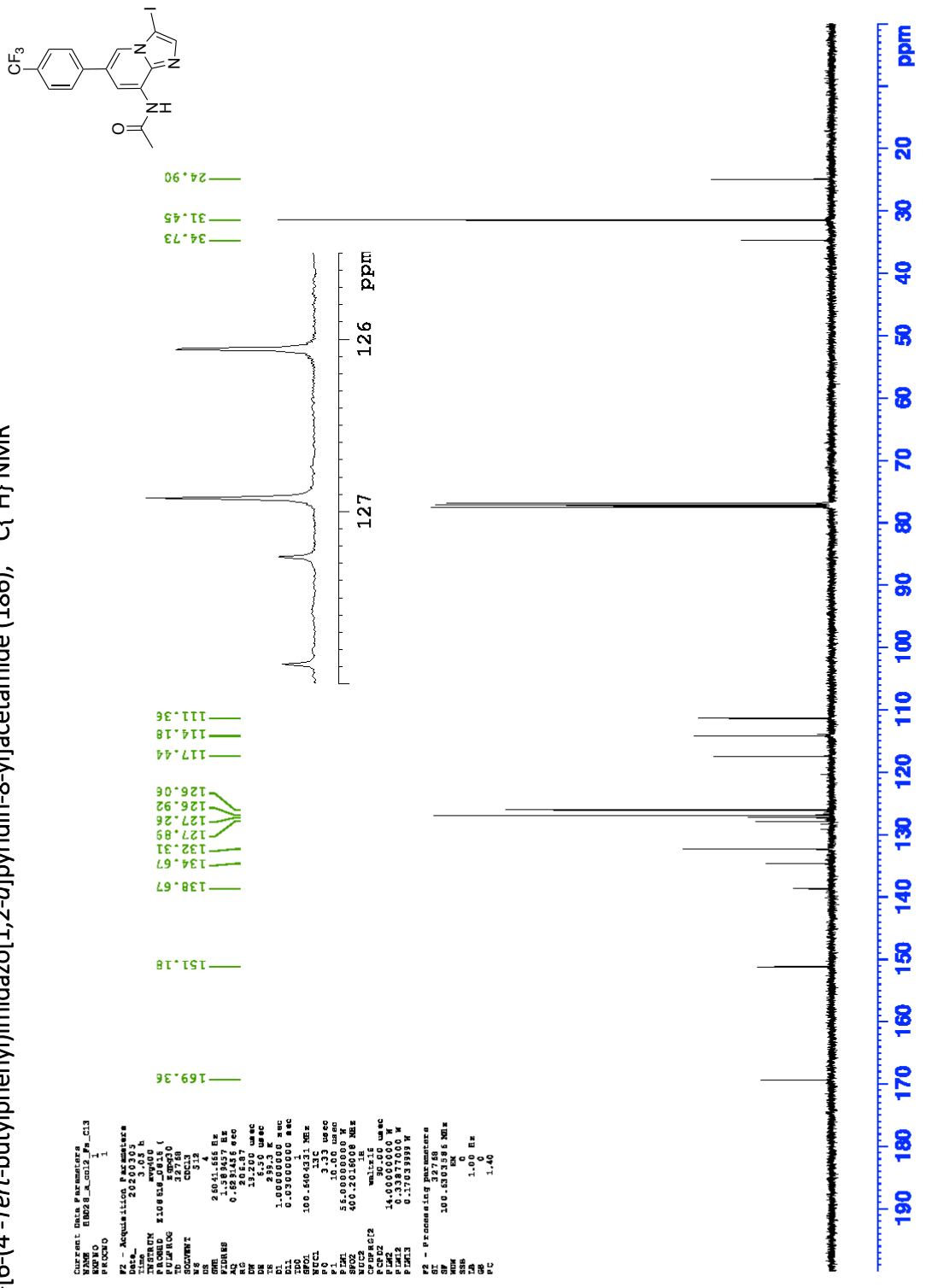
F2 - Acquisition Parameters
Date_         20201221
Time              13.42 h
INSTRUM         avg400
PROBHD     Z108618_0816 (
PULPROG         zgflqn
TD              261912
SOLVENT         CDCl3
NS                16
DS                 4
SWH          131578.953 Hz
FIDRES         1.004757 Hz
AQ             0.9952656 sec
RG              206.87
DW               3.800 usec
DE               6.50 usec
TE              296.7 K
D1               2.00000000 sec
TD0                1
SFO1         376.5359897 MHz
NUC1              19F
P1               15.00 usec
PLW1         20.00000000 W

F2 - Processing parameters
SI              131072
SF           376.5642320 MHz
WDW                EM
SSB                0
LB              0.50 Hz
GB                 0
PC              1.00
```

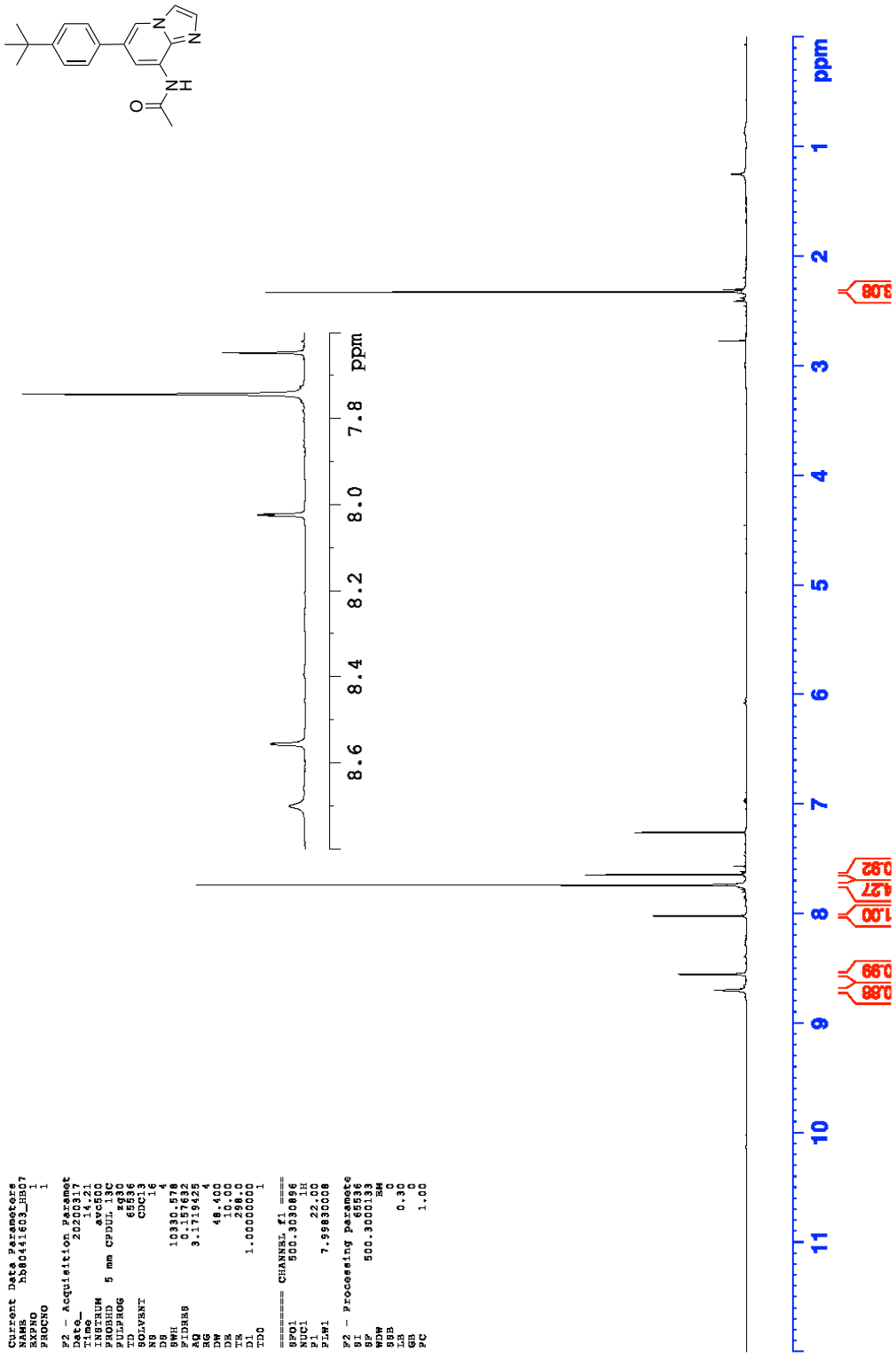
N-[6-(4'-*Tert*-butylphenyl)imidazo[1,2-*a*]pyridin-8-yl]acetamide (186), ^{1}H NMR



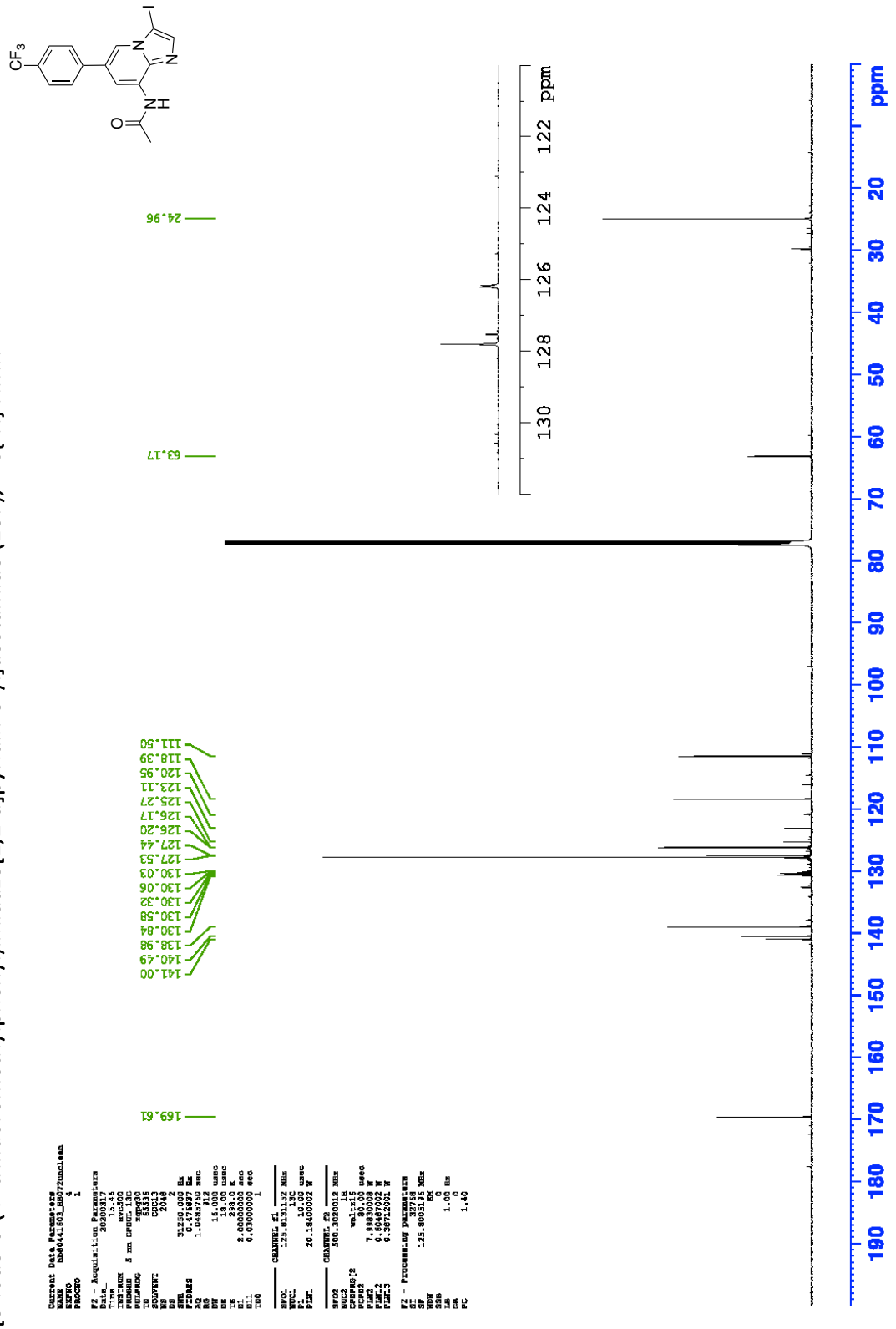
N-[6-(4'-*Tert*-butylphenyl)imidazo[1,2-*a*]pyridin-8-yl]acetamide (186), $^{13}C\{^{1}H\}$ NMR



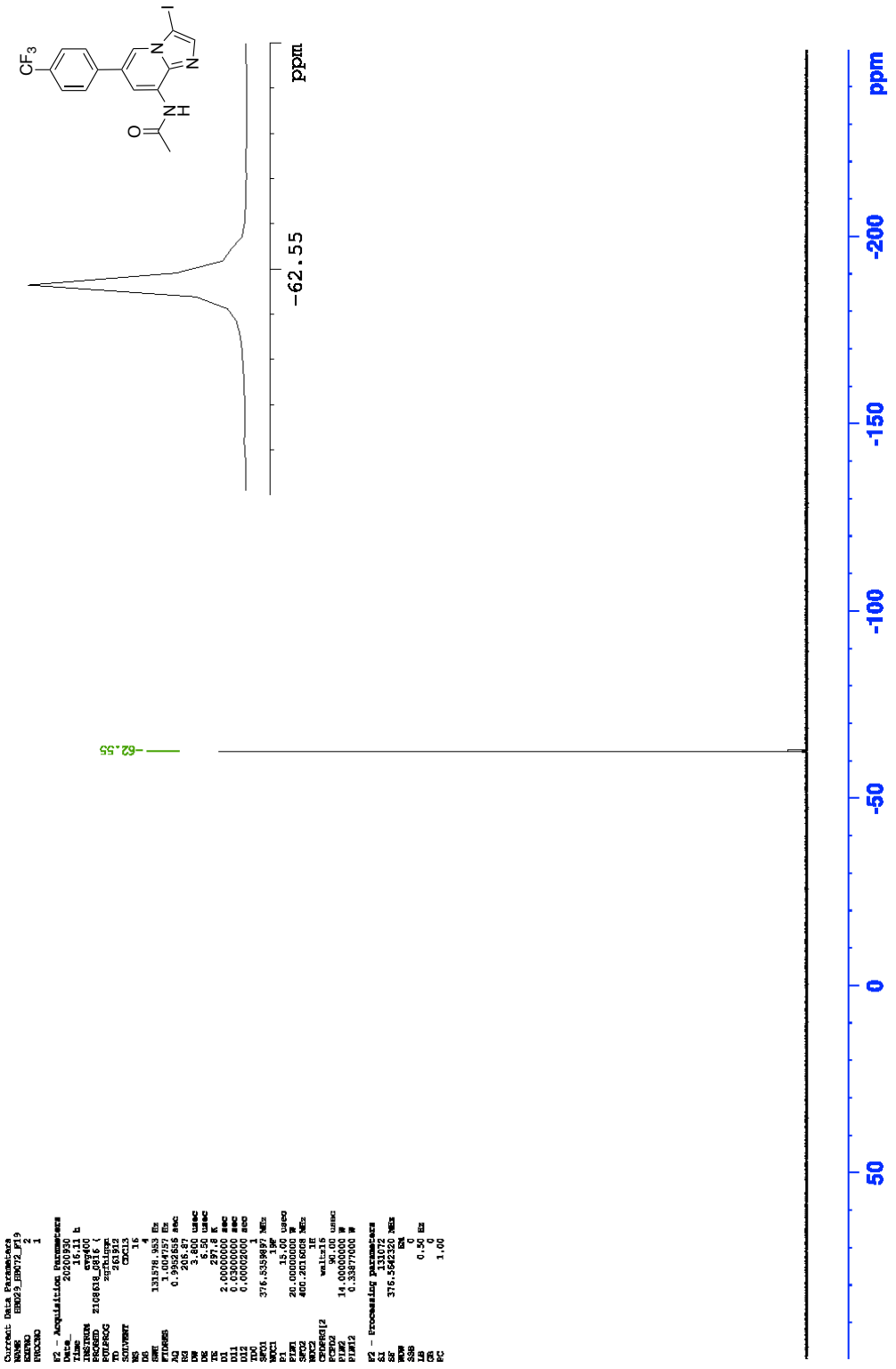
N-[3-Iodo-6-(4'-trifluoromethylphenyl)imidazo[1,2-*a*]pyridin-8-yl]acetamide (187), ^{1}H NMR



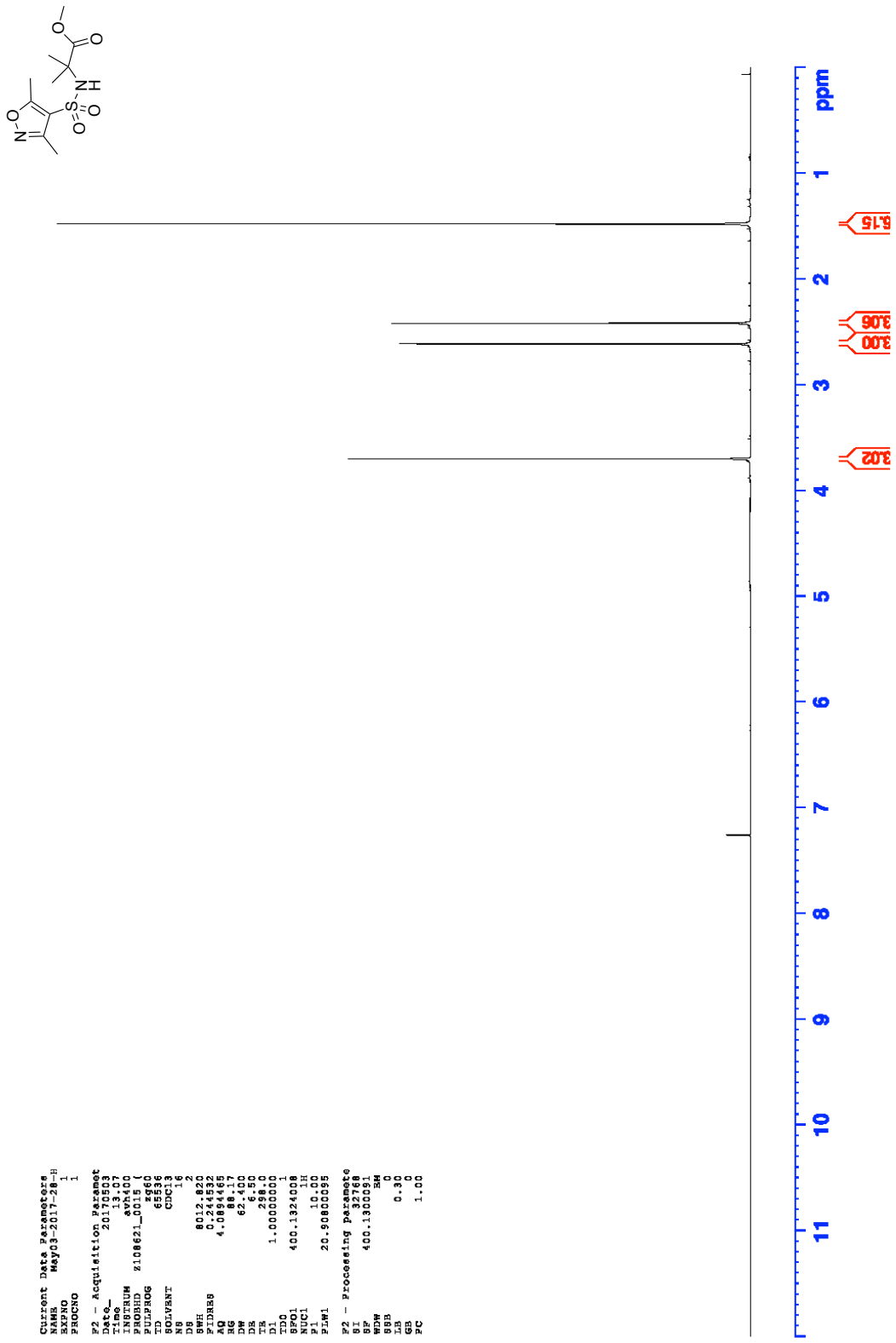
N-[3-Iodo-6-(4'-trifluoromethylphenyl)imidazo[1,2-*a*]pyridin-8-yl]acetamide (187), $^{13}C\{^{1}H\}$ NMR



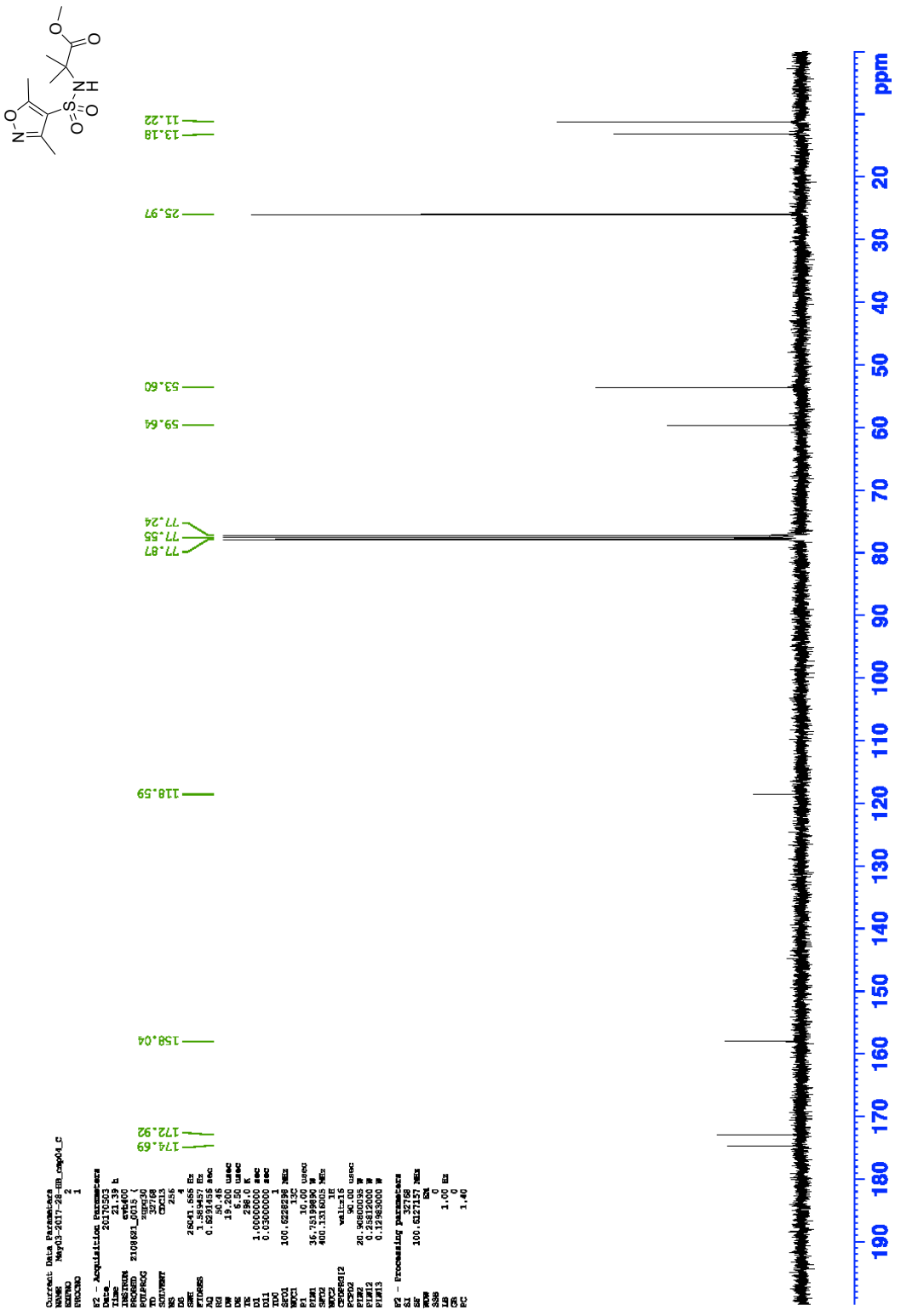
N-[3-Iodo-6-(4'-trifluoromethylphenyl)imidazo[1,2-*a*]pyridin-8-yl]acetamide (187), $^{19}F\{^{1}H\}$ NMR



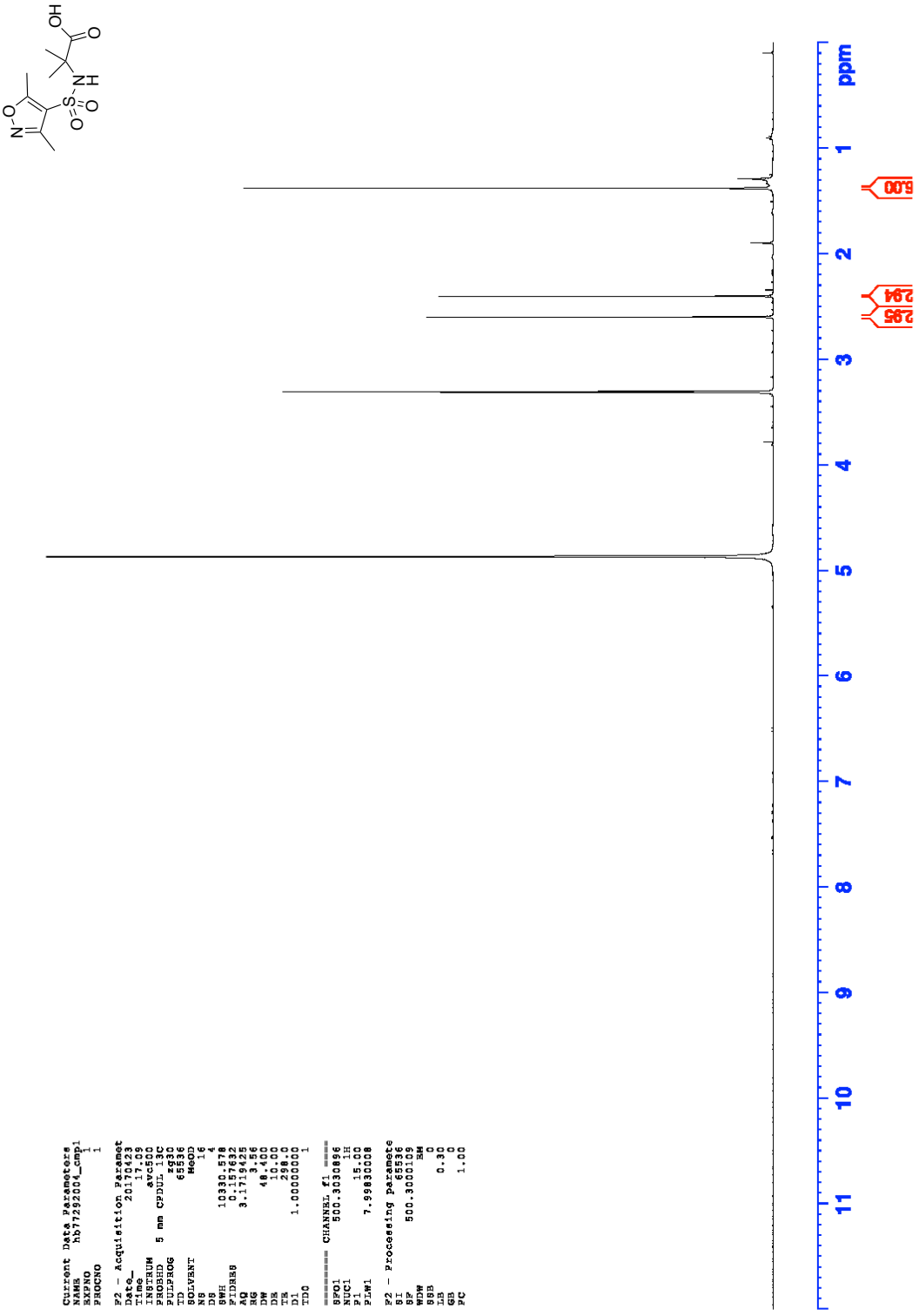
Methyl *N*-((3',5'-dimethyl-1',2'-oxazole-4'-sulfonyl)amino)-2-methylalaninate (195), ^{1}H NMR



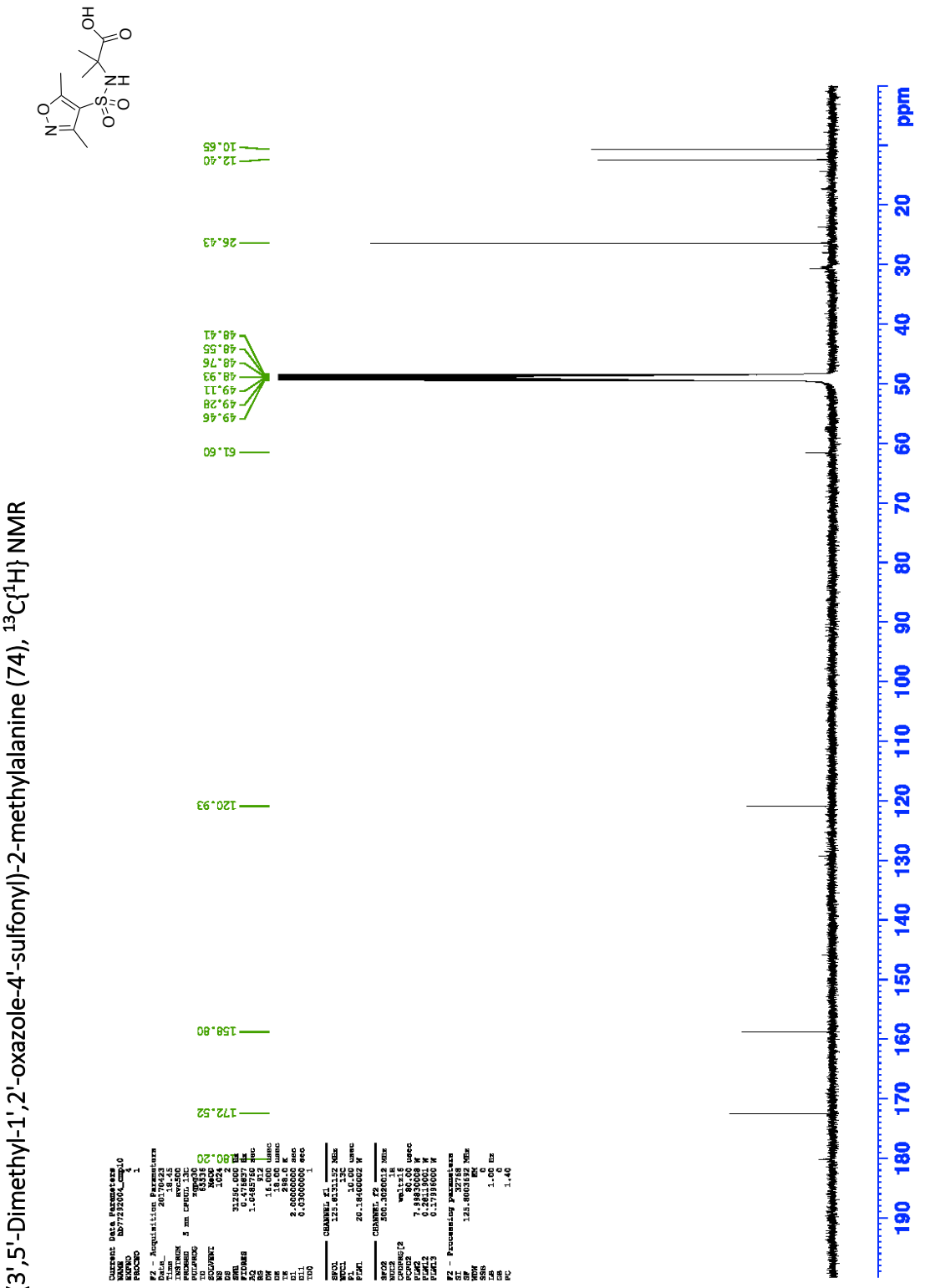
Methyl *N*-((3',5'-dimethyl-1',2'-oxazole-4'-sulfonyl)amino)-2-methylalaninate (195), $^{13}C\{^{1}H\}$ NMR



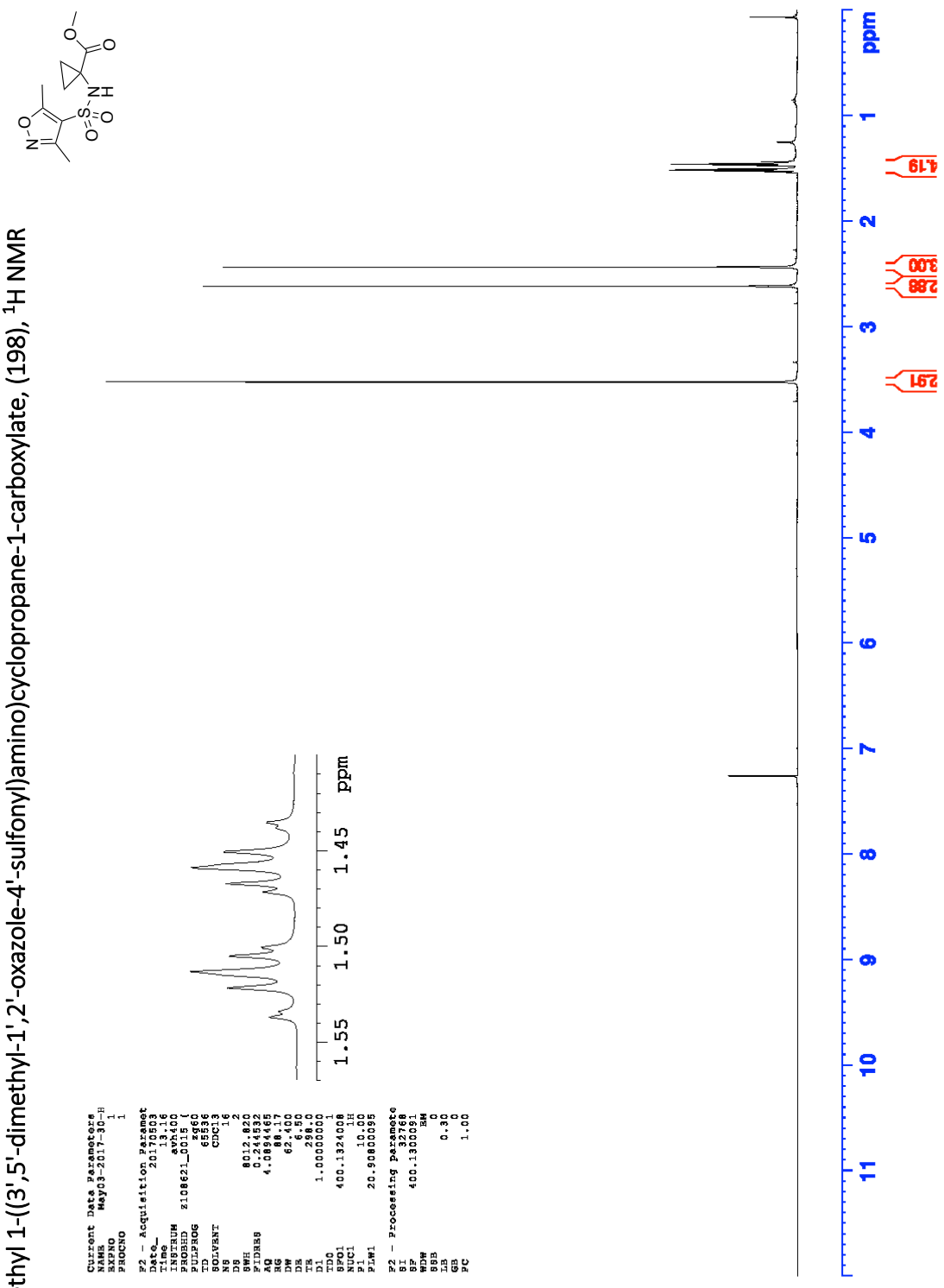
N-(3',5'-Dimethyl-1',2'-oxazole-4'-sulfonyl)-2-methylalanine (74), ^{1}H NMR



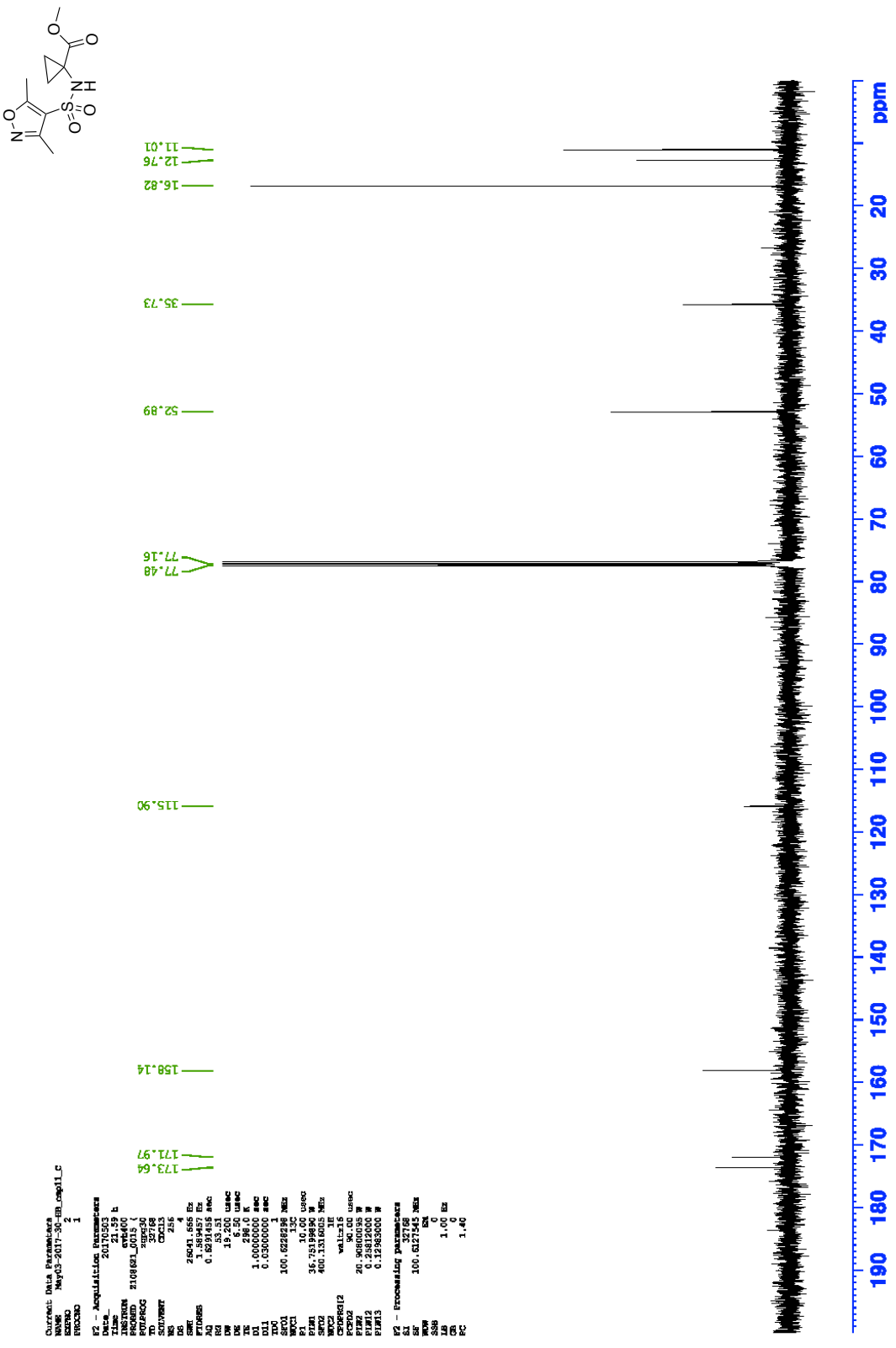
N-(3',5'-Dimethyl-1',2'-oxazole-4'-sulfonyl)-2-methylalanine (74), $^{13}C\{^{1}H\}$ NMR



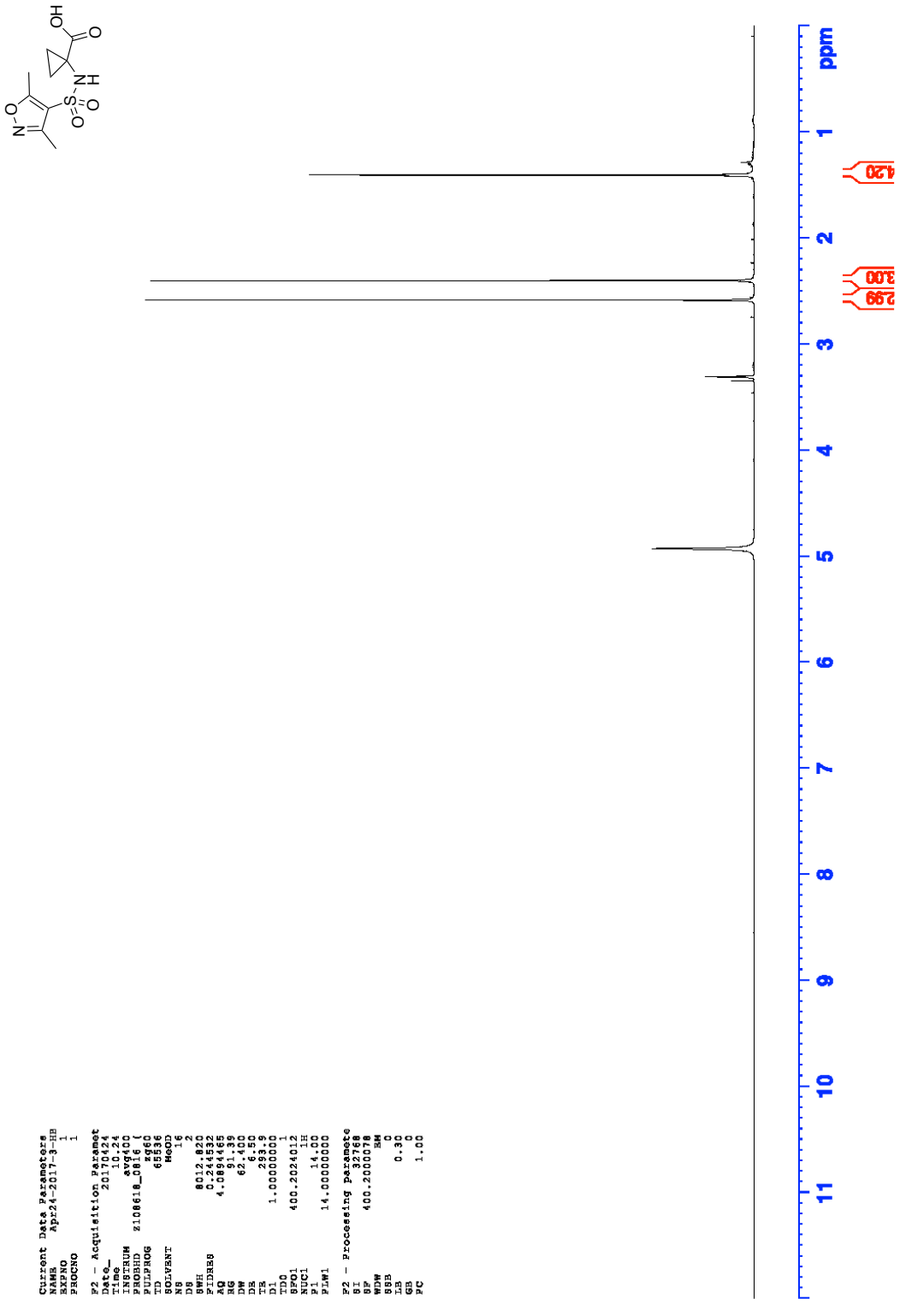
Methyl 1-((3',5'-dimethyl-1',2'-oxazole-4'-sulfonyl)amino)cyclopropane-1-carboxylate, (198), ^{1}H NMR



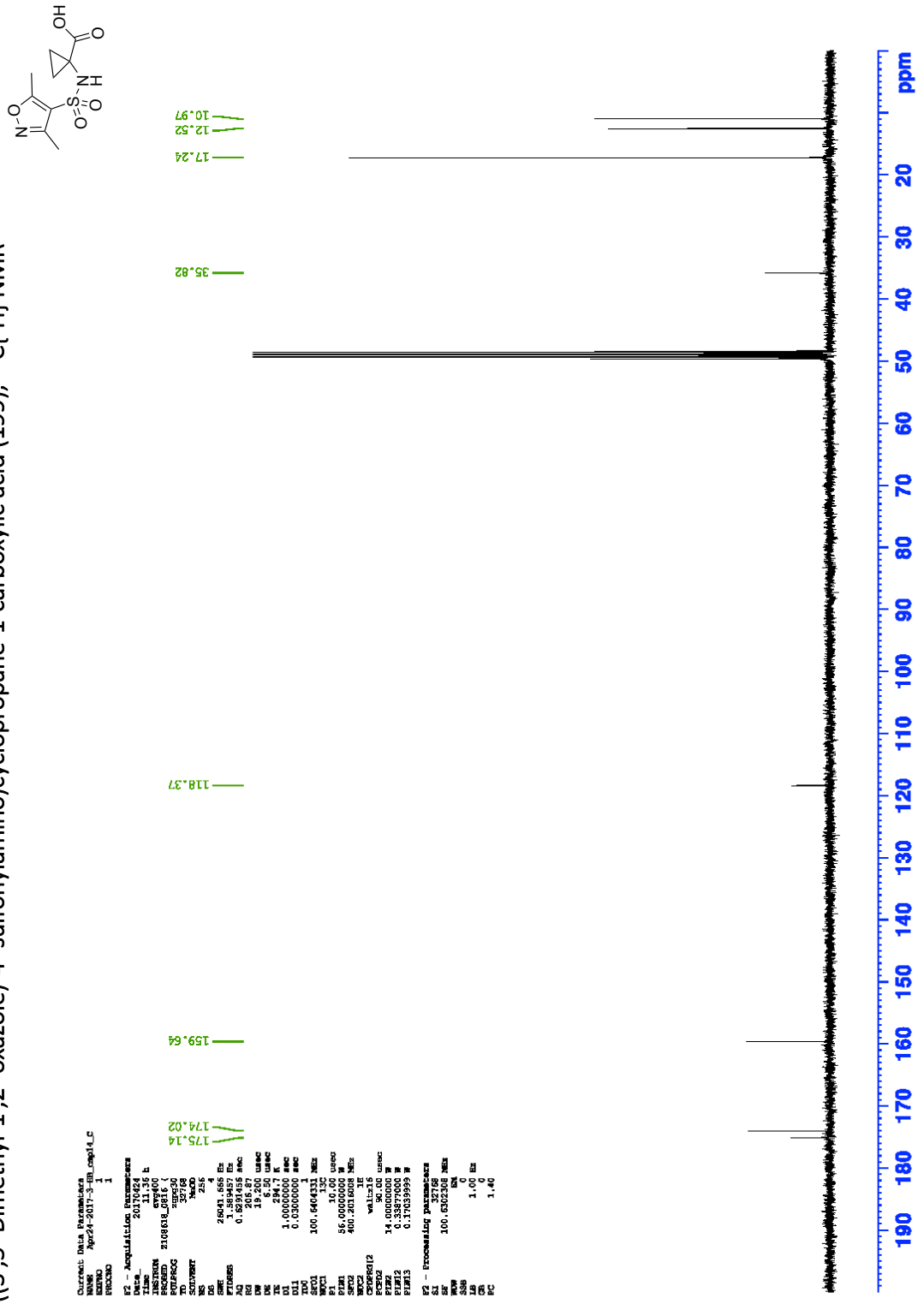
Methyl 1-((3',5-dimethyl-1',2'-oxazole-4'-sulfonyl)amino)cyclopropane-1-carboxylate (198), $^{13}C\{^{1}H\}$ NMR



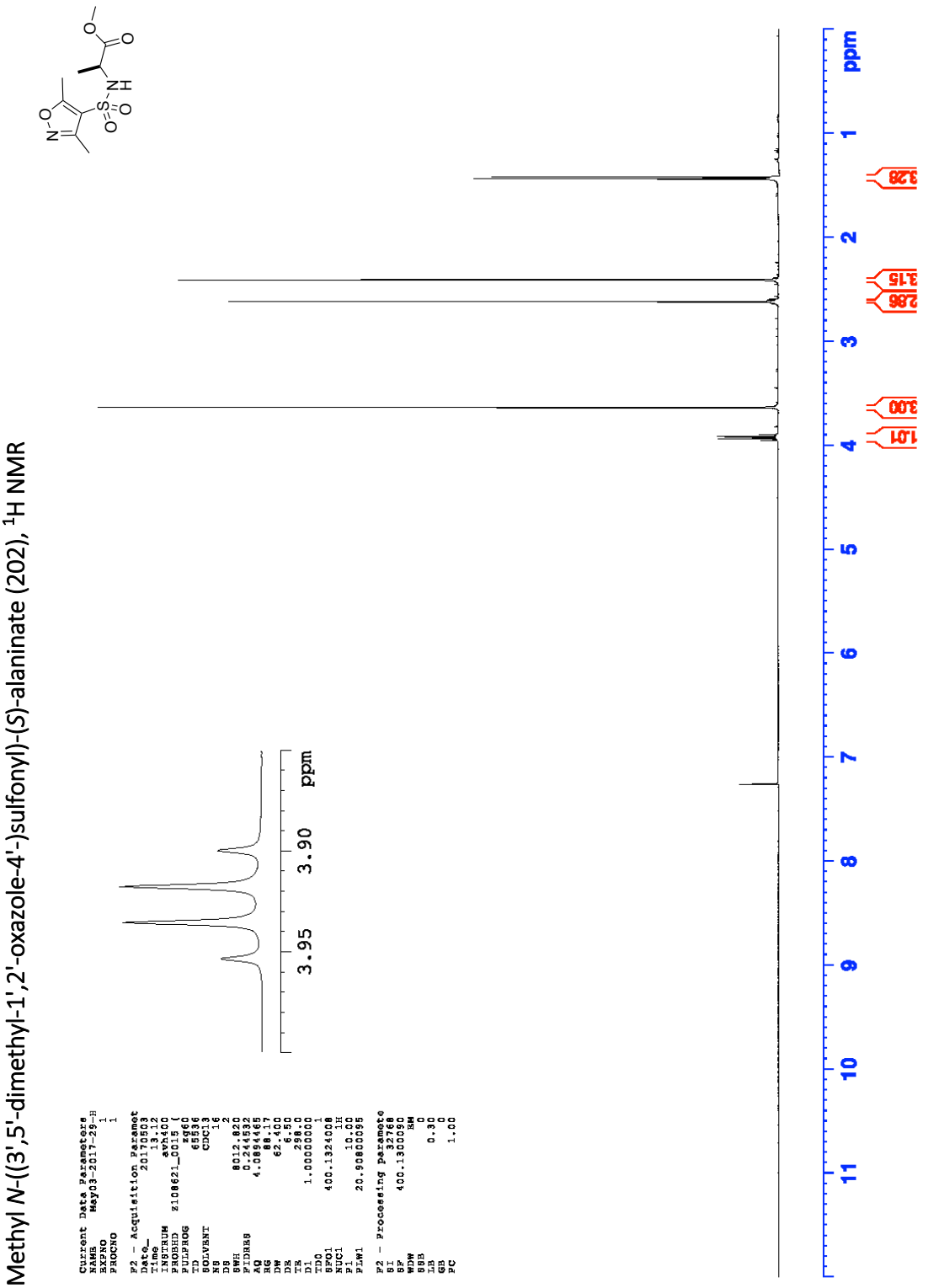
1-((3',5'-Dimethyl-1',2'-oxazole)-4'-sulfonylamino)cyclopropane-1-carboxylic acid (199), ^{1}H NMR



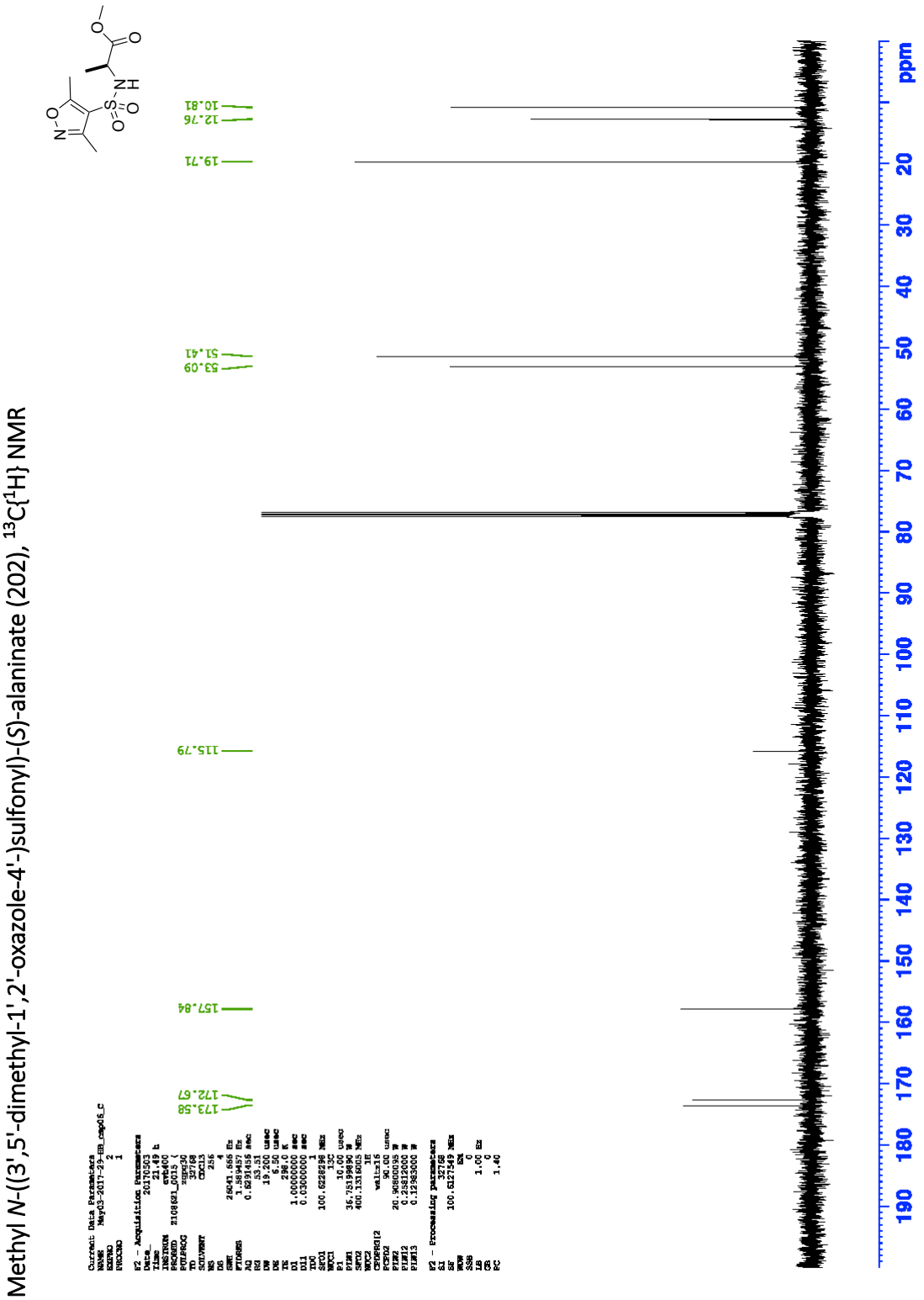
1-((3',5'-Dimethyl-1',2'-oxazole)-4'-sulfonylamino)cyclopropane-1-carboxylic acid (199), $^{13}C\{^{1}H\}$ NMR



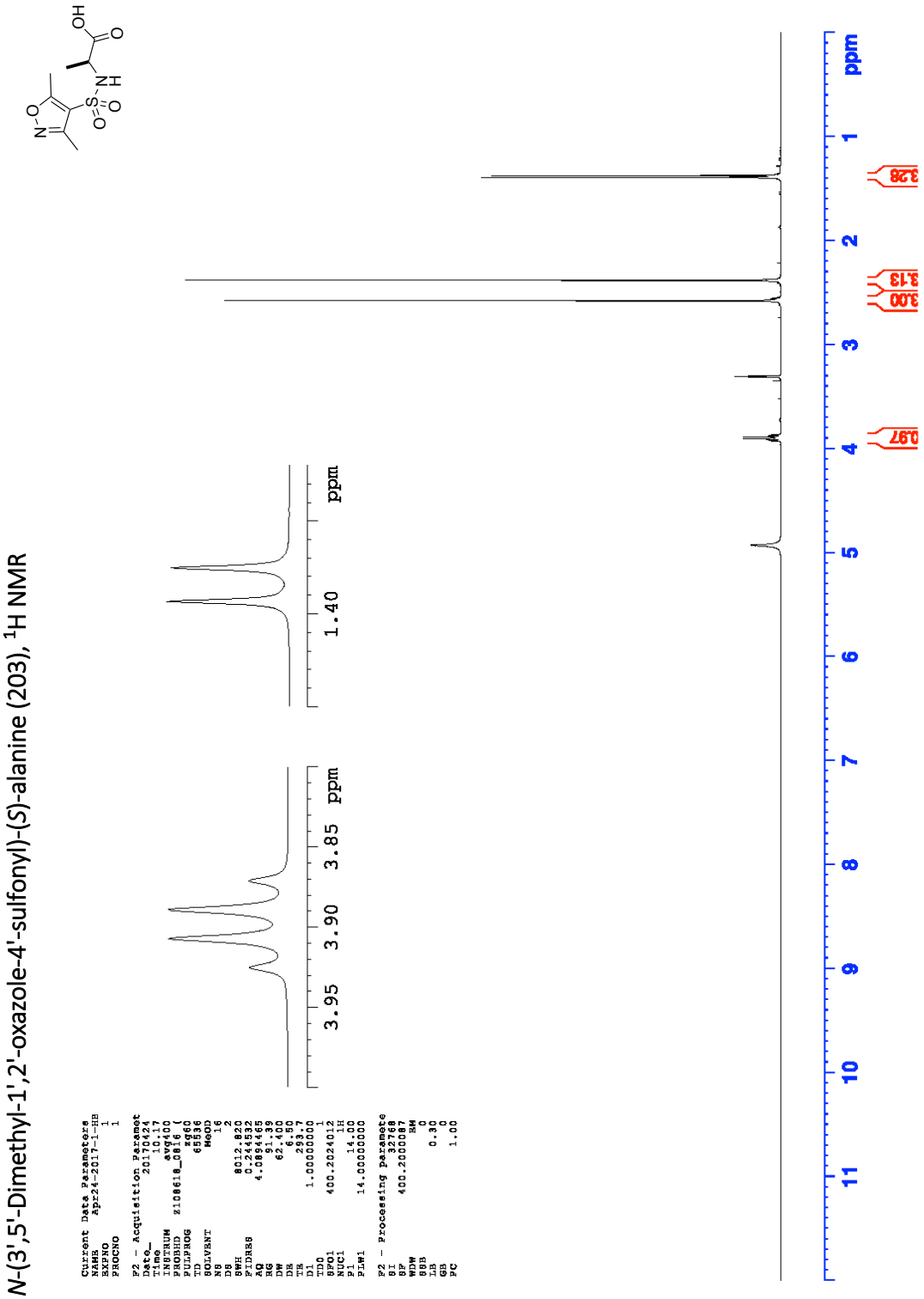
Methyl *N*-((3',5'-dimethyl-1',2'-oxazole-4'-)sulfonyl)-(*S*)-alaninate (202), ^{1}H NMR



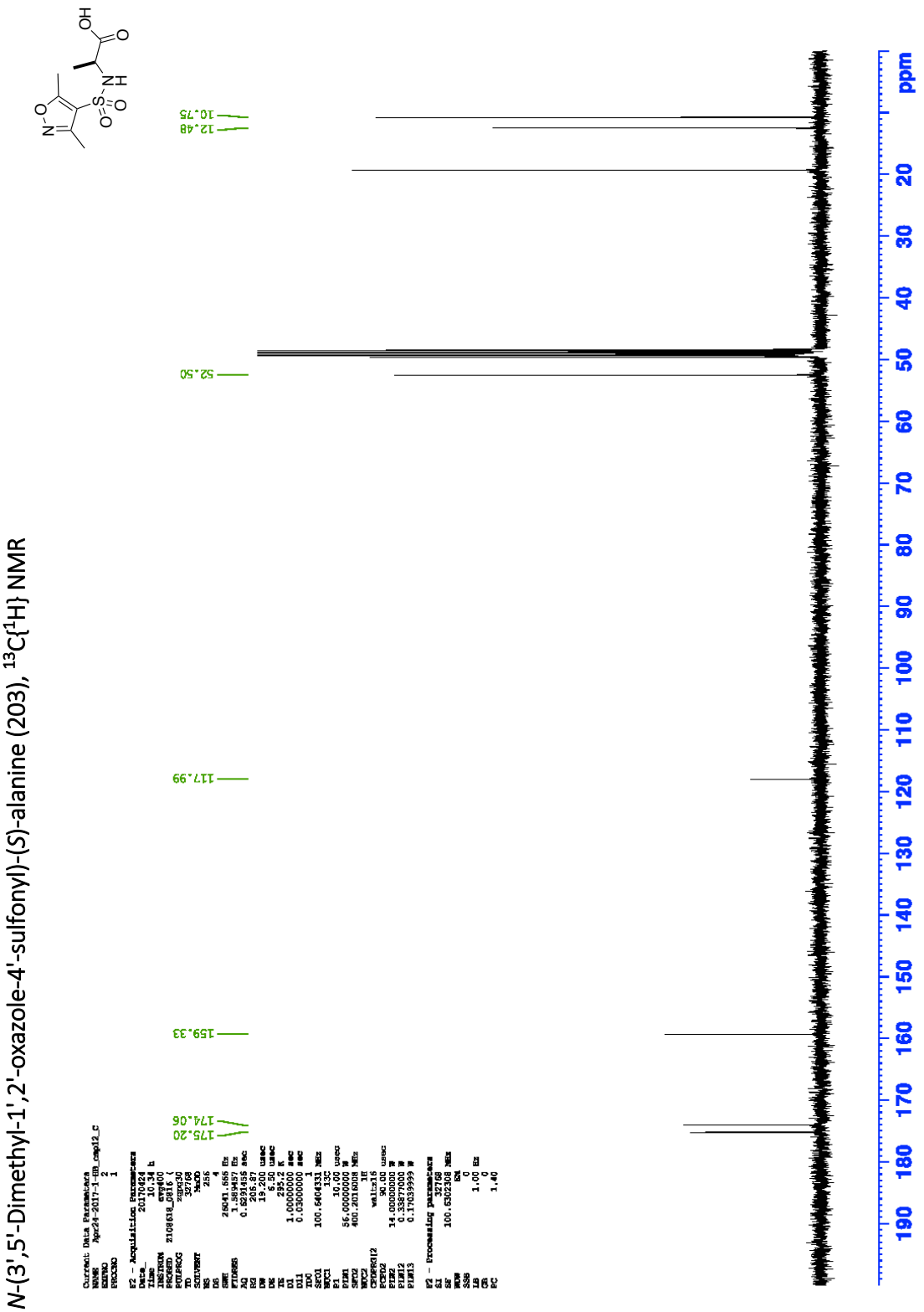
Methyl *N*-((3',5'-dimethyl-1',2'-oxazole-4'-)sulfonyl)-(*S*)-alaninate (202), $^{13}C\{^{1}H\}$ NMR



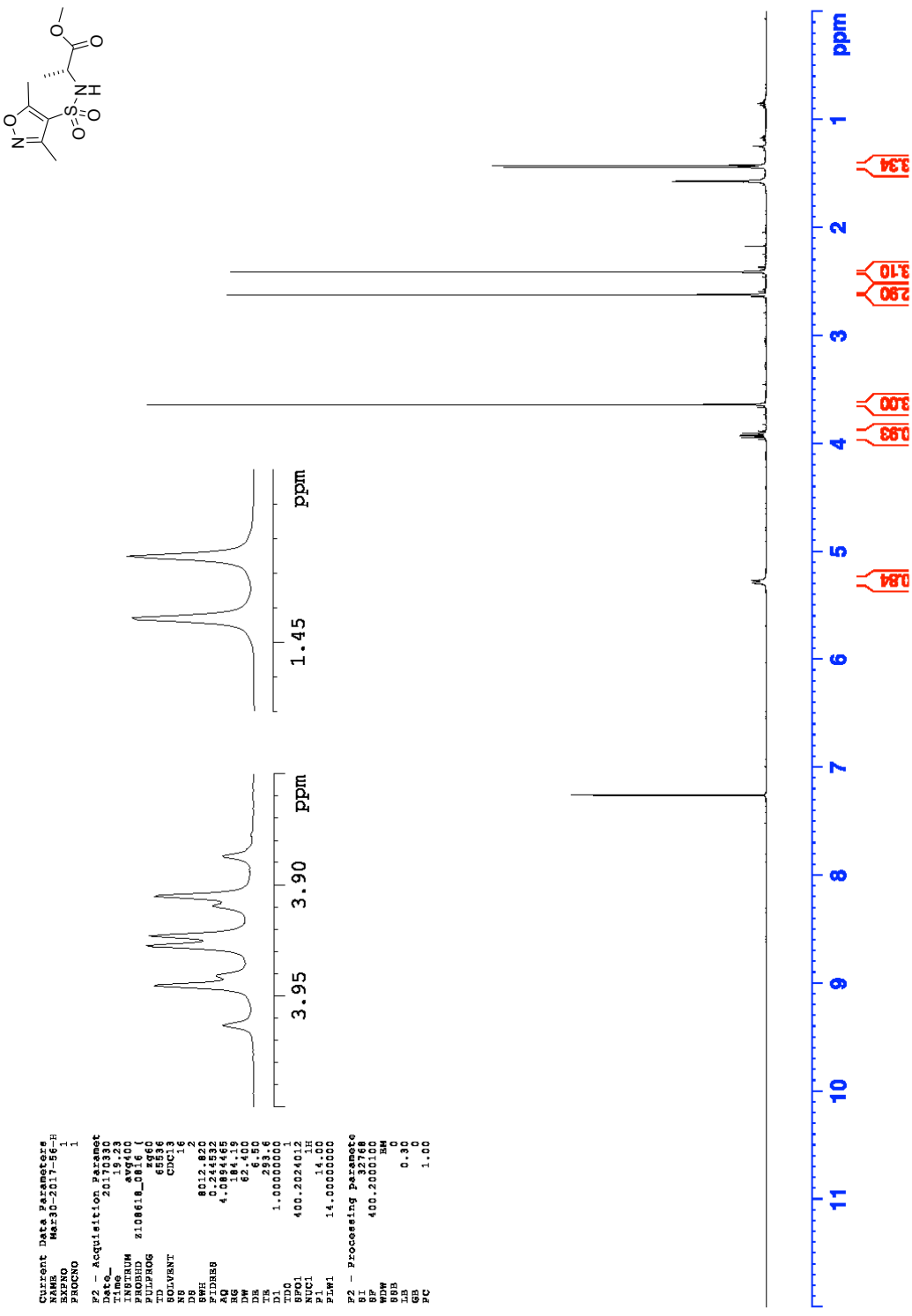
N-(3',5'-Dimethyl-1',2'-oxazole-4'-sulfonyl)-(*S*)-alanine (203), ^{1}H NMR



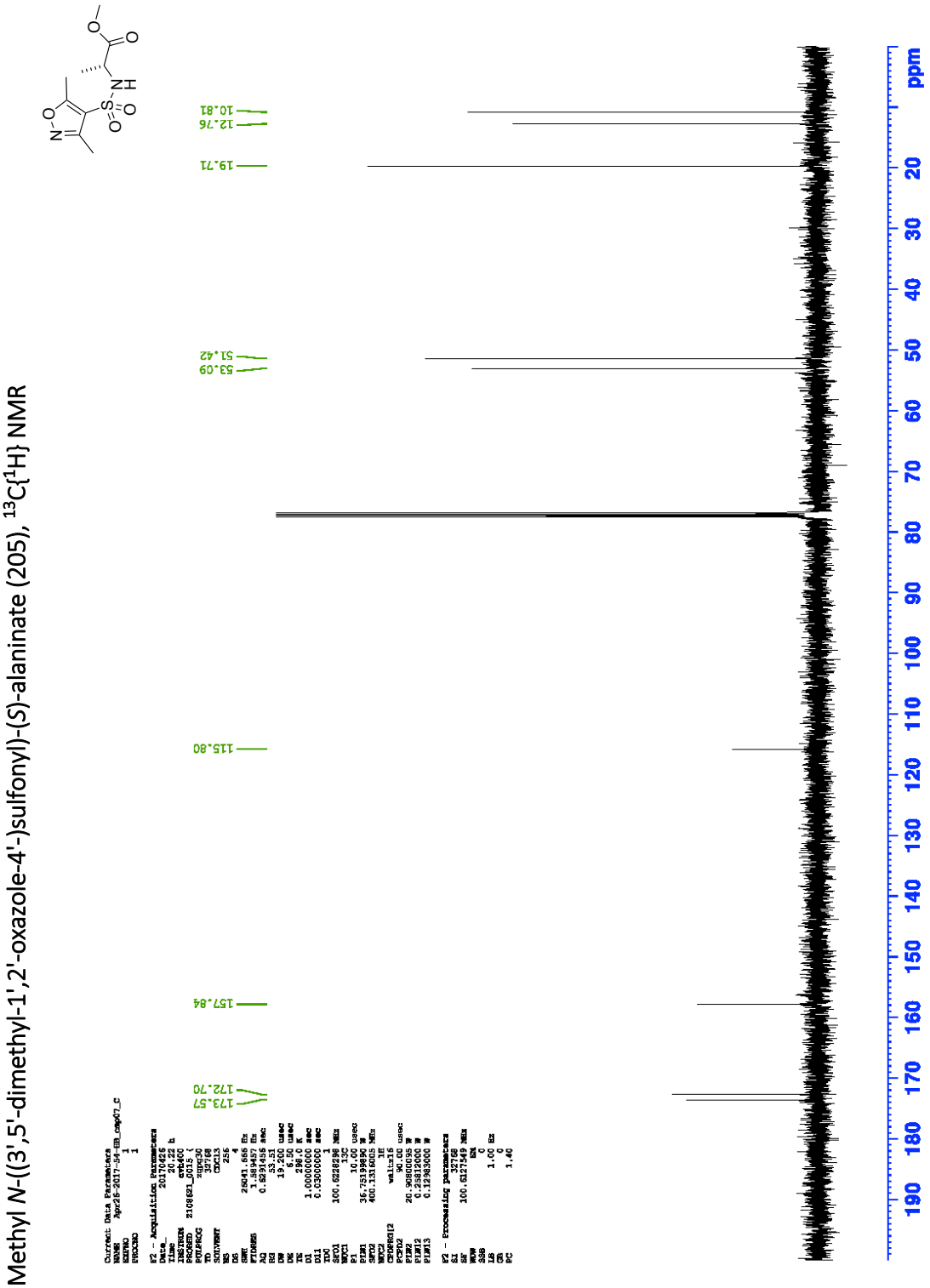
N-(3',5'-Dimethyl-1',2'-oxazole-4'-sulfonyl)-(*S*)-alanine (203), $^{13}C\{^{1}H\}$ NMR



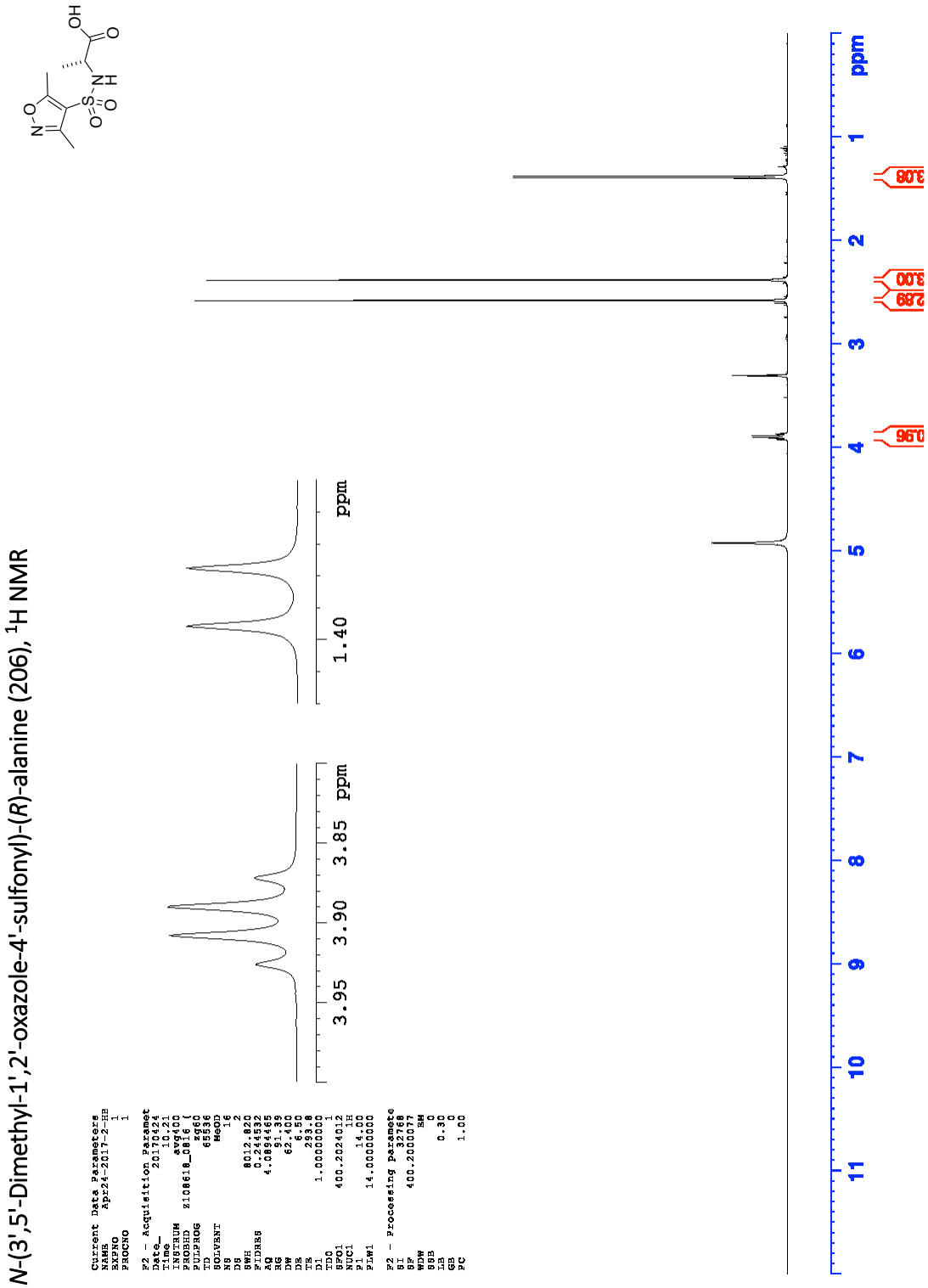
Methyl *N*-((3',5'-dimethyl-1',2'-oxazole-4'-)sulfonyl)-(*R*)-alaninate (205), ^{1}H NMR



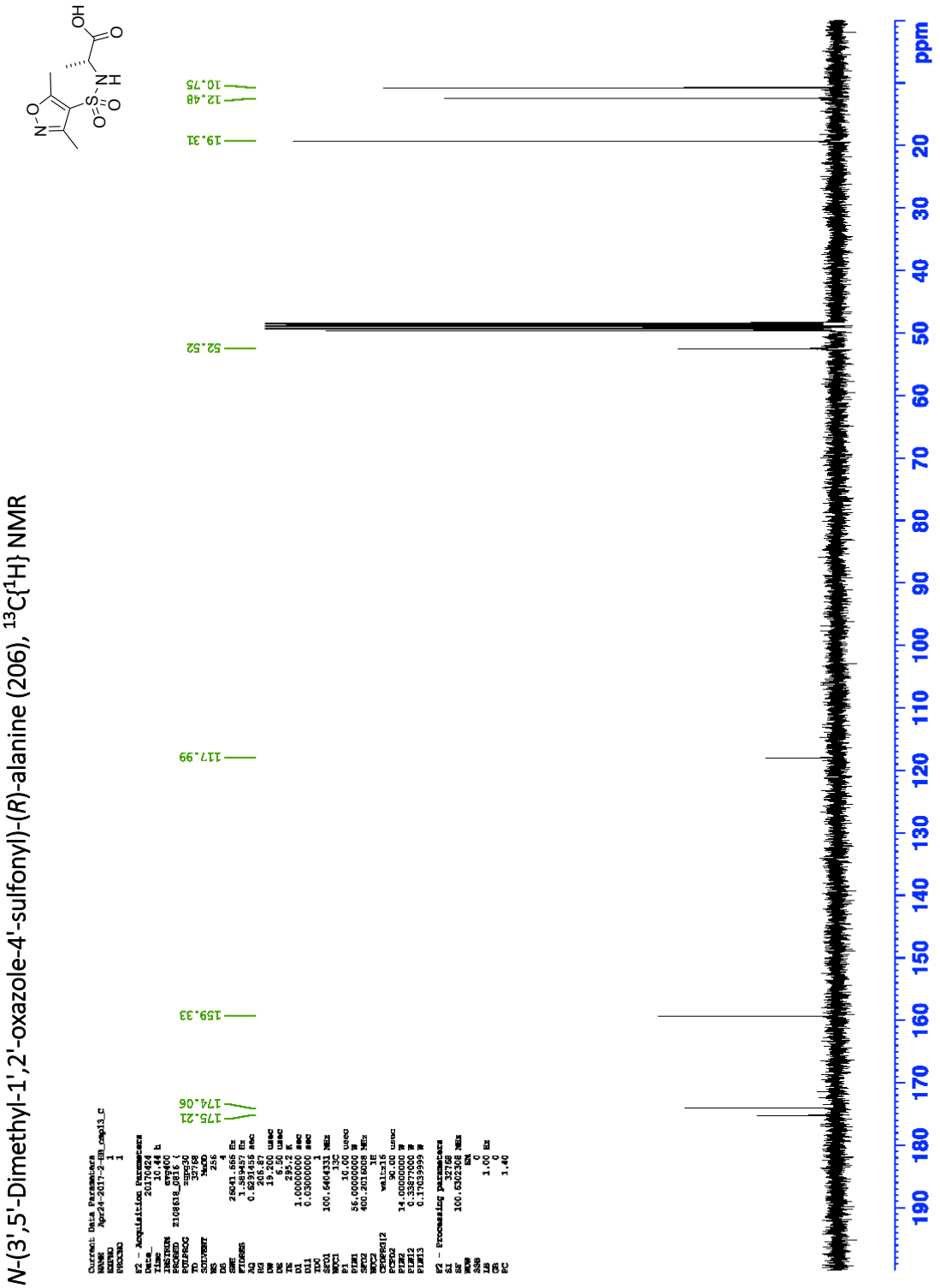
Methyl *N*-((3',5'-dimethyl-1',2'-oxazole-4'-)sulfonyl)-(*S*)-alaninate (205), $^{13}C\{^{1}H\}$ NMR



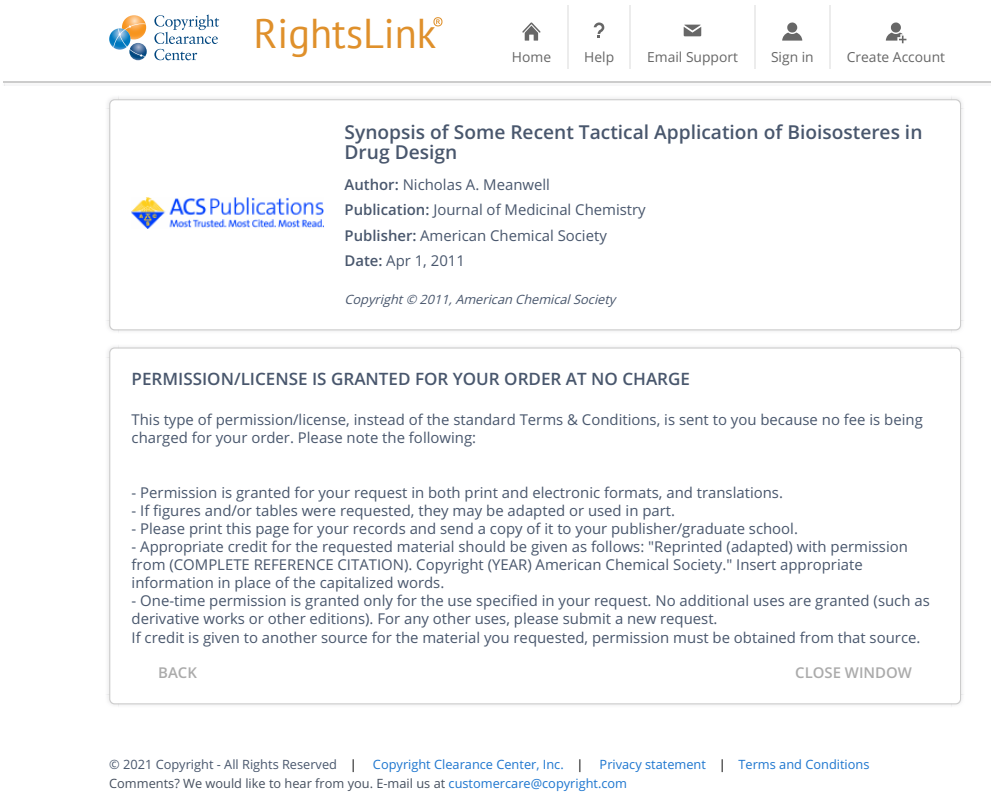
N-(3',5'-Dimethyl-1',2'-oxazole-4'-sulfonyl)-(*R*)-alanine (206), ^{1}H NMR



N-(3',5'-Dimethyl-1',2'-oxazole-4'-sulfonyl)-(*R*)-alanine (206), $^{13}C\{^{1}H\}$ NMR



H: Image Permissions



Copyright Clearance Center RightsLink®

Home | Help | Email Support | Holly Bunce

Chapter: Chapter 11 Protein–Ligand Screening by NMR
Book: High-Resolution NMR Techniques in Organic Chemistry
Author: Timothy D.W. Claridge
Publisher: Elsevier
Date: 2016

Copyright © 2016 Elsevier Ltd. All rights reserved.

Order Completed

Thank you for your order.

This Agreement between Miss. Holly Bunce ("You") and Elsevier ("Elsevier") consists of your license details and the terms and conditions provided by Elsevier and Copyright Clearance Center.

Your confirmation email will contain your order number for future reference.

License Number	4987550423454
License date	Jan 14, 2021

Printable Details

Licensed Content

Licensed Content Publisher	Elsevier
Licensed Content Publication	Elsevier Books
Licensed Content Title	High-Resolution NMR Techniques in Organic Chemistry
Licensed Content Author	Timothy D.W. Claridge
Licensed Content Date	Jan 1, 2016
Licensed Content Pages	35
Journal Type	S&T

Order Details

Type of Use	reuse in a thesis/dissertation
Portion	figures/tables/illustrations
Number of figures/tables/illustrations	1
Format	both print and electronic
Are you the author of this Elsevier chapter?	No
Will you be translating?	No

About Your Work

Title	Development of small molecule, peptide mimetic, activating ligands of the potassium efflux (Kef) system
Institution name	University of Oxford
Expected presentation date	Feb 2021

Additional Data

Portions	Figure 11.21. Magnetisation transfer processes from water to ligand operating in the water-LOGSY experiment.

Requestor Location

Requestor Location	Miss. Holly Bunce Chemistry Research Laboratory Oxford, OX13TA United Kingdom Attn: Miss. Holly Bunce

Tax Details

Publisher Tax ID	GB 494 6272 12

Price

Total	0.00 GBP

Total: 0.00 GBP

CLOSE WINDOW ORDER MORE

© 2021 Copyright - All Rights Reserved | Copyright Clearance Center, Inc. | Privacy statement | Terms and Conditions
Comments? We would like to hear from you. E-mail us at customercare@copyright.com